

Improving the sustainability of heterogeneous catalysis through understanding the role of carbon



Catherine Helen Collett
Supervisor: Dr James McGregor

Department of Chemical and Biological Engineering
University of Sheffield

Thesis submitted for the degree of

Doctor of Philosophy

September 2018

Abstract

Two key challenges facing the chemical industry are tackling climate change and improving sustainability. Improved understanding of the catalytic activity of carbon would assist the development of carbonaceous catalysts sourced from renewable materials, replacing increasingly-scarce metals. The phenomenon of catalytically active coke could also be exploited to improve the efficiency of industrial reactions.

Biochars are by-products of biomass pyrolysis and are attracting increasing interest as catalytic materials. Studies often overlook the impact of feedstock choice, graphitic carbon and trace metal content on catalytic performance. In the present work, the catalytic activity of biochars from four feedstocks before and after surface treatments, alongside a commercial activated carbon, is studied in two reactions utilising waste products as feedstocks, to gain insights into properties influencing catalytic activity.

The catalytic activity of untreated biochar was demonstrated for the first time in the conversion of methanol to dimethoxymethane (DMM) and in the upgrading of glycerol with carbon dioxide (CO₂) to glycerol carbonate and acetins. Potassium content was a key influence: removal of potassium enhanced DMM production, whilst the yields of glycerol carbonate were reduced up to 100 times over demineralised biochar ashes. In addition, methanol conversion over biochar catalysts led to the production of 1,1-dimethoxyethane (1,1-DME), which has not previously been noted in the literature. Production of 1,1-DME may be correlated with more graphitic carbon.

Following development of a novel liquid phase tar impregnation method, pyrolysis of the tar over biochar led to increased surface carbon content. The graphiticity of the surface carbon increased over biochars with higher potassium content, and decreased over biochars with lower potassium content. Over demineralised samples, this trend reversed, implying potassium may influence the formation of graphitic carbon during pyrolysis.

Future studies should consider an application-centred approach to biomass feedstock selection, to realise the full potential of biochars in catalysis.

*To my family and friends, who always believed in me, even when I
lost faith in myself.*

Contents

Abstract	iii
Acknowledgements	vii
Statement of Thesis Length.....	vii
Nomenclature	viii
List of Figures	ix
List of Tables.....	xv
List of Schemes	xv
Chapter 1 – Introduction.....	1
1.1. Context.....	1
1.2. Introduction to heterogeneous catalysis	4
1.3. Catalyst deactivation	5
1.4. CO ₂ utilisation reactions.....	8
1.5. Biochar	10
1.6. Characterisation techniques to be used.....	10
1.7. Aims and Objectives	11
Chapter 2 – Literature Review	13
2.1. Introduction	13
2.2. Applications of carbon in catalysis	14
2.3. Applications of biochar	25
2.4. Role of carbon in CO ₂ utilisation reactions	28
2.5. Characterisation of carbonaceous catalysts	34
2.6. Conclusions	47
Chapter 3 – Experimental Methods.....	53
3.1 Catalyst preparation	53
3.2 Surface treatments.....	56
3.3 Vibrational spectroscopy.....	60
3.4 Composition.....	63
3.5 Adsorption isotherms.....	66
3.6 Reaction studies.....	69
3.7 Summary	76
Chapter 4 – Biochar Characterisation.....	77
Overview.....	77
4.1. Introduction	78
4.2. Methods.....	80
4.3. Results.....	88
4.4. Discussion	108
4.5. Conclusions.....	118
Chapter 5 – Surface Treatments	121
Overview.....	121
5.1. Introduction	122

5.2. Methods.....	124
5.3. Results.....	130
5.4. Discussion	158
5.5. Conclusions.....	173
Chapter 6 – Methanol Conversion.....	177
Overview.....	177
6.1. Introduction	177
6.2. Methods.....	180
6.3. Results.....	183
6.4. Discussion	197
6.5. Conclusions.....	208
Chapter 7 – Glycerol Upgrading.....	211
Overview.....	211
7.1. Introduction	211
7.2. Methods.....	215
7.3. Results.....	219
7.4. Discussion	228
7.5. Conclusions.....	239
Chapter 8 – Discussion.....	242
Overview.....	242
8.1. Introduction	242
8.2. Reliability of results	244
8.3. Potential applications of biochar in catalysis	249
8.4. Implications for carbonaceous catalyst design.....	253
8.5. Potential for exploiting coking	256
8.6. Further considerations.....	258
8.7. Summary	261
Chapter 9 – Conclusions and Future Work.....	263
9.1. Introduction	263
9.2. Characterisation of carbonaceous catalysts.....	264
9.3. Potential applications of biochar in catalysis	269
9.4. Insights for design of carbonaceous catalysts	273
9.5. Suggestions for Future Work.....	277
References	279
Appendix A Characterisation Method Development.....	A-1
Appendix B Surface Treatments	B-1
Appendix C Methanol reaction calibrations	C-1
Appendix D Glycerol reaction calibrations.....	D-1
Appendix E Things Go Better With Coke.....	E-1

Acknowledgements

This project was funded by the EPSRC through a University of Sheffield Doctoral Training Award, which is gratefully acknowledged. The 4CU grant EP/K001329/1 is acknowledged for funding the purchase and use of the SEM.

Thanks to the following members of the Sheffield Catalysis Group, who supported the development of the experimental methods used in this work: Ali Hameed (methanol conversion), Nurul Razali (glycerol upgrading), Laura Quintana-Gomez and Cynthia Kakie Kartey (GCMS analysis).

Special thanks to the following for their training and expertise in the characterisation of my often troublesome biochar samples: Ben Palmer, Yan Yan Farm and Joseph Manning (BET), George Dowson (IGA), Debbie Hammond (XPS), Nik Reeves-McClaren (Raman), Alan Dunbar (SEM-EDX) and Mark Jones (TGA). Very special thanks to the workshop staff at the Department of Chemical and Biological Engineering (particularly Adrian Lumby and Andy Patrick) for their support with maintenance and repairs of the batch reactors.

Thanks to Ondrej Masek and Javier Feroso of the School of Geosciences, University of Edinburgh, for the supply of biochars for this study, and for supervising an eight-week placement at the UK Biochar Research Centre.

Finally to my supervisor, James McGregor, for his incredibly dedicated supervision, generous approach to sharing knowledge, swift and constructive feedback, and unfailing confidence in my abilities.

Statement of Thesis Length

This thesis consists of **78,706** words, excluding references and appendices.

Nomenclature

Abbreviations and Acronyms

AAEM	Alkali and Alkali Earth Metals
AC	Activated charcoal
at%	atom percent
ATR	Attenuated Total Reflectance
BET	Brunauer-Emmett-Teller (isotherm)
EDS/EDX	Energy Dispersive X-ray Spectroscopy
FTIR	Fourier Transform Infrared (Spectroscopy)
GCMS	Gas Chromatography Mass Spectrometry
IGA	Intelligent Gravimetric Analyser
IR	Infrared
m/z	mass to charge ratio
MS	Mass Spectrometry
NLDFT	Non-local density functional theory
OSB	oil seed rape biochar
PGM	platinum group metals
PSD	pore size distribution
RHB	rice husk biochar
rpm	rotations per minute
SEM	Scanning Electron Microscopy
SSB	sewage sludge biochar
SWB	soft wood biochar
TGA	Thermogravimetric Analysis
THz-TDS	Terahertz Time Domain Spectroscopy
TPD	Temperature Programmed Desorption
WSB	wheat straw biochar
wt %	weight percent
XPS	X-ray Photoelectron Spectroscopy
XRD	X-ray Diffraction

Chemicals

DMM	dimethoxymethane
1,1-DME	1,1-dimethoxyethane
DME	dimethyl ether
TMOS	tetramethyl orthosilicate

Suffixes

-###	pyrolysis temperature of biochar (°C)
-A	acetone-washed
-DM	demineralised (treated with hydrochloric acid)
-P	biochar pyrolysed for 1 hour at 550 °C (control test)
-T	tar-impregnated
-T-C	tar-impregnated, followed by pyrolysis

List of Figures

Figure 1-1 The twelve principles of green chemistry (Anastas & Warner 1998). Reproduced with permission of Oxford University Press through PLSclear.	2
Figure 1-2 Kinetic steps in the catalytic cycle. The reaction demonstrated is the oxidation of CO to CO ₂ (filled circles are carbon, open circles are oxygen).....	5
Figure 1-3 schematic of a supported metal catalyst, deactivated by carbon deposition. Figure from Bartholomew (2001), reproduced with permission from Elsevier.	6
Figure 2-1 Schematic of the effect of coking rate on the mechanism of deactivation of catalyst pores. (a) slow coking. (b) rapid coking, leading to pore plugging. Figure adapted from Menon (1990) with permission from Elsevier.....	15
Figure 2-2 The influence of reaction temperature on the structure of carbon deposits formed from cyclohexane on HY zeolite catalysts. Figure produced based on data available in the literature (Menon 1990), and previously published in Catalysis Science and Technology (Collett & McGregor 2016).	15
Figure 2-3 Processes of carbon in the gas phase and the formation of carbon macrostructures (Serp & Figueiredo 2009). Reproduced with permission from John Wiley and Sons Inc.	16
Figure 2-4 Schematic of the facilitation of hydrogen transfer by tetralin. The hydrogen in the saturated ring is activated by the unsaturated ring.	22
Figure 2-5 Model of the palladium surface demonstrating the role of the palladium carbide phase during 1-pentyne hydrogenation (Teschner et al. 2006). The metal carbide phase inhibits the emergence of the dissolved hydrogen, which promotes over-hydrogenation. Reproduced with permission. Copyright 2006 Elsevier.	23
Figure 2-6 Methanol oxidation pathways. Figure reproduced with permission from the Royal Society of Chemistry (Julien Gornay et al. 2010). Dimethoxymethane highlighted for clarity.	29
Figure 2-7 Direct and indirect applications of glycerol carbonate. Figure reproduced with permission from the Royal Society of Chemistry (Sonnati et al. 2013).	32
Figure 2-8 Ideal biochar structure development with highest treatment temperature: (a) increased proportion of aromatic C, highly disordered in amorphous mass; (b) growing sheets of conjugated aromatic carbon, turbostratically arranged; (c) structure becomes graph. Figure reproduced with permission from Routledge through PLSclear (Lehmann & Joseph 2009).	43
Figure 2-9 Schematic representations of the structure of (a) graphitising and (b) non-graphitising carbons, as proposed by Rosalind Franklin (Franklin 1951). Reproduced with permission from The Royal Society.	44
Figure 2-10 The structure of graphite, with the spacing between layers (d_{002}) and the ring size (d_{100}) annotated.	45
Figure 2-11 Schematic of biochar structure at different scales. (a) The macropores are visible in SEM images and are often highly ordered and regular in woody biomass. (b) For non-graphitisable carbons, lamellae are oriented relatively randomly compared to each other. (c) The surface of the biochar contains both flat sides and edges of graphite-like sheets, as well as exposed ash and amorphous carbon/tar. (d) At the atomic scale, a range of functional groups have been observed at the surface, generally at the edges of the sheets. Graphitic, aromatic and amorphous carbon will be present. Some ash will also be present at the surface.	46
Figure 3-1 Schematic of the Stage I Pyrolysis Unit, UK Biochar Research Centre, University of Edinburgh. Figure reproduced with permission from John Wiley and Sons (Crombie et al. 2013).	59
Figure 3-2 Schematic of operating principle of FTIR-ATR.	61
Figure 3-3 Schematic of interaction of incident x-ray (energy $h\nu$) with core level electrons.	64
Figure 3-4 Schematic of batch reactor (Parr Instruments) used for reaction studies.	71
Figure 4-1 Gold sputter coater set-up.	83
Figure 4-2 BET surface area of sieved biochar from different feedstocks, compared with commercial standard AC. Isotherm obtained using N ₂ at 77 K. Error bars calculated from three repeats of WSB-550; standard deviation $\pm 1.25 \text{ m}^2 \text{ g}^{-1}$, percentage error 2.42 %.	89

Figure 4-3 Micropore volume for biochars from different feedstocks. Percentage error of 12.52 % calculated from two repeats of WSB-550 (one anomalous result omitted). No microporosity detected in OSB-550.	89
Figure 4-4 Adsorption and desorption isotherms for biochars and activated carbon. Adsorption data points are open circles (°), desorption data points are crosses (x).	90
Figure 4-5 Reproducibility of pore size distributions for three samples of WSB-550.....	91
Figure 4-6 Pore size distribution for (a) biochars from different feedstocks, and (b) biochars prepared at different pyrolysis temperatures. PSDs calculated from BET isotherms by NLDFT.	92
Figure 4-7 SEM images comparing the structure of sieved biochars from different feedstocks at magnification ×1000. (a) AC, (b) RHB-550, (c) OSB-550, (d) WSB-550, (e) SWB-550 (magnification ×500 to show larger pores) and (f) SWB-550 large particle (×400) before sieving. Pores highlighted with red circles for clarity in (d) and (e).	94
Figure 4-8 Comparison of proximate analysis for biochars from different feedstocks. Error analysis based on two repeats of WSB-550-DM-T-C. Percentage error calculated as: moisture 3.37%, volatiles 3.39%, carbon 0.55% and ash 0.51%.....	95
Figure 4-9 Elemental XPS surveys of biochars of interest. (a) Key elements, C, N, O, Si and K, with ‘other’ elements shown in (b). Data for biochars marked * collected and analysed separately by Dr James McGregor. Error bars calculated from standard deviation of two samples. For SWB-550 and OSB-550, only one sample run; error bars are the average standard deviation calculated from the other samples. No error analysis for Sr and Y elements due to lack of data.	96
Figure 4-10 FTIR-ATR spectra for biochars from different feedstocks pyrolysed at 550 °C, compared with commercial AC.....	97
Figure 4-11 CO ₂ adsorption isotherms for biochars from three feedstocks, compared with commercial AC. Dashed lines to guide the eye only.....	99
Figure 4-12 Raman curve deconvolution data for different biochar feedstocks. The percentage error in each band is estimated from curve deconvolution performed on three spectra from WSB-550-DM.	101
Figure 4-13 A _{D1} /A _G ratio from Raman curve deconvolution data for biochars from different feedstocks. Percentage error of ± 20 % calculated from three repeats of curve deconvolution of WSB-550-DM.....	102
Figure 4-14 Example annotated curve deconvolution for XPS C1s spectra for OSB-700.	103
Figure 4-15 XPS C1s curve deconvolution data for biochars from different feedstocks, comparing the contribution from seven C1 bands. Error bars are standard deviation calculated from curve deconvolution of two spectra for each sample.....	104
Figure 4-16 THz spectroscopy data for biochars from different feedstocks. Data collected and analysed by Dr James McGregor.....	105
Figure 4-17 THz spectroscopy data for sewage sludge biochar pyrolysed at temperatures from 250-750 °C... 106	106
Figure 4-18 Schematic of the surface structures of (a) RHB-550 and (b) SWB-550, using experimental data from Chapter 4.	111
Figure 4-19 Comparison of the proportion of graphitic carbon in biochars as measured by Raman spectroscopy, versus ash content as measured by TGA analysis.	114
Figure 5-1 Composition of ash samples from untreated and demineralised biochars. (a) shows main components of the ash, with trace components (<5 at%) shown in (b). -DM indicates demineralised biochar.	131
Figure 5-2 Quantities of key elements of interest in biochars before and after demineralisation, as measured by XPS elemental survey scans. Error bars are standard deviations based on measurements of two areas of the sample (negligible error detected for P 2p for WSB-550-DM). -DM indicates demineralised sample.....	132
Figure 5-3 BET surface area for biochars before and after demineralisation. Error bars based on percentage error of 2.42% calculated from three repeats of WSB-550.	134
Figure 5-4 Micropore volume of biochars from different feedstocks before and after demineralisation. Percentage error of 12.5 % calculated from two repeats of WSB-550 (third anomalous value omitted).	135
Figure 5-5 Pore size distribution for biochars from different feedstocks before and after demineralisation. ..	135

Figure 5-6 SEM images of biochar grains before and after demineralisation. Two different areas imaged for each sample. Top: (a) RHB-550, (b) RHB-550-DM, middle: (c) OSB-700, (d) OSB-700-DM, bottom: (e) WSB-550, (f) WSB-550-DM.....	136
Figure 5-7 XPS C1s curve deconvolution data for biochar samples before and after demineralisation.	137
Figure 5-8 Thermogravimetric Analysis of biochar samples from different feedstocks before and after acetone washing for (a) untreated and (b) demineralised biochars. Error bars estimated from percentage error for two samples of WSB-550-DM-T-C samples.	138
Figure 5-9 BET surface area measurements for biochars from different feedstocks before and after acetone washing. Error bars estimated from percentage error of 2.42% for three repeats of WSB-550.	139
Figure 5-10 Micropore volume of biochars before and after acetone washing, measured using t-plots.	140
Figure 5-11 Pore size distributions for biochar samples before and after acetone washing. (a) RHB-550, (b) OSB-700 and (c) WSB-550. Solid lines are untreated, dotted lines are acetone-washed.	141
Figure 5-12 FTIR spectra of SWB samples before and after acetone washing. The aromatic C=C band at 1580 cm ⁻¹ is highlighted. -DM indicates demineralised sample.	142
Figure 5-13 Results of TGA proximate analysis for tar-impregnated biochars. -T indicates the tar-impregnated biochar prior to pyrolysis.	143
Figure 5-14 Comparison of experimentally measured RHB-T composition with predicted RHB-T composition, using the results of the RHB acetone control test. A tar loading of 10.2 g per 100 g biochar was calculated to give the observed ash content after tar impregnation.	144
Figure 5-15 TGA proximate analysis data demonstrating the effect of acetone washing and pyrolysis steps on RHB-550. -A indicates acetone-washed, -P indicates pyrolysed, -T-C indicates tar impregnated and pyrolysed.	145
Figure 5-16 XPS elemental analysis of biochars before and after tar impregnation for four key elements of interest: O, C, Si and K. Error bars are standard deviation from two measurements on the sample. -T-C indicates tar-impregnated and pyrolysed samples.	146
Figure 5-17 Tar loading estimates for biochars, calculated by assuming the reduction in percentage ash content after tar impregnation is solely due to additional tar.	147
Figure 5-18 XPS elemental analysis of demineralised biochars before and after tar impregnation and pyrolysis. Error bars are standard deviation from two measurements on the sample.	148
Figure 5-19 BET surface areas for demineralised biochars before and after tar impregnation.	149
Figure 5-20 Micropore volume of demineralised biochar samples before and after tar impregnation and pyrolysis. A logarithmic y-axis is used to allow the clear presentation of large and small values.	149
Figure 5-21 Pore size distributions for demineralised biochar samples before and after tar impregnation. -DM denotes demineralised biochar, -T-C denotes tar impregnated and pyrolysed biochar. Dotted lines are used to distinguish the tar-impregnated biochars.	150
Figure 5-22 Deconvolved Raman spectra for demineralised biochars before and after tar impregnation.	151
Figure 5-23 Effect of tar impregnation over demineralised samples on the ratio of disordered (D1) to graphitic (G) carbon. The percentage error of 20 % was calculated from two repeats of WSB-550-DM.	152
Figure 5-24 XPS C1s curve deconvolution data for demineralised biochars before and after tar impregnation and pyrolysis.	153
Figure 5-25 Normalised FTIR spectra for demineralised biochars before and after tar impregnation and pyrolysis.	154
Figure 5-26 Schematic of the structure of RHB-550 (a) before and (b) after demineralisation using HCl.	162
Figure 5-27 Structure of abietic acid, a component of rosin oil in pine tar.	165
Figure 5-28 Schematic of the surface structure of RHB-550 (a) before and (b) after tar impregnation and pyrolysis.	167
Figure 5-29 Comparison of biochar properties before and after demineralisation and tar impregnation. Green = WSB-550, blue = OSB-700, purple = RHB-550, grey = SWB-550 and black = commercial AC. Open diamonds =	

untreated, filled diamonds = tar-impregnated, open circles = demineralised, filled circles = demineralised and tar-impregnated. The highlighted areas demonstrate that biochars remain clustered by feedstock type.	169
Figure 6-1 Comparison of the GCMS spectra for no catalyst. A logarithmic y-axis is used to allow presentation of both large and small peaks. Peaks as identified by MS are annotated.	184
Figure 6-2 Comparison of GCMS spectra for three biochars, compared with commercial AC. (a) for retention times 3.9-6.0 mins, (b) for 6-9 mins. A logarithmic y-axis scale is used to make the identification of smaller peaks easier.	185
Figure 6-3 Structure of (a) DMM compared with the structure of (b) 1,1-DME.	186
Figure 6-4 Liquid phase products of methanol conversion using biochars produced from different feedstocks. A logarithmic y-axis is used to present large and small concentrations. Percentage errors of 23.3 % for DMM and 20.0 % for 1,1-DME calculated from three repeats of SWB-550 for DMM concentration. Note that the concentration of 1,1-DME is given in arbitrary units.	188
Figure 6-5 GCMS peak areas for the internal standard, 2-propanol, for a set of experiments performed in March 2018.	188
Figure 6-6 Comparison of production of DMM and 1,1-DME with and without CO ₂	190
Figure 6-7 Comparison of production of DMM and 1,1-DME at different reaction pressures, using AC as a catalyst.	191
Figure 6-8 DMM and 1,1-DME production for treated biochar samples. Percentage error of 23.3 % for DMM and 20.0 % for 1,1-DME calculated from three repeats of SWB-550.	192
Figure 6-9 DMM and 1,1-DME production for treated biochar samples. Surface area for SWB-550-acetone not measured. LP indicates low pressure (20 bar, compared to 40 bar).	193
Figure 6-10 Quantity of TMOS produced when using biochars from a range of feedstocks. Percentage error estimated from two repeats of SWB-550 as 39.2 % (third repeat omitted as an outlier).	195
Figure 6-11 Plot of DMM concentration against surface potassium content. Note the logarithmic axis used for potassium content. (Green = WSB-550, blue = OSB-700, purple = RHB-550, grey = SWB-550 and black = commercial AC. Open diamonds = untreated, filled diamonds = tar-impregnated.)	198
Figure 6-12 Comparison of quantities of DMM and 1,1-DME produced in methanol conversion over various biochar catalysts. (Green = WSB-550, blue = OSB-700, purple = RHB-550, grey = SWB-550 and black = commercial AC. Open diamonds = untreated, filled diamonds = tar-impregnated, open circles = demineralised, filled circles = demineralised and tar-impregnated, cross = no catalyst, square = helium atmosphere.)	201
Figure 7-1 Decreasing retention time of the glycerol carbonate peak over time, as measured by calibrations. The position of the glycerol carbonate peak in reaction samples is also given to demonstrate the trend. Line shown to guide the eye only.	218
Figure 7-2 Annotated GCMS chromatograms for reaction products in the absence of catalyst. A logarithmic y-axis is used to allow presentation of both large and small peaks.	220
Figure 7-3 Product peak identification by GCMS for products of glycerol upgrading reaction, using biochars from different feedstocks. GCMS spectra divided into two parts for clarity. Logarithmic y-axis used to allow large and small peaks to be presented.	222
Figure 7-4 Concentrations of liquid phase products in the glycerol upgrading reaction, using biochars from different feedstocks as catalysts. Error bars represent the percentage error, calculated from 3 repeats of OSB-550. Logarithmic y-axis is used to present low and high concentrations of products.	223
Figure 7-5 Comparison of production of glycerol carbonate and acetins using biochars before and after demineralisation. A logarithmic y-axis is used to present high and low concentration products.	225
Figure 7-6 Comparison of production of glycerol carbonate and acetins from biochar ash from different feedstocks. A logarithmic y-axis is used to present high and low concentrations of product.	226
Figure 7-7 Activity of biochar ash before and after demineralisation for glycerol upgrading reaction; -DM indicates demineralised samples. Logarithmic y-axis is used to present high and low concentrations of products.	226

Figure 7-8 Concentration of liquid phase products for RHB-550 after treatment with acetone and tar impregnation.	227
Figure 7-9 Correlations between potassium content and a) glycerol carbonate concentration and b) triacetin concentration for biochar ash. Filled circles = untreated ash, open circles = demineralised ash. Green = WSB-550, blue = OSB-700, purple = RHB-550.	232
Figure 7-10 Structure of potassium silicate.	233
Figure 8-1 Schematic of characterisation techniques for measuring different aspects of graphiticity.	247
Figure 8-2 Proposed catalytic applications of biochar. Highlighted in red are examples from the current work, with further suggestions based on the literature.	249
Figure 0-1 Annotated XPS spectra for survey scan of OSB-700, areas 1 and 2.	A-1
Figure 0-2 Example XPS C1s spectra for OSB-700 run 1 and run 2, calibrated by position of K 2p peaks.	A-2
Figure 0-3 Example XPS C1s deconvolved spectra for OSB-700, run 1 and run 2.	A-2
Figure 0-4 Deconvolved Raman spectra for rice husk biochar samples. (a) RHB-550, (b) RHB-550-DM, (c) RHB-550-T-C, (d) RHB-550-DM-T-C.	A-3
Figure 0-5 Annotated FTIR spectra comparing RHB-550 char and ash samples.	A-4
Figure 0-6 TGA Proximate analysis comparing platinum (Pt) and alumina (Al ₂ O ₃) crucibles for two different biochar samples.	A-5
Figure 0-7 Comparison of TGA Proximate Analysis using methods at the University of Sheffield (UoS) and University of Edinburgh Biochar Research Centre (UKBRC).	A-5
Figure 0-8 TGA analysis of acetone control samples, using RHB. w = washing time, d = drying time. Samples dried in the oven for >2 days had the same composition (shown by red dotted lines), regardless of washing time, implying that differences between other samples are due to the samples not being fully dry.	B-1
Figure 0-9 EDX analysis of OSB-700 samples before and after various surface treatments. Error bars are standard deviation calculated from repeat measurements, analysing different areas of each sample. The number of areas analysed were: 4 × OSB-700, 1 × OSB-700-DM (no error calculated), 3 × OSB-700-ash, 3 × OSB-700-DM-ash, 1 × OSB-700-T-C (no error calculated), 2 × OSB-700-DM-T-C.	B-2
Figure 0-10 Raman curve deconvolution data for biochars from different feedstocks before and after demineralisation. Error bars estimated from percentage error from three repeats of WSB-550-DM.	B-3
Figure 0-11 Raman curve deconvolution data, showing the ratio of the area of the D1 to G bands, for biochars from different feedstocks before and after demineralisation. Error bars estimated from percentage error of 20% from three repeats of WSB-550-DM.	B-3
Figure 0-12 FTIR-ATR spectra for biochars before and after demineralisation.	B-4
Figure 0-13 TGA of pine tar. The majority of the mass is comprised of volatiles (96.62 wt%), with a negligible contribution from ash (0.28 wt%).	B-4
Figure 0-14 Comparison of biochar, liquid and gas yields for Stage I pyrolysis of different biochar materials impregnated with tar.	B-6
Figure 0-15 Proximate analysis for biochar samples before and after demineralisation. This data was used to calculate the percentage of ash content removed from the biochars.	B-6
Figure 0-16 SEM images of tar-impregnated biochars. (a) RHB-550-T-C, (b) RHB-50-DM-T-C, (c) OSB-700-T-C, (d) OSB-700-DM-T-C, (e) WSB-550-T-C, (f) WSB-550-DM-T-C.	B-7
Figure 0-17 Calibration curves for methanol from March 2018, (a) without normalisation and (b) normalised relative to the area of the internal standard peak.	C-1
Figure 0-18 Calibration curves for DMM from March 2018, (a) without normalisation and (b) normalised relative to the area of the internal standard peak.	C-1
Figure 0-19 Calibration curves for triacetin in a pure triacetin sample, and in a calibration sample consisting of 50 % diacetin. The estimated quantity of triacetin in the diacetin sample was adjusted to give the same calibration constant as the pure triacetin sample.	D-1

Figure 0-20 Calibration curves for glycerol, (a) without normalisation and (b) normalised relative to the area of the internal standard peak. D-3

Figure 0-21 Calibration curves for glycerol carbonate, (a) without normalisation and (b) normalised relative to the area of the internal standard peak..... D-3

Figure 0-22 Calibration curves for glycerol monoacetin (a) without normalisation and (b) normalised relative to the area of the internal standard peak..... D-4

Figure 0-23 Calibration curves for glycerol diacetin (a) without normalisation and (b) normalised relative to the area of the internal standard peak. D-4

Figure 0-24 Calibration curves for glycerol triacetin (a) without normalisation and (b) normalised relative to the area of the internal standard peak. D-4

List of Tables

Table 1-1 Industrial reactions using catalysts where carbonaceous deposits have a detrimental effect on catalytic performance.	7
Table 2-1 Reactions where carbon deposits or phases on catalysts have demonstrated catalytic activity.	21
Table 2-2 Characterisation techniques used in the literature for biochars for different applications. Representative examples are given for catalytic and soil remediation applications, with other notable examples also listed.	41
Table 3-1 Standard biochars from UK Biochar Research Centre used in this study.	54
Table 3-2 Chemicals used during the project, with details of concentrations and supplier.	54
Table 3-3 Vibrational modes of CO ₂	60
Table 4-1 BET analysis conditions for N ₂ adsorption and desorption at 77 K.	81
Table 4-2 Protocol for sample preparation before adsorption isotherm measurements.	81
Table 4-3 TGA Proximate Analysis method for the University of Sheffield, using Perkin Elmer TGA 4000.	84
Table 4-4 Settings used for obtaining Raman spectra of biochars.	87
Table 4-5 FTIR peak assignment for biochars and ash samples, with justification from literature sources.	98
Table 4-6 Raman curve deconvolution, peak assignments.	100
Table 4-7 Peak assignment and fitting parameters for XPS C1s curve deconvolution peaks. Adapted from the literature (Smith et al. 2016), with permission from Elsevier.	103
Table 4-8 Summary of characterisation data for biochars studied in Chapter 4.	107
Table 5-1 TGA Pyrolysis/Proximate Analysis method at the University of Sheffield, using Perkin Elmer TGA 4000.	126
Table 5-2 TGA Proximate Analysis method for the University of Edinburgh, using TGA/DSC 1 STAR ^e System.	126
Table 5-3 Ash content of biochars before and after demineralisation, measured using TGA.	130
Table 5-4 Quantities of AAEM elements detected by XPS analysis of chars and ash samples from three feedstocks. -DM indicates demineralised sample.	133
Table 5-5 Percentage increase in volatile component of biochars after acetone washing.	139
Table 5-6 Comparison of the biochar yield from Stage I pyrolysis with the percentage of biochar in the sample.	145
Table 5-7 Summary of key results from effect of various surface treatments on properties of biochar. Shaded boxes indicate data unavailable.	156
Table 6-1 Reaction conditions for the conversion of methanol with CO ₂ to form products.	180
Table 6-2 GCMS method for analysis of undiluted liquid phase products of methanol conversion reaction.	181
Table 6-3 GCMS method for analysis of diluted liquid phase products of methanol conversion reaction.	181
Table 7-1 Reaction conditions for the conversion of glycerol with CO ₂ to form products.	215
Table 7-2 Method used for analysis of products of glycerol upgrading reaction in the GCMS.	216
Table 0-1 Calibration samples prepared for glycerol upgrading reactions in February 2018.	D-2

List of Schemes

Scheme 2-1 Reaction of glycerol with CO ₂ to form glycerol carbonate and water.	31
Scheme 6-1 Formation of dimethoxymethane from methanol oxidation.	178
Scheme 6-2 The production of TMOS from the reaction of silica with DMC.	202
Scheme 7-1 Reactions for the formation of mono-, di- and triacetin from glycerol and acetonitrile.	213

Chapter 1 – Introduction

Chapter 1 – Introduction

In this introductory chapter, the motivation and wider context of the research are set out. First, an introduction to the field of catalysis is given in section 1.2, outlining what catalysts are and how they work. Section 1.3 discusses the process of catalyst deactivation, which affects the majority of heterogeneous catalysts, and particularly deactivation through carbon deposition or coking. The concept of beneficial coking is also introduced. The motivations for studying CO₂ utilisation reactions are outlined in section 1.4, with an introduction to biochar in section 1.5. The use of characterisation techniques in catalysis is briefly discussed in section 1.6. This chapter concludes with an overview of the aims and objectives of the present research in section 1.7, together with an overview of the thesis structure. The literature review then focuses on themes specific to this research project, and follows in Chapter 2.

1.1. Context

Two of the key challenges currently facing the chemical industries are climate change and sustainability. The challenge is to decrease the carbon footprint of industry whilst developing new reaction routes for products previously obtained from fossil resources. Industry is one of the main contributors to global greenhouse gas emissions, with IPCC figures from 2007 putting the contribution from industry at 37 %. This is primarily due to the use of fossil fuels for energy generation and as feedstocks in chemical processing (Worrell *et al.* 2009). Therefore, improving the sustainability of industry could have a real impact on reducing global emissions of greenhouse gases.

First, it is worth considering what is meant by sustainability. Sustainability can be defined as “Development that meets the needs of the present without compromising the ability of future generations to meet their own needs.” (World Commission on Environment and Development 1987) This definition has been further developed for the field of green chemistry by Anastas and Warner, who proposed the 12 principles of green chemistry (Figure 1-1) (Anastas & Warner 1998). These principles have been widely adopted by the chemical industries, for example by Merck and Dow Chemical (Ritter 2017), and provide a framework for sustainable chemical synthesis.

1. It is better to prevent waste than to treat or clean up waste after it is formed.
2. Synthetic methods should be designed to maximize the incorporation of all materials used in the process into the final product.
3. Wherever practicable, synthetic methodologies should be designed to use and generate substances that possess little or no toxicity to human health and the environment.
4. Chemical products should be designed to preserve efficacy of function while reducing toxicity.
5. The use of auxiliary substances (e.g. solvents, separation agents, etc.) should be made unnecessary wherever possible and, innocuous when used.
6. Energy requirements should be recognized for their environmental and economic impacts and should be minimized. Synthetic methods should be conducted at ambient temperature and pressure.
7. A raw material or feedstock should be renewable rather than depleting wherever technically and economically practicable.
8. Unnecessary derivatization (blocking group, protection /deprotection, temporary modification of physical/chemical processes) should be avoided whenever possible.
9. Catalytic reagents (as selective as possible) are superior to stoichiometric reagents.
10. Chemical products should be designed so that at the end of their function they do not persist in the environment and break down into innocuous degradation products.
11. Analytical methodologies need to be further developed to allow for real-time, in-process monitoring and control prior to the formation of hazardous substances.
12. Substances and the form of a substance used in a chemical process should be chosen so as to minimize the potential for chemical accidents, including releases, explosions, and fires.

Figure 1-1 The twelve principles of green chemistry (Anastas & Warner 1998). Reproduced with permission of Oxford University Press through PLSclear.

One area in which the sustainability of chemical industries can be improved is through heterogeneous catalysis. The phenomenon of catalysis is of fundamental importance to the modern world. Examples of its applications are commonplace in everyday life, from catalytic converters in cars to reduce pollution, to the use of nickel catalysts in hydrogenation to produce margarine, to iron catalysts in ammonia synthesis to produce fertilisers, thus greatly

Chapter 1 – Introduction

increasing global food production (Bowker 1998). Today, greater than 80 % of all industrial chemical processes use catalysts (Stevenson 2003). The majority of these are heterogeneous, where the catalyst is in a different phase from the reactants and products – usually, a solid catalyst is used to catalyse a liquid or gas phase reaction.

These catalysts play two key roles, namely enhancing the rate of reaction, and increasing selectivity towards desired products. An enhanced reaction rate makes otherwise slow reactions much more economically viable; for example, this could facilitate the use of renewable feedstocks, as in Principle 7. Enhanced selectivity reduces the energy requirement for separation of the product from the reaction mixture, which is why sustainable catalysts should be “as selective as possible” (Principle 9). As the separation stage is often the most energy intensive step in product synthesis, improved selectivity can significantly reduce the overall energy consumption of the process. Increased selectivity also reduces the amount of raw material that is wasted in forming undesired side-products, thus preventing the formation of waste in accordance with Principle 1. Therefore, catalysis research has the potential to improve the sustainability of the chemical industries in several ways.

The majority of heterogeneous catalysts are metals or metal oxides; however, some metals used in catalysis are growing increasingly scarce – gold and rhenium supplies for example could be depleted by the end of the century (Henckens *et al.* 2014). The development of non-metal-based catalysts from renewable resources could therefore be beneficial for improving the sustainability of heterogeneous catalysis, in accordance with Principle 7.

New classes of catalysts could also open up new reaction routes, which are another tool required for tackling rising CO₂ emissions. The use of CO₂ as a reagent in sustainable reactions is one method for reducing dependence on fossil fuels as feedstocks in chemical synthesis. This is one method of CO₂ utilisation, and part of a range of strategies to reduce the CO₂ emissions which contribute to global warming.

One of the key candidates for the development of non-metal catalysts is carbon. Whilst carbon is already widely used in industry as a support material for metal catalysts, the chemical

properties of carbon make it particularly well-suited to acting as a catalyst. A material which can exist in forms as diverse as coal and diamond, it has a unique chemistry that gives it extraordinary potential as a catalytically active material, which can be sourced sustainably. This project aims to improve the sustainability of the chemical industries through examining the role of carbon in catalysis. In particular, the work aims to identify the factors which make carbonaceous materials catalytically active. This includes carbonaceous deposits which can cause catalyst deactivation, but have also been observed to have beneficial effects. Biochar is used as an example of a carbonaceous material which could find applications in catalysis through a better understanding of the origins of its catalytic activity.

1.2. Introduction to heterogeneous catalysis

Over 80 % of industrial reactions use catalysts, the majority of which are heterogeneous. Whilst most catalysts are made from metals and metal oxides, they are often fixed onto a porous support material, for example platinum supported on alumina. This maximises the available area of the catalytically active material, whilst minimising the amount of the often expensive metals used.

The role of carbon in catalysis is most often as a support material, due to its relative inertness and high porosity. Properties such as porosity and surface acidity can also be tailored to suit the requirements of the process or catalyst (Serp & Figueiredo 2009). However, carbon can also be catalytically active, with industrial applications including the use of activated carbons as catalysts in phosgene synthesis (Schneider *et al.* 2000; Dunlap *et al.* 2010) and flue gas cleaning (Knoblauch *et al.* 1981; Richter *et al.* 1987; Jüntgen *et al.* 1988). The various applications of carbon materials in catalysis are discussed further in section 2.2.

Catalysis can occur via a number of mechanisms, where the overall effect is a reduction in the activation energy required for a reaction to occur. The simplest of these may be visualised using Figure 1-2, where the catalyst may stabilise a favourable configuration, or stabilise reaction intermediates. The catalyst surface is often dynamically involved in the process, with the active site being formed during the reaction (*in situ*), rather than simply being a feature of

Chapter 1 – Introduction

the catalyst surface. An example of this is the formation of the active palladium-carbon phase described by Teschner *et al.* (2006), which would not be detected using an *ex situ* analysis.

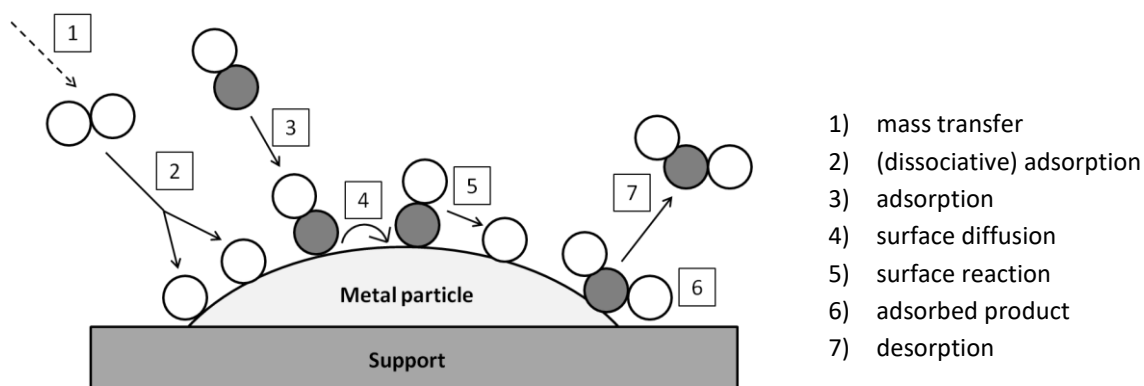


Figure 1-2 Kinetic steps in the catalytic cycle. The reaction demonstrated is the oxidation of CO to CO₂ (filled circles are carbon, open circles are oxygen).

1.3. Catalyst deactivation

As catalysts are not simply static, they will interact with other molecules and change with reaction conditions. As a result, virtually all catalysts will degenerate and become ineffective over time. This process is known as deactivation, and results in the need to periodically replace or regenerate the catalyst. This in turn requires process down-time on a chemical plant, and therefore much research is focused on understanding the causes of catalyst deactivation and mitigating its effects.

1.3.1. Overview of mechanisms

There are several mechanisms of deactivation, which can generally be categorised as thermal, mechanical and chemical mechanisms:

Thermal *e.g.* sintering, collapse of pore structure of support material

Mechanical *e.g.* attrition, fouling

Chemical *e.g.* catalyst poisoning, reaction

A comprehensive review of mechanisms of catalyst deactivation in heterogeneous catalysis can be found in the literature (Bartholomew 2001). In terms of the role of carbon in catalyst deactivation, the principal mechanisms are mechanical and chemical, which are discussed further in section 1.3. Carbon supports are often chosen for their thermal stability, and

therefore this mechanism of deactivation is less relevant to the current work. The applications of carbon as a catalyst support are discussed further in section 2.2.3.

1.3.2. Carbon deposition

A common cause of catalyst deactivation involves carbon deposition, or coking, of heterogeneous catalysts. Organic compounds will undergo cracking reactions on the acidic active sites of the catalyst, leading to the formation of carbon deposits over the active sites and decreased catalytic activity. A schematic demonstrating the process is given in Figure 1-3. As the carbon is deposited over the metal crystallites, the active sites become unavailable for reactants, thereby deactivating the catalyst.

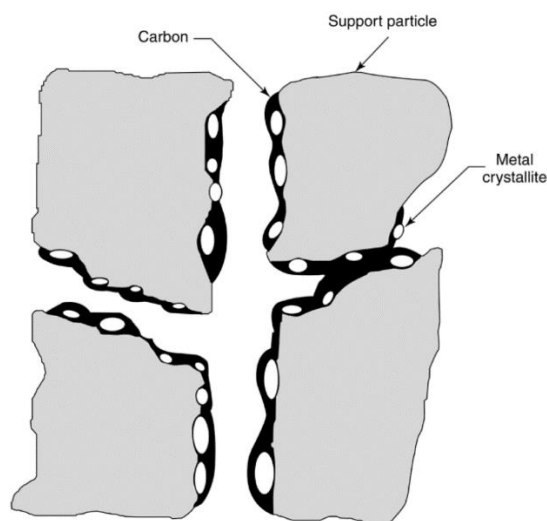


Figure 1-3 schematic of a supported metal catalyst, deactivated by carbon deposition. Figure from Bartholomew (2001), reproduced with permission from Elsevier.

A number of industrial examples of reactions affected by coking are given in Table 1-1, including methanol-to-hydrocarbon conversion, catalytic cracking and steam reforming. This demonstrates the range of reactions which could benefit from an improved understanding of the properties of carbon deposits from a catalytic perspective.

Catalyst deactivation through carbon deposition has been extensively studied, with several possible mechanisms identified. These include poisoning of the active sites, pore blockage, and changes in the number or strength of active sites as a result of carbon laydown (van Donk *et al.* 2001; de Lucas *et al.* 1997). Coking can also result in mechanical damage to the catalyst through the formation of tubular whiskers, or even damage the reactor walls (Menon 1990).

Chapter 1 – Introduction

Table 1-1 Industrial reactions using catalysts where carbonaceous deposits have a detrimental effect on catalytic performance.

Reaction	Catalyst	Source
Catalytic cracking	Silica-alumina Zeolites	(Bartholomew 2001; Mann <i>et al.</i> 1986; Mann 1997; Mann & Thomson 1987)
Fischer-Tropsch synthesis	Cobalt, iron	(Bartholomew 2001)
Oxidative dehydrogenation	VO _x /Al ₂ O ₃	(McGregor, Huang, <i>et al.</i> 2010)
Isomerisation	Sulfated zirconia (solid acid catalysts)	(Li & Gonzalez 1998; van Donk <i>et al.</i> 2001)
Methanol-to-hydrocarbon (MTH) conversion*	HZSM-5, SAPO-34	(Lee <i>et al.</i> 2012; Chen <i>et al.</i> 2012)
Hydrotreating	Supported metal catalysts, e.g. NiMo or CoMo on γ -Al ₂ O ₃	(Pacheco <i>et al.</i> 2011; Snape <i>et al.</i> 2001)
CO ₂ /CH ₄ reforming	Pt Co/ γ -Al ₂ O ₃	(Bitter <i>et al.</i> 1999; Ruckenstein & Wang 2002)
Steam reforming of hydrocarbons	Ni Co	(Vicente <i>et al.</i> 2014; Rostrup-Nielsen 1974)

*deactivation identified as being caused by polycyclic aromatics, as mono- or bi-aromatics did not have significant effects on deactivation

Catalysts have varying sensitivity to the effect of carbon deposition. Some catalysts are completely deactivated by a small amount of coke, perhaps only 2 wt% (de Lucas *et al.* 1997), whilst others used in hydrodesulfurisation processes can reach 10 wt% coke or greater without any noticeable loss in activity (Menon 1990). This demonstrates that the impact of coking is dependent on factors such as the structure and location of the coke, in the context of the particular catalyst and reaction being catalysed (Barbier 1986).

Similarly, whilst there are particular properties and locations of coke which can lead to catalyst deactivation, there are examples where carbon deposition can have beneficial effects. For example, coking can lead to enhanced selectivity, and deposits sometimes even exhibit catalytic activity. As this subject had not been reviewed since 1990, a literature review was carried out to summarise the beneficial roles that carbon deposition can play in heterogeneous catalysis, along with the properties of the coke that are thought to play a role. The key findings are discussed in section 2.2.5.

1.3.3. Implications of research

By understanding the factors which make carbon deposits catalytically active, the sustainability of the chemical industries can be improved in a number of ways. One possibility is that the process of carbon deposition could be exploited to preferentially form catalytically active coke. This would reduce the problem of catalyst deactivation, which would mean not

only less down-time for the process, but also the potential for enhanced activity and selectivity. As discussed in section 1.1, this could reduce the overall energy requirements of the process and reduce the amount of raw materials wasted in the formation of unwanted side-products.

The study of catalytically active coke also has promising implications for the development of carbonaceous, non-metal catalysts. As metal-based catalysts are increasingly becoming unsuitable for commercial use due to their high cost and limited reserves (Ruckenstein & Wang 2002; Kong *et al.* 2014), catalysts made from carbon, either with or without metals present, may provide a more sustainable and economic alternative. This new class of carbon-based catalysts may also open up new reaction pathways utilising more sustainable raw materials instead of fossil fuels (Ampelli *et al.* 2014). Metal carbides for example are able to catalyse many reactions which currently employ rare platinum group metals (PGMs), a phenomenon ascribed to the similarity in electronic structure between carbides and PGMs (Ham & Lee 2009). These new reaction routes could include CO₂ utilisation reactions; this is discussed in section 1.4.

Understanding the role of carbon in catalysis may also allow carbonaceous by-products of the biomass industry, such as biochar, to find applications in heterogeneous catalysis (Kastner *et al.* 2012). Similarly, the study of the catalytic activity of biochar may provide insights into the catalytic activity of carbonaceous deposits. This is the focus of the experimental work in this project.

1.4. CO₂ utilisation reactions

The threat of global warming has fuelled increased research over the past two decades in the field of CO₂ utilisation as a means of combatting increased CO₂ emissions. The potential for atmospheric gases such as CO₂ to block infra-red radiation and cause climate change has been known since at least the 1860s, with Tyndall stating that “the extent alone of the operation remain[s] doubtful” (Tyndall 1861). However, it was not until the 1997 Kyoto Protocol that international action began to be taken on mitigating the effects of global warming and

Chapter 1 – Introduction

reducing greenhouse gas emissions. As a result, CO₂ utilisation is a new and rapidly developing field.

CO₂ utilisation aims to use CO₂ as a more sustainable feedstock for the production of value-added products and chemicals. The CO₂ first has to be captured and separated from other gases, usually from a point source such as a chemical plant or power station. The Gorgon Project in Australia is an example of three major international oil companies (Chevron, Shell and ExxonMobil) working together on developing carbon capture and storage technologies (Flett *et al.* 2009). However, there is also the potential to extract CO₂ directly from the air. The world's first commercial direct air CO₂ capture plant was opened in May 2017 in Zürich by Climeworks (Climeworks 2017).

Once the CO₂ is captured and separated, it can be used as a feedstock in a variety of reactions. Due to the low reactivity of CO₂, CO is more commonly encountered as a feedstock. There are currently limited applications of CO₂ as a carbon source in industrial reactions, though examples include the synthesis of urea and the production of organic carbonates. In the case of organic carbonates, CO₂ is increasingly replacing phosgene as the C1 building unit (Ma *et al.* 2009). However, CO₂ can offer a number of advantages as a feedstock. Besides its green credentials, CO₂ is also cheap, non-toxic and readily available (Sakakura *et al.* 2007). This is driving research into further reactions that could utilise CO₂. Reviews of these areas can be found in the literature (Aresta 2010; Mikkelsen *et al.* 2010; Ampelli *et al.* 2015), including a review on the role of heterogeneous catalysis in CO₂ utilisation (Razali *et al.* 2012).

In this work, two CO₂ utilisation reactions of particular interest in sustainable reaction engineering are studied. The first is the upgrading of glycerol to glycerol carbonate through reaction with CO₂. In this reaction, waste glycerol from biodiesel production is reacted with CO₂ to form glycerol carbonate, which amongst other applications is a precursor for plastics synthesis (Teng *et al.* 2014). The second reaction of interest is between methanol and CO₂ to products. The potential to produce dimethoxymethane (DMM) and dimethylcarbonate (DMC) via this route, using a carbonaceous catalyst, is promising for sustainable reaction engineering. DMM has applications as a fuel additive and in paint, perfume and

pharmaceuticals (Thavornprasert *et al.* 2016), whilst DMC has also gained attention as a 'green' chemical, with potential applications as a reagent, fuel additive and solvent (Keller *et al.* 2010; Tundo *et al.* 2008).

The literature review considers these reactions in more detail, focusing on the potential role of carbon as a catalyst. This is discussed in section 2.2.4.

1.5. Biochar

Biochar is a by-product of biomass pyrolysis, which is a method of biomass gasification. Through heating in the absence of oxygen, the organic structure decomposes to form non-condensable gases, which can be burnt for fuel, as well as condensable organic liquids (Crombie *et al.* 2013). The solid remaining after pyrolysis is a carbonaceous solid termed biochar, which currently has applications in soil remediation and carbon storage. It has also been shown to be catalytically active in a number of reactions – a recent review of the applications of biochar can be found in the literature which summarises the applications of biochar in various catalytic processes, including for syngas cleaning and biodiesel production (Jindo *et al.* 2014). The potential applications of biochar as a catalyst are considered in section 2.3.

1.6. Characterisation techniques to be used

In order to understand the factors affecting catalytic activity, a range of techniques are needed to fully characterise a catalyst. These range from imaging techniques to observe physical structures, to vibrational spectroscopy for characterisation of the chemical structure, to quantitative analysis to determine the composition of a material. In catalysis, it is particularly important to characterise the surface of the material, as this is where the catalysis will take place (see Figure 1-2).

A full understanding of how catalysts work in particular reactions is limited by the techniques available. This is therefore another active area of catalysis research. Particularly in catalysis, the field of *in situ* characterisation is attracting much interest, as the properties of catalysts will change depending on the reaction conditions. Characterising a catalyst under vacuum

Chapter 1 – Introduction

conditions for example will not necessarily give an accurate picture of its properties during a reaction. In some cases, the active phase or site may only be formed *in situ*, such as the active palladium-carbon phase which is formed during selective alkyne hydrogenation (Teschner *et al.* 2006). The application of characterisation techniques to carbonaceous catalysts is the focus of section 2.5, with a particular focus on the characterisation of biochars and carbon deposits.

1.7. Aims and Objectives

The aim of this project is to improve the understanding of the various roles that carbon can play in catalysis, with a view to improving the sustainability of the chemical industries. The three ways in which it aims to achieve this are by:

1. developing a new class of sustainably sourced, non-metal-based catalysts for industrial reactions.
2. investigating the potential of carbonaceous catalysts to open up new reaction routes.
3. enhancing the sustainability of industrial reactions by improving understanding of the origins of catalytic activity in carbonaceous materials, including carbon deposits. This could allow coking in industrial reactions to be exploited for improved catalyst performance, and therefore improved sustainability.

A review of the literature was undertaken to summarise current understanding of the roles of carbon and particularly biochar in catalysis, and is given in Chapter 2. The experimental methods and analysis techniques to be used are developed in Chapter 3, together with a brief overview of the theoretical principles behind them. The results of the experimental work are then presented in Chapters 4-7, and are discussed in Chapter 8. The overall conclusions of the work and recommendations for future work are presented in Chapter 9.

Chapter 2 – Literature Review

Chapter 2 – Literature Review

This literature review will first consider the various roles carbon can play in catalysis. This includes the use of carbon as a catalyst and as a support material, and the detrimental and beneficial effects of carbon deposits, in section 2.2. The applications of biochar as a catalyst will then be considered in section 2.3. The potential of carbonaceous materials to activate CO₂ and therefore catalyse its conversion is considered in section 2.4. The various characterisation methods used in the literature for the study of carbonaceous materials and carbon deposits, including their relative advantages and limitations, are presented in section 2.5. The key findings of the literature review are summarised in 2.5.5, ending with a statement of the aims and objectives of the experimental work.

2.1. Introduction

Carbon is widely studied in catalysis across a number of fields. These range from the synthesis of novel carbonaceous materials, to optimising these materials for desired applications, to studies both aiming to mitigate and exploit carbon deposition on heterogeneous catalysts. These fields are all interlinked, and the insights gained from one field can often be applied to another. The common link is an understanding of the properties of carbon which affect catalytic activity, be this beneficial or detrimental, direct or indirect. For example, intense research efforts are underway to find catalytic applications for novel carbonaceous materials, resulting in the constant production of new knowledge regarding catalytically active carbon. A review of the literature across these fields is therefore required to establish the current state of knowledge of the role of carbon in catalysis.

2.2. Applications of carbon in catalysis

This section includes extracts from a published literature review on catalytically active coke, published in the journal Catalysis Science and Technology (Collett & McGregor 2016); the full paper is given in Appendix E .

The field of carbon in catalysis is broad, and much literature exists in a range of areas. The most commonly encountered case is that of carbon deposits formed on catalysts; the deactivation of catalysts by carbon is therefore considered in section 2.2.1. A brief overview of carbonaceous materials studied in catalysis is given in section 2.2.2, followed by a summary of the key applications of carbon as a support material (section 2.2.3) and as a catalyst in its own right (section 2.2.4). The beneficial and catalytic effects of carbon deposits are considered in section 2.2.5. Finally, the activity of metal-carbon phases, and the influence of trace metal content, is discussed in section 2.2.6. The catalytic potential of a particular carbonaceous material, biochar, is discussed further in section 2.3.

2.2.1. Deactivation by carbon

One of the most common roles of carbon in catalysis is the deactivation of heterogeneous catalysts through the formation of carbon deposits, or ‘coke’. The definition of coke is often somewhat arbitrary; increasingly, coke is characterised in terms of its degree of order or graphiticity (McGregor, Huang, et al. 2010; Serp & Figueiredo 2009). In this work, “coke” is defined as all carbonaceous species which are formed during reaction, either on the catalyst surface or in the sub-surface region and which are not molecular products of the reaction. This therefore includes both deposits and metal carbide phases formed *in situ*.

The impact of coking is dependent on factors such as the structure and location of the coke, which in turn depend on the reaction conditions and the properties of the catalyst. Some catalysts are completely deactivated by a small amount of coke, perhaps only 2 wt% (de Lucas *et al.* 1997). Porous catalysts for example can be deactivated by very low quantities of carbon blocking the entrances to pores; this is a particular problem at high coking rates (see Figure 2-1). However, other catalysts can reach 10 wt% coke or greater without loss of activity (Menon 1990). A comprehensive description of the mechanisms of coke formation and catalyst deactivation can be found elsewhere (Bartholomew 2001).

Chapter 2 – Literature Review

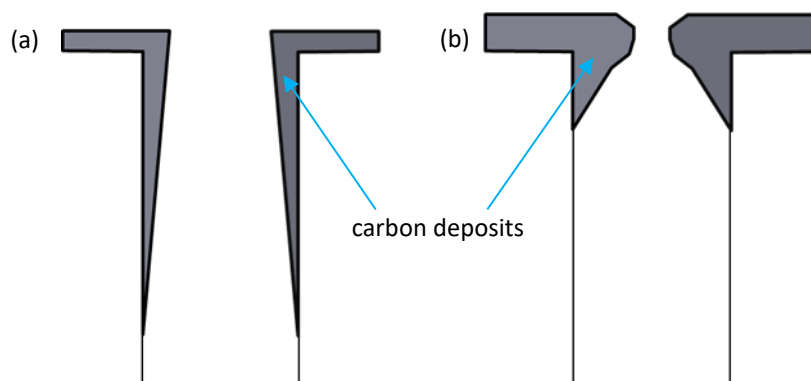
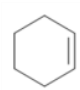
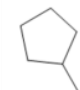
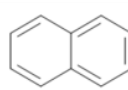
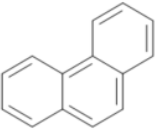
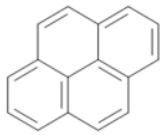
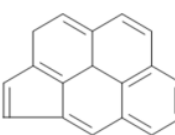


Figure 2-1 Schematic of the effect of coking rate on the mechanism of deactivation of catalyst pores. (a) slow coking. (b) rapid coking, leading to pore plugging. Figure adapted from Menon (1990) with permission from Elsevier.

The graphiticity of carbon structures has been linked to increasing temperatures. For example, in studies of butane dehydrogenation over $\text{VO}_x/\text{Al}_2\text{O}_3$ catalysts, the coke deposits were found to be more graphitic in structure at reaction temperatures above 873 K, as confirmed through THz-TDS studies (McGregor, Huang, *et al.* 2010). Similarly, increasingly complex carbon structures are formed over HY zeolite catalysts from cyclohexane, as demonstrated in Figure 2-2 (Menon 1990). At present, the structure of coke is often studied from the perspective of limiting catalyst deactivation; however, carbon deposits can also be catalytically active. This will be discussed in section 2.2.5.

Process temperature/°C	120	200	350	450
Coke structures formed	 cyclohexene  methylcyclopentane	 naphthalene  phenanthrene	 pyrene	 cyclopentapyrene



 Increasing temperature

Figure 2-2 The influence of reaction temperature on the structure of carbon deposits formed from cyclohexane on HY zeolite catalysts. Figure produced based on data available in the literature (Menon 1990), and previously published in *Catalysis Science and Technology* (Collett & McGregor 2016).

2.2.2. Carbonaceous materials

Carbonaceous materials can be categorised as naturally occurring (for example charcoals and graphites) and synthetic carbons (such as carbon nanostructures and biochars). These carbons possess a range of properties, and can be categorised further by the degree of defined structure, for example, contrasting highly regular graphites with amorphous carbons (Dreyer & Bielawski 2011). Many synthetic carbons are produced on an industrial scale for a range of applications, for example, activated carbons as adsorbents for waste water treatment (Bhatnagar *et al.* 2013).

Several types of carbon have found applications as catalytic materials. The most commonly encountered carbon is activated carbon, *i.e.* carbon that has been chemically or thermally activated to increase the surface area or functionality for catalytic applications (Auer *et al.* 1998). Graphitic and nanostructured carbons have also been studied, although the preparation process is more complex, often requiring a metal template and carbon vapour deposition processes (Serp & Figueiredo 2009). A schematic for the production of carbon nanotubes (CNTs), fullerenes and carbon blacks from hydrocarbons is shown in Figure 2-3. Biochar from biomass provides a sustainable and carbon-neutral source of carbonaceous material, compared to coal, graphite and carbon nanotubes.

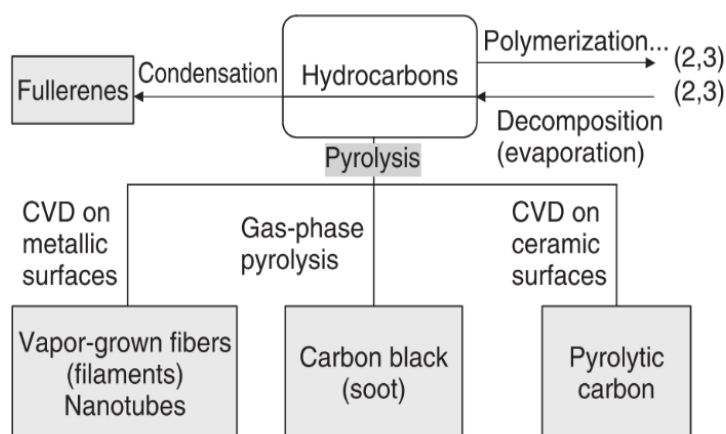


Figure 2-3 Processes of carbon in the gas phase and the formation of carbon macrostructures (Serp & Figueiredo 2009). Reproduced with permission from John Wiley and Sons Inc.

Carbon finds a number of applications in catalysis due to its physical and chemical properties. For example, isotropic or non-graphitisable carbon finds applications as an adsorbent, or as a

Chapter 2 – Literature Review

catalyst support material. Typical sources for this type of carbon include wood or charcoal, nuts, nutshells, low rank coals and synthetic resins (e.g. polyvinylene chloride). (JJ) Carbon structures are stable at temperatures as high as 1000 K, except in the presence of oxygen, and the electron conductivity of graphitic carbons can also be advantageous (Lam & Luong 2014). Carbonaceous materials often possess high surface areas and porosities, which can be tailored easily by altering the feedstock or method of preparation (Dreyer & Bielawski 2011). For example, by altering the temperature of carbonisation, the functionality of the carbon can be drastically altered; aliphatic C-H groups are generated and C=O groups are lost around 400 C, with aromatic groups peaking at temperatures of 450-550 °C (Morterra & Low 1983; Zawadzki 1989). There are also numerous advantages for its application as a support material, which will be considered in section 2.2.3.

2.2.3. Applications as catalyst support

Carbon is commonly encountered in the literature as a support material for precious metal catalysts, and offers some advantages over silica and alumina supports. Carbon for example is resistant to acidic and basic media, and less expensive (Auer *et al.* 1998). The surface functionality and metal adsorption and dispersion can also be easily modified through chemical treatments, leading to improved catalyst performance (Serp & Figueiredo 2009). Carbon is also advantageous for the subsequent recovery of the metal phase, as the support can simply be burnt away, without producing large quantities of solid waste for landfill (Lam & Luong 2014); however this does lead to the emission of CO₂ due to combustion of the carbon. Depending on the source of the carbon, there is therefore potential for carbon supports to improve sustainability through reduced quantities of solid waste during metal recovery (Principle 1) and improved selectivity and performance of the catalyst (Principle 9).

The applications of carbon-supported catalysts are wide-ranging. In a review by Auer and co-workers, over 40 reactions were identified which utilise carbon-supported metal catalysts (Auer *et al.* 1998). Activated carbons are most commonly used, with applications in hydrogenation, dehydrogenation and oxidation reactions. Research continues to investigate the potential of carbon nanostructures and graphite for catalytic applications; progress in these areas can be found in recent literature reviews (Su *et al.* 2012; Kong *et al.* 2014).

A growing area of interest is the use of biochars as carbonaceous support materials. Unlike activated carbons, biochars do not require extensive chemical and thermal treatments, and have been investigated as supports for biomass conversion to products (Lam & Luong 2014). The applications of biochar in catalysis will be considered further in section 2.3.

2.2.4. As a catalyst

Carbon itself can be catalytically active in numerous processes; the use of carbon as a catalyst in its own right is sometimes termed carbocatalysis. The catalytic activity of carbonaceous materials has been demonstrated for a wide range of reactions in the literature, including oxidations, reductions, hydrogenations, dehydrogenations, and other bond-forming and bond-cleaving reactions. Industrial applications of activated carbons include the catalysis of phosgene synthesis (Schneider *et al.* 2000; Dunlap *et al.* 2010) and flue gas cleaning (Knoblauch *et al.* 1981; Richter *et al.* 1987; Jüntgen *et al.* 1988). Graphite and fullerenes have been shown to catalyse the reduction of substituted nitrobenzenes to aniline (Byung *et al.* 1985; Li & Xu 2009), whilst carbon nanotubes catalysed dehydrogenation of *n*-butane to 1-butene (Zhang *et al.* 2008). Graphene oxide in particular has demonstrated ability to catalyse hydration and oxidation reactions, such as alcohols to ketones and aldehydes, alkenes to diones, and alkynes to hydrates (Dreyer *et al.* 2010). Further examples of carbonaceous catalysts can be found in recent literature reviews (Dreyer & Bielawski 2011; Su *et al.* 2012).

The ability of carbon to act as a catalyst is dependent on the availability of active sites. Functional groups containing oxygen and nitrogen may be naturally present, or can be introduced through chemical treatments, and can act as acidic or basic active sites. In graphitic materials, delocalised unpaired electrons at the edge of graphene sheets can act as active sites (Serp & Figueiredo 2009), whilst the conductivity of graphite can facilitate electron transfer between reagents (Larsen *et al.* 2000). The charge distribution of graphite and CNTs can also be modified by doping with heteroatoms, such as nitrogen, sulphur and boron (Liu & Dai 2016). The variety of active sites, and the ease of modification, makes carbonaceous materials versatile catalysts.

Chapter 2 – Literature Review

A further key application of carbon is in the field of electrocatalysis, where carbon is used in place of platinum as an electrode material. This was recently reviewed in the literature (Liu & Dai 2016). Key applications are in the oxygen reduction reaction (ORR), oxygen evolution reaction (OER) and hydrogen evolution reaction (HER). Carbon nanofibers have been reported to demonstrate activity for CO₂ reduction, outperforming silver electrodes, with a negligible overpotential of 0.17 V (Kumar *et al.* 2013). This activity was attributed to the higher binding energy of intermediates to the carbon nanofiber surface, rather than the electronegativity of nitrogen heteroatoms. Whilst electrochemical studies are beyond the scope of this work, the insights from electrocatalytic applications could provide important insights into the properties of carbon influencing catalytic activity.

One of the key challenges in the application of carbon as a catalyst is a lack of reproducibility (Serp & Figueiredo 2009). In samples prepared from biomass, this may be due to the inherent variation in the biomass feedstock, affecting the properties of the catalyst. However, several recent studies have highlighted characterisation as a limiting factor (Nederlof *et al.* 2012; Santiago *et al.* 2005; Suarez-Ojeda *et al.* 2005). This may also indicate a poor understanding of the properties of the carbon which influence catalytic activity. Limitations of characterisation techniques will be discussed further in section 2.5.

Carbonaceous catalysts are sometimes described as 'metal-free', however this term can be misleading. Carbonaceous catalysts may contain trace metal content, for example due to the method used for carbon nanotube preparation, contamination from reactor walls, or due to trace metal content in a biomass feedstock (Dreyer & Bielawski 2011). However, in the examples given here, sufficient evidence exists that the carbon itself is the catalytically active species. The role of trace metal will be considered further in section 2.2.6.

2.2.5. Catalytically active coke

Coking is generally regarded as a detrimental process, often causing deactivation of catalysts by pore blockage or poisoning of active sites. However, coking can also have beneficial effects. This was the subject of a literature review published in *Catalysis Science and Technology* (Collett & McGregor 2016); an overview is given in this section.

Coke deposits may enhance selectivity through the deactivation of non-selective active sites (Fang *et al.* 1999; Beck *et al.* 1999; Bauer *et al.* 2001), and the modification of shape selectivity (Kaeding *et al.* 1981; Bauer *et al.* 2007). Pre-coking is widely used in zeolites to improve selectivity to desired products, such through the Mobil selective toluene disproportionation process (MSTDPTM) and PxMax processes (Bauer *et al.* 2001; Mobil Research and Development 1990; Gonçalves & Rodrigues 2014), ethylbenzene disproportionation, (Pradhan *et al.* 1999), and in transalkylation of heavy aromatics (Chao *et al.* 2008).

Coke deposits can also improve selectivity in catalysts other than zeolites, for example coke was recently shown to decrease catalyst acidity and suppress cracking reactions in $\text{CrO}_x/\text{Al}_2\text{O}_3$ catalysts, improving selectivity to styrene (Gomez-Sanz *et al.* 2016; Gomez-Sanz *et al.* 2015). Similarly, coke deposits and carbides formed in situ have been shown to improve the selectivity of various hydrogenation reactions (McGregor, Canning, *et al.* 2010; McGregor & Gladden 2008; Teschner *et al.* 2008). The case of metal carbides is discussed in more detail in section 2.2.6.

The catalytic activity of carbonaceous deposits has been known since the 1970s, with the first example being the oxidative dehydrogenation of ethylbenzene to styrene (Alkhozov *et al.* 1978). It was noted that carbon deposits did not cause deactivation even after extended times on stream and coke levels as high as 12-13 wt% (Fiedorow *et al.* 1981; Vrieland & Menon 1991; Kim & Weller 1987). Many other oxidative dehydrogenation reactions are now known to be catalysed by carbonaceous materials employed directly as catalysts; a number of examples are discussed in a detailed review (Qi & Su 2014). The potential activity of coke deposits in oxidative dehydrogenation reactions is therefore well-established.

Carbon deposits have since demonstrated activity in further dehydrogenation, ammoxidation, hydrogen transfer and hydrocarbon transfer reactions. The activity of coke deposits is often confirmed through the demonstration of catalytic activity in unsupported (Nederlof *et al.* 2012; McGregor, Huang, *et al.* 2010). A summary of the reactions in which the catalytic activity of coke has been demonstrated can be found in Table 2-1. An in-depth consideration of the various mechanisms is beyond the scope of the present work, however

Chapter 2 – Literature Review

the catalysis of ethylbenzene dehydrogenation over coke deposits has been the subject of several reviews (Lisovskii & Aharoni 1994; Cavani & Trifirò 1995; Chen *et al.* 2014). In brief, the contributing factors are thought to be the oxygenated surface groups (Cavani & Trifirò 1995; Mestl *et al.* 2001; Su *et al.* 2005; Lisovskii & Aharoni 1994; Cadus *et al.* 1990), reduction in surface acidity (Gomez-Sanz *et al.* 2015), and defects in the electron structure (Fiedorow *et al.* 1981; McGregor, Huang, *et al.* 2010; Lisovskii & Aharoni 1994; Cadus *et al.* 1988). Further details are available in the published Literature Review in Appendix E .

Table 2-1 Reactions where carbon deposits or phases on catalysts have demonstrated catalytic activity.

Reaction type	Reaction	Coked catalyst	Reference
Oxidative dehydrogenation	Ethylbenzene to styrene	Metal oxides	(Alkhozov <i>et al.</i> 1978)
		Alumina	(Fiedorow <i>et al.</i> 1981)
		Lanthanide oxide-promoted molybdena-alumina	(Kim & Weller 1987)
Non-oxidative dehydrogenation	Dehydrogenation of cyclohexane	Alumina	(Amano <i>et al.</i> 2001)
	Dehydrogenation of <i>n</i> -butane	VO _x /Al ₂ O ₃	(McGregor, Huang, <i>et al.</i> 2010)
Ammonoxidation	Ammonoxidation of ethylbenzene	Alumina	(Fiedorow <i>et al.</i> 2004)
	Ammonoxidation of toluene	Alumina	(Przystajko <i>et al.</i> 1990)
Hydrogen transfer	Hydrogenation of 2-pentenes	Ni/Al ₂ O ₃	(McGregor & Gladden 2008)
	Selective hydrogenation of alkynes	Pd/θ-Al ₂ O ₃	(Teschner <i>et al.</i> 2006)
Hydrocarbon transfer	Methanol conversion	Zeolites	(White 2011)
	Homologation (methane to C4+ alkanes)	Ni/Al ₂ O ₃	(Liu & Smith 1995)
	Fischer-Tropsch	Iron	(Cruz <i>et al.</i> 2015)
Pore mouth catalysis	Alkylation of <i>p</i> -xylene	Zeolite Y (FCC catalyst)	(Lee <i>et al.</i> 2004)
Isomerisation	Isomerisation of <i>n</i> -heptane	Molybdenum oxycarbide	(Ledoux <i>et al.</i> 1996)

In addition to those reactions outlined in Table 2-1, numerous other reactions have been identified where coke may be catalytically active. In the alkylation of toluene and the isopropylation of naphthalene, conversion was observed to increase with time, despite the micropore volume decreasing to negligible values (Da *et al.* 1999; Guisnet 2002; Magnoux *et al.* 2000). Similarly, in the skeletal isomerisation of *n*-butenes to isobutane, improved selectivity is observed, even when the pores are entirely blocked (Houžvička & Ponec 1997; Guisnet *et al.* 1995; Meriaudeau *et al.* 1997; Xu *et al.* 1995; van Donk *et al.* 2001). Aromatic-structured carbonaceous deposits could also facilitate hydrogen transfer in hydrogenation

and catalytic cracking reactions, in a similar manner to that of tetralin (see Figure 2-4) (Thomson & Webb 1976). In summary, the full potential of catalytically active coke is yet to be realised; it is possible that the reactions discussed in section 2.2.4 could also be catalysed by active coke. Further suggestions for reactions which may be catalysed by active coke can be found in Appendix E .

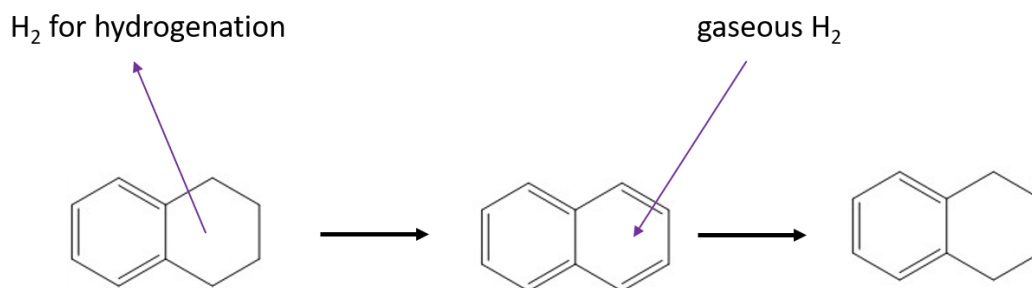


Figure 2-4 Schematic of the facilitation of hydrogen transfer by tetralin. The hydrogen in the saturated ring is activated by the unsaturated ring.

The properties of coke have also been shown to influence the activity of carbon deposits in dehydrogenation reactions. Several studies found that increased graphitic order in carbon deposits or carbonaceous samples correlates with increased catalytic activity (McGregor, Huang, *et al.* 2010; Bayraktar & Kugler 2002; Amano *et al.* 2001; Maldonado-Hódar *et al.* 1999). The extent of graphitisation of carbon deposits required in order to exhibit this activity is unclear, although terahertz spectroscopy studies by McGregor *et al.* indicated that it may require more than 7 aromatic rings (McGregor, Huang, *et al.* 2010). Nitrogen-containing coke may also be more catalytically active than that which does not contain nitrogen, as shown in studies of the ODH of ethylbenzene with nitrobenzene (Fiedorow *et al.* 2004). Similarly, the inclusion of heteroatoms such as nitrogen have been shown to improve the performance of graphene in a range of catalytic applications (Kong *et al.* 2014). The role of heteroatoms and the influence of carbon structure are therefore worthy of further study when considering the activity of carbonaceous deposits and materials.

2.2.6. Active metal-carbon phases

Carbonaceous catalysts and deposits may not consist of pure carbon, and the active component may indeed be a metal or metal carbide. Examples of active iron carbide and

Chapter 2 – Literature Review

molybdenum oxycarbide were given in Table 2-1. A particularly noteworthy example is the formation of palladium carbide in situ, which numerous studies have identified as enhancing the selectivity of alkyne hydrogenation towards alkene formation. The key effects identified in the literature are the destabilisation of alkenes adsorbed on the surface, and inhibition of high energy, unselective, sub-surface hydrogen that promotes over-hydrogenation (García-Mota *et al.* 2010; Teschner *et al.* 2006; Tew *et al.* 2011; Studt *et al.* 2008; Kitchin *et al.* 2005; Yang *et al.* 2016). A schematic of the process can be seen in Figure 2-5. Not all carbides however are active; cobalt carbide for example contributes to deactivation of Fischer-Tropsch catalysts (Karaca *et al.* 2011; Fei Tan *et al.* 2010; Keyvanloo *et al.* 2015). The activity of the metal carbide phase therefore depends not only on the type of carbon, but also on the metal used.

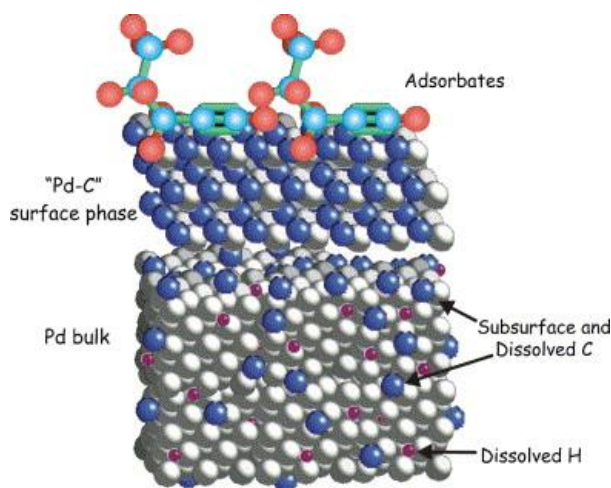


Figure 2-5 Model of the palladium surface demonstrating the role of the palladium carbide phase during 1-pentyne hydrogenation (Teschner *et al.* 2006). The metal carbide phase inhibits the emergence of the dissolved hydrogen, which promotes over-hydrogenation. Reproduced with permission. Copyright 2006 Elsevier.

The activity of metal carbides highlights that the interaction of carbon with other components in the reaction system must be considered. In laboratory research, there are many possible sources of trace metal contamination, which could influence catalytic activity (Ananikov 2016). A key example is the role of metal reactor walls in forming catalytically active coke. In a study by Gornay *et al.*, reactor walls containing Fe and Ni were found to catalyse coke formation during the pyrolysis of octanoic acid; the metal-containing coke then accelerated the pyrolysis of the octanoic acid (J. Gornay *et al.* 2010). Iron impurities have also been detected in carbon nanotubes, due to the use of iron in the production process; however these impurities were shown to decrease selectivity to alkene conversion in the oxidative

dehydrogenation of *n*-butane (Zhang *et al.* 2008). In laboratory studies using quartz or glass reactors, the potential influence of metal reactor walls on catalysis and coke formation should be considered when scaling up for industrial application.

Chapter 2 – Literature Review

2.3. Applications of biochar

Biochar is a carbonaceous material formed by heating biomass in the absence of oxygen, a process known as pyrolysis. Pyrolysis of biomass also produces non-condensable gases, which can be burnt for fuel, as well as condensable organic liquids (Crombie *et al.* 2013). Biomass for these processes can be sourced from a wide range of feedstocks, such as food, animal and municipal waste, as well as plant materials. The applications of biochar are considered in this section, for soil remediation (section 2.3.1), as a catalyst (section 2.3.2) and as a catalyst support (section 2.3.3).

2.3.1. Soil remediation

Biochar has several applications, the most common being soil remediation. Biochar can be used to improve nutrient availability, to adjust the pH of soil, and for the adsorption of pollutants, leading to improved crop yields (Ahmad *et al.* 2014; Hernandez-Mena *et al.* 2014). Biochar also acts as a net carbon sink, with lifecycle analyses estimating carbon savings of 2-19 tonnes of CO₂ per hectare per year through application of biochar to agricultural soils (Gaunt & Lehmann 2008; Woolf *et al.* 2010). This is achieved through the conversion of CO₂ to fixed carbon via photosynthesis, which remains stable in soils for longer periods than other organic matter (Lehmann 2007). Biochar is therefore a sustainable and versatile source of carbonaceous matter, which can itself be used to reduce global CO₂ emissions.

Biochar can be easily modified to suit the desired application, for example through choice of feedstock or pyrolysis conditions. In a study of biochars from 12 feedstocks, properties such as total carbon content and mineral elements were found to be more strongly dependent on feedstock than on pyrolysis temperature (Zhao *et al.* 2013). Notably, ash content can vary from 0 wt% in wood-based chars to over 50 wt% in rice-based chars (Jindo *et al.* 2014; Zhao *et al.* 2013). Increased pyrolysis temperature has been shown to increase the carbon content, ash content, graphiticity, surface area and pH of biochar (Zhao *et al.* 2013; Manyà 2012; Jindo *et al.* 2014; Titirici *et al.* 2015; Zhao *et al.* 2016; Asadullah *et al.* 2010). The effect of pyrolysis conditions and feedstock on catalytic performance however are limited. The ability to modify the properties of biochar could make this material an excellent candidate for catalytic applications.

2.3.2. Catalytic applications

Biochar has found numerous applications in catalytic research, principally as a support and as a functionalised carbon. This is a fast-growing subject of research interest, with a number of reviews published in recent years (Qian *et al.* 2015; Abdullah *et al.* 2017; Lee *et al.* 2017; Cao *et al.* 2017). The key applications of biochar in catalysis will be summarised in this section.

A key area of research is the use of biochar as catalysts for processes closely related to biochar production. These include the reduction of tar (Shen 2015; Liu *et al.* 2011; Abu El-Rub *et al.* 2008) and the conversion of biomass to chemical products (Lam & Luong 2014). The activity of biochar in these processes is often attributed to the mineral or ash content, particularly the potassium and alkali/alkali earth metal (AAEM) content. For example, the CO₂ gasification rate of a spruce wood char was found to increase linearly with Ca and K content (Perander *et al.* 2015). Surface alkali metals in biochars may also be involved in the catalytic decomposition of tar compounds, such as toluene (Mani *et al.* 2013; Feng *et al.* 2018). Biochar may therefore provide a more sustainable source of catalysts for these processes, in place of the currently-used iron- and nickel-based catalysts.

The activity of ash has also been demonstrated in other cases, such as the formation of glycerol from glycerol carbonate over boiler ash (Indran *et al.* 2014), whilst potassium is a known promoter in heterogeneous catalyst design, for example potassium-promoted iron catalysts are used in dehydrogenation of hydrocarbons (Liu & Dai 2016). In methane decomposition, ash content was found to catalyse C-C and C-H bond breakage, with carbon acting as both an active site for methane cracking and as a support for inorganic metals such as Fe, Ca and K; oxygen-containing groups were not found to be involved in the reaction (Klinghoffer *et al.* 2015). In biochar samples, the potassium most likely exists as ions, whilst other alkali earth metals such as calcium and magnesium are more likely bound in organic compounds (Zhao *et al.* 2016). The role of ash content should therefore not be neglected in studies of the catalytic activity of biochar.

Functionalised biochars have also been developed for the production of biodiesel from the transesterification reactions of vegetable oils. This was the subject of a recent literature review

Chapter 2 – Literature Review

(Abdullah *et al.* 2017). Biochars have been used for the production of both solid acid catalysts (Dehkhoda *et al.* 2010; Kastner *et al.* 2012; Yu *et al.* 2011) and solid bases (Bazargan *et al.* 2015; Chakraborty *et al.* 2010; Ofori-Boateng & Lee 2013), and as supports for traditional homogeneous catalysts such as KOH (Riadi *et al.* 2014). Biochars with high AAEM contents are particularly suitable for the formation of solid base catalysts, containing active species such as calcium oxide and potassium carbonate. Solid acid catalysts were generally prepared by treating carbonaceous materials with a sulfonating agent, usually fuming or concentrated sulphuric acid. The ability to form both solid acid and solid base catalysts from biochars is promising for other reactions besides transesterification.

Other applications of biochar catalysts are currently limited. Biochars have been investigated for the production of syngas, and tungsten carbides supported on biochar have been prepared for dry reforming (Lee *et al.* 2017). Solid acid catalysts have been applied for the hydrolysis of cellulose, and therefore the conversion of biomass to chemical products (Ormsby *et al.* 2012). Due to their lower cost, biochars have also been investigated as materials for carbonaceous electrodes, for example in microbial fuel cells, exhibiting higher maximum power densities than Pt/C and graphite electrodes (Lee *et al.* 2017). The full potential of these solid base and solid acid catalysts is yet to be explored.

2.3.3. Catalyst support

As a support material, biochar has found applications in a wider range of reactions, including hydrogenation of phenol to cyclohexanol (Makowski *et al.* 2008), low-temperature selective catalytic reduction of NO (Shen *et al.* 2015), oxidation of glycerol and hydrogenation of levulinic acid (Prati *et al.* 2018). Reproducibility in these applications however can be poor, due to variations in the properties of the biochar used as supports which affect the loading and dispersion of the metal particles; this was noted in the 1990s as being due to commercial carbons not being primarily aimed at the catalytic industries, which is generally still the case (Cameron *et al.* 1990). This variability in properties is likely to also affect the reproducibility of catalytic reactions.

2.4. Role of carbon in CO₂ utilisation reactions

The potential of biochar to catalyse a range of reactions has been demonstrated in the literature. However, one area which is of increasing research interest is that of CO₂ utilisation reactions. The ability of carbonaceous materials to catalyse these reactions has not previously been reported, although carbon electrodes have been used for the reduction of CO₂ to CO in electrocatalysis (Liu & Dai 2016). In this case, the active sites are thought to be positively-charged carbon atoms, which are re-oxidised by the CO₂. The ability of carbonaceous materials to act as CO₂ adsorbents has also been reported in the literature, with potassium content in biomass-derived activated carbon shown to be particularly beneficial (Yin *et al.* 2013). This provides some evidence that biochars may show potential in activating CO₂ for utilisation.

A full consideration of the potential of carbon to catalyse CO₂ utilisation is beyond the scope of this literature review; more comprehensive overviews can be found in the literature (Aresta 2010; Mikkelsen *et al.* 2010; Ampelli *et al.* 2015). Two CO₂ utilisation reactions of interest are considered here. The first is methanol conversion to products, such as dimethoxymethane (DMM) and dimethylcarbonate (DMC). Methanol oxidation is often considered as a probe reaction for the study of catalysts, as the products are highly sensitive to the active sites present (Tatibouët 1997; Sun *et al.* 2009). CO₂ may be able to act as the oxidant in this reaction; this is considered in section 2.4.1. The second reaction is the conversion of glycerol to glycerol carbonate. In this case, the potential of ash containing potassium silicate has already been demonstrated in the literature (Indran *et al.* 2014). The potential of biochars from other feedstocks to catalyse the reaction will be considered in section 2.4.2.

2.4.1. Methanol conversion

Methanol oxidation can be studied as a probe reaction, with the reaction products being highly sensitive to the types of active site present (Tatibouët 1997; Sun *et al.* 2009). The potential products of methanol oxidation are wide ranging, and are summarised in Figure 2-6. Of particular interest is dimethoxymethane (DMM), which has applications in the paint, perfume and pharmaceutical industries, as well as a fuel additive (Thavornprasert *et al.* 2016).

Chapter 2 – Literature Review

The reaction mechanism for the direct conversion of methanol to DMM has been studied over several catalysts, and was recently reviewed in the literature (Thavornprasert *et al.* 2016). Selective oxidation to DMM is thought to occur over catalysts with both redox and acid functionalities; weak acidic sites are required alongside oxidative sites. Methanol is thought to oxidise to formaldehyde before undergoing a condensation reaction to form DMM over bifunctional catalysts. Other potential products are methyl formate and dimethyl ether, formed by the condensation reaction of methanol with the intermediate formic acid – this can occur if sites are too acidic and oxidising for DMM formation (Thavornprasert *et al.* 2016).

Catalysts for this reaction are generally metal oxides, such as molybdenum on silica, and vanadia on titanium oxide (Thavornprasert *et al.* 2016). Other catalysts studied in the literature include supported Re oxides and combined FeMo catalysts (Julien Gornay *et al.* 2010). The role of oxygen in silica supports has been studied through anaerobic studies of the direct methanol conversion reaction. The study found that Si-O groups do not play a role in oxygenation, however, other surface oxygen groups such as V-O may be depleted. This leads to an excess of acidic sites, decreasing activity towards DMM formation (Chen & Ma 2017).

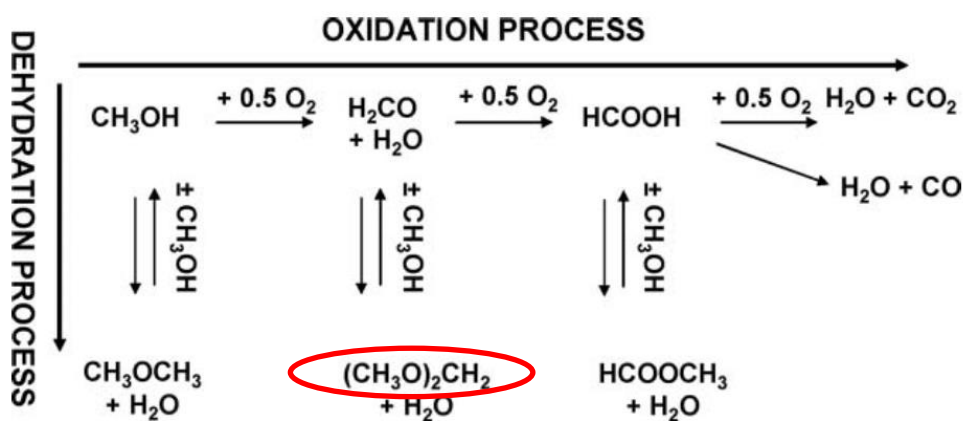


Figure 2-6 Methanol oxidation pathways. Figure reproduced with permission from the Royal Society of Chemistry (Julien Gornay *et al.* 2010). Dimethoxymethane highlighted for clarity.

The reaction of methanol with CO_2 could also lead to the formation of dimethyl carbonate (DMC). This chemical also has potential as a fuel additive, but has generated particular research interest as a 'green' reagent, offering a safer, less toxic alternative to methyl halides and phosgene in methylation and carbonylation reactions (Tundo & Selva 2007). A range of catalysts have been studied for the direct carbonylation of methanol using CO_2 , including

metals, bases, metal oxides and supported metal oxides (Cao *et al.* 2012). Carbonaceous samples have not yet been studied as catalysts for this reaction, however activated carbon has been used as a support material for a PdCl₂-CuCl₂ catalyst (Sakakura & Kohno 2009; Cao *et al.* 2012). Silica supports were found to be too acidic, with no DMC formed; enhanced selectivity was obtained with less acidic alumina-supported catalysts (Aouissi *et al.* 2010).

Many pathways to DMC have been proposed in the literature. The route currently used industrially is the reaction of methanol with phosgene or methyl chloroformate, however due to the high toxicity of these chemicals, the direct oxidative carbonylation route is now preferred (Buysch 2000). The direct carboxylation of methanol using CO has been studied since the 1980s (Hoffman 1982), however CO is also a toxic reagent.

Direct carboxylation of methanol using CO₂ has gained increased interest as a means of reducing greenhouse gas emissions; for example, CO₂ emissions from various processes could be captured and used as a reagent for chemical synthesis. This would be more sustainable according to Principle 7 of the 12 principles of green chemistry (use of renewable feedstocks); by contrast, CO is usually synthesised from coal gasification or steam reforming of natural gas (Bierhals 2001). Other advantages of the CO₂ synthesis route over CO include the lower cost, and the improved safety by replacing toxic CO with the non-toxic CO₂. This is more sustainable according to Principle 3 (less hazardous chemical synthesis).

Two main mechanisms for this pathway have been proposed, depending on the catalyst: acid-plus-base activation of methanol, and double base activation of methanol (Aresta *et al.* 2006). This activation requires strong basic sites to produce methoxy species (Almusaiteer 2009). In these studies, adsorbed methoxy species and activated CO₂ were found to be essential to the process, with concentration being a determining factor. The key disadvantage to this route remains that CO₂ is less reactive than CO, and conversion rates are not yet economically viable for industrial application (Buysch 2000).

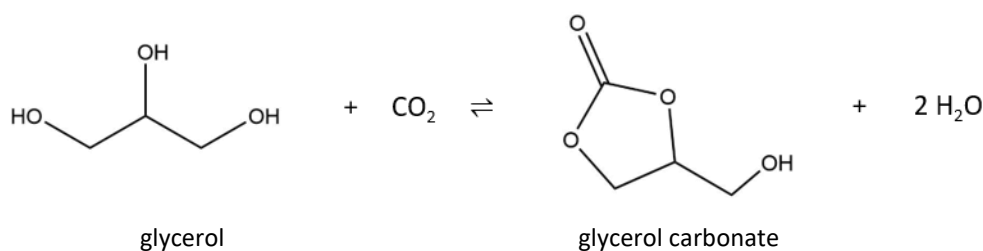
It is possible that DMC may be formed from DMM, although research into this pathway is limited (Fu *et al.* 2005). In general, the formation of DMC is favoured by low temperatures,

Chapter 2 – Literature Review

high pressures and shorter reaction times. The role of dehydration agents in DMC synthesis have also been studied (Sakakura *et al.* 2007; Keller *et al.* 2010). As with DMM synthesis, the reaction is sensitive to catalyst acidity, with likely by-products including dimethyl ether (DME) and methyl formate.

2.4.2. Glycerol upgrading

The reaction of glycerol with carbon dioxide to form glycerol carbonate is a promising avenue of research. Glycerol is an undesired by-product in the manufacture of biodiesel, with 0.1 kg produced per 1 kg of biodiesel (Christoph *et al.* 2006). In addition, CO₂ utilisation is desirable to reduce the impact of CO₂ emissions on climate change. Numerous other reaction pathways to glycerol carbonate have been reviewed in the literature, including synthesis from glycerol and CO, glycerol and phosgene, and glycerol and alkyl and dialkyl carbonates (Sonnati *et al.* 2013). However, direct carboxylation of glycerol using CO₂ offers a promising and sustainable route. The reaction equation is given in Scheme 2-1.



Scheme 2-1 Reaction of glycerol with CO₂ to form glycerol carbonate and water.

Glycerol carbonate has many uses as a feedstock in the chemical industries, for example it is a precursor to the manufacture of epichlorohydrin and glycidol, which are used in polymer production (Sonnati *et al.* 2013; Pagliaro *et al.* 2007). The applications of glycerol carbonate are summarised in Figure 2-7.

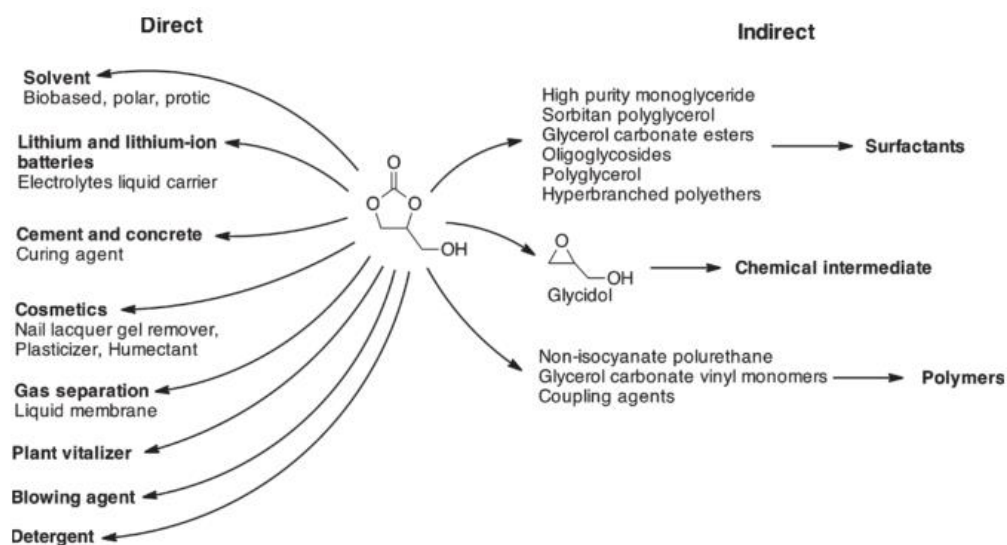


Figure 2-7 Direct and indirect applications of glycerol carbonate. Figure reproduced with permission from the Royal Society of Chemistry (Sonnati *et al.* 2013).

The reaction mechanism for glycerol carbonate formation from glycerol and CO₂ has been proposed in the literature. Glycerol and CO₂ are activated over basic sites, requiring a Brønsted and Lewis base respectively. The CO₂ may form adsorbed C≡O, which is then inserted into the activated glycerol molecule, leading to the formation of glycerol carbonate (Aresta *et al.* 2007). As shown in Scheme 2-1, this leads to the formation of water as a by-product. The production of glycerol carbonate can therefore be favoured through the use of dehydrating agents to remove this water.

A full review of dehydrating agents is beyond the scope of the current work, although further details can be found in the literature (Li *et al.* 2013; Li *et al.* 2015; Razali 2017). Acetonitrile is one such dehydrating agent, which reacts with water to form acetic acid. The acetic acid then reacts with glycerol, leading to the formation of mono-, di- and triacetins. These glycerol acetins are valuable products, with applications as plasticisers, fuel additives and humectants (Kong *et al.* 2016). Whilst monoacetin is thought to be produced in the absence of catalyst, catalysts are reported in the literature to be necessary for the formation of di- and triacetin (Sandesh *et al.* 2015). Selectivity to triacetin has been correlated with Brønsted acidity, although steric hindrance may also play a role in microporous materials (Sandesh *et al.* 2015; Konwar *et al.* 2015).

Chapter 2 – Literature Review

The catalysts used for glycerol upgrading are generally bases such as metal oxides. Metals such as tin and rhodium have been used for the reaction (Sonnati *et al.* 2013), and the effectiveness of zeolites and lanthanum-based catalysts has also been studied (Algoufi & Hameed 2014; Ozorio *et al.* 2015; Razali 2017). Carbonaceous catalysts in the literature have largely been employed as support materials, or as feedstocks for the production of sulfonated carbonaceous catalysts; the use of solid acid catalysts for glycerol acetylation was recently reviewed in the literature (Kong *et al.* 2016). Boiler ash has also been observed to catalyse the reaction, with the activity attributed to potassium silicate (Indran *et al.* 2014). Biochars are yet to be tested for catalytic activity in this reaction.

2.5. Characterisation of carbonaceous catalysts

This section includes extracts from a published literature review on catalytically active coke, published in the journal Catalysis Science and Technology (Collett & McGregor 2016); the full paper is given in Appendix E .

In sections 2.2 and 2.3, it was demonstrated that carbon and particularly carbonaceous deposits can be catalytically active, although the reasons for this are not always clear. Understanding the role of carbon in catalysis requires a full characterisation of the amount, composition, chemical nature and location of the coke (Barbier 1986). Several techniques must be employed as no one technique can capture all of this information. Techniques vary in their ability to measure bulk or surface properties, and some may be invasive or destructive (Serp & Figueiredo 2009). Some recent studies have identified characterisation as a limiting factor, as no differences were identified to explain the higher selectivity or activity of one catalyst over another (Nederlof *et al.* 2012; Santiago *et al.* 2005; Suarez-Ojeda *et al.* 2005). The importance of using a wide range of characterisation methods, ideally conducted simultaneously on the same sample, cannot be overstated.

The aim of this section is to summarise characterisation techniques which have been applied in the literature to carbonaceous samples, including recent advances in the application of these techniques. Vibrational spectroscopy techniques are considered in section 2.5.1, electron spectroscopy methods in section 2.5.2, and further commonly used techniques are discussed in section 2.5.3. Characterisation techniques applied to biochar are considered in particular detail in section 2.5.4, highlighting differences between approaches to characterisation for soil remediation and catalytic applications.

Only brief details on the techniques themselves are provided here; a number of excellent reviews of catalyst characterisation techniques exist in the literature which provide greater detail (Che & Vedrine 2012; Mahmoud & Lobo 2014). The theory behind techniques which will be applied in this work will be outlined in Chapter 3.

2.5.1. Vibrational spectroscopic techniques

Vibrational spectroscopy techniques analyse the interactions between photons or particles with a surface and the resulting excitation or de-excitation. This category of technique

Chapter 2 – Literature Review

includes infrared (IR) spectroscopy, Raman spectroscopy, THz-time domain spectroscopy (THz-TDS), ultraviolet-visible (UV-Vis) spectroscopy and inelastic neutron scattering (INS).

IR spectroscopy is used to identify the functional groups present in a sample, provided the vibration mode produces a change in the dipole moment of the bond. The main application in carbonaceous samples is detection of changes in surface chemistry following surface treatment. This has ranged from treatments with acids and bases (Toles *et al.* 1996; Moreno-Castilla, Carrasco-Marín & Mueden 1997; ShamsiJazeyi & Kaghazchi 2010; Jansen & van Bekkum 1994), to oxidation (Pradhan & Sandle 1999; Koch 1998), heat treatment (Shin *et al.* 1997), microwave treatment (Valente Nabais *et al.* 2004) and heteroatom doping (Gai *et al.* 2016). Adsorption and reaction studies have been coupled with *in situ* IR spectroscopy, allowing the species formed and adsorbed during reaction to be studied (Raymundo-Piñero *et al.* 2001; Guo *et al.* 2010; Al-Khattaf *et al.* 2014; Zawadzki *et al.* 2001; Zawadzki *et al.* 2003). This provides valuable information on the adsorption species and sites on the surface of the carbonaceous sample. However, the highly absorbing nature of carbon samples, which are often black in colour, can obscure key features of the spectrum. It is therefore important to employ methods which can probe optically opaque samples.

Raman spectroscopy is a complementary technique to IR spectroscopy, and is widely used for the study of carbonaceous samples. This is because the Raman scattering effect is dependent on the polarisability of the species, and thus can be used to indicate the degree of graphiticity of a carbon network, where high densities of polarisable electrons are located (Serp & Figueiredo 2009; Haghseresht *et al.* 1999; Ayala *et al.* 2004). The most commonly studied region for carbonaceous samples is from 800-2000 cm^{-1} , where disordered and graphitic carbon bands are observed. Deconvolution of these bands can yield information on the ratio of graphitic to disordered carbon, a key indicator of the extent of graphiticity in carbonaceous and coked catalyst samples. However, no standard exists for the curve deconvolution of carbonaceous samples; for example, methods for analysing carbon films range from fitting 2 to 11 peaks (Ayala *et al.* 2004; Tarrant *et al.* 2004), and for biochars, between 2 and 10 peaks (Zhao *et al.* 2016; Li *et al.* 2006; Zhao *et al.* 2013; Chia *et al.* 2012). The implications of this for biochar characterisation will be discussed in section 2.5.4.

The degree of graphiticity in carbonaceous samples can also be examined quantitatively through terahertz-time domain spectroscopy (THz-TDS) (McGregor, Huang, *et al.* 2010; Arrigo *et al.* 2010; Gomez-Sanz *et al.* 2015). Compared to IR and Raman spectroscopy, THz-TDS probes a lower energy region of the electromagnetic spectrum and is hence ideally suited to characterising low energy modes in extended graphitic-like networks.

Other spectroscopic techniques commonly used in the study of carbon deposits include UV-Vis and inelastic neutron scattering (INS). Typical functionalities which can be identified by UV-Vis spectroscopy include conjugated double bonds, aromatics, and unsaturated carbenium cations (Jiang *et al.* 2007), all of which are relevant to the study of coke deposits. As an example, UV-Vis has been applied to detect an overlayer containing alkenyl carbenium ions on HY-FAU zeolites as a result of hydrocarbon adsorption (Kiricsi *et al.* 2003). INS is an emerging technology, which is particularly suited for analysing hydrogen-rich coke deposits due to the high neutron scattering cross-section of hydrogen. It is also suitable for the analysis of optically absorbing samples (Hamilton *et al.* 2014). Applications include the studies of hydrogen pre-treatment of catalysts (Warringham *et al.* 2015) and hydrogen retention in catalysts (McFarlane *et al.* 2013).

2.5.2. Electron spectroscopy

Electron spectroscopy techniques are highly surface sensitive, and can provide detailed information on the chemical environment of surface atoms. They are commonly used for the study of carbonaceous materials and carbon deposits.

Electron spectroscopy methods, such as Auger electron spectroscopy (AES) and X-ray photoelectron spectroscopy (XPS), can be applied to a variety of samples. In both techniques, electrons are emitted with kinetic energies related to the atomic or molecular environment of the atom of origin, yielding approximate elemental surface composition measurements and oxidation states (Vickerman & Gilmore 2009). XPS for example can quantify the C/H ratio or degree of aromaticity in a coke sample (McGregor, Huang, *et al.* 2010; Grünert 2012). One limitation of XPS is the calibration of the electron binding energies. The position of the adventitious carbon peak is often used, even for carbonaceous samples (Nakayama *et al.* 1990;

Chapter 2 – Literature Review

Jansen & van Bekkum 1995; Chia *et al.* 2012). A detailed study of the C1s peak identified seven components, based on DFT and experimental data (Smith *et al.* 2016). This implies the position of the C1s peak will vary, depending on the relative contribution of these components. As with Raman curve deconvolution, there is little consistency between researchers on curve deconvolution and calibration methods for C1s spectra.

Developments have been made recently in “high pressure” XPS, which enables XPS of catalyst surfaces to be carried out under reaction conditions *i.e.* in a gaseous atmosphere rather than under high vacuum (Knop-Gericke *et al.* 2009). Although not yet used for carbonaceous samples, this technique has been applied to catalytic studies, including CO oxidation on Pt/ceria catalysts (Teschner *et al.* 2007), catalytic oxidation of propane over nickel catalysts (Kaichev *et al.* 2013) and studying deactivation of platinum catalysts (Paál *et al.* 2006). This could improve the utility of XPS for the future study of carbon deposition processes.

Electron spectroscopy also forms the basis of a number of imaging techniques, which can be applied for examining the position of carbon deposits on heterogeneous catalysts. Scanning Electron Microscopy (SEM) and Transmission Electron Microscopy (TEM) use a beam of focused electrons to produce an image of the catalyst surface, and has been applied to image biochar samples in the literature (Chia *et al.* 2012; Ma *et al.* 2016; Han *et al.* 2013). In combination with energy dispersive X-ray spectroscopy (EDX) and Electron Energy Loss Spectroscopy (EELS) it can be used to identify the chemical elements present on a catalyst surface, producing a compositional map on top of the microscope image. These techniques have been applied to produce maps of the position of coke on the catalyst surface (McGregor, Huang, *et al.* 2010). Atomic force microscopy (AFM) can also be used to obtain high resolution images with minimal sample preparation, with applications in studies of carbon films (Ayala *et al.* 2004) and graphene samples (Hong *et al.* 2013).

2.5.3. Additional techniques

Thermal methods involve heating the sample under a controlled atmosphere and either monitoring the species desorbed, for example by mass spectrometry, or monitoring the mass change of the sample. Among the most commonly utilised thermal methods in coke analysis

is temperature programmed oxidation (TPO), which can yield information on the coke type and location on the catalysts; peaks obtained at different temperatures correlate to different coke structures (Querini & Fung 1997; Chen et al. 2013; Sánchez et al. 2009; Bayraktar & Kugler 2002). Temperature programmed desorption (TPD) can yield information on the functional groups present on the surface of the carbonaceous deposit (Muckenhuber & Grothe 2006; Haydar et al. 2000). Other variations include temperature programmed hydrogenation (TPH) and reduction (TPR). Chemical methods can also be used, such as Boehm titration to detect the presence of acidic functional groups on the surface (Serp & Figueiredo 2009; Boehm 1966).

Thermogravimetric analysis (TGA) is widely used to quantify the amount of coke on a surface (Moodley et al. 2007; Pradhan et al. 1999), and to characterise the composition of carbonaceous materials in terms of their fixed carbon content, moisture, ash content and volatile components (Bagreev & Bandosz 2001). Standardised methods for thermogravimetric analysis of carbonaceous materials (coals and cokes) have been developed by the American Society for Testing and Materials (ASTM International 2010), providing the basis of most methods seen in the literature.

NMR techniques have many applications in the study of coke deposits. ^{13}C NMR played a key role in the discovery of the hydrocarbon pool mechanism by which carbon deposits play a catalytic role in the conversion of methanol to higher hydrocarbons (Che & Vedin 2012). In particular, ^{13}C NMR spectroscopy is useful for studying the carbon structure and electronic environment of carbon deposits, but is limited to use at relatively high coke contents, above approximately 3.5 wt% (Hagaman et al. 1998; Haghseresht et al. 1999; van Donk et al. 2001). Other isotopes have also been used to study carbon deposition in zeolites, such as ^{27}Al , ^{129}Xe and ^{131}Xe (Al-Khattaf et al. 2014; Barrage et al. 1990). In studying carbonaceous materials, however, ^{13}C NMR spectra can be composed of very complicated overlapping signals, for example the overlapping of C, CH, CH_2 and CH_3 signals (Hu et al. 2001). NMR is therefore not usually applied to the study of coals and chars.

Interference or diffraction methods, such as X-ray diffraction (XRD) or neutron diffraction, can be used to study the geometry and symmetry of a surface. Since this method relies on the

Chapter 2 – Literature Review

study of diffraction patterns, it is suitable for the study of materials with long-range order which can produce such diffraction patterns, such as carbon fibres (Park *et al.* 2003), ordered coke deposits (Amano *et al.* 2001) and chars and activated carbons with graphitic character (Pradhan & Sandle 1999; Liou & Huang 2013; Yu *et al.* 2011). However, XRD is unsuitable for materials which are polycrystalline or amorphous (Vickerman & Gilmore 2009).

The area of combined techniques is a rapidly developing field. No one individual technique is sufficient to provide all of the information required in order to understand how, for example, surface structure affects chemical reactivity. Demonstrated combinations of analytical techniques include NMR-UV-Vis, UV-Vis-Raman, FTIR-Raman and Raman-XRD (Che & Viedrine 2012). Additionally, a combined NMR/Raman set-up has recently been developed and applied to the study of catalytic metathesis (Camp *et al.* 2014). The application of combined techniques allows coherent and complementary data sets to be obtained under the same reaction conditions and allow connections between two (or more) different sets of data to be drawn with much more confidence. It must be noted however that by combining techniques, a compromise is often required between, (i) the quality of one or more of the data sets, and (ii) the benefits of combined data sets.

2.5.4. Characterisation of biochar

The characterisation of biochar for catalytic applications poses its own challenges. There are many properties of biochar which affect its suitability for catalytic application, and little consistency in how these properties are quantified. There is also a difference in approach between characterisation of biochar for catalysis and characterisation for soil remediation.

There is a difference in approach to biochar characterisation for catalytic applications, and for applications such as soil remediation. Studies of biochar for catalytic applications will often focus on one or two waste materials, and aim to demonstrate their suitability for a given application. The aim of characterisation is to improve the activity of a specific biochar, for example to understand the effect of activation or functionalisation treatments. Examples of this are the development of a sulfonated acid catalyst from pine wood chips for hemicellulose hydrolysis (Ormsby *et al.* 2012), and the use of karanja seeds pyrolysed at different

temperatures for glycerol esterification (Rafi *et al.* 2015). In soil remediation applications, multiple biochars are characterised, in order to choose the biochar with the properties best suited to the application. This can be seen in Table 2-2, where up to 12 biochars are studied, in order to select the feedstock with the most suitable properties. This application-centred approach could be valuable in catalysis research, where characterisation is performed in order to select the best material for the application, rather than the best application for the material.

The characterisation methods themselves vary depending on the application. Some representative examples are given in Table 2-2. In catalytic applications, virtually every study will characterise the surface area, porosity and surface acidity or basicity of a sample, however characterisation of carbon structure is not always performed. Studies often quantify the trace metal content through ICP analysis of elements digested in aqua regia; however, this technique is less effective at removing K and Na from the biochar matrix (Bachmann *et al.* 2016). XPS would also allow surface concentrations to be determined, which is more relevant for catalytic applications. Whilst some factors analysed for soil remediation are not particularly relevant for catalysis, such as the cation exchange capacity, properties such as carbon structure are more often characterised. As discussed in section 2.2, carbon structure and particularly graphitic content may influence catalytic activity, however this is rarely considered in the literature. This may be worthy of further investigation in biochars for catalytic applications.

It is also worth noting that there are no standards for characterisation of biochar, with the result being poor reproducibility between institutions when characterising standardised samples. A recent 'round robin' study found that when three standard biochars were characterised by 22 laboratories in 12 countries, using methods of their choice, reproducibility between laboratories was generally poor, with mean reproducibility standard deviation values over 20 % for most parameters studied (Bachmann *et al.* 2016). Similar problems can be expected in the characterisation of biochars for catalytic applications. As this is a growing area of research, standardised procedures for preparation and characterisation of biochar may be beneficial for comparison of results.

Chapter 2 – Literature Review

Table 2-2 Characterisation techniques used in the literature for biochars for different applications. Representative examples are given for catalytic and soil remediation applications, with other notable examples also listed.

Source	Biochars studied	Target application	Techniques/properties													
			Composition			Structure				Surface chemistry			Other			
			Proximate (TGA)	Ultimate (CHNOS)	Elemental (EDX/XPS/ICP/XRF)	Surface area (BET/N ₂)	Porosity (BJH)	Crystal structure (XRD)	Imaging (SEM/TEM)	Functional groups (FTIR)	Acidity, basicity (TPD/titration)	Carbon content (13C-NMR/Raman/EPR/PAH)	Conductivity (CEC/EC)	Calorimetry	Adsorbance capacity	pH
Catalytic applications																
(Abu El-Rub <i>et al.</i> 2008)	Commercial biomass char (unspecified), pinewood char, pinewood ash	Tar reduction	X	X		X	X									
(Dehkhoda <i>et al.</i> 2010)	Three commercial hardwood chars	Biodiesel production (solid acid catalyst)			X	X					X					
(Kastner <i>et al.</i> 2012)	Pelletised peanut hulls, pine pellets, pine chip char	Esterification of fatty acids (solid acid catalyst)	X	X	X	X	X				X	X				X
(Moussavi & Khosravi 2012)	Pistachio hull biochar	Ozonation of water recalcitrant concentrations	X	X		X					X	X	X			X
(Ormsby <i>et al.</i> 2012)	Pine chip, wood-based AC	Catalyst (solid acid) for hemicellulose hydrolysis	X	X		X	X				X	X				
(Rafi <i>et al.</i> 2015)	Karanja seed shells	Esterification of glycerol with acetic acid	X	X		X		X			X	X	X			
(Shen <i>et al.</i> 2014)	Rice husk char	Conversion of tar using rice husk char-supported nickel-iron catalysts.	X	X	X	X										
(Wang <i>et al.</i> 2014)	Shengli brown coal	Pyrolysis and gasification of biomass			X	X		X	X				X			
(Yu <i>et al.</i> 2011)	Woody biomass	(Solid acid) Transesterification of canola oil	X	X		X	X	X			X	X				
(Shen <i>et al.</i> 2015)	Modified cotton biochar	Low temperature selective catalytic reduction (SCR) of NO			X	X		X			X	X				
(Bazargan <i>et al.</i> 2015)	Calcium oxide-based catalyst from palm kernel shell biochar	Transesterification of sunflower oil with methanol to produce biodiesel	X	X	X	X		X	X		X					

(Chakraborty <i>et al.</i> 2010)	Fly ash and egg shell derived solid catalysts	Solid base catalyst, transesterification of soybean oil to biodiesel				X	X	X	X		X					
(Ofori-Boateng & Lee 2013)	Ash from cocoa pod husks (supported and unsupported)	Transesterification of soybean oil to biodiesel. (Supported and unsupported catalysts)			X	X	X				X					
(Riadi <i>et al.</i> 2014)	Palm bunch ash, support for KOH	Biodiesel synthesis (simultaneous ozonolysis and transesterification)			X	X										
(Feng <i>et al.</i> 2018)	Rice husk biochar	Tar reforming	X	X	X	X				X						
Soil remediation applications																
(Bachmann <i>et al.</i> 2016)	Wood chip, blend of paper sludge and wheat husks, sewage sludge	Soil amendment		X		X						X	X			X
(Crombie <i>et al.</i> 2015)	Pine wood chips, wheat straw and wheat straw pellets	Soil enhancement/C sequestration										X	X			X
(Jindo <i>et al.</i> 2014)	Rice husk, rice straw, apple tree wood chips (<i>Malus pumila</i>), oak tree wood chips (<i>Quercus serrata</i>)	Carbon sequestration/soil fertility	X	X		X	X			X		X				X
(Zhao <i>et al.</i> 2013)	Animal manure (cow, pig), wood waste (sawdust), crop residue (wheat straw, grass), food waste (peanut shell, shrimp hull), aquatic plants (waterweeds, chlorella), municipal waste (wastewater sludge, waste paper, bone dregs)	Soil: carbon sink, contaminant sorbent, soil nutrient amendment	X			X	X			X		X	X			
(Brewer <i>et al.</i> 2011)	corn stover, switchgrass x 3 (different preparation methods)	Soil remediation/carbon sequestration	X	X		X				X		X	X			X
Other applications																
(Danso-Boateng <i>et al.</i> 2015)	Primary sewage sludge	Production of hydrochar as fuel source/soil additive	X	X	X										X	
(Wei <i>et al.</i> 2017)	Rice husk biochar	Adsorbent for acetanilide herbicide metolachlor		X		X				X	X	X				X
(Zhao <i>et al.</i> 2016)	Manchurian walnut	Catalysing pyrolysis (studying effect of pyrolysis temperature on alkali and alkaline earth metallic species)	X	X	X							X				
(Liu <i>et al.</i> 2011)	Rice husks, corn cobs	Adsorbent for phenol (model organic pollutant)	X		X	X				X	X					X
(Zhao <i>et al.</i> 2017)	Corn straw, poplar leaf	Adsorbent for dodecylbenzene sulfonic acid			X	X				X	X		X			

Chapter 2 – Literature Review

2.5.5. Biochar macrostructure

Whilst surface properties are of greater interest in catalytic applications, it is worth considering the bulk structure of chars, as this is what determines the surface area and porosity. Chars are largely amorphous but contain discrete regions or lamellae of graphitic character, of diameter 5-500 nm, consisting of two- to four layers of graphite-like sheets. Chars can be characterised by the extent of the relative orientation of these sheets; in isotropic or non-graphitisable chars the layers are not aligned, whereas when the layers are aligned the result is an anisotropic or graphitizable char. Between these graphitic regions are aromatic and aliphatic carbon compounds, ash and pores. A schematic of the structure of biochar with treatment temperature can be seen in Figure 2-8.

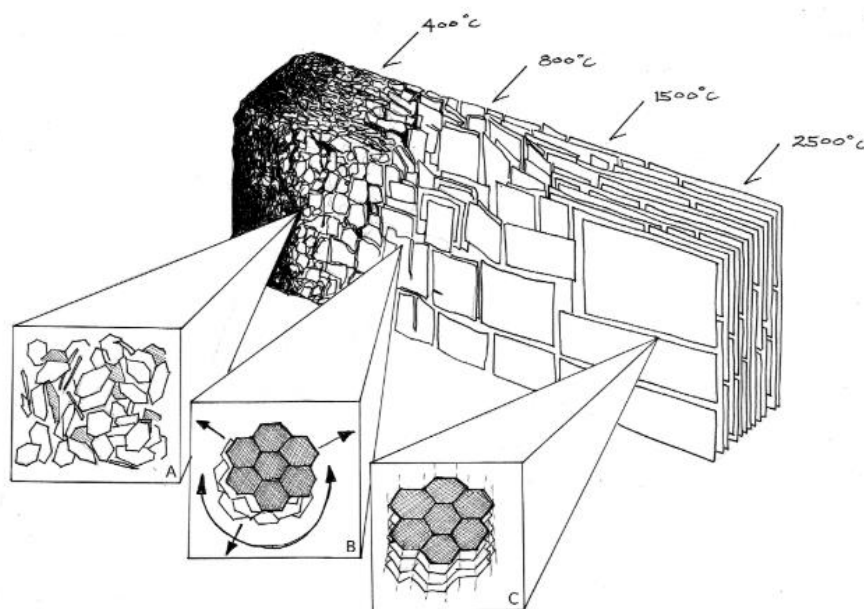


Figure 2-8 Ideal biochar structure development with highest treatment temperature: (a) increased proportion of aromatic C, highly disordered in amorphous mass; (b) growing sheets of conjugated aromatic carbon, turbostratically arranged; (c) structure becomes graph. Figure reproduced with permission from Routledge through PLSclear (Lehmann & Joseph 2009).

The extent of anisotropy in biochars has been found to be dependent on feedstock; biochars with strong cross-linking between layers are non-graphitisable. In graphitizable carbons, the degree of order has been observed to increase with temperature. Rosalind Franklin first demonstrated that non-graphitic carbon could be converted to graphitic carbon through pyrolysis in 1951, through analysis of X-ray diffraction images of various carbons. These included polyvinylidene chloride pyrolysed at 1000 °C, coal and charcoal. The extent of the

relative orientation of these regions was observed to increase with temperature (Franklin 1951). All biochars can be graphitised when heated to 3500 °C. A schematic of graphitizable and non-graphitisable carbon is shown in Figure 2-9.

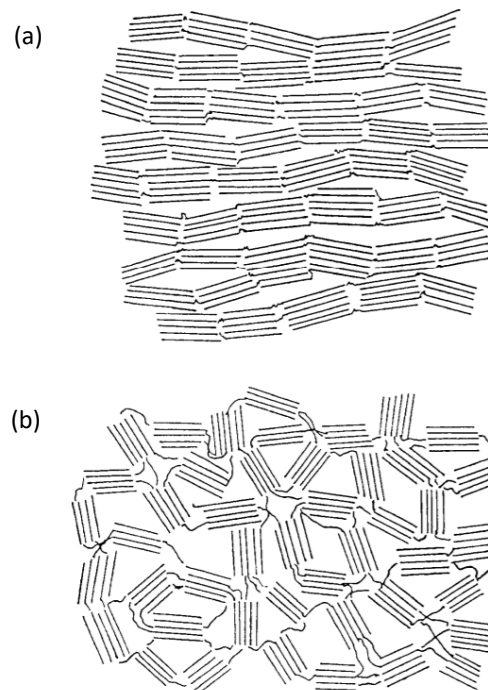


Figure 2-9 Schematic representations of the structure of (a) graphitising and (b) non-graphitising carbons, as proposed by Rosalind Franklin (Franklin 1951). Reproduced with permission from The Royal Society.

Various characterisation techniques are available for the characterisation of the carbon macrostructure of biochars. One key technique is X-Ray Diffraction (XRD), which enables the spacing between graphite layers to be determined from the diffraction patterns of x-rays (see Figure 2-10). For biochar, values between 3.4 and 3.78 Å have been obtained (T. Wang *et al.* 2018; Neeli & Ramsurn 2018). Optical microscopy utilises polarised light to quantify the anisotropy of carbon structures; the colour of the region under polarised light will depend on the orientation of the carbon sheets. The ‘optical texture’ of the biochar can therefore be classified, for example into isotropic, fine and coarse mosaics, granular and lamellar biochars; the classifications can be found in the literature (Grint *et al.* 1979; Moreland *et al.* 1988; Patrick *et al.* 1973).

Chapter 2 – Literature Review

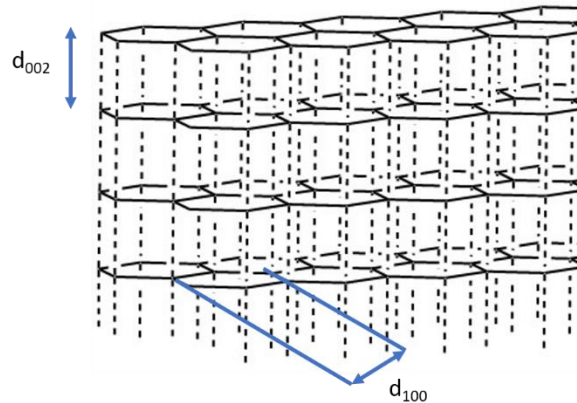


Figure 2-10 The structure of graphite, with the spacing between layers (d_{002}) and the ring size (d_{100}) annotated.

A comprehensive discussion of the known structure of biochar can be found in the literature (Lehmann & Joseph 2009). Figure 2-11 shows a schematic of biochar structure at different scales, based on these literature sources. SEM imaging of biochars is common in the literature, and particularly for woody biomass the structure of macropores is very regular, due to the structure of the xylem cells. The graphitic lamellae can be seen in Figure 2-11b, and are randomly oriented with respect to each other. The meso- and micropores are caused by interstices between the lamellae, but also from vacancies in the graphitic structure, or from the turbostratic alignment of the graphitic sheets. These pores can be filled with ash or tar. From the literature, it is known that functional groups containing oxygen are generally located at the edges of these ordered sheets, and that due to these heteroatoms the spacing between layers is slightly greater than the 0.335 nm obtained for graphite.

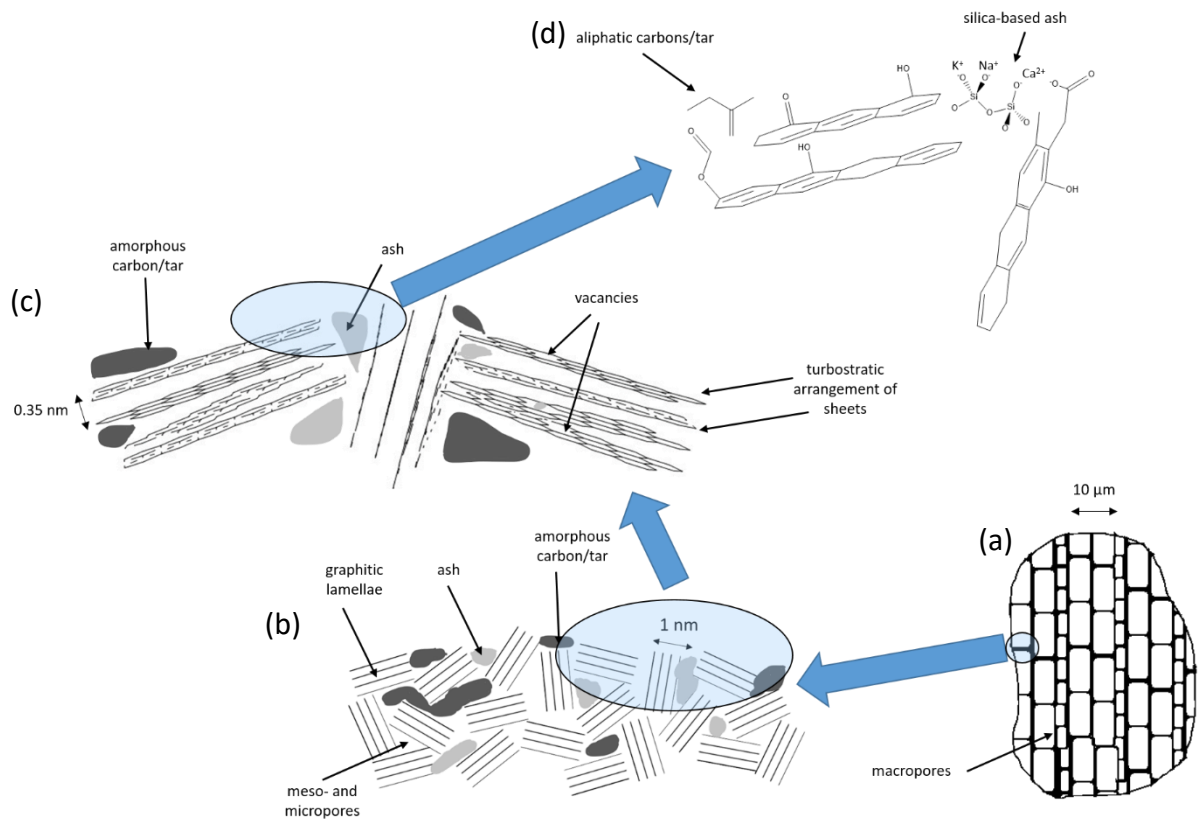


Figure 2-11 Schematic of biochar structure at different scales. (a) The macropores are visible in SEM images and are often highly ordered and regular in woody biomass. (b) For non-graphitizable carbons, lamellae are oriented relatively randomly compared to each other. (c) The surface of the biochar contains both flat sides and edges of graphite-like sheets, as well as exposed ash and amorphous carbon/tar. (d) At the atomic scale, a range of functional groups have been observed at the surface, generally at the edges of the sheets. Graphitic, aromatic and amorphous carbon will be present. Some ash will also be present at the surface.

Chapter 2 – Literature Review

2.6. Conclusions

This literature review has demonstrated the potential of carbon to improve sustainability in heterogeneous catalysis across three key areas: (i) the production of sustainable catalyst materials, (ii) the catalysis of sustainable reaction routes, and (iii) enhancing catalyst performance. The key findings are briefly summarised for each of these areas in section 2.6.1, before highlighting the key challenges and questions remaining in the field of carbonaceous catalysis in section 2.6.2. The proposed experimental work will then be outlined in section 2.6.3, building on the findings of this literature review.

2.6.1. Summary

Sustainable catalyst materials

Metal-based catalysts are increasingly becoming unsuitable for commercial use due to their high cost and limited reserves. Catalysts made from carbon, either with or without metals present, may therefore provide a more sustainable and economic alternative. Carbon has a number of advantages as a catalyst material, not least that it can be sourced sustainably from pyrolysis of waste biomass. Carbonaceous materials have been used as catalysts and catalyst supports since the 1930s. Carbon has been shown to catalyse a range of hydrocarbon transformation reactions: hydrogenations, dehydrogenations, hydrocarbon transfer, oxidations and reductions. In electrocatalysis, carbon is also used for electrodes, where it has been found to outperform silver and platinum electrodes. The variety of possible active sites, such as oxygen-containing functional groups or delocalised electrons in graphitic defects, make carbonaceous materials versatile catalysts.

Biochar is a by-product of biomass pyrolysis, and provides a sustainable and carbon-neutral source of carbonaceous material compared to graphite and coal. Biochar is generally applied as a soil additive, however the study of biochar as a catalytic material is a rapidly growing field, with numerous literature reviews published in recent years (Lee *et al.* 2017; Cao *et al.* 2017; Abdullah *et al.* 2017; Cha *et al.* 2016). The properties of biochar can be easily tailored by altering feedstock or pyrolysis conditions, or applying surface treatments, providing excellent versatility.

The key applications of biochar catalysts are in tar reduction during biomass pyrolysis, and transesterification for biodiesel production. Both solid acids and solid bases have been used in biodiesel production, with solid acids formed by sulfonation of carbonaceous material, and solid bases often produced from the ash content of biochars with high calcium contents. The potential applications of biochars in catalysis have not yet been fully explored.

Sustainable reaction routes

The catalytic potential of carbon has been demonstrated in a range of reactions. However, carbon has not yet been extensively studied for catalytic activity in CO₂ utilisation reactions. An overview of two CO₂ utilisation reactions was given: methanol conversion and glycerol upgrading. Methanol conversion can be used as a probe reaction, with products being highly sensitive to the nature of the active sites present. The production of dimethoxymethane is thought to require weak acidic sites and oxidative sites, both of which should be present in carbonaceous samples. Dimethyl carbonate could also be produced if strong basic sites are present for the activation of methanol and CO₂. In the case of glycerol upgrading, waste boiler ash has been shown to be effective as a catalyst, with activity attributed to the potassium silicate content. Therefore, biochar ash may also be effective in the conversion of glycerol to glycerol carbonate. This new class of carbon-based catalysts may open up new reaction pathways utilising more sustainable raw materials instead of fossil fuels. Consideration should be given to the role not only of carbon structure, but also of the ash content, including the influence of acidic silica content and heteroatoms.

Enhanced catalyst performance

The influence of carbon in catalysis is not only as a support or catalyst material. Carbon deposits formed during reaction can lead to the deactivation of heterogeneous catalysts, however coke can also be beneficial. Pre-coking can be used to improve the selectivity, through improving shape selectivity and selective poisoning of non-selective sites. A wide range of reactions can also be catalysed by carbon deposits, such as dehydrogenation, hydrogenation, ammoxidation, hydrocarbon transfer and hydrogen transfer reactions. Coke may be active in many more reactions, particularly where activity is observed despite high quantities of coke and loss of surface area.

Chapter 2 – Literature Review

The structure of the coke formed is highly variable, and is dependent on the reactant or product from which it formed, the type of active site present, and the reaction conditions. Notably, higher temperatures and pressures lead to increasingly graphitic coke. Increasingly graphitic and paramagnetic coke is thought to be particularly effective in ammoxidation and oxidative dehydrogenation reactions, where it is believed to act as the active site.

Active carbon may not always be metal-free. Metal atoms from the reactor wall may be incorporated in coke deposits, whilst the catalytic activity in graphitic and nanostructured carbon may be attributed activity to trace quantities of metal remaining from the preparation methods used. The potential contribution from trace metal and reactor walls should not be neglected. The deliberate formation of catalytically active coke could be used to enhance activity or selectivity, and therefore the sustainability of the process.

2.6.2. Challenges and Perspectives

One of the key challenges in studying carbon, particularly from biomass, is reproducibility. Commercial activated charcoals and biochars are usually produced for the purpose of soil remediation, and so reproducibility in catalytic applications is not considered. Properties such as porosity and distribution of elements at the surface of the material can have a great impact on the catalytic activity of a sample.

The literature review has also highlighted similarities in approach between the study of carbon deposits and the study of biochar. In both cases, higher temperatures are known to lead to more graphitic structures. Similarly, depending on the feedstock, biomass with lower hydrogen content leads to more graphitic biochars being formed (Titirici *et al.* 2015). It is possible that factors affecting the graphiticity of biochars will also influence the graphiticity of carbon deposits, and therefore potential catalytic activity. This comparison has not previously been made in the literature.

Addressing these challenges may require further development of characterisation techniques, which have been identified as a limiting factor in many coking studies. A wide range of techniques should be applied, as no one technique can fully characterise a sample. Combined

techniques are continually being developed, however these entail a compromise between the quality of data sets and the benefits of a combined data set. Standardisation of characterisation techniques, particularly for biochar in catalytic applications, would facilitate comparisons between different studies; round robin studies have shown inter-laboratory reproducibility to be poor for standard biochars. In Raman and XPS analysis of carbon samples in particular, there was little similarity in curve deconvolution methods used between studies, making comparisons of results difficult.

At present, catalytic studies often focus on optimising a chosen biochar for a particular process, without justifying the choice of biochar. By contrast, in soil remediation studies, biochars are selected from a range of feedstocks for their suitability. This approach better reflects industrial attitudes to catalyst design, however further insights are needed into the properties of biochar which affect catalytic activity in order to adopt this approach. In particular, the influence of carbon structure is not always considered in the literature for catalytic applications.

Additional factors which are often overlooked in the study of biochar catalysts are practical considerations, such as the long-term durability and mechanical strength of the catalysts. Particle attrition for example can be a problem in stirred tank reactors, due to agitation. In addition, chemical activations and surface treatments used in the literature are not always sustainable at larger scales; any sustainability advantages from the improved catalyst may be cancelled out by the volume of waste chemicals produced. The goal of tailor-made catalysts for desired applications can only be realised if the resulting catalysts are cost-effective.

Chapter 2 – Literature Review

2.6.3. Aims and Objectives

This literature review has highlighted a number of ways in which the further study of carbonaceous materials could improve sustainability in heterogeneous catalysis. The objectives of the present work are therefore:

1. To improve understanding of the utilisation of biochar as catalysts, adopting an application-centred approach. This requires a comprehensive characterisation of biochars from a number of feedstocks, and investigating the factors which influence their catalytic activity. This characterisation will include consideration of factors which are often overlooked, such as the role of trace metal content and carbon structure. Surface treatments will be used to study the influence of individual factors.
2. To investigate the potential of biochar as a catalyst for CO₂ utilisation reactions. Biochars are clearly highly versatile carbonaceous materials, which are an area of growing research interest. CO₂ utilisation reactions could increase the economic viability of carbon capture technologies, and decrease dependence on fossil resources; new catalysts are required to make these reactions economically feasible.
3. To apply the insights from these studies to the phenomenon of catalytically active carbon deposits and design of carbonaceous catalysts. Understanding factors which contribute to catalytically active carbon could enhance the design of carbonaceous catalysts, and allow coking of heterogeneous catalysts to be exploited industrially.

These aims and objectives are centred on improving the sustainability of heterogeneous catalysis. It is worth emphasising that the objective of this work is not to design an optimised carbonaceous catalyst for CO₂ utilisation, but to understand the underlying properties of carbonaceous materials which influence catalytic activity. Surface treatments are not carried out with the objective of improving catalyst performance, but to gain insights for the future design of carbonaceous catalysts.

The following chapter will outline the experimental methods that will be used to achieve these objectives.

Chapter 3 – Experimental Methods

This chapter will outline the background theory and rationale for the chosen experimental methods. The materials used in the work will first be described in section 3.1. Section 3.2 then presents the rationale for the various surface treatments that will be applied to the catalysts, including development of the protocols for the surface treatments. In sections 3.3 to 3.5, the characterisation techniques applied to the catalysts are then outlined, which will enable the chemical and physical structure and composition of the biochars to be determined. These include vibrational spectroscopy techniques, XPS, SEM/EDX and adsorption studies. The choice of reaction conditions and liquid phase product analysis techniques are then outlined in section 3.6. The experimental work is then summarised in section 3.7, outlining the structure of Chapters 4-7, where the detailed experimental protocols will be given.

3.1 Catalyst preparation

In the present work, untreated and treated biochars were used as catalysts in two sustainable reactions. The source of the biochar and the chemicals used in these processes are outlined in section 3.1.1. The preparation of powdered biochar is described in section 3.1.2, and the method for preparation of ash samples is justified in section 3.1.3.

3.1.1 Materials

Throughout this project, biochar was sourced from the UK Biochar Research Centre at the University of Edinburgh. The biochar was produced from different feedstocks and at different pyrolysis temperatures in a standardised and reproducible process in a Stage III unit, described elsewhere (Buss *et al.* 2016). The use of standard biochars should enable the results of the studies to be verified in other laboratories.

The biochars used are summarised in Table 3-1. The biochars chosen were generally pyrolysed at 550 °C, as the most significant changes in surface area and carbon content occur between 350-550 °C (Zhao *et al.* 2013). This is a common temperature for biochar pyrolysis in the literature. Four feedstocks were chosen, which were known to exhibit varying compositions and surface areas, following characterisation by the University of Edinburgh (UK Biochar Research Centre 2014). The feedstocks chosen were rice husk biochar, wheat straw biochar, oil seed rape biochar and soft wood biochar. The diverse properties made these biochars an ideal starting point for studying influences on catalytic activity in carbonaceous materials.

Table 3-1 Standard biochars from UK Biochar Research Centre used in this study.

Feedstock	Pyrolysis temperature(s)/°C	Abbreviation
Rice husk	550 & 700	RHB-550 & RHB-700
Wheat straw pellets	550	WSB-550
Oil seed rape	550 & 700	OSB-550, OSB-700
Soft wood	550	SWB-550

The properties of the biochars were compared with a commercial activated charcoal, sourced from Sigma-Aldrich. Other chemicals used during this study are summarised in Table 3-2, and are referred to in the text for the relevant section.

Table 3-2 Chemicals used during the project, with details of concentrations and supplier.

Application of chemical	Grade	Supplier
Characterisation		
Activated charcoal Norit®, from peat (AC)	Steam activated and acid washed, powder	Sigma-Aldrich
Nitrogen gas (for BET)	>99 % purity	BOC
Carbon dioxide gas (for CO ₂ adsorption)	99.99 % purity	BOC
Surface treatments		
Hydrochloric acid (HCl)	37 % concentrate	Sigma-Aldrich
Silver nitrate (AgNO ₃) solution	0.1 M concentration	Sigma-Aldrich
Acetone	>99 % purity	Alfa Aesar
Glycerol upgrading reaction		
Glycerol	>99.0 % purity	Sigma-Aldrich
Glycerol carbonate (4-hydroxymethyl-1,3-dioxolan-2-one)	90 % purity	Acros Organics
Glycerol diacetate	50 % (Technical grade)	Sigma-Aldrich
Glycerol triacetate	99 % purity	Alfa Aesar
Ethanol	>99.0 % purity (HPLC grade)	Fisher Scientific
1-hexanol	98 % (GC grade)	Sigma-Aldrich
acetonitrile	>99.5 % purity	Sigma-Aldrich
Methanol conversion reaction		
Methanol	>99.8 % purity	Sigma-Aldrich
Dimethoxymethane	99 % purity	Sigma-Aldrich
Ethanol	>99.0 % purity (HPLC grade)	Fisher Scientific
Helium gas	99.999 % (CP Grade)	BOC
Other		
Silicone oil	For oil baths Usable range -40 to 200 °C Viscosity 45-55 mm ² s ⁻¹ @ 25 °C	Alfa Aesar

3.1.2 Biochar preparation

Particle size is a key consideration in the preparation of catalyst materials. Larger particle sizes can lead to diffusional limitations, with smaller particle sizes generally possessing larger

Chapter 3 – Methods

surface areas. It is therefore important to standardise the particle sizes used in catalysis studies.

The biochar was supplied in the form of pellets by the UK Biochar Research Centre. These were ground down using a pestle and mortar, and then sieved to particle sizes of less than 90 μm in diameter. By eliminating all particle sizes greater than 100 μm , large particles were no longer present in the experiments. Large particles (*e.g.* with diameters $> 1\text{ mm}$) which could skew the results by having very different properties and surface areas, and could lead to diffusional limitations in catalytic studies (Bachmann *et al.* 2016). The size of biochar pellets also varied between feedstocks, therefore sieving was required to allow comparisons between the biochars. However, particles below 10 μm could be a health and safety risk, causing damage to the lungs (Brown *et al.* 2013). 90 μm was chosen to standardise the particles so that they were the same or similar order of magnitude. All particle sizes less than 90 μm were used, to avoid rejecting material that could be catalytically active.

Biochars were first tested for catalytic activity without pre-treatment, activation, or metal loading. The effect of selected surface treatments on activity was then studied; these surface treatments are discussed in section 3.2.

3.1.3 Biochar ash sample preparation

The potential catalytic role of biochar ash content was studied through the preparation of biochar ash samples. These were prepared through the combustion of biochar in a furnace. The combustion of biochar was carried out at 900 $^{\circ}\text{C}$, consistent with the upper temperature used to evaluate ash content through TGA analysis (see section 3.4.3). However, extended burning can lead to the formation of crystalline silica; this has been observed to form at temperatures between 800-1150 $^{\circ}\text{C}$ (Chandrasekhar *et al.* 2003). Combustion time at 900 $^{\circ}\text{C}$ was therefore limited to 30 mins, to retain the original amorphous form of the silica present in the biochar ash.

3.2 Surface treatments

Various surface treatments were used to test the effect of certain factors on the catalytic activity of biochar. These treatments did not necessarily aim to improve the performance of the biochar catalyst, but to identify whether the treatment led to an improvement or reduction in activity and why. Alongside thorough characterisation, this provided insights into the factors affecting catalytic activity in biochar and other carbonaceous materials.

As discussed in section 2.3, the influence of ash content and carbon structure is of particular interest. The role of ash content was tested by developing demineralisation methods; the rationale for the proposed protocol is outlined in section 3.2.1. Sections 3.2.2-3.2.4 then outline the development of a procedure for the tar impregnation and pyrolysis of biochar, in order to test the influence of biochar properties on the structure of carbon deposits formed.

3.2.1 Demineralisation with HCl

Demineralisation using acid is commonly used in the literature to remove trace metal and ash content from biochar samples (Buczek *et al.* 1999; Liu *et al.* 2011; Santiago *et al.* 2005; Rivera-Utrilla & Sánchez-Polo 2002). The use of acid can however also lead to pore damage, meaning the influence of demineralisation must be decoupled from the influence of the pore structure, and functionalisation of the catalyst. Therefore, the ideal demineralisation method would cause minimal distortion of the pore structure and surface chemistry.

Various acids have been applied as demineralising agents in the literature. One study compared the effect of HF, HCl and HNO₃ on the pore structure and surface chemistry of a low-ash (< 0.1 wt%) activated carbon derived from olive stones. Of the acids tested, HF increased the quantity of C-O groups, and HNO₃ led to the destruction of pore walls. HCl caused only a slight decrease in microporosity, due to the adsorption of chloride ions in the pores (Moreno-Castilla, Carrasco-Marín, Maldonado-Hódar, *et al.* 1997). These excess chloride ions can be easily removed through washing with distilled water (Jensen *et al.* 1998; Jenkins *et al.* 1996). HCl will therefore be used as a demineralising agent in this work.

Chapter 3 – Methods

The protocol for demineralisation using HCl was developed based on the literature (Moreno-Castilla, Carrasco-Marín, Maldonado-Hódar, *et al.* 1997; Nowakowski & Jones 2008; Morgan *et al.* 1981; Raveendran *et al.* 1995). The concentration of acid used in the literature varied from 1-5 M, with washing times of 1 to 48. The acid temperature during demineralisation was generally 60 °C. Washing protocols varied; studies by Jensen and Jenkins indicated that the most effective removal of Cl⁻ ions is achieved through refluxing with distilled water for 1-2 hours, followed by further washing with distilled water (Jensen *et al.* 1998; Jenkins *et al.* 1996). In all cases, samples were washed until Cl⁻ was no longer detected in the washing water using silver nitrate (AgNO₃). The samples were then dried, either in vacuum desiccators at room temperature or in an oven until constant weight.

The protocol used in this work was therefore based on the methods above: washing with concentrated HCl for 36 hours, followed by washing with hot distilled water for 2 hours. Further washing with distilled water was then performed, using 0.1 M AgNO₃ to test for the presence of Cl⁻ in the washing water. The exact protocol is outlined in section 5.2.3.1.

3.2.2 Tar impregnation

A further surface treatment aimed to produce carbon deposits on biochar from tar. Tar reforming is widely studied in the literature, using biochar as a catalyst – this was discussed in section 2.3.2. Studies in the literature generally performed tar pyrolysis using gas-phase naphthalene or other model tar compounds as feedstocks. However, this apparatus was not available for the present work. A liquid phase method of tar impregnation was therefore required, to enable the tar to be pyrolysed in the Stage I pyrolysis unit (see section 3.2.4).

For the tar impregnation and pyrolysis study, commercial pine tar was sourced from Auson (Genuine Pine Tar 850). The composition of the pine tar is complex and includes oxidised acids, esters and fatty alcohols (Auson 2015). This is a biomass-derived tar, and therefore more relevant than the aromatic model tar compounds generally studied (Abu El-Rub *et al.* 2008). In addition, the lack of aromatic molecules in pine tar means that any increases in the graphiticity of biochars can be attributed to changes in the structure of the commercial pine tar, rather than the simple deposit of aromatic molecules. Due to the highly viscous nature of

the tar, the tar was diluted with acetone and contacted with the biochars for 96 hours. This was to allow sufficient time for the viscous tar to impregnate the biochar pores. As no previous methods had been found, the minimum time required was unknown. The protocol for tar impregnation is outlined in further detail in section 5.2.3.3.

3.2.3 Acetone washing

It was found that the acetone used to thin the tar affected the composition of the biochar, and thus the accuracy of the tar loading calculations. This is discussed in section 5.3.2. Therefore, acetone control tests were developed in order to quantify the tar loadings. In addition, the effect of acetone and solvents on carbon composition and surface chemistry had not previously been studied explicitly in the literature. The results were therefore of broader interest in terms of understanding the changes in surface chemistry when carbonaceous catalysts are used *in situ*, for example reactions involving organic and oxygenated substances.

The control test was developed using RHB as the test sample, as this had the highest ash content, making any changes due to acetone easier to detect. 20 g of RHB was washed in a sealed beaker containing 200 ml acetone for 12 hours, 24 hours and 48 hours. A magnetic stirrer was used to ensure the biochar was well mixed with the acetone. Different drying methods were used to determine the most effective method for drying the samples after acetone washing. Samples were dried and tested in the following sequence:

- Drying in air – acetone evaporated on filter paper in the fume cupboard for 24 hours at room temperature. 20 mg removed for immediate TGA proximate analysis.
- Transferred to oven at 110 °C, dried for 3 hours. Another 20 mg removed for immediate TGA proximate analysis.
- Drying in oven at 110 °C for 2-3 days, followed by TGA analysis of a 20 mg sample.

The proximate analysis results were compared with those before acetone washing. This allowed the effect of acetone washing on biochar composition to be investigated. The results from these preliminary method development experiments are given in Appendix B . The drying method chosen for future samples was drying in an oven at 110 °C for 72 hours.

Chapter 3 – Methods

3.2.4 Stage I Pyrolysis Unit

The pyrolysis of tar-impregnated biochars was carried out in a Stage I Pyrolysis Unit at the University of Edinburgh. The unit has been described in detail in the literature (Crombie *et al.* 2013), however a summary of the apparatus is outlined here.

The Stage I pyrolysis unit consists of a quartz sample tube in a furnace, with a series of condensers and cold traps to collect condensable tars produced during pyrolysis. This is shown in the schematic in Figure 3-1. The sample tube had an inner diameter of 50 mm and sample bed depth of 200 mm. Approximately 15-20 g of tar-impregnated biochar was added to the sample tube for each experiment. The temperature and the heating rate of the apparatus can be controlled using the thermocouple. The mass of each component was weighed before and after pyrolysis, allowing the mass of biochar lost and tar produced to be calculated. Compositional analysis of the tars and gases was not carried out as part of the present work.

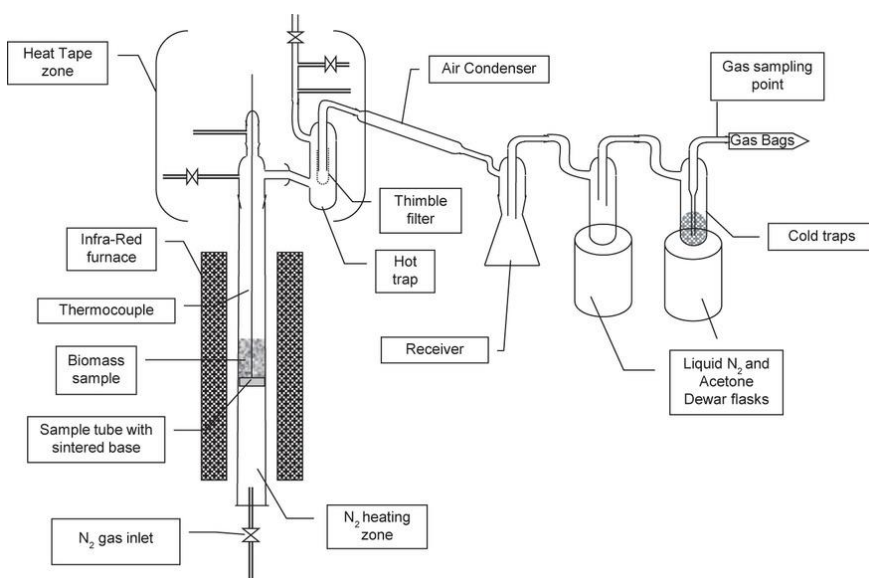


Figure 3-1 Schematic of the Stage I Pyrolysis Unit, UK Biochar Research Centre, University of Edinburgh. Figure reproduced with permission from John Wiley and Sons (Crombie *et al.* 2013).

The heating rate for pyrolysis was set at $10\text{ }^{\circ}\text{C min}^{-1}$, with a pyrolysis temperature of $550\text{ }^{\circ}\text{C}$, consistent with the method used for preparing the biochar feedstocks at UKBRC. The resulting biochars were then characterised by the methods outlined in sections 3.3-3.5, and tested for catalytic activity following the methods outlined in section 3.6.

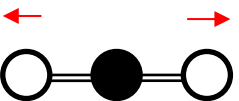
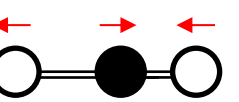

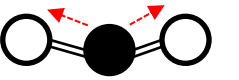
3.3 Vibrational spectroscopy

Vibrational spectroscopy techniques were applied in the characterisation of biochars. These techniques provide insights into the chemical structure of the biochars, for example through the absorption of IR radiation at frequencies corresponding to the vibrational bands of particular functional groups. The advantages of FTIR spectroscopy are outlined in section 3.3.1, and the use of Raman spectroscopy is justified in section 3.3.2.

3.3.1 Fourier Transform Infrared (FTIR) Spectroscopy

FTIR is a technique which characterises the functional groups present at the surface of a sample by measuring the absorption of infra-red radiation by these moieties. The vibrations of functional groups will be IR active if the vibration produces a change in the dipole moment of the group (Williams & Fleming 2008). An example for CO₂ is given in Table 3-3.

Table 3-3 Vibrational modes of CO₂.

Configuration	Vibration mode	IR active?
	symmetric C-O stretch	X
	asymmetric C-O stretch	✓
	y-axis bend	✓
	z-axis bend	✓

A number of different methods can be used to obtain the FTIR spectrum of a sample. In transmission FTIR, the infrared radiation passes through the IR sample, whilst Diffuse Reflectance IR Spectroscopy (DRIFTS) can be used for bulk analysis. In catalytic studies, Attenuated Total Reflectance (ATR) accessories are advantageous as the data collected are

Chapter 3 – Methods

surface sensitive, with minimal sample preparation required (ThermoFisher Scientific 2013). A schematic of an ATR is given in Figure 3-2.

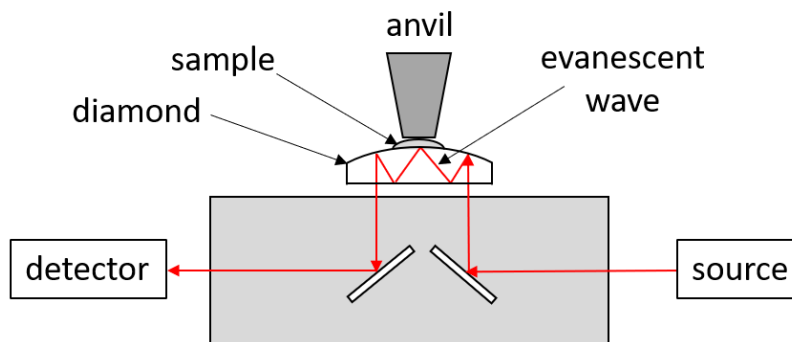


Figure 3-2 Schematic of operating principle of FTIR-ATR.

In ATR, the sample is loaded on an optically dense crystal, for example made from diamond, selenium or germanium, with a high refractive index. The IR beam is directed by a series of mirrors towards the crystal at an angle exceeding the critical angle for internal reflectance. This results in the formation of an evanescent wave which propagates beyond the surface of the crystal and into the sample. In ATR, the distortion of this evanescent wave by the sample is detected, with the signal used to produce an IR spectrum (ThermoFisher Scientific 2013). Due to the rapid degradation of the wave outside the crystal, the wave only penetrates approximately 2 μm into the sample, resulting in a surface-sensitive technique (Scherzer 2002). In this work, diamond is chosen due to its wide spectral range and chemical inertness.

3.3.2 Raman Spectroscopy

Raman spectroscopy is a type of vibrational spectroscopy. When light interacts with a sample, it is usually reflected, transmitted or scattered. The phenomenon of Raman scattering leads to the light being scattered at a different wavelength to the incident radiation, and only occurs for one in every 10^6 photons interacting with a sample. The technique is therefore less sensitive than IR. However, the Raman effect is dependent on the polarizability of the sample, and is therefore particularly useful in the study of graphitic structures, due to the high density of polarisable delocalised electrons.

Fluorescence can pose a major problem in Raman spectroscopy. If the energy of the photons from the laser is sufficiently high, the electrons in the sample atoms could be excited to higher energies, before releasing a photon as they relax. This fluorescence can easily obscure the Raman peaks. Common solutions are to use a lower laser intensity, or to change the laser wavelength. A higher wavelength (such as 325 nm for UV) increases the energy of the photons, but can also move the fluorescence to a different region of the spectrum. A lower wavelength (such as 785 nm for IR) uses lower energy photons, which can either reduce the intensity of fluorescence or prevent the possibility of fluorescence altogether. In the present work, a 514 nm green laser was used, with a low power of 0.2 mW (1 % intensity) to limit fluorescence issues.

Interpretation of Raman spectra for carbonaceous samples can be facilitated through curve deconvolution, as discussed in section 2.5.1. There is little consistency between curve deconvolution methods in the literature, and so the procedure used in this work was developed based on the experimental results obtained. The methods and justification for the curve deconvolution process are therefore detailed in Chapter 4.

Chapter 3 – Methods

3.4 Composition

As described in section 2.3, the composition of biochars can vary depending on the feedstock and pyrolysis conditions used. This is likely to influence the catalytic activity of the biochars. Characterisation of composition is also required to evaluate the effectiveness of surface treatments such as demineralisation, which aim to reduce the ash content of the biochars. XPS was used to quantify the elemental composition at the surface of the biochar, and is outlined in section 3.4.1. SEM/EDX images were also obtained, allowing the structure and composition of the biochars to be visualised; this is described in section 3.4.2. Proximate analysis by TGA was also carried out to quantify the volatile, moisture, ash and fixed carbon content of the samples, and is outlined in section 3.4.3.

3.4.1 XPS

X-ray photoelectron spectroscopy (XPS) analysis of selected biochar and ash samples was carried out in order to quantify the elemental composition of the samples, and to investigate the properties of the carbon species present. In this study, the elemental composition of the ash before and after demineralisation with HCl was of particular interest. High resolution C 1s scans also provided data on the electronic environment of the carbon in the biochars, for example oxygen-containing functional groups and graphitic character.

In XPS, X-rays are fired at the surface of the sample, causing the excitation and ejection of electrons. The energy of these electrons is detected and plotted as a spectrum of electron energy versus intensity. Electrons from deeper within the sample (>10 nm) are less likely to leave the surface without losing energy, resulting in a highly surface-sensitive technique. The energy of the electrons is the energy of the X-ray photon, minus the binding energy required to eject the electron from the sample. This is illustrated in Figure 3-3. The binding energy of the electron is characteristic of the electronic state of the atom, and is therefore characteristic of the element from which it was ejected. This enables the composition of the surface of a sample to be quantitatively studied through XPS.

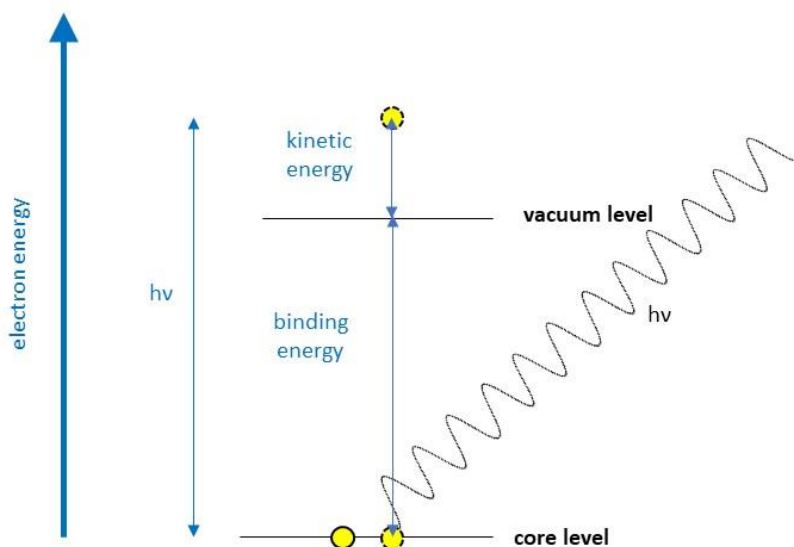


Figure 3-3 Schematic of interaction of incident x-ray (energy $h\nu$) with core level electrons.

The ejection of electrons can lead to the formation of a charged surface, leading to altered electron energies. Charge correction is normally achieved by placing non-conducting samples on conducting surfaces, allowing electrons to be replaced, and calibrating the data by the known position of a peak, often the adventitious carbon peak as discussed in section 2.5.2. The areas of the peaks are calibrated using relative sensitivity factors (RSF), which scale the intensity of a peak to the atomic concentration. The RSF is given relative to the carbon C1 s peak; for example, electrons are less easily removed from O 1s and N 1s, and therefore these elements have higher RSF values of 2.93 and 1.8 respectively. These values have been calibrated using a transmission function, which is characteristic of the instrument used, and are determined using software from NPL (National Physical Laboratory 2012). More detail on RSFs can be found in the literature (Scofield 1976).

3.4.2 Scanning Electron Microscopy (SEM/EDX)

Scanning electron microscopy (SEM) was used to study the physical appearance and macrostructure of the biochar samples. SEM utilises the wave properties of electrons to produce high magnification and resolution images, and has a number of advantages in this study over other imaging techniques. Compared to optical microscopy, SEM can achieve much higher magnifications and resolutions, up to 200 Å (Simon 1969). The depth of focus also enables sharp images to be obtained, even for specimens with large variations in depth.

Chapter 3 – Methods

In SEM, electrons are emitted by a thermionic, Schottky or field emission cathode, and are accelerated through a voltage difference in the range 0.1 to 50 keV. These electrons pass through a two- to three-stage electron lens to produce a probe of diameter 1-10 nm, with a current of 10^{-9} to 10^{-12} A (Reimer 1998). This electron probe can interact with the sample in numerous ways, with each type of interaction providing different information about the material. The electron beam may for example lead to elastic or inelastic scattering, and the emission of further electrons, which can be detected and analysed to produce an image.

The interaction of the electrons with atoms in the sample may cause the ionisation of an inner shell of an atom. When an electron from a higher shell cascades down to fill the vacancy, energy may be emitted as an X-ray with energy equal to the difference between the two energy levels, and is therefore characteristic of the element. This phenomenon is the basis of energy dispersive X-ray spectrometry (EDX or EDS), and can be exploited to provide information on the elemental composition of the sample. The X-rays originate from within a few micrometres of the sample surface, making the technique less surface sensitive than XPS. Further theoretical detail on the principles of SEM/EDX can be found in the literature (Reimer 1998).

3.4.3 Thermogravimetric Analysis (TGA)

TGA is widely used for the proximate analysis of carbonaceous samples, *i.e.* the quantification of moisture, volatile, fixed carbon and ash content. The basic principle is to measure changes in mass as a function of time and temperature. By setting a temperature programme, any changes in composition as a function of temperature can be measured. For the proximate analysis of carbonaceous samples, standards have been developed by ASTM International (ASTM International 2010), which form the basis of most methods seen in the literature. For example, moisture content is evaluated by heating at 107 ± 3 °C for 1 hour, or until constant mass has been achieved.

TGA can also be applied for the study of pyrolysis, by heating a small quantity of sample in a nitrogen atmosphere at a desired temperature with a specified heating rate (Nowakowski & Jones 2008). This was used in the present work to compare the results of Stage I pyrolysis with simulated TGA pyrolysis of tar-impregnated biochar samples.

3.5 Adsorption isotherms

Adsorption is a key process in catalysis, as can be seen in Figure 1-2. As such, the study of the adsorption properties of biochar is an important aspect of their characterisation in studies of their catalytic properties. CO₂ adsorption studies at ambient temperature were conducted in an Intelligent Gravimetric Analyser (IGA-003 Dynamic Analyser supplied by Hiden Isochema) and are discussed in section 3.5.2 below. BET adsorption using nitrogen at 77 K was carried out to determine the surface area of the biochars – this is discussed in section 3.5.1.

3.5.1 BET adsorption isotherms

Biochars are known to exhibit a range of surface areas, from 1 to 500 m² g⁻¹, and surface area is known to be influenced by feedstock and pyrolysis temperature (Zhao *et al.* 2013; Jindo *et al.* 2014). Surface area is a key parameter in catalytic studies, with high surface areas often correlating with higher activities, due to increased access to active sites for catalysis and increased adsorption capacity of reactants. The BET isotherm method is commonly used to obtain surface area data for catalyst samples. The BET surface area and porosity of biochars from different feedstocks and pyrolysis temperatures was therefore quantified, to allow the activity of the biochars in catalytic reactions to be compared.

The BET isotherm assumes multilayer adsorption of gases, and that molecules only interact with adjacent layers (Brunauer *et al.* 1938). Nitrogen is most commonly used, as an inert gas which is unlikely to chemically react with the surface, and BET isotherms are therefore collected at the boiling point of nitrogen, 77 K. This allows the maximum N₂ adsorption capacity of the material to be calculated – at higher temperatures, the N₂ gas molecules may have sufficient kinetic energy to desorb.

The quantity of gas adsorbed on the surface of a sample can be measured at a known temperature and plotted against pressure. The linear region of this graph is assumed to correspond to the formation of a monolayer of nitrogen. The number of atoms or molecules adsorbed in this monolayer can then be calculated, and by knowing the surface area of a nitrogen atom, the surface area of the sample can be estimated (Brunauer *et al.* 1938).

Chapter 3 – Methods

In catalytic applications, micro- and mesoporosity also play key roles, for example by influencing shape selectivity. A range of analysis techniques and models have been developed for the evaluation of porosity from nitrogen adsorption data; further details can be found in the literature (Seaton *et al.* 1989). In this work, two methods developed for the evaluation of porosity in carbonaceous samples are applied, and are outlined briefly below.

There is some debate about how meaningful the BET data obtained for micro- and ultraporous samples are, for example due to the relative size of N₂ and argon atoms compared to the pores, and the possibility of multilayer adsorption in pores. The applicability of BET for the study of microporous materials has been studied in the literature, by comparing theoretical grand canonical Monte Carlo data for perfect Zn₄O Metal Organic Frameworks and zeolites with BET data. The results confirmed that the BET data obtained were a good match for the theoretical values of surface area in microporous materials (Bae *et al.* 2010).

The Harkins-Jura t-plot was developed by studying adsorption behaviours over 200 porous and non-porous samples, including charcoals and carbon blacks (Harkins & Jura 1944). This can be applied to adsorption isotherm data in order to calculate the total micropore volume of a sample.

The non-linear density functional theory (NLDFT) model was developed by Micromeritics for evaluating the pore size distribution of porous carbons from adsorption isotherms (Jagiello & Olivier 2009). Previous models assumed that one-dimensional pores extended infinitely in one dimension. The carbon slit pore model modified this assumption to allow for two-dimensional pores, with heterogeneity in adsorption potential along the pores, and was found to give a better fit with experimental data. This model has since been used in the literature for the analysis of various carbon materials, including activated carbons, carbon xerogel spheres and carbons derived from pyrolysis (Acosta *et al.* 2016; Menéndez *et al.* 2012; Ondarts *et al.* 2018; Hassan & Imran 2018). It should be noted that the drawbacks of the NLDFT model are still being debated in the literature, such as the way non-ideality caused by intermolecular interactions is modelled (G. Wang *et al.* 2018). The NLDFT and t-plot models were applied to

the experimental data collected in this work using Micromeritics 3Flex software. The method used for collecting BET adsorption isotherm data in this work is detailed in section 4.2.1.

3.5.2 Carbon Dioxide adsorption isotherms

CO₂ adsorption isotherms can be used to characterise the CO₂ adsorption capacity of a material. In this work, the objective was to compare the CO₂ adsorption capacity of the biochars with their specific surface area as measured by BET. This would assist in the interpretation of the results of CO₂ utilisation reactions. Whilst much literature exists on the adsorption of CO₂ on carbonaceous materials, particularly for extraction of CO₂ from syngas using activated carbons (Yin *et al.* 2013), a detailed CO₂ adsorption study with isotherm modelling is beyond the scope of the present work. Analysis methods can be found in the literature for the modelling of CO₂ adsorption isotherms on carbonaceous materials, such as the Dubinin-Radushkevich isotherm (Dubinin 1960).

Methods for obtaining CO₂ adsorption isotherms in the literature vary, with temperatures ranging from 0 °C (Moreno-Castilla, Carrasco-Marín, Maldonado-Hódar, *et al.* 1997) to 25 °C (Lithoxoos *et al.* 2010). The study of CO or CO₂ TPD is more common in catalysis (Marchon *et al.* 1988; Zhang *et al.* 2007). A systematic study of the influences on CO₂ adsorption on coals was performed in the literature, with isotherms obtained from 0-20 °C, comparing the effects on biomass-derived and natural coals (Yin *et al.* 2013). The pressure range appears to depend on the region of interest, and the pressure limits of the equipment. Lithoxoos and co-workers studied CO₂ adsorption from 0.01-20 bar, whilst Yin and co-workers studied the region 0.1-1.0 bar.

In this work, the methods were based on those of Lithoxoos on single-walled carbon nanotubes, to allow the results to be compared with literature values across a large range of pressures (Lithoxoos *et al.* 2010). The isotherms were therefore obtained at 25 °C, from 0.004-10.0 bar (the lower and upper pressure limits of the equipment). Detailed methods can be found in section 4.2.2.

Chapter 3 – Methods

3.6 Reaction studies

Two reactions were chosen for testing how the catalytic activity of biochars is affected by variations in composition and structure. These reactions were the conversion of methanol to products in CO₂, and the upgrading of glycerol with CO₂ to glycerol carbonate. The reaction conditions were chosen in consultation with the literature, and are outlined in sections 3.6.1 and 3.6.2. The batch reactor used for catalytic studies is described in section 3.6.3, and the method of preparing liquid phase product samples for analysis is presented in section 3.6.4. The analysis was then carried out by GCMS, the application of which outlined in section 3.6.5.

3.6.1 Methanol conversion

Methanol oxidation can be used as a probe reaction, as the products are highly sensitive to the nature of the active sites present. Possible products include formaldehyde, methyl formate, dimethoxymethane and dimethyl ether, depending on the acidity and availability of redox sites on the catalyst (Thavornprasert *et al.* 2016; Tatibouët 1997).

Dimethoxymethane (DMM) is of particular interest, with applications in the paint, perfume and pharmaceutical industries, as well as a fuel additive (Thavornprasert *et al.* 2016). The formation of DMM is a two-step process, with formaldehyde as an intermediate; the one-step selective synthesis of DMM is therefore a challenge attracting increasing research interest. The use of CO₂ as an oxidising agent could also lead to the production of dimethyl carbonate (DMC), which as discussed in the literature review has attracted research interest as a green solvent and reagent (Bhanage *et al.* 2001; Tamboli *et al.* 2017).

The reaction methods used in this study are adapted from methods in the literature. Several studies utilise continuous fixed-bed reactors operating at atmospheric pressure (Almusaiteer 2009; Chen & Ma 2017); however, higher pressures will shift the equilibrium in favour of the formation of DMM and DMC. Pressures in the literature range from 1-300 bar for the synthesis of DMC (Sakakura & Kohno 2009). A 45 ml batch reactor was used in the present work, capable of achieving pressures up to 50 bar. Further details on the autoclave used are given in section 3.6.3.

The formation of DMM and DMC is thought to be favoured by lower temperatures; DMM is formed by methanol oxidation, and is therefore an exothermic process. However, there is a compromise between equilibrium yield of product and reaction kinetics. A reaction temperature of 200 °C and reaction time of 18 hours were chosen as a compromise; reaction times in the literature vary between 8-140 hours (Sakakura & Kohno 2009). Temperatures in excess of 200 °C are not recommended in the literature (Tatibouët 1997). The optimisation of the reaction conditions for DMM or DMC synthesis was beyond the scope of the current work.

3.6.2 Glycerol upgrading

The reaction of glycerol with CO₂ to form glycerol carbonate was carried out as an example of a CO₂ utilisation reaction. The potential applications were discussed in section 2.4.2.

The experimental method was adapted based on similar studies found in the literature. The formation of glycerol carbonate is favoured by higher temperatures and lower pressures (Li *et al.* 2013). Typical reaction temperatures for the direct synthesis of glycerol carbonate from glycerol range from 80-180 °C, with pressures from 1-50 bar and reaction times from 1-59 hours (Sonnati *et al.* 2013).

The reaction of glycerol and CO₂ is thermodynamically limited (Li & Wang 2011), and therefore a dehydrating agent was used to increase the yield from the reaction by shifting the position of equilibrium. As discussed in section 2.4.2, acetonitrile has the potential advantage of producing valuable by-products, such as triacetin (Kong *et al.* 2016).

The reaction conditions used here are based on those in the literature for the synthesis of glycerol carbonate using acetonitrile as a dehydrating agent (Li *et al.* 2015). A 45 ml stainless steel reactor was used, which is discussed in further detail in section 3.6.3. 4.6 g of glycerol was used, with 5 ml of acetonitrile, with similar reaction pressures, temperatures and reaction times. Modifications were made in consultation with Nurul Razali, whose PhD thesis focuses on the development of lanthanum catalysts for glycerol upgrading, to allow comparison of results (Razali 2017).

Chapter 3 – Methods

3.6.3 Batch Reactors

Both of the reactions outlined in sections 3.6.1 and 3.6.2 were performed in a 45 ml autoclave as batch processes. The autoclave was supplied by Parr Instruments (Model 4714). A schematic of the reactor is shown in Figure 3-4.

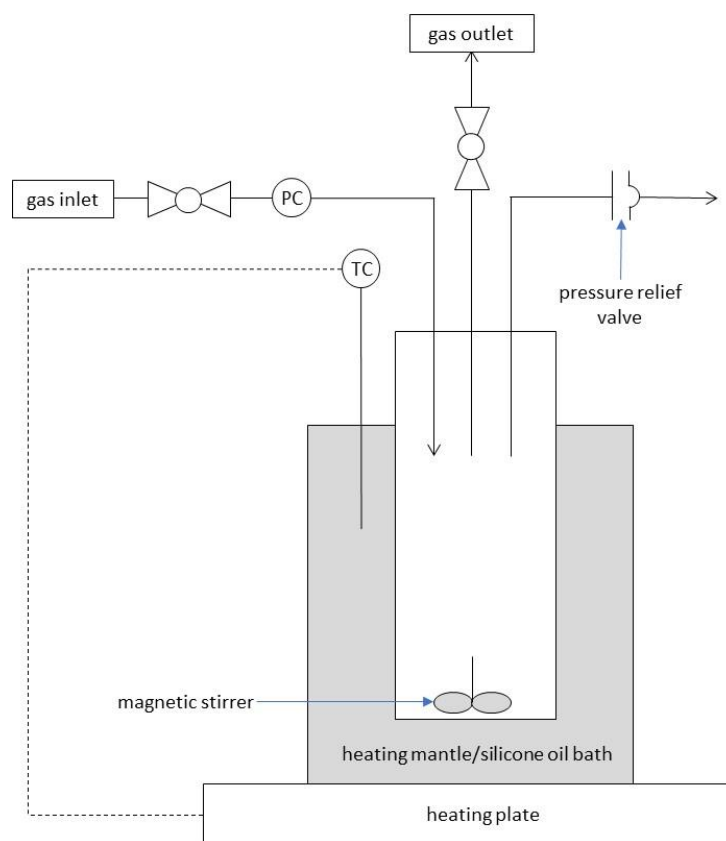


Figure 3-4 Schematic of batch reactor (Parr Instruments) used for reaction studies.

For the glycerol upgrading reaction (Chapter 7), a silicone oil bath was used for heating the reactor, with a thermocouple inserted in the silicone oil for temperature control. For the methanol conversion reaction (Chapter 6), the reactor was heated in an aluminium heating mantle, as the reaction temperature of 200 °C exceeded the upper limit suitable for use of the silicone oil bath. A thermocouple was inserted into the heating mantle.

A magnetic stirring bar was used to stir the contents of the reactor throughout the reaction. The upper pressure limit of the reactor was 100 bar, however the reaction conditions were designed such that the pressure would not exceed 60 bar. Due to the long reaction times, the reactors were often left unsupervised; the pressure relief valve ensured that the reactor did

not reach unsafe pressures. The reactions were carried out in a fume cupboard to ensure any relieved fumes were safely extracted from the laboratory.

In both reactions, the same process was used for purging the reactor of air prior to reaction. This was necessary to remove any oxygen from the reactors. In the case of glycerol upgrading, a standardised CO₂ loading procedure was also required due to the use of acetonitrile as a solvent. CO₂ dissolves in acetonitrile, and therefore it was necessary to ensure that the same quantity of CO₂ was loaded for all reactions. Prior to reaction, the reactors were loaded for 10 seconds with the desired pressure of gas, and then depressurised. This was repeated twice more, before loading the desired pressure of the gas for 30 seconds. This ensured that the reactors were free of oxygen, and loaded with the same quantity of CO₂. The pressure was checked after 15 minutes to ensure that there were no leaks, before heating the reactor to the desired temperature.

The reaction conditions used for each reaction are outlined in the relevant experimental chapter (methanol conversion in Chapter 6, glycerol conversion in Chapter 7). Similar procedures were then used for the preparation of liquid phase samples for GCMS analysis; these are outlined in section 3.6.4.

3.6.4 Liquid phase sample preparation

Following reaction, the reactors were cooled in ice water for 15-30 minutes. The reactor was then depressurised in the fume cupboard, and the liquid phase products were emptied into a glass beaker. In the case of glycerol reactions, the contents of the reactor were mixed with 10 ml of ethanol (Fisher Scientific, >99% purity), to dilute the sample and enable the otherwise highly viscous glycerol mixture to be filtered. Due to the very fine particle size of the biochars, vacuum filtration was insufficient to remove the biochar powder from the liquid phase products. Syringe filtration was therefore used to ensure separation of the finest biochar particles from the liquid phase products (Captiva Premium Syringe Layered Filter, glass microfiber pre-filter, nylon membrane, 15 mm diameter, 0.2 µm pore size). The use of syringe filtration however meant recovery of the catalyst after reaction was not possible.

Chapter 3 – Methods

The filtered liquid phase products were stored in glass vials. Samples were stored in ice water prior to analysis where practical, and GCMS analysis was performed within 12 hours to prevent degradation of the sample. The GCMS analysis methods are considered in section 3.6.5., and the compositions of the liquid phase products analysed by GCMS are presented in the relevant experimental chapters (methanol conversion in Chapter 6, glycerol conversion in Chapter 7).

3.6.5 GCMS analysis

The composition of the liquid phase products was determined by gas chromatography mass spectrometry (GCMS). This technique is able to separate complex mixtures and identify the individual components with a high degree of sensitivity – masses as low as femtograms can now be detected using GCMS (Fialkov *et al.* 2007). The technique is also suitable for use with very small sample sizes, requiring as little as 0.5 μL of sample. This technique is therefore commonly used for the separation and identification of gaseous and liquid phase products from reactions (Annino & Villalobos 1992). The theory behind GCMS is outlined in this section, including justification of the choice of columns for analysis.

The key components of a GC are the injection port, the oven, the GC column and the detector. A small quantity of liquid sample (usually 0.5-5 μL) is injected into the port, where it is vaporised and carried through the stationary phase by the carrier gas, usually an inert gas such as nitrogen or helium (McMaster 2008). Separation then occurs due to the differing affinities of the components with the stationary phase. These interactions between the column and solute could for example be dipole and hydrogen bonding interactions. The separation of the components of the mixture depends on (i) the differing volatilities of the solute (*i.e.* how easily the substance is transported through the column by the mobile phase) and (ii) the difference in the interactions between the solute and stationary phase. More volatile components will be more easily transported through the column in the mobile phase, leading to shorter retention times, whilst solutes with similar polarities to the column will have a stronger affinity and therefore longer retention time in the stationary phase.

In this work, two different columns were chosen for the analysis of products from methanol conversion and glycerol upgrading. The column choice was restricted due to consideration of the requirements of other laboratory users. For glycerol upgrading, an Agilent INNOWax column was used, with a high-polarity polyethylene glycol stationary phase. Due to the incompatibility of the INNOWax column with water, an Agilent DB-1MS column was used for analysing the products of methanol conversion. This was a non-polar column with a dimethylpolysiloxane stationary phase. Further considerations during column selection, such as the role of column internal diameter, length and stationary phase thickness, can be found elsewhere (McMaster 2008). Helium was used as the carrier gas, with a linear flow rate of 30 cm s^{-1} . This is consistent with literature findings that flow rates in the region of $20\text{-}40 \text{ cm s}^{-1}$ are optimal as a compromise between helium efficiency and retention time (Annino & Villalobos 1992).

To identify these separated compounds, gas chromatography is often connected to a detector. These detectors use various physical and chemical properties of the components to identify the solute. Detectors commonly used with GC include Flame Ionisation (FID), Thermal Conductivity (TCD) Electron Capture Detection (ECD) and Mass Spectrometry (MS) (Grob & Barry 2004). Mass spectrometry was used as a detector in this work, as mass spectra would allow the identification of the structure as well as composition of the reaction products, providing key insights into reaction mechanisms. The signal is then plotted against time to give a chromatogram. Calibration is then performed against known concentrations of the component, to convert the peak area to a concentration (Annino & Villalobos 1992).

Mass spectrometry is widely used for the identification of substances. A mass spectrometer operates by ionising the sample and separating the resulting fragments by their mass-to-charge (m/z) ratio. The intensity of each m/z ratio is also recorded, resulting in a mass spectrum, which can be compared with a database to identify the compound. Ionisation is usually achieved by electron ionisation, whereby electrons are fired at a sample to remove electrons from the target molecules, resulting in positively-charged ions (Johnstone & Rose 1996).

Chapter 3 – Methods

Calibration of GCMS data involves running samples of known concentration to calibrate the peak area with the concentration. This should be compared with an internal standard, as this allows variations in the injection volume to be accounted for, and the reliability of the method can be checked. The internal standard should be chemically similar to the compounds of interest, and should be miscible in the solvent, without reacting with any of the components of the mixture. It should also produce a peak in an otherwise clear area of the spectrum. Details of the calibration samples used for each set of reactions are detailed in the relevant experimental chapters (methanol conversion in Chapter 6, glycerol conversion in Chapter 7).

Fresh calibration samples were prepared for each set of reactions, as it is expected that the retention times and sensitivity of the column will vary over time. For column maintenance purposes, the length of the column is slightly decreased each time it is replaced by approximately 5 % (Chromacademy 2018).

A full consideration of the parameters to consider when designing a GCMS method are beyond the scope of the current work; however, key parameters include adjusting the oven temperature, heating rates, holding times and the split ratio (*i.e.* the proportion of the sample injected into the column). The aim of modifying these parameters is to achieve a good separation of the component species, and to avoid distortion of the peak shapes.

3.7 Summary

A range of experimental methods have been developed in order to characterise the properties of biochars and test their catalytic activity. The characterisation will consider the elemental composition, structure, surface chemistry and carbon structure of the biochars. Surface-sensitive techniques will be used to enable the catalytic surface to be characterised.

A wide range of characterisation techniques are available in the literature, and were summarised in section 2.5. Due to limited availability of equipment, some techniques were beyond the scope of the present work. These included temperature-programmed desorption (TPD) studies, which would have provided valuable insights into the surface acidity and basicity of the samples. However, the techniques chosen will include FTIR spectroscopy, deconvolved XPS C1s and Raman spectra, which should provide detailed information regarding the types of functional groups present.

These characterisations will be used to evaluate the effect of various surface treatments. Ash content will be reduced through demineralisation with HCl, following consultation with the literature, and isolated by combustion. Further treatments will include acetone washing, to test the effect of solvent exposure on biochar properties, and tar impregnation and pyrolysis, to test the influence of biochar properties on the structure of carbon deposits formed.

The catalytic activity of the untreated and treated biochars will then be tested in two reactions: methanol conversion and glycerol upgrading. Reaction studies will be performed in batch reactors, enabling elevated reaction pressures and temperatures to be used. The reaction conditions will be broadly comparable with the literature; further optimisation of the reaction conditions is beyond the scope of the current work. The liquid phase products will be analysed by GCMS, allowing the composition to be determined with high accuracy and sensitivity.

The results of the experimental work will now be presented. The results of the characterisation of biochars are presented in Chapter 4, with characterisation of the treated biochars following in Chapter 5. The reaction studies are then presented, with methanol conversion results in Chapter 6 and glycerol upgrading in Chapter 7. The results will be discussed in Chapter 8.

Chapter 4 – Biochar Characterisation

Overview

Biochars have an increasing number of applications, from soil remediation to catalysis. However, the impact of feedstock choice and pyrolysis temperature on catalytic activity is frequently overlooked. In this work, biochars from four feedstocks pyrolysed at 550 °C and 700 °C were extensively characterised: rice husk (RHB-550), oil seed rape (OSB-550 and OSB-700), wheat straw (WSB-550) and soft wood (SWB-550). Their properties were compared with a commercial activated charcoal (AC).

The BET surface areas were lower than for AC (729 m² g⁻¹), with SWB-550 having the highest surface area of 390 m² g⁻¹, and other biochars ranging from 50-120 m² g⁻¹. These values are promising for catalytic applications. TGA proximate analysis and XPS analysis indicated a range of compositions, from SWB-550 consisting of 100 at% C and O, to RHB-550 with 43 wt% ash. Elements including Si, K, Ca, N, P and Cl were detected at the biochar surface, and are likely to influence catalytic activity.

FTIR-ATR spectra for the biochars were broadly comparable. The biochars are highly unsaturated, with C≡C and aromatic C=C detected in all samples. Deconvoluted XPS C1s spectra indicated the presence of C-O, C=O and O-C=O bonds at the surface of WSB-550, OSB-700 and RHB-550, although these were not detected by FTIR-ATR. THz spectra and deconvoluted Raman spectra indicate that feedstock has little influence on graphiticity; the ratio of disordered to graphitic carbon (A_{D1}/A_G) was similar for the biochars studied, around 1.5. AC was found to have a higher A_{D1}/A_G ratio of 2.8. This indicates that biochars may be more graphitic than commercial activated carbons.

This characterisation work will allow the effect of surface treatments to be evaluated in Chapter 5, and the catalytic activity of biochars to be compared in Chapters 6-7.

4.1. Introduction

Biochar is a by-product from biomass pyrolysis, with an increasing number of applications. Biochar has been used commercially in soil remediation and waste water treatment, whilst catalytic applications have included uses as a support material, and as a precursor to functionalised carbon catalysts. However, the catalytic activity of untreated biochar attracts little interest, and the influence of feedstock choice on catalytic properties is rarely considered. This contrasts with studies of biochar for soil remediation purposes, where feedstocks are often compared for the subsequent properties of the biochar, such as mineral content, polycyclic aromatic hydrocarbon content and pH. The potential impact of feedstock on catalytic activity therefore requires further investigation.

Thorough characterisation is required in order to understand the origin of the catalytic activity of biochar. Commonly studied properties are the surface area, porosity and surface acidity of catalysts. Previous studies of biochar catalysts have often focused on preparing one particular feedstock of biochar for one particular reaction, using various chemical and physical activation and functionalisation methods to optimise performance. Catalytic activity is often attributed only to these treatments, with the original activity of the untreated biochar left unexplained. However, the activity of untreated biochar can provide important insights into the activity of catalytically active carbon deposits.

As was seen in the literature review, carbon itself can be catalytically active, for example in oxidative dehydrogenation reactions (Dreyer & Bielawski 2011). Graphitic coke deposits have also demonstrated activity in dehydrogenation reactions (McGregor, Huang, *et al.* 2010). However, the potential role of carbon structure in the catalytic activity of biochar has not previously been explored. The graphitic and disordered bands in Raman spectra are composites of several carbonaceous structures. However, as discussed in section 2.5.1, this is not always performed, particularly when comparing biochars from different feedstocks for catalytic applications. Therefore, a thorough characterisation of the carbon structures in biochars from different feedstocks could assist investigations into the potential contribution of graphitic carbon to catalytic activity in biochar.

Chapter 4 – Biochar Characterisation

It is also worth noting that the potential contribution of ash is often neglected in literature studies. Whilst surface acidity, basicity and functionalities undoubtedly play a role in catalytic activity of biochar, the potential contribution from trace metals and minerals is often neglected. The composition of the biochars from different feedstocks therefore requires thorough characterisation, to allow the effect of surface treatments in Chapter 5 to be evaluated, and so that the full range of factors responsible for catalytic activity to be considered in the reaction studies in Chapter 6 and Chapter 7.

In this chapter, biochars from four different feedstocks will be characterised by several methods. This will allow a comprehensive picture of their catalytic properties to be obtained, covering their structure, surface chemistry, composition and particularly carbon structure. Curve deconvolution will be performed on Raman and XPS C1s spectra, to provide more detail on the carbon structures than is typically seen in the literature on biochars. XPS in particular is highly surface sensitive, providing further detail on carbon structures which may be involved in catalysis at the surface of the biochar. The properties will be compared with a commercial activated charcoal, sourced from peat and acid-washed, to evaluate the potential of the biochars for catalytic application. Repeat measurements will allow the variability of the biochar properties to be accounted for through error analysis.

The characterisation methods for each technique are first outlined in section 4.2. Results are then presented in section 4.3, where techniques are grouped into four areas: techniques quantifying the structure of biochar such as BET analysis (section 4.3.1), techniques studying the composition of the biochars such as TGA proximate analysis and elemental XPS spectroscopy (section 4.3.2), surface-sensitive spectroscopic techniques investigating the surface chemistry of the samples such as FTIR-ATR (section 4.3.3), and techniques to characterise the carbon structure of the materials, such as Raman spectroscopy and high resolution XPS C1s spectroscopy (section 4.3.4). The results are summarised in section 4.3.5 before discussing the implications of the results in section 4.4. This includes implications for carbonaceous catalyst design (section 4.4.1), for the application of biochar as catalysts (section 4.4.2), and limitations of the work and suggestions for future work (section 4.4.4). The conclusions of the chapter are presented in section 4.5.

4.2. Methods

The characterisation techniques used in this chapter were developed and justified in Chapter 3, alongside the background theory. The experimental protocols are outlined here, including analysis methods used for curve deconvolution and to estimate experimental error.

4.2.1. BET isotherms

Approximately 0.2 g of sample was prepared for BET and porosimetry analysis. Before BET analysis, the samples were first thoroughly degassed to ensure the surface was free of moisture and volatiles. This allowed the surface to be clear for N₂ adsorption, and to ensure pores were not blocked by moisture or volatiles. The degassing was completed in two stages: the samples were first placed in a vacuum oven at 120 °C for at least 48 hours, at a vacuum pressure of 0.1 mbar. The samples were then transferred from vials to glass sampling tubes, and transferred to a Micromeritics VacPrep 061 Degasser. They were then further degassed at 250 °C for at least 24 hours, at a vacuum pressure of approximately 0.02 mbar.

Before collecting adsorption and desorption isotherms, the biochars were further degassed in the instrument, under vacuum (approximately 0.133 kPa) at 90 °C for 60 mins, and then 300 °C for 8 hours. Due to difficulties obtaining BET isotherms for OSB-700, an additional heating mantle was used to raise the temperature of the OSB-700 sample tube to 250 °C during the vacuum evacuation stage, prior to degassing. The experimental method for obtaining the BET isotherms is given in Table 4-1. Dead volume space was calibrated after analysis using an estimate of the free space in the tube of 45 cm³.

The experimental error was determined by calculating the average and standard deviation of three repeats of WSB-550. This allowed the natural variation in biochar samples, as well as the experimental error of the equipment, to be accounted for. The standard deviation was used to calculate a percentage error for the BET calculations. Micropore volume was calculated from the adsorption isotherms using Harkins-Jura t-plot, and pore size distributions were determined using the NLDFT model, as discussed in Chapter 3. According to IUPAC standards, micropores are defined as pores with diameters < 2 nm (< 20 Å); mesopores have

Chapter 4 – Biochar Characterisation

diameters of 2-50 nm (20-500 Å); and macropores have diameters > 50 nm (> 500 Å) (IUPAC 1997). At least 5 data points were used for both models, with correlation coefficients > 0.99.

Table 4-1 BET analysis conditions for N₂ adsorption and desorption at 77 K.

Start pressure (p/p ₀)	Pressure increment (p/p ₀)	Ending pressure (p/p ₀)
ADSORPTION		
0.000	0.010	0.100
0.100	0.025	0.300
0.300	0.050	0.800
0.800	0.025	0.900
0.900	0.010	0.990
0.990	0.005	0.995
0.995	0.003	0.998
DESORPTION		
0.998	0.003	0.995
0.995	0.005	0.990
0.990	0.010	0.900
0.900	0.025	0.800
0.800	0.050	0.300

4.2.2. CO₂ adsorption isotherms

The Intelligent Gravimetric Analyser (IGA-003) supplied by Hiden Isochema was used to obtain carbon dioxide adsorption isotherms at 25 °C. The temperature control was performed using a water bath (Grant R2).

Between 50 and 100 mg of each sample was loaded into a stainless steel weighing pan and loaded into an SS316 N reactor. The protocol for sample preparation before CO₂ adsorption is given in Table 4-2.

Table 4-2 Protocol for sample preparation before adsorption isotherm measurements.

Time delay before next step/min	Time elapsed/min	Operation	Set point (°C or mbar)	Ramp rate (°C or mbar/min)
0.1	0.1	Set temperature	80	2
60	60.1	Outgas	N/A	200
30	90.1	Set pressure	999.6	200
60	150.1	Set temperature	20	2
10	160.1	Outgas	N/A	200
60	220.1	Set dry mass	N/A	N/A
5	225.1	End sequence	N/A	N/A

The CO₂ adsorption was performed between 0-10 bar (the upper pressure limit of the apparatus), with data points taken every 0.5-1.0 bar, with additional data points at 0.00439 bar and 0.1 bar. The equilibrium time for each data point was shortened from the ideal of 30 minutes to 20 minutes due to time constraints.

4.2.3. SEM/EDX Analysis

The SEM used in this project is a JEOL JSM-6010LA Analytical Scanning Electron Microscope. The samples were mounted on 10 mm diameter aluminium stubs using carbon-based conductive adhesive discs, and coated with gold using an Agar Sputter Coater (all from Agar Scientific) to improve conductance and therefore image quality.

Using the sputter coater, a gold coating of approximately 10 nm thickness was deposited over the samples – the set-up is shown in Figure 4-1. The sample stubs were placed two at a time in the chamber, with the table set at a height of 25 mm from the target. The chamber was first evacuated to a pressure of under 0.05 mbar, purged using argon at a pressure of greater than 0.4 mbar for at least 10 seconds, and the pressure set to 0.04 mbar for gold coating. A current of 40 mA was used for 5-10 seconds; data provided by Agar engineers in private communications had shown these settings to give a rate of gold deposition of 0.5-1.0 nm s⁻¹.

Chapter 4 – Biochar Characterisation



Figure 4-1 Gold sputter coater set-up.

Images were obtained for biochars at a working distance of 10-12 mm (depending on the sample height), at magnifications between 50×-3000×. A spot size of 50 was used. EDX analysis was carried out over the biochars, allowing maps of elemental distribution and quantitative data to be generated. A working distance of 10 mm was used. The software settings for the EDX analysis can be found in Appendix A, and were chosen as a compromise between detail and time efficiency. High resolutions were not required in this work; the aim was to gain general information on the distribution of elements over the surface of a biochar grain.

4.2.4. TGA

TGA proximate analysis was carried out using a Perkin Elmer TGA (model 4000). An alumina crucible was first weighed whilst empty, to allow the sample weight to be calculated. Approximately 15-20 mg of powdered sample were then loaded into the crucible. To cool the TGA, a cooling jacket was used with tap water at a flow rate of approximately 1 litre/min.

The proximate analysis method is summarised in Table 4-3. The analysis methods used were based on industrial standards for biochar analysis (ASTM International 2010), however the method used here is shortened for time efficiency purposes. For proximate analysis, the

moisture content was evaluated by measuring the mass lost during heating in nitrogen to 110 °C. Volatile content was defined as the mass lost by heating in nitrogen to 900 °C. The fixed carbon content was measured by measuring the mass lost during combustion in oxygen at 900 °C, and the ash was defined as the mass remaining after this combustion step.

Table 4-3 TGA Proximate Analysis method for the University of Sheffield, using Perkin Elmer TGA 4000.

Step	Temperature/°C	Time/mins	Temperature ramp/°C	Heating rate/°C min ⁻¹	Gas	Gas flowrate/ml min ⁻¹
1	30	2			N ₂	20
2			25-110	50	N ₂	20
3	110	5			N ₂	20
4			110-900	100	N ₂	20
5	900	5			N ₂	20
6	900	5			O ₂	50

The experimental error was calculated using two repeats of WSB-550-DM-T-C sample, analysed at the University of Edinburgh. The average and standard deviation for the moisture, volatile, carbon and ash content were calculated, and the standard deviation was expressed as a percentage. This was then used to plot error bars on subsequent TGA spectra.

4.2.5. XPS

In this work, the elemental composition was determined by an elemental scan, and the carbon properties were studied using a high-resolution scan of the C 1s peak. The samples were in powder form, having been ground and sieved to particle sizes less than 90 µm in diameter. Each powder sample was pressed into a piece of soft indium foil, and each mounted sample was placed on a paper label to electrically isolate the samples from each other.

As a paper label was used for electrical isolation, charge neutralisation was necessary to disperse any charge build-up. The XPS instrument used was a Kratos Ultra instrument with a monochromated aluminium source, calibrated using software available from NPL (National Physical Laboratory 2012). Two points were analysed on each sample. Survey scans were collected for binding energies between 1200 and 0 eV, with a 160 eV pass energy and at 1 eV intervals. The high-resolution C 1s spectra were obtained at a pass energy of 20 eV and 0.1 eV intervals, over a range of binding energies from 290 to 280 eV. Two sweeps of the energy

Chapter 4 – Biochar Characterisation

range, each of 5 minutes duration, were carried out for each sample and averaged to obtain the final spectra. Two areas were analysed for each sample to account for heterogeneity.

Analysis and curve deconvolution of the XPS C1s peak were performed using CasaXPS software. Further details on the curve deconvolution method are given in the Results, section 4.3.4, with examples in Appendix A . Error analysis was calculated using the average and standard deviation for the two points on each sample analysed. The standard deviation is plotted as an error bar on XPS data in the results. For some samples marked *, only one measurement was taken. For these samples, the standard deviation marked on the graphs is the average standard deviation calculated for the other biochar samples.

4.2.6. FTIR-ATR spectroscopy

Attenuated Total Reflectance (ATR) was the main method used for the characterisation of the biochar samples, as this required minimal sample preparation, and would give surface-sensitive information relevant to understanding the catalytic activity of the biochar. It is also commonly used in the literature (Han *et al.* 2013; Shin *et al.* 1997).

The ATR accessory used in this work is a Specac Quest with a 1.8 mm diameter diamond crystal capable of obtaining spectra in the range of 7800 to 400 cm^{-1} ; the penetration depth is estimated to be 2.01 μm at 1000 cm^{-1} (Specac 2016). An atmospheric background was used for powdered biochar studies, and the powder was usually used undiluted. For the Specac Quest ATR, no further sample preparation was required.

To load the sample, a small quantity of the pre-sieved biochar powder was applied using a spatula to cover the diamond crystal. In order to ensure a good contact between the sample and the crystal, the sample was loaded as thin layer, which was flattened using the flat of the spatula before applying the pre-set 70 MPa pressure using the anvil.

In analysing the biochar samples, the samples were scanned 16 times using the Happ-Genzel apodization method in transmittance mode. The spectrum obtained was an average of these 16 scans. After use, the crystal and anvil were cleaned with a cotton bud dipped in distilled

water, followed by ethanol, and allowed to dry. A sample scan was performed to check that the surface was dry before loading the next sample – when fully dry, the empty scan would give a flat line due to the background being subtracted.

4.2.7. Raman spectroscopy

In this work, a green laser of wavelength 514 nm was used with a source energy of 20 mW (corresponding to about 12 mW on the sample), at an intensity of 1%. This was found to be low enough in energy to prevent fluorescence from occurring. Fluorescence was an issue when using a higher laser intensity (around 10%). Using a lower intensity of laser power also reduces the risk of damaging the sample.

A Renishaw inVia Raman microscope was used in this experiment. A silicon wafer was used as a calibration source (Renishaw Raman Calibration Source) – analysis of the silicon wafer gives a sharp Raman peak at a shift of 520-521 cm^{-1} , which is used to calibrate the instrument. Calibration using silicon was carried out before each set of experiments.

The samples were analysed in powder form, with particle sizes of less than 90 μm diameter. To prepare the samples, a small amount of powder was squeezed between two glass slides. One slide was then removed, leaving a reasonably flat surface for Raman analysis.

Three different but representative areas were chosen for Raman analysis for each sample. This meant the non-homogeneous nature of the sample could be accounted for. The microscope magnification used was 50 \times . The settings used for obtaining the Raman spectra are given in Table 4-4 for reference. These settings were chosen to provide a compromise between time taken to run a sample and the resulting signal-to-noise ratio. More accumulations would have improved the signal to noise ratio, but would have taken more time. With these settings, sample analysis required approximately 10 minutes to run.

Chapter 4 – Biochar Characterisation

Table 4-4 Settings used for obtaining Raman spectra of biochars.

Laser wavelength/nm	514
Laser power (at 100%)/mW	20
Laser intensity	1%
Number of accumulations	5
Raman Shift range/cm ⁻¹	400-4000

Cosmic Ray Removal was used to mitigate the effect of random atmospheric disturbances, which can create additional intense peaks in the Raman spectra. In Cosmic Ray Removal, three spectra are obtained and the median value for each Raman shift is recorded. This removes the possibility of extreme values appearing in the final spectra. Raman spectroscopy was also carried out in a dark room, with no lights on and the computer monitor switched off, in order to avoid peaks associated with these light sources.

Curve deconvolution was performed for the Raman spectra obtained. This is detailed in the Results, section 4.3.4, with examples given in Appendix A . To estimate the error in the D1/G ratios, three Raman spectra were obtained for three areas of a WSB-550-DM sample. Raman curve deconvolution was then performed and the D1/G area ratio calculated. The average and standard deviation were then calculated. The standard deviation was then expressed as a percentage, and applied to the remaining samples as an estimate of the error involved in the curve deconvolution process, taking into account the natural variation of the sample.

4.3. Results

Interpretation of the catalytic activity of biochar requires a thorough characterisation of the catalysts. In this section, the results of a wide range of characterisation techniques are presented. Data on the surface area and porosity of the catalysts is presented in section 4.3.1; compositional analysis is presented in section 4.3.2; surface chemistry is examined in section 4.3.3; and carbon structure in particular is thoroughly characterised in section 4.3.4. This allows the bulk and surface properties of the biochar to be determined more thoroughly than is typical in the literature for biochar catalysts. This will allow the effect of surface treatments to be studied in Chapter 5, and the origin of catalytic activity in biochars to be determined in Chapters 6 and 7.

4.3.1. Structure of untreated biochars

The structure of the catalysts is characterised in terms of BET surface area, t-plots for micropore volume and NLDFT calculations for mesoporosity. Whilst the porosity of biochars is often characterised for catalytic applications, pore size distributions are rarely compared for different feedstocks. SEM images are also presented to show the macrostructure of the biochars from different feedstocks.

The BET surface areas of biochars from four feedstocks are compared in Figure 4-2, alongside a commercial AC sample. The experimental error was calculated from three repeats of WSB-550, with a percentage error of 2.42 % (calculations in Appendix A). As expected, the activated charcoal has a much higher surface area of $729 \text{ m}^2 \text{ g}^{-1}$, compared to the biochars. Feedstock clearly influences the surface area, as the BET area ranges from $51.7 \text{ m}^2 \text{ g}^{-1}$ for WSB-550 to $389.9 \text{ m}^2 \text{ g}^{-1}$ for SWB-550. An increase in surface area with pyrolysis temperature is also observed for OSB-550 and OSB-700.

Chapter 4 – Biochar Characterisation

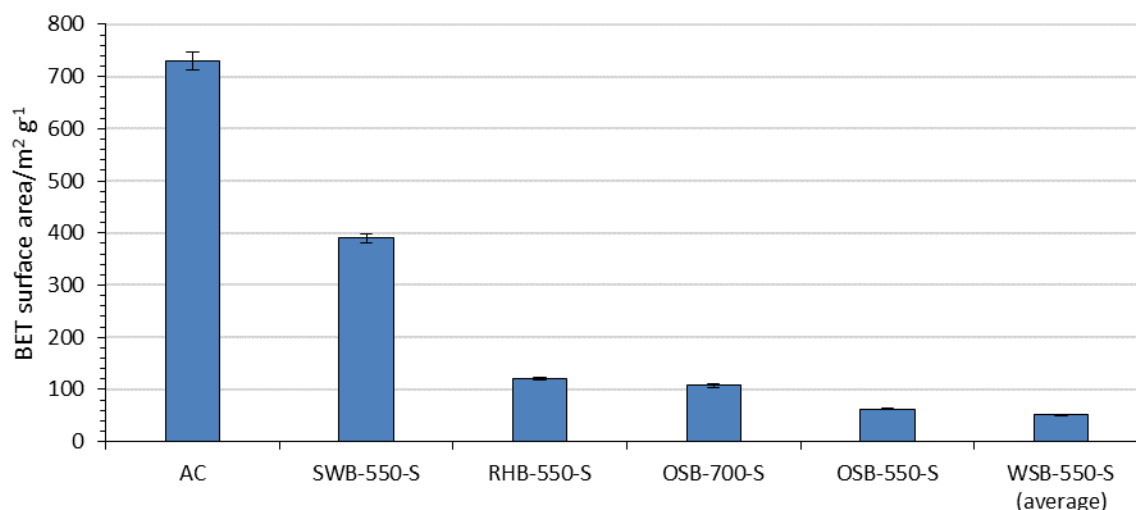


Figure 4-2 BET surface area of sieved biochar from different feedstocks, compared with commercial standard AC. Isotherm obtained using N₂ at 77 K. Error bars calculated from three repeats of WSB-550; standard deviation $\pm 1.25 \text{ m}^2 \text{ g}^{-1}$, percentage error 2.42 %.

The range of surface areas may indicate varying levels of microporosity in the samples; this was investigated using Harkin-Jura t-plots to calculate the total micropore volume. The results are presented in Figure 4-3.

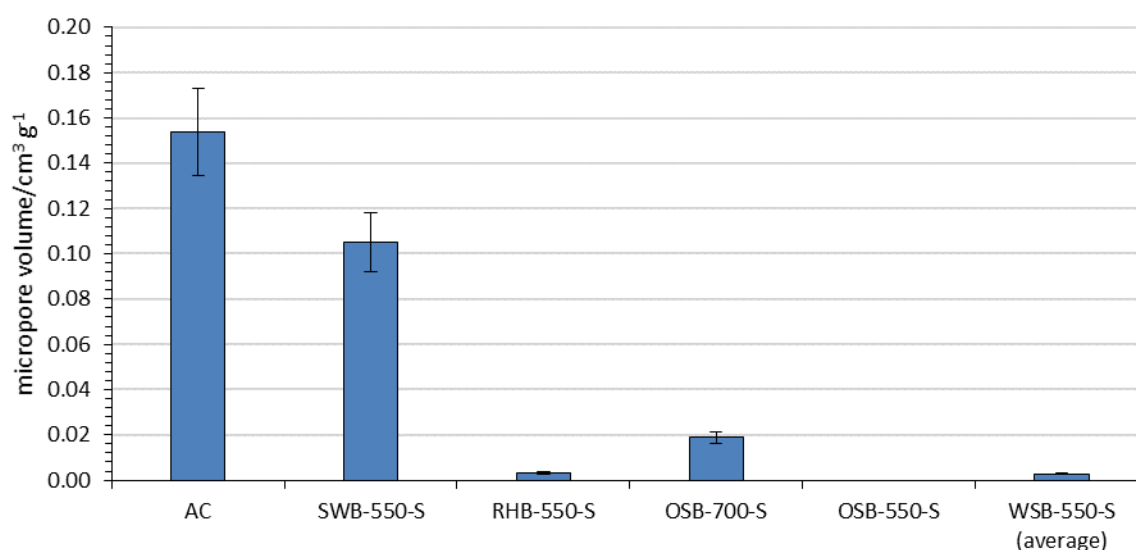


Figure 4-3 Micropore volume for biochars from different feedstocks. Percentage error of 12.52 % calculated from two repeats of WSB-550 (one anomalous result omitted). No microporosity detected in OSB-550.

Similar to the BET surface area, AC and SWB-550 exhibit the highest micropore volume, with volumes in other biochars being much lower. Increased pyrolysis temperature is also seen to lead to a higher micropore volume in OSB-700. However, OSB-550 and WSB-550 did not exhibit microporosity.

The presence of mesoporosity was evidenced by the hysteresis observed in the adsorption isotherms of the biochars (*i.e.* where the adsorption isotherm differs from the desorption isotherm due to capillary condensation in mesopores). This was observed in most biochars except SWB-550. The biochars and activated charcoal exhibited a type II isotherm, corresponding to multilayer adsorption on microporous materials. Example isotherms are presented in Figure 4-4.

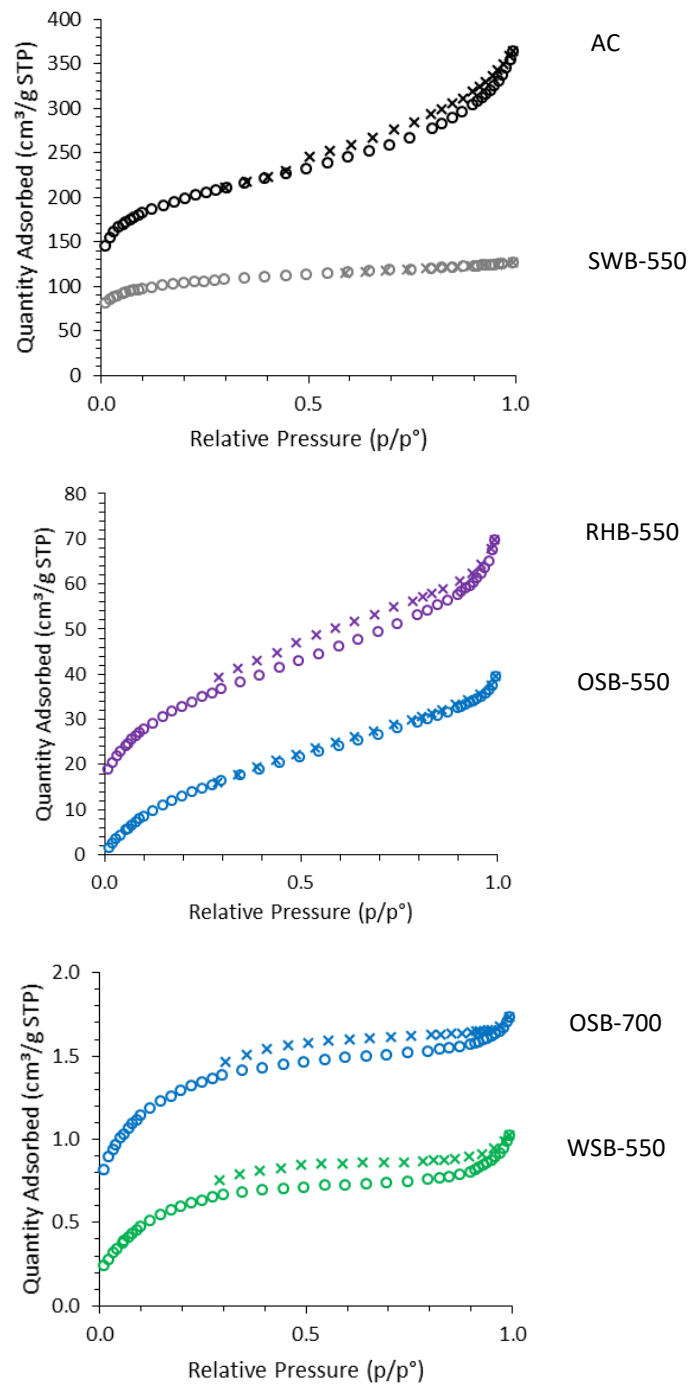


Figure 4-4 Adsorption and desorption isotherms for biochars and activated carbon. Adsorption data points are open circles (°), desorption data points are crosses (×).

Chapter 4 – Biochar Characterisation

SWB-550 was the only sample to show no evidence of mesoporosity through hysteresis. Mesoporosity was further characterised through pore size distributions (PSDs), estimated using a commercial NLDFT model developed by Micromeritics (Jagiello & Olivier 2009). Due to the expected heterogeneity of the biochar samples, the reproducibility of the PSD was first considered by repeating the analysis for three samples of WSB-550; the results are presented in Figure 4-5.

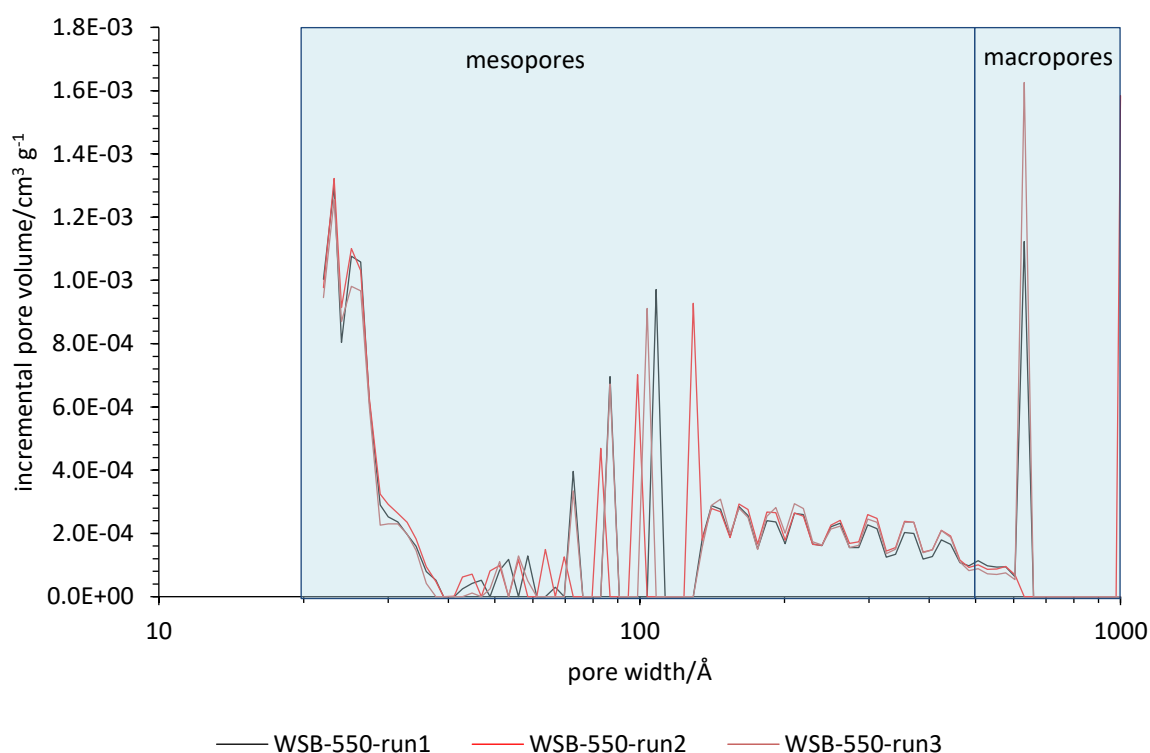


Figure 4-5 Reproducibility of pore size distributions for three samples of WSB-550.

The PSD model appears to be reproducible. Whilst there is slight variation in the position of the peaks, particularly in the region 40-100 Å, the number and intensity of the peaks appears to be consistent. The PSDs for four different feedstocks are compared in Figure 4-6.

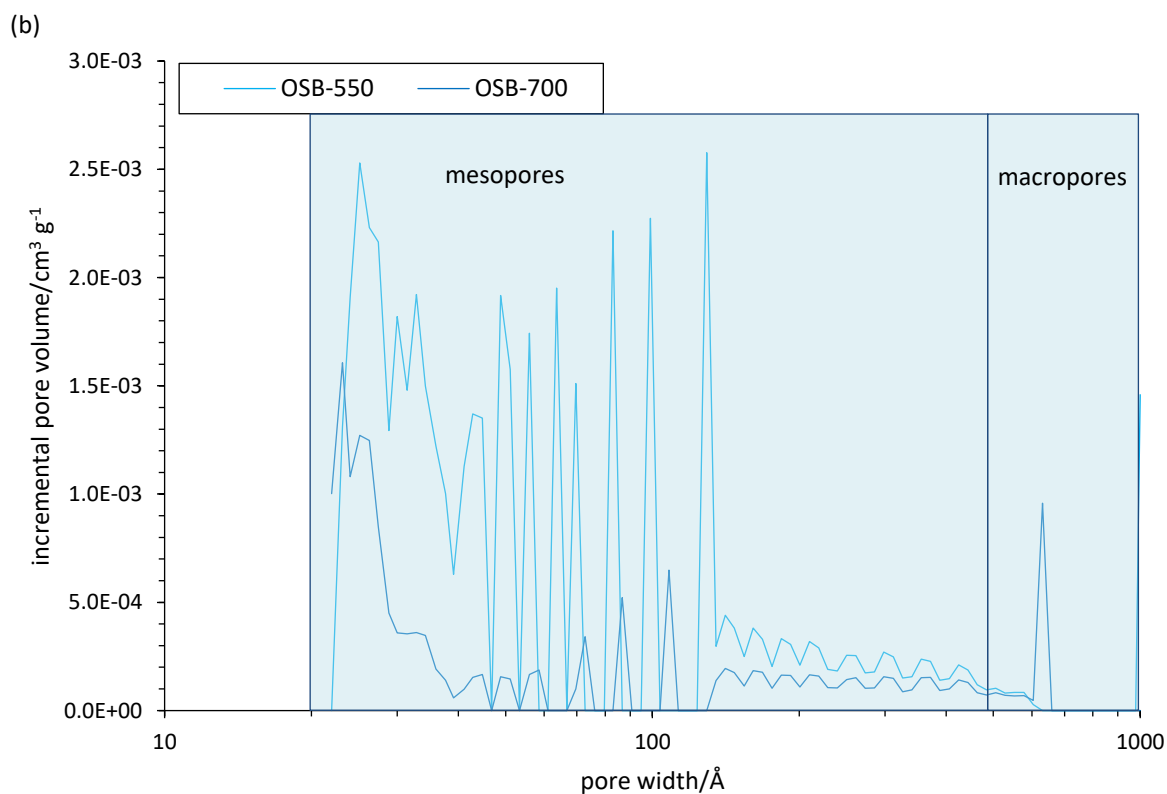
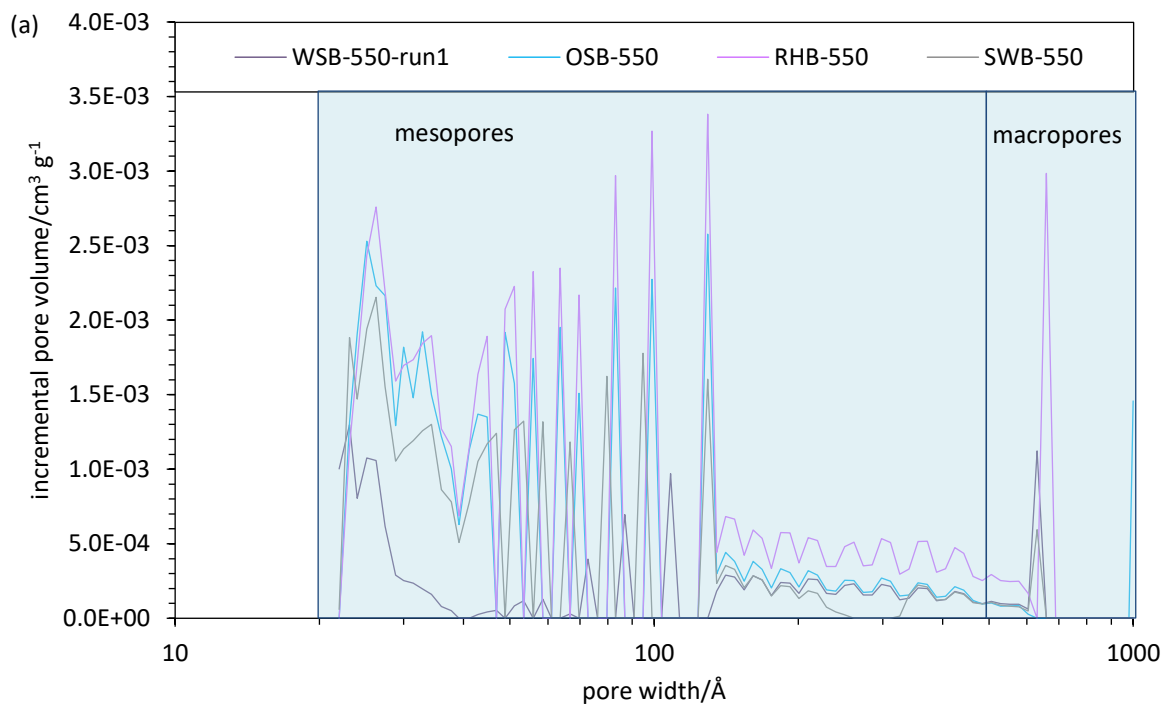


Figure 4-6 Pore size distribution for (a) biochars from different feedstocks, and (b) biochars prepared at different pyrolysis temperatures. PSDs calculated from BET isotherms by NLDFT.

The PSDs demonstrate some consistency between feedstocks; a distinctive ‘step’ pattern is observed in all samples in the region 100-1000 Å; the origin of this regular pattern is unclear. The main differences between feedstocks occur in the region 20-50 Å. In this region, each

Chapter 4 – Biochar Characterisation

feedstock exhibits a different pattern, which is also affected by increasing the pyrolysis temperature.

The differing volume of the mesopores estimated by the NLDFT model is also worth considering. Whilst SWB-550 has a BET area three times that of RHB-550, this appears to be due to microporosity. There is no observable hysteresis for SWB-550, and the NLDFT model also predicts lower volumes of mesopores in SWB-550, particularly in the region 100-500 Å, compared to RHB-550. The NLDFT model calculates that RHB-550 has the highest number and therefore volume of mesopores. The distribution of porosity can therefore vary widely between feedstocks, with some biochars being more micro- or mesoporous than others. Mesoporosity is also shown to decrease with increased pyrolysis temperature, as seen in the pore size distributions of OSB-550 and OSB-700, with some peaks appearing to shift to smaller pore widths.

The structure of the biochars was finally studied using SEM imaging. This allowed variations in particle size, shape and macroporous structure to be observed. The SEM images obtained are shown in Figure 4-7.

All the biochars exhibited a macroporous structure, possibly correlating to cell wall structures, which typically range in size from 10-100 µm. The images also demonstrate the anisotropic structure of the biochars; the macropores are only present in one direction, with sheet-like structures parallel to the pores. There is evidence that the macropores in SWB-550 are considerably larger than those from other feedstocks; however, due to the very small area imaged when using SEM, it is difficult to verify whether this is representative.

The biochars are however distinct from the commercial AC. The commercial AC sample has a much smaller and more uniform particle size, of between 1-15 µm, whilst the biochars contain particle sizes from 1-90 µm. The grinding and sieving process also leads to many smaller and irregularly-shaped fragments. The SEM images demonstrate that at smaller particle sizes, the macroporous structure of the biochars may be lost; the pores are seen more clearly in the larger unsieved SWB-550 sample than the smaller sieved SWB-550 particles.

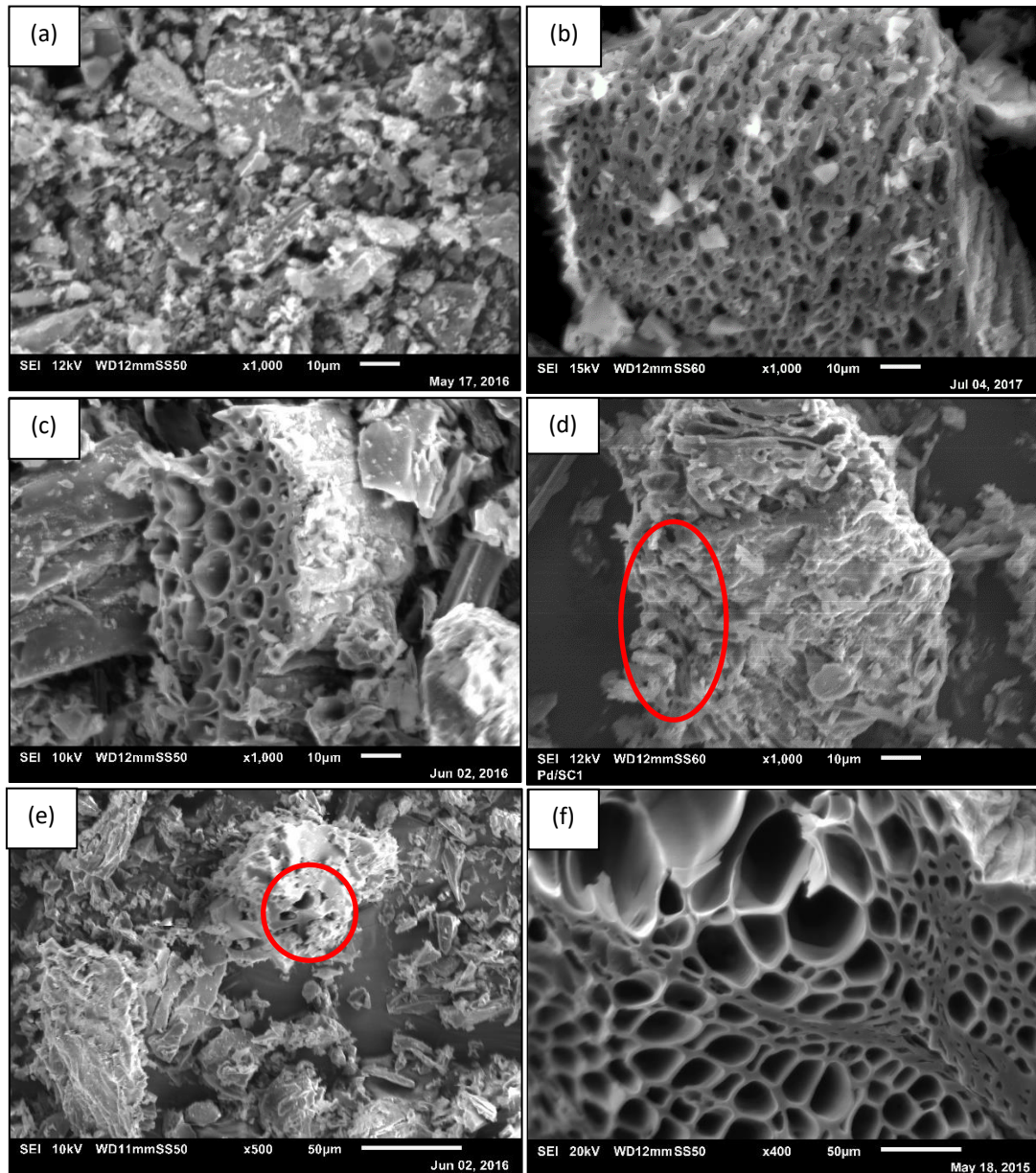


Figure 4-7 SEM images comparing the structure of sieved biochars from different feedstocks at magnification $\times 1000$. (a) AC, (b) RHB-550, (c) OSB-550, (d) WSB-550, (e) SWB-550 (magnification $\times 500$ to show larger pores) and (f) SWB-550 large particle ($\times 400$) before sieving. Pores highlighted with red circles for clarity in (d) and (e).

4.3.2. Composition

The elemental composition was characterised using TGA and XPS analysis. The first stage was to quantify the ash and fixed carbon content in the sample. This was determined using TGA proximate analysis. The results are presented in Figure 4-8.

Chapter 4 – Biochar Characterisation

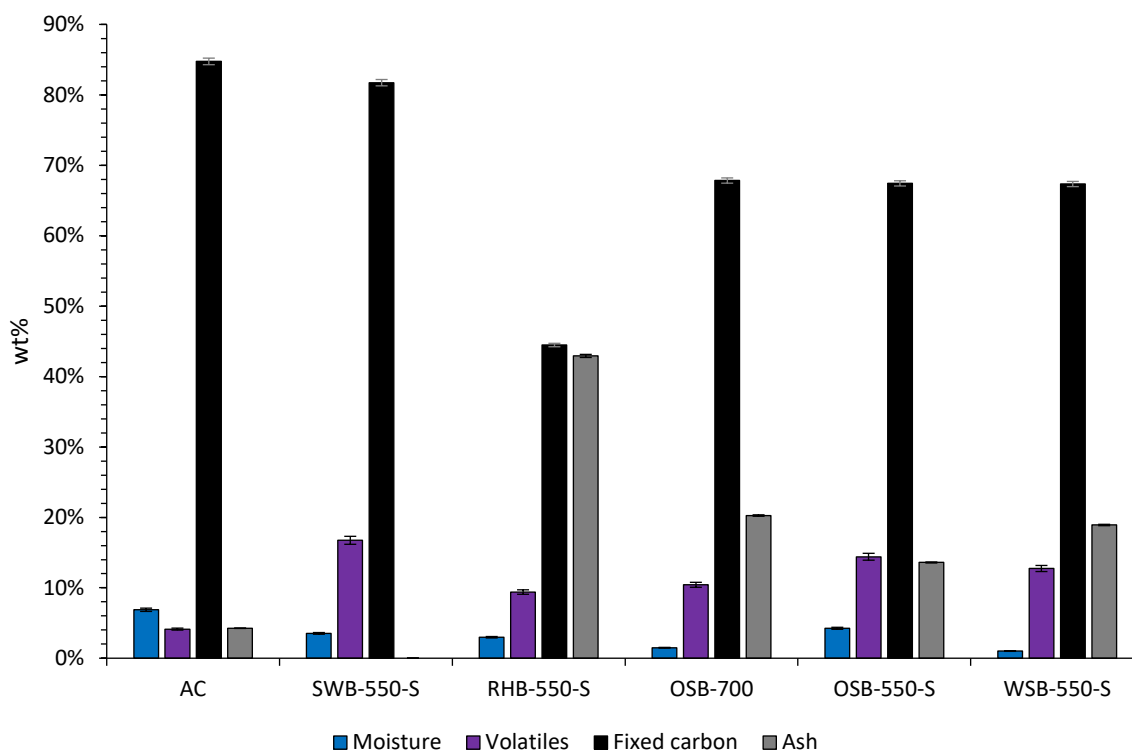


Figure 4-8 Comparison of proximate analysis for biochars from different feedstocks. Error analysis based on two repeats of WSB-550-DM-T-C. Percentage error calculated as: moisture 3.37%, volatiles 3.39%, carbon 0.55% and ash 0.51%.

The proximate analysis demonstrates clear differences between the composition of the biochars, particularly in terms of ash and fixed carbon content. Commercial AC contains the highest levels of fixed carbon content. The biochars however range from very high carbon and low ash content (SWB-550) to very high ash content (42.92 wt% for RHB-550). The choice of feedstock clearly influences the ash content of the biochars. The ash and carbon content of OSB-700 was also higher than that of OSB-550.

Once the proximate composition was known for each sample, the elemental composition of the biochars was next investigated by XPS elemental survey scans. Analysis was first performed on the ash samples to increase confidence in the identification of trace elements, due to the higher concentrations present; the ash composition is presented in Chapter 5. The surface elemental composition of the biochars is shown in Figure 4-9.

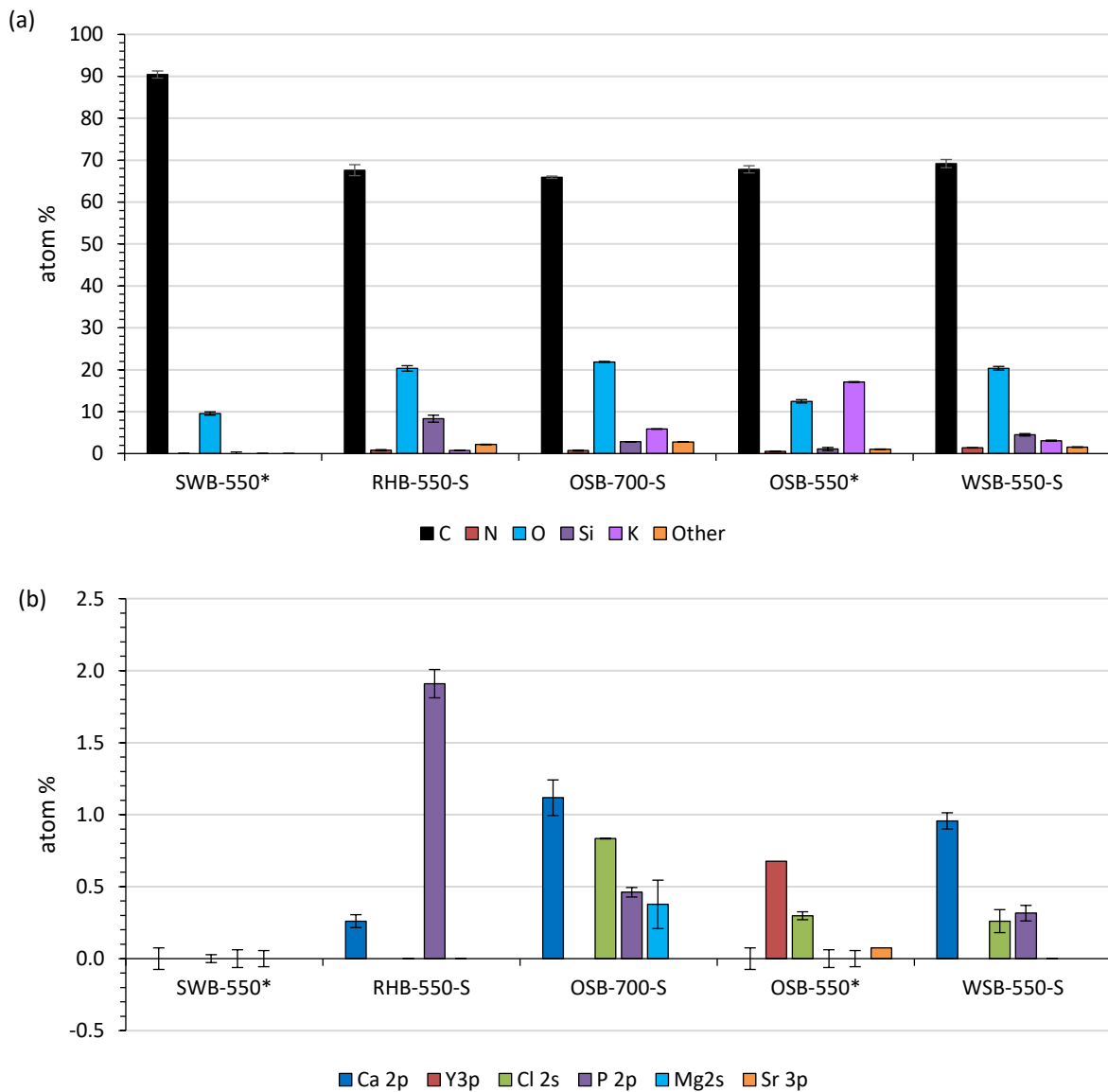


Figure 4-9 Elemental XPS surveys of biochars of interest. (a) Key elements, C, N, O, Si and K, with 'other' elements shown in (b). Data for biochars marked * collected and analysed separately by Dr James McGregor. Error bars calculated from standard deviation of two samples. For SWB-550 and OSB-550, only one sample run; error bars are the average standard deviation calculated from the other samples. No error analysis for Sr and Y elements due to lack of data.

The XPS data in Figure 4-9a confirms that elemental composition varies widely with feedstock. SWB-550 comprises of only C and O, whilst WSB-550 contains at least six other elements: Si, K, N, Ca, P, and Cl. The surface carbon content varies between 67-90 at%, and surface oxygen between 9-20 at%. The potassium content in particular is variable, from 17 at% for OSB-550 to 0 at% for SWB-550. Different elements are identified in OSB-550 and OSB-700 in Figure 4-9b; this is likely due to the different analysis methods used. The same elements would be expected in each sample, although concentration is likely to vary with pyrolysis temperature.

Chapter 4 – Biochar Characterisation

4.3.3. Surface chemistry

The surface chemistry of the biochar samples was tested using FTIR-ATR, a surface-sensitive technique. The effect of feedstock and pyrolysis temperature on surface chemistry is compared in the FTIR spectra shown Figure 4-10.

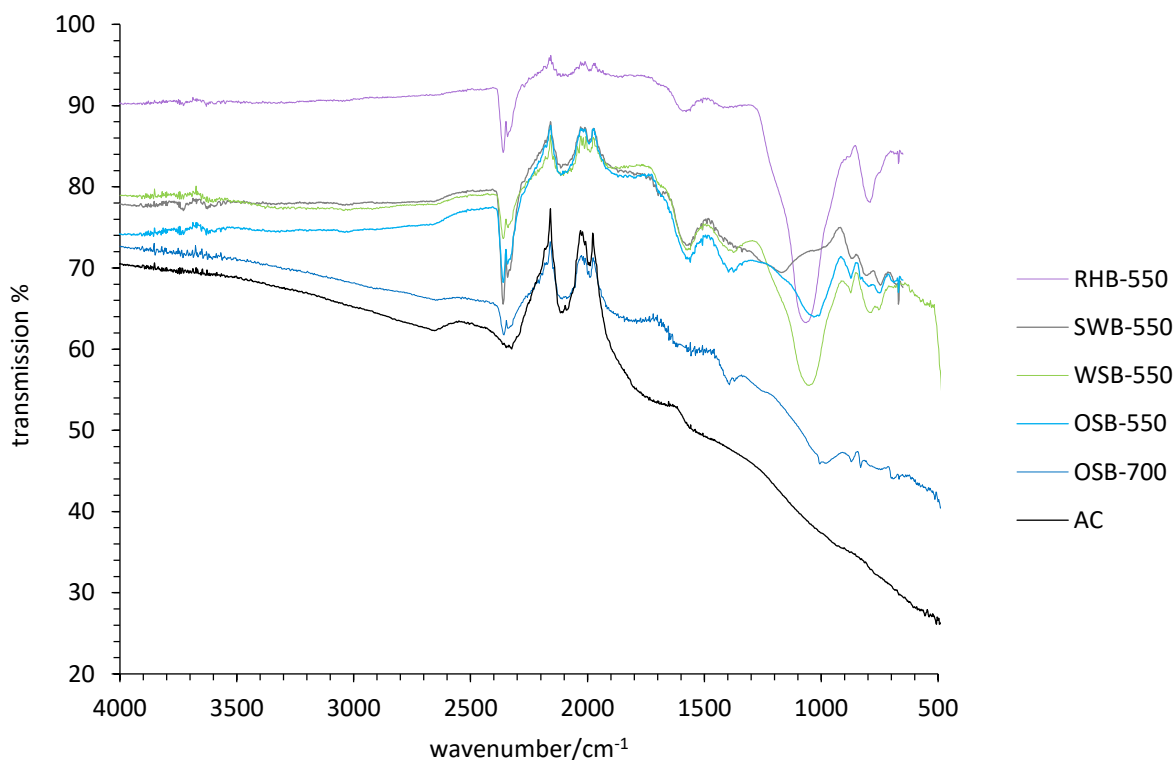


Figure 4-10 FTIR-ATR spectra for biochars from different feedstocks pyrolysed at 550 °C, compared with commercial AC.

The FTIR-ATR spectra are generally similar, independent of the feedstock used. To interpret the FTIR-ATR spectra fully, FTIR analysis of the ash samples was also carried out to verify bands associated with the ash content, versus bands associated with carbon content. This work can be found in Appendix A . The peak assignments and justifications given in Table 4-5 are based on this work, as well as literature references.

Table 4-5 FTIR peak assignment for biochars and ash samples, with justification from literature sources.

Wavenumber/cm ⁻¹	Assignment	Justification
2340	CO ₂ (asymmetric, gas phase)	Present in all samples. Reference: (Williams & Fleming 2008)
2200-2000	C≡C	Present in carbonaceous samples only. Reference: (Williams & Fleming 2008)
1600-1500	Aromatic C=C bending	Present in carbonaceous samples only. Reference: (Qian <i>et al.</i> 2013)
1375	Phenolic O-H bending	Weak. Present in carbonaceous samples only. Reference: (Qian <i>et al.</i> 2013)
1200-900	Si-O-Si symmetric	Much stronger in the ash samples. Reference: (Al-Oweini & El-Rassy 2009)
800	Si-O-Si asymmetric	Much stronger in the ash samples. Reference: (Al-Oweini & El-Rassy 2009)

When comparing the FTIR spectra of the biochars, of particular note is the absence of any C-H or O-H bands in the region 4000-2500 cm⁻¹. Aromatic C-H bonds associated with lignin for example might be expected around 3050 cm⁻¹ (Chia *et al.* 2012), but are not detected. However, C≡C groups are detected in all of the biochars, with the greatest intensity for commercial AC, and lowest in intensity for RHB-550. This indicates that the biochars are highly unsaturated.

There is some evidence for aromatic C=C structures in the biochars, due to the band at weak band at 1600-1500 cm⁻¹. This is similar in SWB-550, WSB-550 and OSB-550, weaker in RHB-550, and not detected in AC. Aromatic C=C is therefore a common feature of biochars, although the extent varies, and further processing of biochar to AC may remove these aromatic properties; this can be seen in the reduced intensity of the aromatic C=C band in OSB-700, compared to OSB-550. The absence of aromatic C-H indicates that there is a high C:H ratio in the biochars.

The key difference between the biochars is in the region 1750-500 cm⁻¹, attributed to silica peaks. This is likely due to the varying ash contents of the samples; the sharpest peaks in the silica region are observed for RHB-550, which has the highest ash content, with virtually no peak observed in this region for AC and SWB. The peak at 1500 cm⁻¹ may also indicate low quantities of phenolic -OH present in OSB-550 and OSB-700, and trace quantities in RHB-550

Chapter 4 – Biochar Characterisation

and WSB-550, which are not present in AC and SWB-550. There is no evidence of a C=O band at 1700 cm^{-1} .

CO_2 adsorption data can give a further indication of differences in surface chemistry. The absorption capacity for CO_2 can indicate the quantity of basic sites for CO_2 adsorption, and whether this is related to the BET surface area. CO_2 adsorption isotherms for three biochars and AC are presented in Figure 4-11.

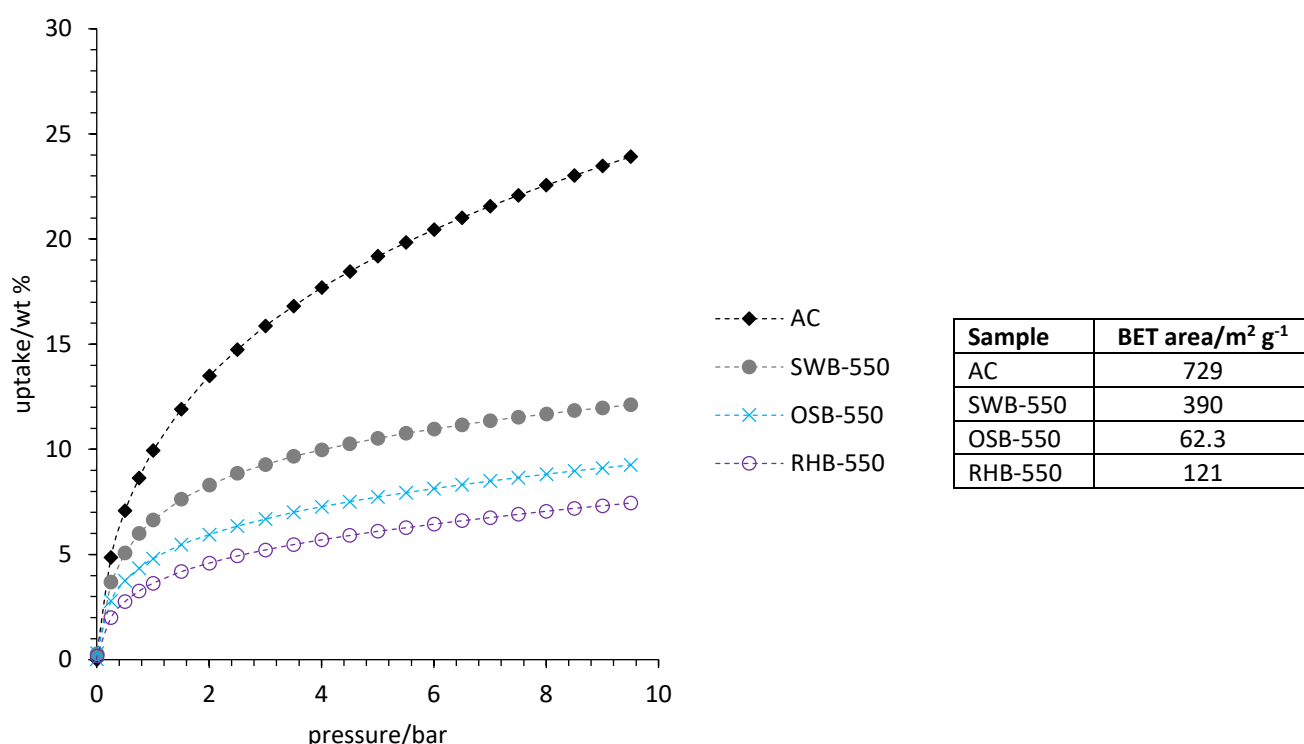


Figure 4-11 CO_2 adsorption isotherms for biochars from three feedstocks, compared with commercial AC. Dashed lines to guide the eye only.

The CO_2 adsorption isotherms are type I, indicating monolayer adsorption, and clearly demonstrate that CO_2 adsorption capacity is not simply correlated with surface area. The surface area of OSB-550 is half that of RHB-550, but clearly has a higher CO_2 adsorption capacity. OSB-550 also has lower micropore and mesopore volume than RHB-550. However, AC and SWB-550 do have the highest surface areas and CO_2 adsorption capacity. Whether high CO_2 adsorption capacity correlates to catalytic activity in CO_2 utilisation will be tested in Chapters 6 and 7.

4.3.4. Carbon structure

From the FTIR-ATR spectra presented in Figure 4-10, some information on the carbon structures present at the surface of the biochars can be gathered. All biochars and particularly AC exhibit C=C bonds, with some evidence of aromatic carbon in the biochars. However, not all carbon structures are IR active. Complementary techniques such as Raman spectroscopy and XPS C1s spectroscopy are therefore used to study the carbon structures in more detail.

Raman spectroscopy is commonly used for quantifying the degree of graphiticity in carbonaceous samples, by detecting graphitic and disordered carbon bands that are IR-inactive. Once the Raman spectra were collected, a curve deconvolution method was developed based on principle of a least curves fit. Six curves were fitted; the band assignments and interpretations are given in Table 4-6, and are based on those identified in the literature sources (see section 2.5.1). Example deconvolved spectra are given in Appendix A .

Table 4-6 Raman curve deconvolution, peak assignments.

Band name	Raman shift/cm ⁻¹	Band interpretation
G _L	1700	Carbonyl group C=O
D2	1620	Graphitic lattice mode; lattice vibration involving graphene layers at surface of graphite crystal. Stretching vibrations of double bonds/olefins.
G	1580	Graphite; aromatic ring quadrant breathing; alkene C=C. In-plane C=C aromatic ring stretching.
V _L	1465	Methylene or methyl; semi-circle breathing of aromatic rings; amorphous carbon structures
D1	1350	Disordered carbon lattice vibration mode (in-plane vibrations of C=C at edge of graphene layer)
D4	1200	C-C and C=C stretching vibration of polyene-like structures.

Curve deconvolution was carried out for the Raman spectra for all biochars. The deconvolved peak areas were summed, and the contribution from each of the six peaks in Table 4-6 was expressed as a percentage. The results for four feedstocks and AC are presented in Figure 4-12.

Chapter 4 – Biochar Characterisation

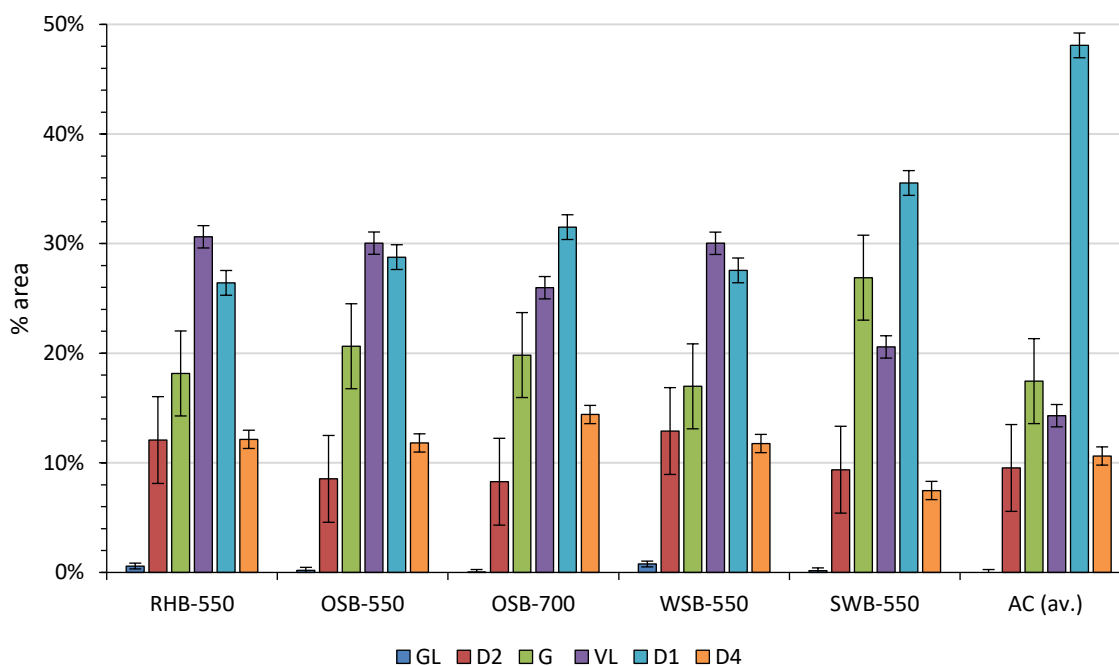


Figure 4-12 Raman curve deconvolution data for different biochar feedstocks. The percentage error in each band is estimated from curve deconvolution performed on three spectra from WSB-550-DM.

From Figure 4-12 there are clear differences between AC, SWB-550 and the other feedstocks. SWB-550 and AC have higher contributions from band D1 and very little evidence of a C=O peak, represented by band GL. AC and SWB-550 also have lower contributions from aromatic VL bands. RHB-550, OSB-550 and WSB-550 have similar carbon structures detected by Raman spectroscopy, indicating that feedstock can but does not necessarily have a strong impact on carbon structure. The effect of pyrolysis temperature can also be seen by comparing OSB-700 and OSB-550; levels of D1 increase and levels of aromatic VL decrease at higher pyrolysis temperatures.

There are similarities between all of the spectra; for example, the main contributions are from VL, D1 and G bands. Levels of D2 and D4 are similar for all of the biochars. There are therefore common features in the carbon structures of biochars from different feedstocks, with significant contributions from a mixture of graphitic (G), disordered (D1) and aromatic structures (VL). The ratio of the area of the D1 and G peaks is commonly used as an indicator of graphiticity. A lower A_{D1}/A_G ratio indicates a more graphitic sample. The A_{D1}/A_G ratios are presented in Figure 4-13.

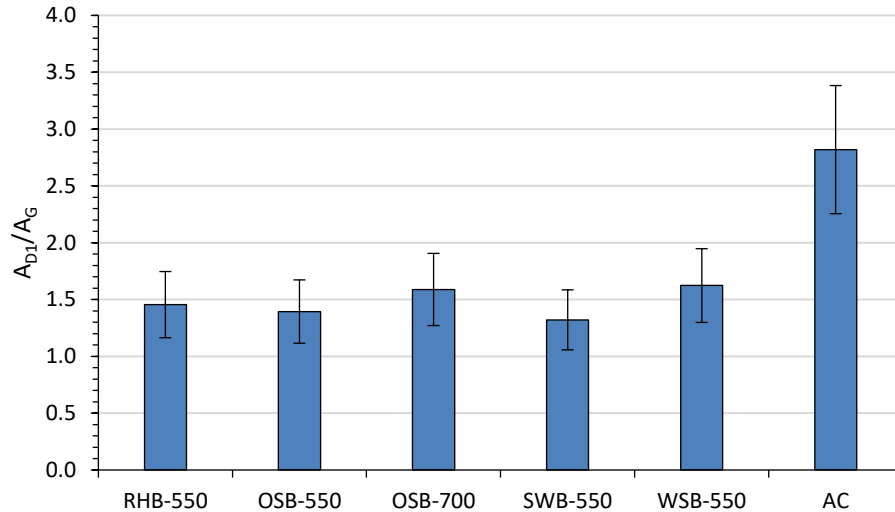


Figure 4-13 A_{D1}/A_G ratio from Raman curve deconvolution data for biochars from different feedstocks. Percentage error of $\pm 20\%$ calculated from three repeats of curve deconvolution of WSB-550-DM.

The biochars exhibit similar levels of graphiticity, with A_{D1}/A_G ratios around 1.5, and are comparable within the estimated experimental error of $\pm 20\%$. SWB-550 may be slightly more graphitic than RHB-550 and OSB-550, whilst WSB-550 is the least graphitic. AC however is significantly less graphitic than the biochars. A comparison with the literature indicates that the biochars are somewhat graphitic; for disordered carbonaceous samples such as soot, A_{D1}/A_G ratios as high as 8 have been calculated (Seong & Boehman 2013).

The Raman spectroscopy results presented here are not surface sensitive, and so whilst the biochars may exhibit similar graphiticities in the bulk, the carbon structures at the surface may vary. High resolution XPS C1s analysis was used to study the carbon structures at the surface of the biochars. Curve deconvolution can be used to give detailed information on the chemical environment of the carbon detected at the biochar surface. Following a similar strategy to that employed for Raman curve deconvolution, C1s peaks and fitting parameters were identified in the literature and are summarised in Table 4-7. These peaks were adapted from the findings of in-depth XPS studies of carbonaceous samples by Smith and co-workers (Smith *et al.* 2016). An example deconvolved spectra for OSB-700 is given in Figure 4-14.

Chapter 4 – Biochar Characterisation

Table 4-7 Peak assignment and fitting parameters for XPS C1s curve deconvolution peaks. Adapted from the literature (Smith et al. 2016), with permission from Elsevier.

Peak #	Assignment	BE/eV	FWHM/eV	G:L (0-1)
I	C-C (low) Cyclopentane rings within cluster. sp ² bonded carbons e.g. graphite	283.4-284.0	1.2-2.0	0-0.3
II	Primary C-C/C-H peak	284.2-284.6	1.2-2.0	0-0.3
III	C-C high C in cycloheptane or larger rings within clusters. C in small clusters containing C=O bonds. Sp ³ bonded carbons.	284.8-285.4	1.2-2.0	0-0.3
IV	C-O, C-O-C Ether and hydroxyl bonded C, C associated with ether bond in lactone/esters	285.9-286.6	1.8-2.2	0-0.1
V	C=O Carbonyl groups and carbons attached to two ether/hydroxyl groups	286.7-287.5	1.8-2.2	0-0.1
VI	C-O=O Carboxyl, lactone and ester groups	288.3-288.9	1.8-2.2	0-0.1
VII	π - π * HOMO-LUMO transition for primary C-C peak; indication of aromaticity	291.0-292.0	2.0-3.0	0-0.1

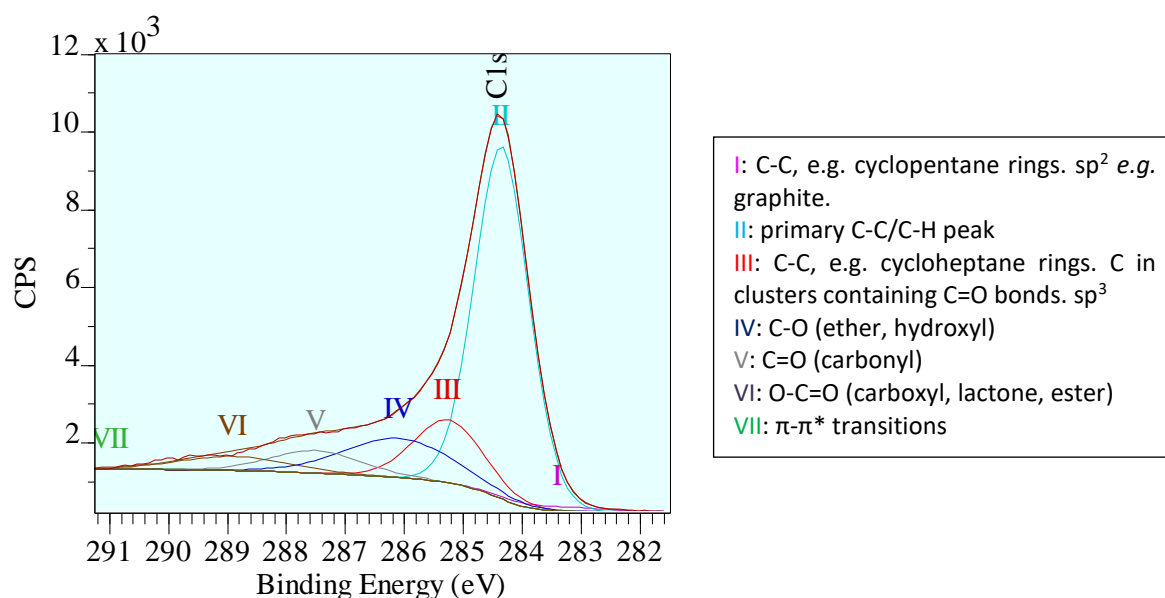


Figure 4-14 Example annotated curve deconvolution for XPS C1s spectra for OSB-700.

XPS C1s spectra were obtained for biochars from three different feedstocks: RHB-550, OSB-700 and WSB-550. These biochars exhibited similar Raman spectra, therefore any differences

in surface carbon were of particular interest. The contribution of each of the carbon bands to the overall C1s peak area were expressed as a percentage; the results are shown in Figure 4-15.

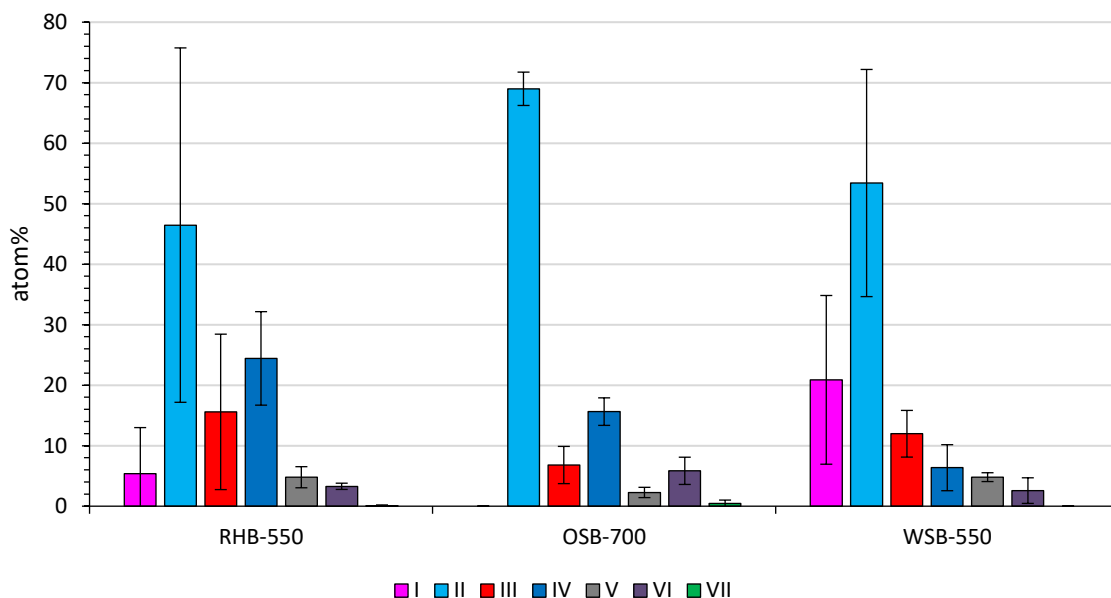


Figure 4-15 XPS C1s curve deconvolution data for biochars from different feedstocks, comparing the contribution from seven C1 bands. Error bars are standard deviation calculated from curve deconvolution of two spectra for each sample.

The XPS C1s data demonstrate that despite similar A_{D1}/A_G ratios measured by Raman spectroscopy, RHB-550 and WSB-550 have differing surface carbon structures. Whilst WSB-550 had the lowest graphiticity measured by Raman, it has the highest contributions from bands I and II, corresponding to graphitic carbon. RHB-550 contains a greater proportion of surface oxygenate groups; band IV is particularly strong for RHB-550, corresponding to C-O groups. There is also an indication of differing aromatic ring size; for RHB-550, the contribution of band III is greater than band I, indicating larger rings such as cycloheptane. For WSB-550, there are more smaller rings from band I, such as cyclopentane. The experimental error however is high, taking into account variation between samples and the reproducibility of the curve deconvolution method.

OSB-700 was prepared at a higher pyrolysis temperature, and has lower contributions from bands I and III, indicating a more regular aromatic six-ring structure. There are also contributions from oxygen-containing groups at the surface, though the contribution of band V (C=O groups) is lower than for the other feedstocks. OSB-700 also has the highest levels of $\pi-\pi^*$ transitions detected. This satellite peak is usually detected in aromatic samples (Serp &

Chapter 4 – Biochar Characterisation

Figueiredo 2009); therefore the results indicate that OSB-700 is the most ordered (graphitic) sample, and WSB-550 the least graphitic. This is consistent with the Raman A_{D1}/A_G ratios presented in Figure 4-13.

A further technique was used to study the effect of feedstock on graphiticity. THz spectroscopic data was collected at the Cavendish Laboratory, University of Cambridge, by Dr James McGregor, and provides an indication of the extent of graphitic networks; higher absorption coefficients corresponds to more extensive graphitic networks. Biochars pyrolysed at 550 °C from four different feedstocks were compared. The results are shown in Figure 4-16.

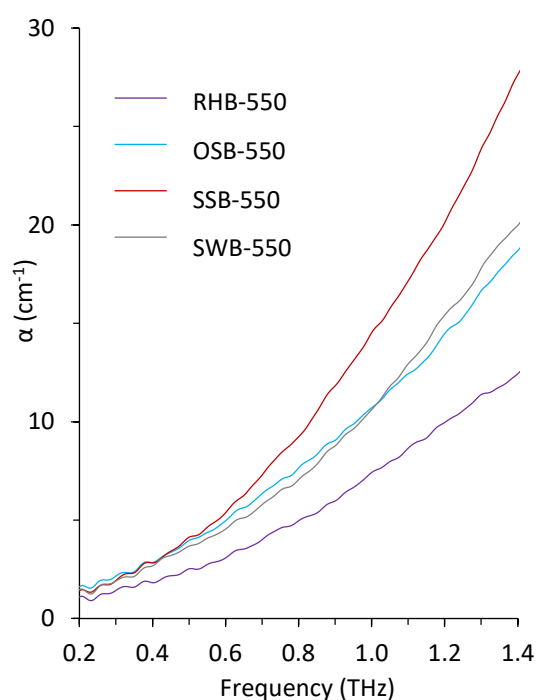


Figure 4-16 THz spectroscopy data for biochars from different feedstocks. Data collected and analysed by Dr James McGregor.

The THz data indicate that absorption coefficients are low for all feedstocks, around 8-15 cm^{-1} at frequencies of 1 THz. In the literature, values of 300 cm^{-1} at 0.5 THz were observed for coked catalysts (Gomez-Sanz *et al.* 2015). Therefore, the feedstock has little effect on the graphiticity of the sample. This is consistent with Raman data, which showed feedstock had little impact on graphiticity. Some differences can be detected: OSB-550 and SWB-550 exhibit similar absorptions across the range of frequencies studied, with SSB-550 the most graphitic and RHB-550 the least graphitic. Pyrolysis temperature however strongly affects the graphiticity of the

samples; this can be seen in the THz spectra in Figure 4-17 for SSB samples pyrolysed at different temperatures.

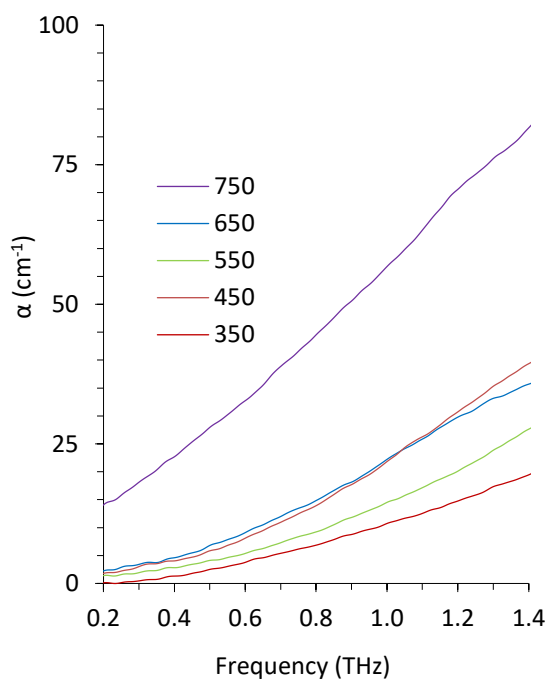


Figure 4-17 THz spectroscopy data for sewage sludge biochar pyrolysed at temperatures from 250-750 °C.

Generally, there is an increase in absorption coefficient and therefore degree of graphiticity with increased pyrolysis temperature, although there are exceptions: SSB-550 has a lower graphiticity than SSB-450, which has a similar graphiticity to SSB-650. This may be due to the inherent heterogeneity of biochar samples. However, there is a notable increase in absorption coefficient for SSB-750. Literature sources also suggest that graphiticity increases with pyrolysis temperature, particularly at temperatures over 700 °C (Gomez-Sanz *et al.* 2015). It would therefore be expected that OSB-700 would have a higher graphiticity than OSB-550.

Chapter 4 – Biochar Characterisation

4.3.5. Summary

Biochars have been characterised using a number of techniques, allowing the structure, elemental composition, surface chemistry and carbon structure to be investigated in detail, before and after various treatments. The key results are summarised in Table 4-8. The possible reasons for these results are discussed in section 4.4.

Table 4-8 Summary of characterisation data for biochars studied in Chapter 4.

Property	RHB-550	OSB-550	OSB-700	WSB-550	SWB-550	AC
STRUCTURE						
BET area/m ² g ⁻¹	121	62.3	107	51.7	390	729
Micropore volume/cm ³ g ⁻¹	3.25E-03	0.00E+00	1.88E-02	2.86E-03	1.05E-01	1.54E-01
Pore volume @ 100 Å/cm ³ g ⁻¹	3.27E-03	2.27E-03	6.48E-04	5.38E-04	1.78E-03	9.15E-02
PROXIMATE COMPOSITION						
Moisture/wt%	2.98	4.25	1.49	1.01	3.52	6.88
Volatile/wt%	9.39	14.4	10.4	12.7	16.7	4.13
Fixed carbon/wt%	44.5	67.4	67.8	67.3	81.7	84.7
Ash/wt%	42.9	13.6	20.3	18.9	0	4.25
SURFACE ELEMENTAL COMPOSITION						
C/at%	67.6	67.8	65.9	69.2	90.4	
O/at%	20.3	12.5	21.9	20.4	9.56	
Si/at%	8.32	1.08	2.83	4.48	0	
K/at%	0.759	17.1	5.85	3.07	0	
Ca/at%	0.261	0	1.12	0.96	0	
Mg/at%	0	0	0.377	0	0	
SURFACE CHEMISTRY						
FTIR functional groups	C≡C, C=C (weak), phenolic (weak), silica	C≡C, C=C, phenolic, silica (weak)	C≡C, C=C, phenolic, silica (weak)	C≡C, C=C, phenolic (weak), silica	C≡C, C=C	C≡C
XPS Bands IV-VI/%	32.5		23.7		13.7	
CO ₂ uptake @ 10 bar/wt%	7.45	9.26			12.1	23.9
CARBON STRUCTURE						
Raman A _{D1} /A _G ratio	1.46	1.39	1.59	1.62	1.32	2.82
THz absorption @ 1 THz	7.40	10.7			10.6	
XPS Band I/%	5.38		0		20.88	
XPS Band VII/%	0.0839		0.457		0	

4.4. Discussion

The characterisation of a range of biochar offers several insights into the wider application of carbonaceous catalysts. The influence of feedstock and pyrolysis temperature provide insights into properties affecting carbonaceous catalyst design, for example how to achieve desired characteristics such as graphitic carbon structure and surface chemistry. This is considered in section 4.4.1. The suitability of biochar for catalytic applications based on the characterisation work completed is considered in section 4.4.2. The implications of this for improving sustainability are discussed in section 4.4.3. Finally the limitations and recommendations for future work are discussed in section 4.4.4, with key conclusions presented in section 4.5.

4.4.1. Implications for carbonaceous catalyst design

The characterisation of the biochars revealed a range of properties, many of which are influenced by feedstock choice and pyrolysis conditions. The factors which influence the properties of biochar have been extensively studied in the literature, particularly the effect of pyrolysis temperature, although this is usually limited to properties influencing their application as soil remediation materials or the optimisation of a particular feedstock for a particular application. The results here are largely in agreement with the literature, for example the finding that surface area, microporosity and ash content increase with pyrolysis temperature (Manyà 2012; Zhao *et al.* 2013); however, some results are worth highlighting in terms of insights for carbonaceous catalyst design.

The choice of feedstock most clearly influences the composition of the biochar, particularly ash content. A range of ash contents were found, from 0-43 wt%. It is also worth noting the increased ash and carbon content of OSB-700 compared to OSB-550 was consistent with literature findings (see section 2.3.1). Similarly, a range of elemental compositions was detected, with elements such as K, Ca and P detected in varying quantities for the different biochars. These elements may contribute to catalytic activity; potassium for example is known to catalyse the pyrolysis of biomass and tar (Mani *et al.* 2013; Perander *et al.* 2015). Therefore, the choice of feedstock for catalyst design should take into account the elemental composition of the biomass.

Chapter 4 – Biochar Characterisation

Similarly, for biochars pyrolysed at the same temperature, a range of surface areas and porosities are recorded, from 50-390 m² g⁻¹. The microporosity of SWB-550 was much higher than that of RHB-550, WSB-550 and OSB-550, for example, with WSB-550 also exhibiting lower mesopore volumes than other feedstocks. Feedstock choice is therefore shown to influence the surface area and porosity of the catalyst – key parameters in heterogeneous catalyst design, which are often tailored using surface treatments.

The presence of mesoporosity and microporosity varied depending on the feedstock used. For example, WSB-550 had the lowest mesopore volume, and no microporosity was detected. This may indicate that shape selectivity could affect the activity of WSB-550; larger molecules for example may be unable to diffuse into and out of the pores. In other samples, such as SWB-550, meso- and microporosity were higher, therefore shape selectivity may not be an issue. Meso- and microporosity is often a key consideration in catalyst design. The choice of feedstock may therefore be worth considering more carefully in terms of the micro- and mesoporosity desired for the application of interest.

There are however properties which are less influenced by feedstock choice, and it is worth noting these common features of biochar catalysts. Macropores were observed in SEM images for all of the biochar samples, with similar pore sizes. This is likely due to the similar scale of plant cells in the raw biomass, which typically range from 10-100 µm. The macropores were however less clear as particle size was decreased. Macropores are of greater importance in soil remediation applications, where they can provide habitats for microorganisms; however, macropores also facilitate gas transport, for example releasing the vapours produced during pyrolysis (Hernandez-Mena *et al.* 2014). They may therefore influence catalytic activity.

Similar surface chemistries and carbon structures were also observed between biochars from different feedstocks. FTIR-ATR spectra of the different biochars were generally comparable, however bands commonly seen in the literature for untreated biochar feedstocks, such as C-O, C=O, O-H and C-H, were not observed here (Manyà 2012; Chia *et al.* 2012; Wei *et al.* 2017). Varying contributions from bands IV-VI were observed in XPS C1s spectra for WSB-550, RHB-550 and OSB-700. This may be because FTIR-ATR is less surface sensitive than XPS, with

estimated penetration depths of 2.01 μm and 1-3 nm respectively. The main difference in the FTIR-ATR spectra was the strength of the silica bands, which was associated with the ash content of the samples. At higher pyrolysis temperatures, the strength of the silica bands in OSB was decreased, despite the increase in ash content as measured by TGA; this may indicate that the silica content was IR-inactive at higher pyrolysis temperatures.

It is worth noting that SWB-550 exhibited a more ordered and graphitic carbon structure than biochars from other feedstocks, as measured by Raman spectroscopy and XPS C1s spectroscopy. This is despite reduced aromatic content as measured by FTIR-ATR and XPS C1s spectroscopy. The reason for this is unclear, as pyrolysis temperature is thought to be a stronger influence on carbon structure (see section 2.3.1). As SWB-550 is the only biochar studied here consisting of only C and O, this may suggest that other elements influence the formation of more disordered carbon, perhaps due to imperfections in the otherwise graphitic structure caused by heteroatoms and ash content. It should be noted however that there is no definitive technique for determining the graphitic character of the biochars, given the different indications from Raman, XPS C1s and THz spectra. This is discussed in section 4.4.4.

Building on the initial schematic of biochar structure given in Figure 2-11, the surface structure of the biochars from different feedstocks can now be visualised. The experimental characterisation work from this chapter is summarised in the schematic in Figure 4-18. The differences in surface structure between RHB-550 and SWB-550 are highlighted. For example, the ash content of RHB-550 was much higher than that of SWB-550, however SWB-550 exhibited a greater extent and quantity of graphitic carbon. The lower ash content is also consistent with the higher micropore volume in SWB-550. Whilst oxygenated functional groups were detected in both biochars, phenolic groups were only detected in RHB-550. This schematic illustrates the key similarities and differences between biochars from different feedstocks, using the experimental data in this chapter.

Chapter 4 – Biochar Characterisation

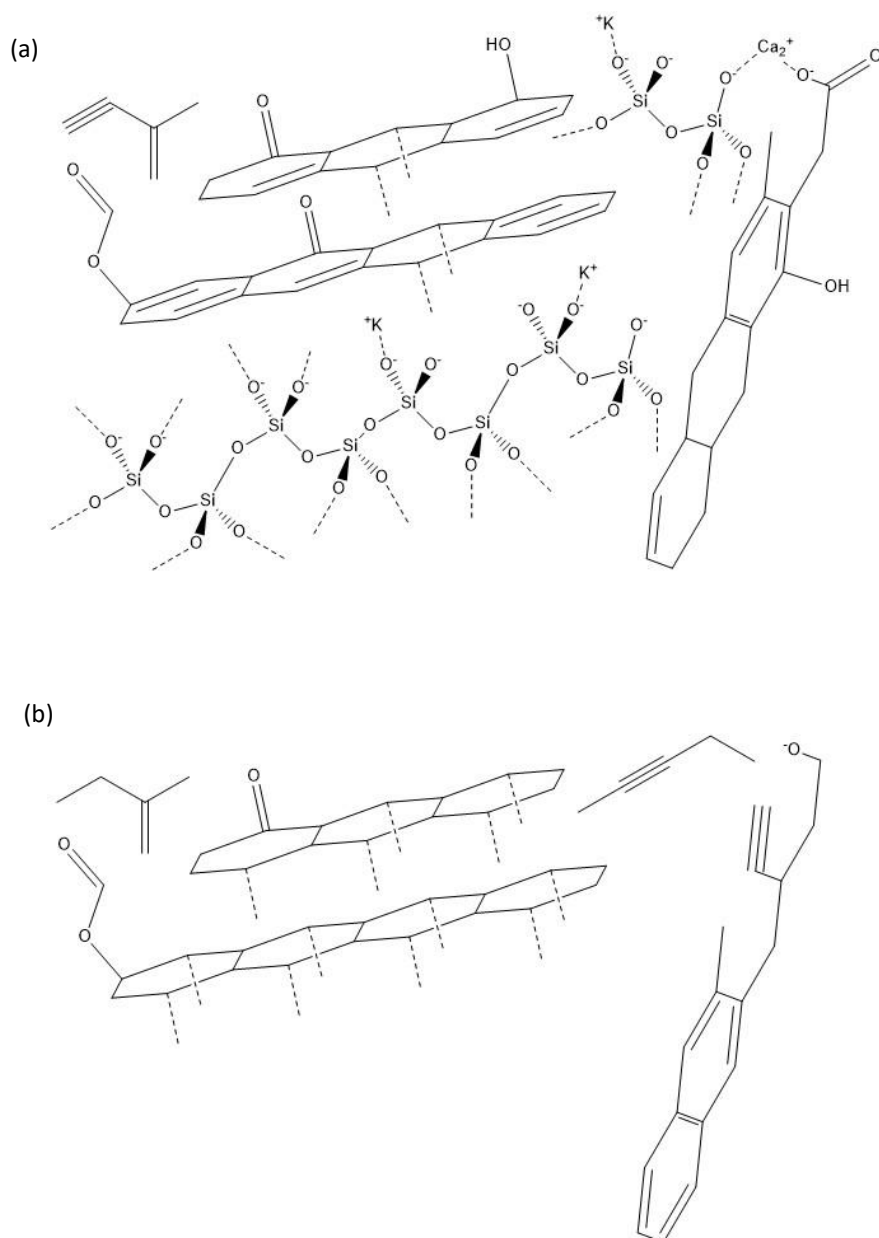


Figure 4-18 Schematic of the surface structures of (a) RHB-550 and (b) SWB-550, using experimental data from Chapter 4.

4.4.2. Implications for catalytic applications

The characterisation of biochars can provide insights into their potential application as catalysts. This includes consideration of key parameters such as surface area, microstructure and surface chemistry, as well as indications of reproducibility.

Potential

The biochars exhibited promising characteristics for application as catalysts. The surface area of over 50 m² g⁻¹ for example is higher than some of those in the literature (Zhao *et al.* 2013);

SWB-550 had a particularly high surface area of $390 \text{ m}^2 \text{ g}^{-1}$. All of the biochars exhibited mesoporosity, with the highest mesopore volume for RHB-550 and lowest for WSB-550. Mesoporosity could be beneficial for avoiding steric hindrance and gas transport limitations. The varied microporosities could lead to varying selectivities, particularly if shape selectivity plays a role.

Influence of ash content

The XPS elemental survey scans demonstrated that ash content is present at the surface of the samples. This may therefore play a role in influencing the catalytic activity of biochars; this is often overlooked in catalytic studies, as discussed in section 2.5.4. Whilst there is also a notable absence of transition metals, which are traditionally used as catalysts, the ash content may be catalytically active. Potassium for example is a known catalyst in tar pyrolysis. The contrast between SWB-550 and RHB-550 may also allow the role of ash content versus carbon content to be considered; SWB-550 was virtually ash-free, whilst the ash content of RHB-550 was very high at 43 wt%. Notably, surface carbon content was similar for the ash-containing samples, ranging from 65-69 at%. SWB-550 likely has a much higher surface carbon content due to the lack of ash.

Variation

As shown by the error analysis, particularly for XPS C1s spectroscopy and Raman curve deconvolution, there is a high degree of error. In these cases, the error has been estimated by analysing two or three areas of a sample, and repeating the curve deconvolution process. The error therefore accounts for variation in the sample, as well as any issues with the deconvolution method. There is evidence that natural variation between samples is responsible for some of the variation. For example, the error for XPS C1s spectra for OSB-700 is much smaller than that for RHB-550, indicating that the error is not solely due to differences in the curve deconvolution method.

This variation within biochar samples may affect the reproducibility of experiments using biochars as catalysts; whilst surface area and mesoporosity appears to be consistent across batches of biochar, as indicated by three repeats of WSB-550, there are clear variations in the

Chapter 4 – Biochar Characterisation

structure and size of individual particles, as shown in SEM images. It is worth noting that bulk analyses were generally reproducible (*e.g.* TGA, BET and FTIR), whilst analyses focused on individual grains were more variable (*e.g.* Raman, XPS). Therefore, whilst samples may look consistent in the bulk, smaller-scale differences could affect the activity of the individual biochar particles, leading to differences in the overall activity of the sample. This is worth bearing in mind when using biochars as catalysts.

Not all properties varied between the biochars; for example, levels of graphiticity were broadly comparable between the biochars, and similar surface functional groups were detected by FTIR-ATR spectroscopy. Some variation in surface C-O, C=O and O-C=O groups was detected by XPS; these groups may act as active sites for reactions, and so the variation in the surface concentration of these groups may influence catalytic activity. In summary, it is expected that not all biochars will be catalytically active for any given reaction, with the variation in surface oxygen groups, elemental composition and structures likely to play a role.

4.4.3. Potential for improving sustainability

Biochars produced from different feedstocks under the same conditions at the same facility have been demonstrated in this chapter to have varying surface compositions, particularly of AAEM elements such as K, Ca and Mg. However, the surface chemistry as detected by FTIR, and the quantity of graphitic carbon as measured by Raman spectroscopy, was comparable. This can be seen in Figure 4-19, where biochars have very comparable A_{D1}/A_G ratios, but where ash content varies widely by feedstock.

As suggested in section 4.4.1, this observation could be used to select the most appropriate feedstock when designing a carbonaceous catalyst. If potassium is detrimental to activity in the reaction of interest, for example, a feedstock such as SWB-550 can be chosen. According to the framework of the twelve principles of green chemistry (Figure 1-1), this would improve the sustainability of the process in accordance with Principle 5 (“the use of auxiliary substances should be made unnecessary”), by eliminating the need for acid treatments to remove trace metal content.

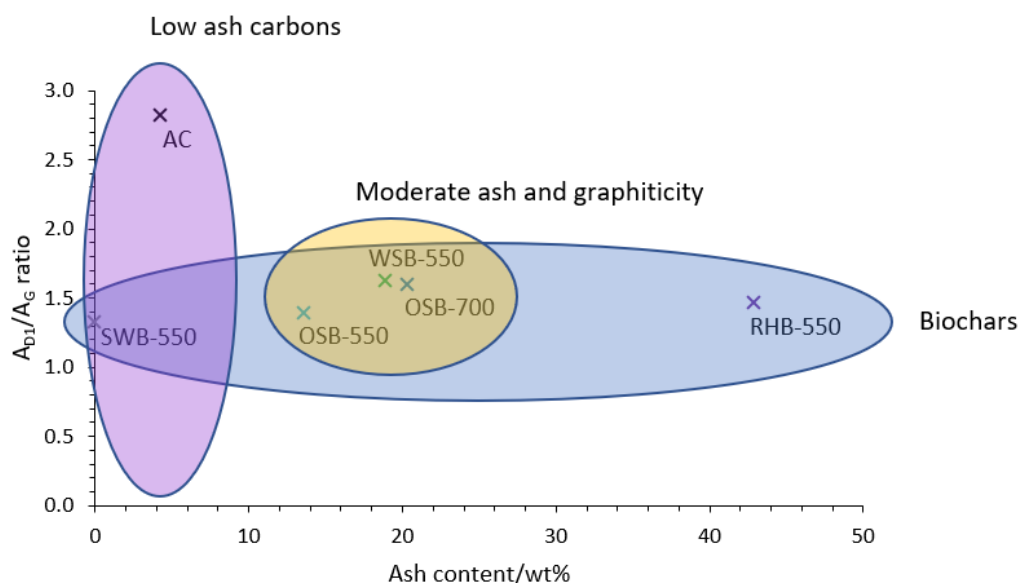


Figure 4-19 Comparison of the proportion of graphitic carbon in biochars as measured by Raman spectroscopy, versus ash content as measured by TGA analysis.

A thorough characterisation of the biochar surface is necessary to analyse which properties of a catalyst are affecting catalytic activity. The results of the experimental work in this chapter will aid the improvement of sustainability by enabling the reaction data from Chapters 6-7 to be interpreted, and will allow the properties influencing selectivity to be identified. This will enable the development of more selective carbonaceous catalysts, and therefore would improve the sustainability of the reaction (Principle 9 of green chemistry – catalysts should be “as selective as possible”).

4.4.4. Limitations and Future Work

Several characterisation techniques have been used to investigate the properties of biochar relevant to catalysis. However, there are improvements which could be made to the analysis techniques used, and additional techniques which could provide additional information relevant to catalysis.

Whilst some of the error in the curve deconvolution of Raman and XPS spectra will be due to natural variations in the samples, inevitably some error will be due to the method of curve deconvolution. For example, parameters such as FWHM were not set for Raman analysis due to a lack of a physical basis; additional peaks such as D3 were not deemed necessary, but may

Chapter 4 – Biochar Characterisation

have improved the curve fit. It is beyond the scope of the current work to perform a detailed analysis of Raman spectra, however there are inevitably further details that could be extracted from more in-depth analysis of the spectra and improved curve-fitting processes. Indeed, methods for curve deconvolution in the literature vary, as highlighted in section 2.5.1.

The calibration of XPS C1s spectra also varies in the literature (see section 2.5.2), with most literature sources using the position of the adventitious carbon peak (284.8 eV) as a reference point for the electron energy in the spectra. However, as shown in the present work, the position of the carbon peak will vary depending on what carbon structures are present. This can clearly affect the curve deconvolution obtained. In this work, the potassium peak was instead used when possible as a reference point; future work may wish to consider using an internal standard for detailed analysis of the C1s peak.

The determination of extent of graphiticity may require further work. In this chapter, several techniques have been used to quantify graphiticity, however the results are not always in alignment. For example, increasing the pyrolysis temperature would be expected to lead to increased graphiticity for OSB-700 compared to OSB-550. This is supported by THz spectroscopy on SSB samples, and the detection of π - π^* transitions in OSB-700. However, FTIR-ATR spectra and Raman spectra indicate a reduction in aromatic bonds for OSB-700, and a decrease in the graphitic G band alongside an increase in band D1. This indicates a reduction in graphiticity. These differences may reflect the varying aspects of graphiticity measured by each technique, for example, THz measures the extent of graphitic networks, whilst FTIR-ATR detects graphitic bonds that are IR-active. The surface sensitivity of the techniques also varies; graphiticity may vary with depth from the surface, meaning each technique will measure different values of graphiticity. There is no definitive technique for measuring graphiticity, as demonstrated by this work, and so care is required in interpreting the data. A combination of techniques is required, and studies may be required on how graphiticity varies in the bulk and at the surface.

Whilst high resolution XPS spectra were obtained for the C1s band, the O1s band could provide more detailed information on the types of C-O bonds present. This could be combined

with TPD measurements to improve knowledge of the surface chemistry of the catalysts, such as surface acidity, basicity and active sites. This is most relevant when optimising catalysts for particular reactions, depending on the active sites required for catalysis. The focus in the present work was on carbon structure, however high resolution O1s could assist investigations into the potential active sites at the surface. It is notable that whilst C-O bands were detected in XPS C1s spectra for the biochars, they were not detected by FTIR-ATR. This may indicate that oxygen is localised at the surface of the biochars, as XPS is much more surface sensitive than FTIR-ATR. Additionally, the possibility of sample contamination cannot be excluded; Cl⁻ for example may be due NaCl transferred from the hands. However, as Na⁺ was not detected, the potential influence of Cl⁻ should be considered when interpreting reaction results.

It is briefly worth noting why different elements were detected for the XPS spectra for OSB-700 and OSB-550. These catalysts were analysed separately, and the raw spectra for OSB-550 was unavailable. The spectra could not therefore be compared to check the identification of the elements. However, the same elements would be expected in both samples, determined by the feedstock used. It is likely that certain elements have been misattributed, for example both Si 2s and Y 3d have binding energies around 160 eV. Without raw spectra, these results are difficult to compare. The variation in the elemental composition is therefore assumed to be an analysis error, which could not be corrected in the present work.

It is also possible that not all mineral elements present in the raw biomass or biochar are present in the ash following combustion. Volatile components may be lost during combustion, for example (Sander & Andrén 1997). However, as trace transition metals were not detected at the surface of the biochars, they are less likely to influence catalytic activity if present.

The FTIR spectra could be improved by performing the analysis under vacuum. CO₂ bands were detected in all spectra, attributed to natural variations in CO₂ in the atmosphere. Performing the analysis under vacuum would purge the atmosphere of CO₂, and eliminate the influence of atmospheric gases on the spectra obtained. *In situ* FTIR, for example DRIFTS analysis, could also be used to test the effect of the reaction atmosphere on the functional

Chapter 4 – Biochar Characterisation

groups detected; for example, in a CO₂ atmosphere, CO₂ may adsorb onto the biochar, changing the potential active sites for catalysis. High resolution FTIR could also determine the mode of adsorption, possibly using ¹³CO₂ for isotopic studies of CO₂ adsorption at the surface. TPD with CO, CO₂ or NH₃ could also provide further information on the types of active sites present at the surface of the biochar.

4.5. Conclusions

The application of biochars as catalysts requires a thorough characterisation of their structure, composition, surface chemistry and carbon structure. In this study, biochars prepared from four different feedstocks were characterised by a variety of methods, and compared with a commercial standard. Carbon structure was characterised in detail, as the potential role of graphitic carbon is often overlooked in catalytic applications.

The key conclusions of the characterisation work were:

- Feedstock influences composition; the biochars exhibited a range of ash contents (from 0 wt% (SWB-550) to 43 wt% (RHB-550)) and compositions. Varying levels of K, Ca, P, Cl, Si and N were detected in surface XPS analysis. Notably, no transition metals were detected in the biochars. Potassium content is of particular interest, as it is known to be catalytically active in biomass and tar pyrolysis. OSB-550 had the highest potassium content (17.1 at%), and SWB-550 the lowest (0.0 at%). As this was detected at the surface, the ash content may influence catalytic activity.
- The biochars exhibited similar surface chemistry. FTIR-ATR spectra mainly varied due to the contribution of silica bands, which varied in strength and position, reflecting the varying contribution of ash to the sample. C≡C and aromatic C=C bonds were detected in all FTIR spectra, with a notable absence of C-O, C=O or C-H bands, indicating the biochars are highly unsaturated. An additional weak phenolic -OH band is detected in OSB-550 and WSB-550. Varying levels of C-O and C=O bands were detected through XPS C1s spectroscopy in RHB-550, WSB-550 and OSB-700; it is possible that these oxygen-containing groups are localised at the surface, and so are not detected by FTIR-ATR.
- Biochars were more graphitic than AC, as measured by Raman spectroscopy, with A_{D1}/A_G ratios of 1.5 compared to 2.8 for AC. Studies also indicated that SWB-550 is the most graphitic of the biochars studied, as measured by Raman and XPS spectroscopy. This may be due to the lack of ash content, as SWB-550 is composed only of C and O; the presence of other elements may lead to imperfections in otherwise graphitic structures.

Chapter 4 – Biochar Characterisation

- Quantification of graphiticity was carried out by several methods, however there was no clear indication across the methods that graphiticity increased with pyrolysis temperature. Whilst a π - π^* transition satellite band was observed in the XPS C1s spectra, and THz spectra for SSB-750 indicated an increase in graphiticity with temperature, Raman spectra indicated increased disordered and decreased graphitic carbon in the OSB-700 sample. There was also very little graphitic Band I detected in the XPS spectra for OSB-700. There is no one technique to measure graphiticity, and a range of methods are required to discern different aspects of graphiticity.
- The relatively high surface areas of the biochars indicate their potential for catalytic applications. Surface areas of at least 50 m² g⁻¹ were calculated for all of the biochars, with SWB-550 having the highest surface area of 390 m² g⁻¹. WSB-550 had the lowest surface area and lowest mesoporosity of the biochars characterised; this may influence activity as well as shape selectivity to reactants.

Three areas were identified for further study. The first was the effect of surface treatments, such as demineralisation, which are often applied to biochar catalysts in order to optimise performance in target reactions. The aim was to identify whether biochars respond differently to surface treatments. Second, the potential influence of organic solvents was studied. Biochar catalysts have not previously been studied *in situ*, however their surface properties may be altered on exposure to organic solvents such as methanol and acetone. The effect of acetone washing on the properties of biochar will therefore be investigated. Thirdly, the potential of potassium and other rare earth and alkali metals to influence carbon structure will be studied. This will build on the literature observation that potassium can catalyse tar pyrolysis, and the results in this work that biochars with no potassium content such as SWB-550 were the most graphitic. This work is presented in Chapter 5. The untreated and treated biochars will then be tested for catalytic activity in two reactions: the conversion of methanol to products (Chapter 6), and the upgrading of glycerol to glycerol carbonate (Chapter 7). The possible contribution of carbonaceous and ash content to the catalytic activity of the biochar samples will be considered.

Chapter 5 – Surface Treatments

Overview

Biochars are diverse carbonaceous materials, with a range of physical and chemical properties. Surface treatments are often studied with the aim of optimising one biochar for a specific application; however, the influence of composition on the effectiveness of these treatments is rarely studied.

In this work, surface treatments are applied to biochars from three different feedstocks, with varying potassium contents: RHB-550 (2.17 at%), WSB-550 (3.07 at%) and OSB-700 (5.85 at%). Demineralisation is used to reduce the ash content of the biochars, and acetone washing is applied to test the effect of organic solvents on biochar properties. A novel liquid phase tar impregnation process is then developed.

The ash content of the biochars was shown to be mostly silica (> 80 at% Si and O). Demineralisation with HCl was therefore of limited success in reducing the overall ash content, with a reduction of only 4.5 % in RHB-550 and 29.9 % in OSB-700. Potassium was completely removed from the biochar surface, with over 80 % removed from the ash. The removal of other AAEM elements varied; this likely depends on the accessibility and solubility of the element (e.g. soluble carbonates in pores vs insoluble phosphates in the bulk). This led to varied effects on surface area and porosity for the different feedstocks.

Acetone washing had similar effects to demineralisation on biochar porosity and surface area, implying a common mechanism of removal of ash from the pore mouths WSB-550 and OSB-700, and possible mesopore mouth blockage from Cl ions or oxygenated groups in RHB-550. Acetone washing did not introduce new functionalities to the surface of the biochars.

Tar loading was performed by diluting pine tar in acetone and contacting with the biochar for 96 hours. The tar loading was estimated using TGA as 10-25 g/100 g of biochar. Conversion of tar during Stage 1 pyrolysis was low, with no overall increase in fixed carbon content detected by TGA. Surface carbon content was shown to increase, using XPS C1s analysis, consistent with the formation of carbon deposits. Carbon deposits were more graphitic in structure for OSB-700, with the highest potassium content. Following demineralisation, none of the biochars increased in graphiticity. This suggests that potassium influences the formation of graphitic carbon.

The modified biochars produced in this chapter will then be studied for catalytic activity in CO₂ utilisation reactions. This is the focus of Chapters 6 and 7.

5.1. Introduction

Biochars are a diverse and versatile source of carbonaceous material for catalyst development. A wide range of feedstocks can be used for the production of biochar, such as plant and municipal waste. As was seen in Chapter 4, these diverse feedstocks influence the composition of the biochars, and even their carbon structures during pyrolysis. Many literature studies focus on optimising one biochar for catalytic application, often as a functionalised carbon or support material; however, the underlying factors influencing the catalytic activity of untreated biochars is poorly understood.

In this chapter, surface treatments are used to modify the properties of biochars, in order to test the influence of individual properties on catalytic activity. Demineralisation will be used to remove mineral and ash content, acetone washing will test whether surface chemistry is affected by the use of biochars in organic solvents, and tar impregnation and pyrolysis will allow the influence of composition on carbon structure to be studied. These modified biochars will then be tested for catalytic activity in two CO₂ utilisation reactions in Chapter 6 and Chapter 7, with the characterisation work in this chapter used to interpret the results.

Biomass ash, in particular potassium, is known to play a role in catalysing the pyrolysis of tar compounds during biomass gasification (Nowakowski & Jones 2008; Trubetskaya *et al.* 2015; Raveendran *et al.* 1995; Jensen *et al.* 1998; Saddawi *et al.* 2012). However, the influence of the feedstock on the structures of carbon deposits formed from the tar has not previously been investigated in detail. Curve deconvolution of Raman spectra for example is rarely carried out, and so detail on the graphitic nature of the carbon structures is limited. In Chapter 4, preliminary results indicated that the carbon structure of SWB-550 was the most graphitic, possibly due to the lack of ash content compared to other biochars. In this work, the carbon deposits formed are extensively characterised, in order to determine the influence of potassium on the graphiticity of the carbon deposits. This could provide insights into how properties of the catalyst affect the structure and therefore catalytic activity of coke formed on heterogeneous catalysts. Insights can also be gained into the design of non-metal-based carbonaceous catalysts.

Chapter 5 – Surface Treatments

To test the influence of potassium and ash content, two methods were used. First, ash samples were produced to enable the influence of potassium to be tested separately from the carbon. A demineralisation method was then developed based on literature sources, as described in section 3.2.1, to remove potassium from the biochars. Hydrochloric acid was chosen due to having fewer detrimental effects on the structure of biochar, as well as for the ease of removal of excess Cl^- ions.

A novel liquid phase tar impregnation method is then developed, in collaboration with the UK Biochar Research Centre at the University of Edinburgh. Existing methods often use gas-phase naphthalene, with specialised experimental set-ups to introduce the naphthalene to the biochars; this equipment was not available, and so a simple liquid-phase method was developed. The tar was diluted in acetone, therefore a control test was used to identify the influence of acetone washing on biochar properties. This also provides insights into how the properties of biochar catalysts can be altered on contact with organic solvents in reaction media. The effectiveness of tar impregnation was tested using TGA, and the tar was then pyrolysed in a Stage 1 unit over three feedstocks with varying levels of potassium content. The subsequent carbon deposits formed on the biochars are then characterised, to identify the influence of feedstock and effect of demineralisation on the effectiveness of tar impregnation, pyrolysis and subsequent carbon structure.

The experimental methods used in this chapter are first outlined in section 5.2, including a brief summary of characterisation techniques from Chapter 4 and detailed descriptions of the surface treatments used. The results are presented in section 5.3 and are divided into four sections. The effect of demineralisation on the properties of the biochars is first considered in section 5.3.1, followed by the impact of acetone washing in section 5.3.2. The effectiveness of tar impregnation is considered in section 5.3.3, and the effect of demineralisation on tar pyrolysis is considered in section 5.3.4. The implications of the results are then discussed in section 5.4, particularly in terms of future catalytic design and catalytic applications. The conclusions are then summarised in section 5.5.

5.2. Methods

Several characterisation and surface treatment techniques were used in the experimental work. Sample characterisation and error analysis was generally performed as described in Chapter 3; where the same technique is used, a summary is provided here for ease of reference. The sample preparation protocols are presented in section 5.2.1, followed by a summary of the characterisation techniques in section 5.2.2. The surface treatment protocols are then outlined in section 5.2.3.

5.2.1. Sample preparation

Samples of biochar were prepared as in Chapter 4, by crushing pellets in a pestle and mortar, followed by sieving to particle sizes of $< 90 \mu\text{m}$ in diameter. The preparation of demineralised and tar-impregnated samples was performed at the University of Edinburgh, where particle sizes between 1.0-1.5 mm were chosen, due to the limited availability of smaller sieves. The impact of this on the results is discussed in section 5.4.7.

Ash samples were prepared by combustion of biochar, using a Carbolite box furnace. Approximately 2 g of sample was placed in a ceramic crucible, and heated to $900 \text{ }^\circ\text{C}$ for 30 mins. This temperature was consistent with the final temperature of the TGA analysis methods, and allowed larger samples of ash to be prepared for further analysis.

5.2.2. Characterisation methods

Characterisation of the biochars was generally performed using the same methods as outlined in Chapter 4. This allowed the impact of surface treatments on the properties of biochar to be evaluated. Where the same characterisation techniques were applied, brief details are provided here for ease of reference; the full protocols can be found in section 4.2.

5.2.2.1. Structure

The structure of the biochars was determined through BET analysis, using a Micromeritics 3Flex instrument. This was used to obtain BET isotherms, with Micromeritics 3Flex software used to obtain t-plots and NLDFT pore size distributions for the biochars studied.

Chapter 5 – Surface Treatments

For SEM analysis, biochar powder was mounted on an aluminium sample stub using a carbon adhesive tab. The stubs were sputter-coated with a layer of gold approximately 10 nm thick. SEM images were obtained at magnifications from $\times 50$ - $\times 5000$, for at least three areas per sample. EDX was performed on the samples at magnifications of $\times 1000$.

5.2.2.2. Composition

Elemental composition was determined through XPS elemental survey scans, as described in Chapter 4. Ash samples were also analysed using the same methods for data collection and analysis.

Proximate analysis and pyrolysis simulations were carried out through TGA both at the University of Sheffield and at the University of Edinburgh. The analysis methods used at each institution were based on industrial standards for biochar analysis (ASTM International 2010), however there are some differences in the proximate analysis methods and the instruments used. The techniques used at each institution are outlined separately below, followed by a comment on the differences between the methods.

University of Sheffield

Experiments at the University of Sheffield were carried out as described in Chapter 4, using a Perkin Elmer TGA (model 4000). Approximately 15-20 mg of powdered sample were loaded into an alumina crucible, with tap water used to cool the instrument. Proximate analysis was carried out as shown in Table 5-1 (step 6 onwards).

An integrated pyrolysis and proximate analysis method was developed, and is shown in Table 5-1. This allowed the ash content of the biochar after pyrolysis to be determined. To simulate the Stage 1 pyrolysis unit used for the experimental work, a heating rate of $10\text{ }^{\circ}\text{C min}^{-1}$ was used. The pyrolysis simulation method was performed in a nitrogen atmosphere and consisted of a temperature ramp to $550\text{ }^{\circ}\text{C}$, one hour hold time at $550\text{ }^{\circ}\text{C}$, followed by cooling to room temperature. The biochar yield from pyrolysis was calculated as the percentage mass remaining after step 5, compared to the initial mass of biochar. Proximate analysis then followed from step 6, using the same method as in Chapter 4.

Table 5-1 TGA Pyrolysis/Proximate Analysis method at the University of Sheffield, using Perkin Elmer TGA 4000.

Step	Temperature/°C	Time/mins	Ramp/°C	Heating rate/°C min ⁻¹	Gas	Flowrate/ml min ⁻¹
1	30	5			N ₂	20
2			25-550	10	N ₂	20
3	550	60			N ₂	20
4			550-25	-100	N ₂	20
5	30	10			N ₂	20
6	30	2			N ₂	20
7			25-110	50	N ₂	20
8	110	5			N ₂	20
9			110-900	100	N ₂	20
10	900	5			N ₂	20
11	900	5			O ₂	50

University of Edinburgh

The instrument used at the University of Edinburgh was a TGA/DSC 1 STAR^e System fitted with Gas Controller GC100, from Mettler Toledo. 150 µl alumina crucibles were used for most samples. For the tar-impregnated samples, 30 µl platinum crucibles were used, to avoid tar becoming impregnated in the porous ceramic crucibles. Preliminary experiments demonstrated that the choice of crucible did not affect the results (see Appendix A). Around 20 mg of each sample was added to the crucibles.

The method used for proximate analysis is detailed in Table 5-2 and comprised a simple temperature ramp under nitrogen flow (around 50 ml min⁻¹) to reach 110 °C. The temperature was held at 110 C for 10 mins, before heating to 900 °C and holding for 30 minutes. The gas flow was then changed to air (50 ml min⁻¹), and the sample was burned for 30 mins. Moisture, volatiles, fixed carbon and ash content were calculated as in Chapter 4.

Table 5-2 TGA Proximate Analysis method for the University of Edinburgh, using TGA/DSC 1 STAR^e System.

Step	Temperature/°C	Time/mins	Temperature ramp/°C	Heating rate/°C min ⁻¹	Gas
1	25	2			N ₂
2			25-110	25	N ₂
3	110	10			N ₂
4			110-900	25	N ₂
5	900	30			N ₂
6	900	30			Air

The experimental error was calculated using two repeats of WSB-550-DM-T-C, analysed at the University of Edinburgh. The average and standard deviation for the moisture, volatile,

Chapter 5 – Surface Treatments

carbon and ash content were calculated, and the standard deviation was expressed as a percentage. This was then used to plot error bars on subsequent TGA spectra.

Comparison between proximate analysis methods

The main difference between the proximate analysis methods was the timings. The instrument at the University of Edinburgh could be used for batch processing of multiple samples overnight, allowing longer methods to be used without compromising on efficiency. At the University of Edinburgh, analysis of one sample required 2 hours, whereas at the University of Sheffield, samples could be run in 30 mins by using shorter hold times and faster heating rates. The results from each method were comparable, as demonstrated in Appendix A .

The starting temperature of the method was slightly higher (30 °C) for the University of Sheffield, as the cooling system was less efficient. 30 °C was considered a safe starting temperature, and again maximised the time efficiency of the experiment.

Finally, air was used for combustion in Edinburgh, whereas oxygen was used for combustion in Sheffield. Both air and oxygen are acceptable for combustion in the standard test methods (ASTM International 2010), however the use of oxygen at the University of Sheffield allowed shorter hold times to be used for combustion.

5.2.2.3. Surface chemistry

Surface chemistry was studied using FTIR-ATR spectra, collected using an IR-Affinity spectrometer and Specac Quest ATR accessory. As in Chapter 4, 16 spectra were collected and averaged to give an overall spectrum for each biochar. Data from high resolution XPS C1s spectroscopy and Raman spectroscopy also gave insights into oxygen-containing functional groups (see section 5.2.2.4).

5.2.2.4. Carbon structure

In addition to FTIR-ATR spectroscopy, two techniques were used for the characterisation of carbon structure: Raman spectroscopy, or analysing the ratio of graphitic to disordered

carbon, and high resolution XPS C1s spectroscopy, for surface-sensitive data on the carbon species present in the biochars. Curve deconvolution and error analysis was carried out for both Raman and XPS C1s spectra, following the methods developed in Chapter 4.

5.2.3. Surface treatments

In order to test the influence of individual factors in the catalytic activity of the biochars, surface treatments were applied. It is worth emphasising that the objective of these treatments was not necessarily to improve the activity of the biochars; for example, demineralisation tested whether ash content contributes to catalytic activity. The demineralisation method was developed based on the literature and is outlined in section 5.2.3.1; the technique for acetone washing is outlined in section 5.2.3.2; the liquid phase tar impregnation method develop is outlined in section 5.2.3.3; and the stage I pyrolysis protocol is outlined in section 5.2.3.4.

5.2.3.1. Demineralisation

Based on previous methods for the removal of ash content from biochar (see section 3.2.1), the following method was developed. A 3 M solution of hydrochloric acid was prepared from a 12 M solution. 200 ml of solution was added to 40 g of crushed and sieved biochar (0.5 – 1.0 mm), and heated and stirred for approximately 36 hours at 60 °C. The solution was then filtered and rinsed with deionised water, and dried overnight in an oven at 105 °C. The sample was then washed further in approximately 500 ml of hot deionised water (80 °C) for 2 hours, and then filtered and rinsed with deionised water to remove any Cl⁻ ions. The rinsing continued until the washing water was free of Cl⁻ ions, detected by adding a few drops of 0.1 M silver nitrate solution; the formation of a white precipitate indicated that Cl⁻ ions were present. The samples were then dried in an oven at 105 °C overnight.

5.2.3.2. Acetone washing

For the tests of the effect of acetone washing on biochar properties, 20 g of biochar were washed in a sealed beaker containing 200 ml acetone for 12 hours. The mixture was stirred at approximately 700 rpm using a magnetic stirrer. The samples were filtered and then left to

Chapter 5 – Surface Treatments

air dry in a fume cupboard for 24 hours, to allow excess acetone to evaporate, before being transferred to a drying oven at 110 °C for 72 hours.

5.2.3.3. Tar impregnation

No liquid-phase methods for the impregnation of biochar with tar were found in the literature – previous studies introduced gaseous naphthalene or toluene as model tar compounds (Frazier *et al.* 2015; Qian *et al.* 2015; Zhang *et al.* 2014). The following method for tar impregnation would allow experiments to be performed with realistic liquid tars.

As tar is very viscous, the tar was diluted in acetone to enable effective mixing with the biochar. 20 g of tar were dissolved in 200 ml of acetone, using a magnetic stirrer, and then 20 g of biochar was added. The beaker was covered in parafilm to prevent the evaporation of acetone, and the mixture was stirred continuously at approximately 700 rpm for 96 hours, allowing plenty of time for the tar to impregnate the biochar. The sample was then filtered without washing, to prevent removal of the tar from the biochar, and dried overnight in an oven at 105 °C. The sample formed a solid disc on the filter paper, which was crushed in a pestle and mortar to form a more uniform powder for pyrolysis and further analysis.

5.2.3.4. Pyrolysis of tar

The tar-impregnated biochar samples were pyrolysed in the Stage I pyrolysis unit at the UK Biochar Research Centre, described in section 3.2.4. Approximately 15 g of tar-impregnated sample was added to the quartz tube and heated in an infrared furnace to 550 °C under nitrogen flow at a rate of 10 °C min⁻¹. The temperature was then held at 550 °C for 1 hour before cooling to room temperature. Liquid products were condensed and collected, with off gases released through the ventilation system. A carbon monoxide monitor was used to ensure that the working environment was safe.

5.3. Results

Three surface treatments were applied to the biochars, and the properties of the biochars were compared before and after treatment. This allowed the effect of the treatments to be evaluated. Demineralisation with HCl was first performed, with the results presented in section 5.3.1. The biochars were then contacted with acetone and dried, before studying the changes in biochar properties. This is presented in section 5.3.2. The biochars were then impregnated with tar and pyrolysed. The results regarding the effectiveness of the tar loading process are presented in section 5.3.3, and the results for the effect of demineralisation on tar impregnation and pyrolysis are shown in section 5.3.4. The results are summarised in section 5.3.5 before being discussed in section 5.4.

5.3.1. Effect of demineralisation

The aim of demineralisation with HCl was to reduce the ash content of the samples, and particularly the AAEM content. The effectiveness of demineralisation in reducing ash content was investigated through TGA proximate analysis, allowing the ash content to be quantified before and after demineralisation. The wt% ash in each sample, and the calculated % ash removed, are presented in Table 5-3.

Table 5-3 Ash content of biochars before and after demineralisation, measured using TGA.

Biochar	wt% ash		% ash removed
	Untreated	Demineralised (-DM)	
RHB-550	42.03%	40.13%	4.50%
OSB-700	20.26%	14.20%	29.91%
WSB-550	18.91%	13.76%	27.26%

The results in Table 5-3 demonstrate that ash content was reduced through demineralisation, however the effectiveness varied in different feedstocks. For example, the ash content of RHB-550 was reduced by only 4.50 wt%, whilst a 29.91 wt% reduction was achieved in OSB-700. This indicates that some components of the ash have been successfully removed, whilst others remain. XPS survey scans were therefore undertaken to study which components of the ash had been removed. Ash samples were prepared as described in section 5.2.1, and the composition of ash from untreated and demineralised samples was compared. The results of the XPS analysis are presented in Figure 5-1.

Chapter 5 – Surface Treatments

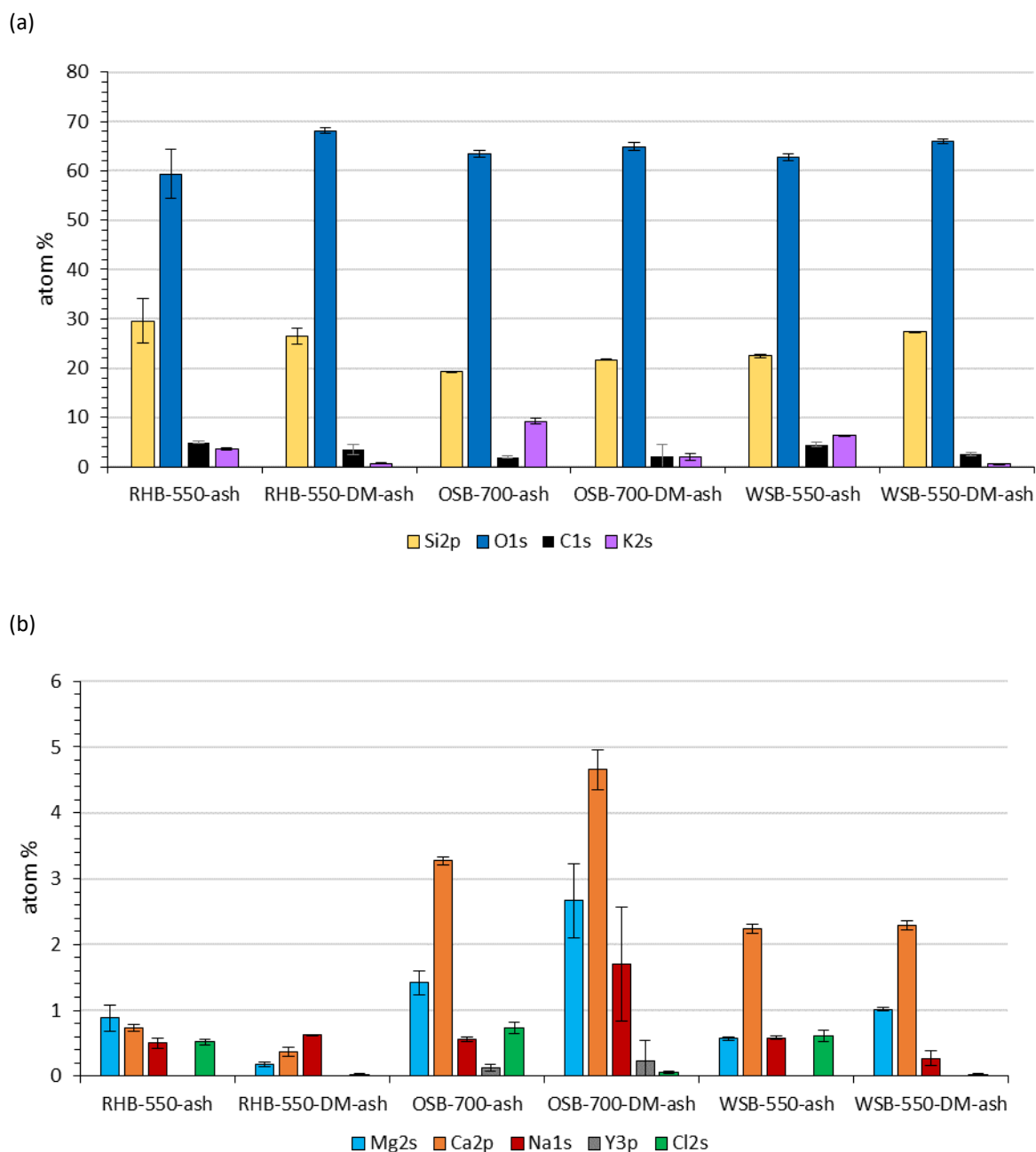


Figure 5-1 Composition of ash samples from untreated and demineralised biochars. (a) shows main components of the ash, with trace components (<5 at%) shown in (b). -DM indicates demineralised biochar.

The XPS analysis demonstrates that many of the components are still present in the ash of the demineralised samples. The largest contribution to the ash content is Si and O, indicating that the main component of the ash is silica, and is unaffected by demineralisation. The contribution from Si and O is slightly higher after demineralisation, most likely as a consequence of other components being removed. Small quantities of carbon (<5 at%)

remain in the biochar ash following combustion, either due to adventitious carbon peaks or due to incomplete combustion.

As the ash samples are effectively bulk samples, it was also important to study the surface composition of the untreated and demineralised biochars. This allowed the effect of demineralisation to be evaluated at the surface and in the bulk, and to determine the actual composition of the surface for catalysis. As in Chapter 4, the analysis of the ash samples enhanced confidence in the identification of trace elements in the chars. The composition of the key elements of interest is presented in Figure 5-2.

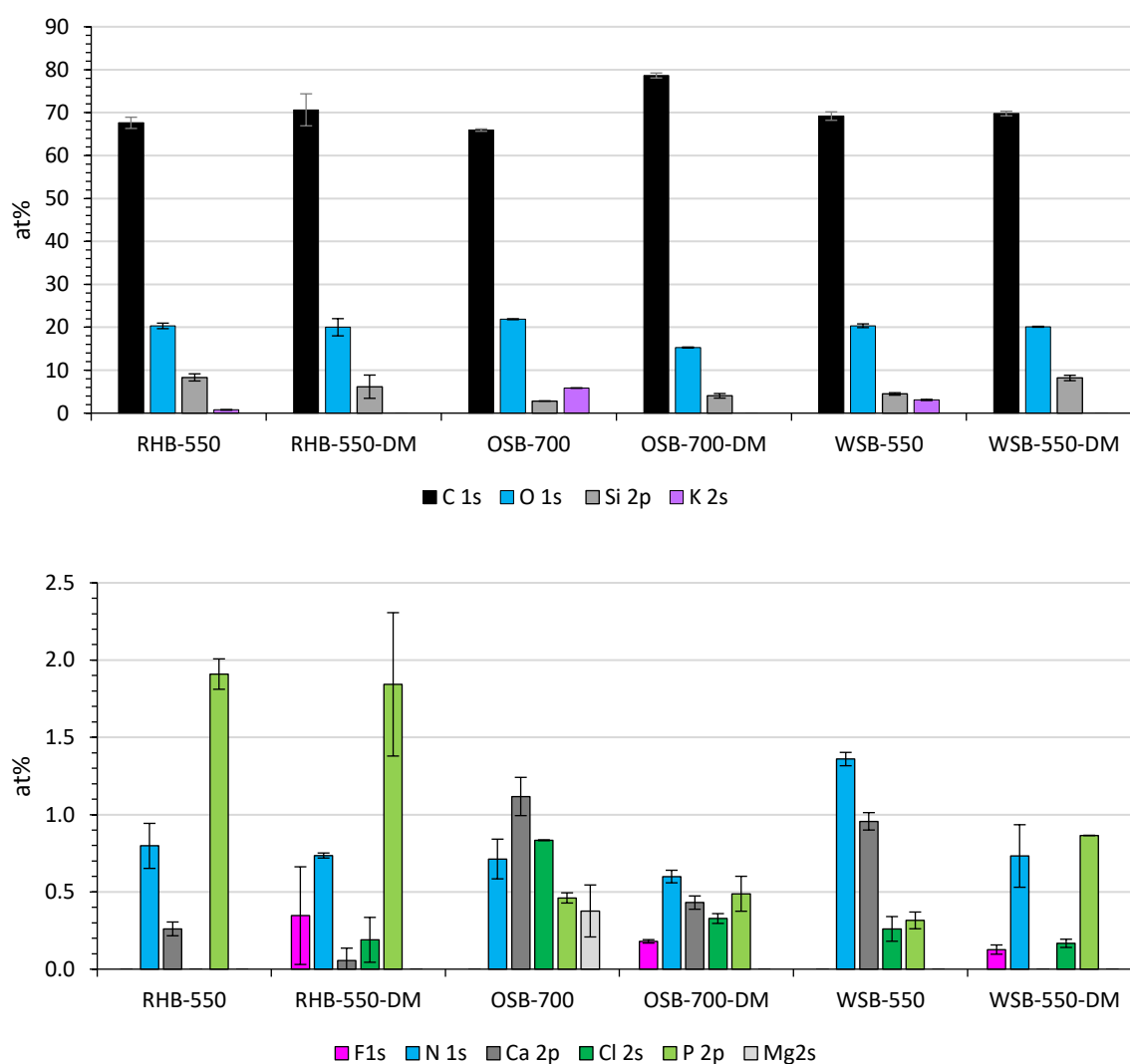


Figure 5-2 Quantities of key elements of interest in biochars before and after demineralisation, as measured by XPS elemental survey scans. Error bars are standard deviations based on measurements of two areas of the sample (negligible error detected for P 2p for WSB-550-DM). -DM indicates demineralised sample.

Chapter 5 – Surface Treatments

Following demineralisation, the surface composition remains largely composed of carbon oxygen and silicon. The overall carbon content is seen to increase within experimental error for WSB-550 and RHB-550, and increase by 12.7 at% for OSB-700. This increase is likely due to the removal of other elements. Elements not present in the ash include phosphorous and nitrogen, neither of which are removed from the surface by demineralisation. Experimental variation is high, however the surface nitrogen content is decreased in all samples, most notably with a 50 % reduction in WSB-550. Fluorine is also detected in the demineralised samples, possibly indicating contamination with tap water – this is discussed in section 5.4.1.

AAEM elements such as K, Ca and Mg are removed to differing extents in the bulk and at the surface of the biochars. A comparison of the removal of AAEM elements from the ash and from the char surface are presented in Table 5-4. The only element consistently removed from the surface is potassium, which is also reduced by 80 at% in the bulk ash content of RHB-550 and OSB-700, and by 90 at% in WSB-550. Surface concentrations of Ca and Mg are reduced in all cases, but not entirely removed; the ash analysis in Figure 5-1 demonstrates that Ca and Mg are only reduced in the bulk of RHB-550.

Table 5-4 Quantities of AAEM elements detected by XPS analysis of chars and ash samples from three feedstocks. -DM indicates demineralised sample.

	K				Ca				Mg			
	Surface		Bulk		Surface		Bulk		Surface		Bulk	
	char at%	% removed	ash at%	% removed	char at%	% removed	ash at%	% removed	char at%	% removed	ash at%	% removed
RHB-550	0.759	100.00	3.498	81.61	0.261	78.38	0.738	49.44	0.000	N/A	0.883	79.41
RHB-550-DM	0.000		0.643		0.056		0.373		0.000		0.182	
OSB-700	5.852	100.00	9.228	79.37	1.118	61.45	3.274	-42.29	0.377	100.00	1.420	-87.71
OSB-700-DM	0.000		1.904		0.431		4.658		0.000		2.665	
WSB-550	3.074	100.00	6.290	89.46	0.957	100.00	2.236	-2.48	0.000	N/A	0.569	-77.92
WSB-550-DM	0.000		0.663		0.000		2.292		0.000		1.013	

As demineralisation was achieved through the use of HCl, the quantity of Cl after demineralisation is of interest. As seen in Figure 5-1, bulk Cl content is reduced after demineralisation in all samples. Figure 5-2 similarly shows a reduction in Cl at the surface, although not a complete removal; indeed the Cl content in RHB-550 increases following

demineralisation. The possible sources of Cl contamination, and the implications of these results for the success of the washing process are discussed in section 5.4.1.

BET analysis was next performed to quantify the effect of ash removal on porosity and surface area. The BET surface areas for the samples before and after demineralisation are shown in Figure 5-3.

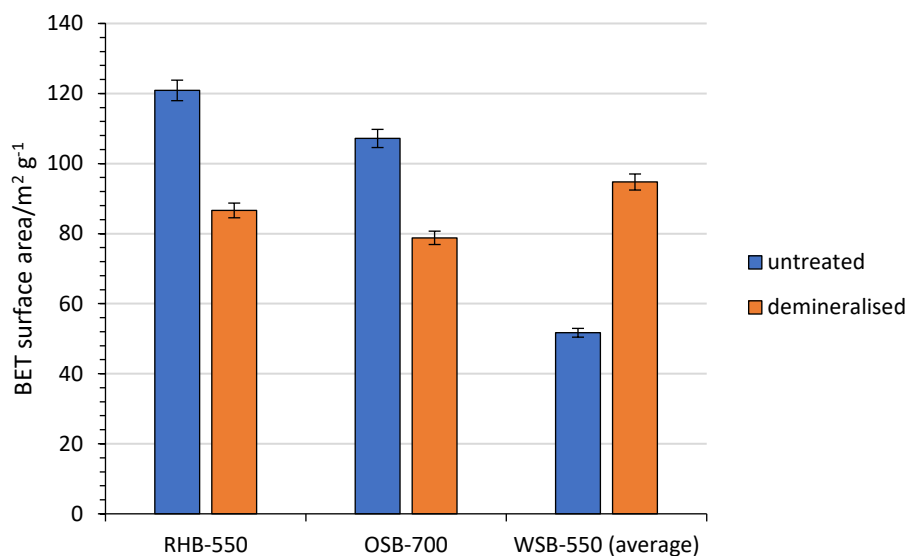


Figure 5-3 BET surface area for biochars before and after demineralisation. Error bars based on percentage error of 2.42% calculated from three repeats of WSB-550.

The BET isotherm data did not indicate a clear trend on the effect of demineralisation on the biochars. Whilst for RHB and OSB the surface area decreased, the surface area almost doubled for WSB. It should be noted that the demineralised samples were comprised of a larger particle size, as discussed in 5.2.1. Notably, the surface areas of the biochars from different feedstocks are comparable after demineralisation.

The micropore volumes calculated from t-plots are shown in Figure 5-4. For RHB-550 and OSB-700, the micropore volume is decreased, and markedly so for OSB-700. However, the micropore volume in WSB-550 is largely unaffected, remaining within experimental error before and after demineralisation.

Chapter 5 – Surface Treatments

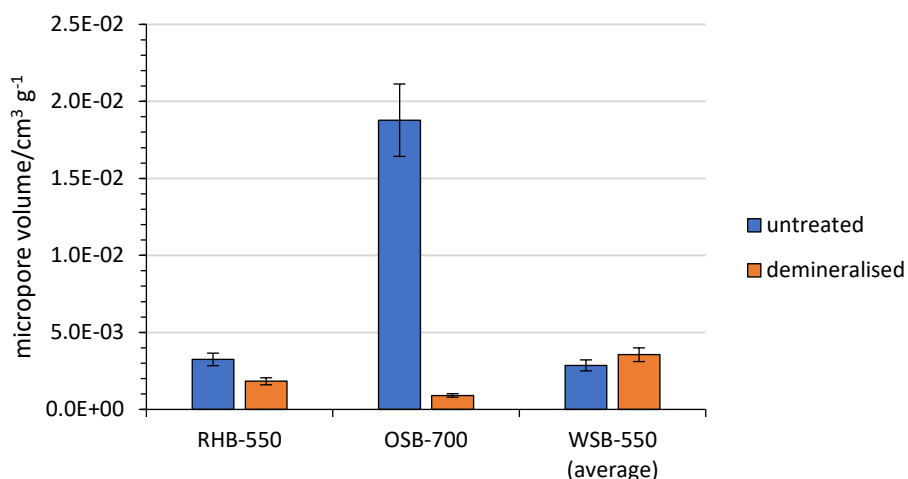


Figure 5-4 Micropore volume of biochars from different feedstocks before and after demineralisation. Percentage error of 12.5 % calculated from two repeats of WSB-550 (third anomalous value omitted).

Mesoporosity was investigated by considering pore size distributions, calculated using a commercial NLDFT model. PSDs are shown for WSB-550, RHB-550 and OSB-700 before and after demineralisation in Figure 5-5.

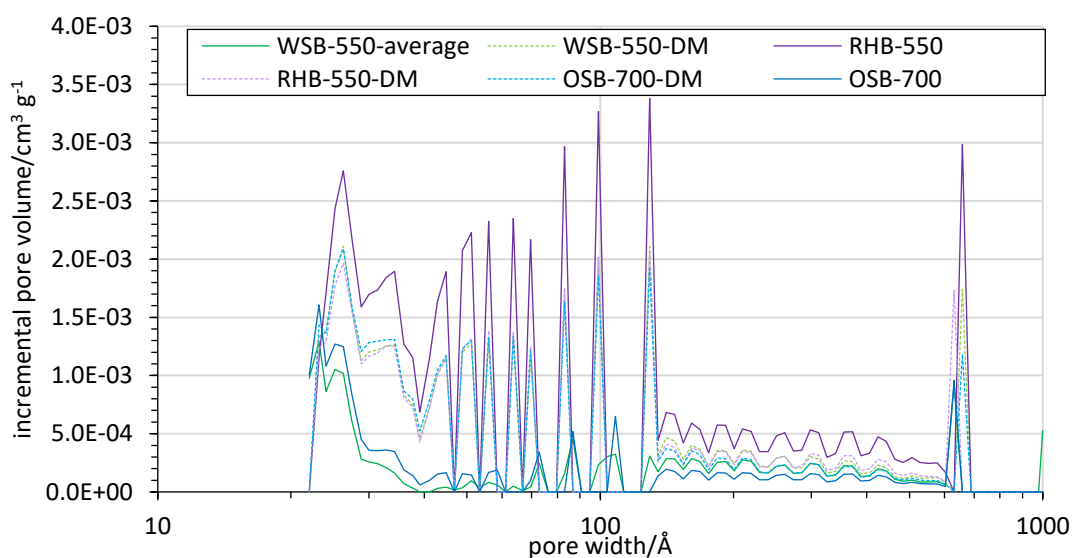


Figure 5-5 Pore size distribution for biochars from different feedstocks before and after demineralisation.

The effect of demineralisation on mesoporosity appears to be feedstock-dependent. The untreated feedstocks exhibited characteristic patterns, particularly in the region 20-100 Å. However, the mesopore volumes of the demineralised samples are comparable across the range of mesopores. Mesopore volume decreases for RHB-550, but increases for OSB-700 and WSB-550, indicating that demineralisation has a different dominant effect on RHB-550.

The effect on macroporosity was briefly considered through SEM imaging of the biochar surfaces. As shown in Figure 5-6, the macroporous structure was retained in the biochars following demineralisation. The results of quantitative EDX analysis were broadly in agreement with XPS analysis, with differences attributable to the use of carbon adhesive tabs and gold coating; these results can be found in Appendix B .

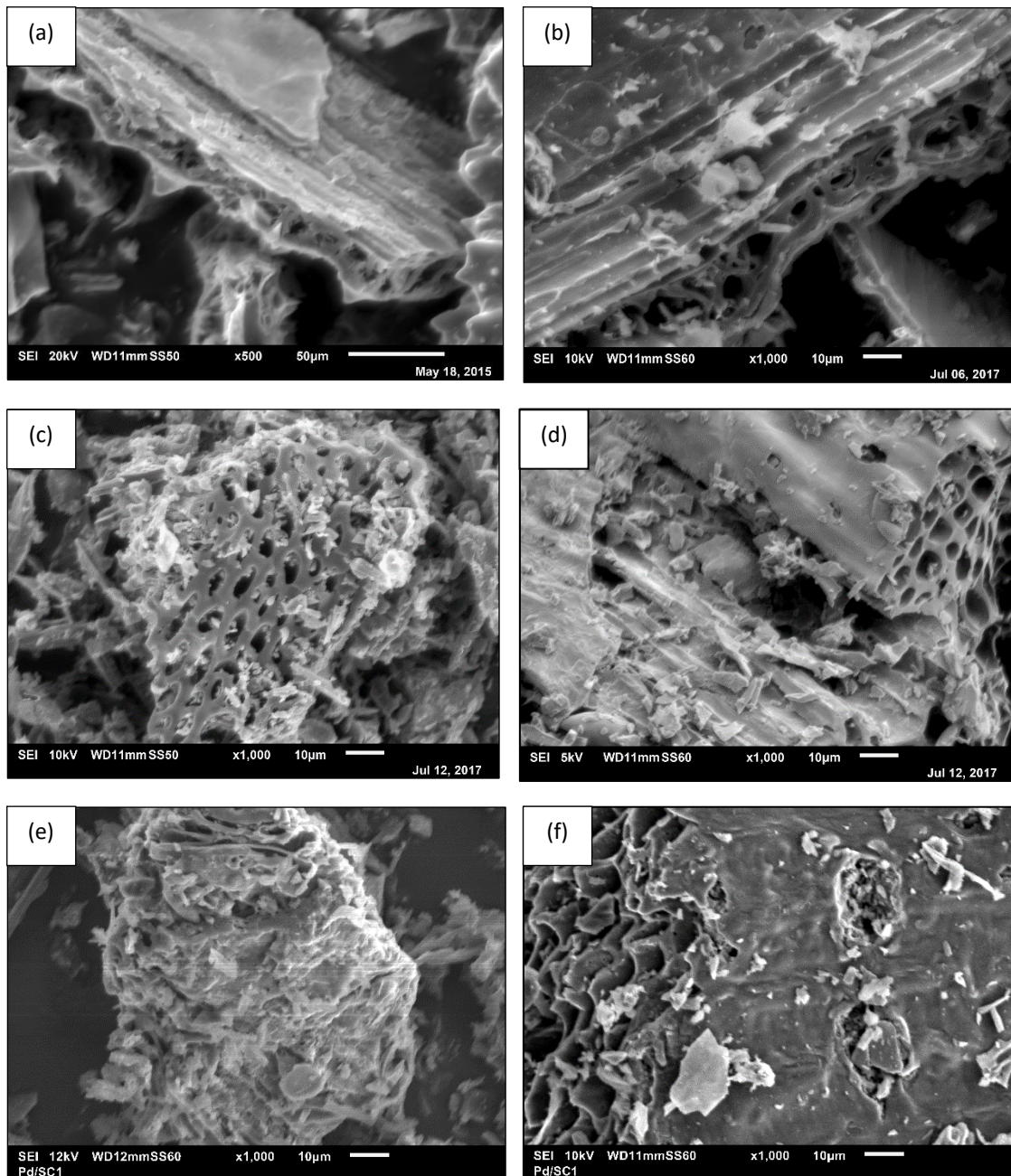


Figure 5-6 SEM images of biochar grains before and after demineralisation. Two different areas imaged for each sample. Top: (a) RHB-550, (b) RHB-550-DM, middle: (c) OSB-700, (d) OSB-700-DM, bottom: (e) WSB-550, (f) WSB-550-DM.

Chapter 5 – Surface Treatments

Whilst the focus of demineralisation was on reducing ash content and removing trace metal content, the impact on carbon structure and surface chemistry was also measured and is briefly considered here. From FTIR-ATR spectra, Raman spectra and XPS C1s spectra it is notable that there were few consistent changes in surface chemistry or carbon structure following demineralisation. No new surface functional groups were introduced, although there is a slight reduction in phenolic O-H bending in all samples, as seen in FTIR-ATR spectra. In terms of carbon structure, the effect on graphiticity and surface oxygen groups was observed to vary; as shown in the deconvolved XPS C1s data in Figure 5-7, for example, band IV increased WSB-550, decreased in RHB-550, and was unchanged in OSB-700. There is an increase in the contribution from band III, in most cases, corresponding to seven-membered rings and greater, and band VII, corresponding to increased π - π^* transitions. However, the experimental error associated with curve deconvolution is high.

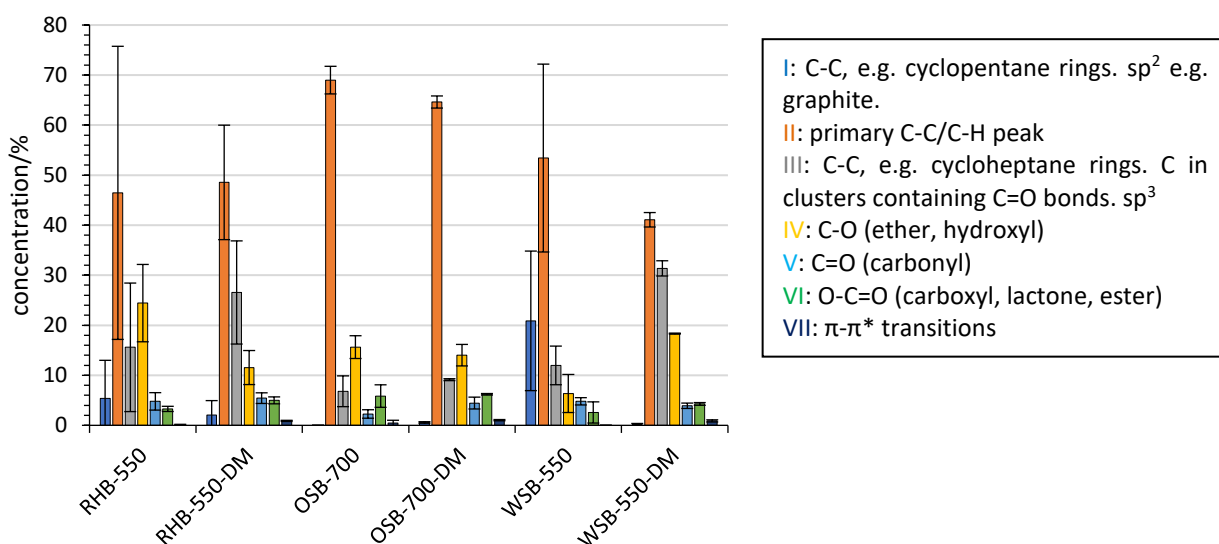


Figure 5-7 XPS C1s curve deconvolution data for biochar samples before and after demineralisation.

Further data on the differing impacts of demineralisation on carbon structure can be found in Appendix B.

5.3.2. Effect of acetone washing

The properties of biochar after exposure to organic solvents have not previously been tested in the literature; however, this can provide important information on their *in situ* properties for catalytic applications. The properties of biochar were therefore tested after exposure to acetone, in terms of changes in surface area, porosity and surface chemistry. This also allowed the effects of tar impregnation to be isolated from those of the acetone solvent used, in sections 5.3.3 and 5.3.4.

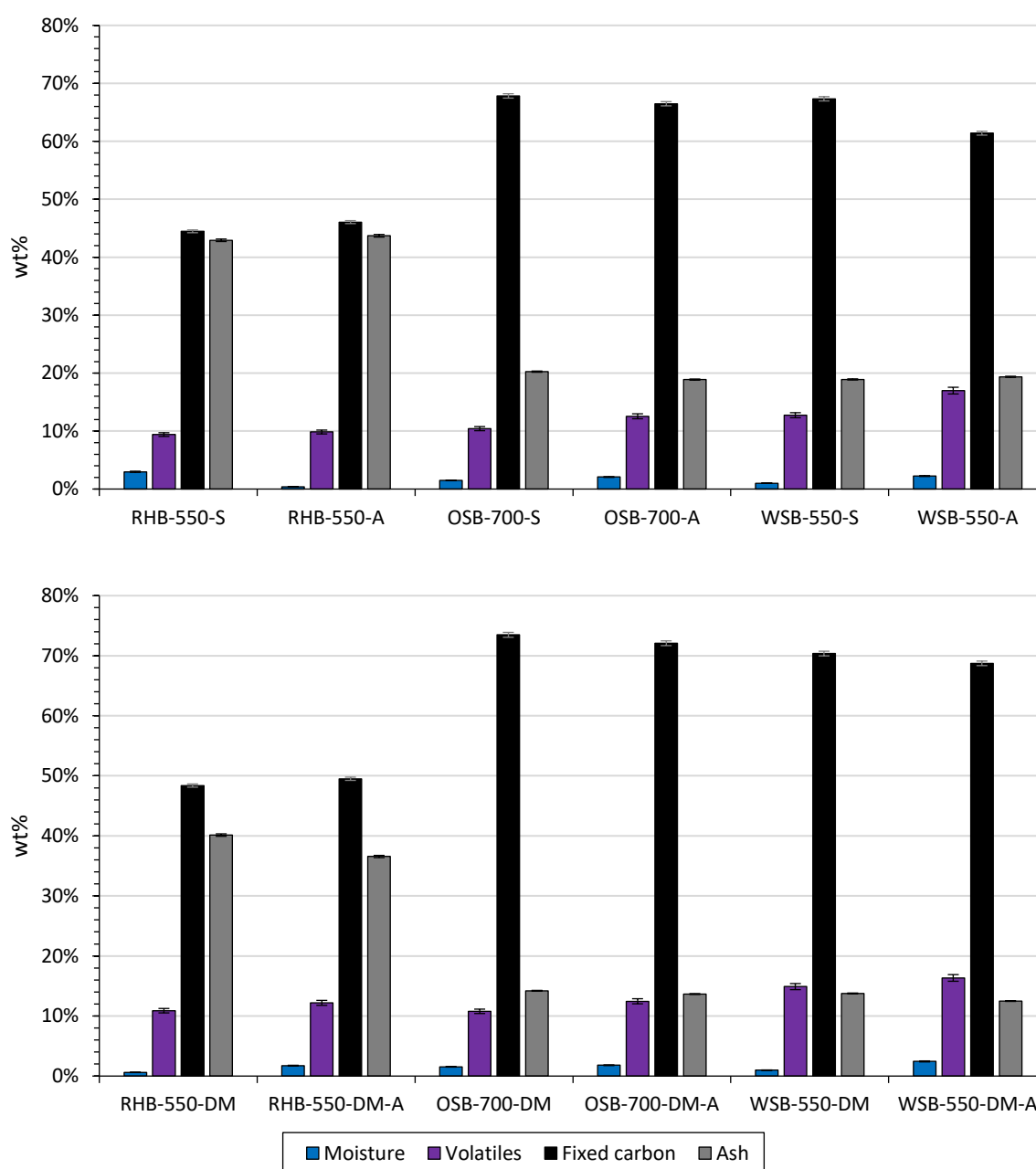


Figure 5-8 Thermogravimetric Analysis of biochar samples from different feedstocks before and after acetone washing for (a) untreated and (b) demineralised biochars. Error bars estimated from percentage error for two samples of WSB-550-DM-T-C samples.

Chapter 5 – Surface Treatments

The bulk composition of acetone-washed samples was first tested by TGA proximate analysis, shown in Figure 5-8 for both untreated and demineralised samples. The only consistent change is the increase in volatiles content, which is highlighted in Table 5-5. The increase in volatiles is greater than the percentage experimental error, estimated at 3.39 %. Fixed carbon content is reduced by 5.96 wt% for WSB-550, contrasting with an increase for RHB-550 of 1.59 wt%.

Table 5-5 Percentage increase in volatile component of biochars after acetone washing.

	Volatile content/wt%		
	untreated	acetone-washed	% increase
RHB-550	9.39%	9.84%	4.78%
RHB-550-DM	10.89%	12.19%	11.98%
OSB-700	10.42%	12.56%	20.47%
OSB-700-DM	10.78%	12.45%	15.53%
WSB-550	12.74%	16.99%	33.33%
WSB-550-DM	14.90%	16.34%	9.69%

The effect on surface area was next studied. As shown in Figure 5-9, there is a decrease in BET surface area after acetone washing across most feedstocks. The extent of the decrease appears to be feedstock-dependent: the decrease of 13 m² g⁻¹ for AC is within experimental error, whilst the surface area of RHB-550 is more than halved (120 m² g⁻¹ to 58 m² g⁻¹). The exception is WSB-550, where a small increase in surface area is observed.

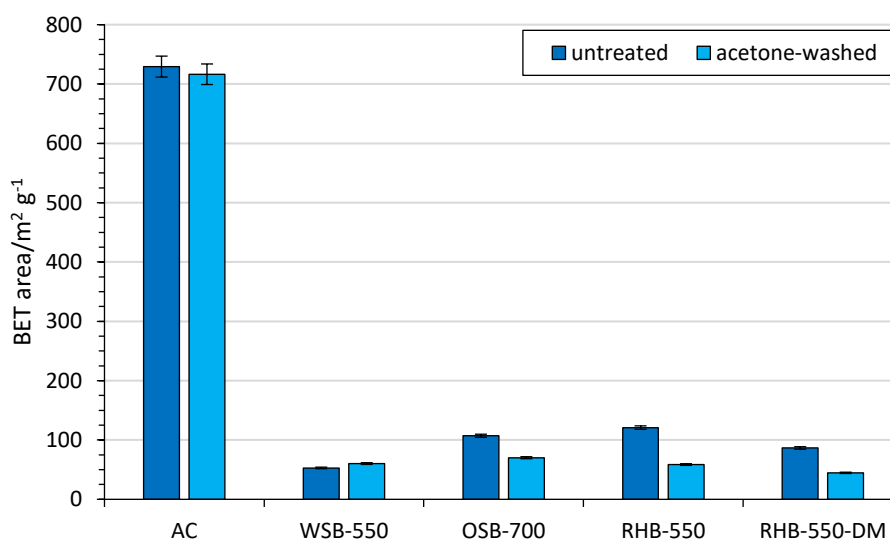


Figure 5-9 BET surface area measurements for biochars from different feedstocks before and after acetone washing. Error bars estimated from percentage error of 2.42% for three repeats of WSB-550.

The effect of acetone washing on microporosity was next considered, with the total micropore volume calculated through the use of t-plots. The results are presented in Figure 5-10. Micropore volume increases for AC, RHB-550 and RHB-550-DM. However, no microporosity is detected after acetone washing in WSB-550 or OSB-700.

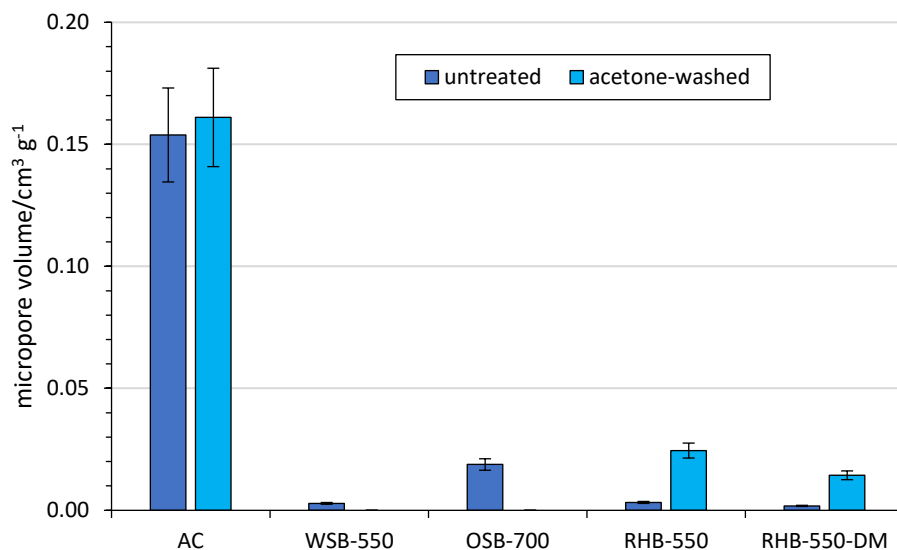


Figure 5-10 Micropore volume of biochars before and after acetone washing, measured using t-plots.

The effect of acetone washing on mesoporosity was next tested by studying PSDs for the biochars before and after acetone washing, shown in Figure 5-11.

Chapter 5 – Surface Treatments

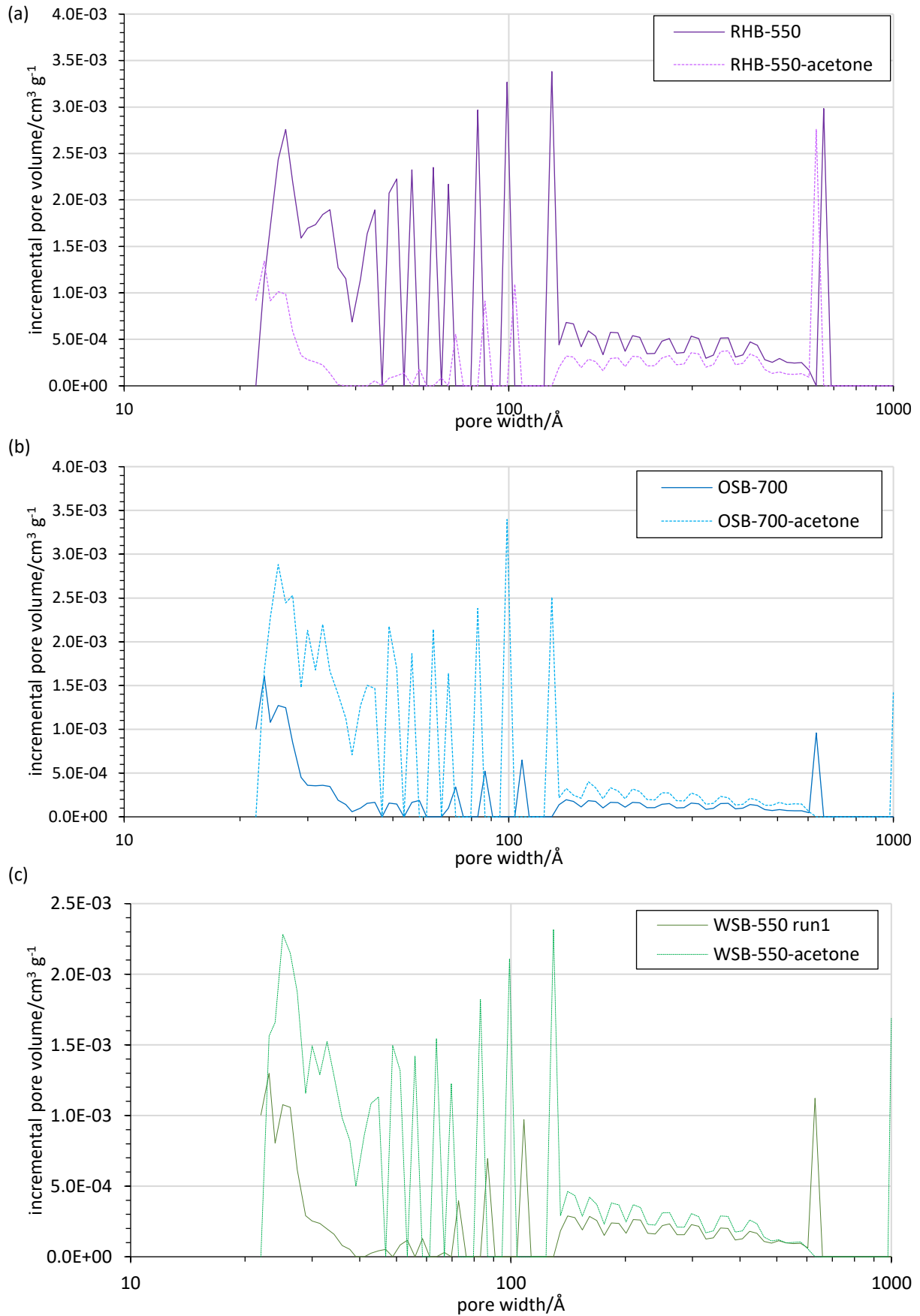


Figure 5-11 Pore size distributions for biochar samples before and after acetone washing. (a) RHB-550, (b) OSB-700 and (c) WSB-550. Solid lines are untreated, dotted lines are acetone-washed.

The PSD demonstrates that acetone washing impacts on mesoporosity, however the effect differs with feedstock. For RHB-550, mesopore volume decreases, with the position of the peaks appearing to shift to the left, indicating a decrease in pore size. However, for OSB-700 and WSB-550, mesopore volume increases after acetone washing, with peaks appearing to shift to the right, indicating an increase in pore size.

Very little change in surface chemistry was detected following acetone washing by FTIR-ATR. The main change detected was in the spectra of SWB-550, shown in Figure 5-12, where a slight decrease is observed in the intensity of the C=C aromatic band at 1580 cm^{-1} . In the remaining FTIR-ATR spectra, the same bands appear with approximately the same intensity after acetone washing; notably, no new oxygen-containing bands are detected. These spectra can be seen in Appendix B .

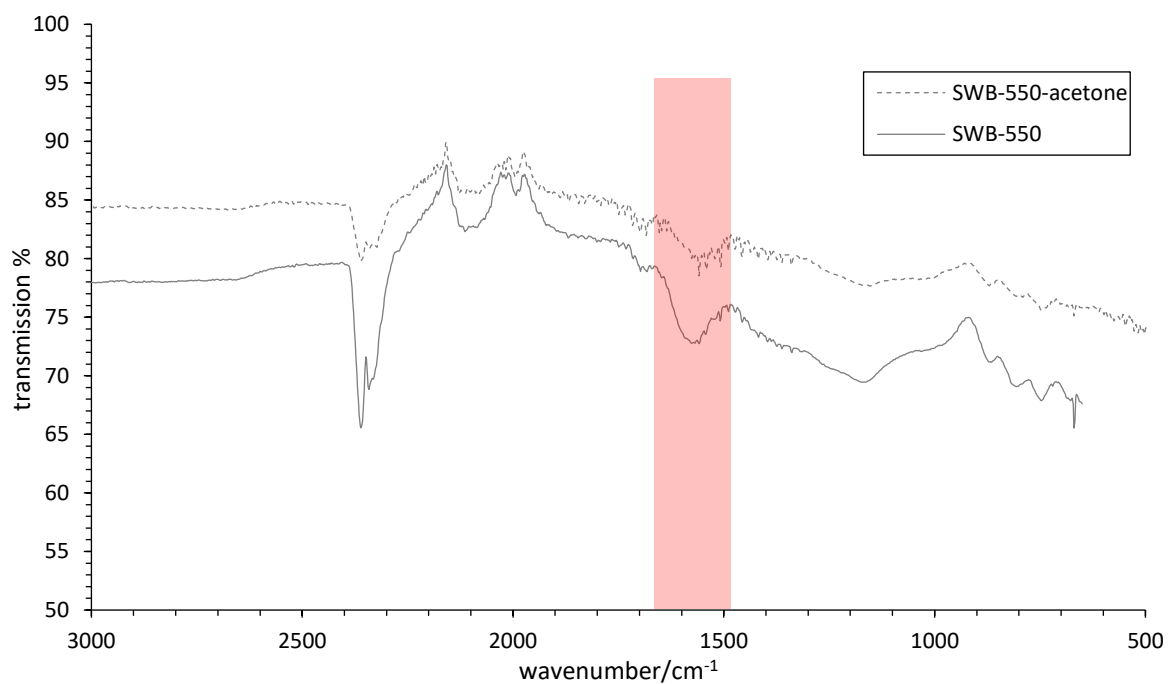


Figure 5-12 FTIR spectra of SWB samples before and after acetone washing. The aromatic C=C band at 1580 cm^{-1} is highlighted. -DM indicates demineralised sample.

Chapter 5 – Surface Treatments

5.3.3. Effectiveness of tar impregnation

In this section, data relating to the effectiveness of the tar impregnation method is presented. The impact on surface area and carbon structure is considered in further detail in section 5.3.4.

The tar loadings were evaluated through proximate analysis of the tar-impregnated biochars, prior to pyrolysis. Preliminary experiments demonstrated that the commercial pine tar consisted of 96.62 wt% volatiles (see Appendix B), therefore an increase in the volatile component would be expected if tar had been successfully impregnated. The TGA proximate analysis is shown in Figure 5-13.

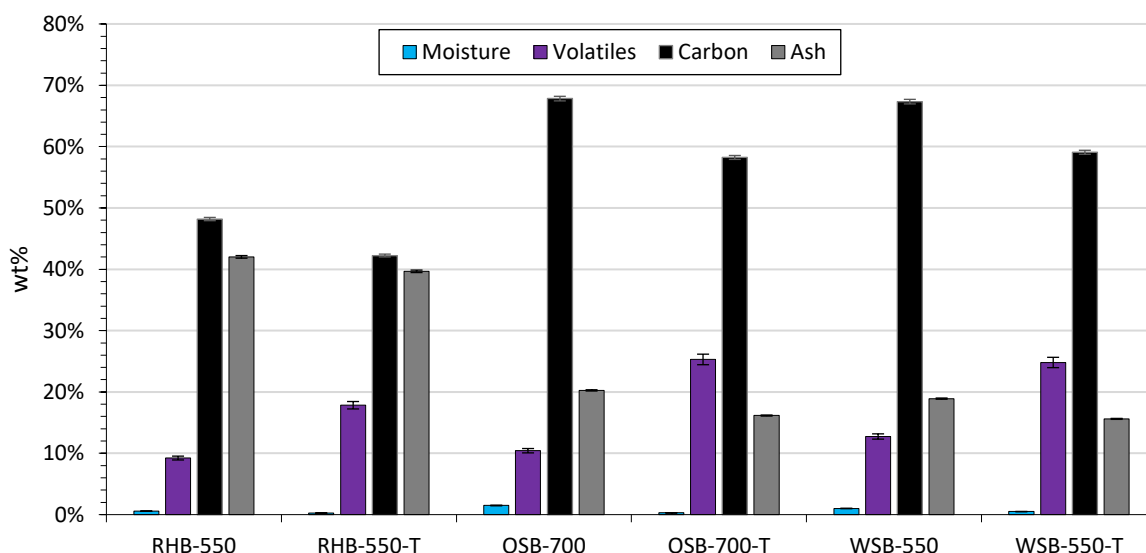


Figure 5-13 Results of TGA proximate analysis for tar-impregnated biochars. -T indicates the tar-impregnated biochar prior to pyrolysis.

A clear increase in volatile content is seen for all the biochar samples, indicating that tar has been successfully impregnated into the biochars prior to pyrolysis. To estimate the quantity of tar loaded, the TGA analysis of the acetone-washed and tar-impregnated samples was compared. The calculation was then performed on the basis that the reduction in ash content following tar impregnation is solely attributable to the additional tar (volatiles) loaded. This assumption was tested by predicting the final composition of the tar-impregnated biochar, using the tar loading calculated. The predicted and actual composition of RHB-550-T are presented in Figure 5-14 as an example – the calculations can be found in Appendix B .

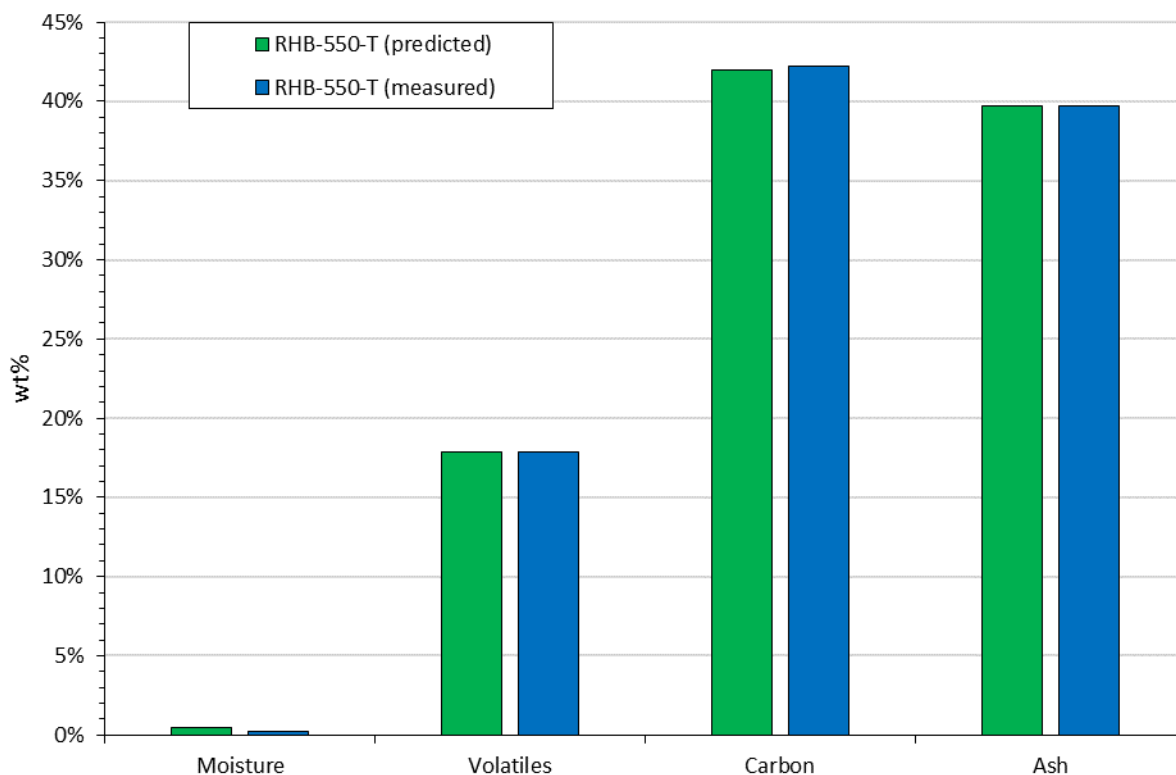


Figure 5-14 Comparison of experimentally measured RHB-T composition with predicted RHB-T composition, using the results of the RHB acetone control test. A tar loading of 10.2 g per 100 g biochar was calculated to give the observed ash content after tar impregnation.

As shown in Figure 5-14, the measured and predicted compositions are highly comparable. The volatile component is most accurately predicted (17.85 wt% predicted, 17.84 wt% measured), with carbon and moisture contents also being very close to the measured values.

The tar-impregnated biochars were next pyrolysed in the Stage I pyrolysis unit at the University of Edinburgh. As part of the analysis of the pyrolysis process, the biochar yield was calculated as follows:

$$\% \text{ biochar yield} = \frac{\text{mass of biochar following pyrolysis}}{\text{starting mass of biochar}} \times 100$$

The liquid and gas yields were also calculated, and can be found in Appendix B .

Chapter 5 – Surface Treatments

The biochar yield was then compared with the estimated quantity of biochar in the tar-impregnated samples, to estimate the conversion of tar to fixed carbon. This comparison is presented in Table 5-6.

Table 5-6 Comparison of the biochar yield from Stage I pyrolysis with the percentage of biochar in the sample.

Biochar	tar loaded/ g tar per 100 g biochar	% tar	% biochar	Stage I % biochar yield
RHB-550-T	10.16	9.22	90.78	86.41
OSB-700-T	16.91	14.46	85.54	80.15
WSB-550-T	24.06	19.39	80.61	78.17

In all cases, the biochar yield calculated was lower than the percentage of biochar present in the sample, indicating that there was an overall loss of biochar mass, rather than an increase due to the conversion of tar to fixed carbon. It was therefore not possible to calculate a theoretical tar conversion percentage. The results indicate that the percentage conversion of tar to solid carbon was very low. The potential reasons for this are discussed in section 5.4.3.

Control tests were next performed on RHB-550, to examine to what extent any changes observed are attributable to tar conversion. The effects of acetone washing and pyrolysis on the proximate composition are shown in Figure 5-15.

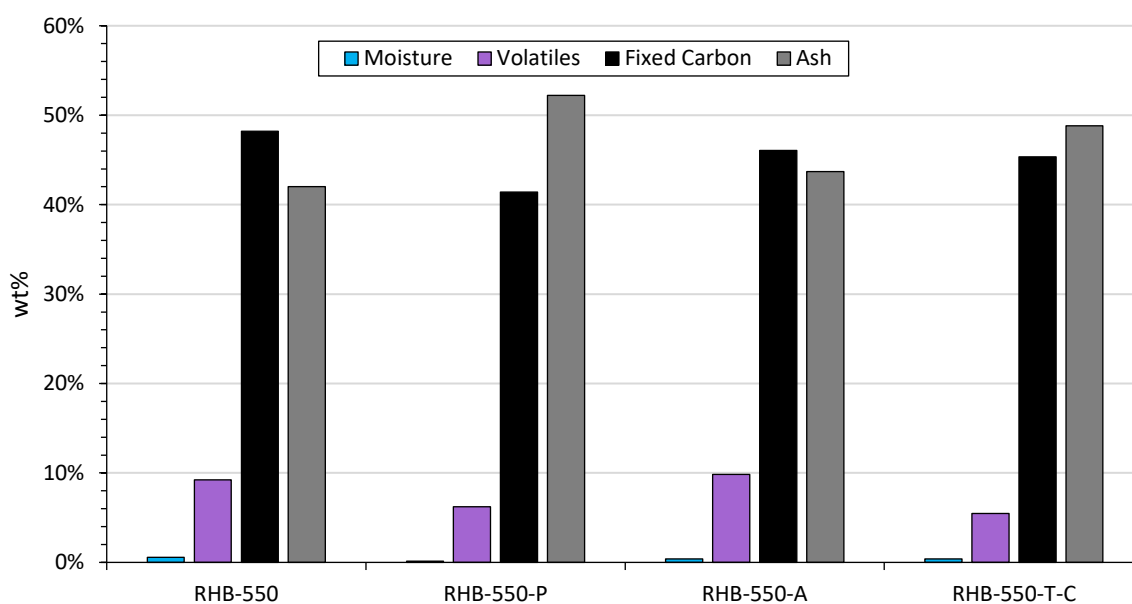


Figure 5-15 TGA proximate analysis data demonstrating the effect of acetone washing and pyrolysis steps on RHB-550. -A indicates acetone-washed, -P indicates pyrolysed, -T-C indicates tar impregnated and pyrolysed.

The case study on RHB-550 demonstrates that pyrolysis alone would lead to a reduction in fixed carbon, volatile and moisture content, leading to an increase in the percentage of ash. Similarly, the tar-impregnated and pyrolysed RHB-550-T-C sample has a lower volatile content, lower fixed carbon content and higher ash content compared to RHB-550-A.

Surface-sensitive methods were next employed to investigate whether carbon content had increased at the surface, consistent with the formation of carbon deposits. XPS elemental survey scan data for biochars before and after tar impregnation are shown in Figure 5-16.

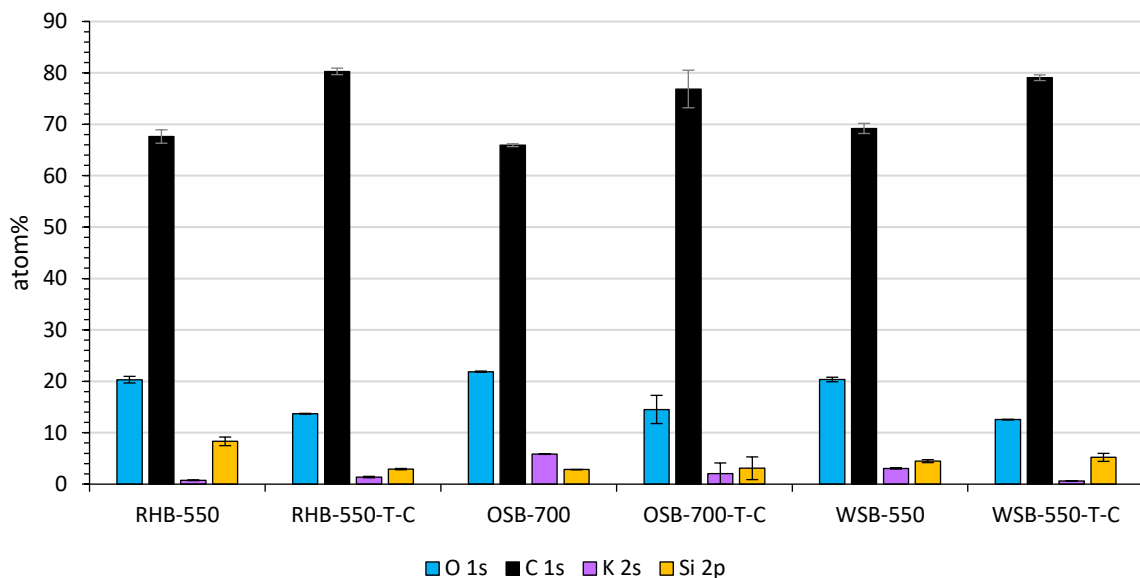


Figure 5-16 XPS elemental analysis of biochars before and after tar impregnation for four key elements of interest: O, C, Si and K. Error bars are standard deviation from two measurements on the sample. -T-C indicates tar-impregnated and pyrolysed samples.

There is a notable increase in surface carbon content in all cases, with carbon content after tar impregnation reaching up to 80 at%. This is accompanied by a decrease in surface oxygen content, to approximately 13 at%. Potassium content decreases in OSB-700 and WSB-550, however a slight increase is observed in potassium content for RHB-550-T-C, from 0.759 at% to 1.378 at%. Silicon content decreases for RHB-550, but remains within experimental error for OSB-700 and WSB-550. The implications for the location of carbon deposits are discussed in section 5.4.3.

Chapter 5 – Surface Treatments

5.3.4. Effect of tar impregnation and pyrolysis on carbon structure

The effect of potassium content on tar impregnation and pyrolysis was studied by examining the quantity and structure of carbon deposits formed on untreated and demineralised biochar samples. A reproducibility study was also performed for WSB-550-DM-T-C; two samples from the same batch of tar-impregnated material were pyrolysed, and the biochars analysed.

The first stage was to examine the success of the tar impregnation over demineralised samples, compared to untreated samples. The tar loadings were calculated from TGA data, as shown in section 5.3.3. The TGA data for the demineralised samples is presented in Appendix B. The estimated tar loadings are compared in Figure 5-17.

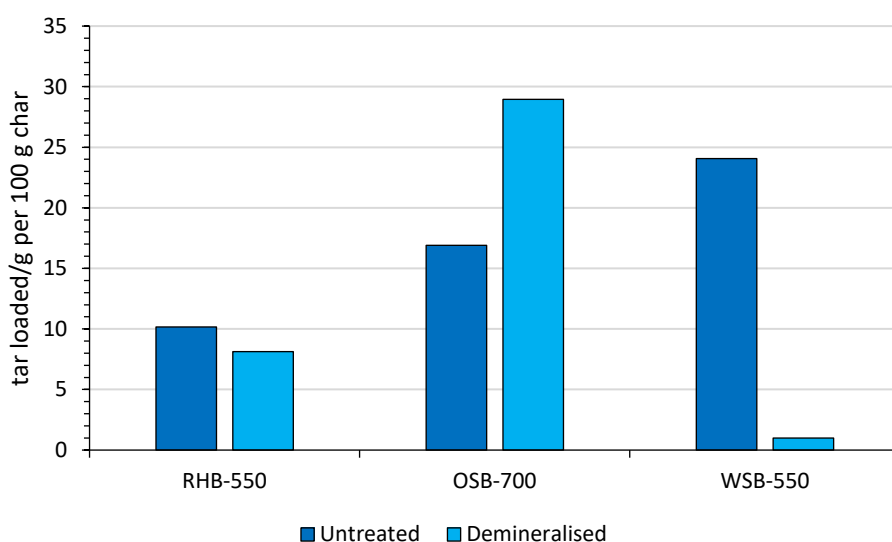


Figure 5-17 Tar loading estimates for biochars, calculated by assuming the reduction in percentage ash content after tar impregnation is solely due to additional tar.

The preliminary results indicate that the tar loading is successful, with at least 10 wt% of tar impregnated (*i.e.* 10 g tar for every 100 g of biochar). The quantity varies with the feedstock used; more than twice as much tar is impregnated on WSB-550 (24.06 g/100 g biochar) than on RHB-550 (10.16 g/100 g biochar). The effect of demineralisation on tar loading is variable; tar loading is greatly increased for OSB-700, and greatly decreased for WSB-550. The tar loadings range from 0.98 g/100 g for WSB-550-DM, to 28.94 g/100 g biochar for OSB-700-DM.

The possible reasons for the changes in tar loading after demineralisation will be discussed in section 5.4.4.

XPS elemental survey scans were next performed to measure the effect of tar impregnation on the surface elemental composition of the biochars; the results are shown in Figure 5-18.

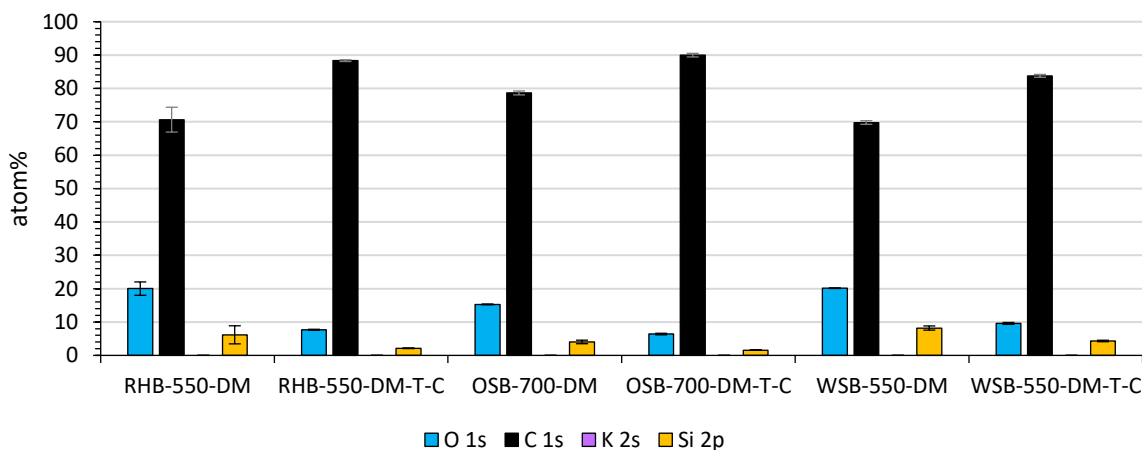


Figure 5-18 XPS elemental analysis of demineralised biochars before and after tar impregnation and pyrolysis. Error bars are standard deviation from two measurements on the sample.

As with the untreated biochars, tar impregnation led to an increase in surface carbon content, with carbon contents up to 90 at% for OSB-700-DM-T-C. This was also the sample with the highest tar loading, as calculated in Figure 5-17. A decrease in surface oxygen content was also observed, consistent with the untreated samples. No surface potassium was detected, and surface silicon was reduced in all cases after tar impregnation.

The effect on surface area was measured by BET isotherms. Over demineralised samples, the increase in surface area was much greater. As shown in Figure 5-19, the surface area of the demineralised samples was 3-4 times higher following tar impregnation, compared to increases of up to 2 times for untreated samples.

Chapter 5 – Surface Treatments

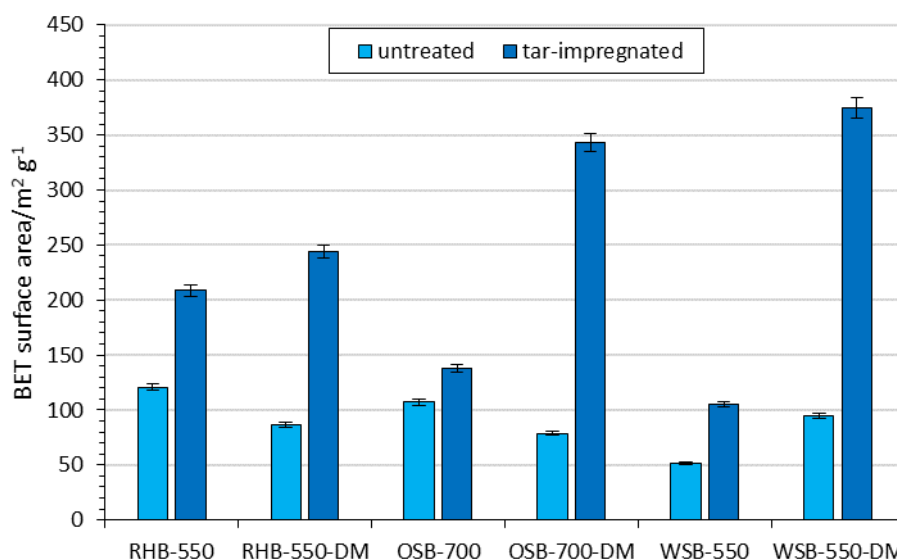


Figure 5-19 BET surface areas for demineralised biochars before and after tar impregnation.

The porosity of the samples before and after tar impregnation was next investigated. Micropore volume was calculated from t-plots; the results are shown in Figure 5-20.

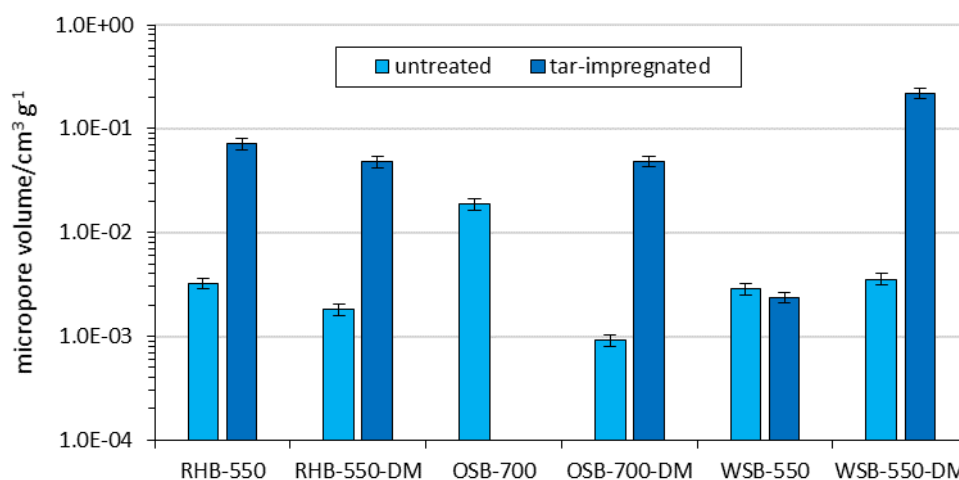


Figure 5-20 Micropore volume of demineralised biochar samples before and after tar impregnation and pyrolysis. A logarithmic y-axis is used to allow the clear presentation of large and small values.

Before demineralisation, the effect of tar impregnation on microporosity varies with feedstock: microporosity is completely lost in OSB-700, slightly decreases in WSB-550, and almost doubles in RHB-550. However, for the demineralised samples, the micropore volume greatly increases. Micropore volume increases by $\times 25$ for RHB-550-DM, $\times 50$ for OSB-700 and $\times 60$ for WSB-550-DM. The micropore volume of OSB-700-DM-T-C is comparable to RHB-550-DM-T-C ($0.0486 \text{ cm}^3 \text{ g}^{-1}$ and $0.0484 \text{ cm}^3 \text{ g}^{-1}$ respectively), however the micropore volume of WSB-550-DM-T-C ($0.221 \text{ cm}^3 \text{ g}^{-1}$) is almost five times' higher.

The effect on the pore size distribution was next considered. The pore size distributions of the demineralised biochars before and after tar impregnation are shown in Figure 5-21.

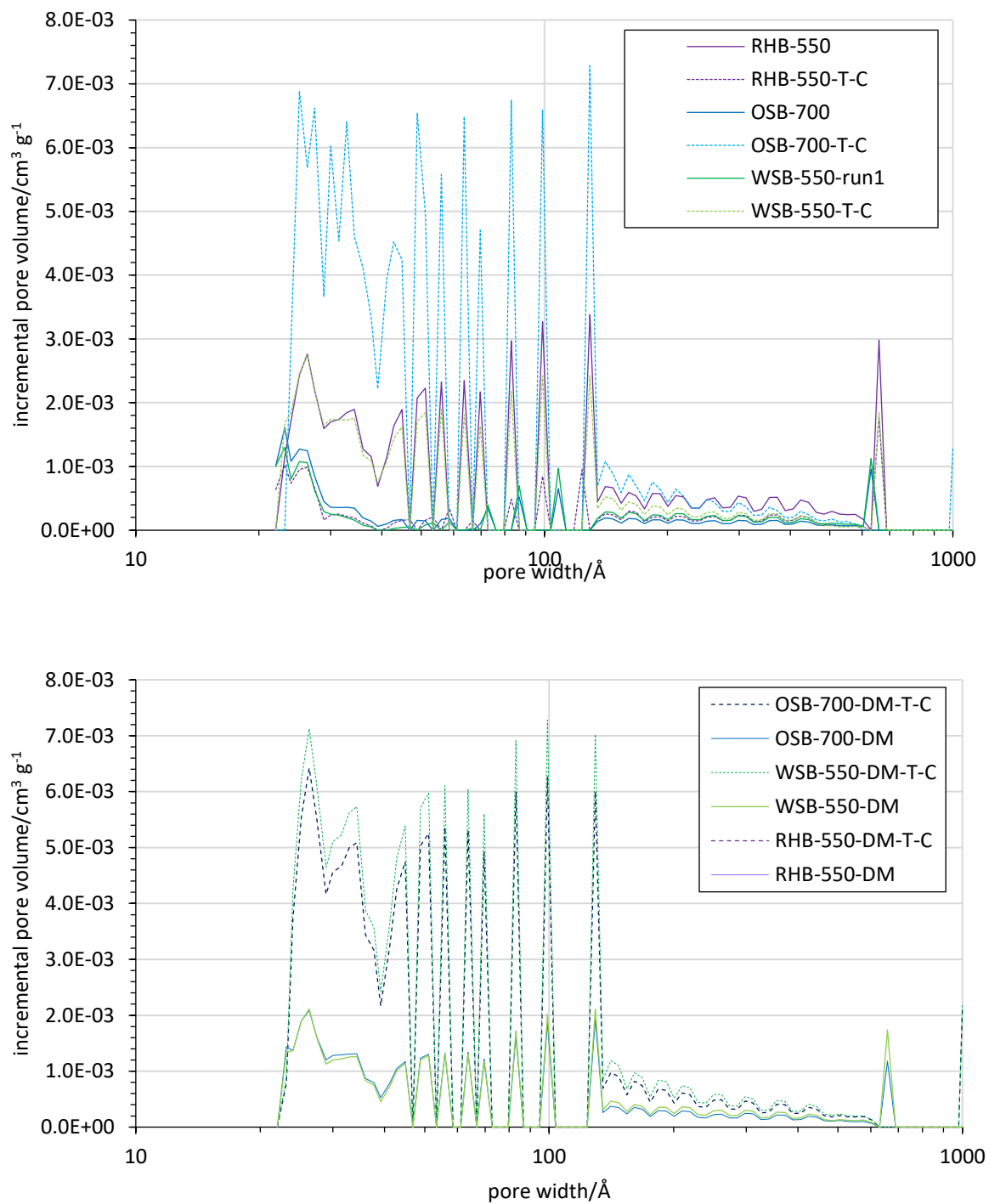


Figure 5-21 Pore size distributions for demineralised biochar samples before and after tar impregnation. -DM denotes demineralised biochar, -T-C denotes tar impregnated and pyrolysed biochar. Dotted lines are used to distinguish the tar-impregnated biochars.

Chapter 5 – Surface Treatments

In all cases, the volume of the mesopores is observed to increase, whilst the peak positions are unchanged. The only notable change is the loss of the peak at the pore width 658 Å in the PSDs for WSB-550-DM-T-C and OSB-700-DM-T-C. The effect on the feedstocks also varies; whilst the demineralised samples had very similar mesopore distributions and volumes, the greatest increases are seen for WSB-550-DM-T-C and OSB-700-DM-T-C. The smallest increase is seen for RHB-550-DM-T-C. The potential reasons for these observations will be discussed in section 5.4.4.

As with the untreated biochars after tar impregnation, Raman analysis was used to examine the graphiticity of the carbon deposits formed. The results of the curve deconvolution are presented in Figure 5-22.

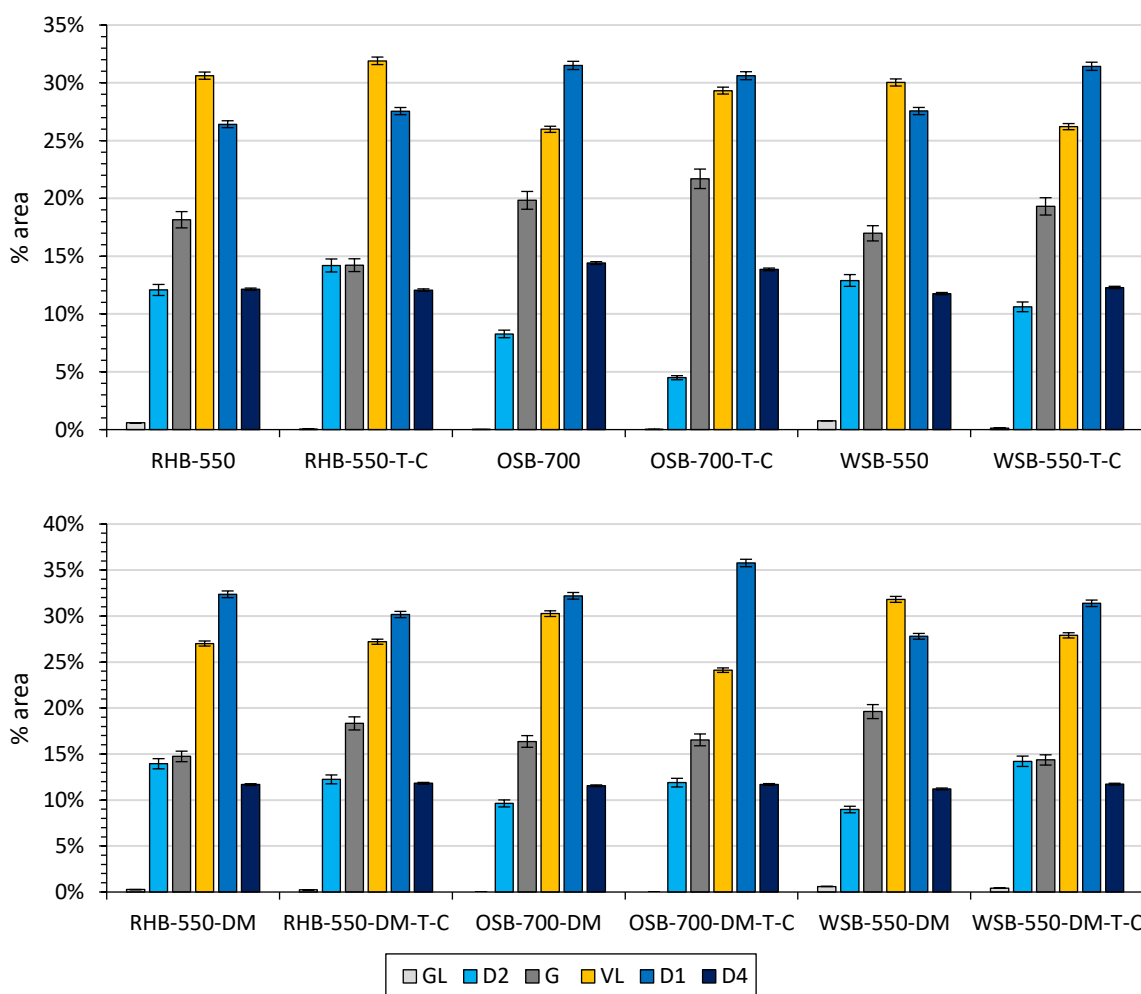


Figure 5-22 Deconvolved Raman spectra for demineralised biochars before and after tar impregnation.

There are few and consistent changes in the deconvolved Raman spectra following tar impregnation. Bands D4 and G_L (C=O) are unchanged in all samples, whilst bands D1 and D2 are observed to increase in OSB-700-DM-T-C and WSB-550-DM-T-C. Only band G increases in RHB-550-DM-T-C. The overall effect of these changes on the A_{D1}/A_G ratio is shown in Figure 5-23.

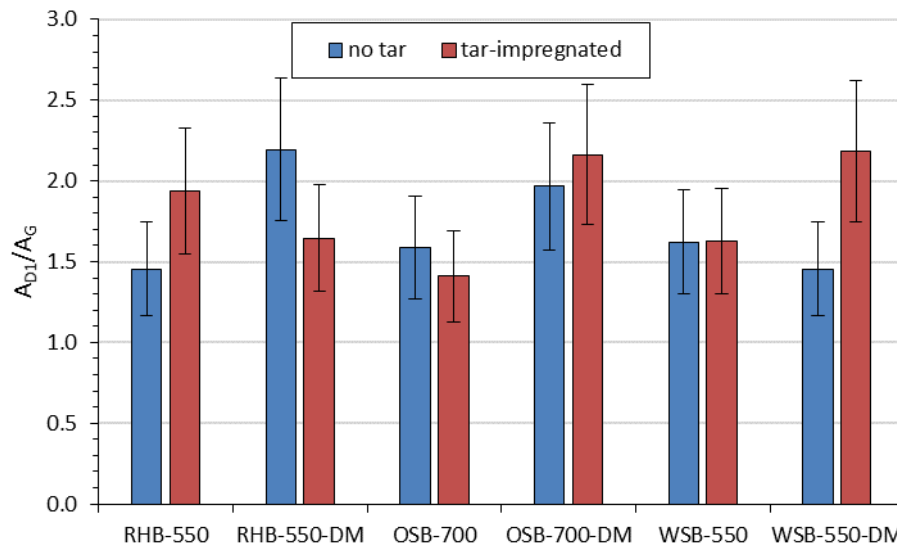


Figure 5-23 Effect of tar impregnation over demineralised samples on the ratio of disordered (D1) to graphitic (G) carbon. The percentage error of 20 % was calculated from two repeats of WSB-550-DM.

As for the untreated biochars, the effects of tar impregnation on the demineralised biochars appear to vary. The A_{D1}/A_G ratio is similar in all cases, with the largest change being a decrease in graphiticity for WSB-550-DM-T-C. Graphiticity decreases for OSB-700-DM-T-C, whilst the graphiticity of RHB-550-DM-T-C increases. These changes are however within the experimental error associated with Raman curve deconvolution and sample variation.

XPS C1s spectra were used to study the effect of tar impregnation on surface carbon groups, including oxygen-containing functionalities. The results are shown in Figure 5-24.

Chapter 5 – Surface Treatments

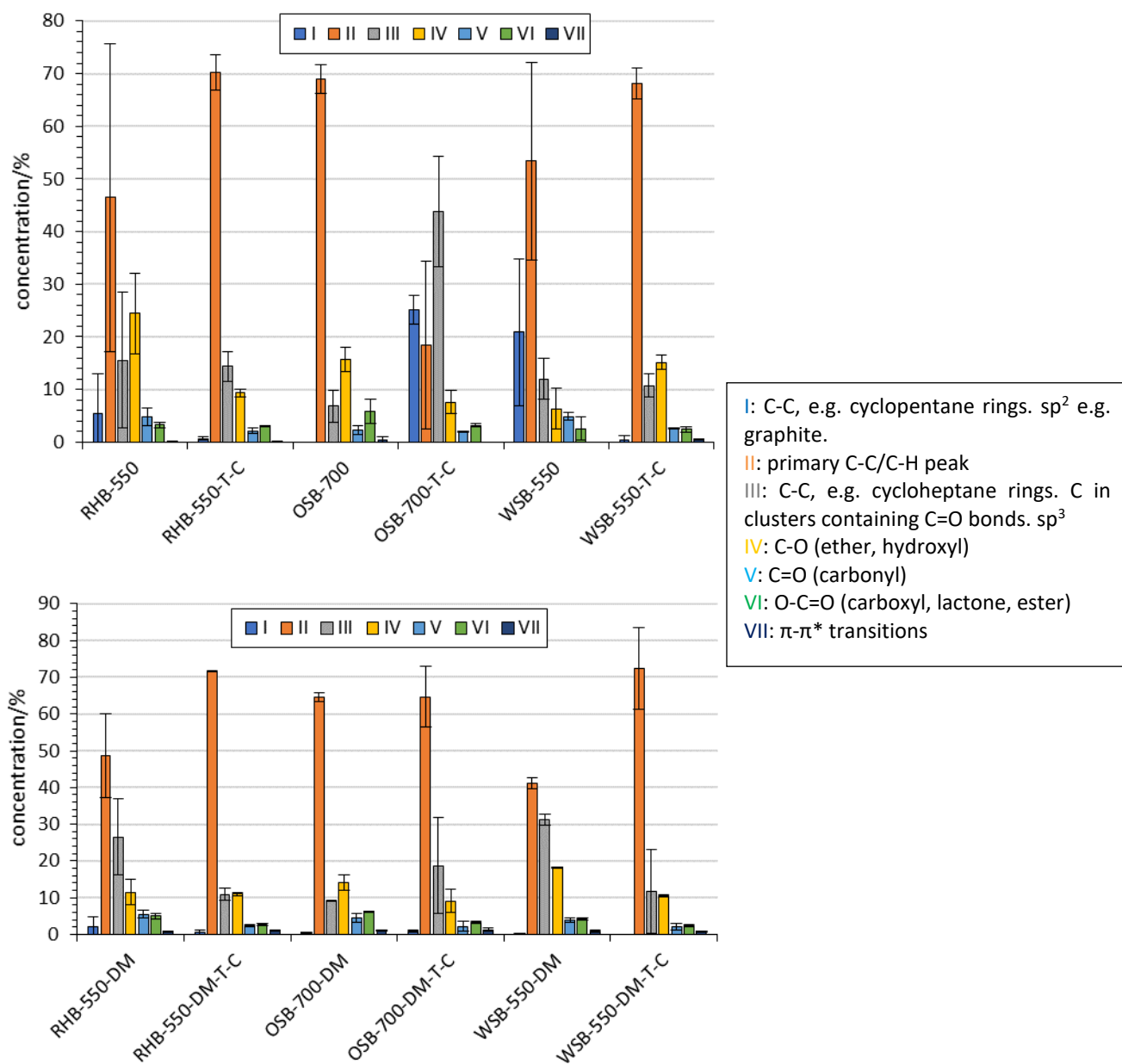


Figure 5-24 XPS C1s curve deconvolution data for demineralised biochars before and after tar impregnation and pyrolysis.

The results for the demineralised samples are more consistent than those for the untreated biochars. In terms of bands which increase, band II (primary C-C) is increased in RHB-550-DM and WSB-550-DM, with a possible increase in band III (C-C in larger aromatic rings) for OSB-700-DM. Experimental error however is high for curve deconvolution, particularly for bands I-III. Also notable is the decrease in surface oxygen groups after tar impregnation: the contribution from bands IV, V and VI were all reduced. The decrease in band IV (C-O) was particularly pronounced for WSB-550-DM. The contribution from π - π^* transitions appears unaffected by tar impregnation.

Few changes are detected through FTIR-ATR spectroscopy of the tar-impregnated samples, shown in Figure 5-25. After tar impregnation, the intensity of the 1550 cm^{-1} aromatic group is reduced in RHB-550-DM-T-C. The 1070 cm^{-1} band attributed to Si-O-Si symmetric stretches is decreased in RHB-550-DM-T-C, but is broader in WSB-550-DM-T-C. There is little observable difference between OSB-700-DM and OSB-700-DM-T-C.

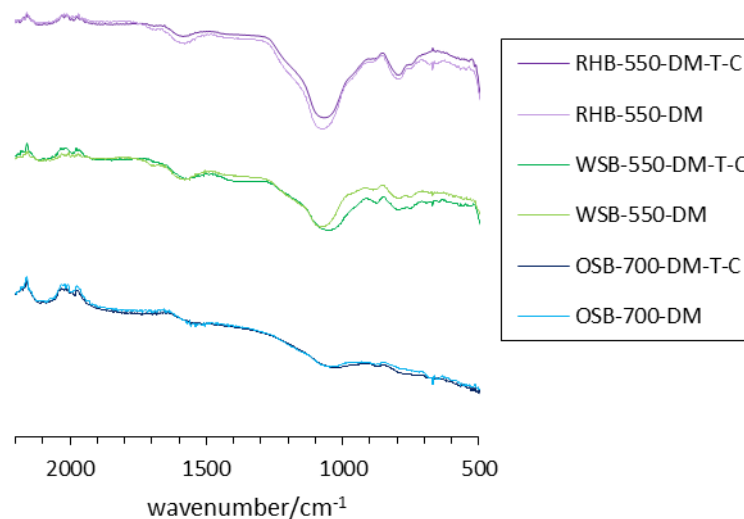


Figure 5-25 Normalised FTIR spectra for demineralised biochars before and after tar impregnation and pyrolysis.

It is worth noting that the tar-impregnated and pyrolysed samples were imaged by SEM to determine whether carbon macrostructures were present on the surface of the biochars. Example images for the tar-impregnated samples are given in Appendix B, and exhibited no changes in the macropores from those shown in Figure 5-6.

Chapter 5 – Surface Treatments

5.3.5. Summary

Biochars have been characterised using a number of techniques, allowing the structure, elemental composition, surface chemistry and carbon structure to be investigated before and after various treatments. Table 5-7 summarises the key findings, which are discussed in section 4.4.

Table 5-7 Summary of key results from effect of various surface treatments on properties of biochar. Shaded boxes indicate data unavailable.

		Demineralisation	Acetone washing	Tar impregnation and pyrolysis (untreated samples)	Tar impregnation and pyrolysis (demineralised samples)
Composition	TGA	Ash content reduced by 4.5 % for RHB-550, 29.9 % for OSB-700, 27.3 % for WSB-550.	Increased V, <5 at%. Reduced fixed C, <6 wt%.	Tar loadings per 100 g biochar: 10 g for RHB-550, 17 g for OSB-700, 24 g for WSB-550.	Tar loadings per 100 g biochar: 29 g for OSB-700-DM, 8 g for RHB-550-DM, 0.98 g for WSB-550-DM.
	(following pyrolysis)			Biochar yields < starting quantity of biochar. RHB-550-P and RHB-550-T-C: reduced C, increased ash.	Biochar yields reduced following demineralisation.
	Non-AAEM (surface)	C increased, Si and O decreased. N reduced in WSB-550, unaffected in RHB-550 and OSB-700. No decrease in P. Additional Cl in RHB-550-DM. Cl reduced ~50 % in OSB-700 and WSB-550. Additional F content (<5 at%).		Increased C, approx.. ~10 at%. Decreased surface oxygen (~5 at%). Decreased surface silicon for RHB-550 (>50 %).	C content increased, 10-20 at%. Surface silica and oxygen contents reduced in all samples by approx.. 50 %.
	Non-AAEM (bulk)	Si and O increased. <5 at% C in ash content. Cl reduction >90 %.			
	AAEM (surface)	All K removed. Ca removed from WSB-550, reduced in OSB-700 and RHB-550. Mg removed from OSB-700.		RHB-550, K increase ~0.6 at%, -60 % in OSB-700, ~80 % in WSB-550.	No K detected.
	AAEM (bulk)	K -80 % (-90 % for WSB-550). Ca and Mg reduced in RHB-550. Na -50 % in WSB-550, no change in RHB-550, OSB-700.			
Structure	BET surface area	RHB-550: -30 %, OSB-700: -30 %, WSB-550-DM: +85 %.	RHB-550: -50 %, OSB-700: -25 %, WSB-550: +15 %, AC: -2 %*.	RHB-550 and WSB-550: +100 %, OSB-700: +30 %.	Increased: WSB-550-DM x4, OSB-700-DM x4, RHB-550-DM x3.

Chapter 5 – Surface Treatments

Structure	Micropore volume	RHB-550: -50 %, OSB-700: -95 %, WSB-550: +25 %*.	RHB-550 and RHB-550-DM, 7.5× increase. No micropores in OSB-700-A and WSB-550-A.	RHB-550: 20× increase. WSB-550: no change*. OSB-700: -100%.	Increased: WSB-550-DM ×60, RHB-550-DM ×25, and OSB-700-DM ×50. WSB-550-DM ×5 greater than RHB-550-DM and OSB-700-DM.
	Mesopore volume	All biochars comparable after demineralisation: same pore volumes and peak positions. Mesopore volume increases for WSB-550 and OSB-700, decreases for RHB-550.	Volume and size decreases for RHB-550, increases for WSB-550 and OSB-700.	Peak positions unchanged. Mesopore volume: increased for WSB-550-T-C, greatly increased for OSB-700-T-C, decreased for RHB-550-T-C.	Increased mesopore volume, unchanged peak positions. Smaller increase for RHB-550-DM-T-C.
	Macropores	No observed changes.		No observed changes.	No observed changes.
Carbon structure	FTIR	C=C (aromatic): RHB-550 increased, OSB-700 unchanged, WSB-550 decreased.	Reduced C=C (aromatic) in SWB-550.	RHB-550 and WSB-550: small decrease in C=C (aromatic). OSB-700: little change.	RHB-550-DM: decrease in C=C (aromatic). OSB-700-DM and WSB-550-DM unchanged.
	Raman Ad_I/Ag ratio	RHB-550-DM increase*, OSB-700-DM increase*, WSB-550-DM decrease*.		RHB-550 increased*, OSB-700 decreased*, WSB-550 unchanged*.	RHB-550-DM decreased*, OSB-700-DM and WSB-550-DM increased*.
	Raman: V_L, D1, D2, D4	RHB-550: V _L reduced, D2 increased, D4 unchanged. OSB-700: V _L increased, D2 increased, D4 decreased. WSB-550: V _L increased, D2 decreased. D4 unchanged.		RHB-550: increases in D2, V _L , D1. OSB-700: increases in V _L , G. WSB-550: increases in G, D1.	RHB-550-DM, increased G. OSB-700 and WSB-550, increased D2 and D1.
	XPS C1s bands I-III, VII	RHB-550: unchanged*. OSB-700: unchanged*. WSB-550: decreased I, increased III, increased VII.		RHB-550-T-C, increased II*. OSB-700-T-C, increased I and III. WSB-550-T-C, increased II* and VII.	RHB-550-DM: increased II. OSB-700: increased III*. WSB-550: increased II. VII unchanged.
Surface chemistry	FTIR	Reduced phenolic -OH bending in WSB-550 and OSB-700. No new groups introduced.	No new groups introduced.	Phenolic -OH band reduced.	RHB-550-DM-T-C: decreased Si-O-Si intensity. OSB-700-DM-T-C: unchanged. WSB-550-DM-T-C: broader Si-O-Si band.
	Raman (band G_L)	Decreased in RHB-550 and WSB-550, removed in OSB-700.		Removed in RHB-550 and WSB-550. Unchanged in OSB-700.	Unchanged.
	XPS C1s bands: IV-VI	RHB-550: unchanged*, OSB-700: unchanged*, WSB-550: increased IV.		RHB-550: IV decreased, V decreased*, VI unchanged*. OSB-700: IV decreased, V unchanged*, VI decreased*. WSB-550: IV increased, V decreased, VI unchanged*.	RHB-550-DM: IV unchanged*, decreased V, VI. OSB-700-DM: decreased IV*, V*, VI. WSB-550-DM: decreased IV, V, VI.

*within experimental error

5.4. Discussion

In this chapter, the response of biochars to surface treatments such as demineralisation and acetone washing have been studied. A novel method of tar impregnation has been tested, and used as part of a pyrolysis study, investigating the influence of biochar composition on the structure of carbon deposits formed. The results presented in section 5.3 indicated that the effect of demineralisation, acetone washing and tar impregnation vary with feedstock, and that demineralisation impacted the structure of the carbon deposits formed. The possible reasons for these findings will now be discussed.

5.4.1. Effect of demineralisation

The quantity of ash removed from the biochars by demineralisation was generally low, and varied with feedstock. The ashes comprised mostly of silica (> 80 at%), which is not removed by HCl. Therefore, the higher silica content of RHB-550 (88.9 at% compared to 82.7 at% for OSB-700-ash) may have contributed to the lower percentage of ash removed (4.5 % of ash compared to 27.3 % from WSB-550 and 29.9 % from OSB-700). Higher quantities of heavier elements were also removed from OSB-700 and WSB-550, such as Ca ($A_r = 40$) and Mg ($A_r = 38$). The effectiveness of demineralisation using HCl is therefore heavily dependent on the composition of the biochars.

The effect of demineralisation on porosity and therefore surface area also varied by feedstock. For RHB-550, the reduction in micro- and mesopore volume is reflected in the decreased surface area, whilst for WSB-550 the mesoporosity increases whilst microporosity is unaffected, leading to an overall increase in BET area. For OSB-700, the micropore volume is reduced by a factor of 10, outweighing the impact of the increased mesoporosity as reflected in the decreased surface area. A decrease in BET area might be expected due to the larger particle size, however the differing effects on porosity indicate that this alone does not explain the changes in surface area. The reasons for these differing responses to demineralisation require further consideration.

The XPS analysis of the surface and bulk of the biochars can give insights into the location of the elements removed by demineralisation. XPS is a highly surface-sensitive technique, with

Chapter 5 – Surface Treatments

a penetration depth of 1-3 nm, meaning elements detected at the surface can be assumed to be accessible to HCl during demineralisation. Any elements remaining at the surface following demineralisation can be assumed to be insoluble. Elements in the prepared ash samples can be considered representative of the bulk ash content, assuming the composition of the ash is homogeneous. These elements may be accessible to HCl if located in pores, or inaccessible if located in the bulk. The XPS spectra of the chars and ashes before and after demineralisation can therefore indicate whether the location and solubility of elements varies between feedstocks.

The XPS analysis illustrates that the location and solubility of AAEM elements varies between feedstocks. The location of Mg varies, being detected in the ash content of all three feedstocks, but only at the surface of OSB-700. The extent of removal also varies, for example, surface calcium is entirely removed in WSB-550 but is only reduced by 60 % in OSB-700. Biochar ash is known to consist primarily of silicates, carbonates, chlorides, sulfates and phosphates (Sander & Andrén 1997), the solubility of which will vary. For example, phosphorous detected in the biochars could indicate the presence of phosphates, which may be insoluble in low concentrations of HCl. The determination of the form of the AAEM elements is beyond the scope of the present work, however the presence of AAEM elements in soluble and insoluble forms may explain the varying degree of removal using HCl.

The differing effects on porosity may be explained by the varying location and solubility of the elements in each feedstock. The microporosity of the samples does not increase, indicating that no new micropores are formed, and that elements are not substantially removed from the micropores of the samples. The mesoporosity of WSB-550 and OSB-700 however is observed to increase; this increase in volume is unlikely to be accounted for by the volume of the atoms removed. This could indicate that elements such as potassium and chlorides have been removed from pore mouths in WSB-550 and OSB-700. However, in RHB-550, the chlorine content is observed to increase following demineralisation; this requires further consideration.

Chlorine content of the biochars and ashes was generally decreased following demineralisation, indicating that washing with distilled water had successfully removed excess Cl from the HCl treatment. However, an increase was recorded for RHB-550-DM-ash. The decrease in the mesopore volume for RHB-550 could indicate that chlorides are blocking the mesopore mouths. As chlorides are expected to be soluble in distilled water, this indicates that the washing process was insufficient. One cause of this could be that biochars have been known to exhibit varying hydrophobicities (Manyà 2012); this could prevent the washing water accessing the micropores sufficiently to remove the chloride ions. The varying hydrophobicity of biochars could explain the differing extent of removal of chloride ions by distilled water.

The demineralisation process also led to the detection of fluorine in demineralised char samples. This is most likely indicative of a contamination issue, possibly from fluoride ions in tap water. Whilst deionised water was used for washing the biochars after acid washing, an alternative source of contamination is glassware which was insufficiently rinsed and dried. Similar levels of fluorine are detected in the biochars, therefore differences in catalytic activity between demineralised samples are unlikely to be attributed to differing levels of contamination.

The measured effect of demineralisation on carbon structure appears to vary depending on the technique used. XPS C1s spectra indicate that band III (C7+ rings) was increased in all cases, whilst band I (graphitic or C5- rings) decreased. Smaller rings may react with HCl due to the higher ring strain, favouring larger ring sizes after demineralisation. The reduction in band I however is not reflected in the Raman spectra; although the contribution of band I is reduced by 20 % in WSB-550-DM, the A_{D1}/A_G ratio is seen to decrease, indicating increased graphiticity. Similar contrasts are seen for aromatic carbon: a slight decrease in the aromatic C=C band is observed in the FTIR spectra for WSB-550, however band V_L (aromatic/amorphous carbon) is not reduced in the deconvolved Raman spectra. These inconsistencies will be considered further in section 5.4.7.

Chapter 5 – Surface Treatments

The effect on surface functional groups also appears to vary with feedstock and measurement technique. For example, band IV (C-O) is only increased in WSB-550-DM. However, reductions in band G_L in the Raman spectra are observed in all biochars, but no decrease is observed in band V (C=O) in XPS spectra. No new functional groups are detected in the FTIR spectra, and the increase in the percentage of band IV (C-O) in WSB-550-DM may be due to decreases in other bands. As XPS is more surface sensitive than FTIR, it is also possible that new C-O groups are highly localised at the surface.

These findings are summarised in Figure 5-26, as a schematic for the effect of demineralisation on RHB-550. In this schematic, the decrease in K⁺ and AAEM metals is observed, whilst silica-based ash is still present. The increase in aromatic content, as observed by FTIR, is also indicated, as well as the slight increase in Cl⁻ ions, which possibly block the mesopore mouths.

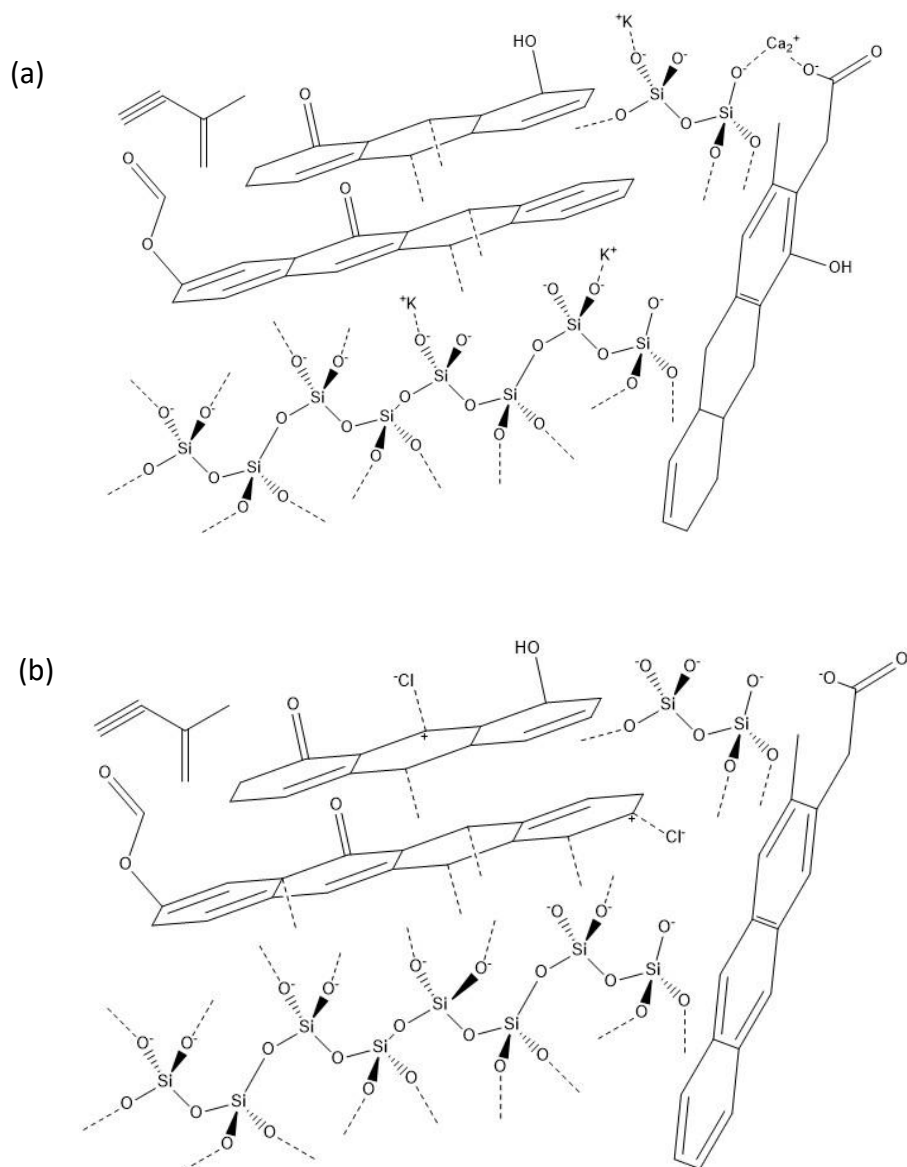


Figure 5-26 Schematic of the structure of RHB-550 (a) before and (b) after demineralisation using HCl.

5.4.2. Effect of acetone washing

Acetone washing was observed to reduce the surface area of RHB-550 by 50 % and OSB-700 by 25 %; however, the surface area of WSB-550 increased by 15 %. This is consistent with the trend in surface areas resulting from demineralisation, and again indicates that the decrease in BET area is not solely due to the decrease in particle size. The surface area of WSB-550 is increased slightly to 60.3 m² g⁻¹ after acetone washing, and to 94.7 m² g⁻¹ after demineralisation. This supports the idea that in WSB-550, pores are being cleared – the effect

Chapter 5 – Surface Treatments

is more pronounced when using acid, however some pore clearing may occur when using acetone. The very small decrease in surface area for AC after acetone-washing (< 2 %) may also suggest that the structure of high-carbon samples is less affected by acetone washing than the structures of high ash samples.

The effect on mesoporosity is also consistent with demineralisation, with increases observed for OSB-700 and WSB-550, and a decrease for RHB-550. This supports the conclusion that material has been cleared from the pore mouths of OSB-700 and WSB-550, and pore mouths are possibly blocked in RHB-550. In this case, however, the blockage cannot be due to insoluble chloride, and may instead be due to oxygenated groups forming on acid sites at the pore mouth. The mesopore mouth openings in RHB-550 may also be narrower, meaning they are more easily blocked.

However, the effect on microporosity differs. Micropore volume was observed to increase for AC, RHB-550 and RHB-550-DM, indicating that either new pores are created or pores are cleared, which are not cleared by demineralisation. As no new micropores are observed in OSB-700-acetone or WSB-550-acetone, it is more likely that the increase in microporosity is due to existing micropores being cleared. These pores may also be cleared by HCl, and subsequently blocked by Cl ions; alternatively, the micropores may be blocked with material only soluble or accessible to acetone. By contrast, the micropores in OSB-700 and WSB-550 are lost, either due to oxygenated groups blocking pore mouths, or due to the microporous structure being destroyed. This would be consistent with the increase in mesoporosity observed in OSB-700-acetone and WSB-550-acetone.

In terms of proximate analysis, acetone remaining after the drying process would be thought to increase the moisture content of biochars, due to its low boiling point of 56 °C. However, the volatiles content was observed to increase in all samples. Whilst part of this increase may be due to the reduction in moisture content (*e.g.* from the extensive drying process), this is insufficient to fully explain the increase. One explanation is that fixed carbon may react with the acetone to form volatile carbon. This could also explain why carbon content is observed to decrease in all samples except RHB-550 and RHB-550-DM.

The FTIR spectra also indicated that C=C aromatic contributions may have been reduced, particularly in SWB-550. Whilst some variation in spectra may be due to the natural heterogeneity of the samples, the reduction in C=C aromatics may be due to volatile aromatic components being dissolved in the acetone solvents. However, acetone does not lead to the creation of new oxygenated surface groups – this is relevant to catalytic studies, as oxygen-containing functional groups were apparently unaffected by immersion in an oxygenated solvent. The surface functionalities of the biochar catalysts may therefore be stable in organic solvents, although dynamic changes will likely occur during catalysis.

5.4.3. Tar impregnation

The tar loading process was shown to be effective by the increased volatiles content in all tar-impregnated samples. Whilst the reproducibility of tar loading has not been quantified, the calculated tar loading values were used to predict the proximate composition of the tar-impregnated char within ± 0.6 %. The results indicate an inverse correlation with BET surface area. RHB-550 for example had the lowest calculated tar loading of 10.16 g/100 g biochar, and the highest surface area of 120.9 m² g⁻¹. The effect of demineralisation on tar loading is also unclear, with tar loading decreasing for WSB-550-DM (24.06-0.98 g/100 g biochar) and increasing for OSB-700-DM (16.91-28.94 g/100 g biochar). The quantity of tar loaded may therefore depend on factors other than available surface area.

The components of tar are long-chain complex molecules, such as polycyclic rosin oil, esters, fatty alcohols and terpenes (Auson 2015). An example component of rosin oil, abietic acid, is shown in Figure 5-27. Steric hindrance may therefore play a role in the micropores, with RHB-550-acetone having a larger micropore volume than WSB-550-acetone and OSB-700-acetone. Tar loading is also likely to be influenced by surface chemistry. For example, oxygenated tar components may adsorb more easily onto acidic sites; the trend in tar loadings may therefore indicate the availability of acidic sites in the biochars, *i.e.* WSB-550 > OSB-700 > RHB-550.

Chapter 5 – Surface Treatments

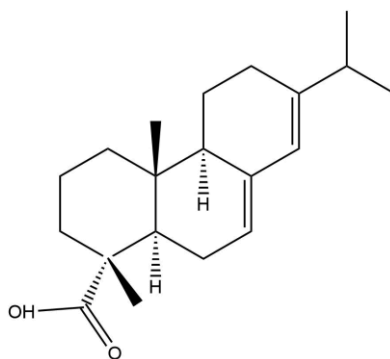


Figure 5-27 Structure of abietic acid, a component of rosin oil in pine tar.

Tar conversion during pyrolysis was very low, with no clear evidence of an increase in carbon content through bulk analysis. The biochar yield was lower than the calculated quantity of biochar in the tar-impregnated samples. This contrasts with the literature, where conversions of. Higher conversions have been achieved in the literature through activation of the tar components in the gas phase, with values of 14 % have been obtained for model tar compounds over untreated biochars, and up to 100 % in treated biochars (Kastner *et al.* 2015; Feng *et al.* 2016). The low conversion of tar in liquid phase analyses may therefore be as expected. For example, the tar may be evaporated before it can be pyrolysed to form carbon deposits. A closed system may be necessary to prevent evaporation of the tar.

Whilst there is little evidence of tar being pyrolysed in the bulk analyses, there is some evidence in the surface analyses. Surface carbon content is observed to increase in XPS analysis, whilst surface silica and oxygen content decreases. This could indicate that carbon has formed on silica and oxygenated sites. However, some of this effect may be attributable to the pyrolysis of the char, rather than the tar; with increased pyrolysis, the ash and carbon content would be expected to increase, whilst surface oxygen content would decrease (Sun *et al.* 2014; Angın & Şensöz 2014; Zhao *et al.* 2016; Tag *et al.* 2016). Similarly, the doubling of BET surface area may be partly attributable to pyrolysis; increases in surface area of up to 30 times with increased pyrolysis temperature have been reported in the literature (Sun *et al.* 2014). Thorough characterisation of pyrolysed control samples is recommended to determine the extent of changes attributable to pyrolysis of tar, versus pyrolysis of char.

The formation of carbon deposits might be expected to lead to a decrease in pore volume, due to pore blockage. However, the effect of tar impregnation and pyrolysis on porosity varies. Consistent with the expected effect of pyrolysis alone, microporosity is seen to increase for RHB-550-T-C, and mesoporosity increases for WSB-550-T-C and OSB-700-T-C. A decrease in mesoporosity is seen for RHB-550-T-C, which may be due to carbon deposits forming in mesopores. There is also no microporosity detected in OSB-700-T-C, suggesting that the micropores in OSB-700 may be blocked by carbon deposits. Alternatively, the micropores may have coalesced during pyrolysis, leading to a loss of microporosity; this is noted as causing a loss of microporosity at higher pyrolysis temperatures in the literature (Angin & Şensöz 2014).

The effect of tar impregnation on the surface of RHB-550 is demonstrated in Figure 5-28 as a schematic. The C=O groups are suggested as sites where amorphous carbon deposits are adsorbed, as indicated by the increase in surface carbon and increase in disordered carbon. The decrease in graphitic and aromatic carbon is illustrated. There is also a slight reduction in surface silica, possibly due to the adsorption of carbon deposits at the surface. The amorphous carbon at the surface may in turn lead to an increased number of interstices, or micropores, explaining the increase in micropore volume and therefore BET surface area.

Chapter 5 – Surface Treatments

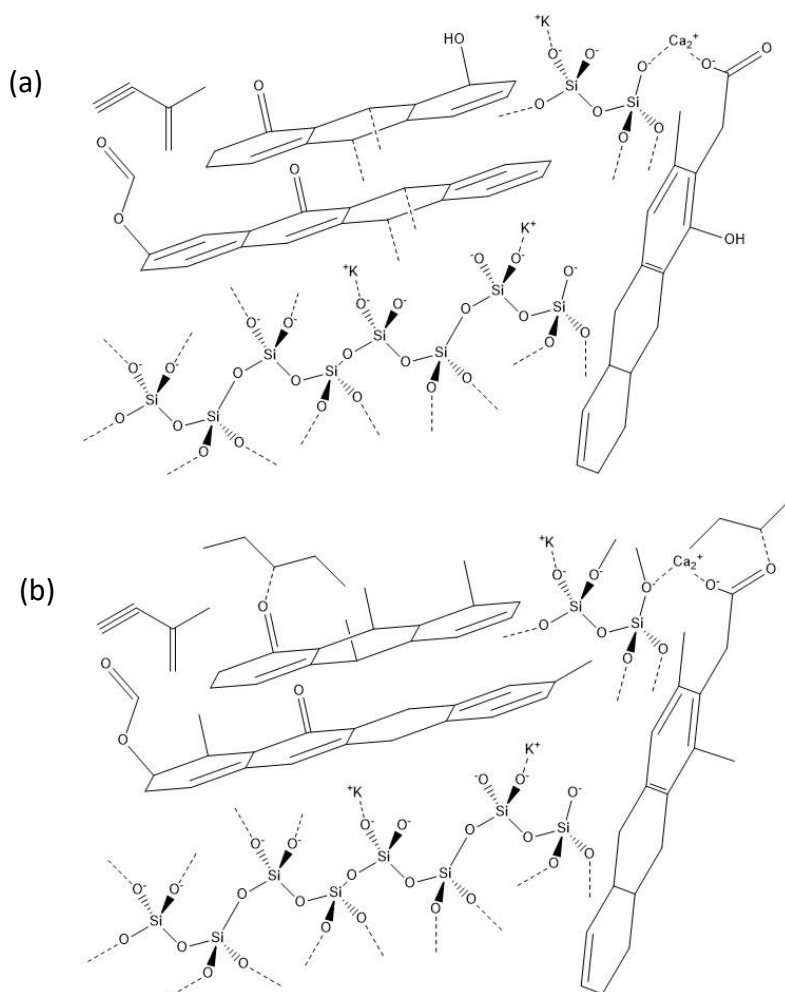


Figure 5-28 Schematic of the surface structure of RHB-550 (a) before and (b) after tar impregnation and pyrolysis.

Although the formation of carbon deposits from the tar cannot be confirmed, the effect of potassium on carbon structure during pyrolysis has been clearly demonstrated. This will be considered separately in section 5.4.4.

5.4.4. Role of potassium in influencing carbon structure

There is clear evidence that potassium influences the carbon structure following pyrolysis. Demineralisation leads to a much greater increase in surface area following tar impregnation and pyrolysis, with BET surface areas tripling or quadrupling. This is greater than the increase expected from pyrolysis alone for these feedstocks, for example the 71 % increase for OSB-700 compared to OSB-550, and may indicate carbon deposits increase the available

area for N₂ adsorption. The impact of tar impregnation and pyrolysis is also highly feedstock-dependent, as shown by the varying effect on mesoporosity.

Potassium content may influence the graphiticity of the carbon structure. Following tar impregnation and pyrolysis, the sample with the highest potassium content (OSB-700) increases in graphiticity, as measured by the A_{D1}/A_G ratio and contribution from band I to the XPS C1s spectra. However, the sample with the lowest potassium content (RHB-550) has increased contributions from disordered carbon. Following demineralisation, this pattern is lost, with OSB-700 decreasing in graphiticity. This could indicate that biochars with higher potassium content promote the formation of more graphitic carbon or carbon deposits following tar pyrolysis.

There is some evidence from XPS survey scans that more carbon is deposited on demineralised samples compared to untreated samples. The percentage increase in atomic carbon content following tar impregnation and pyrolysis is greater for the demineralised samples. However, this is not reflected in the tar loading calculations, which indicated a negligible tar loading for WSB-550-DM, for example. This would be a surprising result, as potassium is thought to catalyse the formation of carbon deposits from tar; if more deposits are formed in the absence of carbon, this implies other factors are stronger influences on tar conversion to carbon deposits.

The location of carbon deposits may also change following demineralisation. In all cases, microporosity is increased, indicating that carbon deposits are not formed in micropores. However, the contribution from band G_L (C=O) to Raman spectra is removed in RHB-550 and WSB-550, but unchanged in the demineralised samples. This could indicate that carbon deposits are no longer forming on C=O, and that the adsorption of carbon to this group is influenced by potassium or AAEM content. However, the same effect is not observed in the XPS C1s data, and may be more indicative of the heterogeneous nature of the biochar surface.

Chapter 5 – Surface Treatments

5.4.5. Implications for catalytic applications

The experimental work has firstly shown that biochars from different feedstocks do not respond in the same way to surface treatments. This is particularly clear for the demineralisation experiments – whilst the surface area of RHB-550 and OSB-700 was reduced, the surface area for WSB-550 increased. It therefore should not be assumed that a treatment developed for the activation of one feedstock will necessarily work in the same way with another feedstock.

Notably, a comparison of the properties after surface treatments indicates that biochars are still predominantly clustered by feedstock type (Figure 5-29). Whilst ash content and graphiticity of biochars was altered by surface treatments, a plot of graphiticity versus ash content demonstrates that the changes were not as significant an influence on properties as the choice of feedstock. The range of graphiticities did not vary significantly from those of untreated biochars, whilst ash contents did not vary enough to compensate for feedstock choice (i.e. the lowest ash content for a treated RHB sample was still higher than for WSB or OSB).

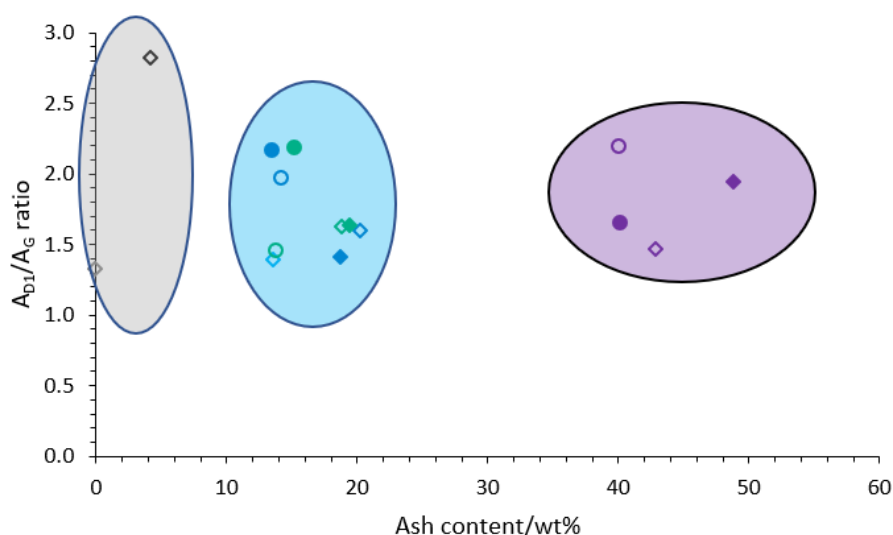


Figure 5-29 Comparison of biochar properties before and after demineralisation and tar impregnation. Green = WSB-550, blue = OSB-700, purple = RHB-550, grey = SWB-550 and black = commercial AC. Open diamonds = untreated, filled diamonds = tar-impregnated, open circles = demineralised, filled circles = demineralised and tar-impregnated. The highlighted areas demonstrate that biochars remain clustered by feedstock type.

In this work, biochars have been formed with higher surface areas, and with reduced ash contents. This may enhance or reduce their catalytic activity for certain applications. Potassium and calcium may also increase the graphiticity of the carbon deposits formed (*e.g.* demineralisation led to reduced graphiticity of carbon deposits, as seen in Figure 5-23) – it is possible they also influence catalytic activity. By testing these modified biochars for catalytic activity, insights can be gained into factors which influence activity in chemical reactions. For example, the removal of potassium content may be detrimental, beneficial, or have no impact. Similarly, the effect of the carbon deposits on the activity of the biochars can be tested.

5.4.6. Implications for sustainability

The primary aim of the experiments in this chapter was to allow the influence of individual properties on catalytic activity to be studied. As stated in the twelve principles of green chemistry, the use of auxiliary substances such as acids to produce catalysts should be avoided (Principle 5). Even after surface treatments such as demineralisation, the main influence on the properties of the biochars was from the feedstock material used (see Figure 5-29). This indicates that a more sustainable route to developing carbonaceous catalysts with desired properties would be the careful selection of a suitable raw material. This would keep additional surface treatments to a minimum. The study of the catalytic activity of carbon deposits may also aid the improvement of sustainable reaction engineering, by improving the energy efficiency of the process (Principle 6) and selectivity of the catalyst (Principle 9).

In this chapter, the structure of the carbon deposits was shown to be influenced by the feedstock; **following demineralisation, the graphiticity of the carbon deposits (as measured by Raman spectroscopy) decreased.** This indicates that catalysts containing AAEM could lead to the formation of more graphitic carbon deposits. Coupled with reaction data, this knowledge could extend the lifetime of industrial catalysts susceptible to coking, thus reducing the quantity of catalyst required (Principle 1 – preventing waste formation). The improved performance of the catalyst would also reduce the energy requirements of the process (Principle 6).

Chapter 5 – Surface Treatments

5.4.7. Limitations and Future Work

During this work, several areas were identified for improvement. These included the quantification of tar loading, the curve deconvolution processes used for Raman and XPS C1s spectra, and suggestions for further characterisation. Future avenues of research are also proposed which are beyond the scope of the current work.

The **demineralisation method** used in the present work did not remove the main component of the ash, which was identified as silica. Some elements may also be present in insoluble forms, or be inaccessible due to pore blockage or hydrophobicity. Silica removal would require chemicals such as NaOH and HF, which would likely disrupt the surface chemistry and pore structure of the char (Moreno-Castilla, Carrasco-Marín, Maldonado-Hódar, *et al.* 1997); further work may be required to identify less disruptive methods for ash and silica removal.

One key area for improvement would be the **choice of solvent for diluting the tar**. Alcohol or turpentine are traditionally suggested as thinning agents (Auson 2015), however acetone was chosen for its availability and known effectiveness as a solvent. The ideal solvent would have minimal effect on the properties of the biochar, allowing the effect of tar impregnation and pyrolysis to be isolated. Studies of the effect of solvents on model carbons, such as graphite, could also advance understanding of the properties of carbonaceous catalysts in reaction media.

The **tar loading process** could be further characterised. Adsorption isotherms could be obtained, by adsorbing small but known quantities of tar onto the surface of the biochars. Reproducibility experiments should also be performed. In the present work, surface-sensitive analysis was not possible, due to the requirement for high vacuums in techniques such as XPS and SEM, making them unsuitable for analysis of highly volatile components. Surface characterisation was therefore performed after pyrolysis. Control experiments are also recommended to isolate the effect of pyrolysis of char from pyrolysis of the loaded tar.

The error bars for the **curve deconvolution of Raman and C1s XPS spectra** were relatively high, particularly for bands where overlap was expected. A systematic analysis could be performed to optimise the curve fitting procedure, such as identifying the physical basis for restricting peak widths. This could aid the development of standard procedures for spectral analysis of carbonaceous materials; as noted in section 2.5, there is currently little consistency in curve deconvolution methods employed. Similarly, standard measures of graphiticity could also aid progress in this area. Analysis of a larger number of sample areas would also allow the natural heterogeneity of samples to be accounted for in error analysis.

As was discussed in Chapter 4, **further characterisation techniques** could be used to develop a more complete picture of the properties of the biochar. Techniques such as TPD and pH tests could test the effect of the surface treatments on the surface acidity, whilst high resolution O1s XPS spectroscopy could provide details on the oxygen sites present. The composition of the prepared ash samples may also require further investigation, as volatile components and dust will be lost during combustion of the biochar (Sander & Andrén 1997). Alternative methods, such as digestion followed by ICP, could allow trace metal content to be quantified more accurately, although these methods would be less surface-sensitive than XPS (Tag *et al.* 2016).

The **properties of the bio-oil** produced in pyrolysis may also be of interest. Potassium is known to influence the yield of biochar, with the yield of bio-oil usually being lower in the presence of a catalyst (Manyà 2012). Bio-oil was not characterised in the present work, however the potential of biochar to catalyse the formation of more useful bio-oil products (*e.g.* products with higher heating values and higher C/O ratios for use as transport fuel), albeit with lower yields, could provide an interesting avenue for further research.

Chapter 5 – Surface Treatments

5.5. Conclusions

In this work, the response of biochars from different feedstocks to surface treatments has been thoroughly characterised. Biochars have been treated with HCl to remove ash content, and with acetone to test the effect of oxygenated organic solvents on biochar properties. A novel liquid phase tar impregnation method was then developed, which was used to produce carbon deposits on biochars before and after demineralisation. The carbon structure of the biochars was characterised in detail, such as the graphiticity and the types of oxygen-containing functional groups present at the surface. The key conclusions of the work are:

- The feedstock dependence of demineralisation and acetone washing indicates that treatments cannot be generalised when applied to biochars – a treatment developed for the optimisation of catalytic activity in one feedstock may have a lesser or even opposite effect on biochars from another feedstock.
- The effectiveness of demineralisation varied from removal of 4.5 wt% ash in RHB-550, to 29.9 wt% ash in OSB-700. The composition of the ash (particularly quantity of silica) has a strong influence on the success of HCl in demineralisation.
- The effect of demineralisation on porosity was varied, and was attributed to the differing extent of removal of AAEM elements, depending on their locations and forms in the chars (*e.g.* soluble carbonates in pores or insoluble phosphates in the bulk). In RHB-550, both micropore and mesopore volume decreased, leading to decreased BET area, whilst in WSB-550, micropore volume was unaffected whilst mesoporosity increased, with an overall increase in BET area. Potassium was the only element consistently removed from the surface of the biochars.
- Most chlorine was removed from the biochars following demineralisation, however the surface chlorine content of RHB-550 was increased. The decreased micro- and mesoporosities of RHB-550-DM may indicate that chlorine from HCl was deposited in the pores. The effectiveness of distilled water washing for chlorine removal may be dependent on the hydrophobicity of the biochars; further research would be required to confirm this.
- Acetone washing had similar effects to demineralisation on structural properties; surface areas were decreased for RHB-550 and OSB-700, and increased for WSB-550.

The same trend in mesoporosity was also observed; this may indicate that the mesopore mouths in RHB-550 are narrower and more prone to blockage, *e.g.* by chlorine or oxygenated groups. The effect on microporosity varied; micropore volume increased in AC, RHB-550 and RHB-550-DM, likely due to existing micropores being cleared. Microporous structure was lost in OSB-700 and WSB-550, possibly due to coalescence of micropores.

- There is little change to surface chemistry following demineralisation and acetone washing. No new functional groups are detected in XPS, FTIR or Raman spectra, although there is a reduction in smaller aromatic rings (five-membered and fewer) after demineralisation, possibly due to the action of Cl⁻. A slight reduction in aromatic C=C was also noted for SWB-550 following acetone washing. There was a slight increase in volatile content of biochars following acetone washing, measured by proximate analysis, indicating fixed carbon may be converted to volatile carbon.
- The novel liquid phase tar impregnation method was shown to be successful through TGA proximate analysis, with tar loadings estimated at between 10-25 g/100 g biochar. The accuracy of the tar loadings was tested by comparing the actual and predicted proximate compositions, assuming that all of the material added was volatile mass. The quantity of tar loaded was inversely correlated with surface area and porosity; it is possible that steric hindrance effects prevent adsorption of tar in materials with higher microporosities, such as RHB-550-acetone.
- Tar conversion following pyrolysis was low, possibly due to evaporation of tar prior to conversion, with no increase in carbon content detected by proximate analysis. However, increases in surface carbon were detected by XPS, consistent with the formation of carbon deposits. Raman studies indicated that demineralisation influenced the structure of these deposits: OSB-700 and WSB-550 increased in graphiticity following tar impregnation and pyrolysis, however OSB-700-DM and WSB-550-DM decreased in graphiticity. Potassium content may therefore be beneficial for the formation of graphitic carbon during pyrolysis.
- Following tar impregnation and pyrolysis, decreases were observed in surface Si and O content, and in the contribution of C-O, C=O and O-C=O functional groups in XPS C1s spectra. Decreases in the contribution of band G_L (C=O) to the Raman spectra

Chapter 5 – Surface Treatments

were also observed. This could indicate that carbon deposits are formed on silica and oxygen-containing functional groups. Following demineralisation, band G_L was unaffected. This may indicate that the location of carbon deposits was also altered by demineralisation.

- The changes in biochar properties following tar impregnation and pyrolysis may be partly attributable to the role of pyrolysis alone. Preliminary tests and literature sources indicate that pyrolysis of char also increases the C:O ratio and ash content. Pyrolysis control tests are therefore recommended to determine the extent of changes attributable to the formation of carbon deposits.

Following on from this study, the catalytic activity of the biochars will now be studied in two reactions. The thorough characterisation work from Chapter 4 will allow the key factors influencing activity to be identified, whilst the surface treatments tested in this chapter will enable the influence of individual factors to be tested. Demineralisation for example will allow the impact of potassium and calcium content on biochar to be investigated, whilst the influence of graphitic and non-graphitic carbon deposits can be tested using the tar-impregnated samples. This work will provide insights into the origins of catalytically active coke, which could then be exploited industrially, as well as demonstrating the potential of biochar from different feedstocks in catalytic applications. These findings will advance the objective of improving the sustainability of heterogeneous catalysis, by improving the energy efficiency of industrial reactions (Principle 6), and facilitating the development of catalysts sourced from a renewable resource (Principle 7).

The first reaction to be studied will be the conversion of methanol to products, using CO₂ as an oxidant, in Chapter 6. Oxidation of methanol is often used as a probe reaction in the characterisation of catalysts (Tatibouët 1997), and therefore studying the range of products will provide insights into the types of active sites on the biochars. A second reaction, the upgrading of glycerol to glycerol carbonate using CO₂, will then be considered in Chapter 7 as an example of the potential of biochar catalysts in CO₂ utilisation reactions.

Chapter 6 – Methanol Conversion

Overview

Methanol conversion to dimethylcarbonate (DMC) is a promising carbon dioxide (CO₂) utilisation reaction, providing a more sustainable pathway to a versatile green reagent. Thus far, investigations into the application of carbon as a catalyst in this reaction are limited, with most heterogeneous catalysts being metal oxides, sometimes on carbon supports. In this chapter, biochar from different feedstocks is tested for catalytic activity in this reaction, with the aim of identifying key factors responsible for the catalytic activity of a carbonaceous catalyst.

Although DMC was not formed, dimethoxymethane (DMM) was shown to be favoured in biochars with low potassium contents, a link not previously made in the literature. The formation of DMM in anaerobic conditions is evidence of active surface oxygen in biochars, and indicates the presence of acidic sites required for the conversion of formaldehyde to DMM. Key by-products in the liquid phase included tetramethylorthosilicate (TMOS), which may have formed through the reaction of any DMC with silica content in the biochar. 1,1-dimethoxyethane (1,1-DME) was an unexpected by-product not observed in the literature, and may be formed from the direct methylation of DMM. In summary, biochars exhibited potential for activating methanol and possibly CO₂ for conversion, and therefore biochar may be active in other CO₂ utilisation reactions. This will be tested in Chapter 7 through the study of glycerol upgrading using biochar catalysts.

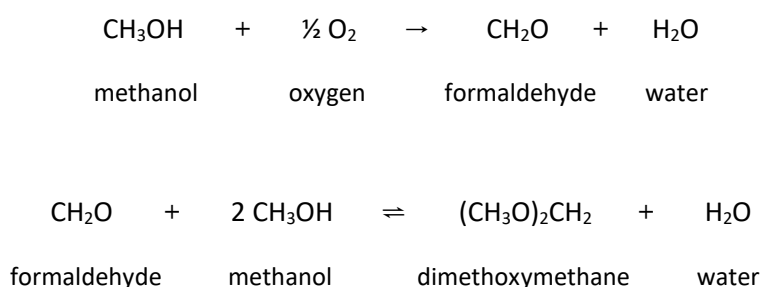
6.1. Introduction

Methanol conversion reactions have the potential to transform the sustainability of the chemical industry. The idea of a ‘methanol economy’ was popularised by Nobel Prize winner George Olah in 2004, to reduce dependence on fossil fuels and instead use methanol as a feedstock, fuel and means of energy storage (Olah 2004). As a chemical that can be renewably sourced (e.g. from biomass and carbon dioxide recycling), methanol conversion reactions could offer new reaction pathways to products that are currently sourced from fossil fuel, and are therefore the subject of intense research interest.

One such set of reactions involves the conversion of methanol to dimethyl carbonate, using carbon dioxide (CO₂) as a feedstock. The application of carbon dioxide as a chemical feedstock was discussed in section 2.4, and has the potential to address the issues of global

warming and sustainability. Dimethyl carbonate (DMC) is of particular interest for its applications as a 'green reagent', being non-toxic, biodegradable and having no irritating or mutagenic effects. The potential of this reaction route to improve sustainability was discussed in section 2.4.1.

The conversion of methanol is often used as a probe reaction to study the properties of catalysts. For example, the selectivity to formaldehyde, methyl formate and dimethoxymethane (DMM) can offer insights into the strength of acidic and basic sites on the catalyst (Thavornprasert *et al.* 2016). DMM in particular has potential applications as a fuel additive. The formation of DMM can proceed via selective oxidation of methanol to formaldehyde (Tatibouët 1997), as shown in Scheme 6-1.



Scheme 6-1 Formation of dimethoxymethane from methanol oxidation.

For biochar catalysts, the study of this reaction and the liquid phase products could improve understanding of the catalytic properties, and therefore provide insights into potential industrial applications as a catalyst. By using a range of feedstocks, and isolating factors for further investigation through surface treatments used in Chapter 5, key properties of the biochar can be identified that determine its catalytic properties, which can be exploited in future catalyst design.

In this chapter, the catalytic properties of biochars are investigated for the conversion of methanol to dimethyl carbonate, using carbon dioxide as a reactant. The aim is to identify which properties of biochars influence the catalytic activity in this CO₂ utilisation reaction, and therefore biochars from a range of feedstocks will be used. In section 6.2, the reaction and analysis methods are developed based on the literature, with results of initial screening and control tests given in section 6.3.1. The role of CO₂ in the reaction is briefly investigated

Chapter 6 – Methanol Conversion

in section 6.3.2. The impact of individual properties is then investigated by using treated biochar samples from Chapter 5; the results of these experiments are presented in section 6.3.3. The activity of biochar towards an unexpected by-product, tetramethylorthosilicate (TMOS), is presented in section 6.3.4 and conversion data considered in section 6.3.5. The implications of the results for catalyst and reaction design are discussed in section 6.4, with the conclusions presented in section 6.5.

6.2. Methods

The experimental work in this chapter involved reaction studies, using biochar as a catalyst in the conversion of methanol to products in a small batch reactor. The reaction method is described in section 6.2.1. Analysis and calibration of the liquid phase products was carried out by GCMS analysis, the theory of which was described in section 3.6.5. The GCMS analysis methods are described in sections 6.2.2 and 6.2.3. Characterisation work from Chapter 4 and Chapter 5 is referred to throughout to interpret the reaction data presented in this chapter.

6.2.1. Reaction method

The reaction conditions used in this study were chosen in consultation with fellow PhD student Ali Hameed, whose PhD focuses on the role of coke in methanol conversion to DMC. The reaction conditions used were intended to facilitate comparison between the studies, and had shown potential for DMC conversion in his preliminary studies. It was beyond the scope of the present work to optimise the reaction conditions further. The reaction methods were adapted from those developed in the literature (Bhanage *et al.* 2001; Almusaiter 2009).

The methanol conversion reaction was carried out in a 45 ml autoclave reactor, as described in section 3.6.3 (Parr, model number 4714). The reaction was carried out on an IKA C-MAG HS 7 Magnetic Stirring plate. 0.20 g of biochar was added to 7 ml of methanol (Sigma Aldrich, purity >99.9%). The reactor was then sealed and loaded with 18 bar of CO₂ (BOC, purity 99.8%). The reaction conditions are summarised in Table 6-1 for reference, and were used unless otherwise stated in the Results.

Table 6-1 Reaction conditions for the conversion of methanol with CO₂ to form products.

Reactor volume/ml	45
CO₂ loading pressure/bar	18
Reaction pressure (approx.)/bar	45
Reaction temperature/°C	200
Quantities of liquid reagents	7 ml methanol
Quantity of catalyst/g	0.20
Reaction time/hrs	18

Chapter 6 – Methanol Conversion

The reactor was placed in an aluminium heating block and heated to 200 °C, controlled using a thermocouple. The reaction time was 18 hours, with a stirring rate of approximately 500 rpm. Following reaction, the reactor was cooled in ice water for 10-15 mins.

6.2.2. Liquid phase product analysis

Two samples of the reaction products were prepared for GCMS analysis. The first sample consisted of 1.5 ml of undiluted liquid products in a 2 ml GCMS vial, with 1.0 µL of 2-propanol used as an internal standard. This was to enable the detection of low-concentration products. The second sample contained 50 µL of liquid product in 1.45 ml of distilled water with 1 µL of internal standard. This allowed the final concentration of methanol to be determined without saturating the detector.

The internal standard of 2-propanol was chosen for its miscibility in ethanol and distilled water, and non-reactivity with the analysis mixture. As shown in section 6.3.1.2 (Figure 6-2), 2-propanol was shown not to be a reaction product, and did not overlap with any of the product peaks in GCMS analysis, thus fulfilling the requirements of an internal standard.

The liquid products were analysed using a GCMS fitted with a DB1-MS capillary column (length 59.7 m, internal diameter 0.25 mm, film thickness 0.25 µm). 0.5 µL of sample were injected into the column. A simple temperature ramp was used for each part of the analysis, and is detailed in Table 6-2 and Table 6-3.

Table 6-2 GCMS method for analysis of undiluted liquid phase products of methanol conversion reaction.

Heating rate/°C min ⁻¹	End T/°C	Hold time/mins
-	40	2
10	120	2
Solvent cut time/mins	3.9	

Table 6-3 GCMS method for analysis of diluted liquid phase products of methanol conversion reaction.

Heating rate/°C min ⁻¹	End T/°C	Hold time/mins
-	40	2
10	100	2
Solvent cut time/mins	0	

6.2.3. Calibration

The two main peaks of interest were the dimethoxymethane peak, as the target product, and the concentration of methanol, which would allow the conversion to be estimated.

Calibration samples were therefore prepared for these two peaks. For each set of reactions, at least three concentrations of calibration sample were prepared to allow the concentrations to be calibrated from the GCMS peak areas. The calibrations were repeated after any column changeovers.

For calibration of DMM, part 1 of the GCMS analysis method (described in Table 6-2) was used. Between 1-15 μL of DMM was dissolved in methanol to give 1.5 ml of calibration sample. For methanol calibration, Part 2 of the GCMS analysis was used (described in Table 6-3), with concentrations ranging from 10-50 μL MeOH per 1.5 ml aqueous sample. For each calibration sample, 1 μL of 2-propanol was added as an internal standard, such that the concentration of internal standard was the same for calibration and reaction samples. The calibration curves can be seen in Appendix C .

Chapter 6 – Methanol Conversion

6.3. Results

The experimental work was divided into three sections: the screening of biochars for catalyst activity (section 6.3.1), experiments to verify the role of CO₂ in the reaction (section 6.3.2), and testing of biochars that had undergone surface treatments (6.3.3). This allowed the factors affecting the catalytic activity of biochar to be identified. The production of TMOS is considered briefly in section 6.3.4, and conversion data is discussed in section 6.3.5. The implications of the results are discussed in section 6.4.

6.3.1. Catalyst screening

The first stage of experimental work was to determine which biochars were effective as catalysts for the conversion of methanol to products. Control tests were run in the absence of catalyst, and the results were compared with the activity of biochars from four different feedstocks, pyrolysed at 550 °C: soft wood biochar (SWB), wheat straw biochar (WSB), rice husk biochar (RHB) and oil seed rape biochar (OSB). The activity of these biochars was then compared with a commercial activated charcoal (AC), before testing the role of CO₂ in the reaction in section 6.3.2.

6.3.1.1. No catalyst

Control tests in the absence of catalyst were performed to verify what products were obtained independently of the biochar catalysts. In particular, the potential catalytic effect of the reactor walls, as described in section 2.2.6, could be eliminated.

The reaction conditions were as described in Table 6-1, but without any catalyst added. The experiment was performed three times, once in each of the three reactors available, to ensure any variation between the reactors was accounted for. Before quantifying, the GCMS spectra were examined to identify any products and contaminants. The GCMS spectra for the three control tests are shown in Figure 6-1.

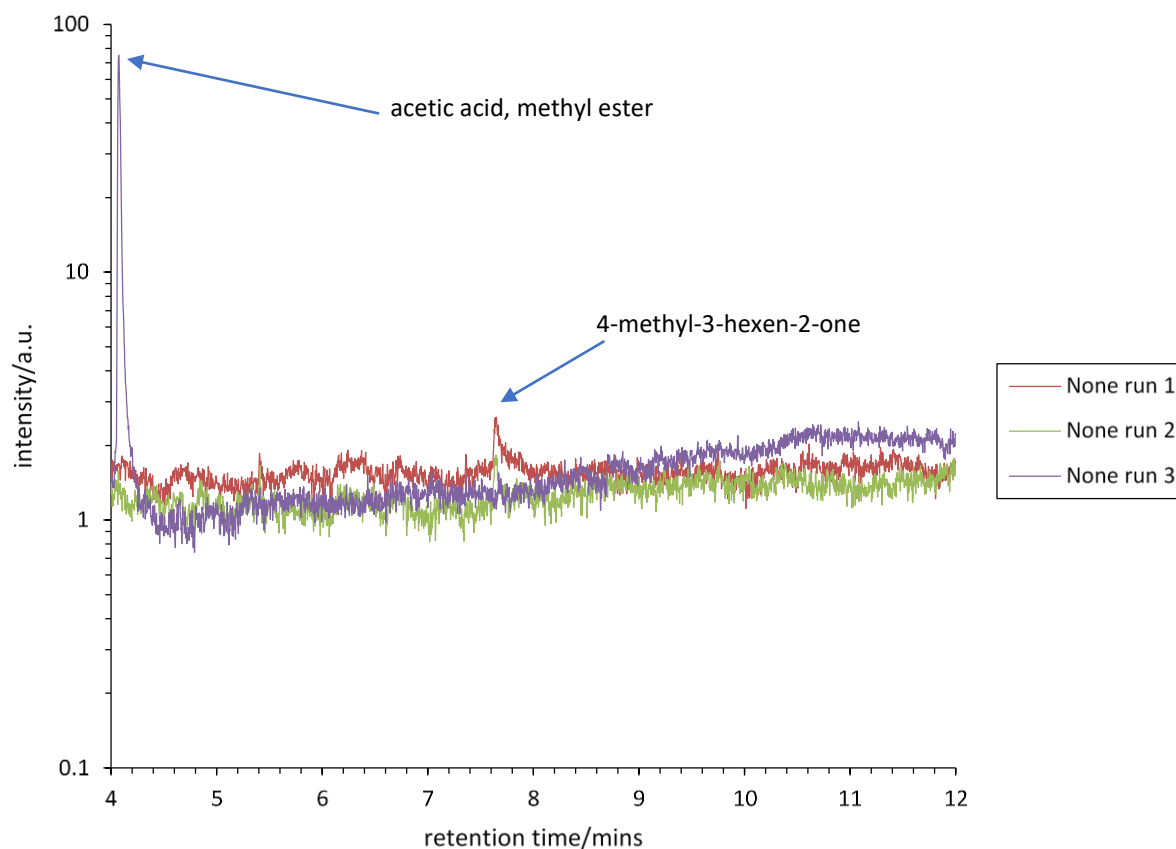


Figure 6-1 Comparison of the GCMS spectra for no catalyst. A logarithmic y-axis is used to allow presentation of both large and small peaks. Peaks as identified by MS are annotated.

From the GCMS spectra in Figure 6-1, it is clear that there are no liquid phase products formed. In particular, there is no DMM or DMC produced. Although two peaks are observed (acetic acid methyl ester in run 3, 4-methyl-3-hexen-2-one in run 1), they are not consistently produced in the absence of catalyst. These peaks can therefore be discounted as contaminants, and any other peaks formed when using biochar catalysts can be attributed to the activity of the biochar.

6.3.1.2. Product identification

The next stage was to assess what liquid phase products are formed when using biochar catalysts, before quantifying and calibrating the products. In this section, the GCMS spectra are analysed to determine which peaks can be attributed to genuine reaction products, and which can be discounted as contaminants. This also allows a 'gap' to be identified in the spectra for an internal standard. The peaks of interest are then calibrated and quantified in section 6.3.1.3.

Chapter 6 – Methanol Conversion

In Figure 6-2, GCMS spectra are shown for four carbonaceous catalysts with a range of ash contents and properties, as was shown in Chapter 4. The results should therefore represent the full range of products expected in these experiments.

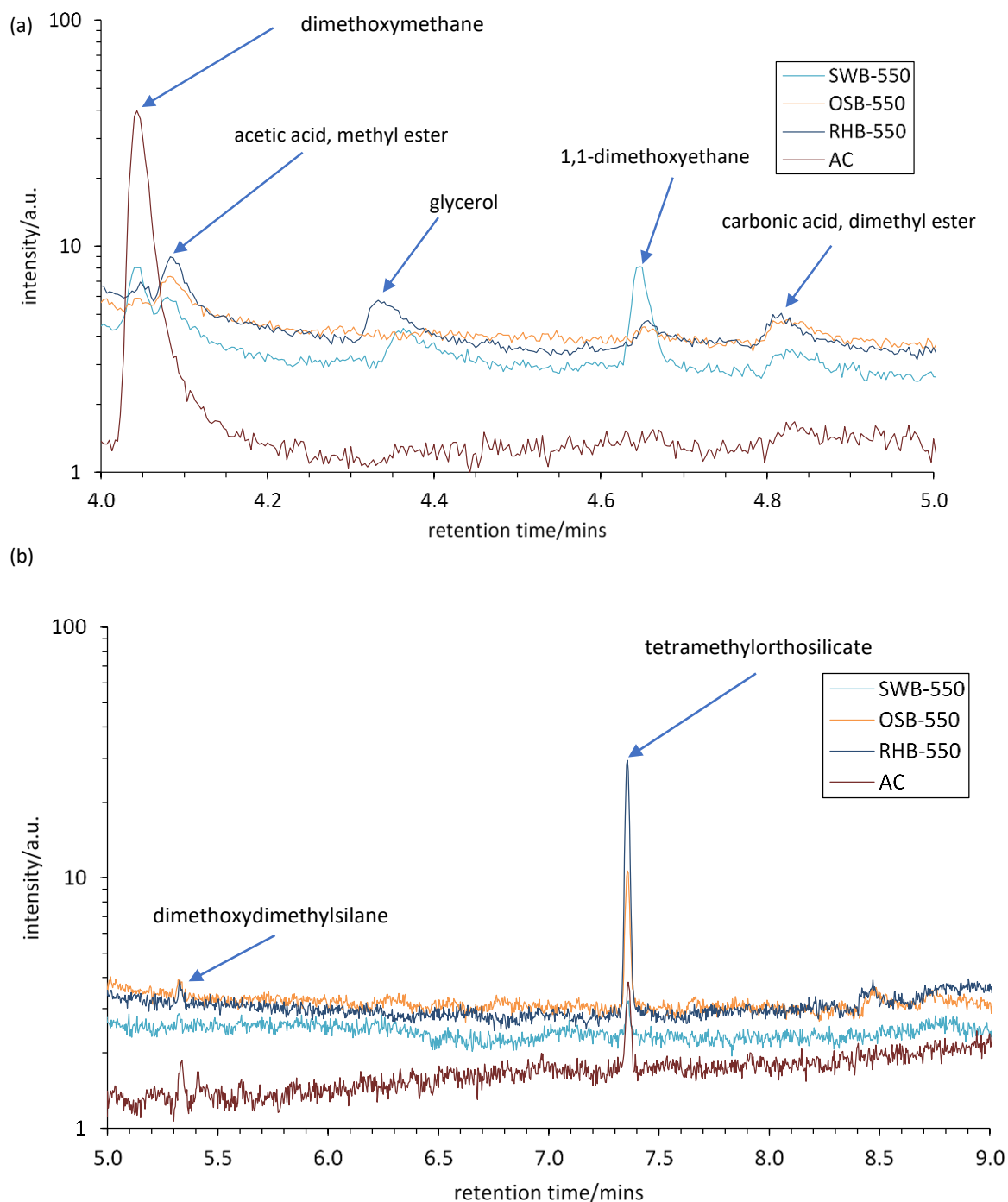


Figure 6-2 Comparison of GCMS spectra for three biochars, compared with commercial AC. (a) for retention times 3.9-6.0 mins, (b) for 6-9 mins. A logarithmic y-axis scale is used to make the identification of smaller peaks easier.

From Figure 6-2a, it is clear that DMM has been produced for AC and SWB-550. This appears to be the main liquid phase product, with no DMC detected. Unexpectedly, 1,1-dimethoxyethane (1,1-DME) also appears to be produced using SWB-550. 1,1-DME is similar in chemical structure to DMM, varying only by the addition of a methyl group to the central carbon in place of a hydrogen atom, as shown in Figure 6-3. The potential mechanisms are considered in section 6.4.2.

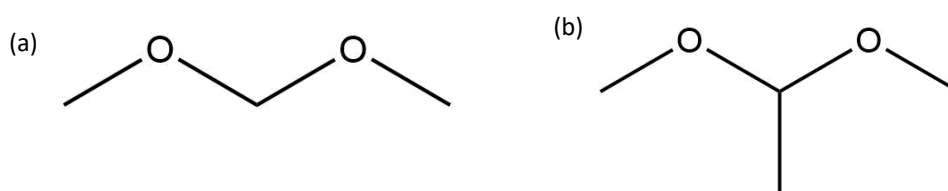


Figure 6-3 Structure of (a) DMM compared with the structure of (b) 1,1-DME.

Acetic acid methyl ester is detected for RHB-550 and OSB-550, however as this is also detected in the absence of catalyst (see Figure 6-1), this may be a contaminant. Glycerol is also likely to be a contaminant from glycerol conversion reactions carried out in these reactors. As will be discussed in Chapter 7, glycerol is highly viscous (approximately 1.41 Pa s), and can be difficult to remove from the reactor pipework.

The presence of product peaks containing silica is of interest, as the source of silica is likely the ash content of the biochars. If the source was the silica-based GCMS column, the silica-containing peaks would be expected in the control experiments and calibration samples, however this is not the case. A very small peak corresponding to dimethoxydimethylsilane can be seen in Figure 6-2a, with a much larger tetramethylsilicate (TMOS) peak observed in Figure 6-2b. It is worth noting that the quantity of TMOS appears at first to correspond with the ash content of the samples, as measured by proximate analysis; AC and SWB-550 are essentially ash-free, whilst RHB-550 exhibits the highest percentage of ash (42.92 wt%). This will be explored further in section 6.3.4.

Chapter 6 – Methanol Conversion

The formation of carbonic acid may be due to the reaction of CO₂ with water produced in the reaction as a by-product (see Scheme 6-1). However, this peak is very small, and difficult to verify as carbonic acid, due to the background MS spectra.

No DMC was detected in the liquid phase products; this chapter focuses on the production of DMM. This product was calibrated as described in section 6.2.3. The quantity of TMOS produced by the various biochar catalysts is considered in section 6.3.4, and methanol and CO₂ conversion data are considered in section 6.3.5.

6.3.1.3. Biochar activity

The calibrated data is presented in this section to allow a comparison of the activity of biochars from different feedstocks towards DMM production. As it has not been possible to calibrate or normalise the peak areas for 1,1-DME, the raw peak area data is used. However, the peak areas seem to be consistent over time; the percentage error for 1,1-DME was calculated as $\pm 20.0\%$ using three repeats of SWB-550 collected over two years. This was lower than the percentage error of the calibrated DMM, 23.3%. The calculations are presented in Appendix C.

In Figure 6-4, the concentration of liquid phase products is shown for five biochars, including OSB pyrolysed at 550 °C and 700 °C, and the commercial standard AC. It is firstly confirmed that DMM and 1,1-DME are only produced in the presence of a catalyst, and that AC is the most active for the formation of DMM. However, SWB-550 is the most active for 1,1-DME formation. SWB-550 is the most active for DMM production of the biochars studied, producing leads to approximately 10 × higher concentrations of DMM than other feedstocks. AC, SWB-550, OSB-700 and WSB-550 are the most active for 1,1-DME formation. RHB-550 and OSB-550 do not lead to high concentrations of DMM or 1,1-DME being produced. The implications of this are discussed further in section 6.4.3.

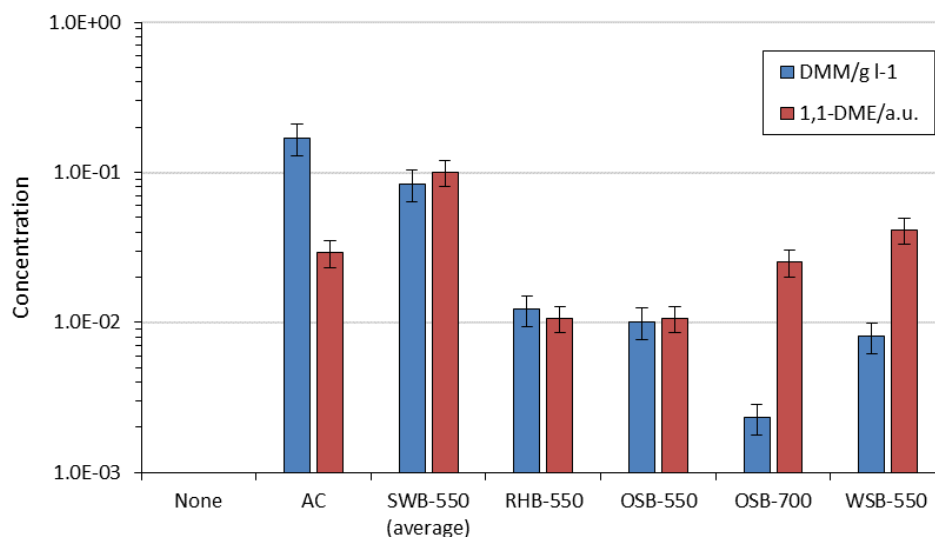


Figure 6-4 Liquid phase products of methanol conversion using biochars produced from different feedstocks. A logarithmic y-axis is used to present large and small concentrations. Percentage errors of 23.3 % for DMM and 20.0 % for 1,1-DME calculated from three repeats of SWB-550 for DMM concentration. Note that the concentration of 1,1-DME is given in arbitrary units.

The internal standard peak area appeared to be highly variable – an example is given in Figure 6-5. This was attributed to experimental error in adding 1.0 μL of standard to the product vial. The precision of the micropipette of 0.5 μL leads to a $\pm 50\%$ error in the quantity of 2-propanol added. Therefore, the calibrated data are presented here without normalisation using the internal standard. The calibration issues are discussed further in section 6.4.5; calibration calculations are compared in Appendix C

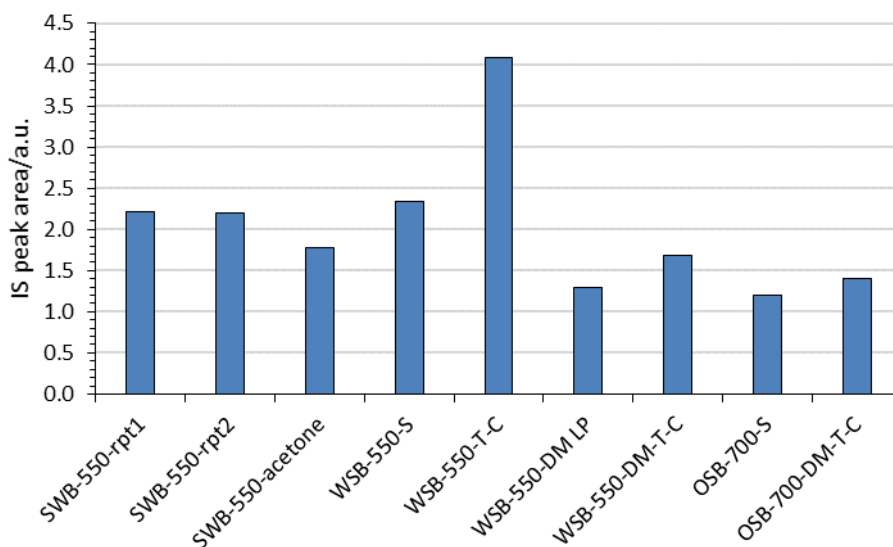


Figure 6-5 GCMS peak areas for the internal standard, 2-propanol, for a set of experiments performed in March 2018.

Chapter 6 – Methanol Conversion

The mechanism of DMM and 1,1-DME formation requires further investigation, in particular whether or not CO₂ plays a role. In section 6.3.2, the role of CO₂ is investigated by repeating the experiment in an inert helium (He) atmosphere. The role of pressure is also briefly investigated.

6.3.2. Influence of gaseous atmosphere

In section 6.3.1, it was found that DMM and 1,1-DME were produced in higher quantities using two of the six carbonaceous catalysts tested. However, no DMC was formed, and the mechanisms for the formation of DMM and 1,1-DME are currently unclear. In this section, the potential role of the gaseous atmosphere is investigated. From the literature review, it is known that the formation of DMC is favoured by higher pressures (see section 2.4.1), whilst DMM can be produced by selective oxidation or via a condensation reaction with methanol and formaldehyde. In section 6.3.2.1 the experiment is repeated in an inert atmosphere to determine the role of CO₂ in the reaction, whilst the effect of reaction pressure is briefly investigated in 6.3.2.2.

6.3.2.1. Role of CO₂

To determine the role of CO₂ in the methanol conversion reaction, the experiment was repeated using the same loading pressure, temperature, reaction time and quantities as per Table 6-1. The only change was the replacement of CO₂ with He gas (BOC, purity > 99.9 %). The reaction pressure was the same as for reaction with CO₂, therefore any changes in catalytic activity are not due to differences in pressure when using He.

Three catalysts were chosen to examine the range of possible effects in an inert atmosphere. AC was previously the most active catalyst for DMM production, SWB-550 was the most active for 1,1-DME production, and RHB-550 performed poorly in both. Therefore, any increase, decrease or lack of change should be apparent by studying these three samples. RHB-550 in particular was chosen due to its very different ash content and composition compared to SWB-550 (see section 4.3.2).

In Figure 6-6, the performance of AC, RHB-550 and SWB-550 in producing DMM and 1,1-DME are compared in CO₂ and He atmospheres. The effect differs by feedstock. SWB-550 produces slightly less DMM in the helium atmosphere, and RHB-550 produces approximately 10 × less DMM. However, the concentration of DMM increases almost by a factor of ten for AC, from 0.169 g l⁻¹ in CO₂ to 1.01 g l⁻¹ in He. 1,1-DME production appears to be less affected by the change to a helium atmosphere. Slight increases in concentration are observed for AC and RHB-550, with a slight decrease for SWB-550. The possible reasons and mechanisms for DMM and 1,1-DME production are discussed in section 6.4.2.

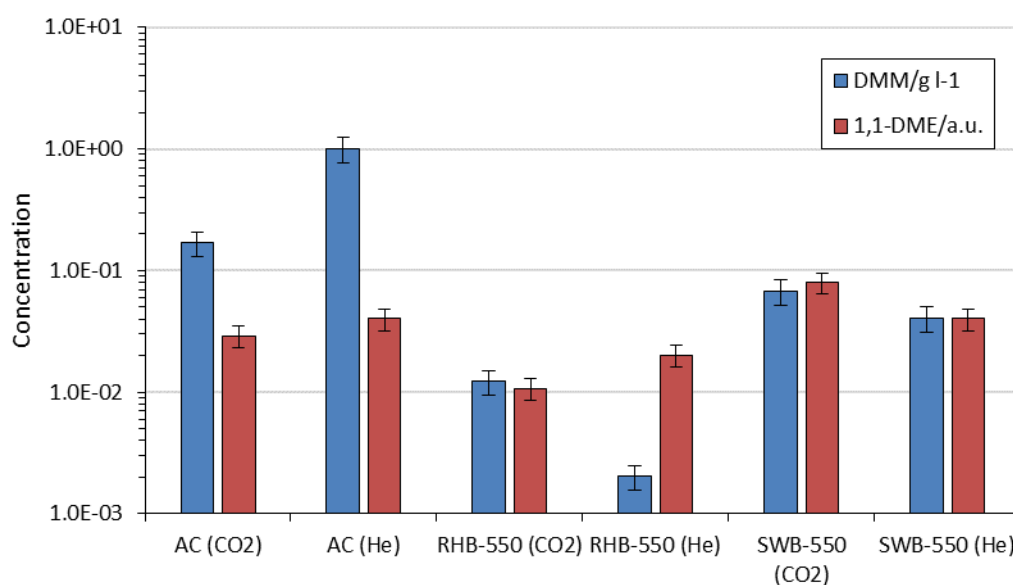


Figure 6-6 Comparison of production of DMM and 1,1-DME with and without CO₂.

As expected, DMC was not produced in the absence of CO₂, as CO₂ is expected to be a reagent in this case. The influence of CO₂ was next tested in terms of reaction pressure in section 6.3.2.2.

6.3.2.2. Role of reaction pressure

The effect of reaction pressure on product concentration is briefly considered in this section. The experiment was repeated using AC as a catalyst in a CO₂ atmosphere, but with a loading pressure of 25 bar, resulting in a reaction pressure of 50 bar.

Chapter 6 – Methanol Conversion

The effect of increased reaction pressure on DMM and 1,1-DME concentration is shown in Figure 6-7. The quantity of DMM is increased by almost four times at the higher pressure of 50 bar, from 0.169 g l⁻¹ to 0.690 g l⁻¹, whilst 1,1-DME is no longer produced. No DMC was produced at the higher pressure of 50 bar, indicating that increased pressure alone is not sufficient to favour the formation of DMC. The reasons for DMM formation and lack of DMC production are discussed in section 6.4.2.

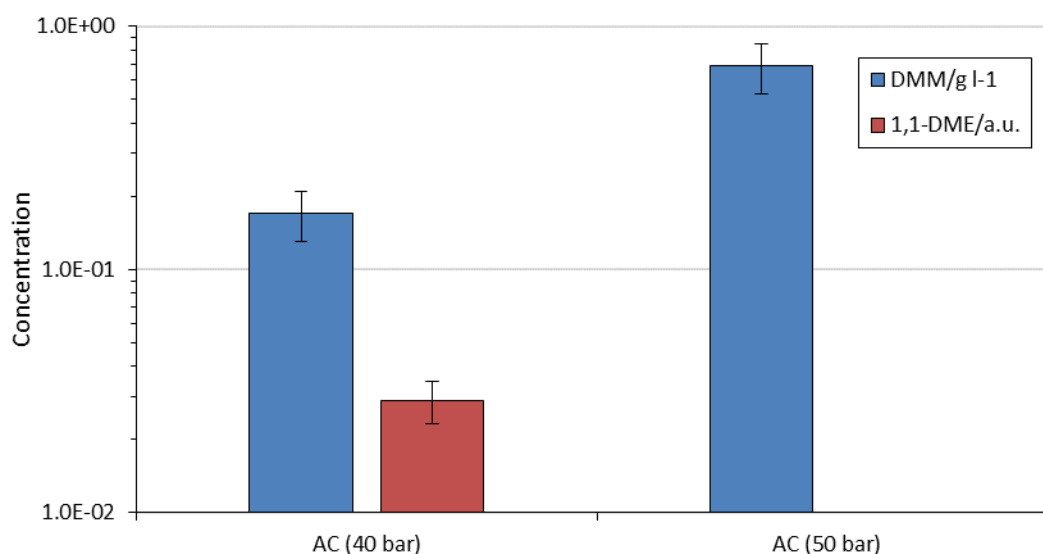


Figure 6-7 Comparison of production of DMM and 1,1-DME at different reaction pressures, using AC as a catalyst.

6.3.3. Effectiveness of treated biochars as catalysts

In order to verify which factors most strongly influenced the catalytic activity of the biochar, samples that had undergone surface treatments were tested for catalytic activity. The first factor studied was the effect of surface area, which is presented in section 6.3.3.1. As these experiments demonstrated that increased surface area was not solely responsible for the improved activity of the treated samples, the effect of acetone washing, demineralisation and tar impregnation on DMM and 1,1-DME production was studied in section 6.3.3.2. Characterisation work from Chapter 4 is referenced throughout to assist the interpretation of the results, with the implications of the results discussed in section 6.4.

6.3.3.1. Effect of surface area

It is expected that a high surface area is beneficial for catalysis, as it allows a greater quantity of material to be adsorbed. From the BET data in Chapter 4, it appears that the catalysts with the greatest surface area are also the most active for DMM formation. The surface area of SWB-550 ($390 \text{ m}^2 \text{ g}^{-1}$) is more than three times that of the next highest biochar, RHB-550 ($121 \text{ m}^2 \text{ g}^{-1}$). It may therefore only be necessary to increase the surface area for catalysis to occur. A table of the surface areas for the samples of interest is presented alongside the figures in this section for ease of reference.

To test this hypothesis, two biochars with increased surface areas after treatment were tested. The surface area of WSB-550-DM-T-C ($374 \text{ m}^2 \text{ g}^{-1}$) and of OSB-700-DM-T-C ($343 \text{ m}^2 \text{ g}^{-1}$) was similar to that of SWB-550 ($390 \text{ m}^2 \text{ g}^{-1}$). It would therefore be expected that if surface area was the dominant factor, a similar concentration of DMM would be obtained for all three samples. The effect of increased pyrolysis temperature on activity was also tested by comparing the activity of OSB-550 with that of OSB-700.

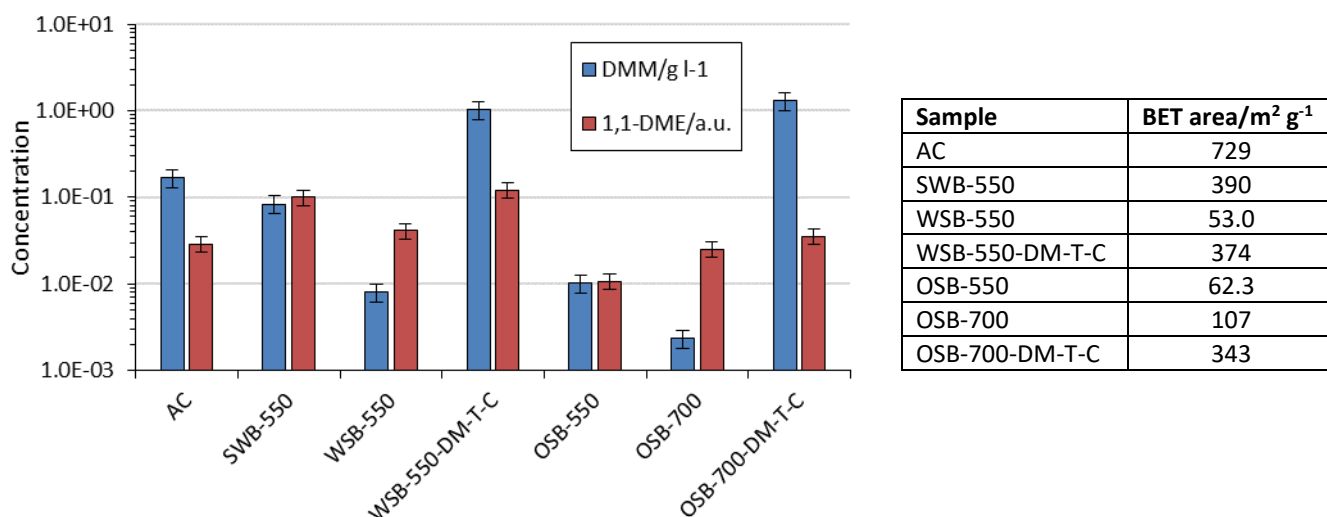


Figure 6-8 DMM and 1,1-DME production for treated biochar samples. Percentage error of 23.3 % for DMM and 20.0 % for 1,1-DME calculated from three repeats of SWB-550.

The data presented in Figure 6-8 firstly demonstrate the effectiveness of surface treatments in activating WSB-550 and OSB-700. Notably OSB-700 was less active than OSB-550, despite having a surface area almost twice as high. The surface treatments applied to WSB and OSB

Chapter 6 – Methanol Conversion

are effective; both WSB-550-DM-T-C and OSB-700-DM-T-C outperform the SWB-550 catalyst by more than 100 times, despite similar surface areas.

As for DMM, the surface treatments applied to WSB-550 and OSB-700 lead to increased production of 1,1-DME, but on a much smaller scale. In this case, the increase for WSB-550-DM-T-C is a factor of 3, whilst for OSB-700-DM-T-C the improvement is only a factor of 1.5. Unlike DMM, the OSB-700 outperforms OSB-550. For 1,1-DME, the improvements may be explained simply by the increased surface area, however the underlying activity still appears to be feedstock-dependent.

6.3.3.2. Effect of surface treatments

As the improved performance of WSB-550-DM-T-C and OSB-700-DM-T-C is not simply explained by increased surface area, the surface treatments must have influenced catalytic activity. In this section, the intermediate treatments used in producing WSB-550-DM-T-C will be studied, to identify which stage had the greatest influence. The implications of the results will be discussed in section 6.4.

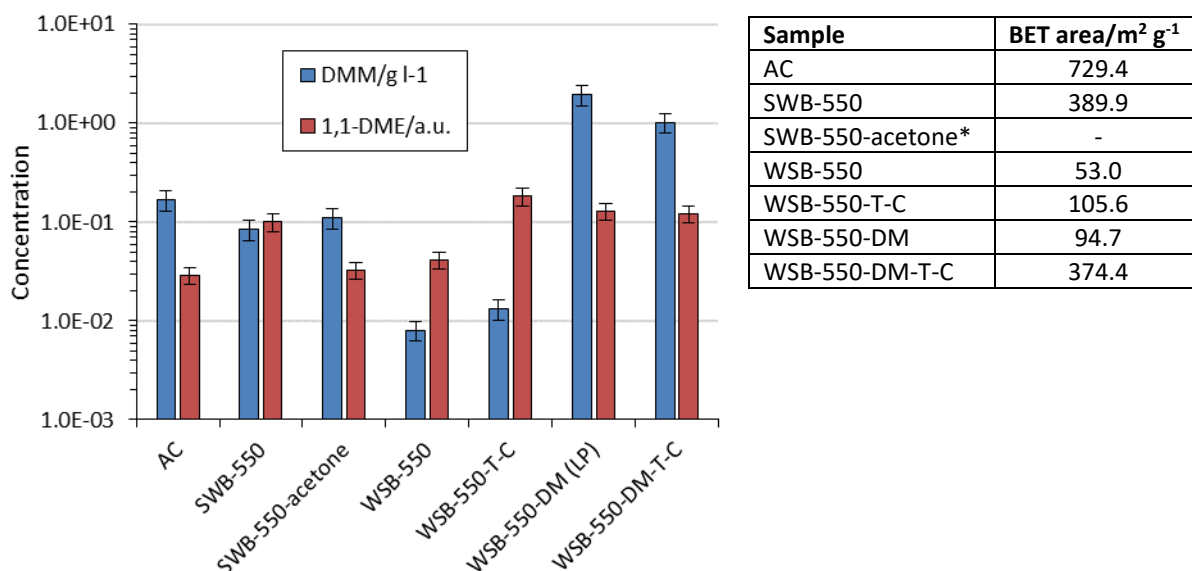


Figure 6-9 DMM and 1,1-DME production for treated biochar samples. Surface area for SWB-550-acetone not measured. LP indicates low pressure (20 bar, compared to 40 bar).

From Figure 6-9 it is clear that demineralisation influences DMM production. The highest DMM concentration was achieved using WSB-550-DM, despite the lower reaction pressure of 20 bar caused by a relief valve fault, and WSB-550-DM-T-C produces 100 times more DMM than WSB-550-T-C. From Figure 6-7, the expectation is that higher pressures favour DMM formation. This should imply that DMM production would be even higher for WSB-550-DM at the intended reaction pressure of 40 bar. The influence of demineralisation on 1,1-DME is less clear; similar quantities of 1,1-DME are produced using WSB-550-T-C and WSB-550-DM-T-C. The highest quantity of 1,1-DME is produced using WSB-550-T-C. For WSB-550-DM (LP), the concentration of 1,1-DME might be expected to be lower at the intended reaction pressure, in accordance with Figure 6-7. The effect of acetone washing was briefly considered using acetone-washed SWB-550. The DMM yield from SWB-550 is slightly improved, shown in Figure 6-9, whilst 1,1-DME production is decreased.

6.3.4. TMOS

Although the formation of tetramethylorthosilicate (TMOS) has not yet been considered, it is worth noting as it was not an anticipated product. It also appears to be a genuine reaction product; although the column is silica based, this peak is only ever observed in reaction products, and not in calibration samples.

As for 1,1-DME, it was not possible to quantify or normalise the amount of TMOS produced in each reaction, however the raw peak area is presented here as an indication of the quantity produced. The quantity is likely to be low, as the peak area is of the same order of magnitude as the internal standard, *i.e.* approximately 0.001 g ml⁻¹.

Chapter 6 – Methanol Conversion

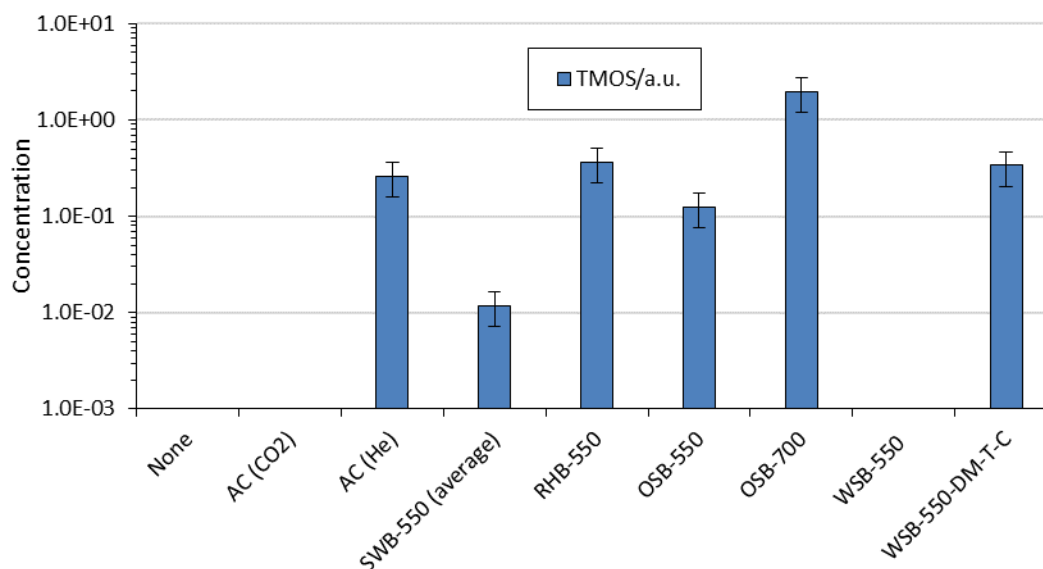


Figure 6-10 Quantity of TMOS produced when using biochars from a range of feedstocks. Percentage error estimated from two repeats of SWB-550 as 39.2 % (third repeat omitted as an outlier).

From Figure 6-10 there is no simple pattern behind the production of TMOS. The quantity of TMOS increases with pyrolysis temperature, as shown by OSB-700 and OSB-550. Surface treatments also appear to activate WSB-550, as no TMOS is produced before surface treatment, whilst WSB-550-DM-T-C produces similar quantities to RHB-550 and AC (He). TMOS is also only detected when using AC in a helium atmosphere, but not in a CO₂ atmosphere. The repeat data for SWB shows that the peak is reliably detected at roughly the same order of magnitude, and the TMOS peak was not detected in any calibration or control samples. This has been identified as an area for further study, and will be discussed in section 6.4.2.3.

6.3.5. Conversion

Methanol conversion to liquid phase products was calculated by comparing the concentration of methanol in the liquid phase products with pure methanol. This was the second stage of the GCMS analysis. Due to calibration issues it has unfortunately not been possible to calculate conversion values for all experiments – the calculations are given in Appendix C .

From the reproducibility experiments on SWB-550, the method of calculating methanol conversion appears to be unreliable. For all experiments, the range of methanol conversion values lies in the range of 10-20%, however for SWB-550 alone there are values between 13% and 20% (see Appendix C). There are also several cases where negative methanol conversions of up to -30 % were calculated. As methanol is a volatile component, there may be a strong time dependence in the GCMS analysis of these samples; if a sample is left for several hours before GCMS analysis, as happens when processing a batch file overnight, it is possible that the methanol will evaporate, leaving a lower concentration in the vial. This same issue may have particularly affected the dilute calibration samples, and therefore it has not been possible to accurately calibrate the methanol conversion.

In terms of CO₂ conversion, as gas phase analysis proved very difficult due to the pressure in the line being too high for MS analysis, the only indicator possible is the final pressure in the reactor, compared to the loaded pressure of 18 bar. This however only gives an indication of whether there are more or fewer moles of gas in the reactor than at the start, and so cannot be used as a measure of CO₂ conversion.

Chapter 6 – Methanol Conversion

6.4. Discussion

The aim of studying the conversion of methanol over biochar was to identify the factors affecting the catalytic activity of the biochar. The objective was to apply the insights gained from these experiments to the design of carbonaceous catalysts, and to identify any insights into the reaction mechanisms of methanol conversion over carbonaceous catalysts. The findings may also aid the understanding of the phenomenon of catalytically active carbon deposits, as discussed in 2.2.5. In this Discussion of the results, the implications of the results are discussed in terms of:

- Which properties of biochar affected DMM and 1,1-DME production, which did not, and possible reasons for this
- The possible mechanism of DMM and 1,1-DME production over the biochars
- The feasibility of using biochar as a carbonaceous catalyst in this reaction and others
- The implications of the work for improving sustainability
- Limitations of the work and recommendations for future work

A summary of the key conclusions of the chapter follows in section 6.5, with a consideration of the questions still to be answered, and which aspects will be investigated in further detail in this Thesis.

6.4.1. Influence of potassium on DMM production

From the experimental work presented in section 6.3, there is clear evidence that potassium is hindering the production of DMM. A plot of DMM concentration against potassium content reveals a negative correlation (see Figure 6-11). This has not previously been noted in the literature; while potassium is a common component of catalysts for DMC production, the exact mechanism is unclear, and the detrimental effect on DMM production has not previously been observed.

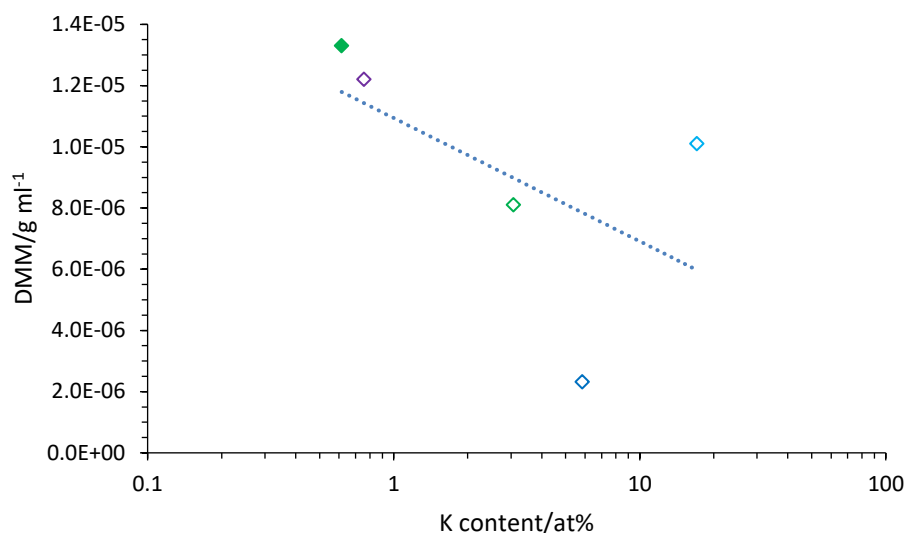


Figure 6-11 Plot of DMM concentration against surface potassium content. Note the logarithmic axis used for potassium content. (Green = WSB-550, blue = OSB-700, purple = RHB-550, grey = SWB-550 and black = commercial AC. Open diamonds = untreated, filled diamonds = tar-impregnated.)

The possible effects of potassium are:

1. Positively charged potassium ions alter the surface electronic environment, preventing the adsorption and/or activation of methanol. For example, the positive charge of K^+ may cause OH^- groups to adsorb too strongly, either preventing reaction of adsorbed methanol or desorption of DMM.
2. Potassium may lead to the formation of more basic sites, such as KOH groups. It is suggested in Chen & Ma that for DMM production in anaerobic conditions, a balance is needed between active surface oxygen and acidic sites. Basic potassium sites may reduce the concentration of acidic sites, which would be detrimental to DMM selectivity (Chen & Ma 2017).
3. The potassium could be enhancing competing reactions. These could be reactions involving intermediates in the production of DMM, or reactions from DMM to other products. In this case, other products would be expected in the liquid and gas phases.

As no other liquid phase products are detected for catalysts high in potassium, the third option seems the least likely. It is however possible that gas phase products were formed,

Chapter 6 – Methanol Conversion

which were not detected in the present work. Further experiments would be needed to distinguish between options 1 and 2 – these are suggested in section 6.4.5.

6.4.2. Reaction mechanisms

The use of surface treatments altered the activity of the biochar catalysts. By considering the impact of surface treatments on DMM production, insights can be gained into the reaction mechanism of methanol conversion over carbonaceous catalysts. The insights into the mechanisms for DMM, 1,1-DME, DMC and TMOS production are considered in this section.

6.4.2.1. DMM

The finding that DMM can be produced in the absence of CO₂ is supported by the literature, where it was found by Chen and Ma that DMM can be produced under anaerobic conditions (Chen & Ma 2017). This implies that the biochar catalysts that can produce DMM must contain a balance of active oxygen sites, which oxidise the conversion of methanol to formaldehyde, and acidic sites, which catalyse the formation of DMM from formaldehyde. The same study found that oxygen from Si-O is inactive, or at least not consumed, in this reaction, and it is therefore likely to be C-O groups providing the active oxygen in this case. This may explain why low-ash, high-carbon compounds were initially found to be the most active for DMM production.

The biochars were found to respond differently to commercial AC in anaerobic conditions, as seen in Figure 6-6, indicating a difference in mechanism. Whilst DMM production was increased in anaerobic conditions for AC, DMM production was lower for the biochars SWB-550 and RHB-550, compared to using a CO₂ atmosphere. It is expected that in anaerobic conditions, the active surface oxygen is depleted, whereas CO₂ may re-oxidise the surface. CO₂ may also react with H₂O by-products, shifting the equilibrium towards the product side (see Scheme 6-1). This explains why the biochars perform better in a CO₂ atmosphere. The potential reasons for why AC performs better in anaerobic conditions will be briefly considered.

The dominant effect over AC may be the adsorption of CO₂ on surface oxygen sites, making the oxygen unavailable for DMM formation. As CO₂ is a Lewis acid, it may adsorb onto oxygen-containing sites, making them unavailable for the oxidation of methanol to DMM. In biochars, the rate-limiting step may be the re-oxidation of the readily available surface oxygen, whereas in AC the limiting step may be the availability of surface oxygen. Therefore, in an anaerobic atmosphere, the surface oxygen in AC is readily available, and DMM production is favoured. This implies that the surface oxygen is totally consumed. This could be tested through a time-on-stream study, to test whether the surface oxygen is fully consumed (*i.e.* whether the catalyst is deactivated).

Alternatively, over AC the DMM may react with CO₂ to form other products. As these were not detected in the liquid phase, the assumption would be that these are gas phase products. It is unclear why this would not occur over biochar catalysts, but may be worthy of further investigation.

6.4.2.2. 1,1-DME

From the reaction data presented in section 6.3, the selectivity to 1,1-DME formation appears to vary. For example, AC produces very high quantities of DMM, but very little 1,1-DME, whilst WSB-550-DM-T-C produces higher quantities of both products. There does not appear to be a correlation between DMM and 1,1-DME production (see Figure 6-12). It is worth considering whether the evidence supports the instinctive hypothesis that DMM is an intermediate in 1,1-DME formation, and if so, what properties of biochar are influencing this process.

Chapter 6 – Methanol Conversion

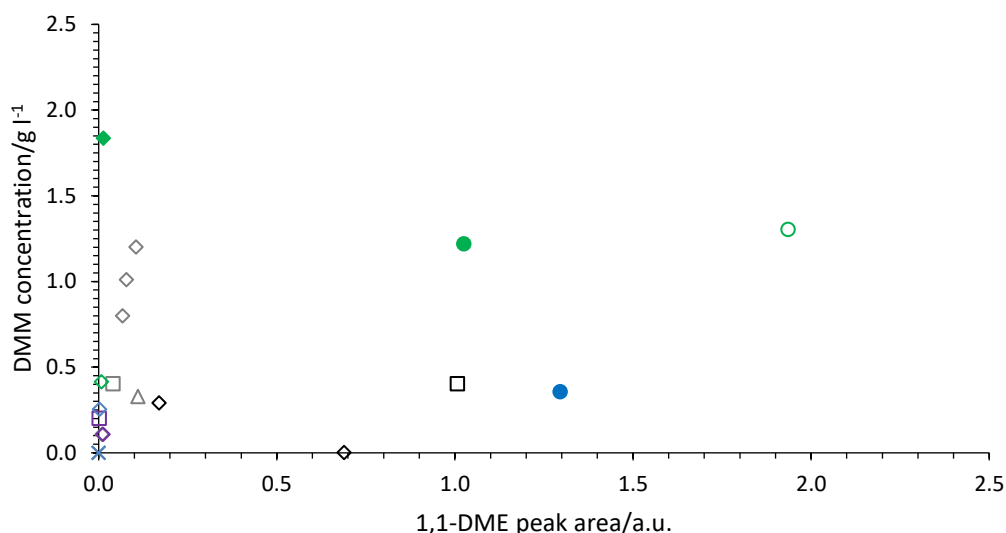


Figure 6-12 Comparison of quantities of DMM and 1,1-DME produced in methanol conversion over various biochar catalysts. (Green = WSB-550, blue = OSB-700, purple = RHB-550, grey = SWB-550 and black = commercial AC. Open diamonds = untreated, filled diamonds = tar-impregnated, open circles = demineralised, filled circles = demineralised and tar-impregnated, cross = no catalyst, square = helium atmosphere.)

The mechanism intuitively appears to be methyl addition to DMM, however, evidence has not been found for this in the literature so far. 1,1-DME is not noted as a potential or notable by-product in the literature for DMM or DMC synthesis. Similarly, DMM is not identified as an intermediate or by-product in the literature regarding 1,1-DME synthesis. Mechanisms are known for the synthesis of 1,1-DME from methanol and acetylene (Trimm *et al.* 2009), and whilst unlikely in these circumstances, acetylene is noted as a possible product of biomass gasification (Ranzi *et al.* 2008). However, in this study, 1,1-DME is never formed without also forming DMM, indicating that DMM may be an intermediate. The absence of the 1,2-DME isomer also indicates that the direct methylation of DMM could be responsible. This appears to be a relatively novel observation, though further experiments would be required to verify this reaction route.

As biochar catalysts contain a variety of active sites, it may be that biochar can catalyse DMM formation, and also a further stage converting DMM to 1,1-DME. It follows that these must be different sites from those forming DMM, as otherwise 1,1-DME would have been observed as a by-product in the literature. The nature of the active site for DMM to 1,1-DME conversion is currently unknown, although it is observed that tar impregnation is beneficial

for 1,1-DME selectivity. The potential reasons for this would be worthy of further investigation.

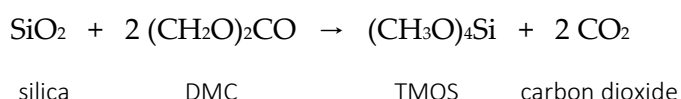
6.4.2.3. TMOS and DMC

It is worth considering why DMC was not detected in this reaction. There are two possibilities: that DMC was not formed at all, or that any DMC formed reacted further to form other products.

In the first case, the reaction conditions chosen may have been unfavourable for DMC formation. The conditions had been shown in preliminary experiments to favour DMC, however these preliminary experiments used a ZSM-5 zeolite catalyst, and so may not apply when using biochar. For example, DMC formation is known to be sensitive to reaction temperature, and the choice of 200 °C may have been too high to favour DMC production. The long reaction time of 18 hours may also have led to hydrolysis of any DMC formed, if water was formed as a by-product (Sakakura *et al.* 2007; Keller *et al.* 2010). It is therefore likely that the reaction conditions could be optimised further for biochar catalysts.

The other likely factor is the surface chemistry of biochar. The formation of DMM indicates that there are surface acid sites, which may be detrimental to DMC selectivity (Aouissi *et al.* 2010). There may be biochar catalysts which possess the required surface chemistry for DMC formation, however they were not found in this study at the reaction conditions studied.

The formation of TMOS indicates a second possibility: that DMC was formed in some cases, and subsequently reacted with silica in the biochars to form TMOS. TMOS is a useful precursor in the ceramics industry, although it is toxic, with tetraethylorthosilicate (TEOS) being a preferred reagent. One possible synthesis route is via the reaction of DMC with SiO₂ (Ono *et al.* 1993), as shown in Scheme 6-2:



Scheme 6-2 The production of TMOS from the reaction of silica with DMC.

Chapter 6 – Methanol Conversion

Rice hull ash has been employed successfully as a silica source for this reaction in the literature (Akiyama *et al.* 1993). It is therefore possible that DMC is being produced, and is reacting with the silica content of the biochars to form TMOS. This could explain why TMOS is observed in greater quantities over catalysts with high silica content, such as RHB-550. However, as DMC is not observed in the liquid phase products, this would require 100 % conversion of DMC. It is also unclear how DMC would be produced in AC in the absence of CO₂, and where the source of silica would be in SWB-550.

6.4.3. Implications for application of biochar as a catalyst

Whilst the focus of the study was on identifying factors which are responsible for the catalytic activity of biochar, it is worth considering the implications of the results for the future application of biochar as a catalyst. The aim of the experiment was not to maximise product yield, methanol conversion, or to demonstrate the commercial viability of the biochars; however, this work may provide the foundation for such studies.

The results have demonstrated that biochars are highly versatile materials for use as catalysts, with a range of compositions, surface chemistry and structures available. These properties can also be tuned using surface treatments – this was seen in Chapter 5. The usefulness of this for catalyst design is seen in the work in this chapter, as these diverse properties are reflected in the differing effectiveness of the biochars for the methanol conversion reaction. However, the potential reactivity of the ash towards DMC was not anticipated; this demonstrates that whilst biochar mostly consists of unreactive carbon, the reactivity of the ash should not be neglected.

Potassium content seemed to influence DMM production more strongly than carbon structure or surface chemistry. Potassium is simple to remove through demineralisation, although industrialisation of this process would be challenging due to the volumes of acid required and waste acid produced. On a smaller scale however, it may offer a simple method to tailor the selectivity of carbonaceous catalysts in this reaction.

Biochar has been successfully applied as a catalyst in methanol conversion, although further work would be needed to make it suitable for industrial application. Methanol was successfully converted to DMM and 1,1-DME, although methanol conversion was limited to 10-20%, and selectivity appears to be low. A higher conversion and selectivity would be required for industrial application, and this could be achieved through surface treatments, for example higher pyrolysis temperatures to increase the surface area. The conversion and range of products may however be suitable for smaller scale applications where purity and reproducibility are of less importance, for example domestic reactors converting waste to fuel, such as those discussed in a recent review by Jouhara and others (Jouhara *et al.* 2017).

Another major challenge facing the application of biochar catalysts is the poor reproducibility in terms of the quantity of products produced. Whilst products can be reliably produced, the repeats with SWB-550 demonstrated that the quantities can vary by a factor of two. Whilst the reproducibility is good enough to be sure of which catalysts are more effective than others, it would be challenging to design an industrial process using biochar catalysts. This appears to be a fundamental problem, as biochar materials are inherently heterogeneous; at the microscale each fragment of biochar will be slightly different, as shown by SEM images in section 4.3.1.

Challenges therefore remain for the industrial application of biochar as a catalytic material. However, it is significant that biochar materials exhibited improved activity following surface treatments. This can be taken as proof of concept that the properties of biochars can be fine-tuned to suit the reaction of interest. Similarly, properties such as potassium content could be used to enhance selectivity towards desired products, for example if DMM is an undesirable side product in the formation of DMC. Therefore, although biochar may not yet be suitable for applications in industry, it has shown potential to be developed as a catalyst in its own right.

6.4.4. Implications for sustainability

The current work has demonstrated that carbonaceous catalysts with low potassium contents can catalyse the formation of dimethoxymethane, although yields and selectivity

Chapter 6 – Methanol Conversion

are low. Depending on the source of the carbon material, carbonaceous catalysts could provide a more sustainable source of catalyst material than currently-used copper and nickel (Principle 7). Copper and nickel are moderately scarce in the earth's crust, and could be depleted in the next 100-1000 years at current rates of extraction, according to analysis by Henckens and co-workers (Henckens *et al.* 2014). Carbon sourced from waste biomass could provide a renewable alternative.

Further, a more sustainable pathway to dimethoxymethane has been demonstrated over carbon catalysts. Dimethoxymethane is usually sourced from non-renewable resources, for example the hydroformylation of alkanes using syngas (Abatjoglou & Miller 2011).

Depending on the source of the methanol, direct carboxylation of methanol could provide a more sustainable pathway to dimethoxymethane by using a renewable resource (Principle 7). Due to the activity of carbon in this reaction for TMOS synthesis, it is possible that low-silica carbon could also catalyse the formation of DMC under different reaction conditions. This would again be a more sustainable pathway to DMC compared to reaction with phosgene (see section 2.4.1), by utilising renewable feedstocks and catalyst materials.

6.4.5. Limitations and Future Work

The aim of the experimental work was to identify factors affecting the catalytic activity of biochar in methanol conversion. This led to a number of limitations in the experimental design, as the focus was not on optimising the reaction conditions or catalyst design. The lack of gas phase data meant that a key by-product, DME, could not be detected. The detection and quantification of DME would have allowed the selectivity of the catalysts to DMM and DME conversion to be calculated, and to verify the reaction route to DMM. Whilst online MS was attempted, the equipment tripped due to the high sensitivity to pressure. To solve this, an additional needle valve to control the gas flow could be fitted to the reactor.

A flaw in the two GCMS methods used is that expected reaction intermediates such as formaldehyde have not been detected. In the concentrated analysis, the detector was only switched on after methanol had left the column, to avoid saturating the detector. However,

intermediates such as formaldehyde will leave the column before methanol, and so are not detected. The dilute method demonstrates that the concentration of any intermediates is too low to be detected. Solutions include turning the detector off only when methanol is expected to leave the column, so that the intermediates can be detected, or reducing the dilution for the second GCMS method. If intermediates are still not detected, the implication is that the intermediates are almost completely converted, giving insights into the kinetics of the process.

An internal standard was used in this work, however the calibration of methanol was found to give a much higher R^2 value without normalising (see Appendix C), indicating that the internal standard was detrimental to accuracy. This indicates that there were precision issues in pipetting the internal standard, and the quantity added varied. When pipetting 1.0 μL of sample, the error could be proportionally higher due to small differences in surface tension, either retaining sample on the inside of the pipette or from additional sample dripping from the outside of the pipette. A higher volume of internal standard (*e.g.* 10.0 μL) could address this issue.

Certain products were not anticipated and therefore were not calibrated, such as 1,1-DME and TMOS. The calibration of these products would again provide insights into the selectivity of the reaction to DMM formation, and the reaction mechanisms of TMOS formation and 1,1-DME formation. The formation of TMOS could be studied further using time-on-stream studies, and by testing whether DMC reacts with silica-containing biochars to form TMOS. This would explain whether the ash-containing biochars are active for DMC formation, but are unsuitable for industrial application due to the reaction of DMC with the ash content. This experiment was not performed here due to the high toxicity of TMOS.

Reaction mechanisms could be investigated in further detail using surface acidity measurements. Time-on-stream studies could indicate whether 1,1-DME is formed *via* DMM. TPD- NH_3 could indicate the effect of surface treatments on acidity, for example the effect of potassium content, and therefore the impact on biochar activity. TPD- CO_2 could also indicate the adsorption strength of CO_2 on the chars, and therefore whether CO_2 is

Chapter 6 – Methanol Conversion

blocking available surface oxygen for DMM formation. The difference between AC and the biochars would be of particular interest here. High resolution XPS O1s spectra could also quantify the types of surface oxygen available in AC and the biochars.

In terms of the factors affecting catalytic activity of biochar, the results have demonstrated activity for methanol conversion is hindered by potassium content. Further work is needed to investigate whether the same properties affect biochar activity in other reactions, for example glycerol upgrading to glycerol carbonate. In this case, glycerol carbonate is not expected to react with the biochar, and so the product should be detected. This reaction is also a CO₂ utilisation reaction involving OH⁻ groups, and would allow the potential of biochar to be demonstrated in a different context. Further, the activity of carbon in this reaction suggests that carbon supports may contribute to the synthesis of dimethoxymethane. This possible contribution should not be neglected in future studies when interpreting reaction data.

6.5. Conclusions

In this Chapter, various biochars have been used as catalysts for the conversion of methanol to dimethoxymethane, in order to identify the key properties of biochars influencing their catalytic activity. The reaction was run in the absence of catalyst as a control test, and biochars from four feedstocks were compared with a commercially activated charcoal sample. Surface treatments were also performed to test the influence of individual properties of the biochar. Characterisation work first performed in Chapter 4 was used to interpret the results of the reaction studies, in terms of surface area, surface chemistry, chemical composition and carbon structure. The key conclusions were:

- Biochar from a range of feedstocks is catalytically active for the conversion of MeOH to DMM, both with and without treatment. None was formed in absence of catalyst, and DMC was not detected.
- Feedstock has a strong influence on the initial catalytic activity of biochar in DMM formation. Whilst AC and SWB-550 were active, RHB, WSB and OSB initially were not. In particular, a higher pyrolysis temperature for OSB did not lead to activity towards DMM formation, indicating the stronger influence was a property of the feedstock itself.
- The activity of feedstocks can be enhanced using surface treatments. Potassium appears to be a key factor, and likely inhibits DMM formation (rather than catalysing a further reaction). SWB and AC are free of potassium, and demineralisation of previously inactive feedstocks such as WSB-550 was shown to improve activity. Tar impregnation may also slightly improve activity through carbon deposits forming over the potassium sites.
- Although the influence of carbon structure was investigated in depth, it appeared to have little influence on DMM production. Increased graphiticity may benefit 1,1-DME production, however this would have to be decoupled from the increased surface areas of the samples tested here.

Chapter 6 – Methanol Conversion

- The formation of DMM in anaerobic conditions indicates that the biochars have available active surface oxygen, used to form formaldehyde, and acid sites, to catalyse the conversion of formaldehyde to DMM. However, it is unclear anaerobic conditions are favourable for DMM production over AC, in contrast to the biochars. AC may have limited surface oxygen available, meaning that if CO₂ adsorbs onto these sites, the surface oxygen is unavailable for DMM formation. TPD-CO₂ could be used to test the adsorption strength of CO₂ on AC, whilst high resolution O1s XPS could quantify the type of surface oxygen available in AC, compared to the biochars.
- Whilst not extensively studied, the formation of 1,1-DME may proceed using DMM as an intermediate, over a different type of active site. 1,1-DME is not produced without observing DMM, however catalysts such as AC are more selective to DMM than 1,1-DME. The absence of 1,2-DME is further evidence that DMM may act as an intermediate. The active site for 1,1-DME production may be affected by acetone washing, and selectivity to 1,1-DME may be enhanced by tar impregnation – again this must be decoupled from the effect of increased surface area.
- Although the aim was to produce DMC, no DMC was observed in the liquid phase. It is known from the literature that DMC is sensitive to the surface acidity of samples, but as DMC was not formed using any of the biochars, it is more likely that the reaction temperature was too high to favour DMC production. It is possible that DMC reacted with the silica content of the biochars to form TMOS, however this is difficult to verify without observing DMC in the liquid phase products.

Several questions following from the results in this chapter are beyond the scope this PhD, such as extensive determination of the reaction mechanisms of DMM, 1,1-DME and TMOS formation, and the precise nature and roles of the active sites. It is also not the focus of the present work to optimise the performance of the catalyst in the reaction for DMM or DMC formation, however the results presented in this chapter may provide the foundation for further study of this reaction using carbonaceous catalysts.

The next stage in the present work focuses on the application of biochar in a different CO₂ utilisation reaction, to identify whether similar factors influence catalytic activity under different conditions. From these conclusions, it is clear that biochar has potential applications in CO₂ utilisation reactions, and that the comparison of different feedstock materials is a viable method for identifying factors which determine the catalytic activity of biochar. This approach will therefore be applied to another CO₂ utilisation reaction of interest, namely the conversion of glycerol to glycerol carbonate. This will be examined in Chapter 7.

Chapter 7 – Glycerol Upgrading

Overview

The conversion of glycerol with CO₂ to glycerol carbonate and acetins is a sustainable route to forming high value products from waste materials. Literature studies have used carbon as a support and sulfonated mesoporous carbons as catalysts for glycerol transesterification reactions, and the activity of waste boiler ash for glycerol carbonate production from urea has also been demonstrated. In this chapter, the potential activity of biochars from different feedstocks is explored. Biochars from four feedstocks are screened for activity, with surface treatments then applied to test the influence of carbon and ash content. In contrast to the methanol conversion reaction, the most active catalysts were those with higher ash contents. The ash content of biochar from several feedstocks was shown to be catalytically active for the production of glycerol carbonate and triacetin, whilst ash-free catalysts such as soft wood biochar and commercial activated charcoal were inactive. The activity of the ash content was reduced following demineralisation, and this has been attributed to the loss of potassium content. The potential beneficial influences of potassium on the reaction mechanism are therefore explored in this chapter. In summary, biochar and biochar ash could find applications as catalysts for glycerol upgrading, with the role of potassium a particular focus for future research.

7.1. Introduction

The conversion of glycerol to glycerol carbonate using carbon dioxide is a reaction which tackles a number of sustainability issues. Firstly, glycerol is a waste product of biodiesel production, the quantities of which are increasing. It has been estimated that the world market supply of glycerol is currently six times' greater than demand (Christoph *et al.* 2006). Secondly, the use of CO₂ as a reagent could facilitate a reduction in CO₂ emissions, necessary to reduce the impact of CO₂ on global warming. In both of these cases, sustainability is improved in accordance with Principle 1 (preventing waste). Finally, glycerol carbonate is a useful precursor for plastics synthesis, and as such this reaction can produce a valuable chemical from renewable feedstocks (Principle 7). This route to plastics would be using a renewable resource, rather than sourcing plastic precursors from oil, and as such would be more sustainable.

Applying a catalyst sourced from renewable materials to this reaction would improve the sustainability even further. As was discussed in section 2.4.2, the direct synthesis of glycerol

carbonate from glycerol and CO₂ is the subject of ongoing research interest. Metals such as tin and rhodium have been used for the reaction (Sonnati *et al.* 2013), and the effectiveness of zeolites has also been studied (Algoufi & Hameed 2014; Ozorio *et al.* 2015; Razali 2017). However, rhodium is a platinum group metal and is very expensive, whilst tin is moderately scarce, and could be depleted in the next 100-1000 years (Henckens *et al.* 2014). Carbonaceous catalysts could therefore improve the sustainability of the process by using catalytic materials from a renewable resource (Principle 7).

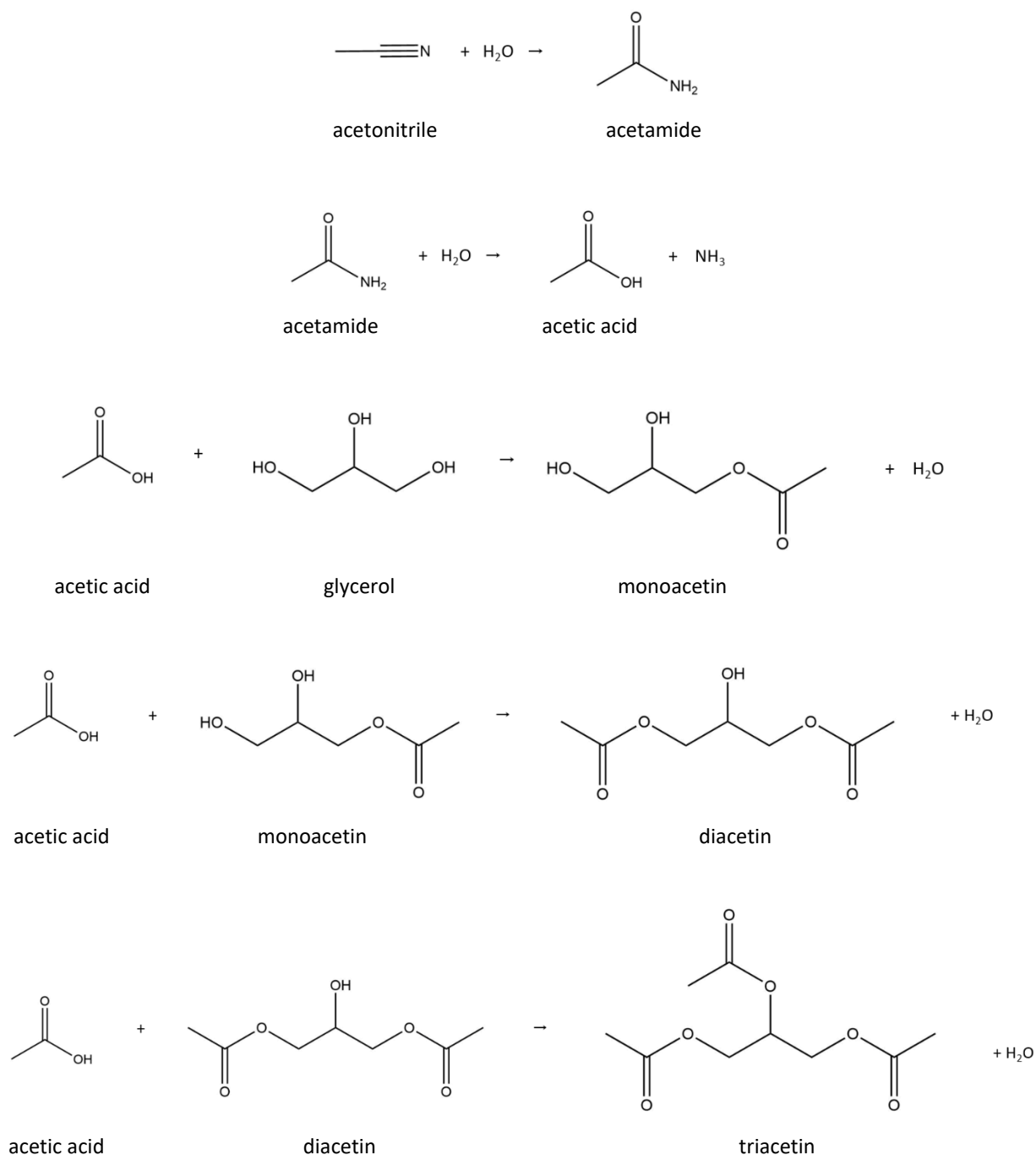
Carbonaceous materials in the literature have largely been employed as support materials, or as feedstocks for sulfonated carbonaceous catalysts (Kong *et al.* 2016). Waste boiler ash from biomass has also demonstrated activity for the synthesis of glycerol carbonate *via* the reaction of glycerol and urea (Indran *et al.* 2014). The potential of untreated biochar to catalyse glycerol conversion has yet to be studied. From Chapter 6, it is known that biochar can catalyse the conversion of a C1 alcohol; in this chapter, the potential of biochar to catalyse the conversion of polyols such as glycerol is considered. This could provide important insights into future catalyst design in this reaction, but also insights for the wider application of carbon catalysts, particularly in CO₂ utilisation reactions.

In the direct synthesis of glycerol carbonate from glycerol and CO₂, direct carbonation of glycerol leads to the formation of water, as was shown in Scheme 2-1. The removal of water can favour the production of glycerol carbonate, as the equilibrium is shifted further towards the product side. In this study, acetonitrile is used as the dehydrating agent, and has been successfully tested in the literature (Li *et al.* 2013; Li *et al.* 2015), although not with carbonaceous catalysts.

An additional benefit of acetonitrile is the production of acetins, such as those shown in Scheme 7-1. The reaction between acetonitrile and water leads to the formation of acetic acid, which then reacts with glycerol. The acetins formed can be mono-, di- or triacetins, depending on the extent of the reaction. These acetins are valuable products, finding applications as plasticisers, fuel additives and humectants (Kong *et al.* 2016). The selective

Chapter 7 – Glycerol Upgrading

production of triacetin is a particular challenge in the literature (Konwar *et al.* 2015). The potential of biochar to catalyse the formation of acetins is therefore of interest.



Scheme 7-1 Reactions for the formation of mono-, di- and triacetin from glycerol and acetonitrile.

This chapter aims to identify the properties of biochar which influence catalytic activity in the glycerol upgrading reaction. Biochars from a range of feedstocks will be screened for catalytic activity, in a similar manner to the screening tests used in Chapter 6. Treated

biochars will then be tested to isolate the effects of individual factors, for example the contribution of ash content to overall activity.

The reaction conditions and analysis methods will be outlined in section 7.2, before presenting the results of the biochar screening and treated biochar experiments in section 7.3. Characterisation work from Chapter 4 and Chapter 5 will be used throughout to assist interpretation of the results, for example by studying the role of surface area, carbon content and elemental composition. The implications of the results will be discussed in section 7.4, with key conclusions drawn in section 7.5.

Chapter 7 – Glycerol Upgrading

7.2. Methods

The experimental work in this chapter involved reaction studies, using biochar as a catalyst in the conversion of glycerol to glycerol carbonate in a small batch reactor. The choice of reaction conditions is described in section 7.2.1. Analysis and calibration of the liquid phase products was carried out by GCMS analysis, the theory of which was described in section 3.6.5. The GCMS analysis methods are described in sections 7.2.2 and 7.2.3. Characterisation work from Chapter 4 and Chapter 5 was used to interpret the reaction data presented in this chapter.

7.2.1. Reaction method

The reaction conditions used in this study were chosen in consultation with fellow PhD student Nurul Razali, whose PhD focused on designing optimal reaction conditions and catalysts for the conversion of glycerol to glycerol carbonate (Razali 2017). The reaction conditions used were intended to facilitate comparison between the studies, and had shown potential for glycerol carbonate formation. It was beyond the scope of the present work to optimise the reaction conditions further. Details of the reactor used and general reactor and liquid phase analysis methods are outlined in section 3.6; details specific to the glycerol upgrading reaction are presented here.

The glycerol upgrading reaction was carried out in a 45 ml autoclave reactor, as described in section 3.6.3 (Parr, model number 4714). The reaction was carried out on an IKA C-MAG HS 7 Magnetic Stirring plate. 0.23 g of biochar was added to 4.6 g of glycerol, with 5 ml of acetonitrile used a dehydrating agent. The reactor was then sealed and loaded with 18 bar of CO₂ (BOC, purity 99.8%). The reaction conditions are summarised in Table 7-1 for reference.

Table 7-1 Reaction conditions for the conversion of glycerol with CO₂ to form products.

Reactor volume/ml	45
CO₂ loading pressure/bar	18
Reaction pressure (approx.)/bar	30
Reaction temperature/°C	160
Quantities of liquid reagents	4.6 g glycerol 5 ml acetonitrile
Quantity of catalyst/g	0.23
Reaction time/hrs	22

The reactor was placed in an aluminium heating block and heated to 160 °C, controlled using a thermocouple. The reaction time was 22 hours, with a stirring rate of approximately 500 rpm. Following reaction, the reactor was cooled in ice water for 10-15 mins.

7.2.2. Liquid phase product analysis

Following syringe filtration, a GCMS vial was prepared for analysis of the liquid phase products. Due to the high viscosity of glycerol (approximately 1.41 Pa s), the sample was first diluted with 10 ml of ethanol in the reactor, to allow the contents to be extracted more easily. Due to the high glycerol concentration and the high retention levels of glycerol in the column, the sample was diluted further: 100 µL were added to 1 ml of ethanol for GCMS analysis, with 1 µL of internal standard.

The internal standard chosen was 1-hexanol (Sigma-Aldrich, 98%). 1-hexanol was chosen due to its similar structure to glycerol (as a 6-carbon alcohol), its non-reactivity with the products or reagents, its miscibility in ethanol, and for the fact that its GCMS peak occurred in an otherwise empty part of the GC spectrum (~8.3 mins retention time). This will be justified in section 7.3.1.2.

The liquid products were then analysed using a GCMS fitted with an HP-INNOWAX capillary column (length 30 m, internal diameter 0.25 mm, film thickness 0.25 µm). 0.5 µL of sample were injected into the column. The GCMS analysis method is detailed in Table 7-2.

Table 7-2 Method used for analysis of products of glycerol upgrading reaction in the GCMS.

Temperature/°C	Hold time/min	Ramp rate/°C min ⁻¹
40	2	10
163	1	50
190	3	10
205	3	10
250	5	N/A

Chapter 7 – Glycerol Upgrading

7.2.3. Calibration

Calibration samples were prepared to relate the GCMS product peak area to the concentration of the product. Whilst several products were obtained, glycerol carbonate and mono-, di- and triacetin were chosen for further study and calibration. The concentration of glycerol after reaction was also calibrated.

For initial calibration runs, separate calibration samples were prepared for each of the products. One complication was that pure calibration samples were unavailable for monoacetin and diacetin. The composition of the diacetin sample therefore had to be calculated. This was achieved by comparing calibrations for a pure triacetin sample with the concentration of triacetin in a 50% diacetin sample. The calculations are outlined in Appendix D . The composition of the acetin sample by weight was estimated to be 50 wt% diacetins, 28.9 wt% triacetin, and 21.2 wt% monoacetin (and other trace acetins).

Once the composition of the acetin sample had been estimated, calibration samples were prepared by dissolving a mixture of glycerol, glycerol carbonate, and glycerol acetins in ethanol. Supplier details and purities are given in section 3.1.1. As glycerol is very viscous, the glycerol quantity was measured by weight. A small amount of glycerol (0.1-0.6 g) was weighed into a 30 ml vial, and 5-10 ml of ethanol was added, such that the concentration ranged from 0.1-0.01 g ml⁻¹. This was then shaken vigorously to dissolve the glycerol in the ethanol. Glycerol carbonate and the acetins were added by volume using micropipettes, such that the concentration of glycerol carbonate and acetins ranged from 0.0005-0.01 g ml⁻¹. At least three different concentrations of calibration mixture were prepared for each calibration. 1.1 ml of each sample was added to a GCMS vial using a micropipette, with 1 µl of 1-hexanol as an internal standard. The concentration of internal standard in the calibration samples was therefore the same as for the reaction samples. An example of calibration sample concentrations is given in Appendix D .

Fresh calibration samples were prepared for each set of reactions, as it is expected that the retention times and sensitivity of the column will vary over time due to column aging. The length of the column is also slightly decreased each time it is replaced. As an example,

Figure 7-1 demonstrates the change in retention time for the glycerol carbonate peak over the course of 50 months, demonstrating the need for repeated calibrations after each column change.

The concentrations quoted in this chapter are for the concentration of sample detected in the diluted product mixtures; due to calibration issues which will be discussed in section 7.4.5, it was not possible to calculate the conversion of glycerol and yield of the products. However, the calibration has allowed the activity of the biochars to be quantitatively compared.

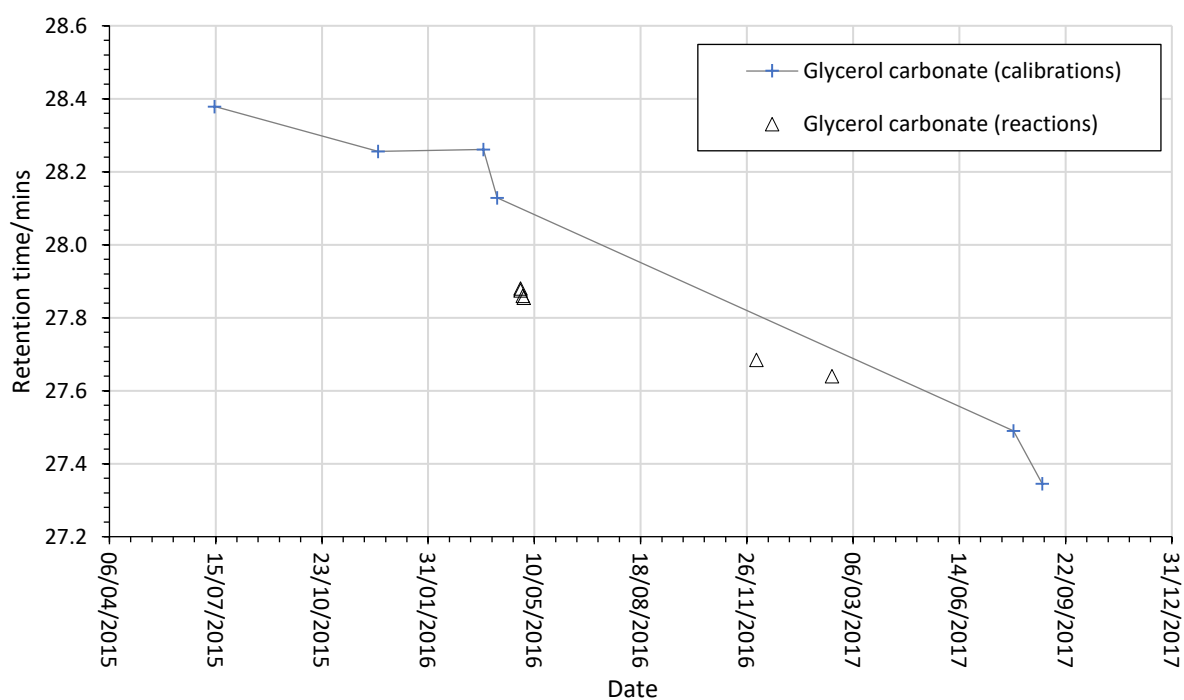


Figure 7-1 Decreasing retention time of the glycerol carbonate peak over time, as measured by calibrations. The position of the glycerol carbonate peak in reaction samples is also given to demonstrate the trend. Line shown to guide the eye only.

Chapter 7 – Glycerol Upgrading

7.3. Results

The experimental work was divided into three sections:

- the screening of biochars for catalyst activity (section 7.3.1), including reproducibility tests, and identification of products for calibration
- experiments to test the effect of demineralisation on catalytic activity (7.3.2), on both the chars and the ash content
- experiments briefly testing the effect of acetone washing and tar impregnation on the catalytic activity of the biochars (7.3.3).

Characterisation work from Chapter 4 and Chapter 5 is included where relevant to the explanation of results in this chapter. Comparisons are also drawn between the results obtained here with results from Chapter 6 in the discussion (section 7.4).

7.3.1. Catalyst screening

The first stage of experimental work was to determine which biochars were effective as catalysts for the upgrading of glycerol to products, and to identify potential reasons for this. Control tests were first run in the absence of catalyst (section 7.3.1.1), before identifying the range of products produced when using biochars from different feedstocks (section 7.3.1.2). The feedstocks studied in this chapter were soft wood biochar (SWB), wheat straw biochar (WSB), rice husk biochar (RHB) and oil seed rape biochar (OSB), pyrolysed at 550 °C. The activity of OSB was also compared at pyrolysis temperatures of 550 °C and 700 °C. These biochars were compared with a commercial activated charcoal sample (AC). Selected products were then calibrated, and the activity of the biochars is compared quantitatively in section 7.3.1.3.

7.3.1.1. No catalyst

Control tests in the absence of catalyst were performed to verify what products were obtained independently of the biochar catalysts. In particular, the potential catalytic effect of the reactor walls, as described in section 2.2.6, could be eliminated. Annotated GCMS spectra for the control tests are shown in Figure 6-1.

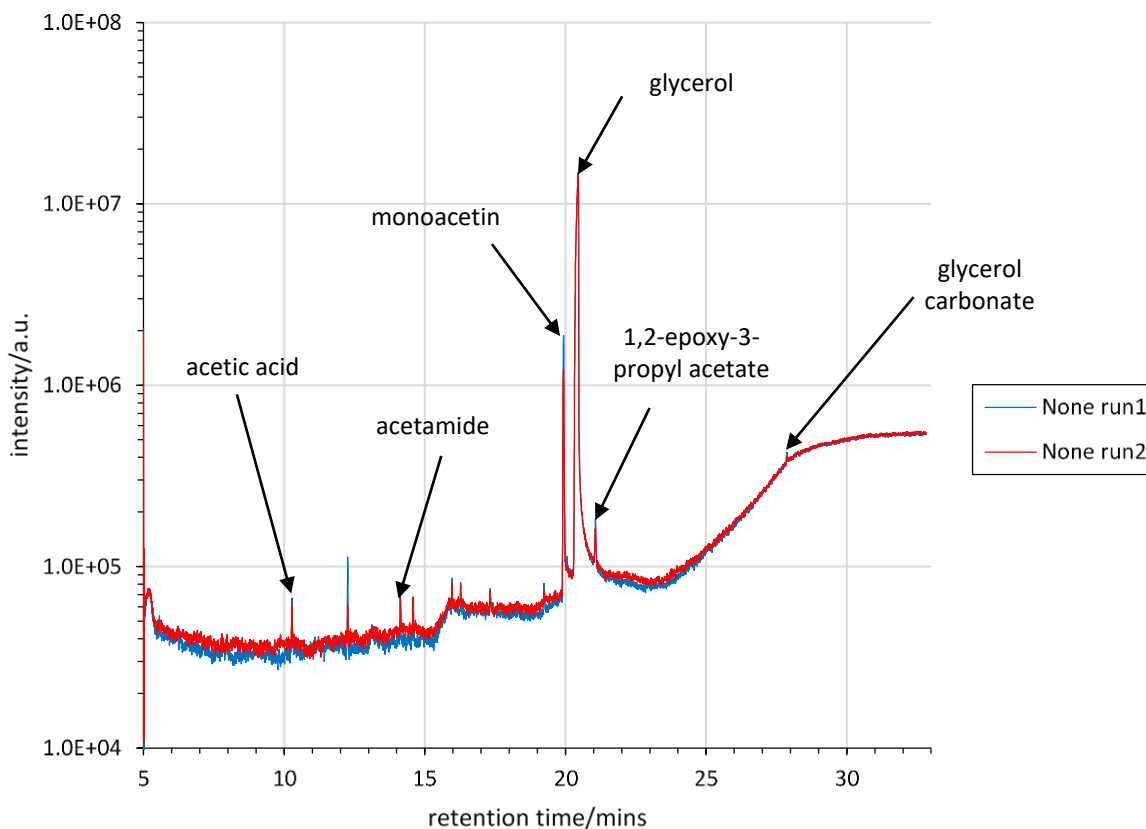


Figure 7-2 Annotated GCMS chromatograms for reaction products in the absence of catalyst. A logarithmic y-axis is used to allow presentation of both large and small peaks.

Whilst there are many smaller peaks in the region 5-15 mins, these peaks vary from run 1 to run 2, and are difficult to identify due to the low signal-to-noise ratio. These peaks were therefore discounted. The largest peak corresponded to glycerol, as expected, though it is worth noting the formation of significant quantities of monoacetin in the absence of catalyst. Small peaks were also identified as the intermediates required for monoacetin formation: acetic acid (10.25 mins) and acetamide (14.2 mins).

A very small peak with the same retention time as glycerol carbonate was also detected, though again it is difficult to verify this due to the low signal-to-noise ratio. There is a small peak overlapping with the glycerol peak, which was tentatively identified as 1,2-epoxy-3-propyl acetate. As the main acetins of interest were mono-, di- and triacetin, 1,2-epoxy-3-propyl acetate was not studied in further detail.

Chapter 7 – Glycerol Upgrading

7.3.1.2. Product identification

The next stage was to assess what liquid phase products are formed when using biochar catalysts, before quantifying and calibrating the products. In this section, the GCMS spectra are analysed to determine which peaks can be attributed to genuine reaction products, and which can be discounted as contaminants. This also allows a 'gap' to be identified in the spectra for an internal standard. The peaks of interest are then calibrated and quantified in section 7.3.1.3.

In Figure 7-3, annotated GCMS spectra are shown for the products obtained when using SWB-550, RHB-550 and OSB-550 catalysts. These catalysts had a range of ash contents, as was shown in Chapter 4, ranging from 0 wt% for SWB-550 to 43 wt% for RHB-550, and so should demonstrate the range of products that can be expected in the liquid phase.

To identify key products of interest from Figure 7-3, peaks that were present in more than one reaction were identified, and were highlighted if the peak was sufficiently large to allow identification by MS. Certain products such as mono-, di- and triacetins and glycerol carbonate were expected, and so could be identified from their retention times, compared with those from calibration samples.

Based on the GCMS spectra shown in Figure 7-3, 1-hexanol was chosen as an internal standard for the reaction. 1-hexanol was known from the column catalogue to have a retention time of approximately 8 mins, which is a clear area of the GCMS spectra, and with six carbons and an alcohol group, is similar in structure to glycerol without being reactive.

The products of interest were therefore identified as glycerol carbonate, mono-, di- and triacetin. To calibrate the quantities of these products, the method outlined in section 7.2.3 was followed. The internal standard allowed the volume of sample injected to be verified, however when calibrating the samples, a higher R^2 value was obtained without the internal standard (see Appendix D). As was the case in section 6.3.1, this may be due to the instrumental precision error in pipetting 1 μL of sample. The calibrations were therefore completed without normalising peak areas relative to the internal standard.

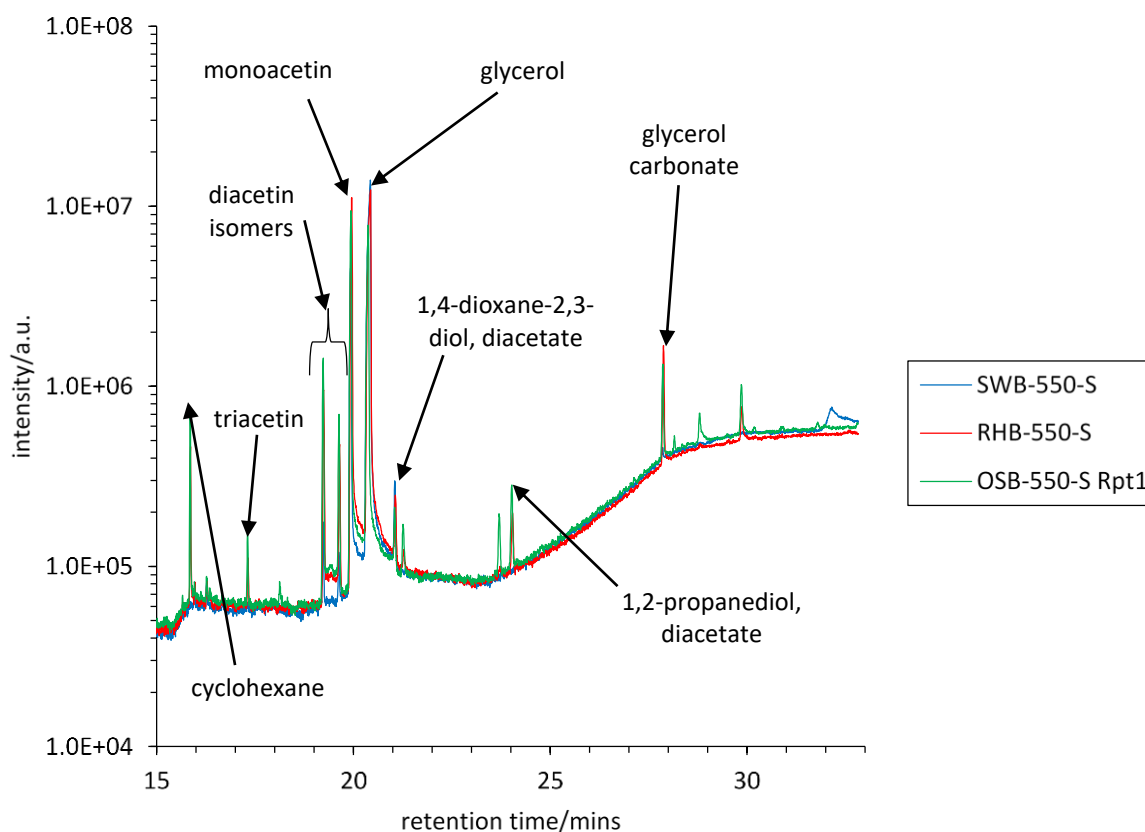
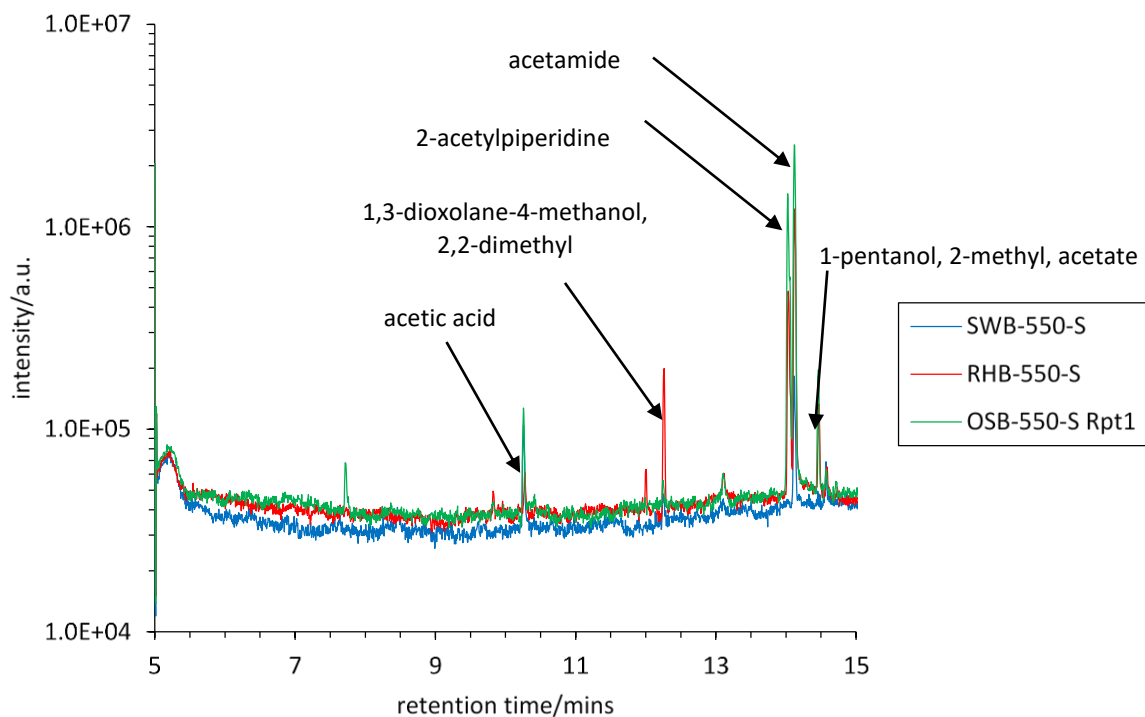


Figure 7-3 Product peak identification by GCMS for products of glycerol upgrading reaction, using biochars from different feedstocks. GCMS spectra divided into two parts for clarity. Logarithmic y-axis used to allow large and small peaks to be presented.

Chapter 7 – Glycerol Upgrading

7.3.1.3. Biochar activity

The calibrated data for glycerol carbonate, monoacetin, diacetin and triacetin are presented in this section to allow a comparison of the activity of biochars from different feedstocks towards the glycerol upgrading reaction. The product concentrations have been calculated in mol ml⁻¹ to allow comparisons on a molar basis. The effectiveness of the feedstocks is compared in Figure 7-4.

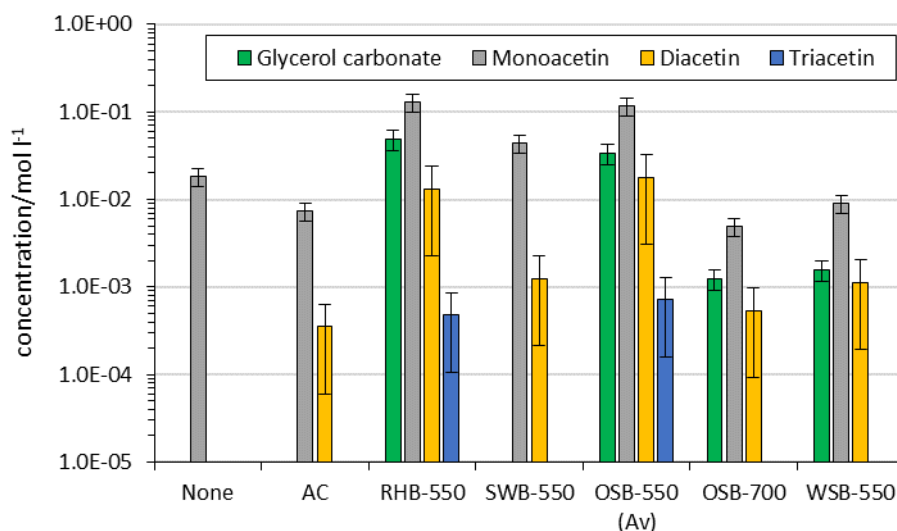


Figure 7-4 Concentrations of liquid phase products in the glycerol upgrading reaction, using biochars from different feedstocks as catalysts. Error bars represent the percentage error, calculated from 3 repeats of OSB-550. Logarithmic y-axis is used to present low and high concentrations of products.

It is firstly worth noting that in the absence of catalyst, the only product of interest formed is monoacetin, although the concentration of monoacetin increases when using RHB-550 and OSB-550. Diacetin, triacetin and glycerol carbonate are only formed in the presence of a catalyst. Figure 7-4 demonstrates that the range of products and concentration is sensitive to the feedstock used. Glycerol carbonate is also produced using most biochars, except SWB-550 and AC. Diacetin is produced using all of the catalysts, however the concentration varies by a factor of 10-100. Triacetin is only produced using RHB-550 and OSB-550. This chapter will aim to identify the potential reasons for this.

The range of products and quantities are also reproducible, shown by the error bars in Figure 7-4. The percentage error was calculated from three repeats of OSB-550, following the

percentage error method outlined in Appendix A . The percentage error is greatest for diacetin and triacetin, and lowest for glycerol carbonate and monoacetin.

It is notable that the increased pyrolysis temperature for OSB-700 greatly reduces its effectiveness as a catalyst for glycerol carbonate production, producing almost 100 times less glycerol carbonate than OSB-550. Triacetin is also only produced when using OSB-550, and is not detected in the reaction products when using OSB-700.

7.3.2. Effect of demineralisation

In this section, the potential role of the ash content of biochar on catalytic activity is investigated. As in Chapter 6, this was firstly tested by comparing the activity of biochars before and after demineralisation. Ash samples were then tested as catalysts before and after demineralisation. As was discussed in Chapter 5, demineralisation reduced the overall ash content of the biochars by 5-30 wt%, although the silica content was largely unaffected. In all samples the potassium content was reduced to levels where it could not be detected, whilst effects on other elements varied. The influence of potassium content in glycerol upgrading can therefore be investigated; this will be discussed in section 7.4.

7.3.2.1. Activity of demineralised biochar

The effectiveness of demineralisation was known to vary depending on the feedstock, as was shown in Chapter 4. Two feedstocks, RHB-550 and OSB-700, were therefore compared, to study the impact of demineralisation on the activity of the biochars. In particular, for RHB-550 only 4 wt% of ash content was removed, whilst the reduction for OSB-700 was closer to 20 wt%. The concentration of the key products of interest is shown in Figure 7-5.

Consistent with the finding that demineralisation had different effects on RHB-550 and OSB-700, the impact of this on the activity of the catalysts is varied. Whilst RHB-550 performs more poorly following demineralisation, the effectiveness of OSB-700 is improved. It is worth noting that the range and concentrations of products from RHB-550-DM and OSB-700-DM are comparable, indicating that the overall effect of demineralisation has been to produce two catalysts from different feedstocks with similar activity. It may be for example

Chapter 7 – Glycerol Upgrading

that the reduction in potassium content of RHB-550 is detrimental, but the clearing of ash from pores in OSB-700 is beneficial.

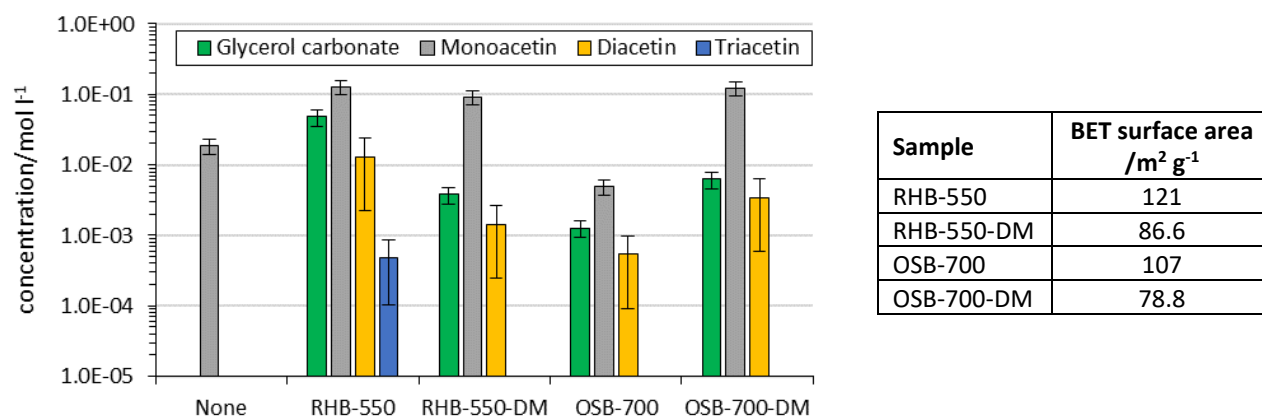


Figure 7-5 Comparison of production of glycerol carbonate and acetins using biochars before and after demineralisation. A logarithmic y-axis is used to present high and low concentration products.

In both cases, the demineralised sample has a lower surface area than the original biochar, partly due to the larger particle sizes used in preparing demineralised samples. Therefore, the change in activity is not simply explained by changes in surface area or microporosity. In particular, the ability of RHB-550 to catalyse the conversion of diacetin to triacetin is reduced by demineralisation, indicating a reduction in the number of Brønsted acid sites. This is despite the use of hydrochloric acid in demineralisation, which might be expected to increase the overall surface acidity.

7.3.2.2. Role of ash content

As demineralisation was found to affect the catalytic activity of biochars, the role of the ash content before and after demineralisation was investigated in more detail. The ash content from RHB-550, OSB-550, OSB-700 and WSB-550 was tested for catalytic activity, as were the ash contents from demineralised samples. The performance of the untreated biochar and ash samples are compared in Figure 7-6.

As shown in Figure 7-6, the ash content is active for the production of glycerol carbonate and acetins, and with the exception of RHB-550-ash, is more active than the original biochar, despite the lower surface area. Notably for OSB-700, triacetin is only produced using the ash

sample; the performance of OSB-550-ash and OSB-700-ash is comparable. The selectivity to glycerol carbonate is also increased in the ash samples, with concentrations exceeding that of monoacetin; this is not the case for any of the chars studied. It is also notable that the most active catalyst tested was WSB-550-ash, despite having the lowest surface area.

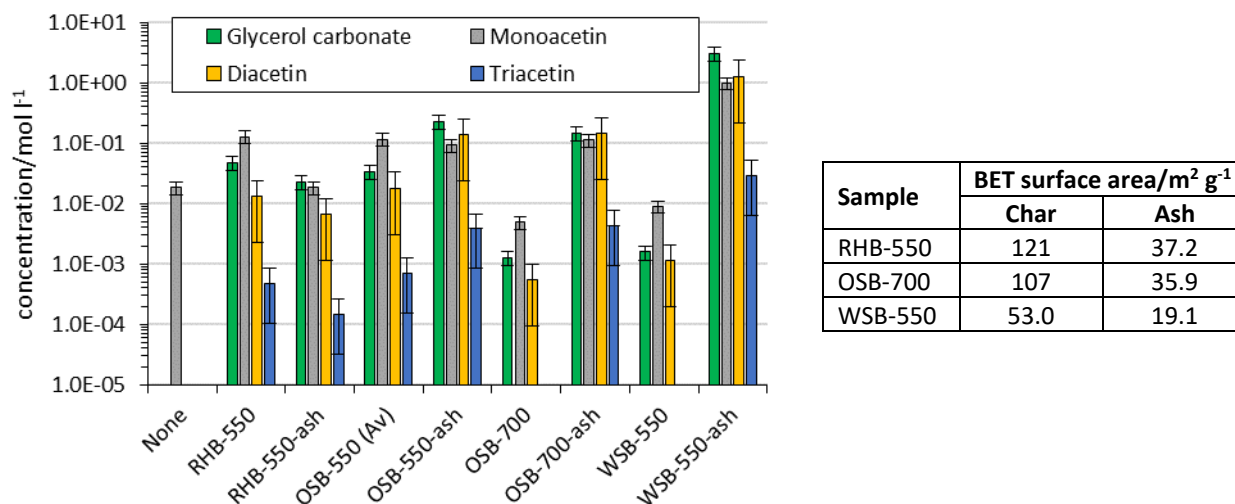


Figure 7-6 Comparison of production of glycerol carbonate and acetins from biochar ash from different feedstocks. A logarithmic y-axis is used to present high and low concentrations of product.

The ash content from demineralised samples was next tested for catalytic activity in this reaction, to determine the influence of potassium and other AAEM elements, which were removed using HCl (see section 5.3.1). The concentrations of the liquid phase products obtained are shown in Figure 7-7.

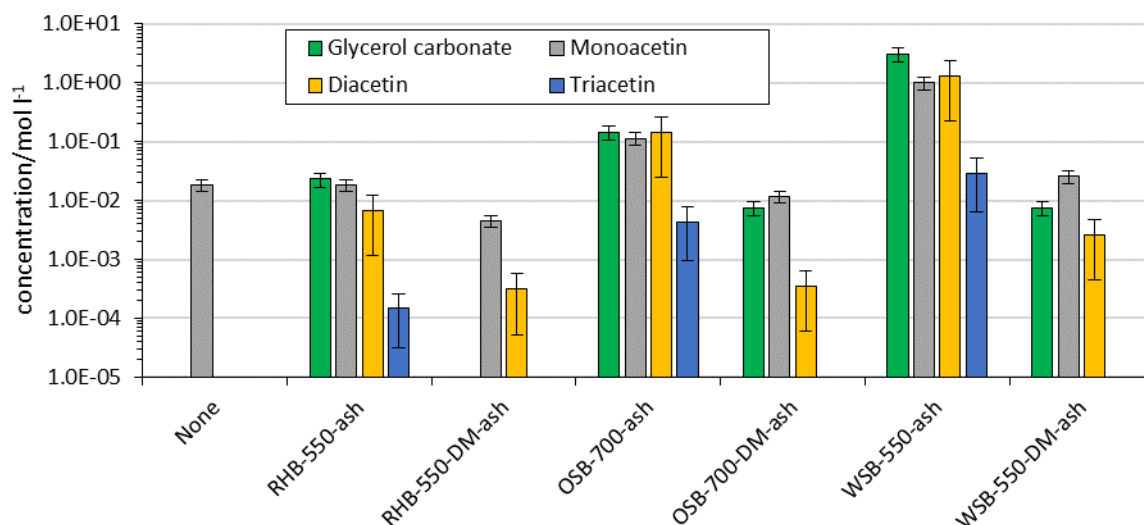


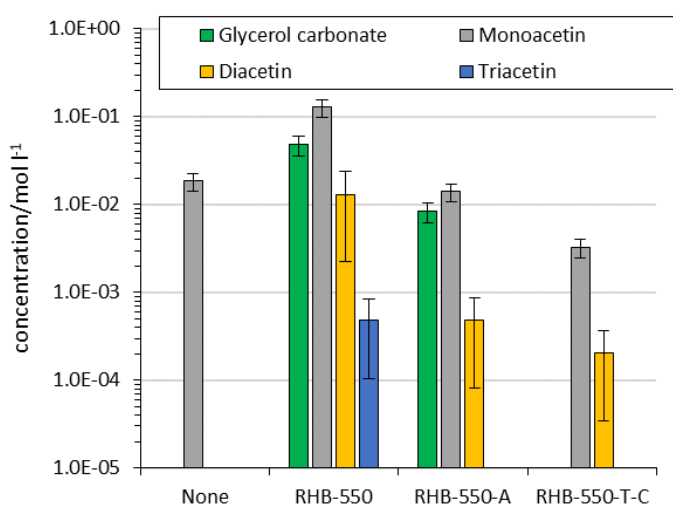
Figure 7-7 Activity of biochar ash before and after demineralisation for glycerol upgrading reaction; -DM indicates demineralised samples. Logarithmic y-axis is used to present high and low concentrations of products.

Chapter 7 – Glycerol Upgrading

In all cases, the ash content is less catalytically active following demineralisation, although not completely deactivated. Selectivity to diacetin and glycerol carbonate is much lower, with yields 10-100 times lower in the demineralised samples; glycerol carbonate is no longer produced by RHB-550-ash after demineralisation. Triacetin is also not produced when using any of the demineralised ash samples.

7.3.3. Role of acetone and tar impregnation

The effect of acetone washing and tar impregnation on catalytic activity was briefly considered. From Chapter 5, it is known that acetone washing does not strongly affect the carbon structure or surface chemistry, whilst tar impregnation leads to increased carbon content and decreased surface oxygen. There is some evidence that surface potassium is reduced for WSB-550 and OSB-700 following tar impregnation, although the quantities are too small (<1 at%) to be certain for RHB-550. In Figure 7-8, the liquid phase products obtained using treated RHB-550 samples are presented.



Sample	BET surface area/m ² g ⁻¹
RHB-550	121
RHB-550-A	59.6
RHB-550-T-C	209

Figure 7-8 Concentration of liquid phase products for RHB-550 after treatment with acetone and tar impregnation.

Both acetone washing and tar impregnation reduce the yield of glycerol carbonate. Acetone washing removes activity towards triacetin, whilst tar impregnation removes activity towards glycerol carbonate production. This is despite the almost-doubled surface area of RHB-550-T-C compared to RHB-550. Monoacetin and diacetin yields are reduced by a factor of almost 100 in RHB-550-T-C, compared to RHB-550.

7.4. Discussion

In this section, the results and limitations of the experimental work are discussed. Firstly, the properties which influence the catalytic activity of biochar are identified in section 7.4.1, and the implications of this for future carbonaceous catalyst design are discussed, including the impact on the study of catalytically active carbonaceous deposits. Insights into the reaction mechanism are then discussed in section 7.4.2, in terms of whether the mechanisms outlined in section 2.4.2 apply over carbonaceous catalysts. The influence of potassium on the mechanism is also considered. The challenges for industrial application of biochar as a catalyst are discussed in section 7.4.3, with implications for sustainability discussed in section 7.4.4. The limitations and future work are presented in section 7.4.5. A summary of the key conclusions of the chapter follows in section 7.5, with a consideration of the questions still to be answered.

7.4.1. Properties of biochar influencing activity

From the experimental work presented in section 7.3, it is clear that biochar from a range of feedstocks is active in the conversion of glycerol to glycerol carbonate, with acetins as by-products. The ash content was also shown to be catalytically active, with demineralisation proving detrimental to the catalytic performance of the ash. Acetone washing and tar impregnation of biochar were also detrimental to catalytic performance. These results can indicate which properties of the catalysts are influencing activity, and the potential factors are considered in this section.

A key influence appeared to be **potassium content**. From the reaction data using ash catalysts, the demineralisation process clearly reduced the catalytic activity of the ash content (see Figure 7-7). As was shown in Chapter 5, the principal effect of demineralisation was the almost complete removal of potassium, with no other elements consistently reduced. It is therefore possible that the removal of potassium in the ash was detrimental to glycerol carbonate and triacetin synthesis – the influence of potassium on the reaction mechanism is considered in section 7.4.2. However, the performance of OSB-700 was improved following demineralisation, suggesting that potassium content is not the only factor.

Chapter 7 – Glycerol Upgrading

From Chapter 5, it was observed that **demineralisation** had differing effects on biochars from different feedstocks. This may explain why demineralisation improved the activity of OSB-700, but was detrimental to the activity of RHB-550. One major difference is the quantity of ash removed: ash content in RHB-550 was reduced by 4%, but in OSB-700 was reduced by 20%. It may be that the ash in OSB-700 was blocking access to active sites on the carbon, and therefore its removal contributed to greater catalytic activity. The higher residual potassium content in the demineralised ash of OSB-700, as detected by XPS, may also have played a role. Whilst potassium removal from the ash was clearly detrimental, other effects of demineralisation, such as clearing pores, may have been beneficial.

It is worth noting that whilst potassium removal is detrimental to performance, **it does not necessarily follow that higher potassium content leads to improved performance**. WSB-550 was the best-performing catalyst for glycerol conversion, despite having a potassium content inbetween that of OSB-700 and RHB-550. It is possible that there is an optimum level of potassium, and that the higher levels of potassium in OSB are detrimental; however there is little supporting evidence for this at present.

Whilst it is clear that ash content contributes to the catalytic activity of biochar, there is also evidence that **carbon plays a role**. Whilst the ash content for OSB-700 and OSB-550 performs similarly, OSB-700 is less effective than OSB-550, despite having a higher ash content. This implies that although the catalytic activity of the ash is similar, the catalytic activity of the carbonaceous component of biochar decreases at higher pyrolysis temperatures. Graphiticity may be an influence, although different aspects of graphiticity may be affected by pyrolysis temperature. Whilst the extent of networks is expected to increase, as seen in THz spectra for SSB-750, Raman and XPS data in section 4.3.4 indicated that OSB-700 was less graphitic than OSB-550. Similar surface functionalities were observed in FTIR-ATR spectra, making graphiticity a plausible candidate for explaining the differing activity.

The tar impregnation study on RHB-550 confirmed that **carbon deposits are not active for the synthesis of triacetin, and are detrimental to the synthesis of glycerol carbonate**. RHB-550-acetone is inactive for triacetin production, as is RHB-550-T-C, despite having a higher

surface area. Similarly, RHB-550-acetone was reduced in effectiveness for glycerol carbonate synthesis, and RHB-550-T-C was inactive for glycerol carbonate synthesis. This indicates that carbon deposits formed on the active sites for glycerol carbonate production, and were not themselves active. From section 5.3.4, it is known that in RHB-550-T-C the quantity of surface oxygen-containing functional groups detected by XPS and Raman spectroscopy decreases after tar impregnation; it is possible that these functional groups are the active sites for glycerol carbonate synthesis, and are blocked by carbon deposits after tar impregnation and pyrolysis. The reaction mechanisms will be considered in section 7.4.2.

7.4.2. Mechanisms of glycerol carbonate and acetin formation

As was discussed in section 7.4.1, biochars from different feedstocks had varying activity towards glycerol carbonate and triacetin synthesis. In particular, surface treatments affected the activity of biochars, with potassium removal from ash proving particularly detrimental. The reaction mechanisms behind glycerol carbonate and triacetin synthesis over carbonaceous catalysts are therefore discussed in this section, with particular consideration of the possible influence of potassium on these mechanisms.

7.4.2.1. Reaction mechanism over carbonaceous catalysts

As was discussed in section 2.4.2, glycerol carbonate synthesis likely occurs via the dissociative adsorption of CO₂ on the catalyst surface, with glycerol activated by basic sites. This leads to the insertion of carbon monoxide into the activated glycerol, and the subsequent formation of glycerol carbonate. As no trace metals were detected in the biochar (see section 4.3.2), this route is more likely than that occurring via metal complexes.

The water formed as a by-product then reacts with acetonitrile to form acetamide, which hydrolyses to acetic acid. The acetic acid then reacts with glycerol to form mono-, di- and triacetin. This pathway is supported by the results, as acetic acid and acetamide were detected in the liquid phase products by GCMS analysis (see Figure 7-3).

From the literature, monoacetin production occurs in the absence of catalyst, whilst triacetin production via the acetic acid pathway is related to the concentration of Brønsted acid sites.

Chapter 7 – Glycerol Upgrading

This is consistent with the result that acetone washing was detrimental to triacetin synthesis, as it can reasonably be expected that the C=O group in acetone may react with Brønsted acid sites, therefore reducing the overall concentration of Brønsted acid sites. Shape selectivity is unlikely to play a role in selectivity to triacetin synthesis here, due to the mesoporous nature of the biochars (see section 4.3.1).

7.4.2.2. Influence of potassium on reaction mechanism

As the reaction mechanisms outlined in the literature review appear to be consistent with the reaction results, it is now worth considering why the removal of potassium content was detrimental for performance. The potential influence of potassium on the reaction mechanisms is therefore considered.

For the experimental work in this chapter, a positive correlation was found between potassium content and glycerol carbonate and triacetin yields, as shown in Figure 7-9. Previous suggestions in the literature for the role of K⁺ in this reaction are unable to explain the results presented in section 6.3. Whilst Indran and co-workers found that potassium silicate was active for glycerol carbonate synthesis from urea (Indran *et al.* 2016), the suggestion that K⁺ acted as a Lewis acid does not appear to fit the proposed mechanism for glycerol carbonate synthesis from CO₂. Similarly, Nosyrev and co-workers suggested that carbonyls could be formed due to the formation and reaction of potassium superoxide (Nosyrev *et al.* 1996), however this seems unlikely in a CO₂ atmosphere. Therefore, a return to general principles is required to explain the role of potassium.

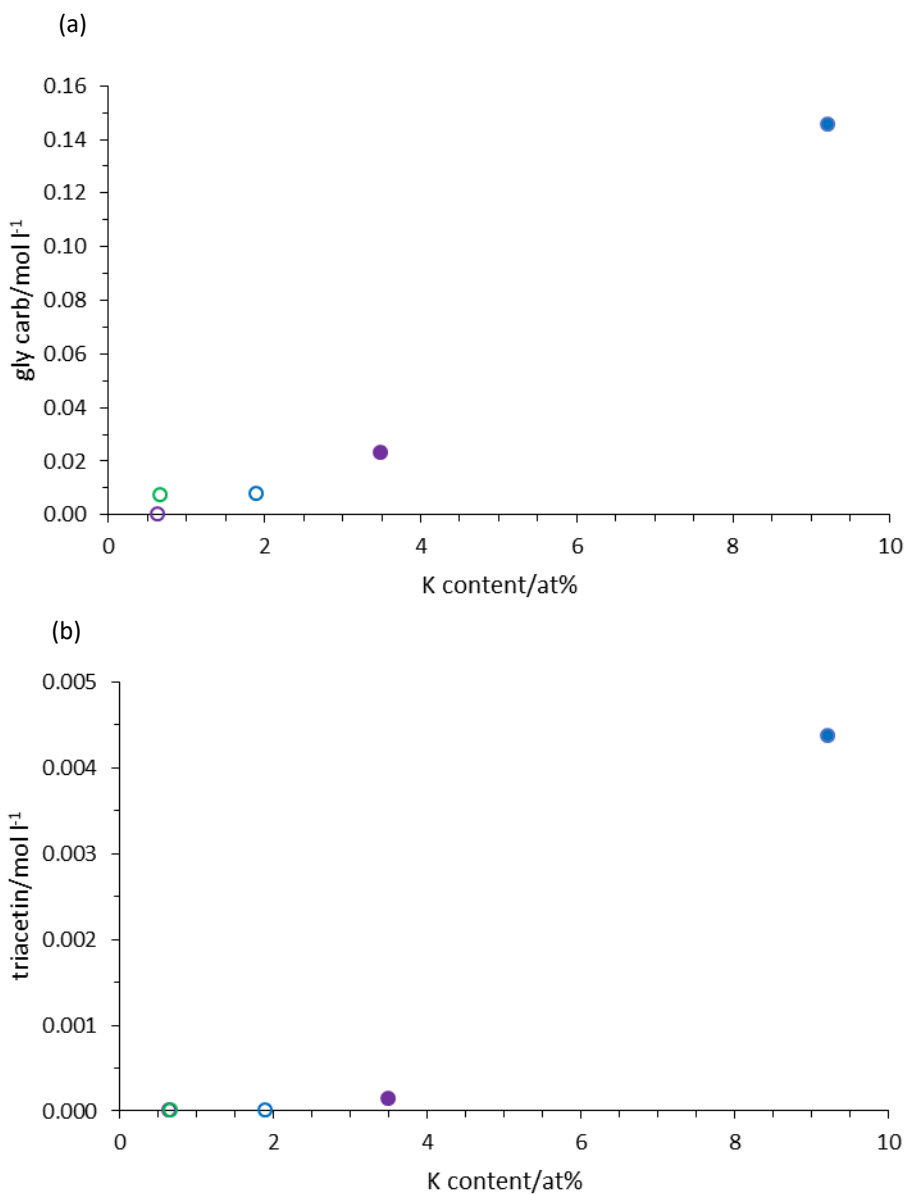


Figure 7-9 Correlations between potassium content and a) glycerol carbonate concentration and b) triacetin concentration for biochar ash. Filled circles = untreated ash, open circles = demineralised ash. Green = WSB-550, blue = OSB-700, purple = RHB-550.

The promoting effect of alkali metals on catalytic performance is often observed, but less well understood. Literature studies often focus on the influence of additional potassium loading on pure metals, particularly the effect on crystal faces and structure. However, catalysts are rarely composed of pure metals and pure potassium – for example, oxides and salts may be present, and so the promotion effect of alkali metals on catalysts *in situ* is poorly understood (Huo *et al.* 2011). The potential effects on carbonaceous catalysts are even less studied. However, the same principles may apply to metals and graphitic carbon, due to their conductive nature.

Chapter 7 – Glycerol Upgrading

In terms of glycerol upgrading over biochar catalysts, the potassium may affect the ability of the catalyst to activate glycerol and CO₂, for example by affecting the local surface chemistry. There are several mechanisms by which this could take place, which were summarised by Huo and co-workers (Huo *et al.* 2011). It is not currently possible to identify which of these mechanisms would be responsible, although direct bonding to K⁺ seems unlikely, as Lewis acidity is not required for activation or reaction.

Assuming potassium alters the surface chemistry of the biochar, the four most likely effects of potassium removal on the glycerol upgrading reaction are summarised below:

1. **Potassium enables O⁻ sites in potassium silicate to activate glycerol.** The structure of potassium silicate is shown in Figure 7-10, and is thought to be present in biochar ash (Indran *et al.* 2016). Potassium silicate contains K⁺ bound to O⁻. The O⁻ acts as a basic site for the activation of glycerol, and may for example form KOH after activation – a known catalyst for glycerol carbonate synthesis, albeit not known to catalyse the direct carboxylation pathway used here (Sonnati *et al.* 2013). When K⁺ is removed, the chemistry of the O⁻ site is altered, and can no longer activate glycerol. An inert silica may be formed through demineralisation, for example. This is only the case for O⁻ sites in potassium silicate – other O⁻ sites are unaffected, so some activity is retained. As well as reduced glycerol carbonate yields, less water is produced as a by-product of glycerol activation, leading to the lower acetin yields observed in the demineralised ash samples.

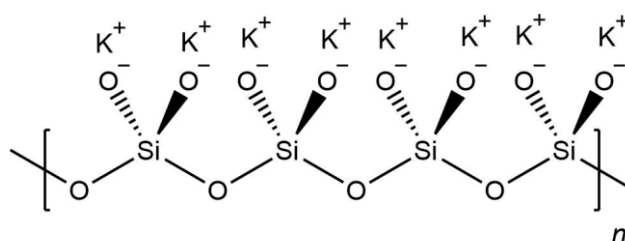


Figure 7-10 Structure of potassium silicate.

2. **K⁺ induces the dissociative adsorption of CO₂.** This is observed in clean metals (Pratt & King 2003), however it has not yet been demonstrated on carbonaceous

samples. The proposed mechanism of glycerol carbonate synthesis using CO₂ on a non-metal catalyst involves the direct insertion of CO, and therefore a dissociative adsorption of CO₂. Removal of K⁺ may reduce dissociative adsorption of CO₂ and therefore glycerol carbonate synthesis. A consequence of this would be that acetin production would be unaffected, as CO₂ adsorption is not required for acetin synthesis. However, if removal of K⁺ also reduces glycerol activation as in Point 1, then acetin synthesis would be reduced. Further experiments would therefore be required to verify the adsorption mode of CO₂ on carbonaceous catalysts.

3. **CO₂ adsorbs on potassium, forming surface K₂CO₃.** K₂CO₃ has been observed in the literature to catalyse glycerol carbonate formation, albeit via the DMC pathway or indirect routes rather than direct carboxylation with CO₂ (Rokicki *et al.* 2005; Gómez-Jiménez-Aberasturi *et al.* 2010). It is also possible that some potassium carbonate is present in the biochar ash, as well as potassium silicate.
4. **Potassium acts as a dehydrating agent.** It is possible that K⁺O⁻ sites in potassium silicate could react with water to form KOH and OH⁻, as suggested by Indran and co-workers (Indran *et al.* 2014). This would supplement the dehydrating action of acetonitrile, and therefore enhance selectivity to glycerol carbonate, as it would consume the water without producing acetins as side products. It is also possible the kinetics of the process would be improved due to the presence of two dehydrating agents, leading to higher conversion. As selectivity to glycerol carbonate could not be measured in this case, further quantitative data would be required to test this effect.
5. **Potassium enhances Brønsted acidity and therefore triacetin production.** As speculated above, it is possible that K⁺O⁻ sites can accept protons from water and/or glycerol to form KOH. If the K⁺O⁻ site can be regenerated, this KOH is effectively a Brønsted acid, re-donating the H⁺. This would increase the Brønsted acid site concentration, thus leading to increased triacetin production. This is supported by the results, as demineralised ashes and chars do not produce triacetin, implying reduced Brønsted acidity according to the literature (Sandesh *et al.* 2015; Konwar *et al.* 2015). However, reduced triacetin production may simply be due to reduced

Chapter 7 – Glycerol Upgrading

glycerol activation, for example via the effect in Point 1. There is also no evidence at present on whether or not K^+O^- sites are regenerated.

In summary, the potential promoter effects of potassium can be explained consistent with the proposed reaction mechanisms. However, the biochar system is very complex, and as shown by the varied reaction results, the effect of potassium may vary depending on the feedstock used. Whilst Point 1 could be sufficient to explain the experimental results, all four effects could be playing a role in explaining why the removal of potassium is detrimental for glycerol carbonate and triacetin synthesis. Further experiments would be required to verify this – suggestions for future work are made in section 6.4.5.

7.4.3. Implications for industrial application of biochar as a catalyst

Although the aim of this work was not to optimise biochar catalysts for industrial application, insights can still be gained regarding the potential of biochar catalysts and key challenges to address.

The most promising result is the demonstration that carbonaceous catalysts can be used for the synthesis of glycerol carbonate and triacetin from glycerol and CO_2 . Whilst conversion and yields were low (not quantified but clearly less than 10%), there could be potential to optimise reaction conditions and catalyst preparation to improve this. Notably, commercial activated charcoal was inactive, demonstrating that the versatile properties of biochar may be beneficial in this reaction. In terms of future catalyst design, the potential promoting effect of alkali metals on carbonaceous catalysts could be investigated in further depth.

Of particular interest is the effectiveness of the ash content of various biochars in catalysing glycerol conversion. Previously, this had only been demonstrated for boiler ash from palm oil industries. This has now been demonstrated to apply to ashes from a wider range of biomass feedstocks. This could have potential for smaller scale domestic or agricultural reactors, for example, using agricultural ash from incinerators to convert waste glycerol to higher value products.

Besides optimising performance, the key challenge to overcome in industrial application would be the reproducibility of the reaction. The same liquid phase products could be reliably produced, at concentrations within an order of magnitude, with glycerol carbonate concentration more reproducible than for diacetin or triacetin. This would be sufficient for small scale reactors, but would be unacceptable in industry. Variation is expected when using biochar samples, due to their inherent heterogeneity, and this would need to be addressed if adapting the biochars for commercial application as catalysts.

7.4.4. Implications for sustainability

As discussed in section 7.1, the conversion of glycerol to glycerol carbonate using CO₂ could address several sustainability issues. In the current work, it has been demonstrated that biochars and particularly biochar ash can catalyse this reaction at moderate temperatures (160 °C) and pressures (30 bar). The operating conditions are an important consideration when discussing the energy requirements of the process (Principle 6). This reaction route is not yet used on an industrial scale, and is the subject of ongoing research, and so a definitive assessment of the improvements to sustainability from this research are not yet possible. However, this reaction route is clearly a candidate for sustainable synthesis of a plastic precursor.

Glycerol carbonate is not yet manufactured on an industrial scale, however the current work has demonstrated that a cheap, biomass-sourced catalyst could be used, thus improving the economic feasibility and sustainability of the process. The yields and selectivity would require improvement in future studies (see section 7.4.5), however the insights gained in the current work from biomass-derived catalysts could provide insights into the design of a renewably-sourced catalyst for the process (see section 7.4.3).

7.4.5. Limitations and Future Work

Notable limitations of the reaction studies included the lack of gas phase data. Gas phase data would have enabled the conversion of CO₂ in the gas phase to be calculated, and to test whether any gas phase products were produced. Whilst the products of interest were in the

Chapter 7 – Glycerol Upgrading

liquid phase, gas phase data would have provided a more complete picture of the reaction mechanisms over biochar catalysts.

Some problems were experienced with quantification of the liquid phase data, for example identification and calibration of the full range of liquid phase products. This can be seen in Appendix D. The concentration of acetic acid and acetamide for example may have provided further insights into the kinetics of the conversion of glycerol to acetins. Additional products of interest such as glycidol, or nitrogen-containing compounds, were also not investigated in detail here. Glycerol conversion was difficult to calculate, partly due to the difficulty of removing it fully from the GCMS INNOWAX column, and therefore glycerol conversion and selectivity to products could not be calculated. More dilute samples may be required for accurate glycerol conversion calculations to be performed.

The results have indicated that potassium removal is detrimental to performance, however the reasons for this would require further investigation. Following the suggestions in section 7.4.2.2, future work could include TPD to measure the number and strength of Brønsted acid sites. This would indicate whether triacetin yield was in this case linked to higher Brønsted acidity, and in particular whether this was affected by potassium removal. The effect of potassium on CO₂ adsorption could be tested by *in situ* FTIR investigations, to detect the type of C-O bonds formed on the catalyst surface and therefore whether dissociative adsorption occurs on carbonaceous samples. The types of active sites could also be investigated in more detail – whilst oxygen is likely to form part of the active site, high resolution XPS O1s spectroscopy could provide further information on the chemical nature of the oxygen sites on the surface of ash and biochar compounds. *In situ* XPS could also measure changes to the oxygen-containing sites during reaction. These experiments are however beyond the scope of the present study, which focuses on properties of biochar which influence catalytic activity, rather than mechanistic studies.

The exact role played by carbon has also been difficult to isolate. Carbon content clearly influences activity, for example by catalysing monoacetin conversion to diacetin in the case of AC and SWB-550. Whilst these samples may have simply lacked suitable active sites for

conversion to triacetin and glycerol carbonate, it is possible that the carbon is actively inhibiting conversion to these products. This would require a deeper understanding of the mechanism of the reaction. In essence, the activity of biochar is complex in this reaction, with contributions from the ash and from the carbon, which vary with feedstock and by pyrolysis temperature. Mechanistic studies focusing on this reaction could prove enlightening for understanding the complex nature of biochar catalysts, and how to design future catalysts.

Chapter 7 – Glycerol Upgrading

7.5. Conclusions

In this chapter, the catalytic activity of biochar has been tested for the upgrading of glycerol and CO₂ to glycerol carbonate, using acetonitrile as a dehydrating agent. Demineralised samples were studied to test the influence of alkali metals such as potassium on activity, and the activity of ash samples was compared with the activity of the char samples to understand the origin of the observed activity. The effect of acetone washing and tar impregnation was also investigated. These results allowed the potential application of carbonaceous catalysts to be evaluated, with consideration of which factors were the most influential in determining their catalytic activity. This also provided insights into the reaction mechanism, and potential insights for future catalyst design and study of catalytically active carbon deposits.

The key conclusions of this chapter are:

- Catalysts are necessary for the production of diacetin, triacetin and glycerol carbonate. Whilst some monoacetin was produced in the absence of catalyst, higher acetins and glycerol carbonate were only produced in the presence of a catalyst.
- Biochars and biochar ash from various feedstocks have potential applications as catalysts for the conversion of glycerol to glycerol carbonate and acetins, including triacetin. The results are reproducible, with a calculated percentage error of $\pm 23.3\%$. Conversion, yield and selectivity are low ($< 10\%$), however the optimisation of the reaction was beyond the scope of the present work.
- Feedstock material clearly affects the activity of the resulting biochar. The most active catalyst before treatment was RHB-550, whilst SWB-550 and AC were inactive for glycerol carbonate and triacetin synthesis. As SWB-550 and AC consist of only C and O, this implies that other properties of biochar are responsible for activity.
- Mono-, di- and triacetin were produced via the acetic acid pathway, confirmed by the detection of acetic acid and acetamide in the liquid phase products. This pathway therefore applies to carbonaceous catalysts as well as previously studied catalysts.
- Ash content contributes to catalytic activity. For the first time, ash content from a range of biochar feedstocks (RHB, WSB and OSB) was shown to be active for glycerol

carbonate and triacetin synthesis, with WSB-550-ash the most active. The ash content of OSB-700 and WSB-550 outperformed the biochar, despite the lower surface area.

- Carbon content also contributes to activity. Whilst the ash content of OSB-550 and OSB-700 performed similarly, OSB-700 was notably poorer than OSB-550, despite a higher ash content. This suggests the higher pyrolysis temperature was detrimental to the activity of the carbon. This is further supported by the finding that OSB-700-DM outperforms OSB-700, despite a lower and less active ash content. Removal of 20 wt% of ash content had a beneficial effect on OSB-700, perhaps by improving access to active sites in the pores for example.
- Potassium removal by demineralisation is detrimental to catalytic activity. This was clearly demonstrated by the reduced activity of demineralised ash samples to triacetin and glycerol carbonate production. Five mechanisms were suggested for this: potassium silicate may be active for glycerol activation, whilst silica is inactive; potassium and alkali metals may induce dissociative adsorption of CO₂ on carbon, allowing carbonylation of activated glycerol; potassium in the ash may be in the catalytically active form of K₂CO₃; potassium may act as a dehydrating agent and form catalytically active KOH; and KOH formed on potassium silicate could act as a Brønsted acid for triacetin synthesis, reforming K⁺O⁻. Further experiments would be required to determine which of these mechanisms is operating here.
- Carbon deposits from tar impregnation are not catalytically active in this reaction, and are deposited on the active sites for glycerol carbonate synthesis. These may be oxygen-containing functional groups, as suggested in section 5.4.3. Whilst acetone washing of RHB removed activity towards triacetin, probably by reducing the number of Brønsted acid sites, tar impregnation also removed activity towards glycerol carbonate, whilst triacetin was still not produced.

There are several questions which remain which are beyond the scope of the present work. Further avenues for research include investigations into the reaction mechanism over carbonaceous catalysts, verification of the influence of potassium on the reaction mechanism, studies of gas phase reaction products and optimisation work with a view to employing biochar catalysts on a larger scale. For example, conversion, yield, selectivity and

Chapter 7 – Glycerol Upgrading

reproducibility would require vast improvements before the use of biochar catalysts in this reaction could be considered commercially viable.

In terms of the present work, biochar has now been shown to be catalytically active in two sustainable reactions: methanol conversion (Chapter 6) and glycerol conversion. In both cases, biochar catalysts had not previously demonstrated catalytic activity without pre-treatment, the effect of feedstock had not been investigated, and potassium content had not been identified as an influential property of the feedstock. It is therefore possible that biochars can open up new reaction routes. Notably, different biochars were active in each reaction: whilst AC and SWB-550 were the most active feedstocks for methanol conversion, they were inactive for glycerol carbonate and triacetin synthesis.

The experimental results obtained in the present work will now be discussed in Chapter 8, in terms of the insights gained for the application of biochar in catalysis, the characterisation of biochar and other carbonaceous materials, and the future design of carbonaceous catalysts.

Chapter 8 – Discussion

Overview

In this Chapter, the experimental results from Chapters 3-6 are discussed in terms of the implications for biochar application as catalysts, carbonaceous catalyst design and exploitation of catalytically active coke. The poor reproducibility of certain results, such as the $\pm 20\%$ error in glycerol carbonate yield, indicate that the biochars are heterogeneous, with properties varying between grains, between samples and between sources of the same feedstock. This poses challenges for the classification of biochars, which are currently identified by their feedstock. The characterisation of graphiticity also requires greater understanding of the aspect of graphiticity being measured by each technique; there is no agreed definition of graphiticity in the literature, and so correlations of catalytic activity with 'graphiticity' may be overly simplified. Based on the reaction studies, a wide range of further catalytic applications are possible for both the carbon and ash content of the biochars; challenges remain however in terms of the reliability of results and yields of product obtained. When designing biochar catalysts, an application-centred approach is recommended for biochar feedstock selection; this applies to biochars as catalysts and as supports. Biochar properties such as trace element concentration may also influence the catalytic activity of carbon deposits, either directly as catalysts or indirectly by influencing the structure of the deposits formed. Further considerations beyond the scope of the present experimental work include consideration of mechanical properties of biochars, and evaluation of the sustainability of the chosen catalyst through lifecycle analysis.

8.1. Introduction

The aim of the present work is to improve understanding of the catalytic properties and potential of biochars, in order to improve the sustainability of heterogeneous catalysis. Four different biochars have been characterised, modified, and tested as catalysts, and compared with a commercial activated carbon. Thus far, the experimental results have been presented across four key areas:

- Characterisation of biochar properties
- Effect of surface treatments on biochar properties
- Activity of biochar in methanol conversion reaction
- Activity of biochar in glycerol upgrading reaction

Chapter 8 – Discussion

Common themes have emerged in the interpretation of the results in each of these chapters. The poor reproducibility of results and contradictory characterisation results have posed challenges throughout the work. In reaction studies, the biochars exhibited very different catalytic properties, with biochars generally being active in either methanol conversion or glycerol upgrading. The overall implications for biochar application, carbonaceous catalyst design and the exploitation of carbon deposits will now be discussed, drawing on the results obtained across the previous four chapters. Throughout, the implications of the findings for improving sustainability will be discussed.

The reliability of the results will be discussed in section 8.2, with particular consideration given to the implications for the heterogeneity of the biochars. The results will then be discussed in section 8.3 in terms of the potential applications of biochar in catalysis, including a discussion of the remaining challenges. In section 8.4, the insights gained into the design of carbonaceous catalysts will be discussed, with particular consideration of the characterisation of graphiticity. The implications for improved understanding of catalytically active coke are then discussed in section 8.5. Further considerations for the application of biochar catalysts, such as mechanical stability and lifecycle analysis, are discussed in section 8.6. The key discussion points are then summarised in section 8.7.

8.2. Reliability of results

Before considering the wider implications of the experimental results, the reliability and reproducibility of the data must first be considered. In section 8.2.1, it will be argued that whilst some variation in results is expected due to experimental error, the error can also be attributed to the heterogeneity of the biochars. The implications of this heterogeneity for the classification of biochars is then discussed in section 8.2.2. The specific challenges encountered in quantifying graphiticity are then considered in section 8.2.3.

8.2.1. Heterogeneity of biochars

Biochars have demonstrated heterogeneity throughout the present work. From reproducibility studies, the percentage error of characterisation work ranged from 2-20 %, and the percentage error of the reaction studies exceeded 20 %. Some of the experimental error will be attributable to variations in curve deconvolution methods and experimental precision. However, the areas analysed by several surface-sensitive techniques are very small, for example probe diameters of < 200 μm in XPS SEM. Biochars are not homogeneous, and elements and functional groups are likely not evenly distributed across the surface of the biochar. Each area analysed will have different properties, each particle will exhibit different catalytic activity, and as a result, each gram of sample will produce slightly different results when tested as a catalyst. Poor reproducibility was observed in several characterisation techniques, and in the catalytic activity of the biochars. The error therefore appears to indicate genuine heterogeneity in the biochar samples, rather than purely experimental error.

The heterogeneity of biochars poses challenges for catalytic applications. Soil remediation applications are less sensitive to small variations in surface composition, however in catalysis this heterogeneity can alter the quantity of product produced by ± 23.3 %, as seen in section 7.3.1.3. The implications of this heterogeneity on catalytic applications will be considered further in section 8.3.3.

It is worth noting that in the repeat reaction studies, the same products were reliably produced, however the quantity of product did vary. This indicates that the same elements

Chapter 8 – Discussion

and functional groups were present in each sample, leading to the same products to be formed, however the quantity or distribution may vary between samples, leading to the variation in conversions and yields observed in the reaction studies.

Challenges also remain for the characterisation of biochars, due to their inherent heterogeneity. Catalysis occurs at the surface and in pores of materials, and therefore surface-sensitive techniques are required, which often only analyse small areas of a sample (as small as 10 μm for XPS). It is therefore recommended to sample a variety of areas of a biochar sample, to better evaluate how representative the results of characterisation are for the sample as a whole.

8.2.2. Classification of biochars

The heterogeneity of biochar is not just seen in individual samples. Rice husks are commonly encountered in the literature as a source of biomass for biochar production, due to their availability as a waste from rice production in China and developing countries (Wei *et al.* 2017; Leng *et al.* 2015). However, depending on the source of the rice husks, such as the species and the soil in which they were grown, the composition will vary. Literature sources for example identify trace quantities of aluminium and iron in their rice husk biochars (Feng *et al.* 2018), which are not detected in the present work. Ash contents also vary, from 14.77 wt% to 44.38 wt% (Leng *et al.* 2015; Wei *et al.* 2017). The varying properties of rice husks were the subject of a recent literature review (Chandrasekhar *et al.* 2003). The properties of biochar can therefore vary greatly, even when sourced from the same plant material and prepared under similar conditions.

The current work therefore raises questions for how best to classify biochar materials for catalysis. In the literature, catalysts are often classed in terms of their catalytic functionality, such as solid acids, bifunctional catalysts and molecular sieves, or as particular classes of materials, such as zeolites and metal oxides. Literature studies have classified biochars by origin of feedstock material, such as the six categories used by Zhao: animal manures, waste wood, crop residues, food waste, aquatic plant and municipal waste (Zhao *et al.* 2013). There is some evidence in the present work to support classification on this basis, as AC and SWB-

550 tended to exhibit similar compositions and catalytic activities, with biochars derived from ash-rich plant materials such as RHB-550, WSB-550 and OSB-700 active in other reactions. However, even these three biochars differed from each other in their response to surface treatments, as shown in Chapter 5. Biochars produced from similar feedstocks can have very different properties, as discussed for rice husks above. Classification should ideally provide insights into the catalytic activity of the material; based on the current work, classification could be recommended based on percentage mineral content, elemental content, or perhaps percentage carbon (or indeed percentage graphitic carbon). Alternate methods include structural classification, such as extent of micro- or mesoporosity.

8.2.3. Defining graphiticity

Throughout the experimental work, it has been observed that measurements of graphiticity often support differing conclusions. As an example, the results for the graphiticity of RHB-550 and WSB-550 in section 4.3.4 will be compared. It was observed that WSB-550 contained a higher proportion of band I graphitic carbon than RHB-550 in XPS C1s spectra. However, RHB-550 resulted in a lower A_{DI}/A_G ratio than WSB-550 in Raman spectra. Therefore, more graphitic carbon was detected at the surface of WSB-550 by XPS, but in bulk Raman analysis, RHB-550 contained a higher proportion of graphitic versus disordered carbon. THz spectra were not available for WSB-550, but would provide another insight into the extent of graphitic networks in RHB-550 and WSB-550. The underlying issue is a lack of understanding of what is meant by graphiticity, and what aspect of graphiticity these techniques measure.

In the scientific literature, graphiticity is rarely defined. Graphite has several characteristic properties, which when shared with other carbonaceous samples may lead to these samples being described as 'graphite-like' or graphitic. These properties include:

- The electronic conductivity of a carbonaceous sample
- The extent of a network of aromatic rings
- The depth of a network of graphene sheets
- The perfection of a network of aromatic rings (*i.e.* how free from defects)

Chapter 8 – Discussion

- The proportion of a material which is (or shares the properties of) graphite

These properties may naturally be interrelated – the perfection of a graphitic network will influence the conductivity, for example. However, when attempting to quantify the ‘graphiticity’ of a sample, it is necessary to define the aspect of graphiticity which is of interest. In catalysis, for example, local graphitic properties such as defects in graphitic materials can act as active sites, whilst longer-range graphitic properties may influence electron transfer in reactions.

Characterisation techniques will also vary in the aspect of graphiticity measured. This is illustrated schematically in Figure 8-1. Not only do techniques such as Raman, XPS and FTIR vary in their penetration depth and spatial resolution, they also vary in what phenomenon they are detecting. The sample may not be homogeneous, meaning that analysis of different areas of the sample may yield varying results. Consideration must therefore be given to how representative the results of characterisation are, both in terms of how reproducible the results are across the surface, and how representative the results are of the aspect of graphiticity of interest.

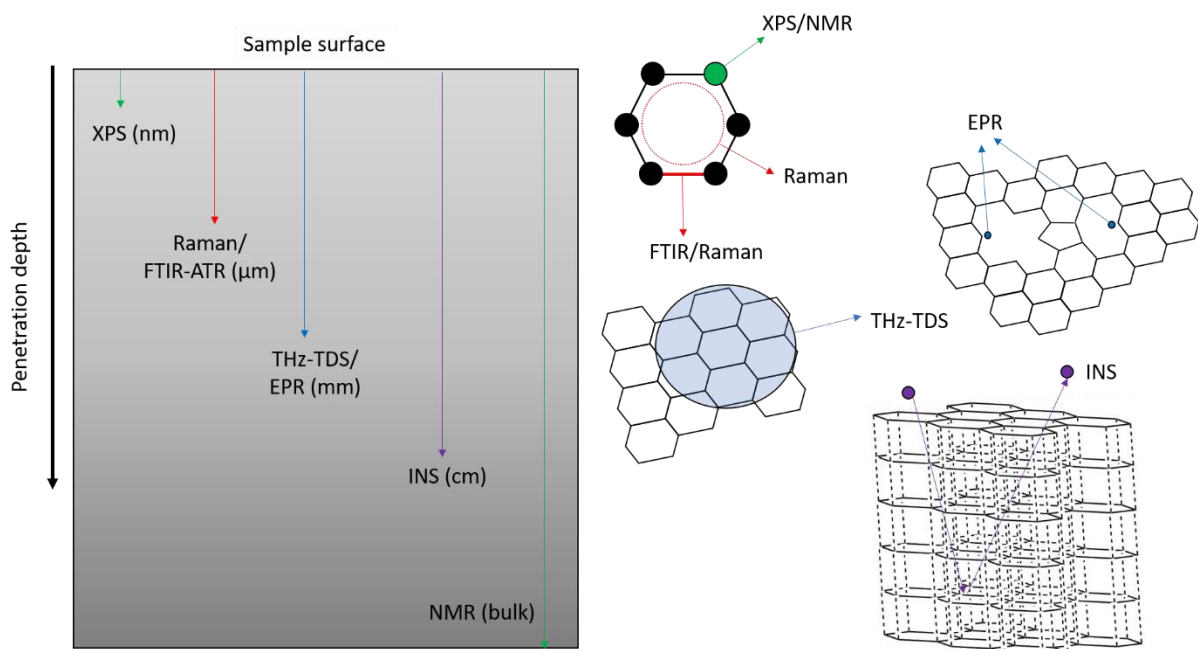


Figure 8-1 Schematic of characterisation techniques for measuring different aspects of graphiticity.

The accurate definition and characterisation of graphiticity has clear implications for the design of carbonaceous catalysts. When designing new catalytic materials and correlating activity with 'degree of graphiticity', it is necessary to identify accurately and precisely which aspect of graphiticity is responsible for the activity. As discussed in section 8.2.1, the properties of biochars vary widely – it is conceivable that if two biochars exhibit increased measures of graphiticity by one technique, they may differ when using another technique. It is therefore misleading and overly simplistic to correlate activity with 'graphiticity'.

Chapter 8 – Discussion

8.3. Potential applications of biochar in catalysis

As discussed in section 8.2, the composition of biochars is highly versatile, likely making them suitable candidates for the production of catalytic materials for a wide range of reactions. In section 2.2, the limited range of reactions in the literature utilising biochar catalysts was explored. The present work has demonstrated two further examples of reactions which could use carbonaceous catalysts derived from biochar: methanol conversion to DMM, and glycerol upgrading to glycerol carbonate. The potential applications of biochar in catalysis are summarised in Figure 8-2, with suggestions for future study based on the experimental results obtained in the present work. Reactions where untreated biochar may exhibit activity are considered in section 8.3.1, and the potential for biochars as support materials is discussed in section 8.3.2. The challenges for the application of biochars in catalysis are then discussed in section 8.3.3.

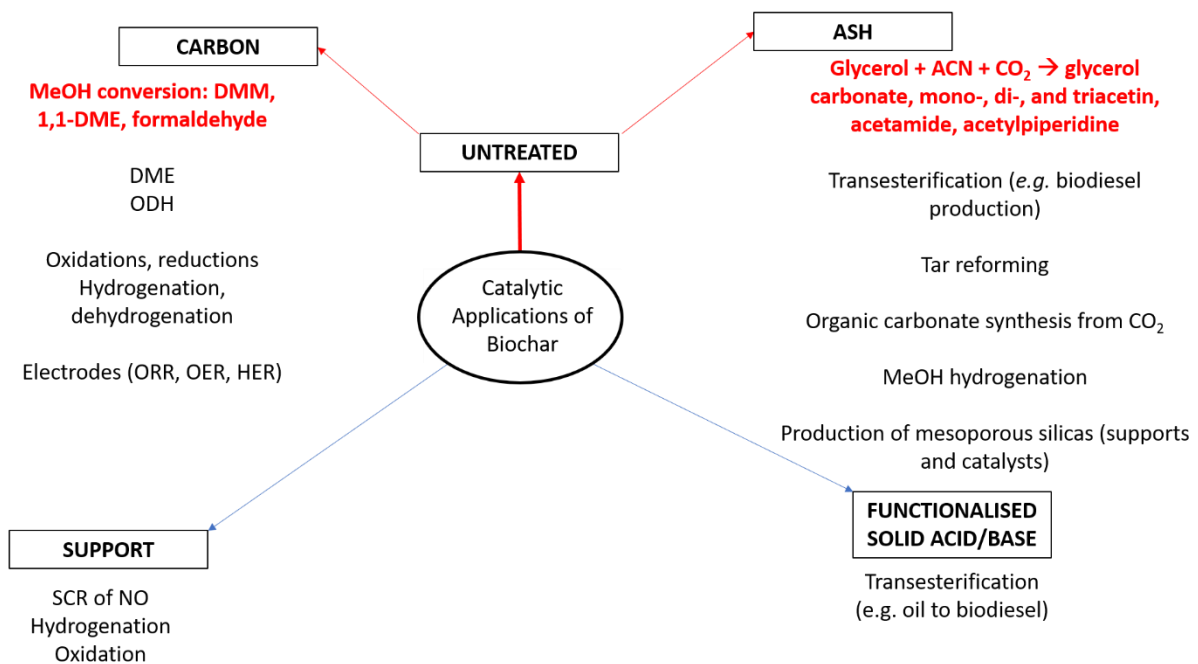


Figure 8-2 Proposed catalytic applications of biochar. Highlighted in red are examples from the current work, with further suggestions based on the literature.

8.3.1. Biochar as a catalyst

CO₂ utilisation reactions are a growing area of research, allowing captured CO₂ to be converted to useful products. Biochar has successfully been applied as a catalyst in the conversion of glycerol and CO₂ to glycerol carbonate, with potassium appearing to be

beneficial for catalytic activity, both in carbonaceous and siliceous materials. As was identified in Chapter 7, the basic sites on biochar may facilitate the activation of CO₂, as well as the activation of glycerol. Biochar ash may therefore find applications in other CO₂ utilisation reactions, such as the formation of cyclic carbonates and the transesterification of alcohols and esters to form biodiesel. The reactivity of the product with silica must be considered, however, as DMC formed in MeOH conversion may have reacted with silica to form TMOS, as suggested in section 6.4.2.3.

The carbon content in biochar was shown to be active in methanol conversion reactions, with liquid phase products including DMM, 1,1-DME and formaldehyde. Gas phase products were not detected, but likely include DME. As discussed in section 2.2.4, carbon has exhibited catalytic activity in a range of reactions, including oxidative dehydrogenations, hydrogenations and dehydrogenations. It could also act as a cheaper alternative to platinum electrodes in electrocatalysis. It is possible carbonaceous biochars may be most promising for activity in these reactions, rather than those with high ash content.

The contribution to activity from fluorine has not been explored in the present work; as discussed in section 5.4.1, fluorine was introduced to the demineralised samples, likely as a result of contamination from tap water. As the levels of contamination were similar in each sample, the effect of fluorine on activity was not considered further. However, the effect of trace quantities of elements is of increasing interest in the literature. The role of trace metals has been explored in influencing the activity of CNTs, as discussed in section 2.2.6. The potential for accidental contamination of catalysts with trace elements must therefore be considered in experimental work, to ensure the origins of catalytic activity are correctly attributed.

8.3.2. Biochars as supports/functionalised carbons

The study of biochars as support materials for catalysis was beyond the scope of the present work, however the full potential of biochars as support materials has yet to be realised. In the literature review, it was reported that biochars have been used as catalyst supports for

Chapter 8 – Discussion

the selective catalytic reduction of NO, and various hydrogenation and oxidation reactions (section 2.2.3). Given the variety of applications of biochars as catalysts (see section 8.3.1), and the range of applications of CNTs and graphitic carbons as supports, it is likely that biochars also have potential as catalyst supports in a wider range of reactions. Implications for the design of biochar catalyst supports and functionalised carbons will be discussed in section 8.4.2.

In particular, when considering the application of biochars as supports or functionalised carbons, the underlying catalytic activity of the biochars should not be neglected. As in section 8.3.1, the ash or carbon content of the biochar may contribute to catalytic activity. Graphitic carbon for example may facilitate electron or hydrogen transfer. It is recommended that the activity of the carbonaceous support is tested separately, to determine what extent of the catalytic activity is due to the loaded metal or treatment applied.

8.3.3. Challenges for application

Key challenges remain for the application of biochar as a catalyst. One of the key variables, beyond the scope of the present work, is the variability in the composition of biochar. For example, this may vary seasonally, and be dependent on the composition of the soil in which it is grown (Dodson *et al.* 2013). As was shown in Chapters 6-7, the catalytic activity of biochar is highly sensitive to composition, with the reduction or removal of AAEM elements proving detrimental for CO₂ utilisation, but possibly enhancing activity in methanol conversion. This variability in composition leads to reproducibility issues, making biochars unsuitable for industrial applications where the quantity and purity of reactant and product streams must be strictly controlled. The insights gained from the study of biochar catalysts however may find applications in the design of industrial carbonaceous catalysts, for example synthesised from graphite or CNTs.

The conversion and yields achieved in the current work are also low. Whilst the aim of the present work was not to optimise the performance of these catalysts, the underlying catalytic activity of these materials has been demonstrated. The use of surface treatments to

achieve desired characteristics is less desirable in terms of sustainability, as this involves the use of additional treatments and the generation of waste, contrary to principles 1 and 5. However, this may be necessary in order to optimise the performance of the most promising catalysts for desired applications. A life cycle analysis would be recommended to quantify the impact on the sustainability of the process for any suggested surface treatments. Quantitative methods for assessing sustainability are discussed further in section 8.6.

Whilst unsuitable for industrial application, biochar catalysts could find applications in reactors where quantity and purity of product do not need to meet such stringent standards. For example, domestic-scale reactors to produce biofuel from waste could be catalysed using incinerated ash waste, or pyrolysed waste to form carbonaceous catalysts, allowing domestic waste (itself having variable compositions) to form more useful products, such as fuels for domestic heating. The ability to catalyse the conversion of waste products, using materials derived from waste products as catalysts, is very appealing from a sustainability perspective in terms of reducing the quantity of waste from a process (Principle 1), and using renewable resources as feedstocks (Principle 7).

Chapter 8 – Discussion

8.4. Implications for carbonaceous catalyst design

The insights from the present work have demonstrated that biochars can be applied as catalysts in a wide range of reactions. These insights can be applied to the design of biochar catalysts, for example through feedstock selection (section 8.4.1). More broadly, in the design of carbonaceous catalysts, the current work has demonstrated inconsistencies in measures of graphiticity, which need to be better understood when designing carbonaceous catalysts. The definition of graphiticity in the context of carbonaceous catalysts is therefore discussed in section 8.2.3. The implications of the experimental results for the design of biochar-based catalyst supports and functionalised biochar catalysts are then discussed in section 8.4.2.

8.4.1. Feedstock selection influences catalytic activity

Biochars have been shown to exhibit a variety of properties, making them highly versatile materials for catalysis. These properties are strongly influenced by the choice of feedstock material, for example, the elemental composition, which in turn may influence the carbon structures formed during pyrolysis, and the catalytic activity of biochar catalysts. The implications of the current research for the selection of biomass feedstocks for design and production of biochar catalysts will be considered in this section.

The catalytic activity of biochars has been demonstrated in two reactions: the conversion of methanol to DMM, and the upgrading of glycerol to glycerol carbonate. Prior to treatment, the biochars which were active in one reaction were inactive in the other. For example, commercial AC was the most effective catalyst for the production of DMM, but inactive in the production of glycerol carbonate. The removal of potassium was demonstrated to have opposite effects in each case: whilst removal of potassium enhanced the yield of DMM from WSB-550 in methanol conversion, removal of potassium led to deactivation of RHB-550-ash in glycerol upgrading, with glycerol carbonate and triacetin no longer produced. This indicates an improved understanding of the catalyst requirements in each case is necessary, in order to select biochar feedstocks with the desired properties for catalysis.

The present work has proposed that AAEM elements such as potassium may influence catalytic activity in carbonaceous materials in the following ways:

- Altering the local surface electronic environment, affecting the adsorption and desorption strength of reactants and products. For example, potassium may induce the dissociative adsorption of CO₂, as found in the literature (Pratt & King 2003). This is comparable to the addition of potassium promoters in the design of traditional metal catalysts. The effect of potassium ‘promoters’ in carbonaceous studies has not previously been studied; biochars are usually loaded with transition metals, or treated to form acidic or basic functionalities.
- Formation or presence of catalytically active materials, such as alkali silicates, alkali hydroxides and alkali carbonates (Indran *et al.* 2016; Sonnati *et al.* 2013). It is worth noting that these materials may form *in situ*, for example, carbonates formed in CO₂ atmospheres, or hydroxides when contacted with water.
- AAEM elements may alter the surface acidity or basicity, for example through the formation of K⁺ ions or KOH. For example, the selectivity of triacetin formation has been noted to be sensitive to the concentration of Brønsted acid sites (Sandesh *et al.* 2015). The formation of KOH at the biochar surface may therefore lower the concentration of surface acid sites.

The present work has demonstrated that biochars are materials with varied and complex compositions. It is therefore feasible that AAEM elements may play different roles in different biochars. These mechanisms may enhance catalysis of a desired reaction, or of competing reactions. The influence of AAEM elements is therefore likely to depend on the particular chemistry of the biochar and of the reaction in question. Whilst the influence of loaded and trace transition metal content is well understood, the influence of AAEM elements on catalytic activity in carbonaceous materials should not be overlooked.

A thorough characterisation of the biochars is also necessary, beyond that usually employed in contemporary catalytic studies. Traditional catalysis research focuses on the optimisation of surface acidity and porosity, often enhancing and tailoring these properties through surface treatments. However, the use of acids and bases as surface treatments leads to the unsustainable production of waste. This waste can be reduced by the selection of suitable feedstocks, which exhibit the required properties for catalysis, thus improving sustainability

Chapter 8 – Discussion

in accordance with Principle 1. The characterisation of mineral content, for example, can enhance understanding of the likely surface chemistry, such as the carbon structures and functional groups which may result from pyrolysis. Characterisation may also be required to identify catalytically active functional groups formed *in situ*, such the carbonates and hydroxides, which were not detected in the *ex situ* FTIR-ATR analysis performed here.

It is also necessary to consider properties which may make a biochar unsuitable for certain applications. The composition of biochars can be complex, and may react with products or side-products of the reaction. For example, the reaction of DMC with silica to form TMOS is well-documented, meaning silica-rich biochars would not be suitable for the production of DMC. Only two reactions have been studied here using four different feedstocks; it is likely that similar effects would be found for the use of biochars from different feedstocks in a wide range of other reactions.

8.4.2. Design of catalyst supports

Carbons are mostly commonly encountered as supports for metal catalysts in the literature, providing a high surface area and easily modifiable surface chemistry which allows the dispersion and loading of metals to be controlled. This was discussed in section 2.2.3. As shown in the present work, however, the response of biochars to surface treatments varies; in Chapter 5, it was shown that WSB-550 increased in surface area following demineralisation, whilst OSB-700 and RHB-550 decreased. This was attributed to differing effects on the porosity of the samples. This in turn would likely affect the loading and dispersion of metal particles on the biochars if they were used as supports. Similarly, biochars are often used in the production of functionalised carbonaceous solid acid catalysts, for example for transesterification reactions. The differing responses to activation treatments should be considered when using biochars as support materials.

The application of biochars from different feedstocks as supports has also yet to be studied. Just as feedstock choice affects catalytic activity, feedstock choice likely influences the properties of biochar as a support material, such as the effectiveness of metal loading and dispersion. Studies of biochar as a support material for SCR of NO, hydrogenation, or

application as an electrode material, generally do not consider the influence of feedstock choice (see Table 2-2). In a similar manner to that outlined in section 8.4.1, a range of feedstocks should be considered, to identify the most desirable properties for the support, and therefore to select a feedstock accordingly. Biochar feedstocks should not be considered interchangeable, and the differences should be considered when selecting a feedstock for use as a catalyst support or functionalised carbon. This process could facilitate the design of catalysts with improved performance, thus improving sustainability (Principle 9), whilst also reducing the quantity of waste generated when producing the catalyst (Principle 1).

8.5. Potential for exploiting coking

The phenomenon of catalytically active coke was outlined in section 2.2.5, however the origin of its catalytic activity requires further study. The present study of biochar can provide insights into properties which may influence the catalytic activity of carbonaceous deposits. For example, just as with biochars, the properties which influence activity are likely to vary depending on the particular material and reaction being studied. The general principles from biochars which may apply to the study of catalytically active coke are outlined below.

The influence of trace elements should also not be neglected. Just as trace metals from reactor walls or from the formation of CNTs can contribute to the catalytic activity of carbons, accidental contamination can enhance the activity of a reaction. As discussed in section 8.4, contaminants such as Pd, F and Cl have been shown in the literature to contribute to the catalytic activity of the studied catalyst. However, the coke may provide a support for this active material, for example electron or hydrogen transfer.

These trace elements may also enhance catalytic activity indirectly. In Chapters 4-5, it was demonstrated that the structure of carbon formed during pyrolysis is influenced by the composition of the biomass. In section 5.3.4, following tar impregnation and pyrolysis, the increase in graphiticity as measured by XPS and Raman spectroscopy corresponded with potassium content. Potassium may therefore influence the graphiticity of carbon deposits. As discussed in section 2.2.5, in certain reactions such as alkane dehydrogenation, the

Chapter 8 – Discussion

graphiticity of carbon may influence catalytic activity. This implies that the presence of trace AAEM elements could induce the formation of catalytically active, graphitic coke.

A complex nature of carbons has provided insights into the varying aspects of graphiticity which may influence catalytic activity. Each characterisation technique provided different insights into the graphiticity of the biochars: whilst exhibiting similar A_{D1}/A_G ratios of approximately 1.5, the contribution of band I (graphitic carbon) to the XPS spectra of RHB-550, WSB-550 and OSB-700 varied from 0-20 at%. Depending on the reaction being studied, the aspect of graphiticity which influences activity may vary; the insights provided in section 8.2.3 may aid the advancement of understanding of the graphiticity of carbon deposits, and therefore understanding of the origin of their catalytic activity.

8.6. Further considerations

The present work has focused on the properties of biochar which directly influence catalytic activity. However, when choosing biochars for industrial applications, there are several other factors to consider which are beyond the scope of the present work. A brief overview of these considerations is provided here.

The mechanical properties of the biochar may dictate whether or not a biochar is suitable for use in a reaction. As noted in their study of the activity of biochar catalysts for esterification, pine chip biochars were found to fragment into fine powder, posing challenges for their proposed application in packed-bed reactors (Kastner *et al.* 2012). This is not a key consideration in soil remediation applications, and further work may therefore be required to evaluate the mechanical strength of carbonaceous samples derived from biomass for catalytic applications. The mechanical strength of the biochars, for example their resistance to shear stress in stirred reactors, should be considered at the screening stage, alongside catalytic activity.

Biochars are often championed as sustainable alternatives to increasingly-scarce metal catalysts. However, the source of the material must be taken into account. Sources of biomass should be non-depleting, and this involves consideration of the alternative uses of the land used for growing the biomass, such as food production. The transport requirements of the feedstock should also be considered, alongside the energy requirements to grow the biomass (*e.g.* production and use of fertiliser, use of fossil fuels to power agricultural machinery). In summary, it is not guaranteed that biomass is a more sustainable source of material than the mining of abundant metals.

Conclusions regarding improvements in sustainability should also be supported by quantitative analysis. Whilst measures such as yield and atom economy can be calculated theoretically, experimental data is needed to evaluate the expected performance in an industrial setting. Possible metrics for the quantification of sustainability for a given reaction route include:

Chapter 8 – Discussion

- **E-factor:** the amount of by-products formed per unit weight of product. This can be quantified using experimental data.
- **Environmental quotient:** this is calculated from multiplying the E-factor by a Q-factor, representing the environmental ‘unfriendliness’ of the by-product. However, there is currently no agreed method by which to calculate Q-factors.
- **Effective mass yield (EMY):** this metric is similar to the E-factor, but does not take into account benign materials such as water, dilute ethanol or acetic acid. This aims to address an issue with E-factor analysis, where large quantities of benign waste can make a process look less sustainable than one which produces smaller quantities of harmful waste.

There is no one metric which provides a definitive measure of sustainability; instead a variety of measures should be used to develop an understanding of the relative advantages and disadvantages of different processes. Further details and examples of these quantitative methods can be found in the literature (Lancaster 2010).

A further example of quantitative analysis is life-cycle analyses (LCA), balancing the energy expended in the production of biochar (including surface treatments applied) with the savings from improved catalytic performance, or compared to the use of a metal catalyst. Whilst limited in the literature, LCAs have been performed comparing biochar with metal catalysts for syngas production, confirming that biochars reduce greenhouse gas emissions by 93 % (Frazier *et al.* 2015). As a further example, rice husk biomass is often sourced from Asia or Japan; for UK-based applications, this distance must be accounted for when quantifying the sustainability of the biochar. An example LCA for biochar production from different feedstocks can be found in the literature (Roberts *et al.* 2010). It may be preferable to use a less catalytically-active but locally-sourced biomass as a feedstock for biochar, to ensure the process is more sustainable than the alternative.

Much of the data needed to quantify the improvement in sustainability was not available for the current work. For example, biochars sourced from the University of Edinburgh are not currently sold commercially; the calibration of reaction products also revealed errors in the

concentration of products of $\pm 20\%$ for repeat measurements, reducing the reliability of the quantitative analysis. Further, the production of glycerol carbonate via CO_2 synthesis is not yet performed industrially, and is still conducted at the laboratory scale by a variety of methods. A quantitative analysis of the improvements to sustainability was therefore beyond the scope of the current work.

Chapter 8 – Discussion

8.7. Summary

The significance of the experimental results obtained in the present work has been discussed across several areas. The reliability of the results was first discussed, with the experimental error being partly attributed to the heterogeneity of the biochars. This variation can be found in individual samples, between samples of the same biochar, and between samples of the same feedstock from different sources. To account for this heterogeneity, it is recommended that future studies analyse several sample areas. The variation between different sources of the same feedstock poses challenges for the classification of biochars as catalysts; suggested methods include classification by composition (*e.g.* ash content or carbon content), or by structure (*e.g.* porosity or graphiticity).

The applications of biochar in catalysis were next considered, particularly the potential of carbon and ash content to catalyse a broader range of reactions than those studied here. Activity in glycerol upgrading suggests that ash content may be active in the synthesis of other organic carbonates from CO₂, and may also be active in transesterification and hydrogenation reactions. Carbon content was shown to be active in methanol conversion to DMM, and may also catalyse the formation of DME. Similar activity may be observed in hydrogenation/dehydrogenation and oxidation/reduction reactions, as well as potential applications as carbonaceous electrodes in place of platinum. Having demonstrated the versatility of untreated biochars as catalysts, further applications may be found as supports and functionalised catalysts, including the production of mesoporous supports from the silica content of biochar ash. Challenges remain however for the application of biochars industrially, due to the low conversions obtained and poor reproducibility.

The insights from the present work can be applied to the design of carbonaceous catalysts and supports. The catalytic activity of biochar was shown to be dependent on composition, which is in turn influenced by feedstock choice. Rather than relying on surface treatments to tailor the properties of biochar to the desired application, the feedstock can be characterised and selected based on the most desirable properties required from the biochar catalyst. This would also improve the sustainability of the process by reducing the need for surface treatments to further modify the biochar (Principle 5). Biochars could be screened for

potential as catalyst supports in a similar way; it is worth emphasising that biochars from different feedstocks should not be treated as interchangeable, but rather as distinct carbonaceous materials with various properties.

The insights gained can also be applied to exploiting the phenomenon of catalytically active coke. As with biochars, the activity may be attributable to trace elemental content, such as K, F or Cl; alternatively or in addition, these elements may influence the structure of the carbon formed. An improved understanding of the term graphiticity is required to understand what aspect of graphiticity is responsible for the observed catalytic activity of the biochars studied here, as well as graphitic carbon deposits. It should also be recognised that different characterisation techniques provide different insights into graphiticity: THz for example provides data on the extent of long-range graphitic networks, whilst carbon atoms in aromatic or graphitic environments can be detected through XPS and ^{13}C -NMR. A combination of characterisation techniques may be required to gain a full picture of the graphitic character of a sample, and therefore which aspect of graphiticity is responsible for the catalytic activity observed.

Finally, further considerations should be taken into account when selecting biochars for catalytic applications. Whilst the parameters affecting catalytic activity have been studied here, the mechanical strength of the biochar material may require characterising to assess the suitability for use in stirred and packed bed reactors. Similarly, life cycle analyses and quantitative metrics such as E-factor analysis may need to be performed to assess the sustainability of the choice of biochar, and any surface treatments performed to it, compared to other alternatives.

Having discussed the wider implications of the work, the final conclusions of the thesis will be presented in Chapter 9, with recommendations for future work.

Chapter 9 – Conclusions and Future Work

In this chapter, the final conclusions of the work will be presented, summarising the new knowledge obtained through the experimental work performed. The aims and objectives of the work are reviewed in section 9.1. In section 9.2, conclusions relating to the characterisation of the biochar catalysts are presented. Conclusions regarding the application of biochars in heterogeneous catalysis are then presented in section 9.3, and insights into the design of carbonaceous catalysts and exploitation of catalytically active coke are summarised in section 9.4. The study of the catalytic activity of biochars is a relatively new field of research, and several recommendations for future practice are made throughout this chapter. New areas of potential research are identified in section 9.5.

9.1. Introduction

In this work, biochars produced from four different feedstocks have been characterised before and after surface treatments, and tested for catalytic activity in two reactions utilising waste materials as feedstocks: the conversion of methanol to products, and the upgrading of glycerol with CO₂ to glycerol carbonate. The feedstocks were supplied by the UK Biochar Research Centre at the University of Edinburgh: rice husks (RHB), wheat straw (WSB), oil seed rape (OSB) and soft wood biochar (SWB). The biochars were produced at pyrolysis temperatures of 550 °C and 700 °C. The catalytic performance and carbon structure of the biochars was compared with a commercial activated charcoal (AC), supplied by Sigma Aldrich.

The objectives of the experimental work, as set out in section 2.6.3, were:

- To improve understanding of the utilisation of biochar in catalysis
- To investigate the potential of biochar as a catalyst for sustainable reaction engineering
- To apply the insights from the activity of biochar to the design of carbonaceous catalysts, and the exploitation of catalytically active coke

The overall aim of the research was to improve sustainability of chemical reaction engineering, by improving understanding of the role of carbon in heterogeneous catalysis. Thorough characterisation of the biochar (section 9.2) has improved understanding of the factors which affect the catalytic activity of biochar; this will enable biochars to be selected for the desired application, reducing waste material and improving energy efficiency. Finding catalytic applications for biochar (section 9.3) could lead to the development of catalysts produced from more sustainable resources; utilising waste materials could be more sustainable than the mining of increasingly-rare metals, though life-cycle analysis would be needed to verify this. Finally, the insights gained from this study could be used to develop improved carbonaceous catalysts (section 9.4). This would improve the efficiency of reactions catalysed by carbonaceous materials, reducing the quantity of energy and materials required for a given reaction. The insights could also be applied to the phenomenon of catalytically active coke on metal-based catalysts, again improving efficiency in a range of catalytic reactions.

In summary, the findings of the current work could find applications in improving sustainability across the chemical industries. The key recommendations for future work needed to realise this are summarised in section 9.5.

9.2. Characterisation of carbonaceous catalysts

The properties of biochars have been thoroughly characterised in the current work, before and after surface treatments. Characterisation has included vibrational spectroscopy, XPS, SEM imaging, TGA, and BET adsorption isotherms. The effect of feedstock choice and pyrolysis conditions on biochars are already well-studied in the context of soil remediation applications, but had not previously been studied with a view to catalytic applications. The experimental work conducted has led to new insights into both the properties of biochars (section 9.2.1), and methods for characterising these properties (section 9.2.2). The implications of the work for sustainability are summarised in section 9.2.3, with recommendations for future practice given in section 9.2.4.

Chapter 9 – Conclusions and Future Work

9.2.1. Properties of biochars

Standard biochars from UKBRC were ground to particle sizes of $< 90 \mu\text{m}$ and characterised for catalytic applications for the first time. The surface areas of the studied materials ranged from 50 to $320 \text{ m}^2 \text{ g}^{-1}$, with micropore volumes from 0.000 to $0.105 \text{ cm}^3 \text{ g}^{-1}$. The highest values were obtained for SWB-550, and were comparable although lower than those found for the AC, with a measured BET surface area of $729 \text{ m}^2 \text{ g}^{-1}$ and micropore volume of $0.153 \text{ cm}^3 \text{ g}^{-1}$. The next highest values were obtained for RHB-550 and OSB-700, with BET surface areas of $121 \text{ m}^2 \text{ g}^{-1}$ and $107 \text{ m}^2 \text{ g}^{-1}$ and micropore volumes of 0.00325 and $0.0188 \text{ cm}^3 \text{ g}^{-1}$ respectively. The lowest values were found for OSB-550 and WSB-550, with surface areas of $62.3 \text{ m}^2 \text{ g}^{-1}$ and $51.7 \text{ m}^2 \text{ g}^{-1}$ respectively, and micropore volume of $0.00286 \text{ cm}^3 \text{ g}^{-1}$ for WSB-550. No microporosity was detected in OSB-550. This demonstrates that biochars can exhibit promising properties for catalysis without further treatments, however these properties do vary with feedstock. It is also notable that the increased microporosity and surface area observed for OSB at higher pyrolysis temperatures is consistent with literature findings.

The composition of the biochar was studied through proximate analysis using TGA, and elemental composition analysis through XPS. The properties again varied with feedstock, as consistent with expectations from the literature; whilst SWB-550 consisted of only C ($90.4 \text{ at}\%$) and O ($10.6 \text{ at}\%$), RHB-550 consisted of only $67.6 \text{ at}\%$ C. The ash content of RHB-550 was evaluated at $42.9 \text{ wt}\%$ by TGA, and comprised of Si, O, K, P and Ca. Indeed, RHB-550 and SWB-550 exhibited very different catalytic activities in the reactions studied; this is considered in section 9.3. Notably, no transition metals with known catalytic activity were detected, such as Fe, Ni or Pd.

The biochars studied in the present work were all plant-derived, and similarities were detected in aspects of carbon structure and surface chemistry. FTIR-ATR spectra indicated similar surface chemistries, with the main differences being in the intensity of silica bands. This was correlated with the ash content of the biochars. Deconvoluted Raman spectra indicated that the area ratio of disordered to graphitic carbon bands ($A_{\text{D1}}/A_{\text{G}}$) were similar for the biochars, at approximately 1.5. Notably no increase in graphiticity was observed with increased pyrolysis temperature for OSB; indeed the ratio increased slightly from 1.39 to

1.59, although this was within the experimental error. The percentage error associated with curve deconvolution and analysis of different areas of the sample was relatively high, at 20 %, however the biochars were clearly more graphitic than the commercial AC, which had a much higher A_{D1}/A_G ratio of 2.82.

The characterisation work indicated that the structure of biochars is heterogeneous, with percentage errors of > 20 % partly attributable to variations in the properties of biochars at the surface. In XPS analysis, for example, two areas of each sample were analysed, and the error was calculated from the standard deviation of the two values measured for each element. In some cases, elements were only detected in one area of the sample, such as Mg in OSB-700. The concentration of elements, and therefore the distribution of functional groups, is very unlikely to be uniform across the surface of the samples. This can be seen in SEM-EDX images, where each particle demonstrated different structures and distributions of elements. This impacts on catalytic performance, as will be shown in section 9.3.

Comparison with biochars in the literature also indicated that the properties of biochars can vary when different sources of the same feedstock are used. Rice husk biochar for example is commonly used in the literature, due to the availability of rice husk waste in Asia. However, the reported properties of RHB in the literature varied in ash content from 14.77 wt% to 44.38 wt% (Leng *et al.* 2015; Wei *et al.* 2017). Composition also varied, with aluminium and iron detected in the literature but not detected in samples from the UKBRC. This variation in properties presents challenges for classification of biochars; recommendations are made in section 9.2.4.

9.2.2. Characterisation of graphiticity

There are currently no standard procedures for characterising the graphiticity of a carbonaceous sample. The ratio of the disordered to graphitic bands in Raman spectra is most commonly used as a measure of graphiticity, however the methods used vary (discussed in section 9.2.3). The term graphiticity has not been defined in the literature in the context of catalysis, and could refer to the extent of graphitic networks, the proportion of a material that is graphite, the perfection (*i.e.* lack of defects) of a graphitic network, and so on.

Chapter 9 – Conclusions and Future Work

The results of the present work provided insights into the various methods for characterising graphiticity in carbonaceous samples.

In the current work, several techniques were applied to the biochars to quantify graphiticity: XPS C1s spectra, Raman spectra, and previously-obtained THz spectra. As each technique measures a different aspect of graphiticity, a more complete picture of the graphitic character of the biochars has been obtained than in previous studies. In OSB-700, no graphitic carbon was detected at the surface, but was detected through Raman spectroscopy. Due to the varying penetration depths of these techniques, this indicates that in OSB-700, graphiticity may only be present deeper within the sample, and not at the surface. Similarly, RHB-550 is more graphitic than WSB-550 when measured using Raman spectroscopy, but less graphitic at the surface as measured by XPS (surface band I content is 5.38 % for RHB-550, versus 20.88 % for WSB-550). This variation is likely to affect other carbonaceous samples besides biochars.

9.2.3. Implications for sustainability

A thorough characterisation of the surface chemistry of biochars has highlighted some of the key similarities and differences between biochars from different feedstocks. For biochars produced under the same conditions at the same facility, the key differences largely related to elemental composition and ash content, whilst surface chemistry and graphiticity were broadly similar. This suggests that when sourcing biochars for catalytic applications, the key consideration should be the elemental composition of the biochar, compared to the requirements of the process. For example, potassium content was beneficial for glycerol carbonate synthesis, and detrimental for methanol conversion. This insight could facilitate the selection and development of biochar catalysts with higher selectivities and conversions, without the use of surface treatments, thus preventing the formation of waste in accordance with Principle 1 of Green Chemistry.

9.2.4. Recommendations for future practice

The principal recommendation for the future study of biochar is to ensure biochars from different materials are not treated as interchangeable. The catalytic properties of biochar can

vary widely with feedstock and pyrolysis temperature, and even with source of feedstock. The composition of plant-based biochar likely also varies seasonally, depending on the composition of the soil. Thorough characterisation is therefore vital when studying biochars in catalytic applications.

An understanding of the heterogeneity of biochar is also essential for catalytic studies. It is recommended that several areas of a sample (at least five) are measured by each characterisation technique, to ensure the results are representative. The use of standard biochars could be used for the development of standardised protocols for the analysis of biochar catalysts, in a similar manner to the ongoing European Cooperation in Science and Technology project (COST Action TD1107) to develop standardised characterisation protocols of biochars for soil remediation applications (Bachmann *et al.* 2016). This should include standardised methods for curve deconvolution and calibration of Raman and XPS C1s spectra, particularly recognising that more than two peaks contribute to the D and G bands observed in Raman spectra. This would ensure that results from across institutions can be compared.

The characterisation of graphiticity in future work should also consider the aspect of graphiticity which is being studied. As shown in the present work, XPS C1s spectroscopy, Raman spectroscopy and THz spectroscopy can produce conflicting results, not all of which may be relevant to the subsequent catalytic activity of the biochar.

The varied properties of biochars sourced from the same feedstock in particular highlights the need for a classification system for biochars. Classification by feedstock type may not be an accurate predictor of catalytic activity; indeed, the plant-based materials used in the present work have exhibited different catalytic activities, as will be shown in section 9.3. Classification by composition, such as carbon or ash content, may provide a more appropriate method for classifying biochars, which might better group together biochars with similar catalytic activities.

Chapter 9 – Conclusions and Future Work

9.3. Potential applications of biochar in catalysis

One of the objectives of the work was to provide insights into the catalytic activity of biochars and therefore other carbonaceous catalysts. In the present work, activity has been studied in two reactions: methanol conversion to DMM, and glycerol upgrading with CO₂ to glycerol carbonate. The conclusions from these studies are presented in section 9.3.1, whilst implications for sustainability are discussed in section 9.3.2. The challenges facing further catalytic applications are considered in section 9.3.3. Recommendations for future practice are given in section 9.3.4.

9.3.1. Biochar in catalysis

In methanol conversion, high carbon contents and low AAEM contents were related to higher catalytic activity. DMM was reliably produced using SWB-550 and AC, however the quantity produced when using RHB-550, OSB-550 and WSB-550 was 10-100 times lower. Following demineralisation, the activity of WSB-550 and OSB-700 was greatly improved, with production of DMM exceeding that of commercial AC. This is consistent with the hypothesis that AAEM elements are detrimental to DMM production.

Another notable product of methanol conversion was the formation of 1,1-DME. This product has not previously been noted in the literature, and may indicate that biochars are able to catalyse the reaction of DMM with methanol to form 1,1-DME; this is supported by the lack of the 1,2-DME isomer in the reaction products. The effect of demineralisation on 1,1-DME yield was less pronounced; increased activity may be related to graphitic carbon content, as the greatest increase in yield was observed for WSB-550-T-C without demineralisation. SWB-550 also produced more 1,1-DME than AC, despite the lower surface area and DMM yield. The reaction mechanism however would require verification, and the increased yield would need to be decoupled from the effect on DMM production.

DMM was produced in helium atmospheres, indicating that the biochars can supply active surface oxygen for the oxidation of methanol. For SWB-550, slightly less DMM was produced in the helium atmosphere, indicating that in the absence of CO₂ to re-oxidise the active sites, the surface oxygen is depleted. As there was little difference in the activity of

RHB-550, it is possible that CO₂ is unable to re-oxidise the active sites, leading to the limited DMM activity observed. This may also be the case for WSB-550, OSB-550 and OSB-700. In the case of AC, DMM yields were higher in the absence of CO₂, possibly indicating that CO₂ is blocking the active sites in AC.

By contrast, the most active biochars for the production of glycerol carbonate from glycerol and CO₂ were RHB-550 and OSB-550. No glycerol carbonate was produced when using SWB-550 and AC as catalysts. In this case, activity is partly attributable to the ash content of the biochars; the ash content of RHB-550, OSB-700 and WSB-550 was demonstrated to be catalytically active. This extends a previous literature observation that boiler ash waste can catalyse the formation of glycerol carbonate from glycerol and urea. The best performance was obtained by WSB-550-ash, which may also have the highest accessible potassium content (as evidenced by the 90 at% removal of K following demineralisation, compared to 80 at% for RHB-550 and OSB-700). Further, demineralisation of the ash reduced the production of glycerol carbonate by a factor of 10-100. The effect of demineralisation was less clear in the biochars, where the glycerol carbonate yield of RHB-550 was reduced by a factor of 10, but increased for OSB-700 by a factor of 10.

Carbon content also appears to play a role in glycerol carbonate synthesis, as OSB-550 was more active than OSB-700, despite the similar performance of the ash contents. Tar impregnation and pyrolysis however decreased the yield of glycerol carbonate from RHB-550, indicating that active sites may have been blocked by carbon deposits. These active sites may be oxygenated functional groups, which decrease in concentration following tar impregnation.

Notably, triacetin production is commonly noted in the literature as being related to Brønsted acidity; however, biochar ash is generally basic in nature, and led to higher quantities of triacetin being produced than the original biochar.

The activity of biochar carbon and biochar ash in these two reactions demonstrates the potential of biochars and carbonaceous materials to catalyse other reactions. For example,

Chapter 9 – Conclusions and Future Work

the production of glycerol carbonate indicates biochars could catalyse the formation of other cyclic carbonates. There is some evidence for this in the formation of TMOS during methanol conversion, which could indicate the formation of DMC, which then reacts with silica. Other potential reactions involving the activation of CO₂ or alcohols, such as transesterification reactions, could be catalysed by biochar ash. The carbonaceous content of biochar could also show potential to catalyse further oxidations, reductions, hydrogenations and dehydrogenations; CNTs and graphite have already demonstrated catalytic activity in these reactions. Biochar could also be used as a catalyst support, or to produce mesoporous silicas as catalyst supports.

9.3.2. Implications for sustainability

In the current work, biochars have demonstrated catalytic activity in two different reactions: methanol conversion and glycerol upgrading to glycerol carbonate. This implies that the full potential of these materials as catalysts is yet to be realised, with further applications likely to be possible. Depending on the source of the biomass and the alternative catalyst, biochars could prove a more sustainable source of catalytic material than increasingly-scarce metals such as copper, nickel and tin. This would improve sustainability by reducing reliance on depleting reserves of metal, in accordance with Principle 7 of Green Chemistry.

The reaction routes themselves are also highly promising for improving the sustainability of industrial reaction engineering. In the current work it has been shown that both pathways can be catalysed by a cheap, biomass-derived catalyst, and thus both reactions are promising areas for future research and catalyst development. The dimethoxymethane product formed in this experimental work is currently sourced from steam reforming or coal gasification, however the current work has shown that methanol could be used as a precursor. Similarly, the formation of glycerol carbonate from waste glycerol utilises a waste product of biodiesel synthesis, whilst also forming a useful precursor for plastic synthesis from a renewable resource, instead of from oil. In both of these reactions, biochar has been shown to be catalytically active for the first time. This insight could facilitate the design of cheap, biomass-derived catalysts to make these sustainable processes economically feasible.

9.3.3. Challenges for application

Although the present work did not aim to optimise the biochars, the yields and selectivities obtained are currently too low to consider industrial applications. Due to calibration issues, there were challenges in calculating the conversion of glycerol and methanol, but the values are likely to be < 10 %. The conversion may however be suitable for the use of waste biomass as a catalyst for the conversion of waste oil to biodiesel in a domestic setting, for example.

The reproducibility of the reactions would also require improvement before applying to industrial applications; the percentage error was estimated from three repeats, and was found to be 23.3 % for DMM production and 26.4 % for glycerol carbonate. For diacetin, the percentage error was even higher, at 82.9 %. This was attributed to biochar heterogeneity.

9.3.4. Recommendations for future practice

The key observation in the present work is that biochars from different feedstocks are not interchangeable. Different biochars exhibited catalytic activity in the two reactions studied: SWB-550 for example was active for methanol conversion, but not for glycerol upgrading. Screening and characterisation are recommended to identify the most promising feedstock for the desired application.

Future experimental work involving GCMS analysis of reaction products should consider the use of internal standards for the accurate calibration of reaction products. To enhance separation of products, columns should also be chosen with similar polarities to the likely reaction products; in the current work, column choice was constrained due to the requirements of other laboratory users.

The potential catalytic influence of metal reactor walls should also be accounted for by carrying out reactions in a quartz or glass lining within the reactor. In this case, control experiments indicated that the reactor walls were not catalytically active. Gas phase analysis of products would also be recommended to ensure the full range of products can be identified, and provide further insights into the reaction mechanism, *e.g.* the detection of DME could enhance understanding of the selectivity of the catalysts to methanol oxidation.

Chapter 9 – Conclusions and Future Work

9.4. Insights for design of carbonaceous catalysts

Biochars from different feedstocks demonstrated catalytic activity in both methanol conversion and in glycerol upgrading. This is the first time that carbonaceous catalysts have been applied in the study of these reactions, and demonstrates that biochars and carbonaceous catalysts could find many more applications than are currently studied in the literature. New sustainable reaction pathways could be opened up through the design of carbonaceous catalysts, with the properties easily modified to optimise production of the desired product. The properties of biochars which influence catalytic activity are presented in section 9.4.1, with the conclusions regarding the effect of surface treatments for modification of biochars presented in section 9.4.2. The implications for sustainability are presented in section 9.4.3, and recommendations for future practice are given in section 9.4.4.

9.4.1. Properties influencing catalytic activity

It is firstly worth noting that classification of biochars by feedstock material or feedstock type is insufficient to predict catalytic activity. The plant-based biochars presented in the present work did not exhibit similar catalytic activity; RHB-550 for example was active for the production of glycerol carbonate, but inactive for DMM production from methanol. The opposite was true of SWB-550. Catalytic activity is rarely compared in the literature for multiple reactions or multiple feedstocks, and this is therefore an important insight for future catalyst design.

In the present work, the key factor affecting catalytic activity in both reactions appeared to be AAEM content. The removal of potassium led to improved activity in methanol conversion, whilst the presence of potassium and AAEM elements in the ash was related to improved performance in glycerol carbonate synthesis. A number of possible mechanisms were proposed, such as alteration of adsorption/desorption strengths, the presence of catalytically active minerals such as alkali hydroxides (possibly formed in situ), and alteration of surface acidity/basicity. Further work would be required to identify which mechanism dominates. It is very possible that different mechanisms dominate in different biochars, due to the complexity and variation in these materials. As elemental composition is

heavily influenced by the feedstock, the most promising biochars for given applications could be selected based on the elemental composition of the biomass.

The graphiticity of carbon structures may also influence catalytic activity. Based on the present work, for example, the yield of 1,1-DME in methanol oxidation may be correlated with increased graphiticity of the carbon. However, it is important to consider the definition of graphiticity, and which aspect of graphiticity is responsible for the improved catalytic performance, as noted in section 9.2.3.

9.4.2. Use of surface treatments

In the literature, surface treatments are commonly used to modify the properties of biochar for catalytic applications. This includes acid washing to remove or reduce ash content, acid or base treatments to introduce new functional groups, and metal loading when biochars are being used as support materials. These surface treatments are often developed to optimise the performance of a particular biochar in a given reaction, however systematic studies of the effect of the surface treatment on different feedstocks are not often performed.

In the present work, three surface treatments were performed on three different biochars. The effect of each surface treatment on the biochar was observed to vary, particularly the effect on surface area and surface chemistry. Some variation in surface area is expected due to the use of different particle sizes for the production of demineralised samples at the University of Edinburgh, however the differing trends indicate that at least the extent of changes in surface area vary widely between biochars.

The effectiveness of demineralisation using HCl to reduce the ash content was observed to vary between biochars. Whilst approximately 30 % of ash was removed from OSB-700 and WSB-550, only 5 % was removed from RHB-550. In demineralisation and acetone washing, the surface area of WSB-550 was increased by 85 % following treatment, despite the larger particle size used, whilst surface area was reduced by 30 % in RHB-550 and OSB-700. The microporosity of OSB-700 in particular was reduced by 95 %. This demonstrates that common acid washing techniques in the literature may have different effects on biochars

Chapter 9 – Conclusions and Future Work

from different feedstocks, and treatments which enhance the activity of one biochar may be ineffective in another.

The demineralisation treatment with HCl was shown to be effective for the removal of surface K, but only partly effective for the removal of Ca and Mg. In addition, washing with demineralised water may not have removed all of the Cl⁻ ions introduced to RHB-550. This may be due to differences in hydrophobicity between the biochars. The influence of trace fluorine introduced during demineralisation was not considered in depth during the present work, however the influence of potential contaminants, such as fluoride ions from tap water, should be considered.

9.4.3. Implications for sustainability

The insights gained from the present work could be used to design carbonaceous catalysts and supports with improved conversions and selectivities, for use in a range of reactions. In some cases, carbonaceous catalysts may be cheaper and more sustainable than metal-based alternatives; in others, cheap carbonaceous catalysts could make processes using renewable feedstocks economically viable, compared to vastly more expensive platinum-group metal catalysts.

The number of reactions which can be catalysed by some form of carbonaceous material is likely to be greater than is currently realised. Many studies focus on pure carbon such as graphite, carbon nanotubes or activated carbons, however in the present work activated carbon was not active for glycerol upgrading. This insight from the present research could inspire research into further reactions where more complex carbonaceous materials could act as catalysts, again facilitating the use of renewably-sourced materials as catalysts (Green Chemistry Principle 7).

9.4.4. Recommendations for future practice

In future studies aiming to design carbonaceous materials for catalytic activity, the varying effects of biochars to surface treatments should be considered. The hydrophobicity of the biochar in particular may influence the effectiveness of aqueous-phase treatments. Ideally,

appropriate biochar feedstocks should be selected to minimise the surface treatments required to produce the desired properties. For example, SWB-550 already contains 0 wt% ash, and so the choice of SWB would eliminate the requirement for a demineralisation process. Lifecycle analyses and E-factor analyses could also be performed to quantify the sustainability of the process, including the use of any surface treatments and transporting the feedstock from the source.

Whilst not detected in the present work, trace quantities of transition metals such as Fe, Mn or Al are often detected in biochars in the literature (Chandrasekhar *et al.* 2003). These elements are known to be catalytically active in a range of organic chemistry reactions, such as hydrogenations, dehydrogenations, oxidations and reductions. The contribution of these elements to any catalytic activity should be considered when interpreting reaction data.

Chapter 9 – Conclusions and Future Work

9.5. Suggestions for Future Work

The present work provides a foundation for future systematic studies of the application of biochar in catalysis. In addition to the insights for future practice provided in sections 9.2.3, 9.3.4 and 9.4.4, several new research questions have been posed by the present work, which could provide the basis for future study. Continued research in these areas is necessary to realise the full catalytic potential of biochar, and the ambition of catalysts made from sustainable carbon. The properties of these catalysts could be modified, using the insights gained from the present work, to catalyse sustainable reaction routes, and improve the sustainability of heterogeneous catalysis.

Characterisation of carbonaceous catalysts *in situ* would advance understanding of reaction mechanisms over carbonaceous catalysts. This could involve the use of reaction cells with FTIR to study changes in surface functionality, for example. Further characterisation of biochars in terms of surface acidity and basicity, for example through TPD studies, would also assist in mechanistic studies of catalytic activity, providing information on possible active sites for reactions.

Similarly, the changes in the properties of biochars on exposure to organic solvents, such as acetone and methanol, should be considered. The current work purposely focused on complex biochar systems, to gain insights into the various influences on carbonaceous materials in catalytic systems. The study of model systems could enable reaction mechanisms to be investigated in more detail. For example, the effect of acetone on the structure and surface chemistry of graphite and amorphous carbon blacks could be studied, and related to the observed effects in the present work of acetone on biochars.

The objective of the present work was not to optimise the performance of the biochars in the reactions of interest, but to investigate the origins of underlying catalytic activity. In order to apply biochars as catalysts, further research would be required into appropriate (and sustainable) activation and functionalisation of biochars, as well as optimisation of the process conditions of the reaction of interest when using biochar catalysts. It is worth emphasising that the results of the present work suggest that biochars are not

interchangeable, and that the optimal reaction conditions for one biochar may not be the optimal conditions for another.

A large-scale systematic study of the catalytic activity of biochar from different feedstocks was beyond the scope of the present work. However, having demonstrated that biochars from similar feedstocks can exhibit differing catalytic activity, there may be benefits to a large-scale study of biochars from different feedstocks. This would benefit from an appropriate system for classifying the biochars, as suggested in section 8.2.2. Predictions could be made for which biochars will exhibit similar activity. The conversion of methanol would provide an ideal model reaction, with the range of reaction products being highly sensitive to surface acidity.

The use of biochar for tar reforming currently focuses on model compounds, usually in the gas phase. A liquid phase method suitable for use with real tar mixtures was developed in the present work, however the conversion of the tar was negligible. A closed system and longer reaction times may be necessary to study conversion of tar in the liquid phase.

The full range of catalytic applications of biochar has yet to be explored. In the present work, untreated biochar has demonstrated activity for methanol conversion and the reaction of glycerol and carbon dioxide to form glycerol carbonate. Due to the demonstrated activity of both the ash and the carbon in various reactions, there is a broad scope for future reactions that could be catalysed by biochar, or use supports produced from biochar. This includes the development of mesoporous silica from biomass for use as catalyst supports. The present work suggests an application-centred approach should be adopted for feedstock selection for biochar, minimising the use of surface treatments and activation processes by selecting the feedstock with the most promising characteristics for the desired reaction. Lifecycle analyses, E-factor analyses and mechanical properties should also be considered to quantify the sustainability and practicality of using the chosen feedstock.

References

References

- Abatjoglou, A.G. & Miller, D.J., 2011. Aldehydes. In *Kirk-Othmer Encyclopedia of Chemical Technology*. Hoboken, NJ, USA: John Wiley & Sons, Inc., pp. 1–12.
- Abdullah, S.H.Y.S., Hanapi, N.H.M., Azid, A., Umar, R., Juahir, H., Khatoon, H. & Endut, A., 2017. A review of biomass-derived heterogeneous catalyst for a sustainable biodiesel production. *Renewable and Sustainable Energy Reviews*, 70, pp.1040–1051.
- Abu El-Rub, Z., Bramer, E.A. & Brem, G., 2008. Experimental comparison of biomass chars with other catalysts for tar reduction. *Fuel*, 87(10–11), pp.2243–2252.
- Acosta, R., Fierro, V., Martinez de Yuso, A., Nabarlatz, D. & Celzard, A., 2016. Tetracycline adsorption onto activated carbons produced by KOH activation of tyre pyrolysis char. *Chemosphere*, 149, pp.168–176.
- Ahmad, M., Rajapaksha, A.U., Lim, J.E., Zhang, M., Bolan, N., Mohan, D., Vithanage, M., Lee, S.S. & Ok, Y.S., 2014. Biochar as a sorbent for contaminant management in soil and water: A review. *Chemosphere*, 99.
- Akiyama, M., Suzuki, E. & Ono, Y., 1993. Direct synthesis of tetramethoxysilane from rice hull ash by reaction with dimethyl carbonate. *Inorganica Chimica Acta*, 207(2), pp.259–261.
- Al-Khattaf, S., D'Agostino, C., Akhtar, M.N., Al-Yassir, N., Tan, N.Y. & Gladden, L.F., 2014. The effect of coke deposition on the activity and selectivity of the HZSM-5 zeolite during ethylbenzene alkylation reaction in the presence of ethanol. *Catalysis Science & Technology*, 4(4), p.1017.
- Al-Oweini, R. & El-Rassy, H., 2009. Synthesis and characterization by FTIR spectroscopy of silica aerogels prepared using several Si(OR)₄ and R'Si(OR)₃ precursors. *Journal of Molecular Structure*, 919(1–3), pp.140–145.
- Algoufi, Y.T. & Hameed, B.H., 2014. Synthesis of glycerol carbonate by transesterification of glycerol with dimethyl carbonate over K-zeolite derived from coal fly ash. *Fuel Processing Technology*, 126, pp.5–11.
- Alkhazov, T.G., Lisovskii, A.E., Ismailov, Y.A. & Kozharov, A.I., 1978. Oxidative dehydrogenation of ethylbenzene on activated carbons. 1. General process relationships. *Kinetics and Catalysis*, 19(3), pp.482–485.
- Almusaiteer, K., 2009. Synthesis of dimethyl carbonate (DMC) from methanol and CO₂ over Rh-supported catalysts. *Catalysis Communications*, 10(7), pp.1127–1131.
- Amano, H., Sato, S., Takahashi, R. & Sodesawa, T., 2001. Dehydrogenation of cyclohexene over carbon deposited on alumina. *Physical Chemistry Chemical Physics*, 3(5), pp.873–879.
- Ampelli, C., Perathoner, S. & Centi, G., 2014. Carbon-based catalysts: Opening new scenario to develop next-generation nano-engineered catalytic materials. *Chinese Journal of Catalysis*, 35(6), pp.783–791.
- Ampelli, C., Perathoner, S. & Centi, G., 2015. CO₂ utilization: an enabling element to move to a resource- and energy-efficient chemical and fuel production. *Philosophical Transactions of the Royal Society of London A: Mathematical, Physical and Engineering Sciences*, 373(2037).
- Ananikov, V., 2016. Plausible role of nanoparticle contamination in the synthesis and properties of organic electronic materials. *Organic Photonics and Photovoltaics*, 4, pp.68–76.
- Anastas, P.T. & Warner, J.C., 1998. *Green chemistry: theory and practice*, Oxford University Press.
- Angin, D. & Şensöz, S., 2014. Effect of Pyrolysis Temperature on Chemical and Surface Properties of Biochar of Rapeseed (*Brassica napus* L.). *International Journal of Phytoremediation*, 16(7–8), pp.684–693.
- Annino, R. & Villalobos, R., 1992. *Process gas chromatography: fundamentals and applications: on-line analysis for process monitoring and control*, Instrument Society of America.
- Aouissi, A., Al-Deyab, S.S., Al-Owais, A. & Al-Amro, A., 2010. Reactivity of Heteropolytungstate and Heteropolymolybdate Metal Transition Salts in the Synthesis of Dimethyl Carbonate from Methanol and CO₂. *International Journal of Molecular Sciences*, 11(7), pp.2770–2779.
- Aresta, M., 2010. Carbon Dioxide: Utilization Options to Reduce its Accumulation in the Atmosphere. In *Carbon Dioxide as Chemical Feedstock*. Weinheim, Germany: Wiley-VCH Verlag GmbH & Co.

- KGaA, pp. 1–13.
- Aresta, M. *et al.*, 2007. Utilisation of CO₂ as a chemical feedstock: opportunities and challenges. *Dalton Transactions*, 98(28), p.2975.
- Aresta, M., Dibenedetto, A., Pastore, C., Pápai, I. & Schubert, G., 2006. Reaction mechanism of the direct carboxylation of methanol to dimethylcarbonate: experimental and theoretical studies. *Topics in Catalysis*, 40(1–4), pp.71–81.
- Arrigo, R., Hävecker, M., Wrabetz, S., Blume, R., Lerch, M., McGregor, J., Parrott, E.P.J., Zeitler, J.A., Gladden, L.F., Knop-Gericke, A., Schlögl, R. & Su, D.S., 2010. Tuning the acid/base properties of nanocarbons by functionalization via amination. *Journal of the American Chemical Society*, 132(28), pp.9616–30.
- Asadullah, M., Zhang, S., Min, Z., Yimsiri, P. & Li, C.-Z., 2010. Effects of biomass char structure on its gasification reactivity. *Bioresource Technology*, 101(20), pp.7935–7943.
- ASTM International, 2010. Standard Test Methods for Proximate Analysis of Coal and Coke by Macro Thermogravimetric Analysis.
- Auer, E., Freund, A., Pietsch, J. & Tacke, T., 1998. Carbons as supports for industrial precious metal catalysts. *Applied Catalysis A: General*, 173(2), pp.259–271.
- Auson, 2015. Genuine Pine Tar 850. *Auson*.
- Ayala, P., Maia da Costa, M.E.H., Prioli, R. & Freire, F.L., 2004. Nano- and micro-scale wear of fluorinated carbon films. *Surface and Coatings Technology*, 182(2–3), pp.335–341.
- Bachmann, H.J. *et al.*, 2016. Toward the Standardization of Biochar Analysis: The COST Action TD1107 Interlaboratory Comparison. *Journal of Agricultural and Food Chemistry*, 64(2), pp.513–527.
- Bae, Y.-S., Yazaydin, A.O. & Snurr, R.Q., 2010. Evaluation of the BET Method for Determining Surface Areas of MOFs and Zeolites that Contain Ultra-Micropores. *Langmuir*, 26(8), pp.5475–5483.
- Bagreev, A. & Bandosz, T.J., 2001. H₂S adsorption/oxidation on unmodified activated carbons: importance of prehumidification. *Carbon*, 39(15), pp.2303–2311.
- Barbier, J., 1986. Deactivation of reforming catalysts by coking - a review. *Applied Catalysis*, 23, pp.225–243.
- Barrage, M.C., Bonardet, J.L. & Fraissard, J., 1990. 129Xe-NMR study of coke distribution in dealuminated HY zeolites. *Catalysis Letters*, 5(2), pp.143–154.
- Bartholomew, C.H., 2001. Mechanisms of catalyst deactivation. *Applied Catalysis A: General*, 212(1–2), pp.17–60.
- Bauer, F., Chen, W.-H., Zhao, Q., Freyer, A. & Liu, S.-B., 2001. Improvement of coke-induced selectivation of H-ZSM-5 during xylene isomerization. *Microporous and Mesoporous Materials*, 47(1), pp.67–77.
- Bauer, F., Chen, W., Bilz, E., Freyer, A., Sauerland, V. & Liu, S., 2007. Surface modification of nano-sized HZSM-5 and HFER by pre-coking and silanization. *Journal of Catalysis*, 251(2), pp.258–270.
- Bayraktar, O. & Kugler, E.L., 2002. Characterization of coke on equilibrium fluid catalytic cracking catalysts by temperature-programmed oxidation. *Applied Catalysis A: General*, 233(1–2), pp.197–213.
- Bazargan, A., Kostić, M.D., Stamenković, O.S., Veljković, V.B. & McKay, G., 2015. A calcium oxide-based catalyst derived from palm kernel shell gasification residues for biodiesel production. *Fuel*, 150, pp.519–525.
- Beck, J.S., Crane, R.A.J., Mathias, M.F., Kowalski, J.A., Lissy, D.N. & Stern, D.L., 1999. Xylene isomerisation.
- Bhanage, B.M., Fujita, S., Ikushima, Y. & Arai, M., 2001. Synthesis of dimethyl carbonate and glycols from carbon dioxide, epoxides, and methanol using heterogeneous basic metal oxide catalysts with high activity and selectivity. *Applied Catalysis A: General*, 219(1), pp.259–266.
- Bhatnagar, A., Hogland, W., Marques, M. & Sillanpää, M., 2013. An overview of the modification methods of activated carbon for its water treatment applications. *Chemical Engineering Journal*, 219, pp.499–511.
- Bierhals, J., 2001. Carbon Monoxide. In *Ullmann's Encyclopedia of Industrial Chemistry*. Weinheim,

References

- Germany: Wiley-VCH Verlag GmbH & Co. KGaA.
- Bitter, J.H., Seshan, K. & Lercher, J.A., 1999. Deactivation and Coke Accumulation during CO₂/CH₄ Reforming over Pt Catalysts. *Journal of Catalysis*, 183(2), pp.336–343.
- Boehm, H.P., 1966. Chemical Identification of Surface Groups. *Advances in Catalysis*, 16, pp.179–274.
- Bowker, M., 1998. *The Basis and Applications of Heterogeneous Catalysis*, Oxford University Press, Incorporated.
- Brewer, C.E., Unger, R., Schmidt-Rohr, K. & Brown, R.C., 2011. Criteria to Select Biochars for Field Studies based on Biochar Chemical Properties. *BioEnergy Research*, 4(4), pp.312–323.
- Brown, J.S., Gordon, T., Price, O. & Asgharian, B., 2013. Thoracic and respirable particle definitions for human health risk assessment. *Particle and fibre toxicology*, 10, p.12.
- Brunauer, S., Emmett, P.H. & Teller, E., 1938. Adsorption of Gases in Multimolecular Layers. *Journal of the American Chemical Society*, 60(2), pp.309–319.
- Buczek, B., Biniak, S. & Świątkowski, A., 1999. Oxygen distribution within oxidised active carbon granules. *Fuel*, 78(12), pp.1443–1448.
- Buss, W., Graham, M.C., MacKinnon, G. & Mašek, O., 2016. Strategies for producing biochars with minimum PAH contamination. *Journal of Analytical and Applied Pyrolysis*, 119, pp.24–30.
- Buysch, H.-J., 2000. Carbonic Esters. In *Ullmann's Encyclopedia of Industrial Chemistry*. Weinheim, Germany: Wiley-VCH Verlag GmbH & Co. KGaA.
- Byung, H.H., Dae, H.S. & Sung, Y.C., 1985. Graphite catalyzed reduction of aromatic and aliphatic nitro compounds with hydrazine hydrate. *Tetrahedron Letters*, 26(50), pp.6233–6234.
- Cadus, L.E., Arrua, L.A., Gorrioz, O.F. & Rivarola, J.B., 1988. Action of activated coke as a catalyst: oxydehydrogenation of ethylbenzene to styrene. *Industrial & Engineering Chemistry Research*, 27(12), pp.2241–2246.
- Cadus, L.E., Gorrioz, O.F. & Rivarola, J.B., 1990. Nature of active coke in the oxydehydrogenation of ethylbenzene to styrene. *Industrial & Engineering Chemistry Research*, 29(7), pp.1143–1146.
- Cameron, D.S., Cooper, S.J., Dodgson, I.L., Harrison, B. & Jenkins, J.W., 1990. Carbons as supports for precious metal catalysts. *Catalysis Today*, 7(2), pp.113–137.
- Camp, J.C.J., Mantle, M.D., York, A.P.E. & McGregor, J., 2014. A new combined nuclear magnetic resonance and Raman spectroscopic probe applied to in situ investigations of catalysts and catalytic processes. *The Review of scientific instruments*, 85(6), p.063111.
- Cao, X., Sun, S. & Sun, R., 2017. Application of biochar-based catalysts in biomass upgrading: a review. *RSC Adv.*, 7(77), pp.48793–48805.
- Cao, Y., Cheng, H., Ma, L., Liu, F. & Liu, Z., 2012. Research Progress in the Direct Synthesis of Dimethyl Carbonate from CO₂ and Methanol. *Catalysis Surveys from Asia*, 16(3), pp.138–147.
- Cavani, F. & Trifirò, F., 1995. Alternative processes for the production of styrene. *Applied Catalysis A: General*, 133(2), pp.219–239.
- Cha, J.S., Park, S.H., Jung, S.-C., Ryu, C., Jeon, J.-K., Shin, M.-C. & Park, Y.-K., 2016. Production and utilization of biochar: A review. *Journal of Industrial and Engineering Chemistry*, 40, pp.1–15.
- Chakraborty, R., Bepari, S. & Banerjee, A., 2010. Transesterification of soybean oil catalyzed by fly ash and egg shell derived solid catalysts. *Chemical Engineering Journal*, 165(3), pp.798–805.
- Chandrasekhar, S., Satyanarayana, K.G., Pramada, P.N., Raghavan, P. & Gupta, T.N., 2003. Review: Processing, properties and applications of reactive silica from rice husk—an overview. *Journal of Materials Science*, 38, pp.3159–3168.
- Chao, P.-H., Lin, H.-W., Chen, C.-H., Wang, P.-Y., Chen, Y.-F., Sei, H.-T. & Tsai, T.-C., 2008. Precoking selectivation for improving benzene product purity in heavy aromatics transalkylation. *Applied Catalysis A: General*, 335(1), pp.15–19.
- Che, M. & Vedrine, J.C., 2012. *Characterisation of Solid Materials and Heterogeneous Catalysts: From Structure to Surface Reactivity, Vol 1&2* M. Che & J. C. Vedrine, eds., Wiley-VCH Verlag GMBH, Germany.
- Chen, D., Holmen, A., Sui, Z. & Zhou, X., 2014. Carbon mediated catalysis: A review on oxidative dehydrogenation. *Chinese Journal of Catalysis*, 35(6), pp.824–841.

- Chen, D., Moljord, K. & Holmen, a., 2012. A methanol to olefins review: Diffusion, coke formation and deactivation on SAPO type catalysts. *Microporous and Mesoporous Materials*, 164, pp.239–250.
- Chen, K., Xue, Z., Liu, H., Guo, A. & Wang, Z., 2013. A temperature-programmed oxidation method for quantitative characterization of the thermal cokes morphology. *Fuel*, 113, pp.274–279.
- Chen, S. & Ma, X., 2017. The role of oxygen species in the selective oxidation of methanol to dimethoxymethane over VOx/TS-1 catalyst. *Journal of Industrial and Engineering Chemistry*, 45, pp.296–300.
- Chia, C.H., Gong, B., Joseph, S.D., Marjo, C.E., Munroe, P. & Rich, A.M., 2012. Imaging of mineral-enriched biochar by FTIR, Raman and SEM–EDX. *Vibrational Spectroscopy*, 62, pp.248–257.
- Christoph, R., Schmidt, B., Steinberner, U., Dilla, W. & Karinen, R., 2006. Glycerol. In *Ullmann's Encyclopedia of Industrial Chemistry*. Weinheim, Germany: Wiley-VCH Verlag GmbH & Co. KGaA.
- Chromacademy, 2018. GC Column Maintenance - Prevention is Better than Cure.
- Climeworks, 2017. Climeworks launches world's first commercial plant to capture CO₂ from air.
- Collett, C.H. & McGregor, J., 2016. Things go better with coke: the beneficial role of carbonaceous deposits in heterogeneous catalysis. *Catal. Sci. Technol.*, 6(2), pp.363–378.
- Crombie, K., Mašek, O., Cross, A. & Sohi, S., 2015. Biochar - synergies and trade-offs between soil enhancing properties and C sequestration potential. *GCB Bioenergy*, 7(5), pp.1161–1175.
- Crombie, K., Mašek, O., Sohi, S.P., Brownsort, P. & Cross, A., 2013. The effect of pyrolysis conditions on biochar stability as determined by three methods. *GCB Bioenergy*, 5(2), pp.122–131.
- Cruz, M.G.A., Bastos-Neto, M., Oliveira, A.C., Filho, J.M., Soares, J.M., Rodríguez-Castellón, E. & Fernandes, F.A.N., 2015. On the structural, textural and morphological features of Fe-based catalysts supported on polystyrene mesoporous carbon for Fischer–Tropsch synthesis. *Applied Catalysis A: General*, 495, pp.72–83.
- Da, Z., Magnoux, P. & Guisnet, M., 1999. Liquid phase alkylation of toluene with 1-heptene over a HFAU zeolite: evidence for transalkylation between toluene and non-desorbed products. *Applied Catalysis A: General*, 182(2), pp.407–411.
- Danso-Boateng, E., Shama, G., Wheatley, A.D., Martin, S.J. & Holdich, R.G., 2015. Hydrothermal carbonisation of sewage sludge: Effect of process conditions on product characteristics and methane production. *Bioresource Technology*, 177, pp.318–327.
- Dehkhoda, A.M., West, A.H. & Ellis, N., 2010. Biochar based solid acid catalyst for biodiesel production. *Applied Catalysis A: General*, 382(2), pp.197–204.
- Dodson, J.R., Cooper, E.C., Hunt, A.J., Matharu, A., Cole, J., Minihan, A., Clark, J.H. & Macquarrie, D.J., 2013. Alkali silicates and structured mesoporous silicas from biomass power station wastes: the emergence of bio-MCMs. *Green Chemistry*, 15(5), p.1203.
- van Donk, S., Bitter, J.H. & de Jong, K.P., 2001. Deactivation of solid acid catalysts for butene skeletal isomerisation: on the beneficial and harmful effects of carbonaceous deposits. *Applied Catalysis A: General*, 212(1–2), pp.97–116.
- Dreyer, D.R. & Bielawski, C.W., 2011. Carbocatalysis: Heterogeneous carbons finding utility in synthetic chemistry. *Chemical Science*, 2(7), p.1233.
- Dreyer, D.R., Jia, H.P. & Bielawski, C.W., 2010. Graphene oxide: A convenient carbocatalyst for facilitating oxidation and hydration reactions. *Angewandte Chemie - International Edition*, 49(38), pp.6813–6816.
- Dubinin, M.M., 1960. The Potential Theory of Adsorption of Gases and Vapors for Adsorbents with Energetically Nonuniform Surfaces. *Chemical Reviews*, 60(2), pp.235–241.
- Dunlap, K.L., Dunlap & L., K., 2010. Phosgene. In *Kirk-Othmer Encyclopedia of Chemical Technology*. Hoboken, NJ, USA: John Wiley & Sons, Inc.
- Fang, L.-Y., Liu, S.-B. & Wang, I., 1999. Enhanced para-Selectivity by Selective Coking during Toluene Disproportionation over H-ZSM-5 Zeolite. *Journal of Catalysis*, 185(1), pp.33–42.
- Fei Tan, K., Xu, J., Chang, J., Borgna, A. & Saeys, M., 2010. Carbon deposition on Co catalysts during Fischer–Tropsch synthesis: A computational and experimental study. *Journal of Catalysis*, 274(2), pp.121–129.

References

- Feng, D., Zhang, Y., Zhao, Y., Sun, S. & Gao, J., 2018. Improvement and maintenance of biochar catalytic activity for in-situ biomass tar reforming during pyrolysis and H₂O/CO₂ gasification. *Fuel Processing Technology*, 172, pp.106–114.
- Feng, D., Zhao, Y., Zhang, Y., Sun, S., Meng, S., Guo, Y. & Huang, Y., 2016. Effects of K and Ca on reforming of model tar compounds with pyrolysis biochars under H₂O or CO₂. *Chemical Engineering Journal*, 306, pp.422–432.
- Fialkov, A.B., Steiner, U., Lehotay, S.J. & Amirav, A., 2007. Sensitivity and noise in GC–MS: Achieving low limits of detection for difficult analytes. *International Journal of Mass Spectrometry*, 260(1), pp.31–48.
- Fiedorow, R., Frański, R., Krawczyk, A. & Beszterda, S., 2004. Carbonaceous deposits on alumina as catalysts and supports. *Journal of Physics and Chemistry of Solids*, 65(2–3), pp.627–632.
- Fiedorow, R., Przystajko, W., Sopa, M. & Dalla Lana, I.G., 1981. The nature and catalytic influence of coke formed on alumina: Oxidative dehydrogenation of ethylbenzene. *Journal of Catalysis*, 68(1), pp.33–41.
- Flett, M., Brantjes, J., Gurton, R., McKenna, J., Tankersley, T. & Trupp, M., 2009. Subsurface development of CO₂ disposal for the Gorgon Project. *Energy Procedia*, 1(1), pp.3031–3038.
- Franklin, R., 1951. Crystallite growth in graphitizing and non-graphitizing carbons. *Proceedings of the Royal Society of London. Series A. Mathematical and Physical Sciences*, 209(1097), pp.196–218.
- Frazier, R., Jin, E. & Kumar, A., 2015. Life Cycle Assessment of Biochar versus Metal Catalysts Used in Syngas Cleaning. *Energies*, 8(1), pp.621–644.
- Fu, Y., Zhu, H. & Shen, J., 2005. Thermal decomposition of dimethoxymethane and dimethyl carbonate catalyzed by solid acids and bases. *Thermochimica Acta*, 434(1–2), pp.88–92.
- Gai, C., Guo, Y., Peng, N., Liu, T., Liu, Z., Ai, Y., Hay, A.G., Zhang, M., Wang, S. & Zheng, B., 2016. N-Doped biochar derived from co-hydrothermal carbonization of rice husk and *Chlorella pyrenoidosa* for enhancing copper ion adsorption. *RSC Adv.*, 6(59), pp.53713–53722.
- García-Mota, M., Bridier, B., Pérez-Ramírez, J. & López, N., 2010. Interplay between carbon monoxide, hydrides, and carbides in selective alkyne hydrogenation on palladium. *Journal of Catalysis*, 273(2), pp.92–102.
- Gaunt, J.L. & Lehmann, J., 2008. Energy Balance and Emissions Associated with Biochar Sequestration and Pyrolysis Bioenergy Production. *Environmental Science & Technology*, 42(11), pp.4152–4158.
- Gómez-Jiménez-Aberasturi, O., Ochoa-Gómez, J.R., Pesquera-Rodríguez, A., Ramírez-López, C., Alonso-Vicario, A. & Torrecilla-Soria, J., 2010. Solvent-free synthesis of glycerol carbonate and glycidol from 3-chloro-1,2-propanediol and potassium (hydrogen) carbonate. *Journal of Chemical Technology & Biotechnology*, 85(12), pp.1663–1670.
- Gomez-Sanz, S., McMillan, L., McGregor, J., Zeitler, J.A., Al-Yassir, N., Al-Khattaf, S. & Gladden, L.F., 2015. A new perspective on catalytic dehydrogenation of ethylbenzene: the influence of side-reactions on catalytic performance. *Catal. Sci. Technol.*, 5, pp.3782–3797.
- Gomez-Sanz, S., McMillan, L., McGregor, J., Zeitler, J.A., Al-Yassir, N., Al-Khattaf, S. & Gladden, L.F., 2016. The enhancement of the catalytic performance of CrO_x/Al₂O₃ catalysts for ethylbenzene dehydrogenation through tailored coke deposition. *Catalysis Science and Technology*, 6(4), pp.1120–1133.
- Gonçalves, J.C. & Rodrigues, A.E., 2014. Simulated moving bed reactor for p-xylene production: Adsorbent and catalyst homogeneous mixture. *Chemical Engineering Journal*, 258, pp.194–202.
- Gornay, J., Coniglio, L., Billaud, F. & Wild, G., 2010. Octanoic acid pyrolysis in a stainless-steel tube: What is the role of the coke formed on the wall? *Journal of Analytical and Applied Pyrolysis*, 87(1), pp.78–84.
- Gornay, J., Sécordel, X., Tesquet, G., Ménorval, B. de, Cristol, S., Fongarland, P., Capron, M., Duhamel, L., Payen, E., Dubois, J.-L. & Dumeignil, F., 2010. Direct conversion of methanol into 1,1-dimethoxymethane: remarkably high productivity over an FeMo catalyst placed under unusual conditions. *Green Chemistry*, 12(10), pp.1833–1837.
- Grint, A., Swietlik, U. & Marsh, H., 1979. Carbonization and liquid-crystal (mesophase) development.

9. The co-carbonization of vitrains with Ashland A200 petroleum pitch. *Fuel*, 58(9), pp.642–650.
- Grob, R.L. & Barry, E.F., 2004. *Modern practice of gas chromatography* 4th ed. R. L. Grob & E. F. Barry, eds., Hoboken, NJ: Wiley Interscience.
- Grünert, W., 2012. Auger Electron, X ray and UV Photoelectron Spectroscopies. In M. Che & J. C. Vedrine, eds. *Characterization of Solid Materials and Heterogeneous Catalysts*. Wiley-VCH Verlag GmbH, Germany, pp. 537–584.
- Guisnet, M., 2002. “Coke” molecules trapped in the micropores of zeolites as active species in hydrocarbon transformations. *Journal of Molecular Catalysis A: Chemical*, 182–183, pp.367–382.
- Guisnet, M., Andy, P., Gnep, N.S., Travers, C. & Benazzi, E., 1995. Origin of the positive effect of coke deposits on the skeletal isomerization of n-butenes over a H-FER zeolite. *Journal of the Chemical Society, Chemical Communications*, (16), p.1685.
- Guo, J., Lou, H., Mo, L. & Zheng, X., 2010. The reactivity of surface active carbonaceous species with CO₂ and its role on hydrocarbon conversion reactions. *Journal of Molecular Catalysis A: Chemical*, 316(1–2), pp.1–7.
- Hagaman, E.W., Murray, D.K. & Del Cul, G.D., 1998. Solid State ¹³C and ¹⁹F NMR Characterization of Fluorinated Charcoal. *Energy & Fuels*, 12(2), pp.399–408.
- Haghseresht, F., Lu, G.Q. & Whittaker, A.K., 1999. Carbon structure and porosity of carbonaceous adsorbents in relation to their adsorption properties. *Carbon*, 37(9), pp.1491–1497.
- Ham, D.J. & Lee, J.S., 2009. Transition Metal Carbides and Nitrides as Electrode Materials for Low Temperature Fuel Cells. *Energies*, 2(4), pp.873–899.
- Hamilton, N.G., Warringham, R., Silverwood, I.P., Kapitán, J., Hecht, L., Webb, P.B., Tooze, R.P., Zhou, W., Frost, C.D., Parker, S.F. & Lennon, D., 2014. The application of inelastic neutron scattering to investigate CO hydrogenation over an iron Fischer–Tropsch synthesis catalyst. *Journal of Catalysis*, 312, pp.221–231.
- Han, Y., Boateng, A.A., Qi, P.X., Lima, I.M. & Chang, J., 2013. Heavy metal and phenol adsorptive properties of biochars from pyrolyzed switchgrass and woody biomass in correlation with surface properties. *Journal of Environmental Management*, 118, pp.196–204.
- Harkins, W.D. & Jura, G., 1944. The Decrease (π) of Free Surface Energy (γ) as a Basis for the Development of Equations for Adsorption Isotherms; and the Existence of Two Condensed Phases in Films on Solids. *The Journal of Chemical Physics*, 12(3), pp.112–113.
- Hassan, S. & Imran, Z., 2018. Adsorption of ionic liquids onto an activated carbon: kinetic modeling studies. *Environmental Science and Pollution Research*, 25(32), pp.32112–32121.
- Haydar, S., Moreno-Castilla, C., Ferro-García, M.A., Carrasco-Marín, F., Rivera-Utrilla, J., Perrard, A. & Joly, J.P., 2000. Regularities in the temperature-programmed desorption spectra of CO₂ and CO from activated carbons. *Carbon*, 38(9), pp.1297–1308.
- Henckens, M.L.C.M., Driessen, P.P.J. & Worrell, E., 2014. Metal scarcity and sustainability, analyzing the necessity to reduce the extraction of scarce metals. *Resources, Conservation and Recycling*, 93, pp.1–8.
- Hernandez-Mena, L.E., Pecora, A. a B. & Beraldo, A.L., 2014. Slow pyrolysis of bamboo biomass: Analysis of biochar properties. *Chemical Engineering Transactions*, 37, pp.115–120.
- Hoffman, W.A., 1982. A convenient preparation of carbonates from alcohols and carbon dioxide. *The Journal of Organic Chemistry*, 47(26), pp.5209–5210.
- Hong, J., Park, M.K., Lee, E.J., Lee, D., Hwang, D.S. & Ryu, S., 2013. Origin of new broad Raman D and G peaks in annealed graphene. *Scientific reports*, 3, p.2700.
- Houžvička, J. & Ponec, V., 1997. Skeletal Isomerization of Butene: On the Role of the Bimolecular Mechanism. *Industrial & Engineering Chemistry Research*, 36(5), pp.1424–1430.
- Hu, J.Z., Solum, M.S., Taylor, C.M. V., Pugmire, R.J. & Grant, D.M., 2001. Structural Determination in Carbonaceous Solids Using Advanced Solid State NMR Techniques. *Energy & Fuels*, 15(1), pp.14–22.
- Huo, C.-F., Wu, B.-S., Gao, P., Yang, Y., Li, Y.-W. & Jiao, H., 2011. The Mechanism of Potassium Promoter: Enhancing the Stability of Active Surfaces. *Angewandte Chemie International Edition*,

References

- 50(32), pp.7403–7406.
- Indran, V.P., Haji Saud, A.S., Maniam, G.P., Yusoff, M.M., Taufiq-Yap, Y.H., Ab. Rahim, M.H., Rahim, M.H.A. & Alloin, F., 2016. Versatile boiler ash containing potassium silicate for the synthesis of organic carbonates. *RSC Adv.*, 6(41), pp.34877–34884.
- Indran, V.P., Syuhada Zuhaimi, N.A., Deraman, M.A., Maniam, G.P., Yusoff, M.M., Yun Hin, T.-Y. & Ab. Rahim, M.H., 2014. An accelerated route of glycerol carbonate formation from glycerol using waste boiler ash as catalyst. *RSC Adv.*, 4(48), pp.25257–25267.
- IUPAC, 1997. *IUPAC Gold Book* 2nd edition. A. D. McNaught & A. Wilkinson, eds., Oxford: Blackwell Scientific Publications.
- Jagiello, J. & Olivier, J.P., 2009. A Simple Two-Dimensional NLDFT Model of Gas Adsorption in Finite Carbon Pores. Application to Pore Structure Analysis. *The Journal of Physical Chemistry C*, 113(45), pp.19382–19385.
- Jansen, R.J.J. & van Bekkum, H., 1994. Amination and ammoxidation of activated carbons. *Carbon*, 32(8), pp.1507–1516.
- Jansen, R.J.J. & van Bekkum, H., 1995. XPS of nitrogen-containing functional groups on activated carbon. *Carbon*, 33(8), pp.1021–1027.
- Jenkins, B.M., Bakker, R.R. & Wei, J.B., 1996. On the properties of washed straw. *Biomass and Bioenergy*, 10(4), pp.177–200.
- Jensen, A., Dam-Johansen, K., Wójtowicz, M.A. & Serio, M.A., 1998. TG-FTIR Study of the Influence of Potassium Chloride on Wheat Straw Pyrolysis. *Energy & Fuels*, 12, pp.929–938.
- Jiang, Y., Huang, J., Reddy Marthala, V.R., Ooi, Y.S., Weitkamp, J. & Hunger, M., 2007. In situ MAS NMR–UV/Vis investigation of H-SAPO-34 catalysts partially coked in the methanol-to-olefin conversion under continuous-flow conditions and of their regeneration. *Microporous and Mesoporous Materials*, 105(1–2), pp.132–139.
- Jindo, K., Mizumoto, H., Sawada, Y., Sanchez-Monedero, M.A. & Sonoki, T., 2014. Physical and chemical characterization of biochars derived from different agricultural residues. *Biogeosciences*, 11(23), pp.6613–6621.
- Johnstone, R.A.W. & Rose, M., 1996. *Mass spectrometry for chemists and biochemists*, Cambridge University Press.
- Jouhara, H., Czajczyńska, D., Ghazal, H., Krzyżyńska, R., Anguilano, L., Reynolds, A.J. & Spencer, N., 2017. Municipal waste management systems for domestic use. *Energy*, 139, pp.485–506.
- Jüntgen, H., Richter, E., Knoblauch, K. & Hoang-Phu, T., 1988. Catalytic NO_x reduction by ammonia on carbon catalysts. *Chemical Engineering Science*, 43(3), pp.419–428.
- Kaeding, W., Chu, C., Young, L.B., Weinstein, B. & Butter, S.A., 1981. Selective alkylation of toluene with methanol to produce para-Xylene. *Journal of Catalysis*, 67(1), pp.159–174.
- Kaichev, V.V., Gladky, A.Y., Prosvirin, I.P., Saraev, A.A., Hävecker, M., Knop-Gericke, A., Schlögl, R. & Bukhtiyarov, V.I., 2013. In situ XPS study of self-sustained oscillations in catalytic oxidation of propane over nickel. *Surface Science*, 609, pp.113–118.
- Karaca, H., Safonova, O. V., Chambrey, S., Fongarland, P., Roussel, P., Griboval-Constant, A., Lacroix, M. & Khodakov, A.Y., 2011. Structure and catalytic performance of Pt-promoted alumina-supported cobalt catalysts under realistic conditions of Fischer–Tropsch synthesis. *Journal of Catalysis*, 277(1), pp.14–26.
- Kastner, J.R., Mani, S. & Juneja, A., 2015. Catalytic decomposition of tar using iron supported biochar. *Fuel Processing Technology*, 130, pp.31–37.
- Kastner, J.R., Miller, J., Geller, D.P., Locklin, J., Keith, L.H. & Johnson, T., 2012. Catalytic esterification of fatty acids using solid acid catalysts generated from biochar and activated carbon. *Catalysis Today*, 190(1), pp.122–132.
- Keller, N., Rebmann, G. & Keller, V., 2010. Catalysts, mechanisms and industrial processes for the dimethylcarbonate synthesis. *Journal of Molecular Catalysis A: Chemical*, 317(1–2), pp.1–18.
- Keyvanloo, K., Fisher, M.J., Hecker, W.C., Lancee, R.J., Jacobs, G. & Bartholomew, C.H., 2015. Kinetics of deactivation by carbon of a cobalt Fischer–Tropsch catalyst: Effects of CO and H₂ partial

- pressures. *Journal of Catalysis*, 327, pp.33–47.
- Kim, J.J. & Weller, S.W., 1987. Oxidative dehydrogenation of ethylbenzene over lanthanide oxide-promoted catalysts. *Applied Catalysis*, 33(1), pp.15–29.
- Kiricsi, I., Pálincó, I. & Kollár, T., 2003. An UV–Vis spectroscopic study on carbenium ions formed on HY–FAU zeolite upon the adsorption of various hydrocarbons. *Journal of Molecular Structure*, 651–653, pp.331–334.
- Kitchin, J.R., Nørskov, J.K., Barteau, M.A. & Chen, J.G., 2005. Trends in the chemical properties of early transition metal carbide surfaces: A density functional study. *Catalysis Today*, 105(1), pp.66–73.
- Klinghoffer, N.B., Castaldi, M.J. & Nzihou, A., 2015. Influence of char composition and inorganics on catalytic activity of char from biomass gasification. *Fuel*, 157, pp.37–47.
- Knoblauch, K., Richter, E. & Jüntgen, H., 1981. Application of active coke in processes of SO₂- and NO_x-removal from flue gases. *Fuel*, 60(9), pp.832–838.
- Knop-Gericke, A. *et al.*, 2009. Chapter 4 X-Ray Photoelectron Spectroscopy for Investigation of Heterogeneous Catalytic Processes. *Advances in Catalysis*, 52, pp.213–272.
- Koch, A., 1998. A study of carbonaceous char oxidation in air by semi-quantitative FTIR spectroscopy. *Fuel*, 77(6), pp.563–569.
- Kong, P.S., Aroua, M.K., Daud, W.M.A.W., Lee, H.V., Cognet, P. & Pérès, Y., 2016. Catalytic role of solid acid catalysts in glycerol acetylation for the production of bio-additives: a review. *RSC Advances*, 6(73), pp.68885–68905.
- Kong, X.-K., Chen, C.-L. & Chen, Q.-W., 2014. Doped graphene for metal-free catalysis. *Chemical Society reviews*, 43(8), pp.2841–57.
- Konwar, L.J., Mäki-Arvela, P., Begum, P., Kumar, N., Thakur, A.J., Mikkola, J.-P., Deka, R.C. & Deka, D., 2015. Shape selectivity and acidity effects in glycerol acetylation with acetic anhydride: Selective synthesis of triacetin over Y-zeolite and sulfonated mesoporous carbons. *Journal of Catalysis*, 329, pp.237–247.
- Kumar, B., Asadi, M., Pisasale, D., Sinha-Ray, S., Rosen, B.A., Haasch, R., Abiade, J., Yarin, A.L. & Salehi-Khojin, A., 2013. Renewable and metal-free carbon nanofibre catalysts for carbon dioxide reduction. *Nature Communications*, 4(1), p.2819.
- Lam, E. & Luong, J.H.T., 2014. Carbon Materials as Catalyst Supports and Catalysts in the Transformation of Biomass to Fuels and Chemicals. *ACS Catalysis*, 4(10), pp.3393–3410.
- Lancaster, M., 2010. *Green chemistry : an introductory text* 2nd ed., Royal Society of Chemistry.
- Larsen, J.W., Freund, M., Kim, K.Y., Sidovar, M. & Stuart, J.L., 2000. Mechanism of the carbon catalyzed reduction of nitrobenzene by hydrazine. *Carbon*, 38(5), pp.655–661.
- Ledoux, M.J., Pham-Huu, C. & Chianelli, R.R., 1996. Catalysis with carbides. *Current Opinion in Solid State and Materials Science*, 1(1), pp.96–100.
- Lee, C.K., Gladden, L.F. & Barrie, P.J., 2004. TEOM studies on the adsorption of p-xylene in coked FCC catalysts: observation of coke promoting chemical reaction. *Applied Catalysis A: General*, 274(1–2), pp.269–274.
- Lee, J., Kim, K.H. & Kwon, E.E., 2017. Biochar as a Catalyst. *Renewable and Sustainable Energy Reviews*, 77, pp.70–79.
- Lee, K.-Y., Kang, M.-Y. & Ihm, S.-K., 2012. Deactivation by coke deposition on the HZSM-5 catalysts in the methanol-to-hydrocarbon conversion. *Journal of Physics and Chemistry of Solids*, 73(12), pp.1542–1545.
- Lehmann, J., 2007. Bio-Energy in the Black. *Frontiers in Ecology and the Environment*, 5(7), pp.381–387.
- Lehmann, J. & Joseph, S., 2009. *Biochar for Environmental Management* J. Lehmann & S. Joseph, eds., London: Earthscan.
- Leng, L., Yuan, X., Zeng, G., Shao, J., Chen, X., Wu, Z., Wang, H. & Peng, X., 2015. Surface characterization of rice husk bio-char produced by liquefaction and application for cationic dye (Malachite green) adsorption. *Fuel*, 155, pp.77–85.
- Li, B. & Gonzalez, R.D., 1998. The effect of coke deposition on the deactivation of sulfated zirconia catalysts. *Applied Catalysis A: General*, 174(1–2), pp.109–119.

References

- Li, B. & Xu, Z., 2009. A Nonmetal Catalyst for Molecular Hydrogen Activation with Comparable Catalytic Hydrogenation Capability to Noble Metal Catalyst. *Journal of the American Chemical Society*, 131(45), pp.16380–16382.
- Li, H., Gao, D., Gao, P., Wang, F., Zhao, N., Xiao, F., Wei, W. & Sun, Y., 2013. The synthesis of glycerol carbonate from glycerol and CO₂ over La₂O₂CO₃–ZnO catalysts. *Catalysis Science & Technology*, 3(10), p.2801.
- Li, H., Jiao, X., Li, L., Zhao, N., Xiao, F., Wei, W., Sun, Y. & Zhang, B., 2015. Synthesis of glycerol carbonate by direct carbonylation of glycerol with CO₂ over solid catalysts derived from Zn/Al/La and Zn/Al/La/M (M = Li, Mg and Zr) hydrotalcites. *Catal. Sci. Technol.*, 5(2), pp.989–1005.
- Li, J. & Wang, T., 2011. Chemical equilibrium of glycerol carbonate synthesis from glycerol. *The Journal of Chemical Thermodynamics*, 43(5), pp.731–736.
- Li, X., Hayashi, J. & Li, C., 2006. Volatilisation and catalytic effects of alkali and alkaline earth metallic species during the pyrolysis and gasification of Victorian brown coal. Part VII. Raman spectroscopic study on the changes in char structure during the catalytic gasification in air. *Fuel*, 85(10–11), pp.1509–1517.
- Liou, Y.J. & Huang, W.J., 2013. Quantitative Analysis of Graphene Sheet Content in Wood Char Powders during Catalytic Pyrolysis. *Journal of Materials Science and Technology*, 29(5), pp.406–410.
- Lisovskii, A.E. & Aharoni, C., 1994. Carbonaceous Deposits as Catalysts for Oxydehydrogenation of Alkylbenzenes. *Catalysis Reviews*, 36(1), pp.25–74.
- Lithoxoos, G.P., Labropoulos, A., Peristeras, L.D., Kanellopoulos, N., Samios, J. & Economou, I.G., 2010. Adsorption of N₂, CH₄, CO and CO₂ gases in single walled carbon nanotubes: A combined experimental and Monte Carlo molecular simulation study. *The Journal of Supercritical Fluids*, 55(2), pp.510–523.
- Liu, Q. & Smith, K.J., 1995. Methane-Propylene homologation and reactivity of surface carbon on modified Ni-Al₂O₃ catalysts. *The Canadian Journal of Chemical Engineering*, 73(3), pp.337–344.
- Liu, W.-J., Zeng, F.-X., Jiang, H. & Zhang, X.-S., 2011. Preparation of high adsorption capacity bio-chars from waste biomass. *Bioresource Technology*, 102(17), pp.8247–8252.
- Liu, X. & Dai, L., 2016. Carbon-based metal-free catalysts. *Nature Reviews Materials*, 1, p.1.
- de Lucas, A., Canizares, P., Durán, A. & Carrero, A., 1997. Coke formation, location, nature and regeneration on dealuminated HZSM-5 type zeolites. *Applied Catalysis A: General*, 156(2), pp.299–317.
- Ma, J., Sun, N., Zhang, X., Zhao, N., Xiao, F., Wei, W. & Sun, Y., 2009. A short review of catalysis for CO₂ conversion. *Catalysis Today*, 148(3–4), pp.221–231.
- Ma, X., Zhou, B., Budai, A., Jeng, A., Hao, X., Wei, D., Zhang, Y. & Rasse, D., 2016. Study of Biochar Properties by Scanning Electron Microscope – Energy Dispersive X-Ray Spectroscopy (SEM-EDX). *Communications in Soil Science and Plant Analysis*, 47(5), pp.593–601.
- Magnoux, P., Guisnet, M. & Ferino, I., 2000. 12th International Congress on Catalysis, Proceedings of the 12th ICC. *Studies in Surface Science and Catalysis*, 130, pp.275–280.
- Mahmoud, E. & Lobo, R.F., 2014. Recent advances in zeolite science based on advance characterization techniques. *Microporous and Mesoporous Materials*, 189, pp.97–106.
- Makowski, P., Demir Cakan, R., Antonietti, M., Goettmann, F. & Titirici, M.-M., 2008. Selective partial hydrogenation of hydroxy aromatic derivatives with palladium nanoparticles supported on hydrophilic carbon. *Chemical Communications*, 0(8), p.999.
- Maldonado-Hódar, F.J., Madeira, L.M. & Portela, M.F., 1999. The use of coals as catalysts for the oxidative dehydrogenation of n-butane. *Applied Catalysis A: General*, 178(1), pp.49–60.
- Mani, S., Kastner, J.R. & Juneja, A., 2013. Catalytic decomposition of toluene using a biomass derived catalyst. *Fuel Processing Technology*, 114, pp.118–125.
- Mann, R., 1997. Catalyst deactivation by coke deposition: Approaches based on interactions of coke laydown with pore structure. *Catalysis Today*, 37(3), pp.331–349.
- Mann, R., Sharratt, P.N. & Thomson, G., 1986. Deactivation of a supported zeolitic catalyst: diffusion, reaction and coke deposition in stochastic pore networks. *Chemical Engineering Science*, 41, pp.711–

- Mann, R. & Thomson, G., 1987. Deactivation of a supported zeolite catalyst: simulation of diffusion, reaction and coke deposition in a parallel bundle. *Chemical Engineering Science*, 42(3), pp.555–563.
- Manyà, J.J., 2012. Pyrolysis for Biochar Purposes: A Review to Establish Current Knowledge Gaps and Research Needs. *Environmental Science & Technology*, 46(15), pp.7939–7954.
- Marchon, B., Carrazza, J., Heinemann, H. & Somorjai, G.A., 1988. TPD and XPS studies of O₂, CO₂, and H₂O adsorption on clean polycrystalline graphite. *Carbon*, 26(4), pp.507–514.
- McFarlane, A.R., Silverwood, I.P., Norris, E.L., Ormerod, R.M., Frost, C.D., Parker, S.F. & Lennon, D., 2013. The application of inelastic neutron scattering to investigate the steam reforming of methane over an alumina-supported nickel catalyst. *Chemical Physics*, 427, pp.54–60.
- McGregor, J., Canning, A.S., Mitchell, S., Jackson, S.D. & Gladden, L.F., 2010. The influence of carbon laydown on selectivity in the hydrogenation of pentenenitriles over supported-nickel catalysts. *Applied Catalysis A: General*, 384(1–2), pp.192–200.
- McGregor, J. & Gladden, L.F., 2008. The role of carbon deposits in the hydrogenation of C₅ hydrocarbons. *Applied Catalysis A: General*, 345(1), pp.51–57.
- McGregor, J., Huang, Z., Parrott, E.P.J., Zeitler, J.A., Nguyen, K.L., Rawson, J.M., Carley, A., Hansen, T.W., Tessonnier, J.-P. & Su, D.S., 2010. Active coke: Carbonaceous materials as catalysts for alkane dehydrogenation. *Journal of Catalysis*, 269(2), pp.329–339.
- McMaster, M.C., 2008. *GC/MS: a practical user's guide*, Wiley-Interscience.
- Menéndez, J.A., Juárez-Pérez, E.J., Ruisánchez, E., Calvo, E.G. & Arenillas, A., 2012. A microwave-based method for the synthesis of carbon xerogel spheres. *Carbon*, 50(10), pp.3555–3560.
- Menon, P.G., 1990. Coke on catalysts-harmful, harmless, invisible and beneficial types. *Journal of Molecular Catalysis*, 59, pp.207–220.
- Meriaudeau, P., Naccache, C., Le, H.N., Vu, T.A. & Szabo, G., 1997. Selective skeletal isomerisation of n-butenes over ferrierite catalyst: Further studies on the possible mechanisms. *Journal of Molecular Catalysis A: Chemical*, 123(1), pp.L1–L4.
- Mestl, G., Maksimova, N.I., Keller, N., Roddatis, V. V. & Schlögl, R., 2001. Kohlenstoffnanofilamente in der heterogenen Katalyse: eine technische Anwendung für neue Kohlenstoffmaterialien? *Angewandte Chemie*, 113(11), pp.2122–2125.
- Mikkelsen, M. *et al.*, 2010. The teraton challenge. A review of fixation and transformation of carbon dioxide. *Energy Environ. Sci.*, 3(1), pp.43–81.
- Mobil Research and Development, C., 1990. Mobil's toluene to PX process proves itself. *European Chemical News*, 54(1418).
- Moodley, D.J., van Schalkwyk, C., Spamer, A., Botha, J.M. & Datye, A.K., 2007. Coke formation on WO₃/SiO₂ metathesis catalysts. *Applied Catalysis A: General*, 318, pp.155–159.
- Moreland, A., Patrick, J.W. & Walker, A., 1988. Optical anisotropy in cokes from high-rank coals. *Fuel*, 67(5), pp.730–732.
- Moreno-Castilla, C., Carrasco-Marín, F., Maldonado-Hódar, F.J. & Rivera-Utrilla, J., 1997. Effects of non-oxidant and oxidant acid treatments on the surface properties of an activated carbon with very low ash content. *Carbon*, 36(1–2), pp.145–151.
- Moreno-Castilla, C., Carrasco-Marín, F. & Mueden, A., 1997. The creation of acid carbon surfaces by treatment with (NH₄)₂S₂O₈. *Carbon*, 35(10–11), pp.1619–1626.
- Morgan, M.E., Jenkins, R.G. & Walker Jr., P.L., 1981. Inorganic constituents in American lignites. *Fuel*, 60(3), pp.189–193.
- Morterra, C. & Low, M.J.D., 1983. IR studies of carbons—II: The vacuum pyrolysis of cellulose. *Carbon*, 21(3), pp.283–288.
- Moussavi, G. & Khosravi, R., 2012. Preparation and characterization of a biochar from pistachio hull biomass and its catalytic potential for ozonation of water recalcitrant contaminants. *Bioresource Technology*, 119, pp.66–71.
- Muckenhuber, H. & Grothe, H., 2006. The heterogeneous reaction between soot and NO₂ at elevated temperature. *Carbon*, 44(3), pp.546–559.

References

- Nakayama, Y., Soeda, F. & Ishitani, A., 1990. XPS study of the carbon fiber matrix interface. *Carbon*, 28(1), pp.21–26.
- National Physical Laboratory, 2012. Calibration software and reference materials for electron spectrometers. *National Physical Laboratory*.
- Nederlof, C., Kapteijn, F. & Makkee, M., 2012. Catalysed ethylbenzene dehydrogenation in CO₂ or N₂—Carbon deposits as the active phase. *Applied Catalysis A: General*, 417–418, pp.163–173.
- Neeli, S.T. & Ramsurn, H., 2018. Synthesis and formation mechanism of iron nanoparticles in graphitized carbon matrix using biochar from biomass model compounds as a support. *Carbon*, 134, pp.480–490.
- Nosyrev, I.E., Gruber, R., Cagniant, D., Krzton, A., Pajak, J., Stefanova, M.D. & Grishchuk, S., 1996. DRIFT spectroscopic characterization of coal samples modified by chemical treatments. *Fuel*, 75(13), pp.1549–1556.
- Nowakowski, D.J. & Jones, J.M., 2008. Uncatalysed and potassium-catalysed pyrolysis of the cell-wall constituents of biomass and their model compounds. *Journal of Analytical and Applied Pyrolysis*, 83(1), pp.12–25.
- Ofori-Boateng, C. & Lee, K.T., 2013. The potential of using cocoa pod husks as green solid base catalysts for the transesterification of soybean oil into biodiesel: Effects of biodiesel on engine performance. *Chemical Engineering Journal*, 220, pp.395–401.
- Olah, G.A., 2004. After oil and gas: methanol economy. *Catalysis Letters*, 93(1–2), pp.1–2.
- Ondarts, M., Reinert, L., Guittonneau, S., Baup, S., Delpeux, S., Leveque, J.-M. & Duclaux, L., 2018. Improving the adsorption kinetics of ibuprofen on an activated carbon fabric through ultrasound irradiation: Simulation and experimental studies. *Chemical Engineering Journal*, 343, pp.163–172.
- Ono, Y., Akiyama, M. & Suzuki, E., 1993. Direct synthesis of tetraalkoxysilanes from silica by reaction with dialkyl carbonates. *Chemistry of Materials*, 5(4), pp.442–447.
- Ormsby, R., Kastner, J.R. & Miller, J., 2012. Hemicellulose hydrolysis using solid acid catalysts generated from biochar. *Catalysis Today*, 190(1), pp.89–97.
- Ozorio, L.P., Pianzolli, R., da Cruz Machado, L., Miranda, J.L., Turci, C.C., Guerra, A.C.O., Souza-Aguiar, E.F. & Mota, C.J.A., 2015. Metal-impregnated zeolite Y as efficient catalyst for the direct carbonation of glycerol with CO₂. *Applied Catalysis A: General*, 504, pp.187–191.
- Paál, Z., Wootsch, A., Bakos, I., Szabó, S., Sauer, H., Wild, U. & Schlögl, R., 2006. Effect of hydrogen pressure on intentional deactivation of unsupported Pt catalyst: Catalytic properties and physical characterization. *Applied Catalysis A: General*, 309(1), pp.1–9.
- Pacheco, M.E., Martins Salim, V.M. & Pinto, J.C., 2011. Accelerated Deactivation of Hydrotreating Catalysts by Coke Deposition. *Industrial & Engineering Chemistry Research*, 50(10), pp.5975–5981.
- Pagliaro, M., Ciriminna, R., Kimura, H., Rossi, M. & Della Pina, C., 2007. From Glycerol to Value-Added Products. *ChemInform*, 38(37).
- Park, S.-J., Seo, M.-K. & Lee, Y.-S., 2003. Surface characteristics of fluorine-modified PAN-based carbon fibers. *Carbon*, 41(4), pp.723–730.
- Patrick, J.W., Reynolds, M.J. & Shaw, F.H., 1973. Development of optical anisotropy in vitrains during carbonization. *Fuel*, 52(3), pp.198–204.
- Perander, M., DeMartini, N., Brink, A., Kramb, J., Karlström, O., Hemming, J., Moilanen, A., Konttinen, J. & Hupa, M., 2015. Catalytic effect of Ca and K on CO₂ gasification of spruce wood char. *Fuel*, 150, pp.464–472.
- Pradhan, A.R., Lin, T.-S., Chen, W.-H., Jong, S.-J., Wu, J.-F., Chao, K.-J. & Liu, S.-B., 1999. EPR and NMR Studies of Coke Induced Selectivation over H-ZSM-5 Zeolite during Ethylbenzene Disproportionation Reaction. *Journal of Catalysis*, 184(1), pp.29–38.
- Pradhan, B.K. & Sandle, N.K., 1999. Effect of different oxidizing agent treatments on the surface properties of activated carbons. *Carbon*, 37(8), pp.1323–1332.
- Prati, L., Bergna, D., Villa, A., Spontoni, P., Bianchi, C.L., Hu, T., Romar, H. & Lassi, U., 2018. Carbons from second generation biomass as sustainable supports for catalytic systems. *Catalysis Today*, 301, pp.239–243.

- Pratt, S.J. & King, D.A., 2003. Coverage dependent promoter action: K coadsorption and reactions with CO and CO₂ on Pd{1 1 0}. *Surface Science*, 540(2–3), pp.185–206.
- Przystajko, W., Fiedorow, R. & Lana, I.G.D., 1990. Ammoxidation of Toluene on Coke-Covered Alumina. *Applied Catalysis*, 59(1), pp.129–140.
- Qi, W. & Su, D., 2014. Metal-Free Carbon Catalysts for Oxidative Dehydrogenation Reactions. *ACS Catalysis*, 4(9), pp.3212–3218.
- Qian, K., Kumar, A., Patil, K., Bellmer, D., Wang, D., Yuan, W. & Huhnke, R., 2013. Effects of Biomass Feedstocks and Gasification Conditions on the Physiochemical Properties of Char. *Energies*, 6(8), pp.3972–3986.
- Qian, K., Kumar, A., Zhang, H., Bellmer, D. & Huhnke, R., 2015. Recent advances in utilization of biochar. *Renewable and Sustainable Energy Reviews*, 42, pp.1055–1064.
- Querini, C.A. & Fung, S.C., 1997. Coke characterization by temperature programmed techniques. *Catalysis Today*, 37(3), pp.277–283.
- Rafi, J.M., Rajashekar, A., Srinivas, M., Rao, B.V.S.K., Prasad, R.B.N. & Lingaiah, N., 2015. Esterification of glycerol over a solid acid biochar catalyst derived from waste biomass. *RSC Adv.*, 5(55), pp.44550–44556.
- Ranzi, E., Cuoci, a, Faravelli, T., Frassoldati, a, Migliavacca, G., Pierucci, S. & Sommariva, S., 2008. Chemical kinetics of biomass pyrolysis. *Energy and Fuels*, 22(6), pp.4292–4300.
- Raveendran, K., Ganesh, A. & Khilar, K.C., 1995. Influence of mineral matter on biomass pyrolysis characteristics. *Fuel*, 74(12), pp.1812–1822.
- Raymundo-Piñero, E., Cazorla-Amorós, D. & Linares-Solano, A., 2001. Temperature programmed desorption study on the mechanism of SO₂ oxidation by activated carbon and activated carbon fibres. *Carbon*, 39(2), pp.231–242.
- Razali, N., 2017. *The Synthesis of Glycerol Carbonate from Glycerol and Carbon Dioxide over Heterogeneous Catalysts*. University of Sheffield.
- Razali, N.A.M., Lee, K.T., Bhatia, S. & Mohamed, A.R., 2012. Heterogeneous catalysts for production of chemicals using carbon dioxide as raw material: A review. *Renewable and Sustainable Energy Reviews*, 16(7), pp.4951–4964.
- Reimer, L., 1998. *Scanning Electron Microscopy* 2nd ed., Berlin, Heidelberg: Springer Berlin Heidelberg.
- Riadi, L., Purwanto, E., Kurniawan, H. & Oktaviana, R., 2014. Effect of Bio-based Catalyst in Biodiesel Synthesis. *Procedia Chemistry*, 9, pp.172–181.
- Richter, E., Knoblauch, K. & Jüntgen, H., 1987. Mechanisms and kinetics of SO₂ adsorption and NO_x reduction on active coke. *Gas Separation & Purification*, 1(1), pp.35–43.
- Ritter, S.K., 2017. Five green chemistry success stories. *Chemical and Engineering News*, 95(26), pp.16–20.
- Rivera-Utrilla, J. & Sánchez-Polo, M., 2002. Ozonation of 1,3,6-naphthalenetrisulphonic acid catalysed by activated carbon in aqueous phase. *Applied Catalysis B: Environmental*, 39(4), pp.319–329.
- Roberts, K.G., Gloy, B.A., Joseph, S., Scott, N.R. & Lehmann, J., 2010. Life Cycle Assessment of Biochar Systems: Estimating the Energetic, Economic, and Climate Change Potential. *Environmental Science & Technology*, 44(2), pp.827–833.
- Rokicki, G., Rakoczy, P., Parzuchowski, P. & Sobiecki, M., 2005. Hyperbranched aliphatic polyethers obtained from environmentally benign monomer: glycerol carbonate. *Green Chemistry*, 7, pp.529–539.
- Rostrup-Nielsen, J.R., 1974. Coking on nickel catalysts for steam reforming of hydrocarbons. *Journal of Catalysis*, 33(2), pp.184–201.
- Ruckenstein, E. & Wang, H.Y., 2002. Carbon Deposition and Catalytic Deactivation during CO₂ Reforming of CH₄ over Co/γ-Al₂O₃ Catalysts. *Journal of Catalysis*, 205(2), pp.289–293.
- Saddawi, A., Jones, J.M. & Williams, A., 2012. Influence of alkali metals on the kinetics of the thermal decomposition of biomass. *Fuel Processing Technology*, 104, pp.189–197.
- Sakakura, T., Choi, J.-C. & Yasuda, H., 2007. Transformation of Carbon Dioxide. *Chemical Reviews*, 107, pp.2365–2387.
- Sakakura, T. & Kohno, K., 2009. The synthesis of organic carbonates from carbon dioxide. *Chemical*

References

- Communications*, 0(11), p.1312.
- Sánchez, B., Gross, M.S., Costa, B.D. & Querini, C.A., 2009. Coke analysis by temperature-programmed oxidation: Morphology characterization. *Applied Catalysis A: General*, 364(1–2), pp.35–41.
- Sander, M.-L. & Andrén, O., 1997. Ash from Cereal and Rape Straw Used for Heat Production: Liming Effect and Contents of Plant Nutrients and Heavy Metals. *Water, Air, and Soil Pollution*, 93(1/4), pp.93–108.
- Sandesh, S., Manjunathan, P., Halgeri, A.B. & Shanbhag, G. V., 2015. Glycerol acetins: fuel additive synthesis by acetylation and esterification of glycerol using cesium phosphotungstate catalyst. *RSC Adv.*, 5(126), pp.104354–104362.
- Santiago, M., Stüber, F., Fortuny, A., Fabregat, A. & Font, J., 2005. Modified activated carbons for catalytic wet air oxidation of phenol. *Carbon*, 43(10), pp.2134–2145.
- Scherzer, T., 2002. Depth profiling of the conversion during the photopolymerization of acrylates using real-time FTIR-ATR spectroscopy. *Vibrational Spectroscopy*, 29(1–2), pp.139–145.
- Schneider, W., Diller, W., Schneider, W. & Diller, W., 2000. Phosgene. In *Ullmann's Encyclopedia of Industrial Chemistry*. Weinheim, Germany: Wiley-VCH Verlag GmbH & Co. KGaA.
- Scofield, J.H., 1976. Hartree-Slater subshell photoionization cross-sections at 1254 and 1487 eV. *Journal of Electron Spectroscopy and Related Phenomena*, 8(2), pp.129–137.
- Seaton, N.A., Walton, J.P.R.B. & Quirk, N., 1989. A new analysis method for the determination of the pore size distribution of porous carbons from nitrogen adsorption measurements. *Carbon*, 27(6), pp.853–861.
- Seong, H.J. & Boehman, A.L., 2013. Evaluation of Raman Parameters Using Visible Raman Microscopy for Soot Oxidative Reactivity. *Energy & Fuels*, 27(3), pp.1613–1624.
- Serp, P. & Figueiredo, J.L., 2009. *Carbon Materials for Catalysis* 1st ed. P. Serp & J. L. Figueiredo, eds., Hoboken, New Jersey: John Wiley and Sons Inc.
- Shamsijazeyi, H. & Kaghazchi, T., 2010. Investigation of nitric acid treatment of activated carbon for enhanced aqueous mercury removal. *Journal of Industrial and Engineering Chemistry*, 16(5), pp.852–858.
- Shen, B., Chen, J., Yue, S. & Li, G., 2015. A comparative study of modified cotton biochar and activated carbon based catalysts in low temperature SCR. *Fuel*, 156, pp.47–53.
- Shen, Y., 2015. Chars as carbonaceous adsorbents/catalysts for tar elimination during biomass pyrolysis or gasification. *Renewable and Sustainable Energy Reviews*, 43, pp.281–295.
- Shen, Y., Zhao, P., Shao, Q., Ma, D., Takahashi, F. & Yoshikawa, K., 2014. In-situ catalytic conversion of tar using rice husk char-supported nickel-iron catalysts for biomass pyrolysis/gasification. *Applied Catalysis B: Environmental*, 152, pp.140–151.
- Shin, S., Jang, J., Yoon, S.-H. & Mochida, I., 1997. A study on the effect of heat treatment on functional groups of pitch based activated carbon fiber using FTIR. *Carbon*, 35(12), pp.1739–1743.
- Simon, R., 1969. Resolving Power of the Scanning Electron Microscope. *Journal of Applied Physics*, 40(7), p.2851.
- Smith, M., Scudiero, L., Espinal, J., McEwen, J.-S. & Garcia-Perez, M., 2016. Improving the deconvolution and interpretation of XPS spectra from chars by ab initio calculations. *Carbon*, 110, pp.155–171.
- Snape, C.E., Diaz, M.C., Tyagi, Y.R., Martin, S.C. & Hughes, R., 2001. *Catalyst Deactivation 2001, Proceedings of the 9th International Symposium*, Elsevier.
- Sonnati, M.O., Amigoni, S., Taffin de Givenchy, E.P., Darmanin, T., Choulet, O. & Guittard, F., 2013. Glycerol carbonate as a versatile building block for tomorrow: synthesis, reactivity, properties and applications. *Green Chem.*, 15(2), pp.283–306.
- Specac, 2016. *The Specac Quest: How the ATR accessory works*,
- Stevenson, R., 2003. The Changing Face of Catalysis. *Science*.
- Studt, F., Abild-Pedersen, F., Bligaard, T., Sørensen, R.Z., Christensen, C.H. & Nørskov, J.K., 2008. On the role of surface modifications of palladium catalysts in the selective hydrogenation of acetylene. *Angewandte Chemie (International ed. in English)*, 47(48), pp.9299–302.

- Su, D.S., Maksimova, N., Delgado, J.J., Keller, N., Mestl, G., Ledoux, M.J. & Schlögl, R., 2005. Nanocarbons in selective oxidative dehydrogenation reaction. *Catalysis Today*, 102–103, pp.110–114.
- Su, D.S., Perathoner, S. & Centi, G., 2012. Catalysis on nano-carbon materials: Going where to? *Catalysis Today*, 186(1), pp.1–6.
- Suarez-Ojeda, M.E., Stüber, F., Fortuny, A., Fabregat, A., Carrera, J. & Font, J., 2005. Catalytic wet air oxidation of substituted phenols using activated carbon as catalyst. *Applied Catalysis B: Environmental*, 58(1–2), pp.105–114.
- Sun, Q., Liu, J., Cai, J., Fu, Y. & Shen, J., 2009. Effect of silica on the selective oxidation of methanol to dimethoxymethane over vanadia–titania catalysts. *Catalysis Communications*, 11(1), pp.47–50.
- Sun, Y., Gao, B., Yao, Y., Fang, J., Zhang, M., Zhou, Y., Chen, H. & Yang, L., 2014. Effects of feedstock type, production method, and pyrolysis temperature on biochar and hydrochar properties. *Chemical Engineering Journal*, 240, pp.574–578.
- Tag, A.T., Duman, G., Ucar, S. & Yanik, J., 2016. Effects of feedstock type and pyrolysis temperature on potential applications of biochar. *Journal of Analytical and Applied Pyrolysis*, 120, pp.200–206.
- Tamboli, A.H., Chaugule, A.A. & Kim, H., 2017. Catalytic developments in the direct dimethyl carbonate synthesis from carbon dioxide and methanol. *Chemical Engineering Journal*, 323, pp.530–544.
- Tarrant, R.N., McKenzie, D.R. & Bilek, M.M.M., 2004. Raman characterisation of PIII multilayer carbon films. *Diamond and Related Materials*, 13(4–8), pp.1422–1426.
- Tatibouët, J.M., 1997. Methanol oxidation as a catalytic surface probe. *Applied Catalysis A: General*, 148(2), pp.213–252.
- Teng, W.K., Ngoh, G.C., Yusoff, R. & Aroua, M.K., 2014. A review on the performance of glycerol carbonate production via catalytic transesterification: Effects of influencing parameters. *Energy Conversion and Management*, 88, pp.484–497.
- Teschner, D., Borsodi, J., Wootsch, A., Révay, Z., Hävecker, M., Knop-Gericke, A., Jackson, S.D. & Schlögl, R., 2008. The roles of subsurface carbon and hydrogen in palladium-catalyzed alkyne hydrogenation. *Science (New York, N.Y.)*, 320(5872), pp.86–9.
- Teschner, D., Vass, E., Hävecker, M., Zafeiratos, S., Schinorch, P., Sauer, H., Knopgericke, A., Schlogl, R., Chamam, M. & Wootsch, A., 2006. Alkyne hydrogenation over Pd catalysts: A new paradigm. *Journal of Catalysis*, 242(1), pp.26–37.
- Teschner, D., Wootsch, A., Pozdnyakovatellinger, O., Krohnert, J., Vass, E., Hävecker, M., Zafeiratos, S., Schinorch, P., Jentoft, P. & Knopgericke, A., 2007. Partial pressure dependent in situ spectroscopic study on the preferential CO oxidation in hydrogen (PROX) over Pt/ceria catalysts. *Journal of Catalysis*, 249(2), pp.318–327.
- Tew, M.W., Janousch, M., Huthwelker, T. & van Bokhoven, J.A., 2011. The roles of carbide and hydride in oxide-supported palladium nanoparticles for alkyne hydrogenation. *Journal of Catalysis*, 283(1), pp.45–54.
- Thavornprasert, K., Capron, M., Jalowiecki-Duhamel, L. & Dumeignil, F., 2016. One-pot 1,1-dimethoxymethane synthesis from methanol: a promising pathway over bifunctional catalysts. *Catal. Sci. Technol.*, 6(4), pp.958–970.
- ThermoFisher Scientific, 2013. *Introduction to FT-IR Sample Handling: How does it work?*,
- Thomson, S.J. & Webb, G., 1976. Catalytic hydrogenation of olefins on metals: a new interpretation. *Journal of the Chemical Society, Chemical Communications*, (13), p.526.
- Titirici, M.-M., White, R.J., Brun, N., Budarin, V.L., Su, D.S., del Monte, F., Clark, J.H. & MacLachlan, M.J., 2015. Sustainable carbon materials. *Chemical Society Reviews*, 44(1), pp.250–290.
- Toles, C., Rimmer, S. & Hower, J.C., 1996. Production of activated carbons from a washington lignite using phosphoric acid activation. *Carbon*, 34(11), pp.1419–1426.
- Trimm, D., Cant, N. & Lei, Y., 2009. Oxygenated fuel additives: The formation of methyl vinyl ether and 1,1-dimethoxyethane by the catalysed reaction of acetylene with methanol. *Catalysis Today*, 145(1–2), pp.163–168.

References

- Trubetskaya, A., Jensen, P.A., Jensen, A.D., Steibel, M., Spliethoff, H. & Glarborg, P., 2015. Influence of fast pyrolysis conditions on yield and structural transformation of biomass chars. *Fuel Processing Technology*, 140.
- Tundo, P., Aricò, F., Rosamilia, A.E., Grego, S. & Rossi, L., 2008. Dimethyl Carbonate: Green Solvent and Ambident Reagent. In *Green Chemical Reactions*. Dordrecht: Springer Netherlands, pp. 213–232.
- Tundo, P. & Selva, M., 2007. Dimethyl Carbonate as a Green Reagent. In *Methods and Reagents for Green Chemistry: An Introduction*.
- Tyndall, J., 1861. The Bakerian Lecture: On the Absorption and Radiation of Heat by Gases and Vapours, and on the Physical Connexion of Radiation, Absorption, and Conduction. *Source: Philosophical Transactions of the Royal Society of London*, 151, pp.1–36.
- UK Biochar Research Centre, 2014. UK Biochar Research Centre - Standard Biochars.
- Valente Nabais, J.M., Carrott, P.J.M., Ribeiro Carrott, M.M.L. & Menéndez, J.A., 2004. Preparation and modification of activated carbon fibres by microwave heating. *Carbon*, 42(7), pp.1315–1320.
- Vicente, J., Montero, C., Ereña, J., Azkoiti, M.J., Bilbao, J. & Gayubo, A.G., 2014. Coke deactivation of Ni and Co catalysts in ethanol steam reforming at mild temperatures in a fluidized bed reactor. *International Journal of Hydrogen Energy*, 39(24), pp.12586–12596.
- Vickerman, J.C. & Gilmore, I., 2009. *Surface Analysis - The Principal Techniques* 2nd ed., John Wiley & Sons Inc.
- Vrieland, G.E. & Menon, P.G., 1991. Nature of the catalytically active carbonaceous sites for the oxydehydrogenation of ethylbenzene to styrene: A brief review. *Applied Catalysis*, 77(1), pp.1–8.
- Wang, F.J., Zhang, S., Chen, Z.D., Liu, C. & Wang, Y.G., 2014. Tar reforming using char as catalyst during pyrolysis and gasification of Shengli brown coal. *Journal of Analytical and Applied Pyrolysis*, 105.
- Wang, G., Tian, Y., Jiang, J. & Wu, J., 2018. Multimodels computation for adsorption capacity of activated carbon. *Adsorption Science & Technology*, 36(1–2), pp.508–520.
- Wang, T., Li, C., Wang, C. & Wang, H., 2018. Biochar/MnAl-LDH composites for Cu (II) removal from aqueous solution. *Colloids and Surfaces A: Physicochemical and Engineering Aspects*, 538, pp.443–450.
- Warringham, R., Hamilton, N.G., Silverwood, I.P., How, C., Webb, P.B., Tooze, R.P., Zhou, W., Frost, C.D., Parker, S.F. & Lennon, D., 2015. The application of inelastic neutron scattering to investigate a hydrogen pre-treatment stage of an iron Fischer–Tropsch catalyst. *Applied Catalysis A: General*, 489, pp.209–217.
- Wei, L., Huang, Y., Li, Y., Huang, L., Mar, N.N., Huang, Q. & Liu, Z., 2017. Biochar characteristics produced from rice husks and their sorption properties for the acetanilide herbicide metolachlor. *Environmental Science and Pollution Research*, 24(5), pp.4552–4561.
- White, J.L., 2011. Methanol-to-hydrocarbon chemistry: The carbon pool (r)evolution. *Catalysis Science & Technology*, 1(9), p.1630.
- Williams, D.H. & Fleming, I., 2008. *Spectroscopic methods in organic chemistry*, McGraw-Hill.
- Woolf, D., Amonette, J.E., Street-Perrott, F.A., Lehmann, J. & Joseph, S., 2010. Sustainable biochar to mitigate global climate change. *Nature Communications*, 1(5), pp.1–9.
- World Commission on Environment and Development, 1987. *Our common future.*, Oxford University Press.
- Worrell, E., Bernstein, L., Roy, J., Price, L. & Harnisch, J., 2009. Industrial energy efficiency and climate change mitigation. *Energy Efficiency*, 2(2), pp.109–123.
- Xu, W.-Q., Yin, Y.-G., Suib, S.L. & O'Young, C.-L., 1995. Coke Formation and Its Effects on Shape Selective Adsorptive and Catalytic Properties of Ferrierite. *The Journal of Physical Chemistry*, 99(2), pp.758–765.
- Yang, B., Burch, R., Hardacre, C., Hu, P. & Hughes, P., 2016. Importance of Surface Carbide Formation on the Activity and Selectivity of Pd Surfaces in the Selective Hydrogenation of Acetylene. *Surface Science*, 646, pp.45–49.
- Yang, Z.-Z., He, L.-N., Liu, A.-H. & Li, Y.-N., 2012. Catalytic Fixation of Carbon Dioxide Into Fuel and

- Chemicals. In *Kirk-Othmer Encyclopedia of Chemical Technology*. Hoboken, NJ, USA: John Wiley & Sons, Inc., pp. 1–27.
- Yin, G., Liu, Z., Liu, Q. & Wu, W., 2013. The role of different properties of activated carbon in CO₂ adsorption. *Chemical Engineering Journal*, 230, pp.133–140.
- Yu, J.T., Dehkhoda, A.M. & Ellis, N., 2011. Development of Biochar-based Catalyst for Transesterification of Canola Oil. *Energy & Fuels*, 25(1), pp.337–344.
- Zawadzki, J., 1989. Infrared spectroscopy in surface chemistry of carbons. *Chemistry and Physics of Carbon*, 21, pp.147–380.
- Zawadzki, J., Wiśniewski, M. & Skowrońska, K., 2003. Heterogeneous reactions of NO₂ and NO–O₂ on the surface of carbons. *Carbon*, 41(2), pp.235–246.
- Zawadzki, J., Wiśniewski, M., Weber, J., Heintz, O. & Azambre, B., 2001. IR study of adsorption and decomposition of propan-2-ol on carbon and carbon-supported catalysts. *Carbon*, 39(2), pp.187–192.
- Zhang, J., Liu, X., Blume, R., Zhang, A., Schlögl, R. & Su, D.S., 2008. Surface-Modified Carbon Nanotubes Catalyze Oxidative Dehydrogenation of n-Butane. *Science*, 322(5898), pp.73–77.
- Zhang, J., Wang, H. & Dalai, A.K., 2007. Development of stable bimetallic catalysts for carbon dioxide reforming of methane. *Journal of Catalysis*, 249(2), pp.300–310.
- Zhang, Y.L., Luo, Y.H., Wu, W.G., Zhao, S.H. & Long, Y.F., 2014. Heterogeneous cracking reaction of tar over biomass char, using naphthalene as model biomass tar. *Energy and Fuels*, 28(5), pp.3129–3137.
- Zhao, L., Cao, X., Masek, O. & Zimmerman, A., 2013. Heterogeneity of biochar properties as a function of feedstock and production temperatures. *Journal of Hazardous Materials*, 256–257, pp.1–9.
- Zhao, N., Yang, X., Zhang, J., Zhu, L. & Lv, Y., 2017. Adsorption mechanisms of dodecylbenzene sulfonic acid by corn straw and poplar leaf biochars. *Materials*, 10(1119), pp.1–15.
- Zhao, Y., Feng, D., Zhang, Y., Huang, Y. & Sun, S., 2016. Effect of pyrolysis temperature on char structure and chemical speciation of alkali and alkaline earth metallic species in biochar. *Fuel Processing Technology*, 141, pp.54–60.

Appendix A Characterisation Method Development

A-I EDX Analysis: software settings

EDX Quantitative Analysis:

Scan time: 60 s

Resolution setting T3

Select elements: Manual (*e.g.* C, N, O, Na, Si, Cl, K)

Method: ZAF

Calculation method: pure

EDX Qualitative Maps:

Resolution setting T4

Pixels 512 × 384

Sweeps: 5

Dwell: 0.2 ms

Select elements: Manual (*e.g.* C, N, O, Na, Si, Cl, K)

A-II XPS Survey Scans: Raw Spectra

Example for OSB-700 Areas 1 and 2

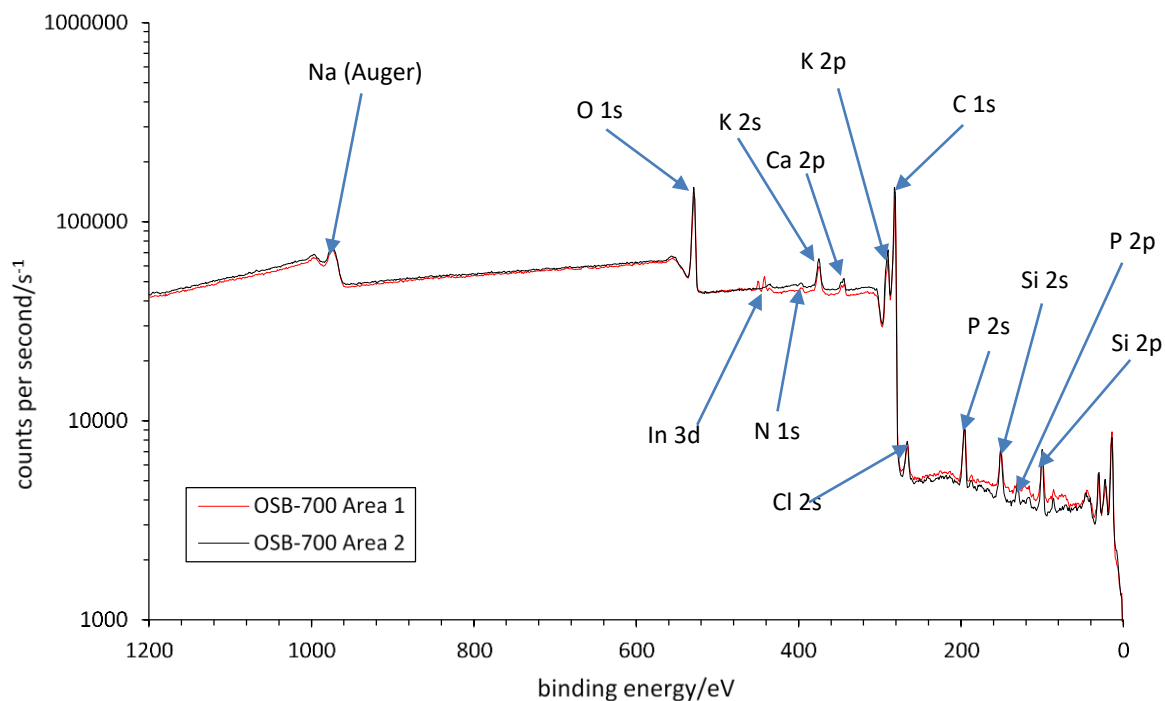


Figure 0-1 Annotated XPS spectra for survey scan of OSB-700, areas 1 and 2.

A-III XPS C1s Curve Deconvolution

Example XPS C1s spectra for OSB-700, areas 1 and 2:

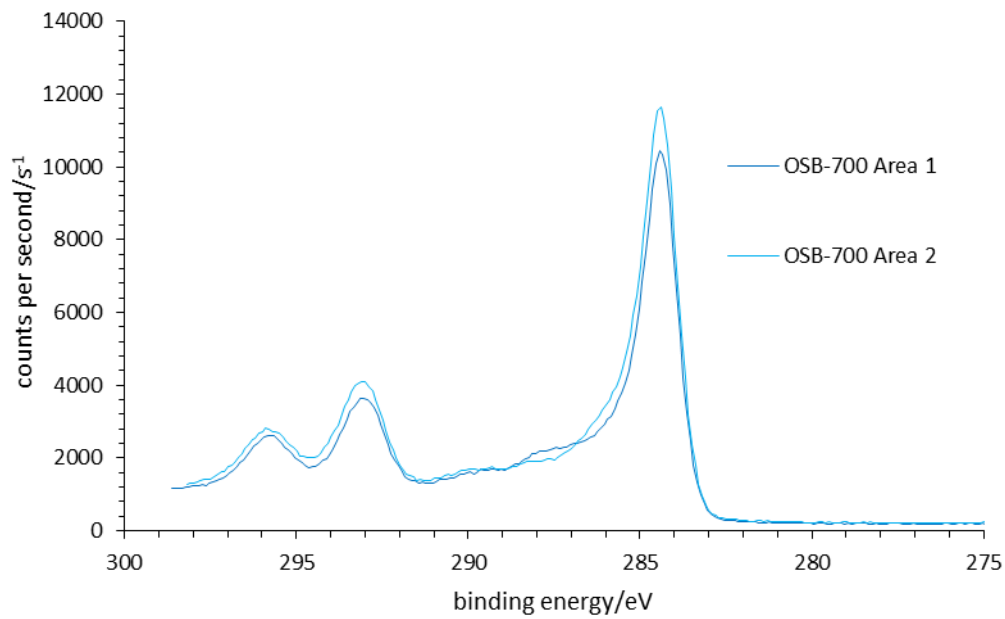


Figure 0-2 Example XPS C1s spectra for OSB-700 run 1 and run 2, calibrated by position of K 2p peaks.

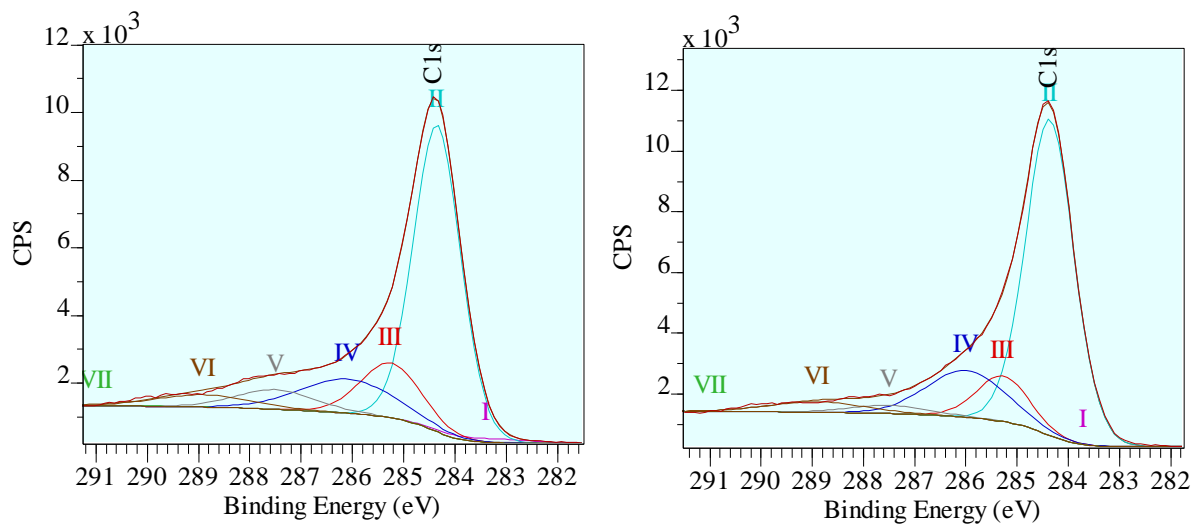


Figure 0-3 Example XPS C1s deconvoluted spectra for OSB-700, run 1 and run 2.

A-IV Curve deconvolution (Raman)

Example deconvolved spectra for rice husk biochar samples:

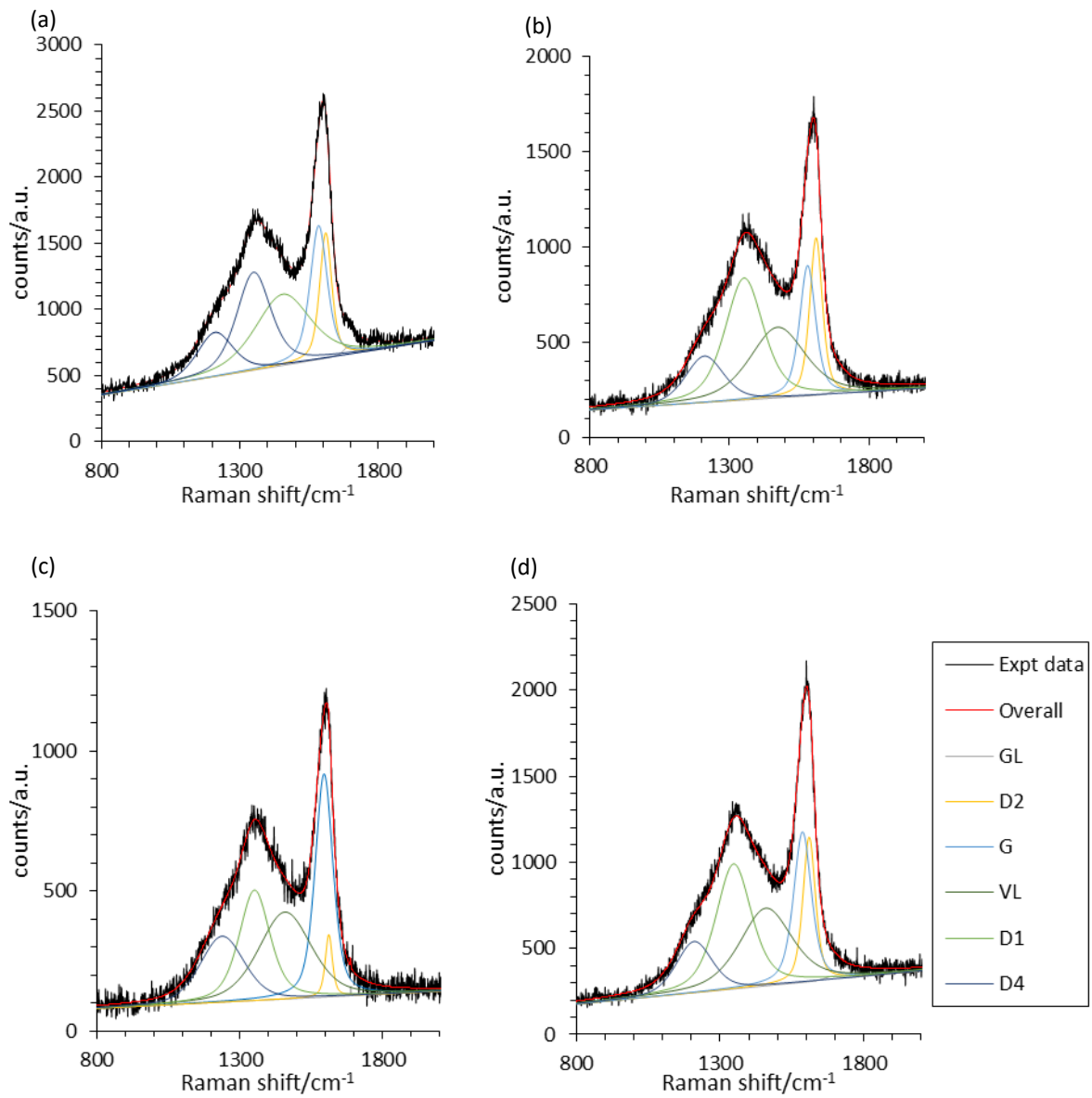


Figure 0-4 Deconvolved Raman spectra for rice husk biochar samples. (a) RHB-550, (b) RHB-550-DM, (c) RHB-550-T-C, (d) RHB-550-DM-T-C.

A-V Percentage Error Calculations

Example for BET analysis of three repeats of WSB-550.

	BET surface area/m ² g ⁻¹	Micropore volume/cm ³ g ⁻¹
WSB-550-run1	53.0	0.00261
WSB-550-run2	50.5	0.000859 (anomalous)
WSB-550-run3	51.6	0.00311
Average (μ)	51.7	0.00286
Standard deviation (σ)	1.25	0.000358
% error (= σ/μ)	2.42 %	12.52 %

The same method is applied to calculate percentage errors when applying the error from one set of biochars to other biochars.

For XPS analysis, two repeats were performed for each sample; in these cases, the standard deviation of the two results is used as the calculated error value.

A-VI FTIR of biochar ash samples (band identification)

By comparing the FTIR-ATR spectra of char and ash samples, it was possible to confirm which bands corresponded to carbonaceous functional groups, and which bands correspond to silica groups. In ash samples, the carbonaceous groups are no longer present due to combustion.

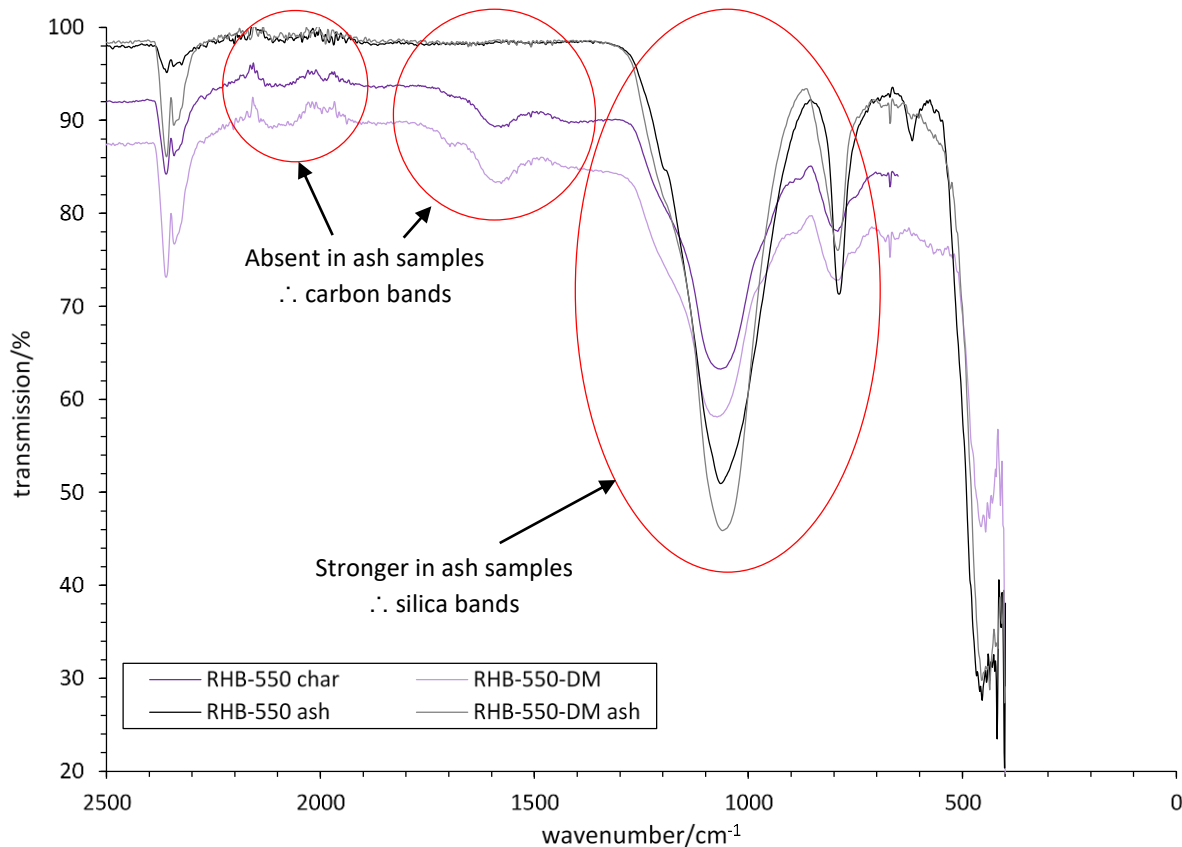


Figure 0-5 Annotated FTIR spectra comparing RHB-550 char and ash samples.

A-VII TGA for change in crucible type

At the University of Edinburgh, TGA for tar-impregnated samples was performed in platinum (Pt) crucibles, to prevent tar impregnation in porous alumina (Al_2O_3) crucibles. The TGA results for OSB-700 and RHB-550 were compared in alumina and platinum crucibles, to confirm that the change in crucible did not affect the results of proximate analysis.

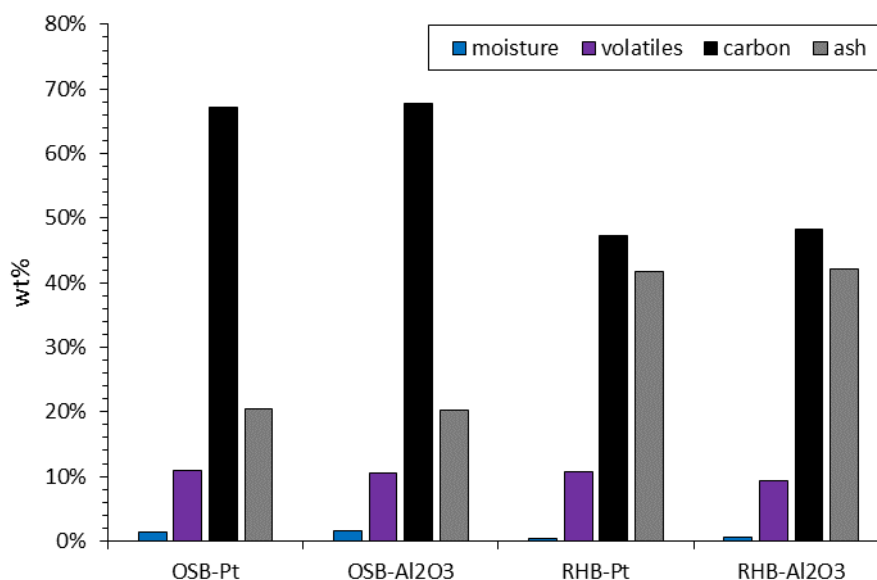


Figure 0-6 TGA Proximate analysis comparing platinum (Pt) and alumina (Al_2O_3) crucibles for two different biochar samples.

A-VIII TGA Edinburgh vs Sheffield

TGA analysis methods differed slightly at the University of Edinburgh and University of Sheffield, as described in section 5.2.2.2. The methods were compared at the University of Sheffield to confirm that the analysis methods produced comparable results.

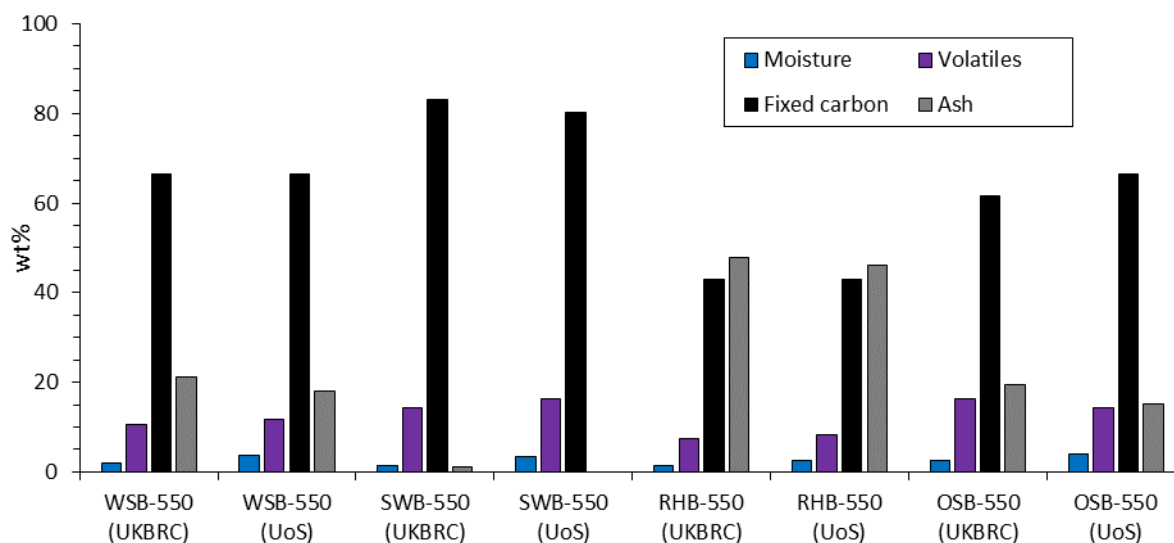


Figure 0-7 Comparison of TGA Proximate Analysis using methods at the University of Sheffield (UoS) and University of Edinburgh Biochar Research Centre (UKBRC).

Appendix B Surface Treatments

B-I Acetone washing preliminary experiments

Experiments to determine the optimal experimental method for preparing acetone-washed control samples. Whilst tar impregnation took place over 96 hours, washing times in acetone of 12 hours were found to give the same result as washing for 48 hours, provided samples were fully dried in an oven.

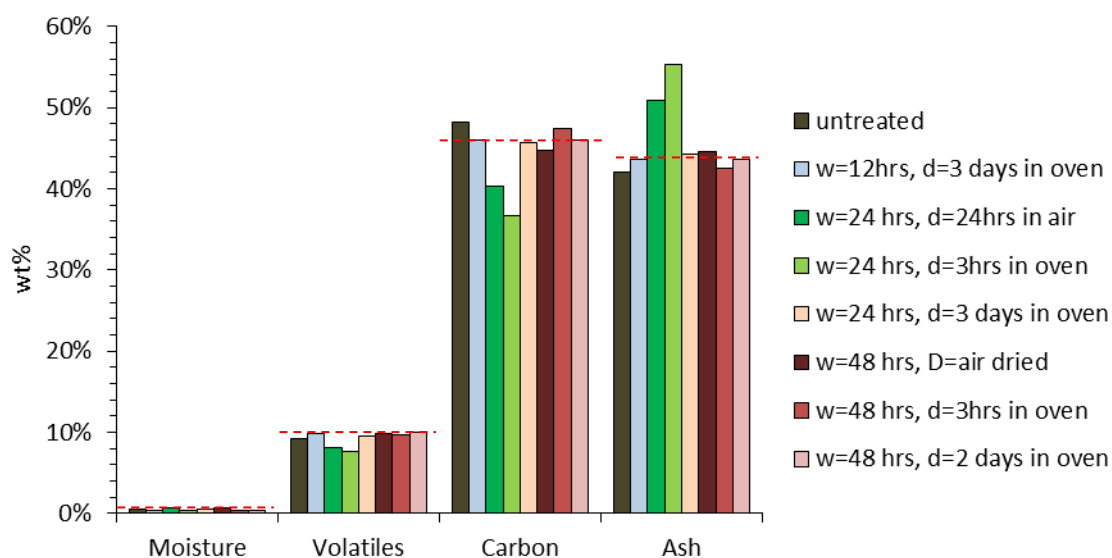


Figure 0-8 TGA analysis of acetone control samples, using RHB. w = washing time, d = drying time. Samples dried in the oven for >2 days had the same composition (shown by red dotted lines), regardless of washing time, implying that differences between other samples are due to the samples not being fully dry.

B-II Quantitative EDX vs XPS

EDX analysis was carried out alongside SEM to quantify the surface composition of the biochars. Due to the use of carbon tab adhesives and gold coatings, the absolute values were not used in the main data analysis, however the data were compared with XPS data to confirm the effects of surface treatments, such as demineralisation and tar impregnation. Example results for OSB-700 are shown in Figure 0-9, and demonstrated that potassium and calcium were reduced by demineralisation, and surface silicon may be reduced after tar impregnation.

The error associated with quantitative EDX was high, with elements sometimes only detected in one of the four areas analysed. This may be further evidence of the heterogeneity of the biochars, however may also be due to varying thicknesses of gold coating, and therefore varying sensitivities in detection limits.

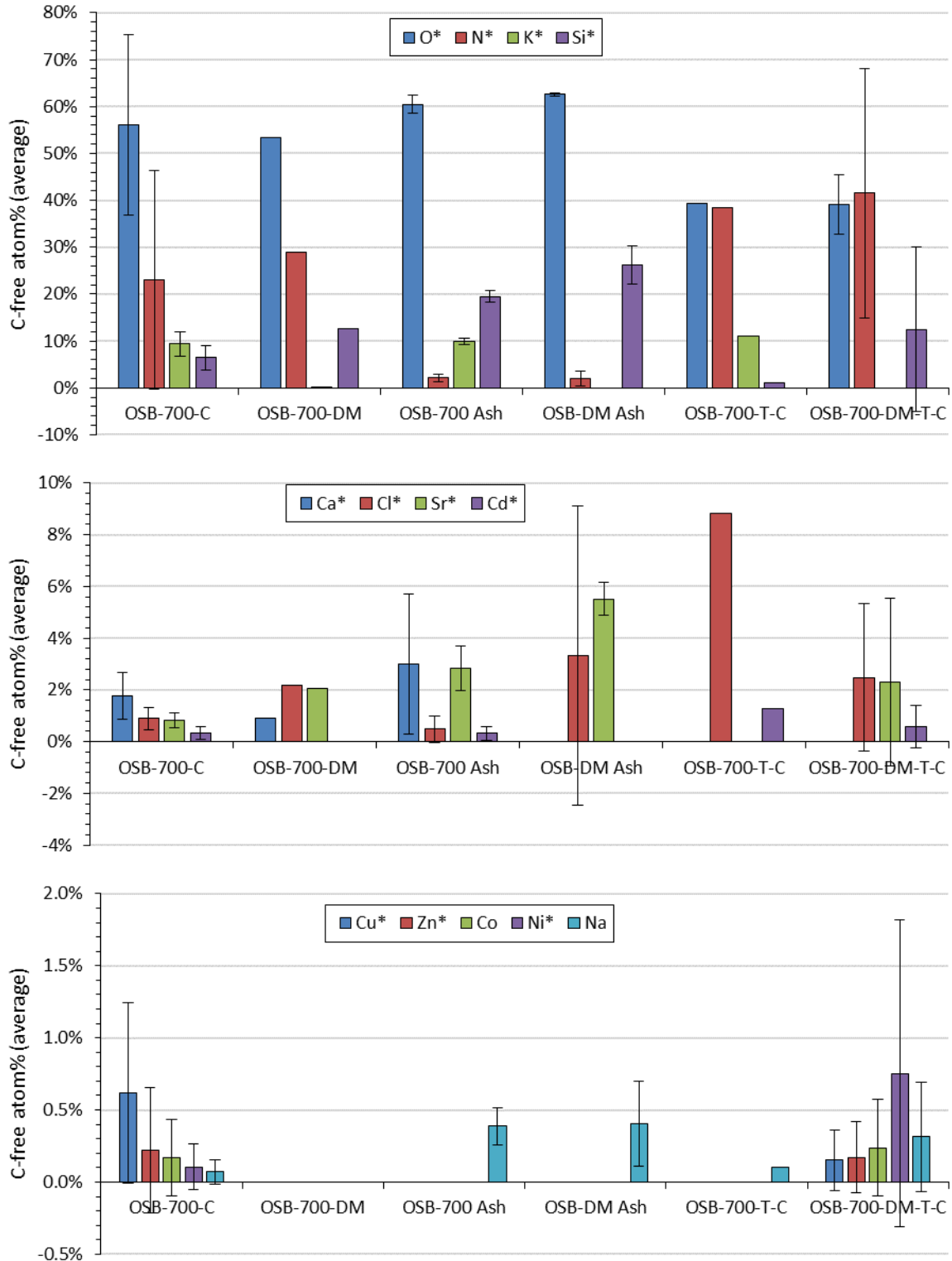


Figure 0-9 EDX analysis of OSB-700 samples before and after various surface treatments. Error bars are standard deviation calculated from repeat measurements, analysing different areas of each sample. The number of areas analysed were: 4 × OSB-700, 1 × OSB-700-DM (no error calculated), 3 × OSB-700-ash, 3 × OSB-700-DM-ash, 1 × OSB-700-T-C (no error calculated), 2 × OSB-700-DM-T-C.

B-III Effect of demineralisation on carbon structure

Additional characterisation data of demineralised samples, investigating the effect of demineralisation on carbon structure. The effect on graphiticity and surface chemistry was observed to vary depending on the feedstock, with no systematic changes observed.

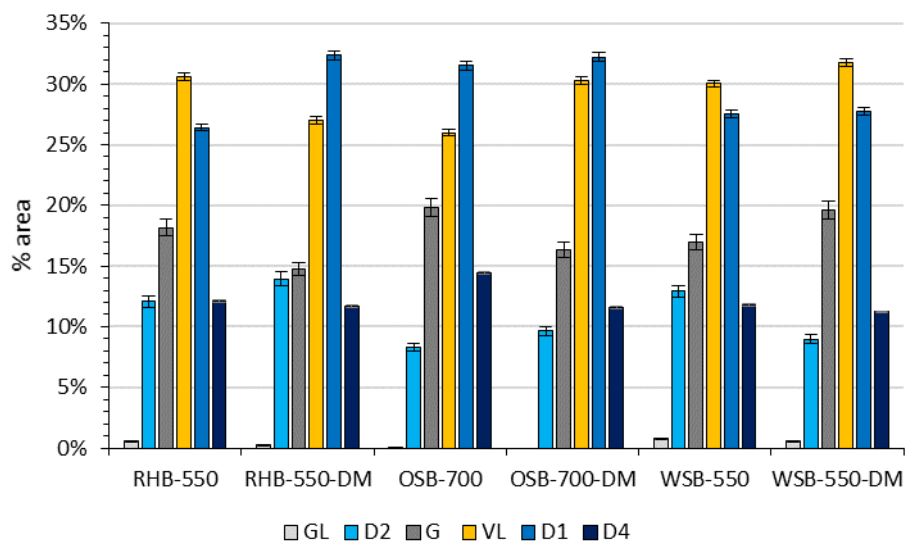


Figure 0-10 Raman curve deconvolution data for biochars from different feedstocks before and after demineralisation. Error bars estimated from percentage error from three repeats of WSB-550-DM.

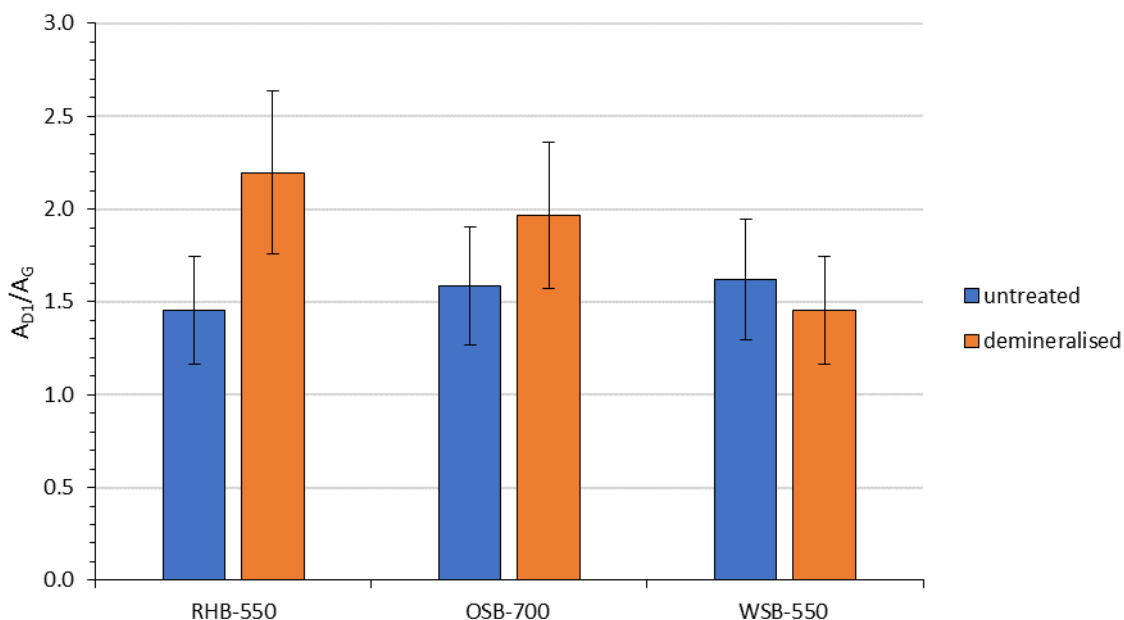


Figure 0-11 Raman curve deconvolution data, showing the ratio of the area of the D1 to G bands, for biochars from different feedstocks before and after demineralisation. Error bars estimated from percentage error of 20% from three repeats of WSB-550-DM.

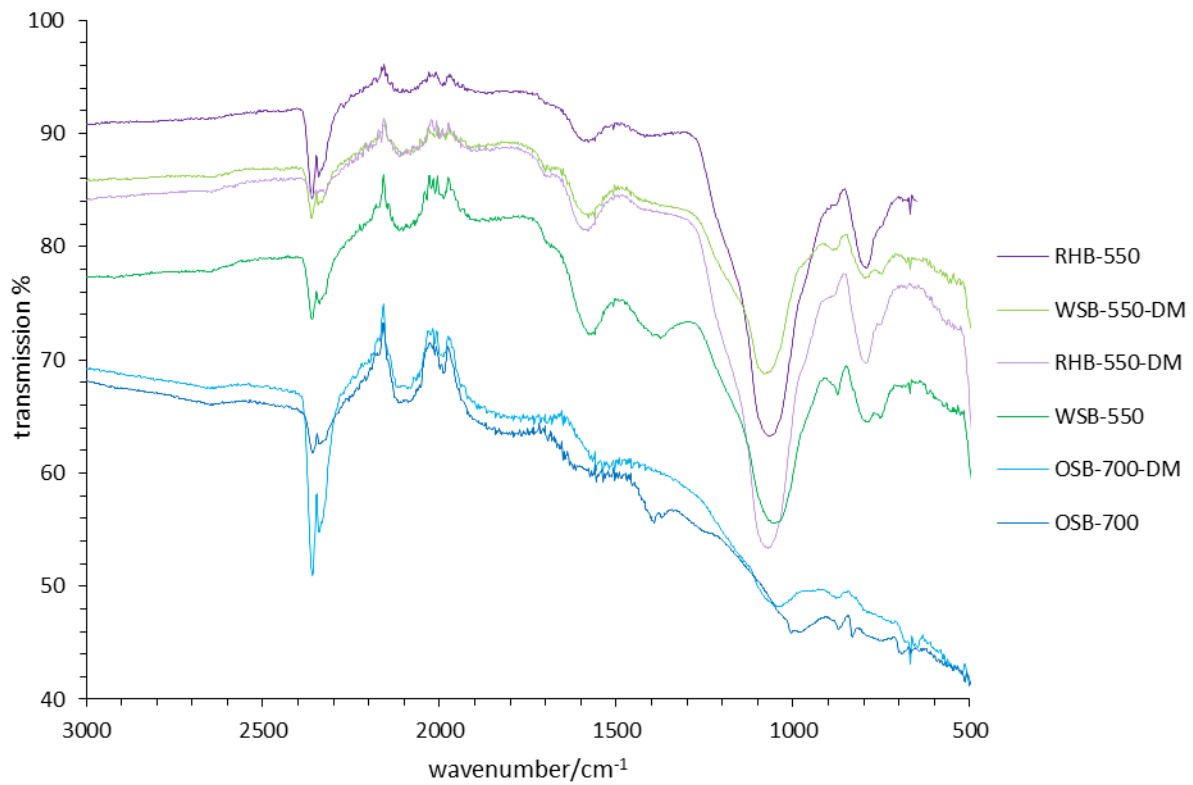


Figure 0-12 FTIR-ATR spectra for biochars before and after demineralisation.

B-IV Pine tar TGA

Proximate analysis of the commercial pine tar supplied by Auson, demonstrating that the pine tar was mostly comprised of volatile components (96.62 wt%), with negligible ash content (0.28 wt%).

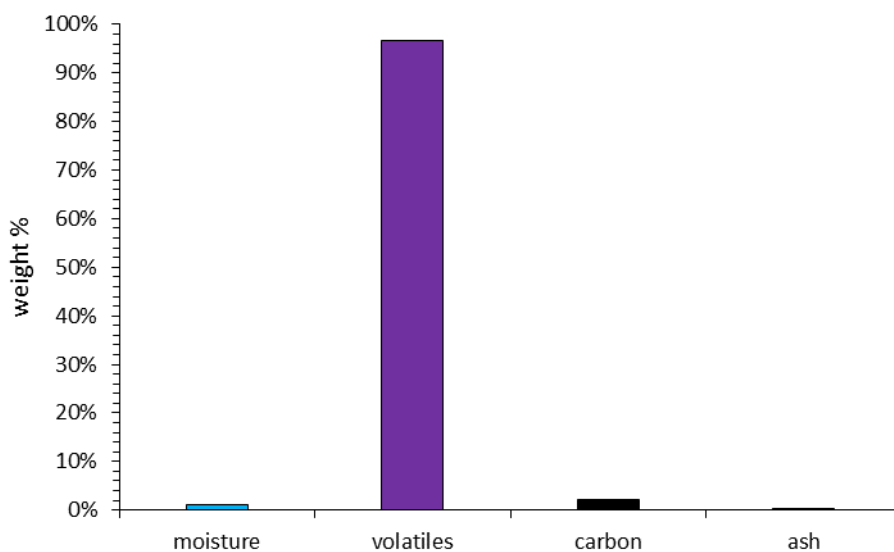


Figure 0-13 TGA of pine tar. The majority of the mass is comprised of volatiles (96.62 wt%), with a negligible contribution from ash (0.28 wt%).

B-V Example tar loading calculations

Example calculations for the quantity of tar loaded on biochar samples. Calculations assume that the decrease in ash content is solely due to the increase in volatile content associated with the tar (see Figure 0-13).

	wt%			wt%	
	RHB-A	RHB-T		OSB-A	OSB-T
Moisture	0.40%	0.25%	Moisture	2.07%	0.30%
Volatiles	9.84%	17.84%	Volatiles	12.56%	25.30%
Carbon	46.06%	42.24%	Carbon	66.48%	58.24%
Ash	43.70%	39.67%	Ash	18.89%	16.15%
Per 100g untreated sample:			Per 100g untreated sample:		
Ash	43.70		Ash	18.89	
Mass of tar-impregnated sample required to reduce % ash content:			Mass of tar-impregnated sample required to reduce % ash content:		
	=43.70/0.3967			=18.89/0.1615	
	110.16			116.91	
Mass of tar added per 100g char:			Mass of tar added per 100g char:		
	10.16			16.91	
Mass of tar	10.16		Mass of tar	16.91	
Mass of biochar	100		Mass of biochar	100	
% biochar	90.78%		% biochar	85.54%	
% tar	9.22%		% tar	14.46%	

Calculations for predicted composition of RHB-550-T:

	RHB-550-A	Tar	tar added (g/100g biochar)	total mass/g	RHB-550-T (predicted)
Moisture	0.40%	1.07%	0.108	0.51	0.46%
Volatiles	9.84%	96.62%	9.816	19.66	17.85%
Carbon	46.06%	2.03%	0.207	46.26	42.00%
Ash	43.70%	0.28%	0.028	43.73	39.70%
TOTAL:			10.160	110.16	100.0%

B-VI Pyrolysis yields of biochar, liquid and gas

The yield of solid, liquid and gas phase products from Stage I pyrolysis of the tar-impregnated biochars. Solid (biochar) yield was calculated from the mass remaining in the quartz sample tube after pyrolysis (see the Stage I pyrolysis set-up in Figure 3-1). Liquid yield was calculated from the increase in mass of the condenser tubes. Gas yield was estimated from the remaining mass lost from the solid biochar. The error in the repeats of WSB-550-DM-T for the liquid and gas phase yield cast doubt on the reliability of the results for the remaining samples.

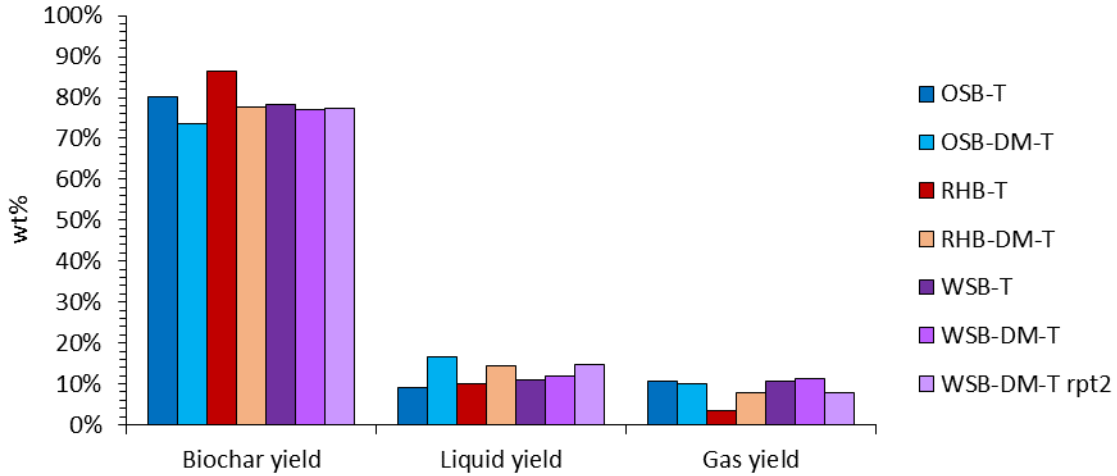


Figure 0-14 Comparison of biochar, liquid and gas yields for Stage I pyrolysis of different biochar materials impregnated with tar.

B-VII TGA for demineralised samples

Proximate analysis was carried out by TGA on biochars before and after demineralisation. This allowed the ash content to be quantified, and therefore the quantity of ash removed by demineralisation to be calculated.

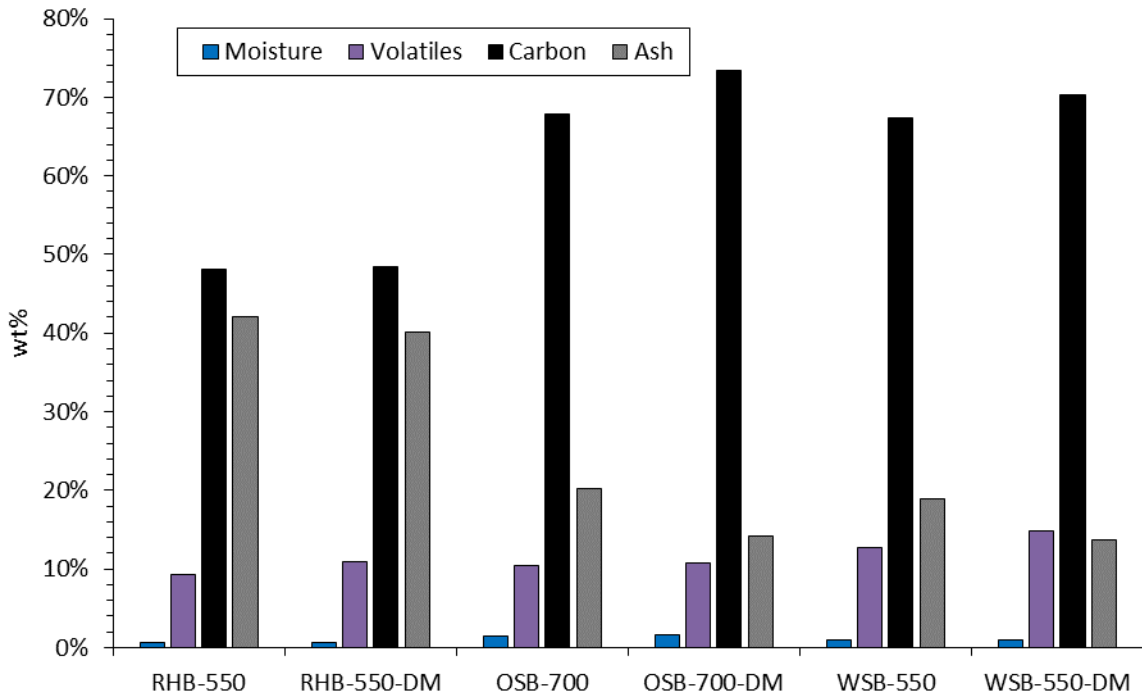


Figure 0-15 Proximate analysis for biochar samples before and after demineralisation. This data was used to calculate the percentage of ash content removed from the biochars.

B-VIII SEM of tar-impregnated samples

SEM images were collected for biochar samples after tar impregnation and pyrolysis to investigate any changes in the macrostructure of the biochars. The images demonstrate that the macropores remained free, and were not blocked by carbon deposits.

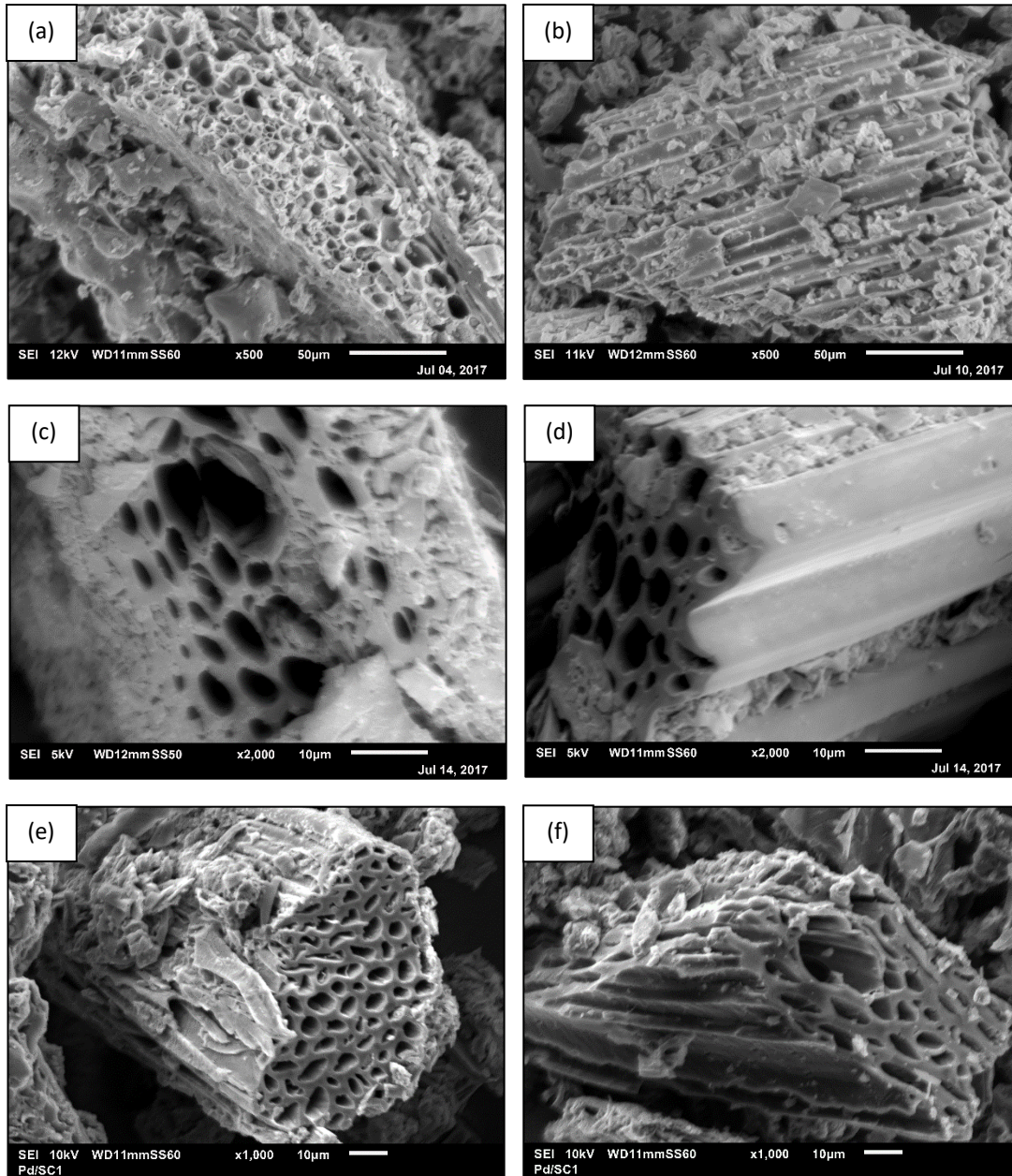


Figure 0-16 SEM images of tar-impregnated biochars. (a) RHB-550-T-C, (b) RHB-50-DM-T-C, (c) OSB-700-T-C, (d) OSB-700-DM-T-C, (e) WSB-550-T-C, (f) WSB-550-DM-T-C.

Appendix C Methanol reaction calibrations

C-I Methanol calibrations

Example calibration curves for methanol and DMM, obtained in March 2018. Calibration of reaction data was carried out without normalising peak areas relative to the internal standard, due to the much lower R^2 value associated with the methanol calibrations when using an internal standard ($R^2 = 0.990$ without internal standard, 0.740 with internal standard). This indicated an error in the quantity of internal standard added to the calibration samples – this is discussed in section 6.4.5.

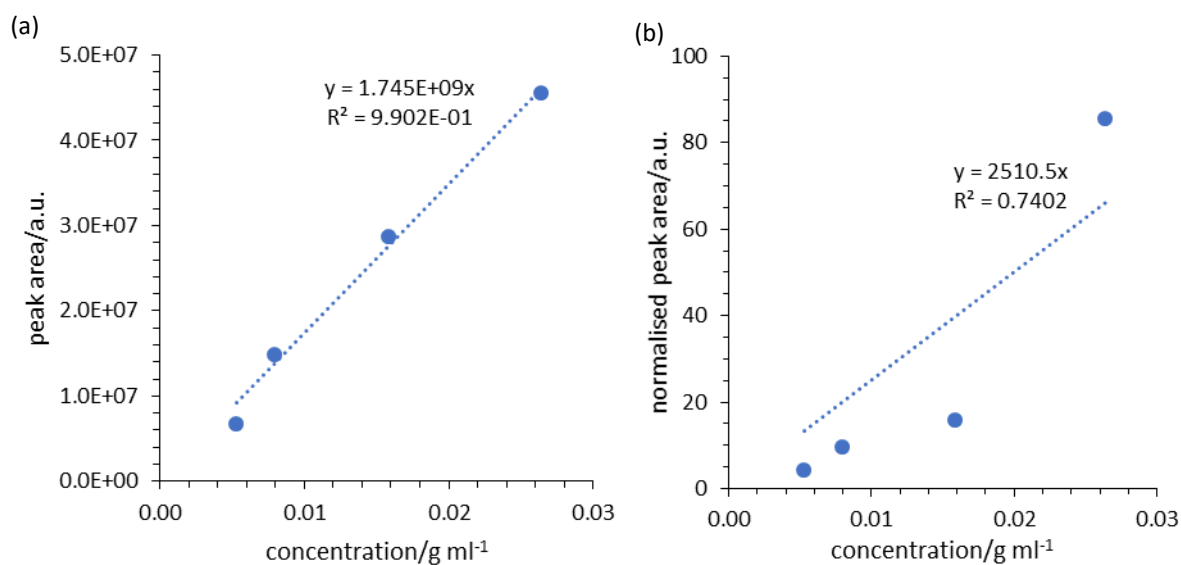


Figure 0-17 Calibration curves for methanol from March 2018, (a) without normalisation and (b) normalised relative to the area of the internal standard peak.

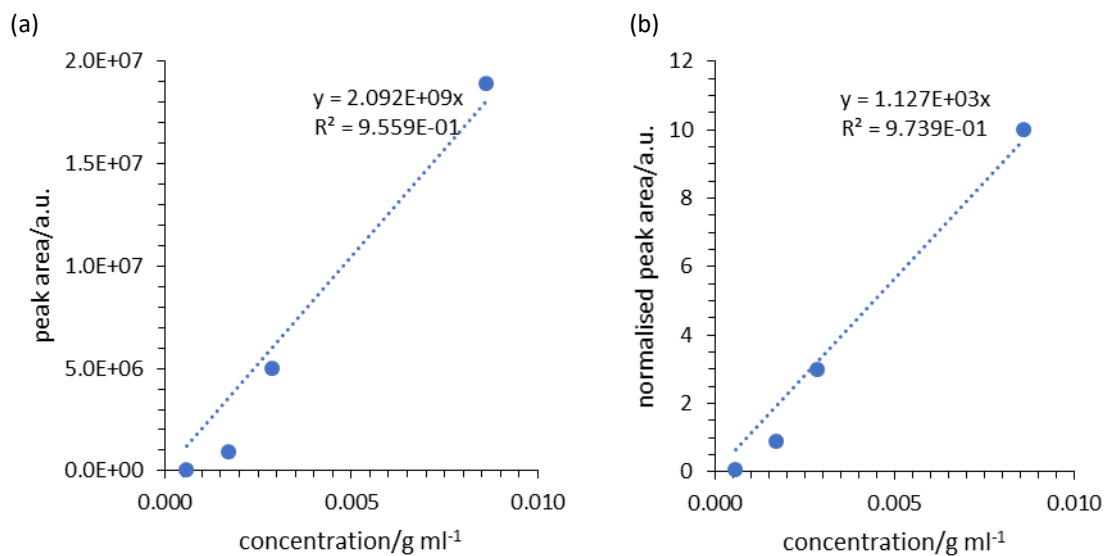


Figure 0-18 Calibration curves for DMM from March 2018, (a) without normalisation and (b) normalised relative to the area of the internal standard peak.

C-II Conversion calculations

Methanol concentration was calculated from GCMS analysis of dilute samples. The conversion of methanol was then calculated, however the error associated with the calculation was too high to draw any meaningful conclusions; for example, the highest and lowest methanol conversions were obtained from the same sample.

Initial concentration of methanol in dilute sample:

Volume of methanol in reactor = 7 ml

Density of methanol = 0.792 g ml⁻¹

Volume of product added to calibration sample = 50 µL

∴ Mass of methanol added to calibration sample = 0.0396 g

Volume of distilled water added for analysis = 1.45 ml

Volume of product added = 50 µL

Internal standard = 1 µl

∴ Total volume of calibration sample = 1.501 ml

∴ Initial concentration = 0.0396/1.501 = 0.0264 g ml⁻¹

To calculate conversion of methanol,

$$X_{MeOH} = \frac{\text{initial concentration} - \text{final concentration}}{\text{initial concentration}} \times 100$$

In some cases, the calculated methanol concentration in the product mixture was higher than the initial concentration of methanol. This led to the calculation of negative conversions, for example:

Calibration constant:	1.05E+09		
	MeOH peak area/a.u.	Concentration/g ml ⁻¹	Conversion
AC (50 bar)	3.05E+07	0.0289	-13.3%
None run1	2.59E+07	0.0246	3.6%
None run2	2.67E+07	0.0254	0.7%
None run3	3.52E+07	0.0334	-30.7%
SWB-550	3.71E+07	0.0352	-37.7%
OSB-550	3.92E+07	0.0372	-45.6%
RHB-550	3.24E+07	0.0308	-20.5%
AC (40 bar)	3.49E+07	0.0331	-29.7%

The error associated with the three control experiments with no catalyst was too high, and the conversion calculations were considered unreliable as a basis for comparing experimental data. The high error in calibrating methanol was attributed to the volatility of methanol and lack of gas phase data, as discussed in section 6.4.5.

C-III Experimental error

Calculations of percentage error in the quantity of each product of methanol conversion, using three repeats of SWB-550.

Experimental error	DMM conc/g ml ⁻¹	1,1-DME peak area/a.u.
SWB-550 run1	6.75E-05	79888
SWB-550 run2	7.80E-05	100901
SWB-550 run3	1.05E-04	120078
Average (μ)	8.36E-05	100289
Standard deviation (σ)	1.95E-05	20102
% error ($=\sigma/\mu$)	23.3%	20.0%

Appendix D Glycerol reaction calibrations

D-I Acetin calibration

The precise composition of the acetin mixture used for calibration was unknown: the mixture was known to be 50 % diacetin, but the concentration of mono- and triacetin was unknown. For calibration purposes, the composition was estimated from a sample of 99+ % triacetin. The quantity of triacetin in the calibration sample was calculated to give the same calibration constant as the pure triacetin sample. This is shown in Figure 0-19.

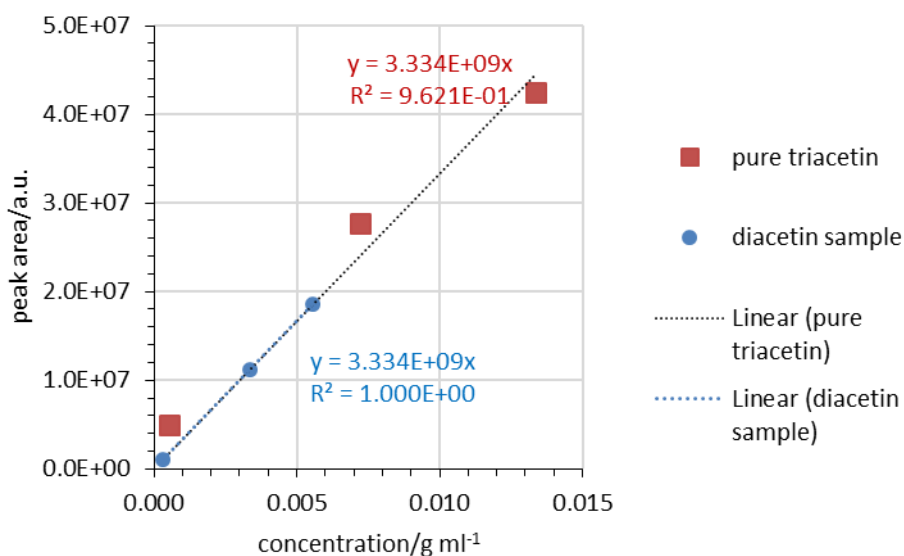


Figure 0-19 Calibration curves for triacetin in a pure triacetin sample, and in a calibration sample consisting of 50 % diacetin. The estimated quantity of triacetin in the diacetin sample was adjusted to give the same calibration constant as the pure triacetin sample.

As an example, for the first data point in the diacetin sample (Calibration sample 1):

Peak area of triacetin in diacetin sample = 1.02×10^6

Calibration constant for triacetin = 3.334×10^9

Concentration of triacetin = peak area/calibration constant = $3.05 \times 10^{-4} \text{ g ml}^{-1}$

From this data, the percentage of triacetin in the diacetin sample could be calculated:

0.001 ml acetins = 0.0017 g acetins

Total liquid volume = 1.1 ml + 10 μL 1-hexanol + 0.001 ml acetins = 1.111 ml.

\therefore Concentration of triacetin = $3.05 \times 10^{-4} \text{ g ml}^{-1}$

\therefore mass of triacetin in calibration sample = $3.05 \times 10^{-4} \text{ g ml}^{-1} \times 1.111 \text{ ml} = 3.38 \times 10^{-4} \text{ g}$

Total mass of acetin added = 0.00117 g

\therefore wt% triacetin = $3.38 \times 10^{-4} \text{ g} / 0.00117 \text{ g} = 28.9 \%$

By definition, wt% diacetin = 50 %

\therefore wt% monoacetin (and others) = $100 - 50 - 28.92 = 21.1 \%$

It is worth noting that other acetins may be present in the calibration sample. The overall density of the calibration sample was quoted as 1.17, however the calculated density based on the estimated composition was calculated as 1.19:

	Density:	Mass (per 100 g sample):	Volume (per 100 g sample):
Pure monoacetin	1.22	21.1	17.3
Pure diacetin	1.19	50	42.0
Pure triacetin	1.16	28.9	24.9
		total volume per 100 g/ml	84.2
		overall sample density/g ml⁻¹	=100/84.2
			=1.19

There may therefore be a significant contribution from lower-density acetins, such 1,2-propanediol diacetate, with a density of 1.05 g ml⁻¹. Precise quantification of the acetin mixture was beyond the scope of the present work; more important was comparison of the trends in acetin production between biochars, and accurate calibration of diacetin and triacetin, which were only produced in the presence of a catalyst.

D-II Glycerol calibration samples

Calibration samples were produced for the quantification of reaction products from the glycerol upgrading reactions in Chapter 7. These calibration samples consisted of a mixture of glycerol, glycerol carbonate, and acetins. The quantity of acetins is based on the estimated composition, calculated in section D-I. An example is given for calibration samples prepared in February 2018 in Table 0-1.

Table 0-1 Calibration samples prepared for glycerol upgrading reactions in February 2018

Sample composition					Sample concentration				
Cal. #	Vol. EtOH/ml	Glycerol/g	Glycerol carbonate/ μ L	Acetins/ μ L	Glycerol/g ml ⁻¹	Glycerol carbonate/g ml ⁻¹	Monoacetin/g ml ⁻¹	Diacetin/g ml ⁻¹	Triacetin/g ml ⁻¹
1	10	1.20	70	240	0.1070	0.008694	0.005251	0.012455	0.007204
2	10	0.95	55	180	0.0865	0.007127	0.004036	0.009573	0.005537
3	10	0.70	35	120	0.0661	0.004701	0.002761	0.006548	0.003787
4	10	0.45	20	65	0.0431	0.002679	0.001557	0.003694	0.002136
5	10	0.20	4	10	0.0210	0.00055	0.000242	0.000575	0.000332

D-III Glycerol calibration curves

Example calibration curves for the products of glycerol upgrading reactions from February 2018. Calibrations are presented with and without normalisation using an internal standard, 1-hexanol. Higher R^2 values were obtained in the absence of an internal standard; this was attributed to the high retention rates of glycerol in the INNOWax column, as discussed in section 7.4.5.

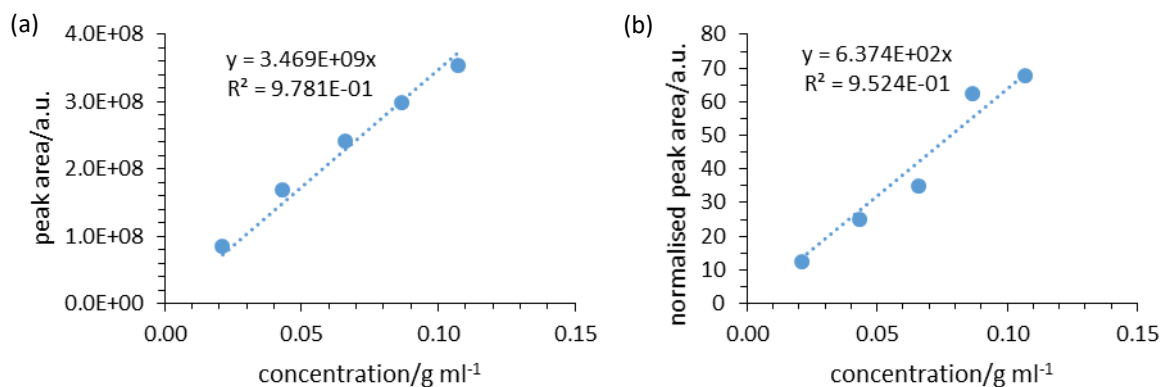


Figure 0-20 Calibration curves for glycerol, (a) without normalisation and (b) normalised relative to the area of the internal standard peak.

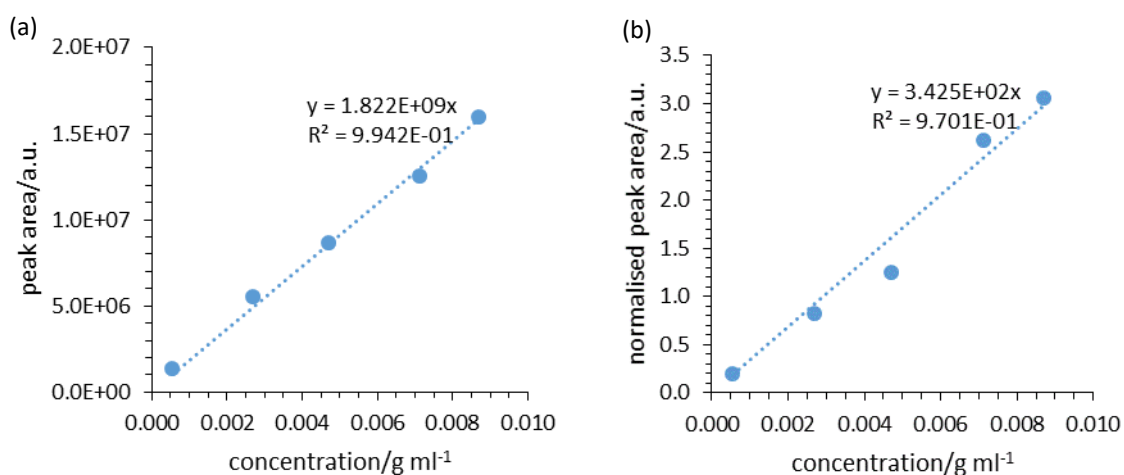


Figure 0-21 Calibration curves for glycerol carbonate, (a) without normalisation and (b) normalised relative to the area of the internal standard peak.

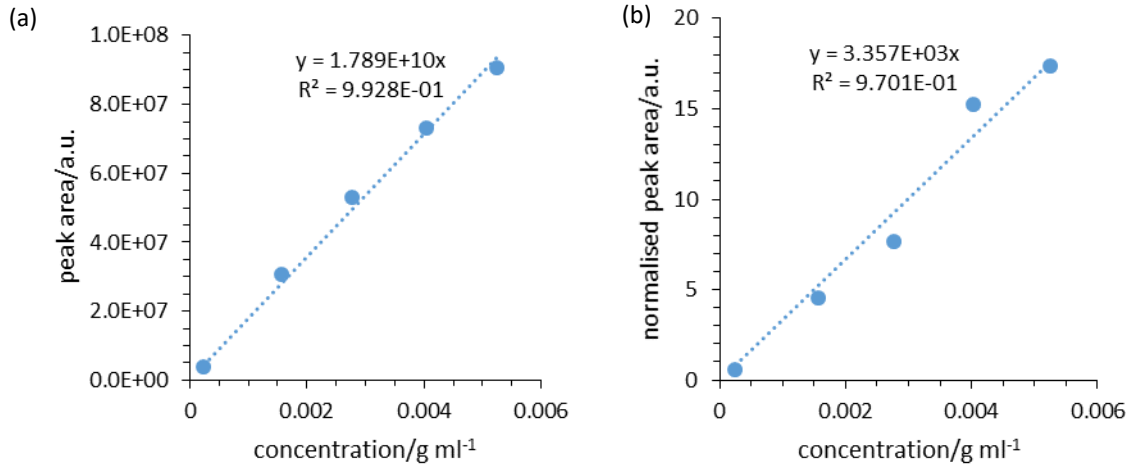


Figure 0-22 Calibration curves for glycerol monoacetin (a) without normalisation and (b) normalised relative to the area of the internal standard peak.

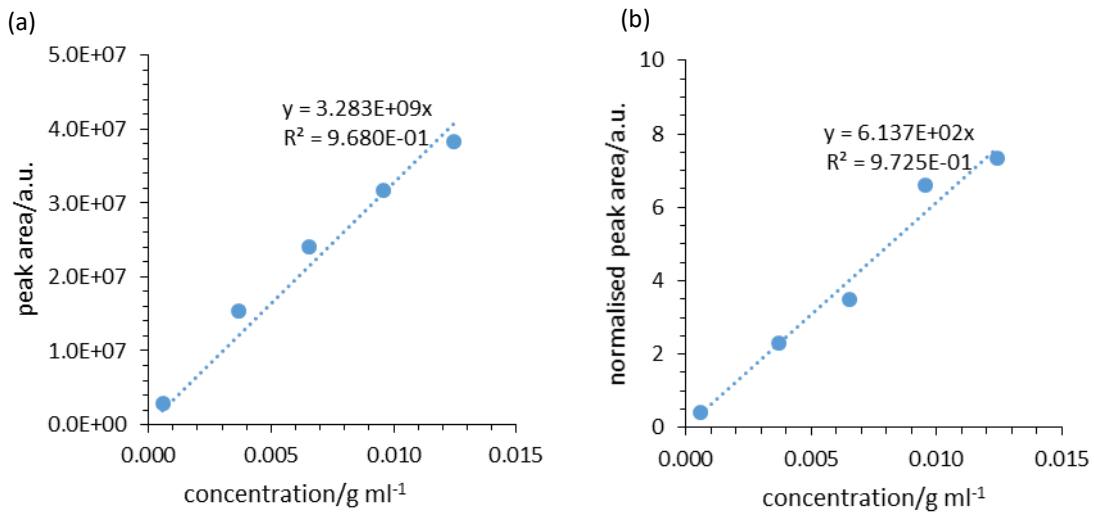


Figure 0-23 Calibration curves for glycerol diacetin (a) without normalisation and (b) normalised relative to the area of the internal standard peak.

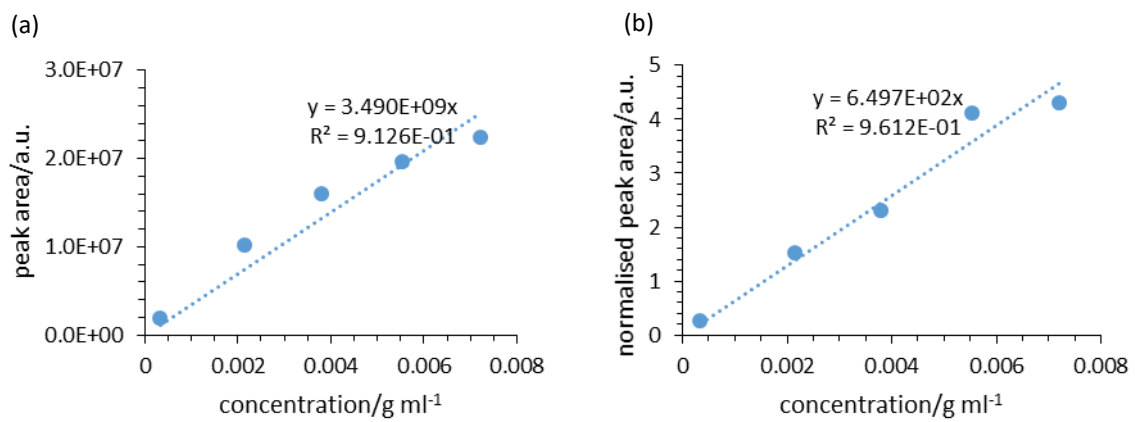


Figure 0-24 Calibration curves for glycerol triacetin (a) without normalisation and (b) normalised relative to the area of the internal standard peak.

D-IV Experimental error

Calculations of percentage error in the quantity of each product of glycerol upgrading, using three repeats of OSB-550.

Catalyst	Concentration/mol l ⁻¹				
	Glycerol	Glycerol carbonate	Monoacetin	Diacetin	Triacetin
OSB-550-S rpt1	0.2562	0.0329	0.0980	0.0188	0.0006
OSB-550-S rpt2	0.3285	0.0257	0.1479	0.0325	0.0013
OSB-550-S rpt3	0.5575	0.0436	0.1030	0.0027	0.0002
Average (μ)	0.3807	0.0340	0.1163	0.0180	0.0007
Standard deviation (σ)	0.1573	0.0090	0.0275	0.0149	0.0006
% error ($=\sigma/\mu$)	41.3%	26.4%	23.6%	82.9%	78.1%

Appendix E Things Go Better With Coke

Reproduced from reference (Collett & McGregor, 2016) with permission from The Royal Society of Chemistry.

CrossMark
click for updatesCite this: *Catal. Sci. Technol.*, 2016,
6, 363

Things go better with coke: the beneficial role of carbonaceous deposits in heterogeneous catalysis

C. H. Collett and J. McGregor*

Carbonaceous or hydrocarbonaceous deposits formed on the surface of heterogeneous catalysts during reaction are typically associated with catalyst deactivation through coking. However, there are a number of cases where such deposits may enhance catalytic performance. This includes: coke deposits acting directly as the catalytically active site, e.g. in alkane dehydrogenation reactions; the selective deactivation of non-selective surface sites thereby increasing catalytic selectivity; and the participation of deposits in the reaction mechanism, including hydrogen and hydrocarbon transfer and the well-documented hydrocarbon pool in methanol-to-hydrocarbon conversion. The *in situ* formation of metal carbides also plays a key role in many reactions including alkyne hydrogenation and Fischer-Tropsch synthesis. These phenomena have been observed over all solid catalyst types including supported metals and metal oxides and zeolites. It is highly likely that there are many systems in which coke plays a positive role which have not yet been reported due to difficulties in deconvolving this from the role coke plays in deactivation. This review summarises the, at present disparate, literature in this important area and highlights how this understanding can be used to inform the rational design of catalysts and catalytic processes.

Received 31st July 2015,
Accepted 10th October 2015

DOI: 10.1039/c5cy01236h

www.rsc.org/catalysis

1 Introduction

The effects of carbonaceous deposits, or “coke”, on catalyst performance have been extensively studied over the past five decades, with the principle focus on the role of coke in catalyst deactivation. There is an evident commercial need to understand the mechanisms by which coke causes catalyst deactivation, in order to optimise process efficiency. Coke deposition, however, can also have beneficial effects on catalyst performance. For instance, it can enhance the selectivity of the catalyst, e.g. through selective poisoning of high-energy active sites which promote undesirable side reactions. Additionally, thermal effects associated with carbon deposition may help to moderate exothermic processes and thus prevent sintering, or carbon deposits may isolate metallic particles, thus preventing sintering by geometric effects.¹ It is also becoming increasingly evident that carbon deposits can exhibit direct catalytic activity in a wide range of systems, for example in oxidative dehydrogenation, isomerisation, hydrogenation and Fischer-Tropsch reactions.

This review seeks to provide an overview of the, at present, disparate, reports on the beneficial role that coke deposits can play such that this knowledge can inform improved design of catalysts and catalytic processes. This is crucial not only in improving the sustainability of existing industrial processes, many of which rely on fossil resources, but also in

developing new processes such as those utilising renewable feedstocks. A particular focus of the review is on those cases where coke has been shown, or has the potential, to play a direct role in the catalytic reaction; in particular providing active sites or reacting with adsorbed reactant species to form the desired product. Much progress has been made since the last major review of this area,² for example, the discovery of the hydrocarbon pool mechanism in methanol-to-olefin reactions,³ and the activity of coke deposits in non-oxidative dehydrogenation reactions.⁴ The catalytic activity of carbon based materials, e.g. activated carbons, carbon nanotubes, graphene *etc.*, has been thoroughly discussed in a number of excellent recent reviews^{5–8} and hence only the catalytic behaviour of carbonaceous deposits formed *in situ* on the surface of a heterogeneous catalyst will be discussed herein.

1.1 Definition and structure of “coke”

The definition of coke is often somewhat arbitrary, and may be loosely correlated with structural parameters of the deposits. The terms young, medium and old coke have been used to describe coke in terms of decreasing hydrogen content with ‘age’ or time spent on the catalyst;^{2,9} whilst hard coke is distinguished from soft coke by its insolubility in chloroform or organic solvents.¹⁰ Increasingly, advanced characterisation techniques are being used to provide quantitative information allowing coke to be described in terms of its degree of order or graphiticity.^{7,11} For the purposes of this review, we will consider the role played by all carbonaceous

Department of Chemical and Biological Engineering, The University of Sheffield, Mappin Street, Sheffield S1 3JD, UK. E-mail: james.mcgregor@sheffield.ac.uk

species which are formed during reaction either on the catalyst surface or in the sub-surface region and which are not molecular products of the reaction. This therefore encompasses both deposits which are traditionally termed as “coke”, but also, *e.g.*, metal carbide phases which may form *in situ*. This attests to the nature of heterogeneous catalysts as dynamic entities which evolve throughout a reaction.

The structure of carbonaceous deposits depends on the reactant, and product, species from which they derive and from the nature of the site at which they form. For instance, coke deposited from linear molecules such as butadiene may be more linear in structure than that formed from cyclic or aromatic molecules.¹² However, even from a single reactant and a single catalyst there are many different coke structures that can be formed at different temperatures; they may vary for instance in terms of their reactivity towards oxygen, hydrogen and steam.² Considering the influence of the active site, it is noted that cracking plays a key role in coke formation at acidic metal oxide or metal sulphide sites, while metallic sites may form coke through hydrogenolysis reactions.^{2,13} Metal sites can also help to stabilise dehydrogenated carbonaceous deposits,^{14,15} and large metal particles are known to stimulate coke formation.^{16,17} A fuller description of the proposed mechanisms of coke formation can be found elsewhere.¹⁵

Another key factor in determining the structure of the coke formed is the reaction conditions employed. The role of temperature and pressure in determining the macrostructure of carbon deposits has been extensively studied. For example, studies of propylene pyrolysis on iron foil identified seven different macrostructures as temperature increased, from tubular whiskers around 723 K to spherical carbon particles above 823 K.² Studies of carbon deposits formed from steam reforming of hydrocarbons over nickel catalysts identified similar structures.¹⁸ Of note is the finding that increasing temperatures and pressures give rise to increasingly complex and graphitic coke nanostructures. Fig. 1 shows the increasingly complex structure of the carbon deposits formed from

cyclohexane on HY zeolite catalysts with increasing temperature.² Elsewhere, in studies of carbon deposits formed from steam reforming of hydrocarbons over nickel catalysts, pyrolytic (or graphitic) carbon was identified as being formed above 873 K. Similarly, in studies of butane dehydrogenation over $\text{VO}_x/\text{Al}_2\text{O}_3$ catalysts, the coke deposits were found to be more graphitic in structure at reaction temperatures above 873 K, as confirmed through THz-TDS studies.¹¹

2 Characterisation techniques

Understanding the role of carbon deposits in catalysis requires a full characterisation of the amount, composition, chemical nature and location of the coke.¹⁴ Several techniques must be employed as no one technique can capture all of this information. Techniques vary in their ability to measure bulk or surface properties, and some may be invasive or destructive.⁷ It is noteworthy that some recent studies have identified characterisation as a limiting factor, as the characterisation of catalysts did not reveal any differences that would explain the higher selectivity or activity of one catalyst over another.^{19–21} The importance of using a wide range of characterisation methods, ideally conducted simultaneously on the same sample, cannot be overstated.

The most common methods used in the surface characterisation of coke can be broadly categorised as described below. Only brief details are provided here; a number of excellent reviews of catalyst characterisation techniques exist in the literature which provide greater detail.^{22,23}

Vibrational spectroscopy

Vibrational spectroscopy techniques analyse the interactions between photons or particles with a surface and the resulting excitation or de-excitation. This category of technique includes infrared (IR) spectroscopy, Raman spectroscopy, THz-time domain spectroscopy (THz-TDS), ultraviolet-visible (UV-vis) spectroscopy and inelastic neutron scattering (INS). Additionally, electron energy loss spectroscopy (EELS) is also considered a vibrational technique; this is typically carried out in conjunction with transmission electron microscopy (TEM); *vide infra*.

IR spectroscopy can be used to identify the functional groups present in a sample, as these moieties will absorb IR radiation and produce a characteristic spectrum. However, this technique is only of limited use in the study of carbon deposits, due to the highly absorbing nature of coked catalyst samples which are often black in colour. Additionally, in the case of supported catalysts, strong absorptions from the support may obscure key features in the spectrum of adsorbed species. It is therefore important to also employ methods which can probe optically opaque samples.

Raman spectroscopy is of particular relevance in the study of coke, as the Raman scattering effect is dependent on the polarisability of the species, and thus can be used to indicate the degree of graphiticity of a carbon network.^{7,24,25}

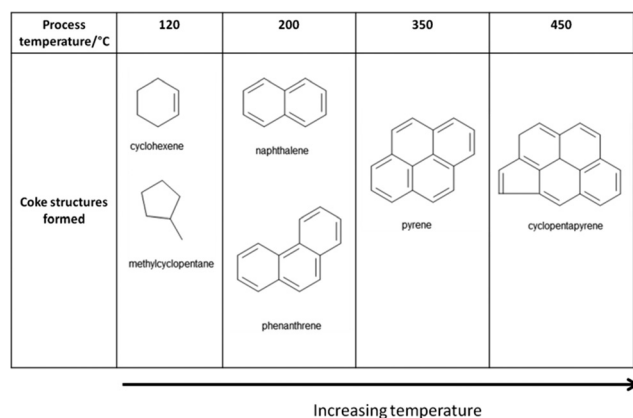


Fig. 1 The influence of reaction temperature on the structure of carbon deposits formed from cyclohexane on HY zeolite catalysts. Figure produced based on data available in Menon (1990).²

THz-TDS can also provide quantitative information on the degree of graphiticity in coke samples.^{11,26,27} Compared to IR and Raman spectroscopy, THz-TDS probes a lower energy region of the electromagnetic spectrum and is hence ideally suited to characterising low energy modes in extended graphitic-like networks.

UV-vis spectroscopy has found many applications in the study of coke deposits. Typical functionalities which can be identified by UV-vis spectroscopy include conjugated double bonds, aromatics, and unsaturated carbenium cations,²⁸ all of which are relevant to the study of coke deposits. Studies utilising UV-vis have identified polycyclic aromatics such as polymethylantracenes, dienylic and trienylic carbenium ions, dienes and polyalkylaromatics.^{28,29} UV-vis has also been used to detect an overlayer containing alkenyl carbenium ions on HY-FAU zeolites as a result of hydrocarbon adsorption.³⁰

Inelastic neutron scattering (INS) is an emerging technology in this field and can be applied to a range of materials. Due to the high neutron scattering cross-section of hydrogen it is particularly suited for analysing hydrogen-rich coke deposits. As with Raman spectroscopy, it is also able to probe optically absorbing samples.³¹ INS can provide information on how hydrogen is incorporated in a catalyst, which has applications in studying the role of hydrocarbonaceous deposits in catalysis, for example, in how they may facilitate hydrogen transfer. It has already been used in studies of hydrogen pre-treatment of catalysts³² and hydrogen retention in catalysts.³³

Thermal methods

Thermal methods involve heating the sample under a controlled atmosphere and either monitoring the species desorbed, for example by mass spectrometry, or monitoring the mass change of the sample. Among the most commonly utilised thermal methods in coke analysis is temperature programmed oxidation (TPO), which can yield information on the coke type and location on catalysts as peaks obtained at different temperatures correlate to different coke structures.^{34–37} Temperature programmed desorption (TPD) can yield information on the functional groups present on the surface of the carbonaceous deposit,^{38,39} such as carboxylic acids, lactones and quinones. Other variations on the above techniques include temperature programmed hydrogenation (TPH) and temperature programmed reduction (TPR).

Thermogravimetric analysis (TGA) is also widely used to quantify the amount of coke on a surface,^{40,41} and to characterise the composition of carbonaceous materials in terms of their fixed carbon content, moisture, ash content and volatile components.⁴²

Mass spectrometry methods

Mass spectrometry methods, such as secondary ion mass spectrometry (SIMS), can be used to analyse the deposits

present on the surface of a used catalyst by bombarding it with energetic primary particles and measuring the mass spectra of the secondary particles emitted. When combined with ion sputtering experiments (dynamic SIMS), this results in a technique with even higher resolution and sensitivity⁴³ which can reveal information about the chemical species present in coke. For example, it has been used to compare the chemical species present in coked alumina with anthraquinone thereby highlighting the similarity in structure between coke and anthraquinone in this case.⁴⁴

Electron microscopy and scanning probe microscopy

Scanning probe microscopy methods, such as atomic force microscopy (AFM) and scanning tunnelling microscopy (STM), are valuable techniques for obtaining high resolution images of the surface topography with minimal sample preparation. They are also relatively low cost as the equipment is relatively easy to construct and operate. Both AFM and STM work as stylus-style instruments, where a sharp probe scans the surface of the sample to detect changes in the surface and generate a signal. AFM detects the interaction force between the probe and the surface, whilst STM measures the surface electron density. Although imaging individual atoms is theoretically possible using AFM, it is in practise easier to achieve higher resolution images using STM, provided the sample is conductive.⁴³ Scanning Electron Microscopy (SEM) produces similar results to the above, but uses a beam of focused electrons rather than a scanning probe to produce an image, and can produce maps of the position of coke on the catalyst surface.¹¹

Transmission electron microscopy (TEM) can provide even higher resolution images, theoretically down to the atomic level, although in reality due to imperfections in manufacture or sample preparation this is not achieved. This has applications in studying changes in catalyst surfaces that occur as a consequence of reaction.¹¹ In combination with energy dispersive X-ray spectroscopy (EDX) and electron energy loss spectroscopy (EELS) it can be used to identify the chemical elements present on a catalyst surface, producing a compositional map on top of the microscope image. EDX is particularly sensitive to heavier elements, whilst EELS is better suited to those with lower atomic numbers, particularly from carbon to the 3d transition metals; in particular, EELS data can distinguish between different forms of carbon, such as amorphous and graphitic carbon, which has clear benefits in the study of carbon deposits.⁴⁵

Electron spectroscopy methods

Electron spectroscopy methods, such as Auger electron spectroscopy (AES) and X-ray photoelectron spectroscopy (XPS), can be applied to a variety of samples. These methods are typically associated with the production of ultraviolet (UV) radiation, which may cause disadvantages such as damage to sensitive materials. In XPS, the surface is irradiated with X-rays, which causes the emission of electrons due to

the excitation of core-level electrons. The kinetic energy of these electrons is related to the atomic or molecular environment of the atom of origin, and so can be used to identify the elements in the sample. This is particularly useful for quantifying the C/H ratio or degree of aromaticity in a coke sample.^{11,46} The number of electrons can provide information on the concentration of the emitting atom. AES works on a similar principle, but is based on the analysis of secondary electrons emitted following irradiation of the sample, known as Auger electrons. The energy of Auger electrons is characteristic of the element from which they were emitted. These techniques can provide information up to a depth of around 10 nm for atoms with a concentration greater than 1 mol% and can therefore, *e.g.*, yield approximate elemental surface compositions and oxidation states.⁴³

Developments have been made recently in “high pressure” XPS, which enables XPS of catalyst surfaces to be carried out under reaction conditions *i.e.* in a gaseous atmosphere rather than under high vacuum.⁴⁷ This technique has already been applied to studies of metal surface oxidation at mbar pressures to study oxidation states, oxide layer formation and kinetics.^{48–51} Applications of the technique in catalytic studies include CO oxidation on Pt/ceria catalysts,⁵² catalytic oxidation of propane over nickel catalysts⁵³ and the role of hydrogen pressure in the deactivation of platinum catalysts.⁵⁴

Ion scattering methods

The operating principle behind ion scattering methods is that the collision of an ion with a solid surface can provide information on the atomic masses on the surface (*e.g.* the amount of coke deposited) by measuring the spectra produced as a result of the impact. As these impacts happen on a faster timescale than thermal vibrations or collision cascades, the results are considered as indicative of the instantaneous condition of the surface. Examples include low-energy ion scattering (LEIS) or ion scattering spectroscopy (ISS), which uses low energy ions to gain information on the first and sometimes second and third atomic layers. Medium energy ion scattering (MEIS) and Rutherford backscattering (RBS) are examples of higher energy methods which provide information on deeper atomic layers.⁴³

Interference (diffraction) techniques

Interference or diffraction methods, such as X-ray diffraction (XRD) or neutron diffraction, are used to study the geometry and symmetry of a surface. A beam of X-rays or neutrons is incident on the sample, and the intensities of the diffracted beams are studied to give an indication of bulk structure. The method can be adapted to give information on the surface structure, such as symmetry and atom coordination number.

Since this method relies on the study of diffraction patterns, it is only suitable for the study of materials with long-range order which can produce such diffraction patterns – it is therefore unsuitable for materials which are polycrystalline

or amorphous, *e.g.* glasses or gels,⁴³ but can have applications in the study of ordered coke deposits.

Nuclear magnetic resonance (NMR) spectroscopy

NMR techniques have many applications in the study of coke deposits. Brønsted acid sites for example can be investigated using a number of techniques, such as ¹H, ²H, ¹³C, ¹⁵N or ³¹P NMR. ¹³C NMR played a key role in the discovery of the hydrocarbon pool mechanism by which carbon deposits play a catalytic role in the conversion of methanol to higher hydrocarbons²² – this process is discussed in section 3.3.2. In particular, ¹³C NMR spectroscopy is useful for studying the carbon structure and electronic environment of carbon, but is limited to use at relatively high coke contents, above approximately 3.5 wt%.^{24,55,56} ²⁷Al NMR has also been used to study changes in the aluminium chemical environment in zeolites due to coke deposition.⁵⁷

¹²⁹Xe and ¹³¹Xe isotopes also find applications in the study of coke deposits. These isotopes are particularly sensitive probes of their local chemical environment due to their large electron cloud, resulting in a large chemical shift range, and provide a solution to the problem of the inherently low sensitivity of most NMR techniques. They have for example been used in studies of coke formation inside zeolite cages.⁵⁸

Other techniques

A variety of additional methods are employed in the characterisation of coke deposits. Chemical methods such as Boehm titration are common for detecting the presence of acidic functional groups on the surface.^{7,59} Electron paramagnetic resonance (EPR), also known as electron spin resonance (ESR), spectroscopy can give information on the electronic structure and symmetry of a paramagnetic centre. It has therefore been used to study paramagnetism in coke samples (see section 3.2.1). Various elemental analysers are also available for measuring the elemental composition of a carbon sample, for example, the C:H ratio.

Combined techniques

The area of combined techniques is a rapidly developing field. No one individual technique is sufficient to provide all of the information required in order to understand how, for example, surface structure affects chemical reactivity. Demonstrated combinations of analytical techniques include NMR–UV-vis, UV-vis–Raman, FTIR–Raman and Raman–XRD.²² Additionally, a combined NMR–Raman set-up has recently been developed and applied to the study of catalytic metathesis.⁶⁰ The application of combined techniques allows coherent and complementary data sets to be obtained under the same reaction conditions and allow connections between two (or more) different sets of data to be drawn with much more confidence. It must be noted however that by combining techniques, a compromise is often required between, (i) the quality of one or more of the data sets, and (ii) the benefits of combined data sets.

3 The beneficial role of coke in catalysis

The beneficial role played by coke in heterogeneous catalytic reactions can take a variety of forms. Coke deposits may for instance enhance selectivity, either through improving the shape selectivity of zeolite pores or through selective poisoning of non-selective active sites; or the coke itself may be catalytically active, forming new active sites *in situ* for the reaction. The coke may instead facilitate hydrogen or hydrocarbon transfer or act as an intermediate in a variety of reactions. The various beneficial roles that coke deposits can play in a range of reactions are described below.

3.1 Enhancing selectivity through coke deposition

It is now well-established that coke deposits can lead to enhanced selectivity of products in a variety of reactions. A particularly well-studied example is the selectivation of HZSM-5 zeolites by pre-coking, particularly for isomerisation reactions such as xylene isomerisation.^{61,62} Reduced yields of undesired side products such as toluene and trimethylbenzene are obtained as a consequence of the formation of carbon deposits on non-selective acid sites which would otherwise promote undesired side-reactions such as transalkylation. There may also be shape selectivation effects due to pore narrowing and steric hindrance caused by the carbon deposits.⁶³ Coke deposits have also been proposed to act directly as the catalytically active sites in isomerisation reactions. This is discussed in section 3.3.3.

Pre-coking to improve selectivity in toluene disproportionation has been practiced industrially by ExxonMobil since the early 1990s through its Mobil selective toluene disproportionation process (MSTDPTM), where the catalyst is pre-coked with aromatic feedstocks at elevated temperature during the initial stages of the treatment; and subsequently through its Pxmax processes.^{62,64,65} Fig. 2 demonstrates how the pre-coking process reduces the yield of side-products over an HZ20 zeolite catalyst.

Fang and co-workers developed a five-stage reaction mechanism to explain how coke deposited during toluene disproportionation reactions led to an increase in *p*-xylene selectivity. This was attributed to the formation of coke on external catalytic sites on the zeolite as, in the initial stages of the reaction, coke was preferentially deposited on Brønsted acid sites in the channels, but no increase in selectivity was observed. This external coke modifies the surface acid properties of the zeolite, thus preventing secondary isomerisation reactions, leading to an increase in selectivity to *p*-xylene.⁶⁶ Similarly, the selectivity to *p*-xylene in toluene methylation reactions over ZSM-5 can also be increased through pre-coking of the zeolite.⁶⁷ This improvement is assigned to improved shape selectivity and deactivation of non-selective acidic sites.

The beneficial effects of coke on zeolite catalysts have also been demonstrated in ethylbenzene disproportionation,

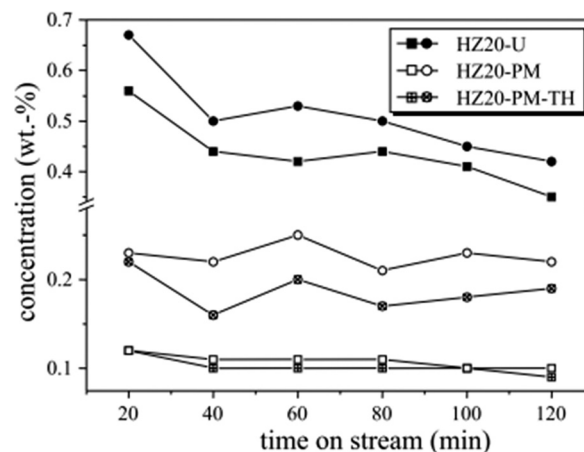


Fig. 2 Yields of by-products (squares = toluene; circles = trimethylbenzenes) for unmodified (HZ20-U), pre-coked (HZ20-PM) and hydrogen-treated (HZ20-PM-TH) catalysts in xylene isomerisation at 673 K. Lower concentrations of by-products result in improved selectivity to *p*-xylene.⁶² Reproduced with permission. Copyright 2001 Elsevier.

where coke is reported to be useful as a modifying agent for selectivation over H-ZSM-5.⁴¹ Pre-coking is also reported to improve selectivity towards benzene in the transalkylation of heavy aromatics. This however only occurs when pre-coking takes place in a hydrogen (rather than helium) atmosphere.⁶⁸ Elsewhere, pre-coking has been successfully applied to the isomerisation of *n*-butene^{69–71} over ferrierite catalysts. In this case, coke blocks the porous channels suppressing dimerization reactions.

It is not only on zeolites where pre-coking, and coke deposits laid down *in situ*, can improve selectivity. Ethylbenzene dehydrogenation to styrene over CrO_x/Al₂O₃ catalysts has recently been shown to proceed through a non-selective cracking regime prior to the dehydrogenation regime.²⁷ Coke deposition during the cracking period was speculated to decrease the catalyst acidity and to effect a reduction in chromium oxidation state thereby diminishing the competition between acid and metal sites, hence favouring the dehydrogenation reaction. Subsequent studies demonstrated that pre-coking with aromatics improved dehydrogenation activity and suppressed cracking.⁷²

Coke deposits have also been linked to changes in selectivity in hydrogenation reactions, *e.g.* of pentenenitrile over supported nickel catalysts.^{73,74} Additionally, the selective hydrogenation of alkynes to alkenes, which has important industrial applications, is also strongly influenced by carbon deposited during reaction. Over palladium catalysts, sub-surface carbon derived from the reactant acts to reduce over-hydrogenation of the alkene to the alkane.⁷⁵ This is discussed more fully in section 3.3.1.

3.2 “Active coke” on catalyst surfaces

The earliest unambiguous demonstration of the ability of coke to provide catalytically active sites dates from the 1970s;

namely the observation of the activity of carbonaceous deposits in the oxidative dehydrogenation (ODH) of ethylbenzene (EB) to styrene.⁷⁶ Since that time, further research has also identified the potential of coke deposits to catalyse non-oxidative dehydrogenation, while ammoxidation reactions on alumina were shown to proceed only when a certain amount of carbon had accumulated on the otherwise inert support.⁷⁷

It is however not surprising that coke deposits can directly catalyse reactions. The catalytic activity of unsupported carbon is well established, with carbonaceous materials known to catalyse a wide range of reactions, including oxidative dehydrogenation, alcohol dehydration, SO_x oxidation, NO_x reduction, catalytic wet air oxidation, halogenations and dehalogenation, decompositions of hydrazines and esterification of organic acids.⁷ It is therefore very likely that coke deposits play an important role in reactions beyond those described here.

3.2.1 Dehydrogenation and oxidative dehydrogenation.

The dehydrogenation of light alkanes is important in the chemical industry for the production of unsaturated hydrocarbons which are valuable as feedstocks for the production of other chemicals, such as plastics and polymers. The typical reaction temperature of this process is in excess of 873 K. As an endothermic process, it is however very energy intensive, while the high temperatures also contribute to deactivation of the catalyst. Oxidative dehydrogenation has therefore been investigated as an exothermic process that can be carried out at lower temperatures of around 623 K. The role of coke deposits in both oxidative and non-oxidative dehydrogenation will now be discussed in more detail.

Oxidative dehydrogenation. The first observation of the catalytic activity of coke deposits was in the oxidative dehydrogenation (ODH) of ethylbenzene (EB) to styrene. It was noted that carbon deposits did not cause deactivation even after extended times on stream.^{78,79} Subsequent studies by Kim and Weller showed that there was no loss of BET surface area or activity over 20 hours, even though coke was continually deposited, reaching levels of 12–13 wt%.⁸⁰ The conclusion that activity was due to the deposited carbonaceous material was subsequently reinforced by the demonstration that activated carbon and carbon fibres are active catalysts for this reaction.^{81–91}

The mechanism by which coke, and unsupported carbon catalysts, catalyse EB ODH has been extensively investigated. Coke deposits reduce the acidity of the alumina catalyst, which is thought to be beneficial for dehydrogenation activity.²⁷ However, it has also been shown that ethylbenzene reacts with quinolinic oxygen functionalities formed on the carbon surface to produce styrene. The reduced surface is then re-oxidised by gas phase oxygen or another oxidant.¹² This area has been the subject of several reviews,^{92–94} and methods of exploiting the role of coke in this reaction continue to be the focus of several contemporary studies.^{19,95}

Carbon deposits may also play a role in catalysing the ODH of *n*-butane, as these reactions have been shown to be

catalysed by coals, where the reaction selectivity is increased as the coal rank is increased, although the overall butane conversion is decreased.⁹⁶ Many other oxidative dehydrogenation reactions have been shown to be catalysed by carbonaceous materials employed directly as catalysts. A number of examples are discussed in a detailed review by Qi and Su including the carbon nanotube-catalysed conversions of ethane to ethene, propane to propene, butane to butene, butane to butadiene, ethanol to acetaldehyde and 9,10-dihydroanthracene to anthracene.⁹⁷ Other catalytically active carbonaceous materials in ODH reactions include graphene oxide in the conversion of isobutane to isobutene, and amorphous carbon in the ODH of 2-butanol to 2-butanone.⁹⁷ It is therefore feasible that coke deposits may be catalytically active in these reactions.

Non-oxidative dehydrogenation. Non-oxidative dehydrogenation (DH) reactions have also been shown to be catalysed over carbon deposits. In a study by Amano and co-workers, the dehydrogenation of cyclohexane was observed to occur on a coked alumina catalyst under non-oxidative conditions, but only isomerisation reactions were observed on the pure alumina catalyst.⁴

Considering the DH of *n*-butane over VO_x/Al₂O₃ catalysts, it was found that the increase in butadiene production with time-on-stream was not concurrent with a decrease in the selectivity towards 1-butene, indicating the formation of a new catalytic site during reaction, *i.e.* carbonaceous deposits.¹¹ A schematic of this is shown in Fig. 3. The studies also found that the coke completely encapsulated the vanadium oxide catalyst, preventing access to VO_x sites, but without deactivating the catalyst, thus providing further evidence for the catalytic role of the coke deposits. The catalytic activity of coke deposits in ODH and DH reactions was confirmed by comparing the activity of coke deposits with that of unsupported carbon nanofibres, which were also shown to be catalytically active.^{11,19}

Nature of active sites. Some studies on oxidative dehydrogenation reactions concluded that the active sites for

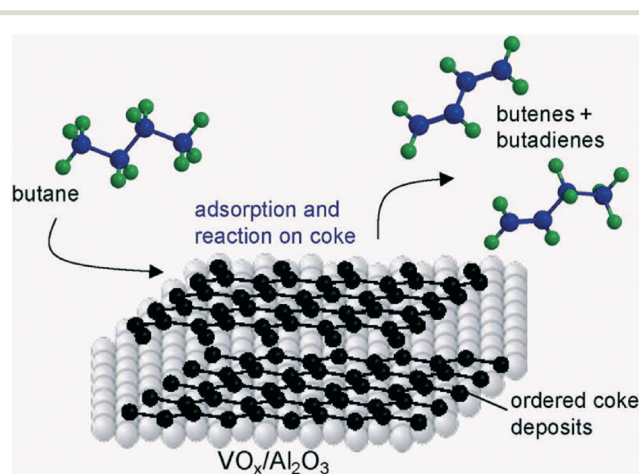


Fig. 3 Coke deposits on VO_x/Al₂O₃ provide the catalytically active sites for *n*-butane dehydrogenation at 973 K. Reproduced with permission.¹¹ Copyright 2010 Elsevier Inc.

such reactions over coked catalysts are oxygen-containing surface groups, such as quinones or hydroxyls.^{44,78,85,86,92,93,98} However, studies of the catalytic activity of carbon deposits in dehydrogenation reactions under non-oxidative atmospheres showed that they exhibit very similar behaviour (albeit at a higher temperature than ODH), although no oxygen is present in the coke deposits.¹⁹ In the latter case at least, it is therefore likely that defects in the coke structure form the active sites.

The formation of these defects may include the breaking of carbon-carbon bonds in otherwise ordered carbon deposits, and thus the presence of unpaired electrons, or paramagnetism. The degree of paramagnetism has been linked to the catalytic activity of coke samples using EPR, thereby suggesting they may act as the active sites.^{11,78,84,92} Similar behaviour was also found on zirconia catalysts, on which the active site had previously been identified as tetragonal phase zirconia. However, carbon deposition was a common feature which better explained the similarities in dehydrogenation behaviour.⁹⁹ Further experimental and theoretical investigations are required in order to definitively identify the role of defects and paramagnetism in the catalytic activity of coke deposits.

Role of graphitic structure. Catalytic activity in non-oxidative dehydrogenation also appears to be related to the structure of the coke deposits formed, with several studies finding that increased graphitic order in carbon deposits correlates with increased catalytic activity.^{11,37} The extent of graphitisation required in order to exhibit this activity is however unclear, although terahertz spectroscopy studies by McGregor *et al.* indicated that it was likely to require more than 7 aromatic rings.¹¹ Carbon deposits shown to be active in non-oxidative cyclohexene dehydrogenation were also characterised as having a graphite-like structure.⁴ Considering ODH, studies on coal samples in the ODH of *n*-butane also found increased selectivity to butane with increased graphiticity, although a lower overall conversion was achieved.⁹⁶

3.2.2 Ammoxidation. Ammoxidation is the reaction of *e.g.* carbons with a mixture of ammonia and air, typically at temperatures between 523 and 673 K.¹⁰⁰ Carbonaceous deposits formed in alumina pores have been shown to be catalytically active for the ammoxidation of ethylbenzene⁷⁷ and toluene.¹⁰¹ Alumina is inactive until a certain quantity of carbon has accumulated on the acid sites of the inert support; the carbon deposits then provide active sites in a similar manner to dehydrogenation reactions (section 3.2.1), with catalytic activity again correlated with the concentration of carbon radicals, *i.e.* the degree of paramagnetism.¹⁰¹ It has been noted both in ammoxidation reactions and elsewhere that nitrogen-containing coke can be more catalytically active than that which does not contain nitrogen. For example, in the ODH of ethylbenzene with nitrobenzene, the use of nitrogen-containing cokes (produced using nitrobenzene and aniline) resulted in a higher conversion than coke which contained negligible nitrogen.⁷⁷ The structure and role of nitrogen

moieties in catalytic carbons has previously been the subject of in-depth characterisation.²⁶ Elsewhere, the inclusion of heteroatoms such as nitrogen have been shown to improve the performance of graphene in a range of catalytic applications.⁸

3.3 Hydrogen and hydrocarbon transfer

Reactions involving hydrogen and hydrocarbon transfer are widely used in the chemical industries to produce a variety of chemicals. Hydrogen transfer reactions may include hydrogenation and dehydrogenation, whilst hydrocarbon transfer reactions are important for the conversion of hydrocarbons to other chemicals, for example methanol-to-olefin reactions. These types of reactions are widely studied and the roles of carbon deposits in facilitating and catalysing these reactions are increasingly well understood, and are discussed further below.

3.3.1 Hydrogen transfer reactions. Carbonaceous deposits can facilitate hydrogen transfer in both alkene hydrogenation and catalytic cracking reactions, in addition to effecting the reduction of a catalytic metal site. In processes such as coal liquefaction, both hydrogenation and cracking reactions are involved.¹⁰² Thomson and Webb were among the first to suggest that the hydrogenation of alkenes on metals may not be the result of direct addition of hydrogen from the gas phase to the adsorbed alkene, but instead a hydrogen transfer reaction between an adsorbed hydrocarbon and the adsorbed alkene.¹⁰³ This mechanism may be behind the reported insensitivity of some alkene hydrogenation reactions to the nature of the metal used.^{103,104}

Hydrogen transfer from adsorbed carbon species also has analogies to liquid-phase hydrogenation systems where hydrogen-donating solvents such as tetralin are employed. The hydrogen-donating ability of tetralin is due to the hydrogens in the saturated ring being activated by the adjacent aromatic ring. This leads to a reduction in non-selective coke formation in hydrogenation and cracking reactions, as the tetralin donates hydrogens to satisfy the supply of free radicals formed.^{102,105} It has been suggested that the hydrogen carrier is the ethylidene radical.¹⁰⁶ Upon hydrogen-transfer, tetralin is dehydrogenated to naphthalene, which is then rehydrogenated to tetralin by the gaseous hydrogen supplied, usually in the presence of a palladium catalyst.¹⁰⁷ As aromatic rings are a common feature of coke molecules, it is likely that aromatic coke molecules can act as hydrogen-donors in a similar manner to the more established mechanism involving aliphatic carbon deposits.

The nature of the coke precursor plays an important role in determining the influence of coke deposits on reaction. For example, carbonaceous deposits from *cis*-2-pentene were shown to activate the hydrogenation reactions of *trans*-2-pentene to *n*-pentane, and *vice versa*.⁷⁴ A similar effect was found for the catalytic wet air oxidation of phenol reaction, whereby the origin of the coke had a greater influence on the subsequent phenol conversion than any surface modifications made to it.²⁰

3.3.2 Hydrocarbon transfer reactions

Methanol-to-hydrocarbons. Methanol-to-olefin (MTO), methanol-to-aromatics (MTA) and methanol-to-hydrocarbon (MTH) reactions – generally MTX – are of increasing industrial interest as a means to generate valuable products in the so-called “methanol economy”. Significant industrial application of this process is already established. MTX processes provide a means to form longer chained products from a C1 substrate.³ Hydrocarbonaceous deposits play a key role in these reactions as part of the hydrocarbon pool mechanism.^{3,108,109}

In the hydrocarbon pool mechanism methanol is first adsorbed onto the surface of the catalyst, typically ZSM-5 or SAPO-34, where it is subsequently converted to carbonaceous deposits to form a hydrocarbon pool. This pool then plays a role in the conversion of further methanol molecules to higher hydrocarbons, which then desorb from the hydrocarbon pool as products, as indicated schematically in Fig. 4. The structure of this pool is thought to be methyl-aromatic in nature (*e.g.* xylene, toluene).¹¹⁰ Fig. 5 shows a detailed proposed mechanism, indicating the role that both hydrocarbon and hydrogen transfer processes play in the production of olefins. In MTO it has been observed that the activity and selectivity over a zeolite catalyst increases with coke content

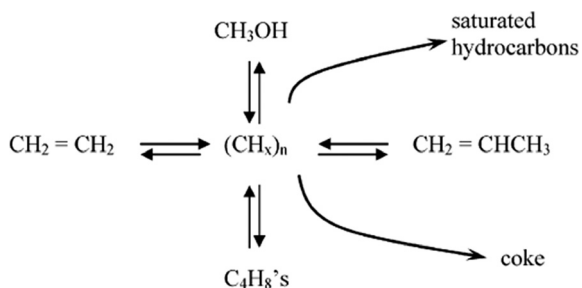


Fig. 4 The simplified hydrocarbon pool mechanism over SAPO-34, as proposed by Kolboe;¹⁰⁸ figure taken from.³ Reproduced with permission. Copyright 2011 Royal Society of Chemistry.

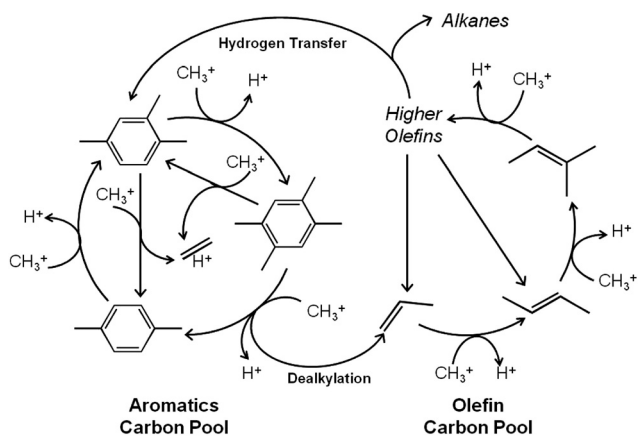


Fig. 5 The hydrocarbon pool mechanism over HZSM-5.¹¹² Reproduced with permission. Copyright 2013 American Chemical Society.

up to 5 wt% coke,¹¹¹ correlating with the formation of the pool. It is worth noting that not all of the hydrocarbon pool is reactive or accessible, as shown in ¹³C NMR studies.²²

It has been speculated that the initial hydrocarbon pool may form as a result of trace impurities in the feed, such as aldehydes, ketones and higher alcohols, rather than from the methanol directly.¹¹³ In one study, in the absence of a hydrocarbon pool, the conversion of methanol to hydrocarbons over a solid acid catalyst was only 0.0026%, but after three identical pulses of methanol, the conversion dramatically increased to almost 10%, indicating that the adsorbed impurities had a catalytic effect on MTX reactions.¹¹³

Homologation. Homologation reactions are reactions in which large molecules react with smaller fragments to form the next molecule in the homologous series.^{114,115} Menon proposed a two stage mechanism for methane homologation whereby CH_4 initially reacts with the catalyst to form carbidic coke, with the coke then reacting with hydrogen to form ethane.¹¹⁶ The same process also applies to alkene homologation. That reactive carbon plays a role in homologation is supported by the finding that the quantity of reactive carbon formed in methane-propylene homologation correlated with the C4 yield.¹¹⁷ The ease of migration of carbon from the metal to the support is thought to be responsible for the greater selectivity in these reactions, however this depends on the type of support, which determines the reactivity of the coke formed.¹¹⁸

3.3.3 Pore mouth catalysis. Coke molecules located at pore openings (*i.e.* the pore mouth) may interact with protonic sites. These hybrid organic-inorganic sites have been proposed as selective active sites for the conversion of methanol over SAPO-34, for isomerisation reactions and for alkylation processes.¹¹⁹ Examples of these are now discussed below.

Isomerisation. The skeletal isomerisation of *n*-butenes to isobutene is an important reaction as isobutene is employed in the production of MTBE (methyl *tert*-butyl-ether), an octane enhancer for petrol.¹²⁰ Improvements in selectivity have been documented to coincide with the formation of carbonaceous deposits.^{70,121–123} While it had been proposed that this was due to modification of the pore diameter in the HFER zeolite catalysts employed,^{71,124–126} it was observed that high selectivities were obtained even with the pores entirely blocked.⁵⁶ It was therefore proposed that the reaction proceeds *via* the formation of carbocations from the carbon deposits, which act as the active site.^{122,127} A schematic of this process is shown in Fig. 6. Pore-mouth catalysis has also been implicated in the hydroisomerisation of long-chained alkanes. For example, employing platinum modified zeolite catalysts at temperatures of 453–550 K, Marten and co-workers obtained yields of branched alkenes inconsistent with a classic bifunctional reaction mechanism, implicating pore-mouth catalysis as the key step in the process.¹²⁸

Alkylation. Pore mouth catalysis is also believed to play a role in alkylation reactions, such as the alkylation of toluene and the isopropylation of naphthalene. The former reaction is of commercial interest as the product, *p*-xylene, is an

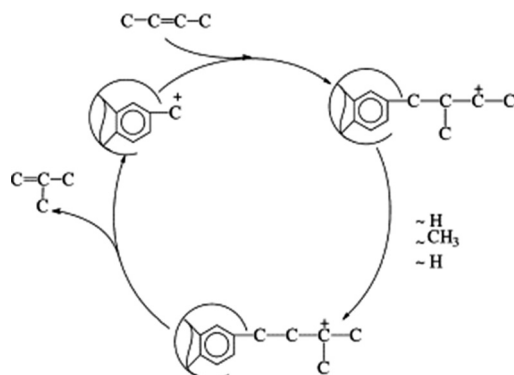


Fig. 6 Schematic of the mechanism of pore mouth catalysis in isomerisation reactions. Reproduced with permission.¹¹⁹ Copyright 2002 Elsevier.

important precursor for the production of polyester fibres. Da and co-workers investigated the alkylation of toluene with 1-heptene at 363 K, observing that the concentration of bi- and tri-alkylated toluene molecules trapped within the pores decreased over time, even after total consumption of 1-heptene had occurred, as a result of the transalkylation with toluene at the pore mouth.¹²⁹ This also suggests a mechanism whereby catalysts which have been deactivated through pore blockage can be regenerated through treatment with toluene, thereby removing trapped molecules *via* this same process. The isopropylation of naphthalene over HFAU and HBEA zeolites shows an increase in conversion with time, despite a rapid decrease in the micropore volume of the catalysts accessible to nitrogen to a negligible value. This is consistent with the involvement in the reaction mechanism of alkylated naphthalenic species trapped at the pore mouth.¹¹⁹ Another study identified pore mouth catalysis as the mechanism of alkylation of naphthalene and toluene.¹³⁰

Coke has also been observed to cause the alkylation of *p*-xylene in FCC catalysts through TEOM (tapered element oscillating microbalance) studies. In the absence of coke, no reaction was observed. It was also observed that acidic sites were necessary for this process, as when the sites were neutralised with quinoline, no alkylation activity was observed.¹³¹ This indicates that coke deposits can be catalytically active in alkylation reactions, and appear to facilitate alkylation in the presence of acidic sites.

3.4 *In situ* carbide formation

Increasingly, studies are investigating the role that metal carbides may play in catalysing reactions. In addition to their application as catalysts directly, metal carbides can also be formed *in situ* from the reaction of hydrocarbons with metal atoms, and may form in a wide range of reactions. It is therefore important to understand their effects on catalytic processes.

3.4.1 Selective alkyne hydrogenation over PdC_x. Selective hydrogenation of alkynes is a particularly important process for improving the quality of alkene streams, particularly the removal of acetylene impurities in ethylene feeds,¹³² and to

prevent the poisoning of polymerisation catalysts by alkynes.¹³³ A particularly noteworthy example of catalytically active carbides and related species is the formation of a PdC_x phase, which has been shown to enhance the selectivity of alkyne hydrogenation towards alkenes. The selectivity of non-promoted palladium to alkenes is fairly low (*e.g.* selectivity to propene is less than 20% when the H₂:propyne ratio is greater than 2¹³²), but the formation of carbide phases leads to an increase in alkene selectivity by destabilising alkenes adsorbed on the surface (*i.e.* they desorb before further hydrogenation can occur), and by inhibiting the formation of the high energy, unselective, sub-surface hydrogen that promotes over-hydrogenation.^{132–134} Smaller palladium particles reduce the amount of coke formed, and thus inhibit the formation of the PdC_x phase, leading to a decrease in the selectivity of the reaction towards alkenes.¹³⁵ Other experimental studies observed that less carbon was dissolved in the palladium catalyst during unselective hydrogenation as compared with selective hydrogenation.⁷⁵

DFT studies have confirmed this hypothesis, for example, one study found that the formation of subsurface carbides and hydrides improves selectivity of acetylene hydrogenation by weakening the surface-adsorbate bond,¹³⁶ and recently published work by Yang and co-workers has also concluded that a carbide phase forms the catalytically active phase in the selective hydrogenation of acetylene through studies of Pd(100) and Pd(111).¹³⁷ Kitchin and co-workers also found that the formation of a metal carbide phase inhibits the formation of non-selective sub-surface hydrogen in other early transition metals, implying that this may be relevant to alkyne hydrogenation over catalysts besides palladium.¹³⁸ A schematic of the palladium surface structure can be seen in Fig. 7.

Particular examples of reactions where the PdC_x phase has been shown to improve catalytic performance include the selective hydrogenation of butadiene,¹³⁹ propyne¹³² and

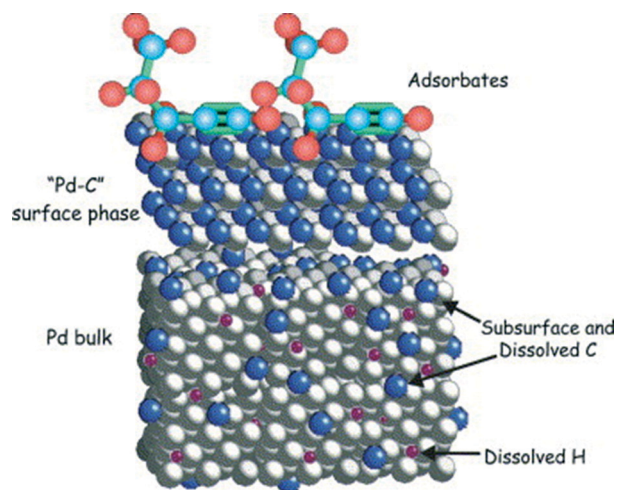


Fig. 7 Model of the palladium surface demonstrating the role of the palladium carbide phase during 1-pentyne hydrogenation.¹³⁴ Reproduced with permission. Copyright 2006 Elsevier.

1-pentyne.^{75,134,140,141} This phase has also been shown to form during the decomposition of acetylene¹⁴² and the acetoxylation of ethylene.¹⁴³ The mechanism of the formation of the PdC_x phase is still being studied, but is thought to involve hydrocarbon fragmentation to form atomic carbon, which penetrates the palladium lattice, thereby preventing the formation of a sub-surface hydride phase.^{134,141} Heating the lattice leads to a decrease in catalytic activity, suggesting that the phase is only metastable.¹³⁴

3.4.2 Fischer–Tropsch synthesis and CO methanation.

Fischer–Tropsch (FT) synthesis is the processes whereby carbon monoxide and hydrogen are converted into a variety of hydrocarbonaceous products, most commonly on ruthenium, iron and cobalt catalysts.¹⁴⁴ FT reactions were noted to be ‘coke-insensitive’ by Menon, meaning that the deposition of coke did not lead to a decrease in catalytic activity.² The formation of carbon deposits could also have beneficial effects, such as preventing the formation of metal carbonyls and their subsequent volatilisation, which can lead to as much as 40 wt% loss of the metal.¹⁴⁵

There is a general consensus in the literature that whilst graphitic carbon can deactivate the catalyst used in FT synthesis, carbidic carbon formed *in situ* on iron catalysts may act as an intermediate.^{2,146} Studies employing isotopically labelled carbidic carbon noted that the ¹³C was contained mostly in the methane, rather than in higher hydrocarbons, directly implicating carbides in the methanation reaction; itself an important process as well as a side-reaction in FT.¹⁴⁷ Additionally, a reactive carbonaceous pool has been proposed as part of the mechanism for the synthesis of aromatics from FT.²

The role of carbides is dependent upon the metal employed; it is generally accepted that iron carbide, rather than metallic iron, is the stable and active phase in ferrous catalysts, although the particular form which is responsible for the activity is still a matter of debate.^{148,149} Cobalt carbides however are inactive in FT synthesis,¹⁵⁰ and the formation of carbon deposits and carbides on cobalt catalysts contributes to their deactivation.^{151,152}

Iron carbide nanoparticles may also act as active sites for the chemisorption of CO to form monomers for polymerisation, leading to the formation of higher hydrocarbons.^{153–158} Methanation may also be more likely to occur at iron carbide sites, whereas lower olefins may be produced at terraced sites promoted by alkali metals.¹⁵⁹ The factors affecting catalyst performance in FT synthesis are the subject of a recent review, and further developments in catalysts for Fischer–Tropsch synthesis can be found therein.¹⁴⁴ While CO is typically the carbon source in FT and methanation reactions, increasingly CO₂ is being employed as a feedstock in these processes, with a view to utilising gas captured from point sources. The reaction mechanism for CO₂ involves breakdown to CO,¹⁶⁰ hence carbides will play the same role in these processes as they do for conventional CO reactions.

3.4.3 Molybdenum oxycarbides. The catalytically active molybdenum oxycarbide has been shown to improve

selectivities in isomerisation of *n*-heptanes and higher hydrocarbons, a significant advancement over other studies which claimed that this could not be performed selectively over acid catalysts without excessive side-product formation due to cracking.¹⁶¹ The carbon atoms are thought to fill some of the vacancies in the molybdenum oxide phase, stabilising the phase and leading to the formation of a catalytically active carbide phase *in situ*. Ledoux *et al.* proposed a bond-shift mechanism for the selective isomerisation of alkanes over molybdenum oxycarbide.¹⁶¹ The same oxycarbide phase has also been demonstrated to be selective for the dehydrogenation of short-chain alkanes.

3.5 Other reactions

Coke has the potential to be catalytically active in other reactions as indicated by the wide application of carbon based catalysts. This section introduces a number of systems where coke is known to, or may, play a key role; although in some cases further mechanistic investigations may be required in order to elucidate the true reaction mechanism.

3.5.1 Oxidative coupling. Oxidative coupling is used to produce a variety of important chemicals, such as imines for the synthesis of nitrogen-containing compounds for the biological and pharmaceutical fields,¹⁶² while the oxidative coupling of methane (OCM) followed by oligomerisation has been proposed as a means to exploit stranded natural gas fields.¹⁶³ These reactions are typically catalysed by transition metals, but carbon-based catalysts have also found applications in this area. For example, oxidative coupling of phenol is known to occur on activated carbon catalysts, leading to the formation of phenol dimers and phenolic polymers.¹⁶⁴ The role of carbon, either from coke or as a catalyst, in this process is as an oxygen radical generator, causing the formation of dimers and phenolic polymers by oxidative coupling, which ultimately leads to the deactivation of the catalyst through pore blockage.^{20,21} In studies of OCM over metal catalysts using ¹³C-labelled methane it was shown that the carbon formed was a reactive intermediate in methane oligomerisation and methane-alkene coupling reactions;^{116,165} coke deposits are likely to participate in a similar way. OCM continues to be a topic of contemporary interest, *e.g.* through the recent EU Framework 7 OCMOL project.^{166–168}

3.5.2 Metathesis. Metathesis reactions involve the exchange of bonds or substituents between two molecules. It is thought that hydrogen transfer, possibly facilitated by coke deposits, plays a role in deactivating the non-selective active sites, allowing metathesis to occur.^{126,169} Metathesis catalysts such as WO₃/SiO₂ do not appear to exhibit deactivation, even at coke contents as high as 49 wt%; although the coke was deposited on the silica support rather than the tungsten in this study.⁴⁰ Other studies have found that tungsten oxide is inactive for metathesis.^{170,171} If active sites are still available for the metathesis reaction at such high coke contents, it is plausible that the carbonaceous deposits are in fact providing them.

3.5.3 Reforming. Carbon deposits have also been recognised as having a positive role in hydrotreating

processes. Hydrotreating involves the reduction of sulphur, nitrogen and aromatic content in crude oil refining. It is assumed that the carbon enhances the number, rather than nature, of the active sites, as there is no evidence of the carbon deposits facilitating an increase in selectivity. This leads to a reported 60% increase in catalytic activity, whilst carbon-free catalysts show a noticeable deactivation of 25% after 18 hours on stream. Pore plugging has been ruled out in this case as there was no significant change in porosity of the catalyst. Both aliphatic and aromatic carbon were detected by ^{13}C NMR, and it was suggested by the authors that the carbon deposits improved the stability of the active phase by restricting the migration of $(\text{Co})\text{MoS}_2$.¹

It is also noteworthy that carbon has shown beneficial properties in several studies as a support material for hydro-treating catalysts, as they are resistant to coke deposition and have a higher catalytic activity per unit mass of catalyst in comparison with traditional alumina-supported hydrotreating catalysts.^{172–174} The active site however is believed to be Ni, Mo and S nanoparticles,¹⁷² but the carbon does play a chemical role by inhibiting metal–support interactions, thus improving sulfidation.¹⁷⁵ Aryee *et al.* report that several forms of carbon have been used as supports for hydrotreating catalysts, including activated carbon and carbon nanotubes.¹⁷⁵ However, it is expected that alumina will continue to be the more popular choice of catalyst support due to its higher mechanical strength and functionality *versus* that of activated carbon.¹⁷²

3.5.4 Reactor wall coking. Coke formation on reactor walls may also play a role in promoting reactions. In these cases the material out of which the reactor is constructed can have a significant effect on the reaction, as stainless steel reactors, for example, may catalyse the formation of catalytically active coke on the walls.¹⁷⁶ In such examples, the incorporation of metal from the reactor wall into the coke may strongly influence catalytic behaviour. However, the unrecognised participation of the reactor walls in reactions makes it difficult to determine the proportion of the reactivity coming from the catalyst as opposed to from the walls.¹⁷⁷

A study carried out by Gornay *et al.* aimed to determine the role of the carbon deposited on the walls in the pyrolysis of octanoic acid.¹⁷⁸ The reactor walls were found to catalyse coke formation, particularly reactor walls containing Fe and Ni, but it was then found that the coke deposits had an ‘accelerating’ effect on the pyrolysis of octanoic acid. This was attributed to the Fe and Ni metal content of the coke, which was incorporated into the coke from the reactor walls;¹⁷⁸ these metals are known to be catalytically active.

Note that while most industrial reactors are fabricated from metallic materials such as stainless steel, many laboratory research reactors are constructed from quartz or other glass. In these cases, while the laboratory studies provide insights into the fundamental reactions occurring on the catalyst surface they will not identify the potential role of the reactor wall, and any coke formed there, in industrial application.

Studies have also been carried out on the influence of metal impurities in carbon nanotube catalysts, as they are often prepared using supported-metal catalysts, which may remain as metallic contaminants.⁸⁸ This has been investigated by treating carbon nanotubes through refluxing in strong acid to remove metal contaminants; the quantity of residual metal was then measured by X-ray fluorescence spectroscopy. These studies confirmed that the quantity of metal was very low (around 0.1%), and that it was not present on the surface, only in the bulk. Further studies deliberately added iron to carbon nanotubes, and concluded that the selectivity to alkene conversion decreased with increasing iron content.⁸⁸

4 Implications for process development

A better understanding of the role of catalytically active coke deposits holds much potential for improving the efficiency and sustainability of catalytic processes, as well as the development of novel catalytic materials. These implications are discussed below.

Tailored materials synthesis

The deliberate exploitation of carbon deposits has promise for future catalytic process development, with the ability to tailor different carbon (nano)structures for specific purposes. Additionally, the understanding gained from these studies can in some cases inform the design of novel catalysts based on the beneficial coke structures observed. In a study on oxide/carbide transition reactions on iron surfaces, carbide particles were shown to catalyse graphitic filament growth.¹⁷⁹ Other studies have investigated the use of lasers to produce carbon composites with particular nanostructures, for example, incorporating metal ions to increase heat dissipation and thus enhance graphitisation of the carbon matrix,¹⁸⁰ or functionalisation of carbon nanotubes for use as catalysts for a number of applications, *e.g.* in fuel cells.^{181,182}

Another method for producing materials with desired characteristics is by using surface treatments. These can be generally classified into chemical, physical and biological types. When considering chemical surface treatments, acidic treatments for example can provide materials with more hydrophilic surfaces and more acidic character, whilst basic treatments may produce catalysts well suited for adsorbing negatively-charged species in greater amounts.¹⁸³

Sustainability

Through understanding the role of carbon, the sustainability of heterogeneous catalysis can be improved in a number of ways.

Metal-based catalysts are increasingly becoming unsuitable for commercial use due to their high cost and limited reserves,^{8,16} and so catalysts made from carbon, either with or without metals present, may provide a more sustainable and economic alternative. This new class of carbon-based

catalysts may also open up new reaction pathways utilising more sustainable raw materials instead of fossil fuels.¹⁸⁴ Furthermore, metal carbides are able to catalyse many reactions which currently employ rare platinum group metals (PGMs), a phenomenon ascribed to the similarity in electronic structure between carbides and PGMs.¹⁸⁵ Elsewhere, understanding the role of carbon may also allow carbonaceous by-products of the biomass industry, such as biochar, to find applications in heterogeneous catalysis,¹⁸⁶ or it may aid in the catalytic conversion of biomass to useful raw materials, such as the hydrogenation of cellulose.¹⁸⁴

The deliberate formation of catalytically active coke could also be used to enhance activity or selectivity.⁷⁴ Improving the selectivity of reactions reduces the amount of raw material that is wasted, and also reduces the energy and economic costs needed to separate the desired products, thus improving the sustainability of the process.

5 Conclusions and outlook

Whilst coke is perhaps best known for causing catalyst deactivation, this review has shown that coke can also play various beneficial roles in catalysis in a wide range of reactions and through a variety of mechanisms. Pre-coking of zeolites is commonly used industrially to improve the selectivity of isomerisation reactions, whilst in other processes the coke may be catalytically active and provide the active sites for reaction. This can result in increased selectivity and/or catalytic activity, depending on the process and the particular mechanism by which coke catalyses the reaction. The range of reactions known to be catalysed by structures or phases formed as a result of carbon deposition includes ODH (e.g. ethylbenzene to styrene, butane to butene, ethanol to acetaldehyde), non-oxidative dehydrogenation, hydrogenation, ammoxidation, methanol-to-hydrocarbon reactions, homologation, isomerisation, alkylation, Fischer-Tropsch synthesis, CO methanation, oxidative coupling, metathesis and reforming.

Given that coke can be catalytically active in such a wide range of processes, it is unsurprising that the mechanisms by which it can enhance catalytic activity vary between processes, and as a result, different coke structures can be beneficial depending on the particular reaction. For example, polyaromatic coke deposits may facilitate hydrogen transfer in hydrogenation reactions, whilst the formation of a metal carbide phase has been shown to enhance the selectivity of alkyne hydrogenation. Increasingly graphitic and paramagnetic coke is thought to be particularly effective in ammoxidation and oxidative dehydrogenation reactions, where it is believed to act as the active site. The hydrocarbon pool mechanism in methanol-to-hydrocarbon reactions, whereby coke is involved in the reaction mechanism through hydrocarbon transfer reactions, is another example of the activity of carbonaceous deposits.

Active coke deposits need not form only on the catalyst surface. Coke formed on reactor walls can also play a

catalytic role. In these cases some metal atoms from the reactor wall may be incorporated in the coke deposits. In other systems the inclusion of heteroatoms such as nitrogen, oxygen, boron or sulphur in carbon structures can increase catalytic activity.

Through understanding the beneficial role of coke deposits in catalysis, there are many implications for future process development. For example, it may lead to the development of nanostructures tailored for specific reactions. It could also lead to improved process sustainability; metal-based catalysts are becoming increasingly unsuitable due to their limited reserves, making carbon catalysts a more sustainable alternative. This could include the use of carbonaceous by-products such as biochar as catalysts, for example. These new catalysts may also open up more sustainable reaction routes, using more sustainable feedstocks or lower energy pathways. Increased selectivity also has clear advantages for reducing separation costs and the associated energy costs, resulting in a more sustainable and economic process.

Acknowledgements

The authors acknowledge the many and varied inputs from colleagues and collaborators over a number of years which have contributed to the development of this field.

References

- 1 C. Glasson, C. Geantet, M. Lacroix, F. Labruyere and P. Dufresne, *J. Catal.*, 2002, **212**, 76–85.
- 2 P. G. Menon, *J. Mol. Catal.*, 1990, **59**, 207–220.
- 3 J. L. White, *Catal. Sci. Technol.*, 2011, **1**, 1630.
- 4 H. Amano, S. Sato, R. Takahashi and T. Sodesawa, *Phys. Chem. Chem. Phys.*, 2001, **3**, 873–879.
- 5 R. Schlögl, in *Advances in Catalysis*, 2013, vol. 56, pp. 103–185.
- 6 P. Serp and E. Castillejos, *ChemCatChem*, 2010, **2**, 41–47.
- 7 P. Serp and J. L. Figueiredo, *Carbon Materials for Catalysis*, John Wiley and Sons Inc., Hoboken, New Jersey, 1st edn., 2009.
- 8 X.-K. Kong, C.-L. Chen and Q.-W. Chen, *Chem. Soc. Rev.*, 2014, **43**, 2841–2857.
- 9 J. G. McCarty and H. Wise, *J. Catal.*, 1979, **57**, 406–416.
- 10 C. E. Snape, M. C. Diaz, Y. R. Tyagi, S. C. Martin and R. Hughes, *Catalyst Deactivation 2001, Proceedings of the 9th International Symposium*, Elsevier, vol. 139, 2001.
- 11 J. McGregor, Z. Huang, E. P. J. Parrott, J. A. Zeitler, K. L. Nguyen, J. M. Rawson, A. Carley, T. W. Hansen, J.-P. Tessonnier and D. S. Su, *J. Catal.*, 2010, **269**, 329–339.
- 12 A. E. Lisovskii and C. Aharoni, *Catal. Rev.: Sci. Eng.*, 1994, **36**, 25–74.
- 13 Y. M. Zhorov and L. A. Ostrer, *Khim. Tekhnol. Topl. Masel*, 1990, **5**, 11–13.
- 14 J. Barbier, *Appl. Catal.*, 1986, **23**, 225–243.
- 15 C. H. Bartholomew, *Appl. Catal.*, A, 2001, **212**, 17–60.
- 16 E. Ruckenstein and H. Y. Wang, *J. Catal.*, 2002, **205**, 289–293.

- 17 J. R. Rostrup-Nielsen, in *Catalysis Science & Technology*, ed. J. R. Anderson and M. Boudart, Springer Berlin Heidelberg, Berlin, Heidelberg, 1984, pp. 1–118.
- 18 C. H. Bartholomew, *Catal. Rev.: Sci. Eng.*, 1982, **24**, 67–112.
- 19 C. Nederlof, F. Kapteijn and M. Makkee, *Appl. Catal., A*, 2012, **417–418**, 163–173.
- 20 M. Santiago, F. Stüber, A. Fortuny, A. Fabregat and J. Font, *Carbon*, 2005, **43**, 2134–2145.
- 21 M. E. Suarez-Ojeda, F. Stüber, A. Fortuny, A. Fabregat, J. Carrera and J. Font, *Appl. Catal., B*, 2005, **58**, 105–114.
- 22 M. Che and J. C. Vedrine, *Characterisation of Solid Materials and Heterogeneous Catalysts: From Structure to Surface Reactivity, Vol 1&2*, Wiley-VCH Verlag GMBH, Germany, 2012.
- 23 E. Mahmoud and R. F. Lobo, *Microporous Mesoporous Mater.*, 2014, **189**, 97–106.
- 24 F. Haghseresht, G. Q. Lu and A. K. Whittaker, *Carbon*, 1999, **37**, 1491–1497.
- 25 P. Ayala, M. E. H. Maia da Costa, R. Prioli and F. L. Freire, *Surf. Coat. Technol.*, 2004, **182**, 335–341.
- 26 R. Arrigo, M. Hävecker, S. Wrabetz, R. Blume, M. Lerch, J. McGregor, E. P. J. Parrott, J. A. Zeitler, L. F. Gladden, A. Knop-Gericke, R. Schlögl and D. S. Su, *J. Am. Chem. Soc.*, 2010, **132**, 9616–9630.
- 27 S. Gomez-Sanz, L. McMillan, J. McGregor, J. A. Zeitler, N. Al-Yassir, S. Al-Khattaf and L. F. Gladden, *Catal. Sci. Technol.*, 2015, **5**, 3782–3797.
- 28 Y. Jiang, J. Huang, V. R. Reddy Marthala, Y. S. Ooi, J. Weitkamp and M. Hunger, *Microporous Mesoporous Mater.*, 2007, **105**, 132–139.
- 29 Y. Jiang, J. Huang, J. Weitkamp and M. Hunger, *Stud. Surf. Sci. Catal.*, 2007, **170**, 1137–1144.
- 30 I. Kiricsi, I. Pálinkó and T. Kollár, *J. Mol. Struct.*, 2003, **651–653**, 331–334.
- 31 N. G. Hamilton, R. Warringham, I. P. Silverwood, J. Kapitán, L. Hecht, P. B. Webb, R. P. Tooze, W. Zhou, C. D. Frost, S. F. Parker and D. Lennon, *J. Catal.*, 2014, **312**, 221–231.
- 32 R. Warringham, N. G. Hamilton, I. P. Silverwood, C. How, P. B. Webb, R. P. Tooze, W. Zhou, C. D. Frost, S. F. Parker and D. Lennon, *Appl. Catal., A*, 2015, **489**, 209–217.
- 33 A. R. McFarlane, I. P. Silverwood, E. L. Norris, R. M. Ormerod, C. D. Frost, S. F. Parker and D. Lennon, *Chem. Phys.*, 2013, **427**, 54–60.
- 34 C. A. Querini and S. C. Fung, *Catal. Today*, 1997, **37**, 277–283.
- 35 K. Chen, Z. Xue, H. Liu, A. Guo and Z. Wang, *Fuel*, 2013, **113**, 274–279.
- 36 B. Sánchez, M. S. Gross, B. D. Costa and C. A. Querini, *Appl. Catal., A*, 2009, **364**, 335–341.
- 37 O. Bayraktar and E. L. Kugler, *Appl. Catal., A*, 2002, **233**, 197–213.
- 38 H. Muckenhuber and H. Grothe, *Carbon*, 2006, **44**, 546–559.
- 39 S. Haydar, C. Moreno-Castilla, M. A. Ferro-García, F. Carrasco-Marín, J. Rivera-Utrilla, A. Perrard and J. P. Joly, *Carbon*, 2000, **38**, 1297–1308.
- 40 D. J. Moodley, C. van Schalkwyk, A. Spamer, J. M. Botha and A. K. Datye, *Appl. Catal., A*, 2007, **318**, 155–159.
- 41 A. R. Pradhan, T.-S. Lin, W.-H. Chen, S.-J. Jong, J.-F. Wu, K.-J. Chao and S.-B. Liu, *J. Catal.*, 1999, **184**, 29–38.
- 42 A. Bagreev and T. J. Bandosz, *Carbon*, 2001, **39**, 2303–2311.
- 43 J. C. Vickerman and I. Gilmore, *Surface Analysis - The Principal Techniques*, John Wiley & Sons Inc, 2nd edn., 2009.
- 44 L. E. Cadus, O. F. Gorriz and J. B. Rivarola, *Ind. Eng. Chem. Res.*, 1990, **29**, 1143–1146.
- 45 J. M. Thomas, B. Williams and M. Uppal, *Philos. Trans. R. Soc., A*, 1984, **311**, 271–285.
- 46 W. Grünert, in *Characterization of Solid Materials and Heterogeneous Catalysts*, ed. M. Che and J. C. Vedrine, Wiley-VCH Verlag GMBH, Germany, 2012, pp. 537–584.
- 47 A. Knop-Gericke, E. Kleimenov, M. Hävecker, R. Blume, D. Teschner, S. Zafeiratos, R. Schlögl, V. I. Bukhtiyarov, V. V. Kaichev, I. P. Prosvirin, A. I. Nizovskii, H. Bluhm, A. Barinov, P. Dudin and M. Kiskinova, *Adv. Catal.*, 2009, **52**, 213–272.
- 48 H. Gabasch, W. Unterberger, K. Hayek, B. Klötzer, E. Kleimenov, D. Teschner, S. Zafeiratos, M. Hävecker, A. Knop-Gericke, R. Schlögl, J. Han, F. H. Ribeiro, B. Aszalos-Kiss, T. Curtin and D. Zemlyanov, *Surf. Sci.*, 2006, **600**, 2980–2989.
- 49 D. Zemlyanov, B. Klötzer, H. Gabasch, A. Smeltz, F. H. Ribeiro, S. Zafeiratos, D. Teschner, P. Schnörch, E. Vass, M. Hävecker, A. Knop-Gericke and R. Schlögl, *Top. Catal.*, 2013, **56**, 885–895.
- 50 H. Bluhm, M. Hävecker, A. Knop-Gericke, M. Kiskinova, R. Schlögl and M. Salmeron, *MRS Bull.*, 2011, **32**, 1022–1030.
- 51 A. Y. Klyushin, T. C. R. Rocha, M. Hävecker, A. Knop-Gericke and R. Schlögl, *Phys. Chem. Chem. Phys.*, 2014, **16**, 7881–7886.
- 52 D. Teschner, A. Wootsch, O. Pozdnyakovatellinger, J. Krohnert, E. Vass, M. Hävecker, S. Zafeiratos, P. Schnörch, P. Jentoft and A. Knopgericke, *J. Catal.*, 2007, **249**, 318–327.
- 53 V. V. Kaichev, A. Y. Gladky, I. P. Prosvirin, A. A. Saraev, M. Hävecker, A. Knop-Gericke, R. Schlögl and V. I. Bukhtiyarov, *Surf. Sci.*, 2013, **609**, 113–118.
- 54 Z. Paál, A. Wootsch, I. Bakos, S. Szabó, H. Sauer, U. Wild and R. Schlögl, *Appl. Catal., A*, 2006, **309**, 1–9.
- 55 E. W. Hagaman, D. K. Murray and G. D. Del Cul, *Energy Fuels*, 1998, **12**, 399–408.
- 56 S. van Donk, J. H. Bitter and K. P. de Jong, *Appl. Catal., A*, 2001, **212**, 97–116.
- 57 S. Al-Khattaf, C. D'Agostino, M. N. Akhtar, N. Al-Yassir, N. Y. Tan and L. F. Gladden, *Catal. Sci. Technol.*, 2014, **4**, 1017–1027.
- 58 M. C. Barrage, J. L. Bonardet and J. Fraissard, *Catal. Lett.*, 1990, **5**, 143–154.
- 59 H. P. Boehm, *Adv. Catal.*, 1966, **16**, 179–274.
- 60 J. C. J. Camp, M. D. Mantle, A. P. E. York and J. McGregor, *Rev. Sci. Instrum.*, 2014, **85**, 063111.
- 61 J. S. Beck, R. A. Crane Jr., M. F. Mathias, J. A. Kowalski, D. N. Lissy and D. L. Stern, WO1999052842, Mobil Oil Corporation, 1999.

- 62 F. Bauer, W.-H. Chen, Q. Zhao, A. Freyer and S.-B. Liu, *Microporous Mesoporous Mater.*, 2001, **47**, 67–77.
- 63 F. Bauer, W. Chen, E. Bilz, A. Freyer, V. Sauerland and S. Liu, *J. Catal.*, 2007, **251**, 258–270.
- 64 C. Mobil Research and Development, *Eur. Chem. News*, 1990, 54.
- 65 J. C. Gonçalves and A. E. Rodrigues, *Chem. Eng. J.*, 2014, **258**, 194–202.
- 66 L.-Y. Fang, S.-B. Liu and I. Wang, *J. Catal.*, 1999, **185**, 33–42.
- 67 W. Kaeding, C. Chu, L. B. Young, B. Weinstein and S. A. Butter, *J. Catal.*, 1981, **67**, 159–174.
- 68 P.-H. Chao, H.-W. Lin, C.-H. Chen, P.-Y. Wang, Y.-F. Chen, H.-T. Sei and T.-C. Tsai, *Appl. Catal., A*, 2008, **335**, 15–19.
- 69 M. Guisnet, P. Andy, N. S. Gnep, E. Benazzi and C. Travers, *J. Catal.*, 1996, **158**, 551–560.
- 70 W.-Q. Xu, Y.-G. Yin, S. L. Suib and C.-L. O'Young, *J. Phys. Chem.*, 1995, **99**, 758–765.
- 71 P. Cañizares, A. Carrero and P. Sánchez, *Appl. Catal., A*, 2000, **190**, 93–105.
- 72 S. Gomez-Sanz, L. McMillan, J. McGregor, J. A. Zeitler, N. Al-Yassir, S. Al-Khattaf and L. F. Gladden, *Catal. Sci. Technol.*, 2015, DOI: 10.1039/C5CY01157D.
- 73 J. McGregor, A. S. Canning, S. Mitchell, S. D. Jackson and L. F. Gladden, *Appl. Catal., A*, 2010, **384**, 192–200.
- 74 J. McGregor and L. F. Gladden, *Appl. Catal., A*, 2008, **345**, 51–57.
- 75 D. Teschner, J. Borsodi, A. Wootsch, Z. Révay, M. Hävecker, A. Knop-Gericke, S. D. Jackson and R. Schlögl, *Science*, 2008, **320**, 86–89.
- 76 T. G. Alkharov, A. E. Lisovskii, Y. A. Ismailov and A. I. Kozharov, *Kinet. Catal.*, 1978, **19**, 482–485.
- 77 R. Fiedorow, R. Frański, A. Krawczyk and S. Beszterda, *J. Phys. Chem. Solids*, 2004, **65**, 627–632.
- 78 R. Fiedorow, W. Przystajko, M. Sopa and I. G. Dalla Lana, *J. Catal.*, 1981, **68**, 33–41.
- 79 G. E. Vrieland and P. G. Menon, *Appl. Catal.*, 1991, **77**, 1–8.
- 80 J. J. Kim and S. W. Weller, *Appl. Catal.*, 1987, **33**, 15–29.
- 81 M. F. R. Pereira, J. J. M. Orfão and J. L. Figueiredo, *Appl. Catal., A*, 2000, **196**, 43–54.
- 82 M. F. R. Pereira, J. J. Orfão and J. L. Figueiredo, *Appl. Catal., A*, 2001, **218**, 307–318.
- 83 J. A. Maciá-Agulló, D. Cazorla-Amorós, A. Linares-Solano, U. Wild, D. S. Su and R. Schlögl, *Catal. Today*, 2005, **102–103**, 248–253.
- 84 L. E. Cadus, L. A. Arrua, O. F. Gorris and J. B. Rivarola, *Ind. Eng. Chem. Res.*, 1988, **27**, 2241–2246.
- 85 D. S. Su, N. Maksimova, J. J. Delgado, N. Keller, G. Mestl, M. J. Ledoux and R. Schlögl, *Catal. Today*, 2005, **102–103**, 110–114.
- 86 G. Mestl, N. I. Maksimova, N. Keller, V. V. Roddatis and R. Schlögl, *Angew. Chem.*, 2001, **113**, 2122–2125.
- 87 D. Su, N. I. Maksimova, G. Mestl, V. L. Kuznetsov, V. Keller, R. Schlögl and N. Keller, *Carbon*, 2007, **45**, 2145–2151.
- 88 J. Zhang, X. Liu, R. Blume, A. Zhang, R. Schlögl and D. S. Su, *Science*, 2008, **322**, 73–77.
- 89 J. J. Delgado, X.-W. Chen, B. Frank, D. S. Su and R. Schlögl, *Catal. Today*, 2012, **186**, 93–98.
- 90 H. Yuan, H. Liu, J. Diao, X. Gu and D. Su, *Carbon*, 2014, **67**, 795.
- 91 H. Yuan, H. Liu, J. Diao, X. Gu and D. Su, *Xinxing Tan Cailiao*, 2013, **28**, 336–341.
- 92 A. E. Lisovskii and C. Aharoni, *Catal. Rev.: Sci. Eng.*, 1994, **36**, 25–74.
- 93 F. Cavani and F. Trifirò, *Appl. Catal., A*, 1995, **133**, 219–239.
- 94 D. Chen, A. Holmen, Z. Sui and X. Zhou, *Cuihua Xuebao*, 2014, **35**, 824–841.
- 95 V. Zarubina, C. Nederlof, B. van der Linden, F. Kapteijn, H. J. Heeres, M. Makkee and I. Melián-Cabrera, *J. Mol. Catal. A: Chem.*, 2014, **381**, 179–187.
- 96 F. J. Maldonado-Hódar, L. M. Madeira and M. F. Portela, *Appl. Catal., A*, 1999, **178**, 49–60.
- 97 W. Qi and D. Su, *ACS Catal.*, 2014, **4**, 3212–3218.
- 98 A. Schraut, G. Emig and H.-G. Sockel, *Appl. Catal.*, 1987, **29**, 311–326.
- 99 J. Park, J. Noh, J. Chang and S. Park, *Catal. Lett.*, 2000, **65**, 75–78.
- 100 J. Bimer, P. D. Salbut, S. Berlozecki, J. P. Boudou, E. Broniek and T. Siemieniowska, *Fuel*, 1998, **77**, 519–525.
- 101 W. Przystajko, R. Fiedorow and I. G. D. Lana, *Appl. Catal.*, 1990, **59**, 129–140.
- 102 D. C. Cronauer, D. M. Jewell, Y. T. Shah and R. J. Modi, *Ind. Eng. Chem. Fundam.*, 1979, **18**, 153–162.
- 103 S. J. Thomson and G. Webb, *J. Chem. Soc., Chem. Commun.*, 1976, 526–527.
- 104 G. C. A. Schuit and L. L. Van Reijen, *Adv. Catal.*, 1958, **10**, 242–317.
- 105 C. S. Carlson, A. W. Langer, J. Stewart and R. M. Hill, *Ind. Eng. Chem.*, 1958, **50**, 1067–1070.
- 106 D. Godbey, F. Zaera, R. Yeates and G. A. Somorjai, *Surf. Sci.*, 1986, **167**, 150–166.
- 107 T. Kabe, O. Nitoh, E. Funatsu and K. Yamamoto, *Fuel Process. Technol.*, 1986, **14**, 91–101.
- 108 I. Dahl and S. Kolboe, *J. Catal.*, 1996, **161**, 304–309.
- 109 I. Dahl and S. Kolboe, *J. Catal.*, 1994, **149**, 458–464.
- 110 T. Xu and J. L. White, *US Pat.* 6734330, ExxonMobil Chemical Patents Inc., 2004.
- 111 D. Chen, K. Moljord and A. Holmen, *Microporous Mesoporous Mater.*, 2012, **164**, 239–250.
- 112 S. Ilias and A. Bhan, *ACS Catal.*, 2013, **3**, 18–31.
- 113 W. Song, D. M. Marcus, H. Fu, J. O. Ehresmann and J. F. Haw, *J. Am. Chem. Soc.*, 2002, **124**, 3844–3845.
- 114 G. C. Bond, *Appl. Catal., A*, 1997, **149**, 3–25.
- 115 J. Matos, P. S. Poon, S. Lanfredi and M. A. L. Nobre, *Fuel*, 2013, **107**, 503–510.
- 116 P. G. Menon, *Appl. Catal., A*, 1992, **86**, N6–N7.
- 117 Q. Liu and K. J. Smith, *Can. J. Chem. Eng.*, 1995, **73**, 337–344.
- 118 G. Boskovic and K. J. Smith, *Catal. Today*, 1997, **37**, 25–32.
- 119 M. Guisnet, *J. Mol. Catal. A: Chem.*, 2002, **182–183**, 367–382.
- 120 P. Meriaudeau, R. Bacaud, L. N. Hung and A. T. Vu, *J. Mol. Catal. A: Chem.*, 1996, **110**, L177–L179.

- 121 J. Houzvička and V. Ponec, *Ind. Eng. Chem. Res.*, 1997, **36**, 1424–1430.
- 122 M. Guisnet, P. Andy, N. S. Gnep, C. Travers and E. Benazzi, *J. Chem. Soc., Chem. Commun.*, 1995, 1685.
- 123 P. Meriaudeau, C. Naccache, H. N. Le, T. A. Vu and G. Szabo, *J. Mol. Catal. A: Chem.*, 1997, **123**, L1–L4.
- 124 W.-Q. Xu, Y.-G. Yin, S. L. Suib, J. C. Edwards and C.-L. O'Young, *J. Catal.*, 1996, **163**, 232–244.
- 125 B. S. Kwak and J. Sung, *Catal. Lett.*, 1998, **53**, 125–129.
- 126 Z. Finelli, N. Figoli and R. Comelli, *Catal. Lett.*, 1998, **51**, 223–228.
- 127 P. Andy, N. S. Gnep, M. Guisnet, E. Benazzi and C. Travers, *J. Catal.*, 1998, **173**, 322–332.
- 128 J. A. Martens, R. Parton, L. Uytterhoeven, P. A. Jacobs and G. F. Froment, *Appl. Catal.*, 1991, **76**, 95–116.
- 129 Z. Da, P. Magnoux and M. Guisnet, *Appl. Catal.*, **A**, 1999, **182**, 407–411.
- 130 P. Magnoux, M. Guisnet and I. Ferino, *Stud. Surf. Sci. Catal.*, 2000, **180**, 275–280.
- 131 C. K. Lee, L. F. Gladden and P. J. Barrie, *Appl. Catal.*, **A**, 2004, **274**, 269–274.
- 132 M. García-Mota, B. Bridier, J. Pérez-Ramírez and N. López, *J. Catal.*, 2010, **273**, 92–102.
- 133 M. W. Tew, M. Janousch, T. Huthwelker and J. A. van Bokhoven, *J. Catal.*, 2011, **283**, 45–54.
- 134 D. Teschner, E. Vass, M. Havecker, S. Zafeiratos, P. Schinorch, H. Sauer, A. Knopgericke, R. Schlogl, M. Chamam and A. Wootsch, *J. Catal.*, 2006, **242**, 26–37.
- 135 S. Jackson, G. D. McLellan, G. Webb, L. Conyers, M. B. T. Keegan, S. Mather, S. Simpson, P. B. Wells, D. A. Whan and R. Whyman, *J. Catal.*, 1996, **162**, 10–19.
- 136 F. Studt, F. Abild-Pedersen, T. Bligaard, R. Z. Sørensen, C. H. Christensen and J. K. Nørskov, *Angew. Chem., Int. Ed.*, 2008, **47**, 9299–9302.
- 137 B. Yang, R. Burch, C. Hardacre, P. Hu and P. Hughes, *Surf. Sci.*, 2015, DOI: 10.1016/j.susc.2015.07.015.
- 138 J. R. Kitchin, J. K. Nørskov, M. A. Barteau and J. G. Chen, *Catal. Today*, 2005, **105**, 66–73.
- 139 T. Ouchaib, J. Massardier and A. Renouprez, *J. Catal.*, 1989, **119**, 517–520.
- 140 D. Teschner, Z. Révay, J. Borsodi, M. Hävecker, A. Knopgericke, R. Schlögl, D. Milroy, S. D. Jackson, D. Torres and P. Sautet, *Angew. Chem., Int. Ed.*, 2008, **47**, 9274–9278.
- 141 D. Teschner, J. Borsodi, Z. Kis, L. Szentmiklósi, Z. Révay, A. Knopgericke, R. Schlögl, D. Torres and P. Sautet, *J. Phys. Chem. C*, 2010, **114**, 2293–2299.
- 142 A. Frackiewicz and A. Janko, *Acta Crystallogr., Sect. A: Cryst. Phys., Diffr., Theor. Gen. Crystallogr.*, 1978, **34**, S377–S378.
- 143 A. H. Zaidi, *Appl. Catal.*, 1987, **30**, 131–140.
- 144 Q. Zhang, W. Deng and Y. Wang, *J. Energy Chem.*, 2013, **22**, 27–38.
- 145 J. G. Goodwin, D. O. Goa, S. Erdal and F. H. Rogan, *Appl. Catal.*, 1986, **24**, 199–209.
- 146 M. G. A. Cruz, M. Bastos-Neto, A. C. Oliveira, J. M. Filho, J. M. Soares, E. Rodríguez-Castellón and F. A. N. Fernandes, *Appl. Catal.*, **A**, 2015, **495**, 72–83.
- 147 M. Araki and V. Ponec, *J. Catal.*, 1976, **44**, 439–448.
- 148 E. de Smit and B. M. Weckhuysen, *Chem. Soc. Rev.*, 2008, **37**, 2758–2781.
- 149 Q. Zhang, J. Kang and Y. Wang, *ChemCatChem*, 2010, **2**, 1030–1058.
- 150 H. Karaca, O. V. Safonova, S. Chambrey, P. Fongarland, P. Roussel, A. Griboval-Constant, M. Lacroix and A. Y. Khodakov, *J. Catal.*, 2011, **277**, 14–26.
- 151 K. Fei Tan, J. Xu, J. Chang, A. Borgna and M. Saeys, *J. Catal.*, 2010, **274**, 121–129.
- 152 K. Keyvanloo, M. J. Fisher, W. C. Hecker, R. J. Lancee, G. Jacobs and C. H. Bartholomew, *J. Catal.*, 2015, **327**, 33–47.
- 153 R. A. van Santen, M. M. Ghouri, S. Shetty and E. M. H. Hensen, *Catal. Sci. Technol.*, 2011, **1**, 891.
- 154 O. R. Inderwildi, S. J. Jenkins and D. A. King, *Angew. Chem., Int. Ed.*, 2008, **47**, 5253–5255.
- 155 C.-F. Huo, Y.-W. Li, J. Wang and H. Jiao, *J. Phys. Chem. C*, 2008, **112**, 14108–14116.
- 156 S. Shetty, A. P. J. Jansen and R. A. van Santen, *J. Am. Chem. Soc.*, 2009, **131**, 12874–12875.
- 157 M. Ojeda, R. Nabar, A. U. Nilekar, A. Ishikawa, M. Mavrikakis and E. Iglesia, *J. Catal.*, 2010, **272**, 287–297.
- 158 C. Yang, H. Zhao, Y. Hou and D. Ma, *J. Am. Chem. Soc.*, 2012, **134**, 15814–15821.
- 159 H. M. Torres Galvis, J. H. Bitter, T. Davidian, M. Ruitenbeek, A. I. Dugulan and K. P. de Jong, *J. Am. Chem. Soc.*, 2012, **134**, 16207–16215.
- 160 J.-Y. Lim, J. McGregor, A. Sederman and J. S. Dennis, *Chem. Eng. Sci.*, 2015, in press.
- 161 M. J. Ledoux, C. Pham-Huu and R. R. Chianelli, *Curr. Opin. Solid State Mater. Sci.*, 1996, **1**, 96–100.
- 162 J. M. Bermudez, J. A. Menendez, A. Arenillas, R. Martinez-Palou, A. A. Romero and R. Luque, *J. Mol. Catal. A: Chem.*, 2015, **406**, 19–22.
- 163 S. Suzuki, T. Sasaki, T. Kojima, M. Yamamura and T. Yoshinari, *Energy Fuels*, 1996, **10**, 531–536.
- 164 D. O. Cooney and Z. Xi, *AIChE J.*, 1994, **40**, 361–364.
- 165 T. Koerts and R. A. Van Santen, *Stud. Surf. Sci. Catal.*, 1993, **75**, 1065–1078.
- 166 V. I. Alexiadis, J. W. Thybaut, P. N. Kechagiopoulos, M. Chaar, A. C. Van Veen, M. Muhler and G. B. Marin, *Appl. Catal.*, **B**, 2014, **150–151**, 496–505.
- 167 P. N. Kechagiopoulos, J. W. Thybaut and G. B. Marin, *Ind. Eng. Chem. Res.*, 2014, **53**, 1825–1840.
- 168 J. W. Thybaut, J. Sun, L. Olivier, A. C. Van Veen, C. Mirodatos and G. B. Marin, *Catal. Today*, 2011, **159**, 29–36.
- 169 S. C. Fung and C. A. Querini, *J. Catal.*, 1992, **138**, 240–254.
- 170 R. Thomas, J. A. Moulijn, V. H. J. De Beer and J. Medema, *J. Mol. Catal.*, 1980, **8**, 161–174.
- 171 N. Tsuda, T. Mori, N. Kosaka and Y. Sakai, *J. Mol. Catal.*, 1985, **28**, 183–190.
- 172 Y. Shi, J. Chen, J. Chen, R. A. Macleod and M. Malac, *Appl. Catal.*, **A**, 2012, **441–442**, 99–107.
- 173 I. Eswaramoorthi, V. Sundaramurthy, N. Das, A. K. Dalai and J. Adjaye, *Appl. Catal.*, **A**, 2008, **339**, 187–195.

- 174 S. K. Maity, L. Flores, J. Ancheyta and H. Fukuyama, *Ind. Eng. Chem. Res.*, 2009, **48**, 1190–1195.
- 175 E. Aryee, A. K. Dalai and J. Adjaye, *Top. Catal.*, 2013, **57**, 796–805.
- 176 D. L. Trimm, *Appl. Catal.*, 1983, **5**, 263–290.
- 177 G. E. Keller and M. M. Bhasin, *J. Catal.*, 1982, **73**, 9–19.
- 178 J. Gornay, L. Coniglio, F. Billaud and G. Wild, *J. Anal. Appl. Pyrolysis*, 2010, **87**, 78–84.
- 179 F. Bonnet, F. Ropital, P. Lecour, D. Espinat, Y. Huiban, L. Gengembre, Y. Berthier and P. Marcus, *Surf. Interface Anal.*, 2002, **34**, 418–422.
- 180 Y. M. Foong, A. T. T. Koh, H. Y. Ng and D. H. C. Chua, *J. Appl. Phys.*, 2011, **110**, 054904.
- 181 K. B. Liew, W. R. Wan Daud, M. Ghasemi, K. S. Loh, M. Ismail, S. S. Lim and J. X. Leong, *Int. J. Hydrogen Energy*, 2015, **40**, 11625–11632.
- 182 W. Y. Wong, W. R. W. Daud, A. B. Mohamad, A. A. H. Kadhum, E. H. Majlan and K. S. Loh, *Diamond Relat. Mater.*, 2012, **22**, 12–22.
- 183 A. Bhatnagar, W. Hogland, M. Marques and M. Sillanpää, *Chem. Eng. J.*, 2013, **219**, 499–511.
- 184 C. Ampelli, S. Perathoner and G. Centi, *Cuihua Xuebao*, 2014, **35**, 783–791.
- 185 D. J. Ham and J. S. Lee, *Energies*, 2009, **2**, 873–899.
- 186 J. R. Kastner, J. Miller, D. P. Geller, J. Locklin, L. H. Keith and T. Johnson, *Catal. Today*, 2012, **190**, 122–132.